AGARD-LS-39-70

AGARD-LS-39-70

AGARD

ADVISORY GROUP FOR AEROSPACE RESEARCH & DEVELOPMENT

7 RUE ANCELLE 92 NEUILLY-SUR-SEINE FRANCE

LECTURE SERIES No. 39

on

Advanced Compressors

NORTH ATLANTIC TREATY ORGANIZATION

NORTH ATLANTIC TREATY ORGANIZATION

ADVISORY GROUP FOR AEROSPACE RESEARCH AND DEVELOPMENT

(ORGANISATION DU TRAITE DE L'ATLANTIQUE NORD)

ADVANCED COMPRESSORS

The material in this book has been assembled to support a Lecture Series under the sponsorship of the Propulsion and Energetics Panel and the Consultant and Exchange Programme of AGARD.

The material in this publication has been composed directly from copy supplied by each author.

Published August 1970

621.438.031.3

Printed by Technical Editing and Reproduction Ltd
Harford House, 7-9 Charlotte St, London. W1P 1HD

FOREWORD

Upon invitation of National Delegates of Belgium and Norway, Lecture Series 39 on "Advanced Compressors" was presented in Brussels, Belgium, and in Bolkesjø, Norway, in June 1970.

This Lecture Series was sponsored by the Propulsion and Energetics Panel and the Consultant and Exchange Programme of AGARD.

During the past few years, significant progress has been made in the design and development of high performance axial and radial compressors, in response to the increasing demand from jet engine and gas turbine manufacturers and to the broadening interest for such machines for closed cycle gas turbine application for atomic power plants.

The development of digital computers has enabled the use of more and more sophisticated design methods which are now paying off. Significant improvements have also been obtained for the compressor operation in the transonic and supersonic range. Interest in the long forgotten radial compressors has been revived, for small gas turbine application, and startling improvement in performance has been obtained, both in efficiency and in maximum pressure ratio obtainable.

It was felt by AGARD that a review of the recent progress and of the prospects for the future was appropriate.

The Lecture Series, which was presented by leading experts in the field, covered advanced information on radial and axial flow compressors, including application of through-flow methods of calculation to axial and radial transonic and supersonic compressors, flow in supersonic bladings (cascade performance and mass flow limitations), flow in subsonic bladings with a local supersonic region, secondary flows and losses, advanced design of radial flow compressors, supersonic vaneless and vaned diffusers.

The Lecture Series was concluded by a round-table discussion.

Scientists and Engineers from 10 NATO Nations participated in this Lecture Series.

ROLLAND A. WILLAUME
Director, Plans and Programmes, AGARD

AVANT-PROPOS

Sur l'invitation des délégués nationaux de la Belgique et de la Norvège, la série de conférences No.39 consacrée aux "Compresseurs d'Avant-garde" fut présentée à Bruxelles, Belgique, et à Bolkesjø, Norvège en juin 1970.

La présente série de conférences fut placée sous l'égide de la Commission "Propulsion et Energétique" et du "Programme Consultatif et d'Echange" de l'AGARD.

Au cours de ces dernières années, des progrès importants ont été réalisés en matière de la conception et de la mise au point des compresseurs axiaux et radiaux à rendement élevé, et ce pour répondre à la demande toujours croissante de la part des fabricants de moteurs à réaction et de turbines à gaz, ainsi qu'à l'intérêt de plus en plus large porté à de telles machines pour application aux turbines à gaz à cycle fermé destinées aux centrales nucléaires.

L'évolution des ordinateurs numériques a permis l'utilisation de techniques d'étude de plus en plus raffinées qui commencent à s'amortir. Une amélioration sensible du fonctionnement du compresseur en régime transsonique et supersonique a également été obtenue. On porte un nouvel intérêt aux compresseurs de type radial, oubliés depuis longtemps, pour application aux turbines à gaz de petite taille, et dans le domaine des performances, aussi bien le rendement que le rapport maximum de pression réalisable se sont trouvés améliorés de facon saisissante.

Il a semblé opportun à l'AGARD de passer en revue les proprès enregistrés jusqu'à présent et les perspectives d'avenir.

La série de conférences, présentée par les grands spécialistes en la matière, a fourni des renseignements avancés sur les compresseurs à écoulement tant axial que radial, y compris l'application aux compresseurs transsoniques et supersoniques à écoulement axial ou radial de procédés de calcul utilisant un écoulement droit; l'écoulement dans les aubages supersoniques (performances des grilles et limitations à d'écoulement massique); l'écoulement dans les aubages subsoniques ayant une zone supersonique locale; les écoulements secondaires et les pertes; l'étude évoluée des compresseurs à écoulement radial; les diffuseurs supersoniques sans et avec aubes.

La série de conférences s'est terminée par une "Table Ronde", et a réuni des scientifiques et ingénieurs venant de 10 pays membres de l'OTAN.

ROLLAND A.WILLAUME
Directeur, Plans et Programmes, AGARD

CONTENTS

PARTICIPANTS

Lecture Series Director: Professor J. Chauvin
Von Kármán Institute
Rhode-Saint-Genèse
Belgium

Speakers:

Mr J. Fabri
Chef de Division de Recherches
ONERA
Châtillon-sous-Bagneux
France

Dr H. Griepentrog
Gutehoffnungshütte Sterkrade
Oberhausen
Germany

Mr D. P. Kenny
Supervisor, Compressor Research
United Aircraft of Canada Ltd
Longueuil, Quebec
Canada

Dr H. Marsh
Engineering Department
University of Cambridge
UK

Mr H. Starken
Institut für Luftstrahlantriebe
DFVLR
Porz-Wahn
Germany

Professor M. H. Vavra
US Naval Postgraduate School
Monterey, California
USA

INTRODUCTORY REMARKS

RECENT PROGRESS IN AERODYNAMIC DESIGN OF COMPRESSORS.

J..CHAUVIN

Professor, Head Turbomachinery Laboratory
von Karman Institute

S U M M A R Y

The progress made during the last few years in compressor performance is briefly reviewed. The reasons behind this progress (systematic use of transonic or supersonic blading, improvement in understanding of the flow behaviour, development of sophisticated theories, availability of large computers) are reviewed and briefly discussed.

The course content is presented, and justified, starting from a physical description of the flow in turbomachines and of the resulting flow models and some of the critical areas for future research are presented.

S O M M A I R E

Les progrès réalisés dans l'accroissement des performances des compresseurs au cours de ces dernières années sont passés en revue. Les bases de ces progrès (utilisation systématique d'aubages transsoniques et supersoniques, meilleure compréhension des mécanismes d'écoulement, développement de théories plus complexes, utilisations d'ordinateurs à grande capacité) sont présentées.

On présente ensuite le contenu du cours, au départ d'une description physique des écoulements dans les turbomachines et des modèles d'écoulement qui en découlent. On présente ensuite quelques-uns des domaines de recherches critiques pour les développements futurs.

LIST OF FIGURES

I. INTRODUCTION

During the last decade, considerable success has been achieved in the improvement of compressor performance. The development of successful axial compressors has continued to follow its steady place of the years 50, and, due to a strong revival of interest for many applications, the radial compressor has seen its rate of progress accelerated considerably.

As in the past, most of the improvement has come from the exacting requirements of the aircraft industry, but, at the same time, the knowledge gained in this privileged sector has been diffusing, at an increasing rate, into the more conventional industry, with some degree of original achievements ((1), for instance).

The evolution of axial compressors for the large and medium size jet engines is summarized in figs. 1 and 2, replotted partly from (2), with additional data on comparable machines coming from tests carried out at VKI. Within the last 10 years, a 60% increase in stage pressure ratio has been achieved, mainly through an increase of the average Mach number level, relative to the rotor bladings, while maintaining practically the same efficiency. The maximum pressure ratio of multistages machines has been raised from 10 about to 27, and could reach more if this was requested by the gas turbine cycle. This fact proves that the interstage matching problem has been largely mastered. The progress has been obtained in the whole ranges of stage types, from the front fan with very low hub to tip ratio (down to 0.3) and high relative rotor inlet Mach number (up to 1.7 at the tip), where the streamline equilibrium problem is predominant, to the high hub to tip ratio (up to 0.9), subsonic rear stages, where end wall effects is the most important factor.

Similar if not larger progress has been achieved in the field of small turbojet and of small gas turbines (500 to 2000 HP) for plane, helicopter or terrestrial propulsion, as witnessed by fig. 3 replotted from (3) and completed. The progress has been stimulated by intelligent government sponsored programs such as the U.S. Army Advanced Component Technology program (4), and it is not unrealistic to predict that, within the next decade, the gas turbine will compete successfully with the diesel engine for many classical applications (5). Although the increase of turbine inlet temperature is the key element for success, it would be fruitless without a parallel increase in compressor pressure ratio, as shown in fig. 4. Due to the small volume flow involved, blade size is always small and end wall effects are predominant, whatever the type of compressor used.

The trend of increasing the average blade Mach number is the same as for the compressors for the larger engines, and even more pronounced, for the advanced projects, which show the first practical application of truly supersonic compressors (6,7,8,9,10).

The progress accomplished with radial compressors is particularly noteworthy. Pressure ratios of the order of 12 per stage have been achieved, with efficiencies in the 70-75% bracket (fig. 5). The feasibility of such high pressure ratios has clearly been established (1,8,9,10) . The aim is now to improve the efficiency at design point. A typical contemporary target is 8/1 pressure ratio and 80% adiabatic efficiency and 10/1 at 75% efficiency.

Already at this stage, new concepts have been introduced in wheel, and especially, in diffuser design ((8,10) and fig. 6).

The past decade has thus been extremely fruitful for the compressor designer, and still more important progress lies ahead. The reason behind this progress will be discussed in par. IV after a physical description of the flow in compressors.

II. PHYSICAL DESCRIPTION OF THE FLOW

The flow through a compressor blade row is essentially three dimensional in nature. In an axial machine, the through flow direction is axial, and varies along the stream direction, except for very particular cases. The flow is deflected tangentially through the blading, and, for a force to be exerted on the blading, a circumferential variation of the velocities must occur between the pressure side of one blade and the suction side of the next one, leading to distortion of the stream surface (induced radial component) (fig. 7). Hub and casing curvature induce further radial components, and, even in a cylindrical channel, the streamlines must assume some curvature in the radial direction, for the flow continuity and conservation of momentum to be satisfied.

In contemporary machines, the flow is always compressible, and very often, local supersonic regions, terminated by shocks appear in the blade passages (fig. 8), or even, for transonic and supersonic compressors, a significant part of the flow at the inlet and in the passage is supersonic and affected by shocks. Boundary layers develop on the blade surfaces and merge in the wakes. They also develop on the hub and casing. Those boundary layers are strongly affected by the shocks, in the compressible regime.

Interaction between hub or casing and blade boundary layers is significant, as shown in fig. 9. The hub and casing boundary layers are submitted to the circumferential pressure gradients existing between the pressure side of one blade and the suction side of the next one. As the velocity is reduced in the boundary layers, a transverse motion

is generated, and the boundary layer material accumulates in the corner formed by the blade suction surface and the hub or casing, where it rolls up in a vortex, very often inducing an extensive separation of the blade boundary layer. An important secondary flow is thus superimposed on the main flow, resulting in the formation of large zones of low energy viscous material and of important local changes of velocity, influencing the bulk of the flow by blockage and swirl induction.

Clearance effects also produce a corner vortex (fig. 10) and deflection of the hub and casing boundary layer existing prior to entrance to the blading induce bulk vortices, whose main effect is to modify the flow direction. An additional secondary flow is due to the centrifugation of the blade boundary layer on the rotor blades, of of their motion towards the hub, due to the radial pressure gradient, in the stators (12,13).

We thus have a fully three dimensional, compressible, viscous type of flow. It is also generally unsteady even for the first rotor row (unsteady motion in absolute coordinates (14)) and quite clearly for all the following blade rows, even for a steady operation of the machine. Any blade row is in relative motion with respect to the preceding one. The flow coming out of this latter is essentially non uniform, and due to the relative motion, feeds the next blade with a flow periodic in time. In particular, it can be shown (15,16) that the wakes coming from the upstream blade row maintain their individuality through one or more successive blade rows, while hub and casing boundary layers are re-energized and mixed (17,18).

Other types of unsteady flow occur in the rotating stall and surge regime of operation. They are also mostly periodic (19,20).

In a radial machine, a similar type of flow exists. The inducer part, which is quite extended in modern compressors has a flow field very closely related to the flow in an axial compressor rotor. The inlet flow is either in the high subsonic range, or partly supersonic, or entirely supersonic (21,8,9,10). In the radial part of the impeller, the flow is also of a tri-dimensional character. In addition to the main radial flow, circumferential variations must exist to produce the force on the blade. Viscous effects and boundary layer interaction are also present. Additionnally, it can be shown both theoretically and experimentally (21) that, due to the rapid area increase with the radius, separation occurs often in the passage between two blades, introducing important secondary flows, with re-circulation inside the blading.(fig. 11 to 14). In particular, at the wheel outlet, the flow can be considered as being made of two jets, one with a high velocity, the other with a small or even zero velocity. Due to clearance effects, a return flow from exit to outlet can exist near the casing. Reference 22 gives detailed velocity distribution in a wheel of large dimensions, rotating at very low speed (the observer sits in the wheel). Figure 15 shows a typical result.

The diffuser is attacked by a heavily unsteady flow, under a high swirl angle (from the axial direction) with velocities in the sonic and, very often, supersonic range to be diffused practically to a zero velocity. Past the entrance region (fig. 16) affected by shocks, the diffuser behaves like a curved pipe or diffuser of rectangular cross section, with the usual secondary flows.

III. DEFINITION OF THE FLOW MODELS

The three dimensional, unsteady, viscous and compressible flow that we have described corresponds to the full Navier-Stokes equations, which cannot be solved - at least now. The detailed flow mechanism is even not yer fully understood. Flow models have to be defined, based on some hopefully justified hypothesis, to allow for a satisfactory solution of the design problem; and an understanding, as complete as possible of the most significant phenomenon occuring in the machine. The basis of the most used one has been established some 20 years ago by Wu (25) but its application is continuously improved.

The first approximation introduced is that, for steady operation of the machine, the flow is steady. We have seen that this was by no means true. However, from our present knowledge about unsteady viscous flows (24) it appears that the reduced frequency of the flow phenomena is such that the steady flow value of the force acting on the bladings, the velocities, etc. are close to the average value of the same parameter in the unsteady flow. This might be questionable, however, for the case of the vaned diffuser of radial compressors. The approximation finds a partial justification in that the machines built on the resulting flow model have achieved, in general, a satisfactory level of performance. It is quite sure, however, that additional progress will be gained when the full impact of the unsteady character of the flow will be understood. This point attracts an increasing amount of research effort.

The second approximation consists in replacing the three dimensional flow by the superposition of two two-dimensional flows.

The first one is the "flow in the meridional plane " (fig. 17) assuming the flow to be axisymmetric (all derivatives are zero in the peripheral direction). This is coherent with the steady flow approximation. It is supposed to represent the flow on a mean stream surface containing the axis (26) or its projection on a plane defined by the axis of the machine and a radius (27,28,29).

The use of this two-dimensional model was initially limited to the calculation of simple isentropic radial equilibrium (no entropy variation along the radius, blade rows considered as isolated, calculations outside the blade region, no streamline curvature, subsonic velocities) which gave rise to the classical forms of swirl distribution (free vortex, constant α_2, etc.). With the advent of digital computers, it has now be allowed to develop computing tools (through-flow methods of calculation) incorporating radial variations of entropy and enthalpy, matrix solutions for multistage machines considered globally, blade regions, streamline curvatures and transonic and supersonic flows. Apart the difficulties inherent to numerical iterative solutions of the flow equations, the single more important difficulty is the evaluation of the entropy variation along the radius, always considerable near the ends of the blades, and all along the radius, for small, highly loaded bladings.

The second two-dimensional model is the "blade to blade flow" (fig. 18), considering the flow on a cylindrical or conical surface centered on the axis, i.e., on an axisymmetric stream surface. The inlet flow is generally supposed to be uniform and defined by the flow in the meridional plane, although this model is now frequently used with non-uniform and unsteady flows to try to gain a better understanding of the unsteady effects.

This model neglects the stream surface distorsion mentioned above (fig. 7). For axial machines, where stre mline shift in the radial direction can usually be neglected, a further simplification can be used (development of the stream surface onto a plane), leading to the well known cascade model. This type of model is valid for stator and approximates relatively well the relative flows in rotor blade sections, when the energy addition in the relative system of coordinates can be neglected (small change in radius of the streamline through the blading). The cascade model seems to be as useful, for the theoretical and experimental investigation for the highly loaded transonic and supersonic blading as it was for the more conventional subsonic bladings (30). It is widely used to gain a better understanding of the flow mechanism and gather data on the losses, pressure increase and turning produced by given blade sections, as examplified in the contribution of MM Starken and Griepentrog to this course. It is also fit to develop optimum blade design procedure, as examplified in (31) and (32). The experimental model can also be used to investigate a certain number of aspects of the secondary flows. This is most useful to help evaluating the entropy variation for the preceding model.

The cascade model cannot be used, of course, to simulate the flow in radial compressor rotors, as there the mechanism of creation of the force on the blading and of energy transfer by rotation cannot be separated anymore (change in radius), except for the inducer part, where the flow strongly resembles the flow in an axial compressor rotor, as already mentioned.

In the radial part, the blade to blade flow is most often considered in the calculations as to be approximated by a linear variation of velocity across the blade passage.

Combining the two two-dimensional flow models it is possible, with some corrections for end wall effects (33,34) to reconstitute an approximate picture for design or analysis purposes (prediction of off-design performance).

This type of approach has been used for the past twenty years, and has been shown to be valid as well for advanced machines, operating in the transonic and supersonic ranges. It is flexible enough to incorporate information coming from a better understanding of thee flow phenomena as they come. It will probably be used for a rather long period of time in the future, although one must try to lift the restriction inherent to the unsteady flow assumption. A further reason of studying the unsteady flow arises from the need to reduce engine noise (35).

IV. ORIGIN OF THE PROGRESS IN COMPRESSOR AERODYNAMIC DESIGN

As mentioned above, the contemporary to compressor design is not new. The most sophisticated equations involved were explicited by Wu (25) in 1950 already. They could not be exploited, however, as no sufficient means were available to perform their numerical solution on the one hand, and as the understading of the phenomena were not sufficient to give the necessary input for their solution.

The slide rule operator could solve the "isentropic simple radial equilibrium" equation, for instance

$$V_u \frac{\partial V_u}{\partial R} + \frac{V_u^2}{R} + V_a \frac{\partial V_a}{\partial R} \qquad (1)$$

(V_u, V_a tangential and axial components of velocity; R, radius), which led to the classical whirl distribution (free vortex, etc.) but could not tackle the generalised radial equilibrium equation.

$$\frac{\partial H}{\partial R} = T \frac{\partial S}{\partial R} + V_u \frac{\partial V_u}{\partial R} + \frac{V_u^2}{R} + V_a \frac{\partial V_a}{\partial a} - V_a \frac{\partial V_R}{\partial a} \qquad (2)$$

(H, total enthalpy; T, absolute temperature; S, entropy; V_R radial velocity; a, coordinate in the axial direction), which describes more accurately the flow characteristics, with its energy and entropy gradients, and the streamline curvature effect. The introduction of the total enthalpy gradient, for instance, is a powerful tool for the designer (35) giving him an additional degree of freedom. Hub and casing contouring (corresponding to the terms in V_a in (2)) are also important.

Thus, one of the main agents in the progress is the digital computer, which gave the possibility of working with equations like (2) in complex systems which will be discussed by Dr Marsh.

The computer will, however, only give back to you the data fed to it, in another form, and its output is worth only what the inputs are worth (entropy gradients, for instance). A correct quantitative description of the flow can thus only come from a good qualitative understanding of its characteristics, allowing in turn to feed in correct numerical inputs.

Among the factors of progress in the understanding of the flow behaviour, the most predominants can be listed as follows:

- better knowledge of boundary layers in general (31,32,36) and in particular of boundary layer shock interaction, and end wall boundary layers (11,33)
- better appreciation of the mode of operation of blades in the supersonic range, i.e., inlet flow mechanism, shock patterns in passages, back pressure effects which led to the design of new types of bladings, reducing shock strength and with a subsonic outlet flow for axial flow compressors, leading to new design for vaned diffusers in radial compressors. A satisfactory fully theoretical method is not yet available however.
- more detailed knowledge of the flow in bladings attacked at highly subsonic Mach number, and having high loading (more correct limit loading factors, inclusion of shock boundary layer interaction, etc.)
- better understanding of the mechanism of secondary flows and of the parameters influencing them, particularly loading and aspect ratio (blade height to blade chord ratio).Semi-empirical correlations are still the basis of quantitative data, however. Fragmentary but significant progress was made also in the understanding of noise generation, stall, stall flutter and surge.

PRESENTATION OF THE COURSE CONTENT

This course is the result of a recommendation of the Propulsion and Energetics Panel of AGARD, energetically and efficiently put into action by AGARD Plans and Programs. The Panel felt that the beginning of the 70th decade was a good time to present a review of the fundamental aspects of the progress which has lead to the impressive improvement in performance of the aircraft and gas turbine compressor.

For this purpose, a group of leading experts in the field was picked up. Each of them has made, to different degrees, original contributions to the development of the modern compressor. They are research people and scholars, but with a deep knowledge of the "hardware" side, through their active contacts with the industry.

Their mission is limited in time and scope. The course is limited to the aerodynamic design aspects and only the most basic aspects will be covered and namely:

For axial compressors:

Dr Marsh will deal with the thorough flow methods of calculation, including losses and end wall boundary layer, and with particular emphasis on the application of the methods to transonic and supersonic compressors.

MM Starken and Fabri will deal with the fundamental aspects of the flow in bladings submitted to a supersonic inlet velocity: mass flow limitation, detailed structure of the inlet flow field and the corresponding methods of calculation, effects of axial velocity ratio on losses and diffusion.

Dr Griepentrog will present the problems associated with the flow in bladings submitted to a high subsonic flow with local supersonic regions contained into the passages between two blades. This is a relevant problem for the root section of transonic rotors and for the stators of all highly loaded machines. He will also discuss the problems of secondary flows and losses, and present semi-empirical correlations showing the factors affecting the losses, mainly the loading the loading and aspect ratio.

For radial compressors:

Professor Vavra will deal with the basic elements for advanced design n the basis of dimensionless parameters, and loss relationships. He will then introduce the through flow theory for radial wheel calculations showing in particular the effects of the simplification introduced into the calculation.

Mr D. Kenny will discuss the very important aspect of diffuser flow for advanced radial compressors, operating in the supersonic region.

The problems associated with stall and surge inlet maldistribution, noise (i.e., unsteady flows in general) have been left out. They would justify a full course by themselves as well as the problem linked to structural integrity and technology (materials, vibration, shaft, bearing, manufacture processes, etc.)

AREAS FOR FUTURE RESEARCH

The course will be concluded by a round table discussion, which will allow a confrontation of the authors' point of view, but also stress out the areas where research is urgently needed.

Tentatively, I would personally suggest that the following points, related to the problems dealt with here still need a lot of clarification:

- secondary flows: no satisfactory theoretical method is available for the moment, and the prediction of flow direction in the secondary flow region is still very inaccurate;
- flow in bladings with supersonic inlet flow: here again, there is no way of predicting accurately the shock pattern inside the blade passages. Shock boundary layer interactions are a key factor, especially for long passages.
- for radial machines, and to a lower extent, for axial machines, the rotor-diffuser or rotor stator interaction are still to be fully understood. It is obvious (9) that good radial machines are obtained only by half empirical matching of diffusers to a particular wheel concept.
- taking into account the unsteady flow phenomenon might be a key to future improvements and the knowledge is still fragmentary.

To quote Professor Vavra, 90 % efficiency, as achieved in many instances, seems to be pretty high, but, frankly, 10% of wasted energy is a very large amount, and we have a long way to go, and hard work lying ahead to improve the situation.

LIST OF REFERENCES

1. HORTOBAGYI, F.: Application des compresseurs supersoniques d'une nouvelle conception à l'industrie du froid.
Conférence de l'Industrie du Froid, Madrid.

2. NEWTON, A.G.: The axial compressor. Problems of design and application.
Lecture given at the von Karman Institute, Rhode Saint Genèse, Belgium, 12th December 1967 - Rolls Royce Publication.

3. ELLIS, C.W., ACURIO, J., SCHNEIDER, J.J.: Helicopter propulsion trends,in Helicopter Propulsion Systems.
AGARD Conference Proceedings 31, June 1968.

4. WHITE, J.W.: Advanced army components technology program.
SAE, Preprint 650707. Combined Powerplant and Transportation Meeting, Cleveland Ohio, Oct. 18-21, 1965.

5. CHAUVIN, J.: Perspectives d'avenir des turbines à gaz et des compresseurs à hautes performances.
IVK, TM 18, juillet 1966.

6. SABATINK, A.: The development of supersonic axial compressor boost stages for small gas turbines.
ASME P 69-GT/44.

7. Research Program: FN-IVK, Private communication.

8. MORRIS, R.E. & KENNY, D.P.: High pressure ratio centrifugal compressors for small gas turbine engines, in Helicopter Propulsion Systems.
AGARD Conference Proceedings 31, June 1968.

9. SCHORR, P.G., WELLIVER, A.D., WINSLOW, L.J.: Design and development of small high pressure ratio single stage centrifugal compressors.
The Boeing Company, Seattle, Washington, March 11, 1969.

10. ERWIN, J.R. & VITALE, N.G.: The radial outflow compressor.
Paper presented at the ASME 1969 Gas Turbine Conference, March 9-13, 1969, Cleveland, Ohio.

11. Centrifugal Compressor Program. US Army AVLABS.

12. HORLOCK, J.H.: Boundary layer problems in axial turbomachines, in Flow Research in Blading, L.S. Dzung, editor; Elsevier Publishing Cy, Amsterdam, 1970, p.322-357.

13. HANSEN, A.G. & HERZIG, H.Z.: Secondary flows and three dimensional boundary layer effects; Chapter XV, NASA SP 36, 1970.

14. HORLOCK, J.H.: Unsteady flows,in Unsteady Flows in Axial Compressors.
VKI, LS 20, 1970.

15. SOVRANO, R. & LE BOT, Y.: Contribution à l'étude des compresseurs supersoniques.
ONERA TP 669, 1969.

16. KERREBROCK, J.L. & MIKOLAYCZAK: Intra-stator transport of rotor wakes and its effect on compressor performance.
Paper presented at the ASME 1970 Gas Turbine Conference, Brussels, Belgium, May 1970.

17. MAGER, A.: Discussion of boundary layer characteristics near the wall of an axial flow compressor.
NACA TR 1085, 1952.

18. SMITH, L.H. Jr: Casing boundary layers in multistage axial flow compressors, in Flow Research in Blading, L.S. Dzung, editor, Elsevier Publ. Cy, Amsterdam, 1970, p. 275-299.

19. FABRI, J.: Le décollement tournant dans les compresseurs axiaux.
ONERA TP 497, 1967 - VKI LS 20, 1970.

20. MORITZ, R.R.: Axial compressor stall,in Unsteady Flows in Axial Compressors.
VKI LS 20, 1970.

21. SCHNELL, E.: Recherches théoriques et expérimentales sur les compresseurs radiaux à charge limite. 1ère partie: Ecoulement au travers de roues radiales à charge limite.
VKI CN 53a, March 1965.

22. FOWLER, H.S.: An investigation of the flow processes in a centrifugal compressor impeller.
NRC Mech.Engrg Report ME 220, July 1966.

24. SMOLDEREN, J.J.: Mathematical basis of unsteady flow treatment.
Unpublished lecture.

25. WU, Chung Hua: A general theory of three-dimensional flow in subsonic and supersonic turbomachines of axial, radial, and mixed flow type.
NACA TN 1795, 1950.

26. MARSH, H.: A digital computer programme for the through flow fluid mechanics in an arbitrary turbomachine using a matrix method.
NGTE Report R 282, July 1966.

27. NOVAK, R.A.: Streamline curvature computing procedures for fluid flow problems.
VKI CN 59; also, ASME Paper 66-WA/GT3.

28. SMITH, L.H. Jr: The radial equilibrium equation of turbomachinery.
Jnl of Engineering for Power, ASME Transact. Series A, vol. 18, 1951, p.1-12.

29. VAVRA, M.H.: Aerothermodynamics and flow in turbomachines.
Wiley & Sons, 1960.

30. MIKOLAYCZAK, A.A.; MORRIS, A.L., JOHNSON, B.V.: Comparison of performance of supersonic blading in cascade and in compressor rotors.
Paper presented at the 15th ASME Gas Turbine Conference, Brussels, May 1970.

31. LE FOLL, J.: A theory of representation of the properties of boundary layers on a plane.
Proceedings Seminar on Advanced Problems in Turbomachinery. K. Cassady and J. Chauvin, editors, VKI 1965.

32. PAPAILIOU, K.: Optimisation d'aubages de compresseur à forte charge sur la base des théories de couches limites. Ph.D. Thesis, Univ. Liège, 1969, also
VKI TN 55, 1969.

33. STRATFORD, B.S.: The use of boundary layer techniques to calculate the blockage from the annular boundary layers in a compressor.
ASME P 67-WA/GT-7, November 1967.

34. NOVAK, R.A. & JANSEN, W.: The application of end wall boundary layer effects in the performance analysis of axial compressors.
ASME 67-WA/GT-11, November 1967.

35. HETHERINGTON, R.: Engine component design problems associated with large subsonic transports.
Lecture given at the von Karman Institute, 23rd April 1969 - Rolls-Royce Publ. also, VKI LS 16 : High Reynolds number aerodynamics, 1969.

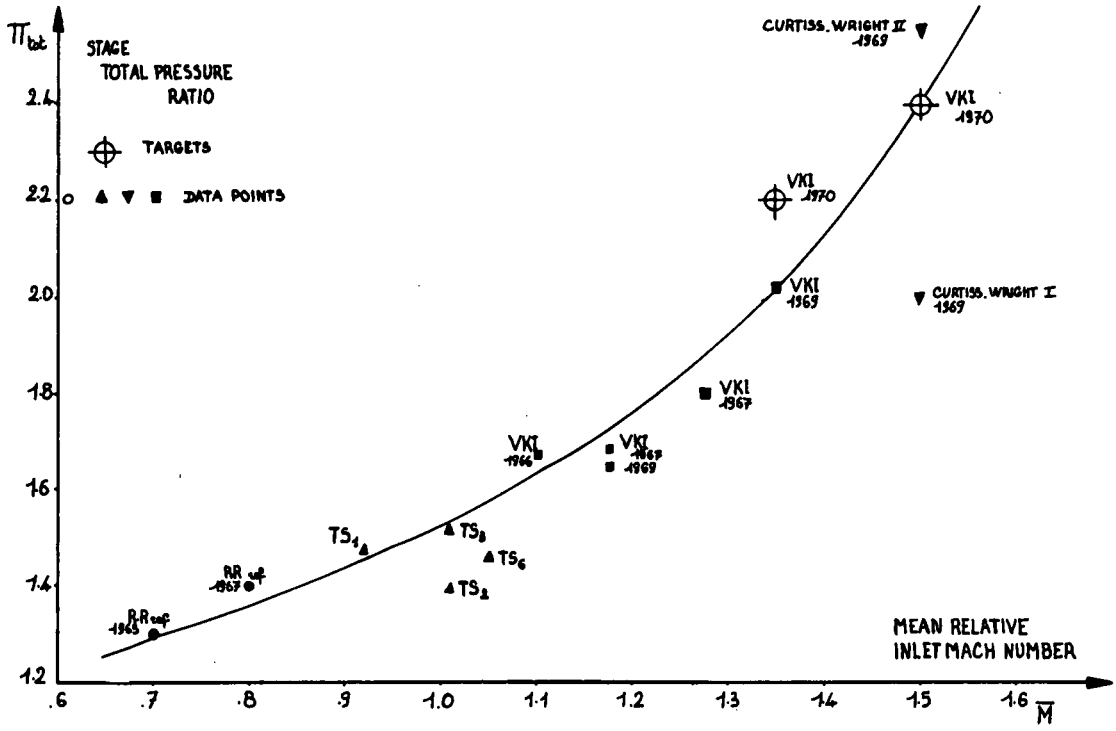

Figure 1

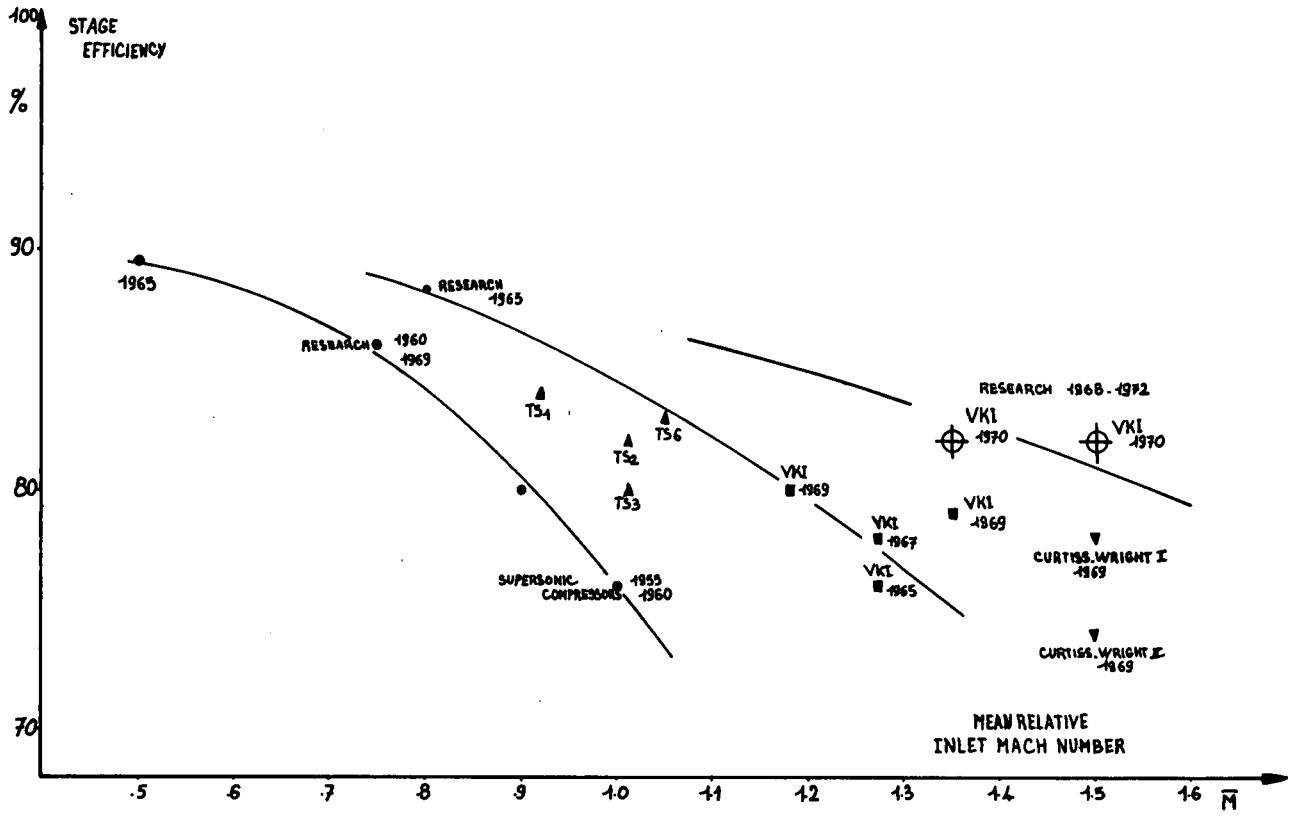

Figure 2

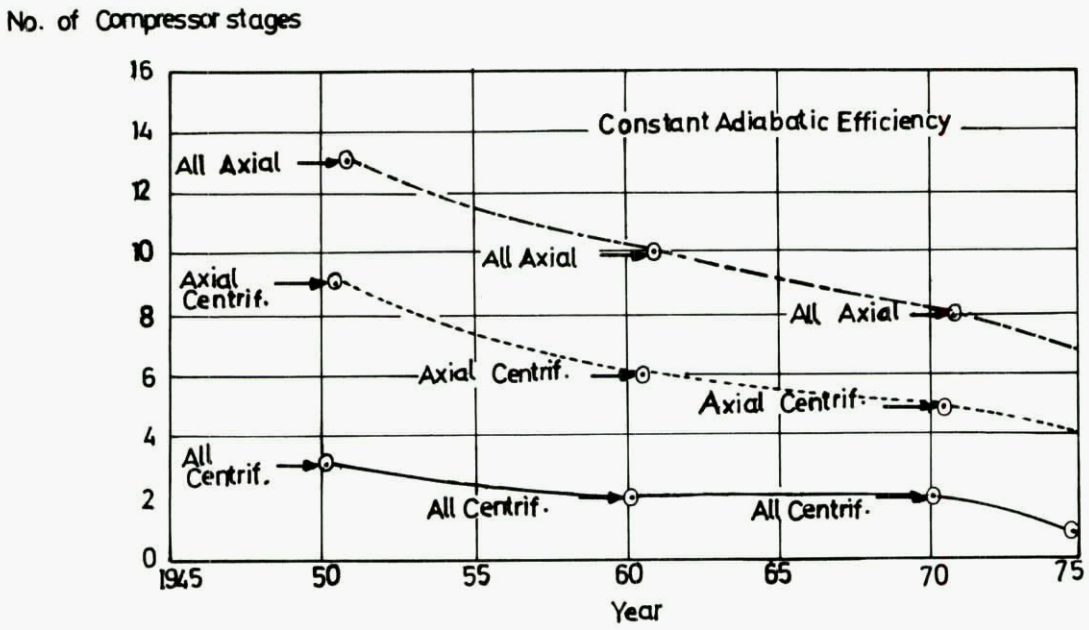

Figure 3

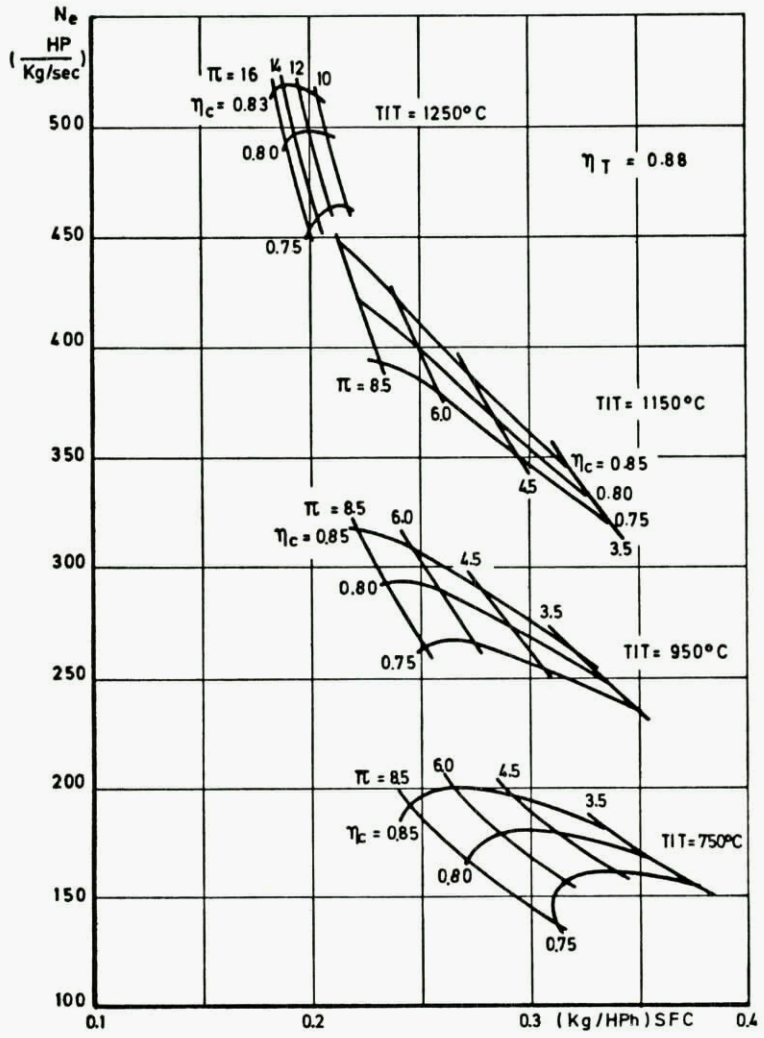

Figure 4

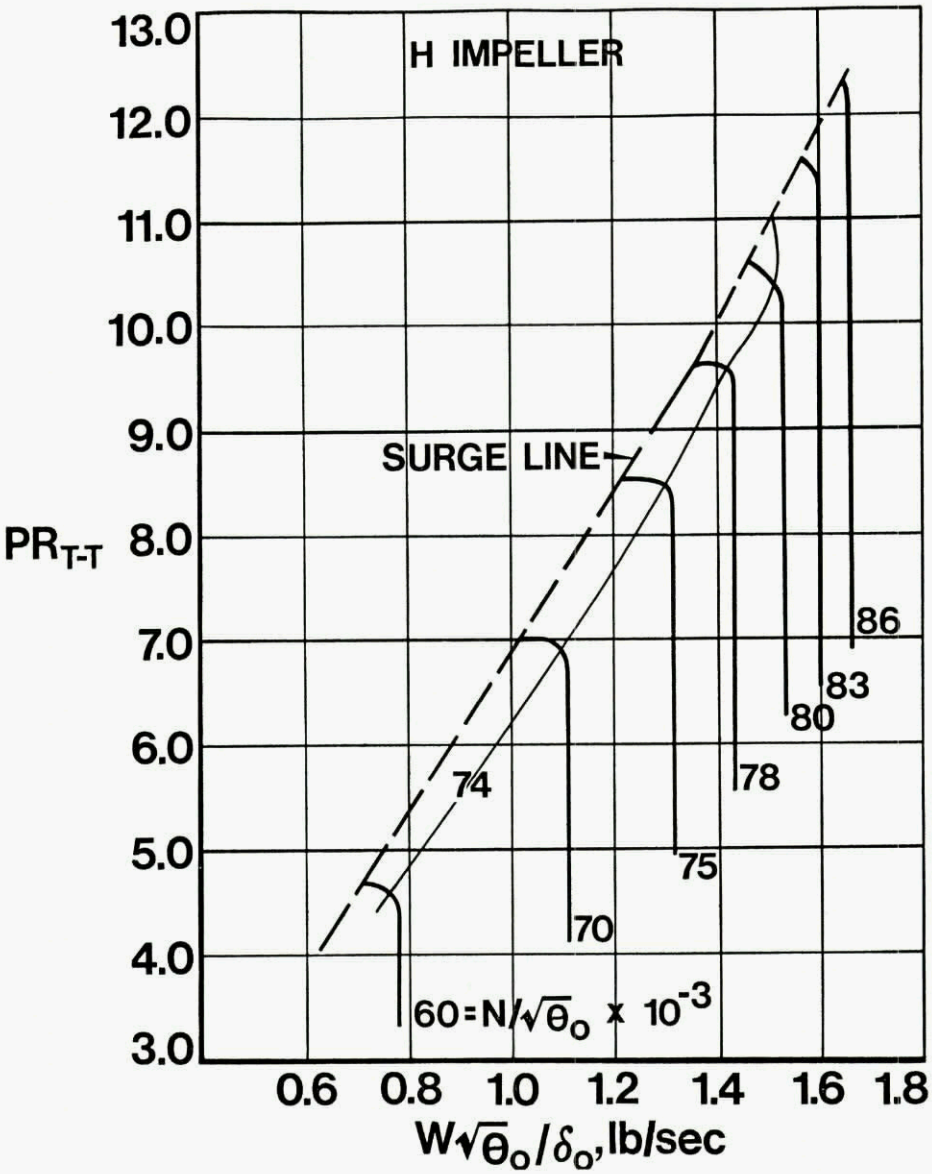

Figure 5

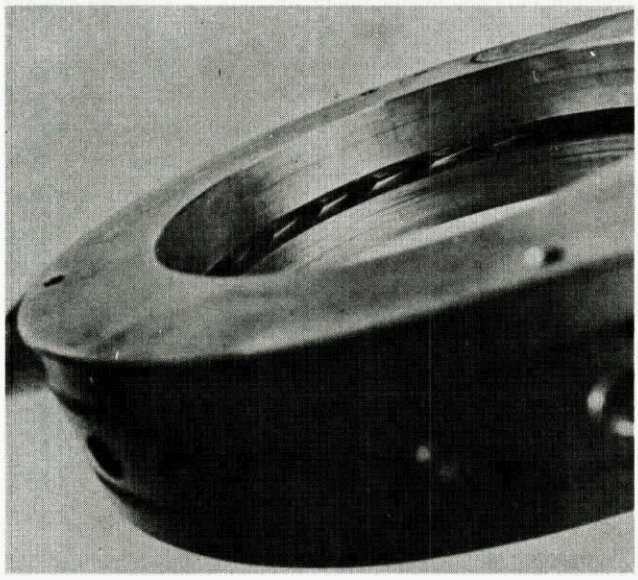

Figure 6

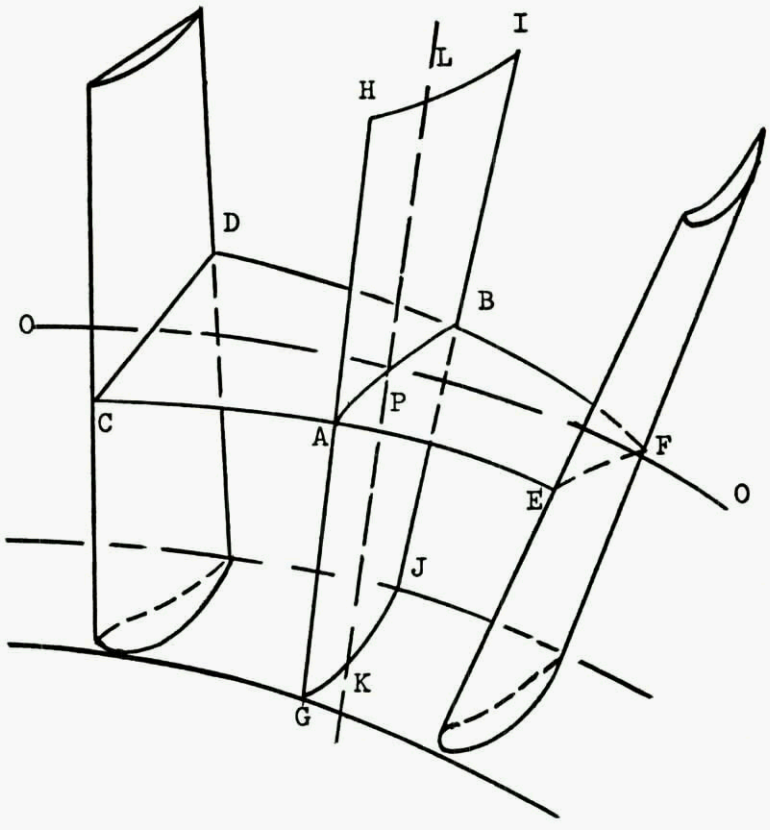

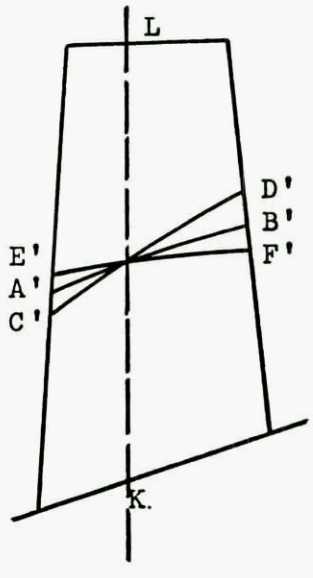

Figure 7

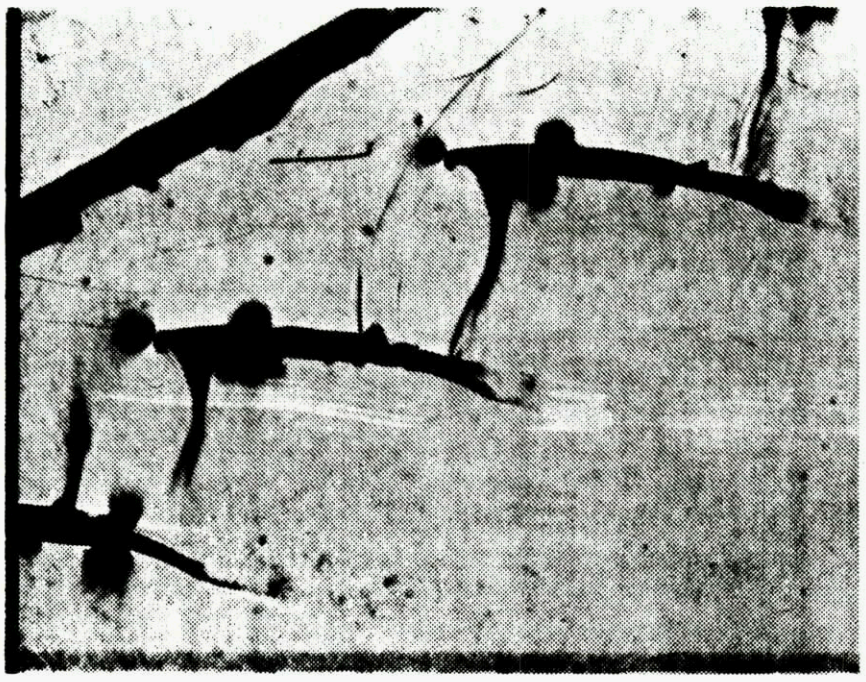

M1 =.824

M1 = .835

Figure 8

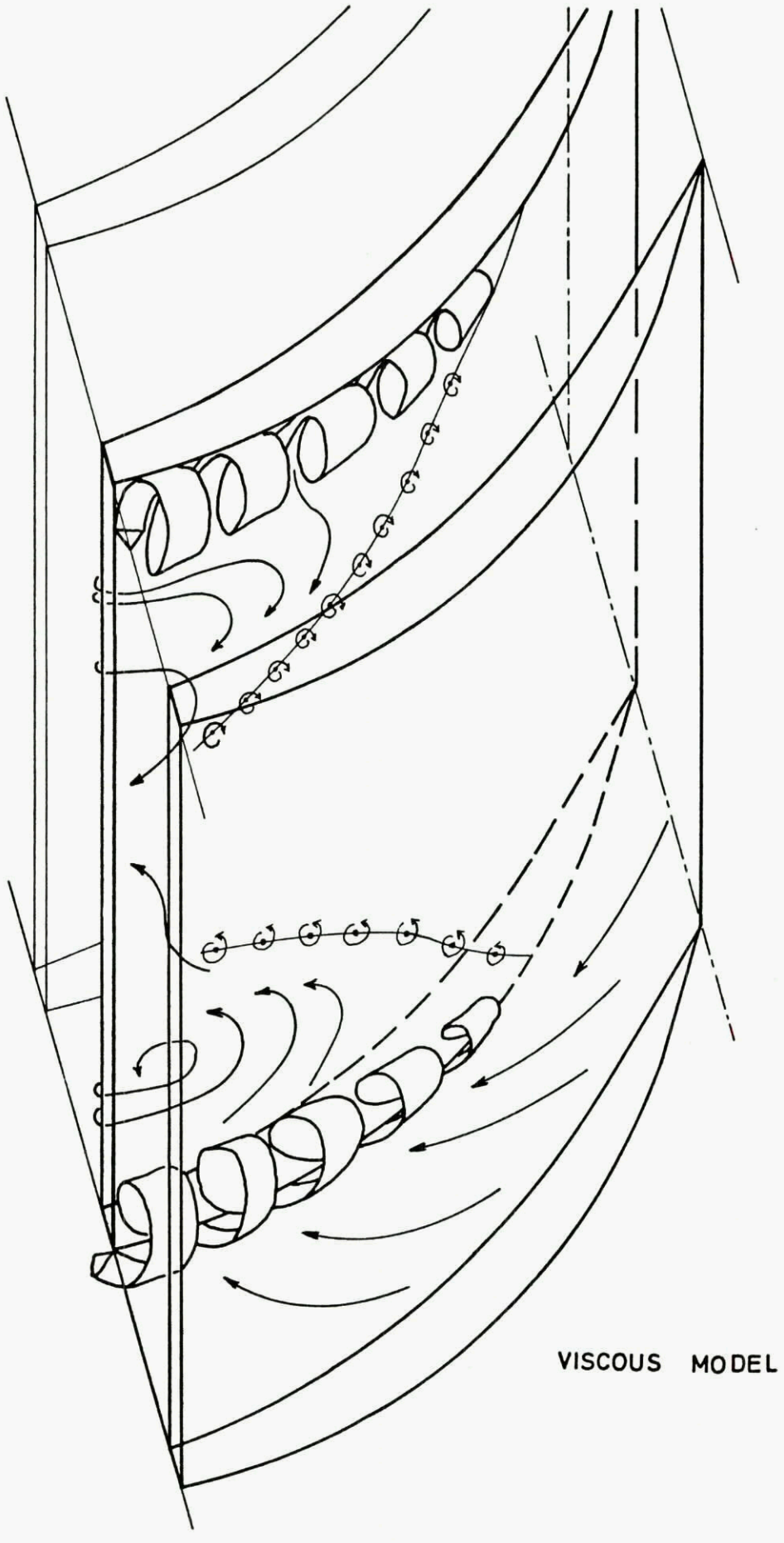

Figure 9

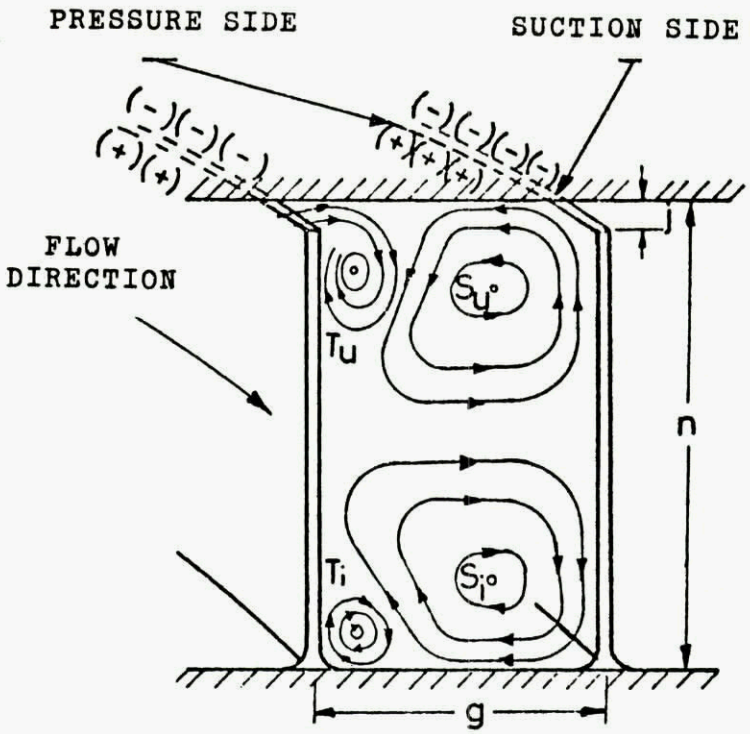

Figure 10

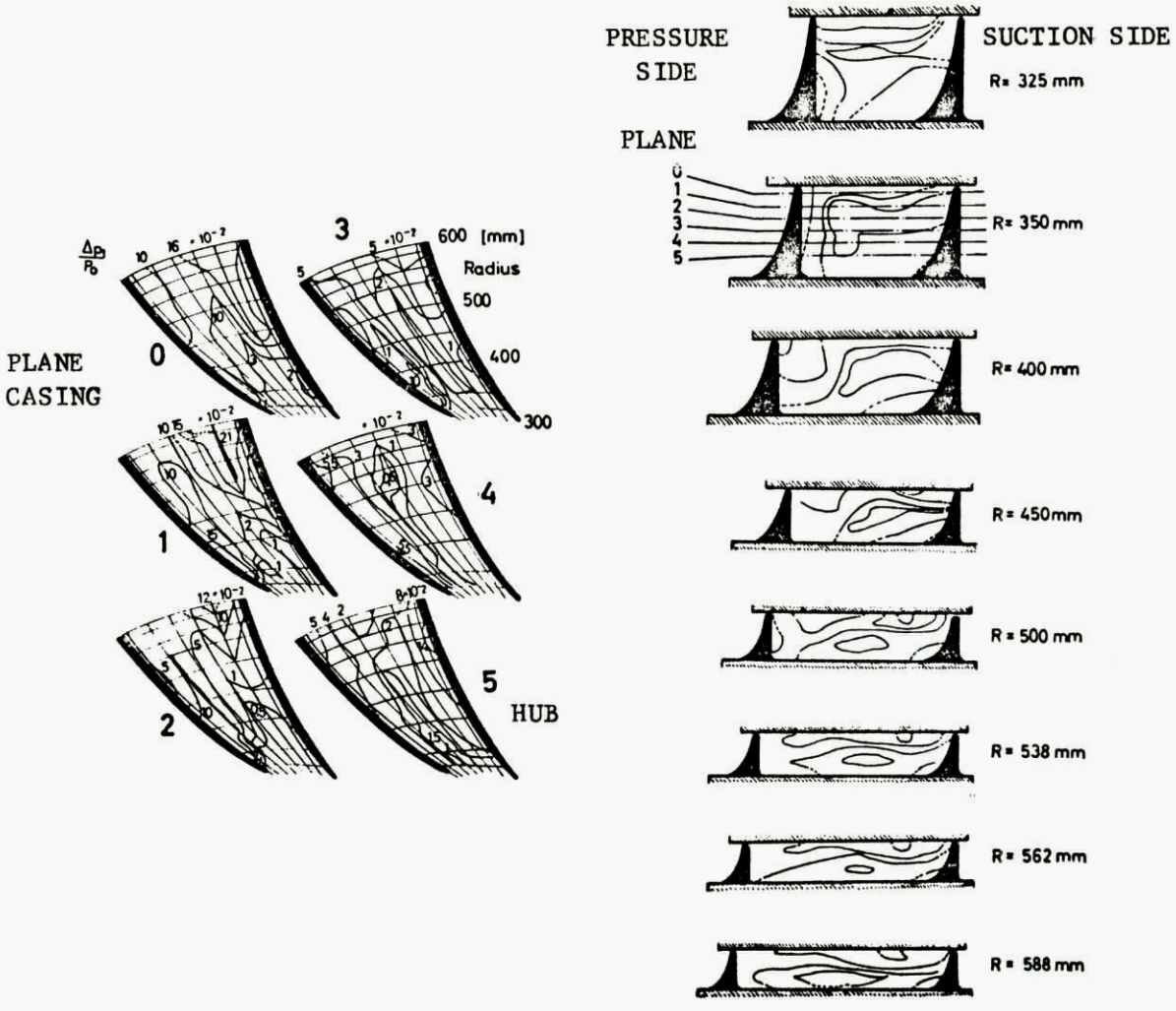

Figure 11

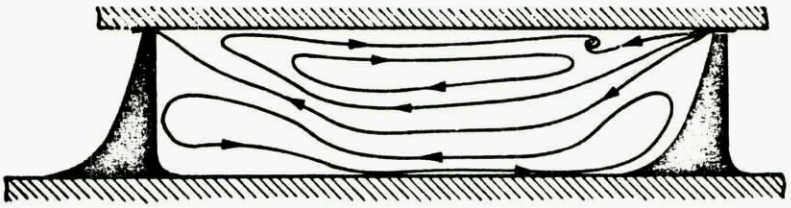

SECONDARY FLOWS AT WHEEL EXIT (RADIAL COMPRESSOR)

Figure 12

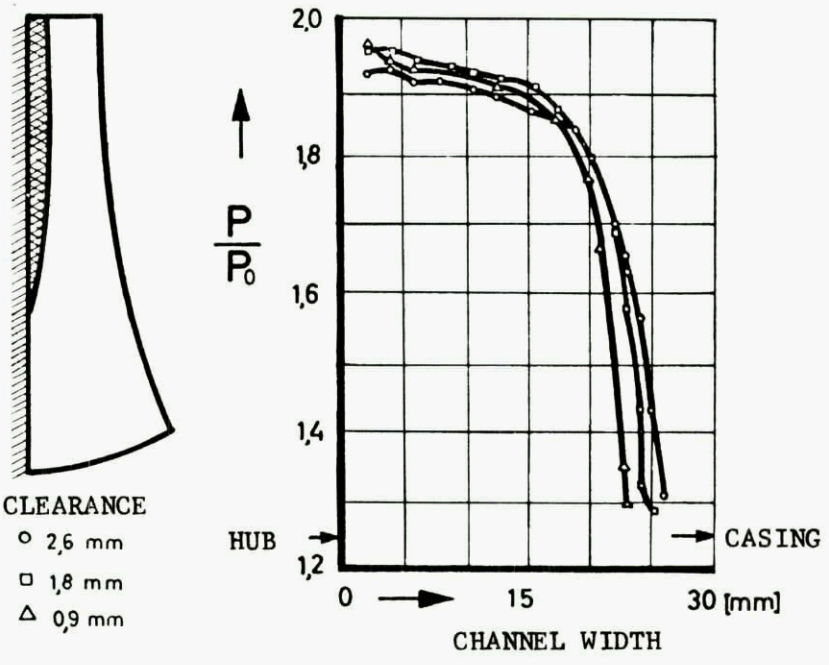

Figure 13

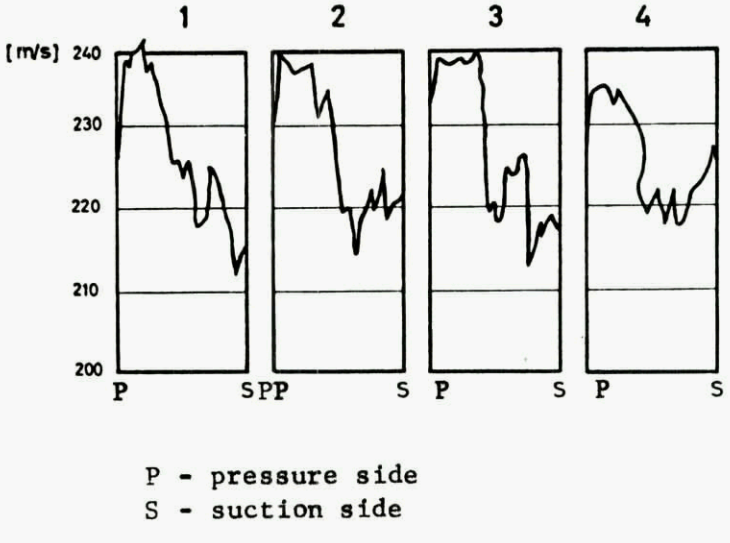

P - pressure side
S - suction side

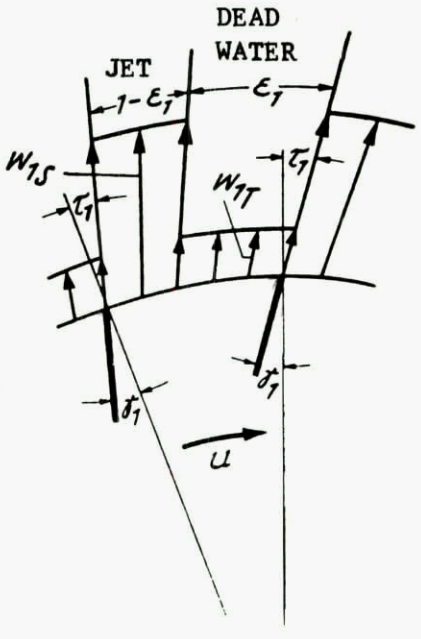

Figure 14

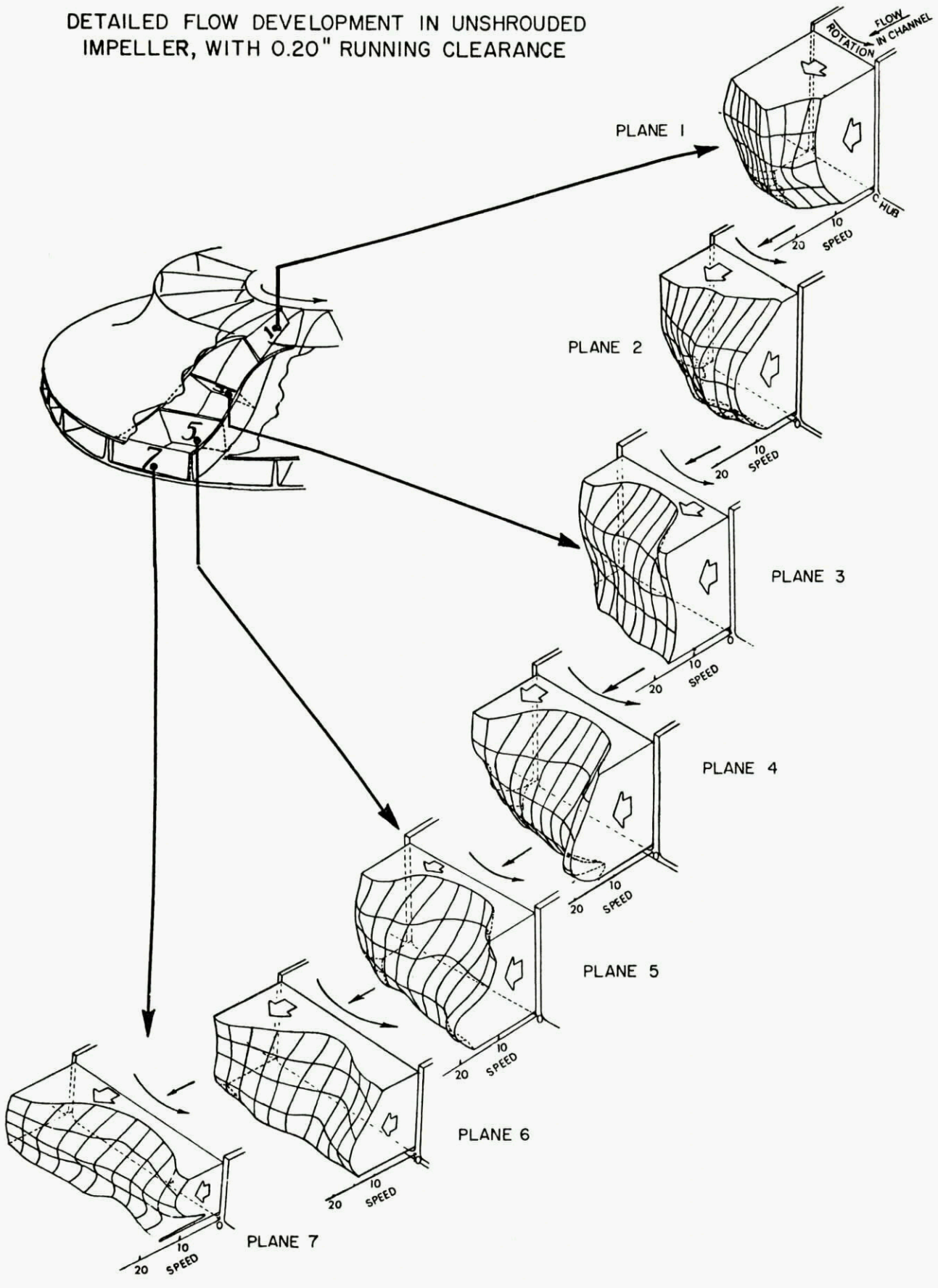

Figure 15

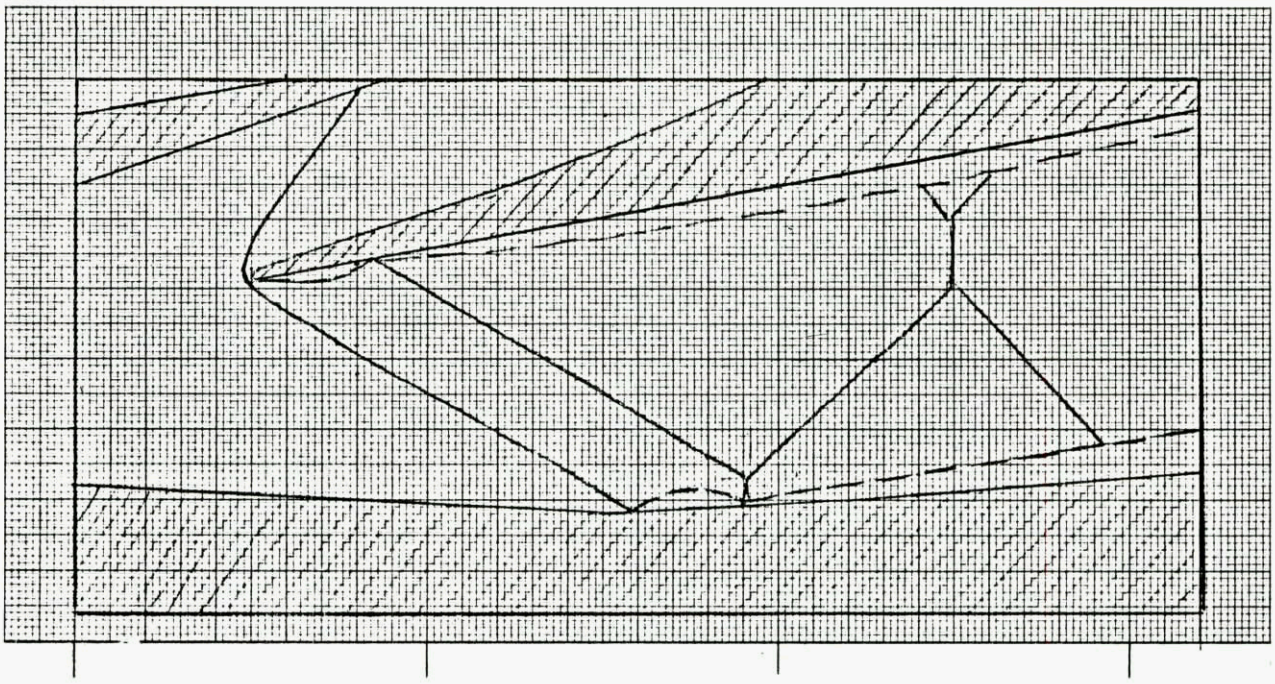

Figure 16

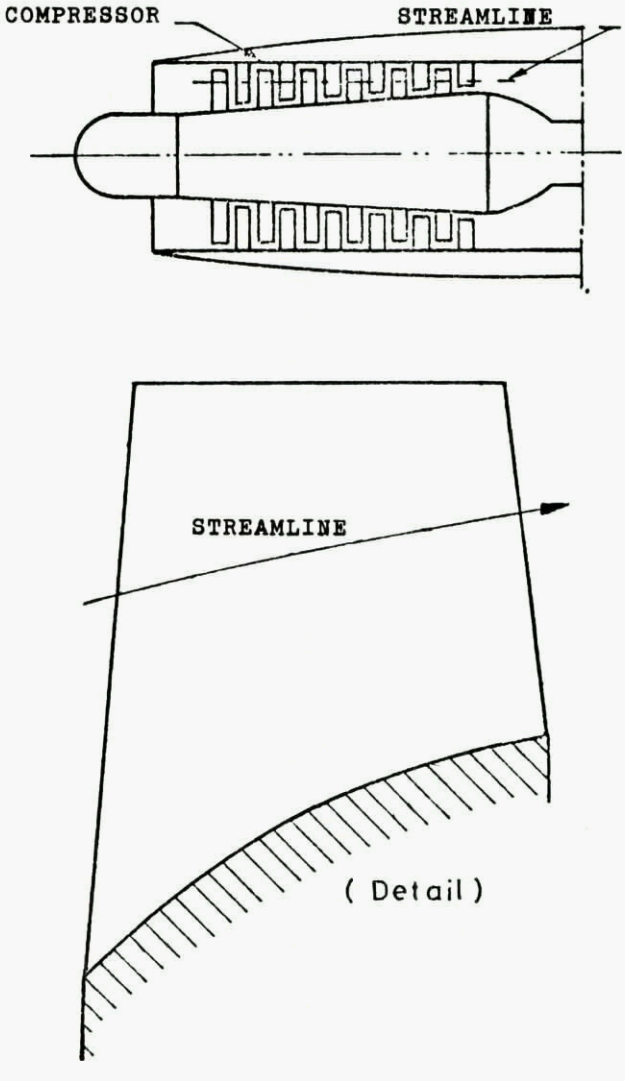

Figure 17

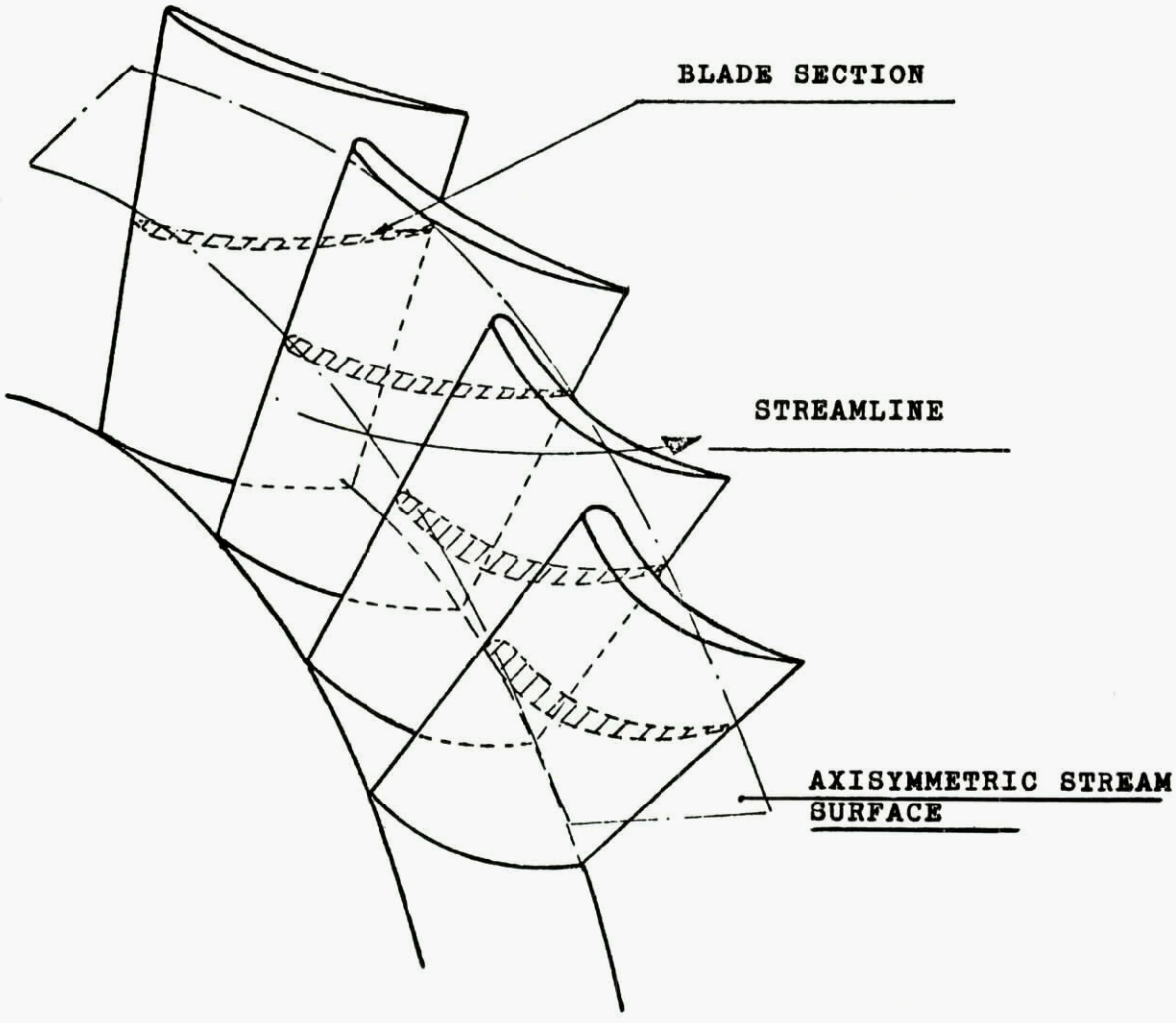

Figure 18

The Through-flow Analysis of Axial Flow Compressors

by

H. Marsh *

* Cambridge University Engineering Department.

Summary

Methods for predicting the performance of axial flow compressors are described in detail and it is shown that the methods of streamline curvature and matrix through-flow analysis are based on the same mathematical model for flow on the mean stream surface. The need for an accurate loss model is emphasised and the Mach number limitations of these two methods of analysis are defined. Methods for predicting the development of the wall boundary layers are discussed and the simple theory of Stratford (10) is shown to be in agreement with experimental results obtained for flows with low angles of swirl. The work of Gregory-Smith (11) suggests that if an accurate estimate of the wall boundary layer can be obtained, then it is possible to predict the flow pattern across the entire annulus.

Notation

a	local velocity of sound,
B	surface thickness parameter,
c	chord,
D_{eq}	equivalent diffusion factor,
$\bar{F}$	force vector,
h	static enthalpy,
H	stagnation enthalpy,
i	incidence,
I	relative stagnation enthalpy (rothalpy) $I = H - \omega r V_\theta$,
K_i	constants,
M_m	meridional Mach number,
M_{rel}	relative Mach number,
$\bar{n}$	vector normal to the mean stream surface,
p	pressure,
r	radius,
R	gas constant,
R_m	radius of curvature of meridional streamlines,
s	entropy,
S	mean stream surface,
T	temperature,
U_m	blade speed at mean radius,
$\bar{V}$	velocity vector,
$\bar{W}$	relative velocity vector,
β	air angle,
δ	deviation,
λ, μ	angles defining the local mean stream surface,
ρ	density,
σ	solidity (chord/pitch),
ϕ	slope of the meridional streamlines,
ψ	stream function,
$\bar{\omega}$	angular velocity,
ω	total pressure loss coefficient,

Subscripts

1	inlet,
2	outlet,
r	radial,
z	axial,
θ	circumferential.

Notation (Cont.)

Boundary Layer

δ^* displacement thickness,

θ momentum thickness,

τ shear stress,

τ_w wall shear stress.

Introduction

The ultimate objective of the through-flow analysis is to predict the performance of a turbomachine so that the design engineer can ensure an efficient machine with the minimum time for development. During the past forty years, methods of flow analysis for turbomachines have progressed from the basic mean line analysis, first to the method of simple radial equilibrium, which was necessary to deal with machines of low hub to tip ratio, then to actuator disc theory, which contributed to our understanding of blade row interaction, and finally to the numerical methods of streamline curvature and matrix through-flow analysis which both use digital computers to solve the equations of fluid motion. The calculation of the flow pattern remains a very difficult mathematical problem and a complete explanation of the flow requires an understanding of several branches of fluid dynamics.

Until 1960, the mathematical model for the flow in turbomachines was more advanced than the methods of computation; for example, the computing facilities available in 1952 were not adequate for obtaining general solutions to the governing equations derived by Wu (1). It is only during the past decade that computers have been developed having sufficient speed and storage capacity to deal economically with these problems of flow calculation. The techniques now exist for calculating the flow in turbomachines on the basis of a flow model which includes the effects of compressibility, radial variations of lift and losses, blade row interaction, secondary flow effects and the development of the wall boundary layers. This flow model is based on our understanding of the flow through cascades, isolated blade rows and single stage machines; it is a model which is continually being revised and improved.

Methods of Flow Calculation

There are two methods of flow calculation for turbomachines and they both attempt to obtain information about the overall flow pattern without including the effects of time dependent flows. These methods, often called streamline curvature and matrix through-flow, are based on the same mathematical model, but differ in their numerical techniques. Although these two methods of analysis were developed independently and are usually treated separately, they have much in common and the following discussion is an attempt to show their relationship to each other.

In Wu's general theory for the flow in turbomachines, reference 1, the equations of fluid motion are satisfied on two intersecting families of stream surfaces, the complete three-dimensional flow field being obtained by an iterative process between solutions for the flow on the two sets of surfaces. Throughout the analysis, it is assumed that the flow is steady. However, at exit from a blade row, the flow and the gas state vary circumferentially and if the following blade row has a motion relative to the first, then it is subject to a time dependent inlet flow. It follows that the general theory is therefore only applicable to the flow through an isolated blade row. The theory is general in the sense that it is a general method for estimating a steady three-dimensional flow by calculating the flow on two intersecting sets of stream surfaces.

The through-flow theory is similar to the general theory, but the equations of fluid motion are only solved for the steady flow on a mean stream surface. The flow and fluid state on this surface may be regarded as average values for the flow within the blade passage. For a multi-stage turbomachine, the time dependence of the flow is removed by treating the through-flow solution as an axially symmetric flow for the duct region between each pair of blade rows. In the analysis which follows, the equations governing the flow on the mean stream surface are derived and the two methods of solution are discussed in detail.

In a coordinate system rotating with the blade row at an angular velocity ω, any steady reversible, inviscid flow is governed by the equation of motion

$$2\bar{\omega}\times\bar{W} - \bar{W}\times(\nabla\times\bar{W}) = -\nabla I + T\nabla s \qquad (1)$$

where $\bar{W}$ is the relative velocity vector. In the r, θ, z coordinate system, the equations of continuity, motion, energy and state are

Continuity

$$\frac{1}{r}\frac{\partial}{\partial r}(r\rho W_r) + \frac{1}{r}\frac{\partial}{\partial\theta}(\rho W_\theta) + \frac{\partial}{\partial z}(\rho W_z) = 0 \qquad (2)$$

Motion

$$-\frac{W_\theta}{r}\left[\frac{\partial}{\partial r}(rV_\theta) - \frac{\partial W_r}{\partial\theta}\right] + W_z\left[\frac{\partial W_r}{\partial z} - \frac{\partial W_z}{\partial r}\right] = T\frac{\partial s}{\partial r} - \frac{\partial I}{\partial r} \qquad (3)$$

$$\frac{W_r}{r}\left[\frac{\partial}{\partial r}(rV_\theta) - \frac{\partial W_r}{\partial\theta}\right] - W_z\left[\frac{1}{r}\frac{\partial W_z}{\partial\theta} - \frac{\partial W_\theta}{\partial z}\right] = \frac{T}{r}\frac{\partial s}{\partial\theta} - \frac{1}{r}\frac{\partial I}{\partial\theta} \qquad (4)$$

$$-W_r\left[\frac{\partial W_r}{\partial z}-\frac{\partial W_z}{\partial r}\right]+W_\theta\left[\frac{1}{r}\frac{\partial W_z}{\partial \theta}-\frac{\partial W_\theta}{\partial z}\right]=T\frac{\partial s}{\partial z}-\frac{\partial I}{\partial z} \tag{5}$$

Energy (adiabatic)

$$W_r\frac{\partial I}{\partial r}+\frac{W_\theta}{r}\frac{\partial I}{\partial \theta}+W_z\frac{\partial I}{\partial z}=0 \tag{6}$$

State (perfect gas)

$$\rho=f(h,s)=A\,h^{\frac{1}{\gamma-1}}e^{-\frac{s}{R}} \tag{7}$$

where h is the static enthalpy per unit mass. These equations together with their boundary conditions define the steady flow through any blade row or duct.

In the through-flow analysis, the governing equations are only solved for the flow on the mean stream surface which is defined as

$$S(r,\theta,z)=0 \tag{8}$$

or

$$\theta=\theta(r,z) \tag{9}$$

where it is assumed that the surface is single valued in θ.

If $\frac{\overline{\partial q}}{\partial r}$ and $\frac{\overline{\partial q}}{\partial z}$ are partial derivatives taken along the stream surface, then

$$\left.\begin{aligned}\frac{\overline{\partial q}}{\partial r}&=\frac{\partial q}{\partial r}-\frac{n_r}{n_\theta}\frac{\partial q}{r\partial\theta}\\ \frac{\overline{\partial q}}{\partial z}&=\frac{\partial q}{\partial z}-\frac{n_z}{n_\theta}\frac{\partial q}{r\partial\theta}\end{aligned}\right\} \tag{10}$$

where n_r, n_θ and n_z are the components of the unit vector $\bar{n}$ normal to the surface. These special derivatives are taken on the stream surface and must be distinguished from ordinary partial derivatives. The special derivative $\frac{\overline{\partial q}}{\partial r}$ is the rate of change of q with r on the stream surface at a given value of z, whereas $\frac{\partial q}{\partial r}$ is the rate of change of q with r at given values of z and θ.

The equations governing the flow may now be expressed in terms of the special derivatives for the flow on the mean stream surface,

Continuity

$$\frac{1}{r}\frac{\overline{\partial}}{\partial r}(r\rho W_r)+\frac{\overline{\partial}}{\partial z}(\rho W_z)=-\frac{\rho}{rn_\theta}\left[n_r\frac{\partial W_r}{\partial\theta}+n_\theta\frac{\partial W_\theta}{\partial\theta}+n_z\frac{\partial W_z}{\partial\theta}\right]$$

Motion

$$=\rho\,C(r,z) \tag{11}$$

$$-\frac{W_\theta}{r}\frac{\overline{\partial}}{\partial r}(rV_\theta)+W_z\left[\frac{\overline{\partial W_r}}{\partial z}-\frac{\overline{\partial W_z}}{\partial r}\right]=T\frac{\overline{\partial s}}{\partial r}-\frac{\overline{\partial I}}{\partial r}+F_r \tag{12}$$

$$\frac{W_r}{r}\frac{\overline{\partial}}{\partial r}(rV_\theta)+\frac{W_z}{r}\frac{\overline{\partial}}{\partial z}(rV_\theta)=F_\theta \tag{13}$$

$$-W_r\left[\frac{\overline{\partial W_r}}{\partial z}-\frac{\overline{\partial W_z}}{\partial r}\right]-\frac{W_\theta}{r}\frac{\overline{\partial}}{\partial z}(rV_\theta)=T\frac{\overline{\partial s}}{\partial z}-\frac{\overline{\partial I}}{\partial z}+F_z \tag{14}$$

where

$$\bar{F}=-\frac{1}{r\rho n_\theta}\frac{\partial p}{\partial\theta}\,\bar{n}$$

Energy

$$W_r\frac{\overline{\partial I}}{\partial r}+W_z\frac{\overline{\partial I}}{\partial z}=0 \tag{15}$$

In an inviscid flow, the force vector $\bar{F}$ is normal to the stream surface S and is therefore normal to the relative velocity vector,

$$W_r F_r + W_\theta F_\theta + W_z F_z = 0 \tag{16}$$

It is convenient to define the local form of the stream surface by two angles λ and μ where

$$\left.\begin{aligned} \text{Tan}\,\lambda &= \frac{n_r}{n_\theta} = \frac{F_r}{F_\theta} \\ \text{Tan}\,\mu &= \frac{n_z}{n_\theta} = \frac{F_z}{F_\theta} \end{aligned}\right\} \tag{17}$$

The three velocity components are then related by

$$W_\theta = -W_r \,\text{Tan}\,\lambda - W_z \,\text{Tan}\,\mu$$

which is the geometrical condition that the flow follows the mean stream surface.

Following Wu's analysis, an integrating factor B is introduced such that the equation of continuity becomes

$$\frac{\overline{\partial}}{\partial r}(r B \rho W_r) + \frac{\overline{\partial}}{\partial z}(r B \rho W_z) = 0 \tag{18}$$

the factor B being given by

$$\frac{W_r}{B}\cdot\frac{\overline{\partial B}}{\partial r} + \frac{W_z}{B}\cdot\frac{\overline{\partial B}}{\partial z} = -C(r,z) \tag{19}$$

The equations indicate that B is proportional to the local angular thickness of the stream surface and as a first approximation, the thickness of the stream surface is assumed to be proportional to the width of the blade passage,

$$B = \frac{\text{circumferential width of the blade passage}}{\text{blade pitch}}$$

For the flow in a duct region, where there are no blades, the parameter B is taken as unity.

The through-flow analysis has been presented here for the flow on the mean stream surface without assuming axial symmetry, so that this can be seen to be the first stage in applying the general theory. However, if axial symmetry were assumed and a distributed body force introduced to represent the blade force, then the governing equations are of the same form, but with the special derivatives replaced by ordinary partial derivatives. It follows that the same flow pattern is obtained by assuming axial symmetry, or by solving for the flow on the mean stream surface and then treating this as an axially symmetric solution. The same solution for the flow pattern is obtained irrespective of whether the assumption of axial symmetry is made before or after the equations are solved.

There are two methods for solving the governing equations, namely the method of streamline curvature and the matrix method. The method of streamline curvature is based on the radial equation of motion,

$$T\frac{\overline{\partial s}}{\partial r} - \frac{\overline{\partial I}}{\partial r} + F_r = -\frac{W_\theta}{r}\frac{\overline{\partial}}{\partial r}(rV_\theta) - W_z\frac{\overline{\partial W_z}}{\partial r} + W_z\frac{\overline{\partial W_r}}{\partial z} \tag{20}$$

The last term on the right hand side can be expressed in terms of the meridional velocity W_m and the slope and curvature of the meridional streamlines

$$W_z\frac{\overline{\partial W_r}}{\partial z} = W_m\frac{\overline{\partial W_r}}{\partial m} - W_r\frac{\overline{\partial W_r}}{\partial r} \tag{21}$$

where m is measured in the direction of the meridional streamline. Introducing the streamline slope ϕ and radius of curvature R_m, this term can also be written as

$$\left[\frac{1}{R_m} = -\frac{\overline{\partial \phi}}{\partial m}\right], \qquad W_z\frac{\overline{\partial W_r}}{\partial z} = -\frac{W_m^2 \,\text{Cos}\,\phi}{R_m} + W_m\frac{\overline{\partial W_m}}{\partial m}\cdot\text{Sin}\,\phi - W_r\frac{\overline{\partial W_r}}{\partial r} \tag{22}$$

so that the radial equation of motion becomes

$$T\frac{\overline{\partial s}}{\partial r} - \frac{\overline{\partial I}}{\partial r} + F_r = -\frac{W_\theta}{r}\frac{\overline{\partial}}{\partial r}(rV_\theta) - W_m\frac{\overline{\partial W_m}}{\partial r} - \frac{W_m^2 \,\text{Cos}\,\phi}{R_m} + W_r\frac{\overline{\partial W_m}}{\partial m} \tag{23}$$

The last term on the right hand side can be evaluated from the equations of continuity and energy, much algebra being omitted,

Continuity

$$\frac{W_m}{\rho}\cdot\frac{\overline{\partial \rho}}{\partial m} = -\frac{W_z}{r}\frac{\overline{\partial}}{\partial r}(r\,\mathrm{Tan}\,\phi) - \frac{W_m W_r}{W_z R_m} - \frac{\overline{\partial W_m}}{\partial m} - \frac{W_m}{B}\cdot\frac{\overline{\partial B}}{\partial m} \qquad (24)$$

Energy

$$W_m\frac{\overline{\partial h}}{\partial m} = -W_m^2\frac{\overline{\partial W_m}}{\partial m} - W_\theta F_\theta + \frac{W_r V_\theta^2}{r} \qquad (25)$$

If the working fluid is a perfect gas then

$$\frac{1}{\rho}\cdot\frac{\overline{\partial \rho}}{\partial m} = \frac{1}{a^2}\cdot\frac{\overline{\partial h}}{\partial m} - \frac{1}{R}\frac{\overline{\partial s}}{\partial m} \qquad (26)$$

and substituting from the equations of continuity and energy

$$\left[1-M_m^2\right]\frac{\overline{\partial W_m}}{\partial m} = \frac{W_m}{R}\frac{\overline{\partial s}}{\partial m} - \frac{W_z}{r}\frac{\overline{\partial}}{\partial r}(r\,\mathrm{Tan}\,\phi) - \frac{W_m W_r}{W_z R_m} - \frac{W_m}{B}\frac{\overline{\partial B}}{\partial m} + \frac{W_\theta F_\theta}{a^2} - \frac{W_r W_\theta^2}{r a^2} \qquad (27)$$

The radial equation of motion can therefore be written as

$$T\frac{\overline{\partial s}}{\partial r} - \frac{\overline{\partial I}}{\partial r} + F_r = -\frac{W_\theta}{r}\frac{\overline{\partial}}{\partial r}(rV_\theta) - W_m\frac{\overline{\partial W_m}}{\partial r} - \left(\frac{M_r^2}{1-M_m^2}\right)\cdot\frac{V_\theta^2}{r} - \left(\frac{1-M_z^2}{1-M_m^2}\right)\frac{W_m^2}{R_m\cos\phi} + \left(\frac{M_r M_\theta}{1-M_m^2}\right)\cdot F_\theta + \left(\frac{W_r}{1-M_m^2}\right)\left[\frac{W_m}{R}\frac{\overline{\partial s}}{\partial r} - \frac{W_z}{r}\frac{\overline{\partial}}{\partial r}(r\,\mathrm{Tan}\,\phi) - \frac{W_m}{B}\cdot\frac{\overline{\partial B}}{\partial m}\right] \qquad (28)$$

or

$$W_m\cdot\frac{\overline{\partial W_m}}{\partial r} + W_m^2\cdot K(r) + L(r) = 0 \qquad (29)$$

This is the form of the radial equilibrium equation as derived by Smith (2), Novak (3) and Silvester and Hetherington (4).

The method of solution assumes that an estimate of the flow pattern is known, so that the functions $K(r)$ and $L(r)$ can be evaluated. At any position in the flow field, a value for W_m is chosen at some position such as the mid-span and the equation for W_m is integrated radially to obtain the axial velocity profile. The mass flow rate across the calculating plane is then computed and compared with the upstream mass flow rate. If necessary, a new value for W_m is chosen and the calculations repeated until the required mass flow rate is obtained. When the axial velocity profiles are known throughout the machine, then the new streamline pattern can be calculated and new values obtained for the functions $K(r)$ and $L(r)$. The complete cycle of calculations is repeated until a convergence criterion is satisfied. The numerical procedure can become highly unstable and it is usually necessary to restrict the calculation to small changes in the flow pattern between successive iterations.

The major difficulty in applying this method is that it is necessary to evaluate the streamline slope and curvature. A commonly used approximation for the shape of the streamlines is that of a spline fit through points of equal stream function on neighbouring calculating planes. This spline curve is sometimes differentiated to obtain both the slope and the curvature, but Shaalan and Daneshyar (5) suggest that a more accurate estimate of the curvature is obtained by fitting a second spline curve to the variation of slope and then differentiating to obtain the curvature. The authors refer to this as a double spline fit. Perhaps the most important feature of the work by Shaalan and Daneshyar is that concerning the ratio of the spacing of the calculating planes to the wavelength of the streamline pattern. It is shown that whereas a single spline fit requires about ten points per wavelength in order to obtain a good estimate of the curvature, the double spline fit requires only four or five points. In a multistage turbomachine, the basic wavelength may correspond to the length of a stage and it then follows that a good estimate for the curvature of the streamlines can only be obtained by taking calculating planes within the blade rows. This is relatively simple for subsonic flows, but in a transonic flow with shocks, the mathematical model is not adequate. It is therefore common to analyse the flow in transonic compressors by placing the calculating planes outside the blade rows and treating the blade rows as devices which have a specified behaviour, even though this may reduce the accuracy of the overall calculation.

The alternative method of solving the equations governing the flow on the mean stream surface is to define a stream function ψ where

$$\left.\begin{aligned} \frac{\partial \psi}{\partial r} &= r B_\rho W_z \\ \text{and} \quad \frac{\partial \psi}{\partial z} &= -r B_\rho W_r \end{aligned}\right\} \qquad (30)$$

The radial equation of motion (12) can then be expressed as

$$\frac{\partial^2 \psi}{\partial r^2} + \frac{\partial^2 \psi}{\partial z^2} = \frac{\partial \psi}{\partial r} \cdot \frac{\partial}{\partial r}\left[\ln(r B_\rho)\right] + \frac{\partial \psi}{\partial z} \cdot \frac{\partial}{\partial z}\left[\ln(r B_\rho)\right] + \frac{r\rho B}{W_z}\left[\frac{\partial I}{\partial r} - T\frac{\partial s}{\partial r} - F_r - \frac{W_\theta}{r} \cdot \frac{\partial}{\partial r}(r V_\theta)\right] \qquad (31)$$

or

$$\frac{\partial^2 \psi}{\partial r^2} + \frac{\partial^2 \psi}{\partial z^2} = q(r,z) \qquad (32)$$

Equation (31) is often referred to as Wu's principal equation; it is a non-linear equation, but it can be solved by the repeated solution and correction of the quasi-linear equation (32). A solution for the stream function ψ is obtained for a given distribution q(r,z), the function q(r,z) is then corrected using the improved solution for ψ and the process is repeated until a convergence criterion is satisfied, as described by Marsh (6).

Mathematically, Wu's analysis is extremely simple, but the difficulty lies in obtaining numerical solutions for the stream function. Many finite difference approximations use a rectangular grid of points, since this leads to simple expressions for the inter-dependence of the function values at neighbouring points. However, for calculating the flow through an axial flow compressor, a more suitable form of grid is a distorted or non-rectangular mesh which is straight in only one direction. Figure 1 shows a distorted grid with parallel radial lines having equally spaced points between the inner and outer casings. By definition, the machine casings form curved grid lines and there are no additional difficulties for grid points which lie close to or on the boundaries. There is an automatic refining of the grid as the annulus height is reduced.

There is clearly no difficulty in forming finite difference approximations for the radial derivatives, but there are no simple expressions for derivatives with respect to z. Reference (6) describes a general method for obtaining the finite difference approximations in the distorted mesh and this can form part of the computer program. The finite difference approximation for the principal equation (32) and its boundary conditions can be written in the matrix form

$$[M][\psi] = [Q] \qquad (33)$$

where $[\psi]$ and $[Q]$ are column vectors and $[M]$ is a band matrix which remains unchanged throughout the calculation. Only one band of non-zero elements is formed and stored in the computer. The method of solution is to solve for the stream function with a given vector $[Q]$, to correct $[Q]$ using the new flow pattern and then to repeat the cycle of calculation until convergence is obtained.

The matrix method has certain limitations on the Mach number, which occur in the calculation of the local density. At each point in the mesh, there are two possible flow solutions, one corresponding to a meridional or relative Mach number less than unity and the other to meridional or relative Mach number greater than unity. To avoid ambiguity and to ensure that the principal equation remains elliptic, the computer program of reference (6) is restricted to flows where

a) in a duct region $M_m \leqslant 1$

b) in a blade row $M_{rel} \leqslant 1$

It has been suggested that these Mach number limitations might be relaxed by modifying the procedure by which the density and velocity components are calculated.

The numerical stability of the matrix method is dependent on the problem which is being solved and although a considerable degree of under-relaxation of the stream function is usually required, in a few problems it has been possible to use over-relaxation. Radial grid lines are usually positioned both in the duct regions and within the blade rows and there does not appear to be any difficulty in obtaining

numerical solutions, provided that the machine boundaries form smooth curves.

It is important to realise that the method of streamline curvature and the matrix through-flow analysis are merely two different numerical techniques for solving the same set of equations governing the flow on the mean stream surface. When applied to the same flow problem with the same mesh, then the two methods of calculation must lead to the same solution. The major difference between the two methods as they are now applied, is that the method of streamline curvature usually places the calculating planes only in the duct regions, while the matrix method includes calculating planes within the blade rows. This is, however, a difference of no great significance in that either method can be applied with or without calculating planes inside the blade rows.

The Loss Model

One difficulty in calculating the flow pattern is that it is necessary to estimate the loss of relative stagnation pressure, or the entropy change, on passing through the blade rows. This problem is perhaps best phrased in terms of entropy in that it is then clear that the effect of loss in a multi-stage compressor is cumulative. It is the radial gradient of entropy which enters directly in the governing equations for the matrix method, while the method of streamline curvature requires both the radial and meridional gradients of entropy. As the flow passes through each blade row, then for an adiabatic flow, the entropy increases monotonically along the streamlines. The changes in entropy and the entropy gradient in an isolated blade row are usually small, but when the flow has passed through a large number of blade rows, then the entropy gradient term in the governing equations becomes more important. For a multi-stage machine, the flow calculations require an extremely accurate definition of the loss model for each blade row.

It might be argued that since both methods of flow calculation do not include any frictional force terms, then the calculations are only valid for a reversible flow. For example, from equations 12, 13, 14 and 15 it is possible to derive an entropy equation,

$$T W_m \frac{\partial \bar{s}}{\partial m} = 0 \qquad (34)$$

which is only valid for a reversible adiabatic process. The problem is to determine whether the use of some empirical relationship for the entropy changes in a turbomachine, based on cascade data, is consistent with the method of calculation. This can readily be determined by considering the equations which are used in the calculation,

1) Continuity,
2) Radial equation of motion,
3) Tangential equation of motion,
4) Energy,
5) State,
6) Entropy (empirical).

For an axial flow machine, the axial equation of motion is not used in either method of calculation. It can thus be argued that the changes of entropy which occur are caused by frictional force terms in the equation of motion which is not required. The loss model therefore assumes that the frictional force acts only in the axial direction and the flow calculations are consistent with this model. An alternative argument is that the local frictional force terms are sufficiently small to be neglected in the three equations of motion, but their cumulative effect is a change of entropy which cannot be neglected.

The simplest method for including losses in the flow calculation is to define a polytropic efficiency which can vary throughout the flow field in accordance with the known behaviour of similar turbomachines. This model has great simplicity and was therefore used in some of the early calculations of reference (6). However, this was quickly superseded by incorporating Lieblein's (7) loss correlation as a loss subroutine in the computer programs for both methods of flow calculation.

Lieblein (7) studied the flow through two dimensional cascades at low speeds and found that there was a relationship between the suction surface diffusion ratio and the ratio of the wake momentum thickness to the blade chord. It was shown that Lieblein's equivalent diffusion parameter could be correlated with the wake momentum thickness parameter θ/c such that the loss coefficient ω could be expressed as

$$\frac{\theta}{c} \simeq \frac{\omega \cos \beta_2}{2\sigma} \left[\frac{\cos \beta_2}{\cos \beta_1} \right]^2$$

The losses in this model are those caused by fluid friction at the blade surface, flow separation and wake mixing. In the discussion of Lieblein's paper Klapproth suggested a modified equivalent diffusion factor

$$D_{eq} = \frac{V_{z1}}{V_{z2}} \frac{\cos\beta_2}{\cos\beta_1} \left\{ K_1 + K_2 (i - i^*)^{K_3} + \frac{K_4 \cos^2\beta_1}{\sigma} \left[\tan\beta_1 - \frac{r_2 V_{z2}}{r_1 V_{z1}} \tan\beta_2 - \frac{\omega r_1}{V_{z1}} \left(1 - \frac{r_2^2}{r_1^2} \right) \right] \right\} \qquad (36)$$

where i^* is the minimum loss incidence. This modified diffusion factor includes the effects of axial velocity change across the blade row and the radial displacement of the streamlines.

Swan (8) later showed that for subsonic flow, a similar correlation to that of Lieblein could be obtained for compressor data. Swan's correlation is in two parts, the first relating the wake momentum thickness parameter to the equivalent diffusion factor for operation at the condition of minimum loss,

$$\left(\frac{\theta}{c}\right)^* \text{ vs. } D_{eq}^*$$

the asterisk denoting minimum loss. The correlation shows that the radial position of the blade element affects the loss. The second correlation was for off-minimum loss operation and related the changes in the wake momentum thickness and diffusion parameters,

$$\left(\frac{\theta}{c}\right) - \left(\frac{\theta}{c}\right)^* \text{ vs. } D_{eq} - D_{eq}^*$$

This second correlation gave curves which were independent of radial position, but very dependent on the Mach number.

Swan also suggested that the Lieblein loss model could be extended to transonic blade rows by adding a shock loss coefficient directly to the profile loss coefficient predicted from D_{eq},

$$\omega_{total} = \omega_s + \omega_p \qquad (37)$$

where ω_s and ω_p are the shock and profile loss coefficients. Swan proposed a shock model in which a bow wave is attached to the leading edge and this is followed by a Prandtl - Meyer expansion along the suction surface until an expansion wave intersects the next blade. A normal shock is assumed to occur across the channel at the position of minimum flow area. The Swan - Lieblein loss model has been found to give good agreement between the predicted and observed performance of compressors.

The shock loss model of Swan and the correlations given by Lieblein are best regarded as a temporary general approximation for the loss model. The shock model is much simplified and the correlations may not cover the entire range of interest, but in the absence of accurate loss data for a particular blade element, this may be the best available method for calculating the losses. This is clearly one part of the calculation for which more detailed information is required.

The Definition of the Mean Stream Surface

The methods of streamline curvature and matrix through-flow both require that the flow angles are specified within, or at exit from, a blade row. The data obtained from testing a stationary linear cascade can give a reasonable approximation for the mean stream surface, but in a turbomachine, these flow angles are influenced by the local flow pattern. The papers by Lieblein and Swan contain a correlation of the deviation with the equivalent diffusion factor and Horlock (9) suggests that the deviation can be related to the axial velocity ratio, AVR, by

$$\delta = \delta' + 10\,(AVR - 1) \qquad (38)$$

where δ' is the deviation for unity axial velocity ratio. The computer program can be arranged so that between the main iterations, the flow pattern is examined and the new air exit angles estimated for the next cycle of calculations. It is thus possible to modify the original definition of the mean stream surface during the calculation, so that the final stream surface is consistent with the local flow pattern.

Annulus Wall Boundary Layers

In order to predict the flow pattern over the entire annulus, it is necessary to combine the through flow analysis with some method for calculating the development of the annulus wall boundary layers. Stratford (10) has proposed a simple model for calculating the development of the axial component of the boundary layer and this model has been compared with experimental results by Gregory-Smith (11) (12). The axial equations of motion for the flow in the mainstream and boundary layer regions are, from equation (14)

Mainstream (m.s.)

$$-\frac{1}{\rho}\frac{\overline{\partial p}}{\partial z} + F_z = W_z \frac{\overline{\partial W_z}}{\partial z} + W_r \frac{\overline{\partial W_z}}{\partial r} \qquad (39)$$

Boundary Layer (b.l.)

$$\frac{1}{\rho}\frac{\partial \overline{\tau_z}}{\partial r} - \frac{1}{\rho}\frac{\partial \overline{p}}{\partial z} + F_z = W_z\frac{\partial \overline{W_z}}{\partial z} + W_r\frac{\partial \overline{W_z}}{\partial r} \tag{40}$$

where τ_z is the axial component of the shear stress. Following boundary layer theory, it is assumed that the pressure does not vary through the boundary layer,

$$\left.\begin{aligned} \left(\frac{\partial p}{\partial z}\right)_{b.l.} &= \left(\frac{\partial p}{\partial z}\right)_{m.s.} \\ \text{and} \qquad \left(F_\theta\right)_{b.l.} &= \left(F_\theta\right)_{m.s.} = -\frac{1}{r\rho}\frac{\partial p}{\partial \theta} \end{aligned}\right\} \tag{41}$$

If there is no distortion of the mean stream surface in the boundary layer, then

$$\left(\frac{1}{\rho}\frac{\partial p}{\partial z}\right)_{b.l.} = \left(\frac{1}{\rho}\frac{\partial \overline{p}}{\partial z} - F_z\right)_{b.l.} = \left(\frac{1}{\rho}\frac{\partial \overline{p}}{\partial z} - F_z\right)_{m.s.} \tag{42}$$

and it follows from these assumptions that

$$\frac{1}{\rho}\left(\frac{\partial \overline{\tau_z}}{\partial r}\right)_{b.l.} = \left[W_z\frac{\partial \overline{W_z}}{\partial z} + W_r\frac{\partial \overline{W_z}}{\partial r}\right]_{b.l.} - \left[W_z\frac{\partial \overline{W_z}}{\partial z} + W_r\frac{\partial \overline{W_z}}{\partial r}\right]_{m.s.} \tag{43}$$

By integrating through the boundary layer, Stratford derived the momentum integral equation for the axial direction which can be written as

$$\frac{\tau_{wz}}{\rho} = \frac{d}{dz}\left(\theta W_z^2\right) + \delta^* W_z \cdot \frac{dW_z}{dz} \tag{44}$$

where τ_{wz} is the axial component of the wall shear stress. Additional information on the skin friction coefficient and the shape factor parameter is obtained from experimental data on the flow over a flat plate with a pressure gradient (10).

In order to apply this method of calculation, the boundary layer must be specified at some upstream position, ahead of the first row of blades. A streamline curvature or matrix through-flow program is used to calculate the flow pattern and this provides data on the flow close to the wall. This information is then used in the calculation of the development of the wall boundary layer. For the flow through a rotor row, the calculation is made in a coordinate system which rotates with the blade row.

Gregory-Smith (11), (12) has reported experiments with an isolated rotor row to test the predictions obtained from Stratford's theory. The apparatus is the rotating cascade wind tunnel at Cambridge University, the overall design being as shown in figure 2, a complete description being available in reference (13). The large inlet leads to a working section with a hub diameter of 2 ft. and a tip diameter of 5 ft., a hub to tip ratio of 0.4. The tunnel has two independent rotors, one being the research rotor and the other being an auxiliary fan which is placed far downstream. The combination of a variable speed research rotor, an auxiliary fan with variable pitch and speed and an exit throttle allows this apparatus to operate over a very wide range of flow conditions. An unusual feature of the apparatus is that the research rotor is fitted with a multi-channel pressure transfer device which transmits pressures from the rotating blades to stationary manometers.

Preliminary experiments with a row of inlet guide vanes had shown that if there was a large radial gradient of axial velocity, then it was difficult to define the edge or the boundary layer. It was therefore decided to test the theory against experiments with an isolated rotor row of free vortex design and later to extend the experiments to a complete free vortex stage. The design flow coefficient was $V_z/U_m = 0.7$, where U_m is the blade speed at the mid-span position. Rotating stall with a single cell was observed at $V_z/U_m = 0.39$ and detailed measurements of the wall boundary layer development were taken at $V_z/U_m = 0.5$, 0.7 and 0.8. For this range of flows the mainstream shear remains small. All experiments were performed at a constant Reynolds number of 300,000, this being based on the blade chord and the relative velocity at the blade mid-span.

The pressure distribution around the rotor blades was measured at fourteen radial positions in the mainstream and wall boundary layer regions. It was found that for both on-design and off-design operation, there was very little variation of pressure through the boundary layer, as assumed in the theory. One particularly interesting result was that there was very little difference between the pressure distributions measured at the edge of the boundary layer and at a position 0.15 in. from the tip of the blade, the tip clearance being 0.1 in. and the blade chord being 6 in. Further work is now being carried out to determine the effect of tip clearance.

Figure 3 shows a comparison of the predicted and experimental development of the wall boundary layer, as measured by Gregory-Smith (12) for operation at $V_z/U_m = 0.5$.

There is good agreement between the theory and the experimental results at the outer wall, but at the inner wall, where the swirl angle is high, the agreement is only fair. It has been found that, in general, the theory provides a good estimate for the development of the wall boundary layers when the swirl angle is small, but there is a progressive deterioration in the predictions as the swirl angle is increased. Stratford's model has simplicity and gives a first approximation for the development of the wall boundary layer, but there is clearly a need for an improved model, particularly for flows at high swirl angles.

Two alternative methods for estimating the growth of the wall boundary layer are the correlation of cascade data by Hanley (14) and an extension of Hoadley's analysis for boundary layers in swirling flows in a diffuser (15). Hanley has correlated end wall loss data from linear cascades, relating the changes in the boundary layer displacement thickness and profile parameter with the free stream loading. It might be possible to check the experimental results of Gregory-Smith against Hanley's correlation. Hoadley's analysis was originally developed for swirling flow in a diffuser, but it can be extended to flows in turbomachines by using a distributed body force to represent a blade row. Horlock (16) has found that Hoadley's analysis gives good agreement with Gregory-Smith's experimental results when the swirl angle is small, but as with Stratford's method, the agreement worsens rapidly as the swirl angle is increased.

Secondary Flows

One of the assumptions in Stratford's boundary layer theory is that the flow angle does not vary through the boundary layer. However, it is well known that large variations in the flow angle can occur close to the annulus walls. Following the work of Hawthorne (17), Gregory-Smith (12) has computed the secondary flow in the isolated rotor row described earlier and by averaging the induced secondary velocities across the pitch, he has obtained the variation in flow angle. These calculations are described in detail in reference (11). For the analysis, the axial velocity profile of the wall boundary layer was assumed to remain unchanged through the blade row and equal to the observed axial velocity profile at exit from the blade row. Figure 4 shows that at the outer wall, there is good agreement between the predicted and measured variation of relative flow angle at exit from the rotor row, there being underturning caused by the component of relative streamwise vorticity at inlet to the blades. At the inner wall, where the deflection of the flow is larger, the agreement is only fair at the low flow coefficient $V_z/U_m = 0.5$. The experimental results at the inner wall may be influenced by the presence of a short gap between the rotor hub and the stator hub, the probe traverse position being a short distance downstream of this gap.

Calculation of the Complete Flow Pattern

One procedure for calculating the flow through turbomachines, including losses, the development of the wall boundary layers and secondary flow effects, might be as follows:-

1. Calculate the mainstream flow, neglecting the boundary layer, using either of the through-flow methods of analysis. This computer program would include a loss subroutine based on the work of Lieblein (7) and Swan (8).

2. Using the solution for the flow on the mean stream surface, stage 1, calculate the development of the annulus wall boundary layers. Stratford's theory (10) gives a simple method for calculating the development of the boundary layer and it is possible that better methods may become available.

3. Hawthorne's (17) secondary flow theory can be used to predict the variation of flow angle close to the walls. This requires data from the boundary layer calculations of stage 2, or from experimental velocity profiles.

4. Using the information on the boundary layer, stage 2, together with the variation of flow angle predicted in stage 3, the flow pattern can be re-calculated for the entire annulus.

5. If necessary, the cycle of calculation, steps 2, 3 and 4 can be repeated.

Gregory-Smith (11) has reported calculations of the flow in the entire annulus, following steps 1 to 4 outlined above. The matrix through-flow program was used with a mesh consisting of unevenly spaced points on radial lines, the radial grid spacing being small in the boundary layer regions and large in the mainstream. In step 1, the matrix through-flow program is used to calculate the flow pattern and to form the data required for the boundary layer program of step 2. The downstream axial velocity profile predicted in step 1 for the isolated rotor row operating off-design, $V_z/U_m = 0.5$, can be seen in figure 5. The corresponding prediction of the development of the boundary layer using Stratford's theory is as shown in figure 3. In order to test the secondary flow theory, the experimental boundary layer profile was used in the calculation of the variation of flow angle, step 3, the results being shown in figure 4. The data from the secondary flow calculations and the observed boundary layer development was fed back into the through-flow program, step 4, and the flow pattern was then predicted for the entire annulus. Figure 5 shows the predicted and experimental axial velocity profiles 15.8 inches downstream of the isolated rotor row. It is clear that the inclusion of boundary layer effects leads to better agreement between the theoretical and experimental

results.

For the present, it has been necessary to base the calculations on the observed development of the wall boundary layers. However, this work by Gregory-Smith shows that if an accurate method of prediction can be developed for the annulus wall boundary layers, then it should be possible to estimate the complete flow pattern in a turbomachine and thereby obtain a more reliable prediction of performance.

Mach Number Limitations

The streamline curvature and matrix through-flow methods have Mach number limitations and at present, the flow pattern in a transonic compressor can only be calculated by treating the blade rows as devices with a specified behaviour and by not placing calculating planes within the blade rows. The major difficulty can best be illustrated by considering the flow in an axisymmetric convergent-divergent nozzle, a turbomachine with no blades and no hub. The streamline curvature and matrix methods can both predict the flow pattern when the entire flow is subsonic, but neither method can deal with the more general problem when there is supersonic flow following the throat and a shock down to subsonic flow. It is unlikely that the present methods of flow calculation will be able to deal with this problem and it may therefore be necessary to develop a new numerical method for flows which include regions of subsonic and supersonic flows and shocks. It may be possible to extend to turbomachinery flows the methods of calculation based on solving the time dependent equations of motion to obtain the ultimate steady state flow pattern. References (18) and (19) describe a numerical technique for calculating the flow in one-dimensional and two-dimensional convergent-divergent nozzles with regions of subsonic flow, supersonic flow and a shock. Figure 6 compares the numerical solution for the pressure distribution in a one-dimensional nozzle with that obtained analytically. There is seen to be close agreement between the two solutions; the shock is smeared, but the main features of the flow are preserved. Stable numerical solutions have also been obtained by Merryweather (19) for the flow in two-dimensional nozzles. It is important to realise that these solutions are based only on the equations of continuity, motion, energy and state, together with the boundary conditions of the upstream stagnation state and the downstream exit pressure. It is hoped that this numerical technique might be extended to flows in turbomachines and thus remove the present Mach number limitations.

Conclusions

During recent years, two methods have been developed for solving the equations governing the flow in turbomachines, namely streamline curvature and matrix through-flow analysis. In this paper it has been shown that these two approaches to turbomachinery flow calculations are based on the same mathematical model; they are merely two different techniques for obtaining numerical solutions to the same set of equations. With the computer programs based on these methods of flow calculation, it is now possible to estimate the performance of a turbomachine operating on-design or off-design. However, the accuracy of these predictions is dependent on the mathematical model. There remains a need for more accurate methods for predicting losses and for predicting the development of the wall boundary layers. More work is also required on the effects of turbulence on the performance of a blade row, the behaviour of a cascade in an unsteady flow, such as that produced by an upstream blade row, and the flow in transonic blade rows. Research is being carried out on several of these problems and as our understanding of the flow improves, then we may expect to see further improvements in the prediction of the performance of turbomachines. In the past, methods of computation were not adequate to deal with the flow model for turbomachines, whereas at present, the means of calculation exist and it is the mathematical model of the flow which requires further improvement.

References

1. Wu, C-H — A general theory of three dimensional flow in subsonic and supersonic turbomachines of axial, radial and mixed-flow types, N.A.C.A. TN 2604, 1952

2. Smith, L.S. — The radial equilibrium equation of turbomachinery, Trans. A.S.M.E., Series A, Vol. 88, 1966.

3. Novak, R.A. — Streamline curvature computing procedures for fluid flow problems. A.S.M.E., Paper 66 - WA/GT-3, 1966.

4. Silvester, M.E. and Hetherington, R. — Three-dimensional compressible flow through axial flow turbomachines, in 'Numerical Analysis - An Introduction' Academic Press 1966.

5. Shaalan, M.R.A. and Daneshyar, H. — Methods of calculating slope and curvature of streamlines in fluid flow problems, Cambridge University Engineering Department Report, CUED/A - Turbo/TR2, 1969.

6. Marsh, H. — A digital computer program for the through-flow fluid mechanics in an arbitrary turbomachine using a matrix method. N.G.T.E. Report R282, 1966, also Aero. Res. Coun. Rep. Memor. 3509, 1968.

7. Lieblein, S. — Loss and stall analysis of compressor cascades, Trans. A.S.M.E. Series D, Vol, 81, 1959.

8. Swan, W.C. — A practical method of predicting transonic compressor performance, Trans. A.S.M.E., Series A, Vol. 83, 1961.

9. Horlock, J.H. — Some recent research in turbomachinery, Proc. Instn. Mech. Engrs. Vol. 182, 1968.

10. Stratford, B.S. — The use of boundary layer techniques to calculate the blockage from the annulus boundary layers in a compressor, A.S.M.E., Paper 67 - WA/GT - 7, 1967.

11. Gregory-Smith, D.G. — Annulus wall boundary layers in turbomachines, Ph.D. dissertation, Cambridge University, 1970.

12. Gregory-Smith, D.G. — An investigation of annulus wall boundary layers in axial flow turbomachines, To be published by A.S.M.E. May 1970.

13. Oxford, J.T.B. — A rotating cascade wind tunnel and a rotating aerofoil in rotational flow, Ph.D. dissertation, Cambridge University, 1965.

14. Hanley, W.T. — A correlation of end wall losses in plane compressor cascades, Trans. A.S.M.E., Series A, Vol. 90, 1968.

15. Hoadley, D. — Three dimensional turbulent boundary layers in an annular diffuser, Ph.D. dissertation, Cambridge University, 1969.

16. Horlock, J.H. — Private communication, 1969.

17. Hawthorne, W.R. and Novak, R.A. — The aerodynamics of turbomachinery, Annual Review of Fluid Mechanics, Annual Reviews Inc., Vol. 1., 1969.

18. Marsh, H. and Merryweather, H. — The calculation of subsonic and supersonic flows in nozzles, Cambridge University Engineering Department Report, CUED/A - Turbo/TR3, 1969.

19. Merryweather, H. — The calculation of subsonic and supersonic flows in ducts, Ph.D. dissertation, Cambridge University 1969.

Acknowledgement

The author would like to thank Mr. D.G. Gregory-Smith for permission to quote the experimental and theoretical work of reference (11).

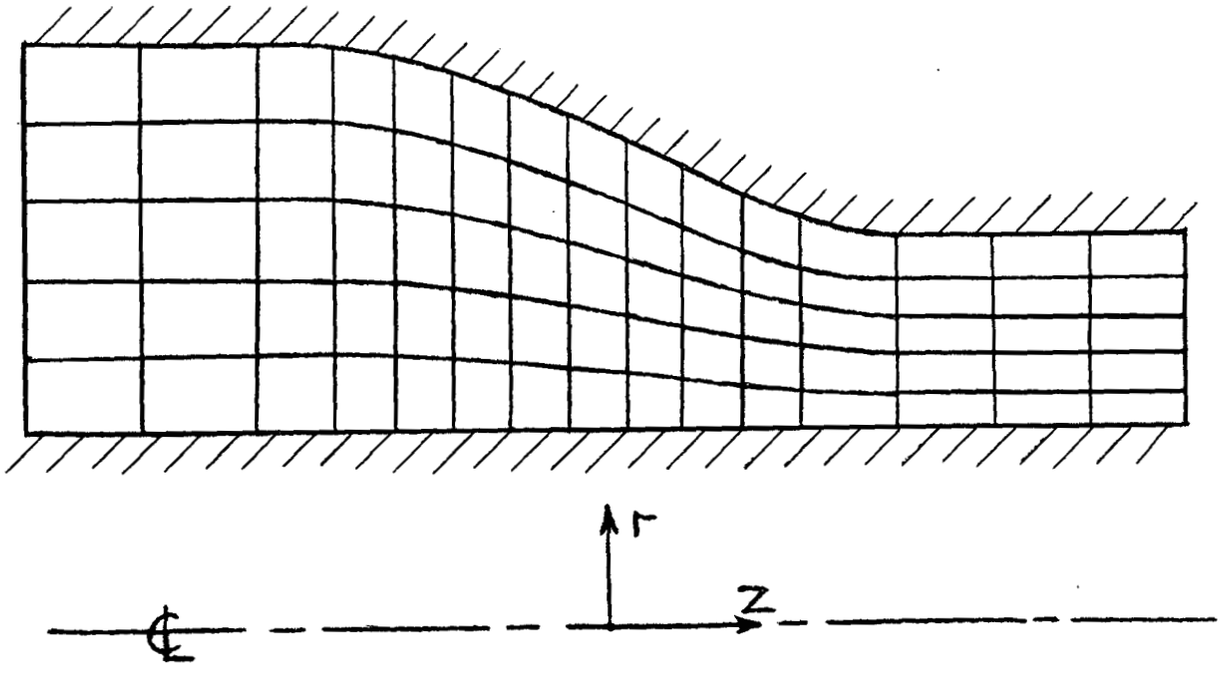

FIGURE 1 DISTORTED GRID

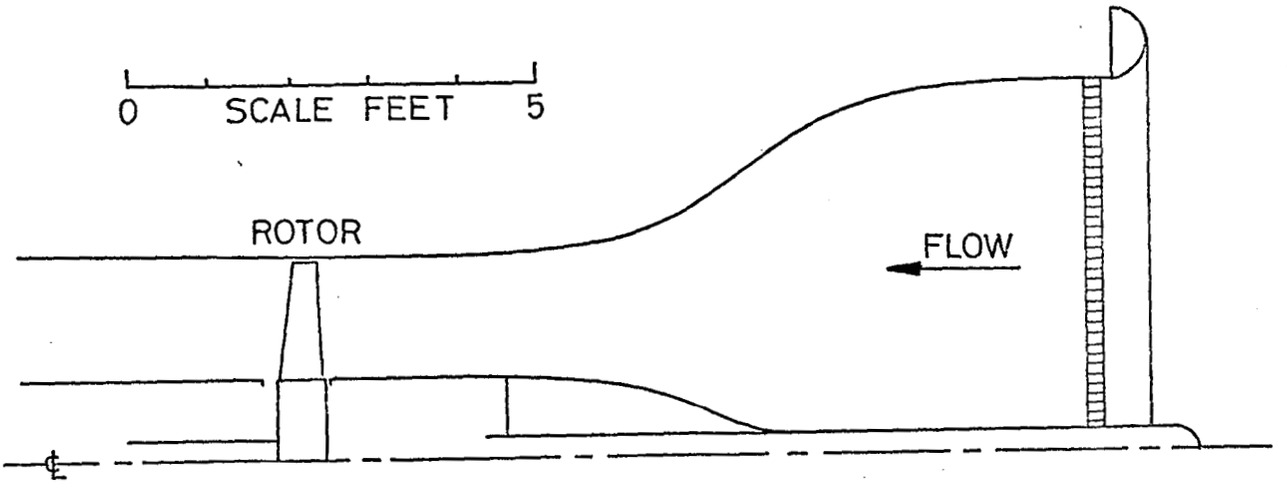

FIGURE 2 ROTATING CASCADE WIND TUNNEL

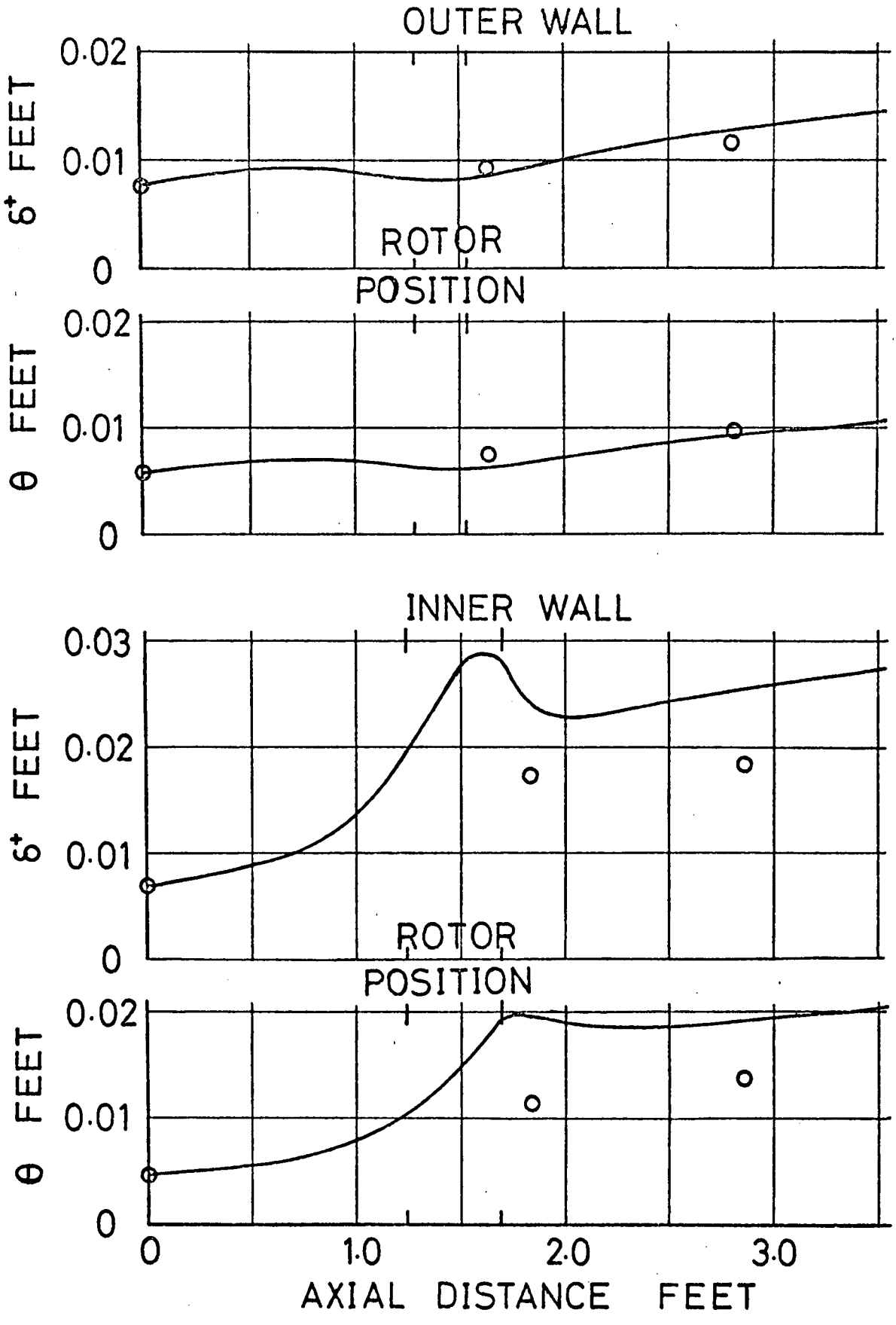

FIGURE 3 ISOLATED ROTOR
BOUNDARY LAYER GROWTH AT $V_z/U_m = 0.5$

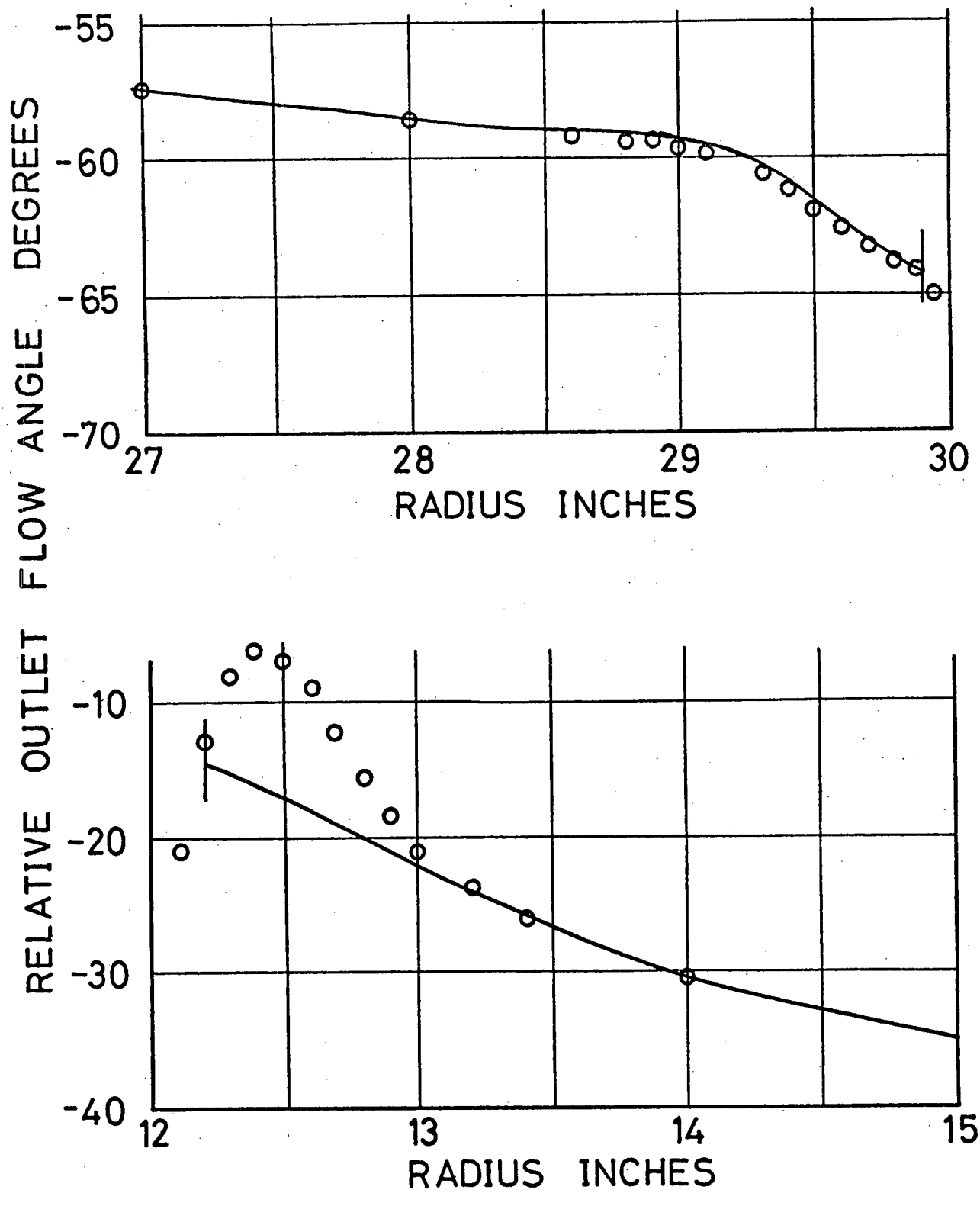

FIGURE 4 ISOLATED ROTOR
SECONDARY FLOWS AT Vz/Um = 0.5

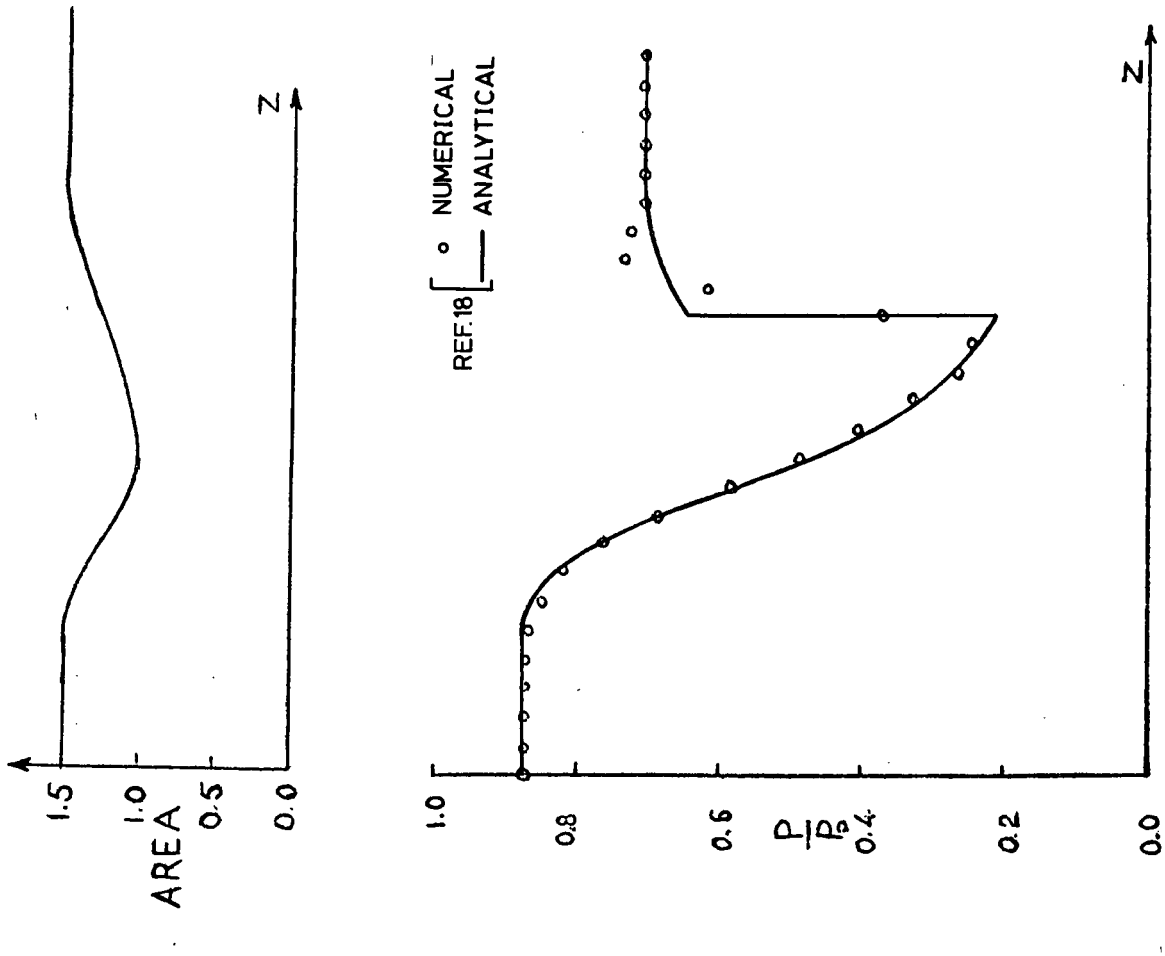

FIGURE 6
PRESSURE VARIATION IN A NOZZLE

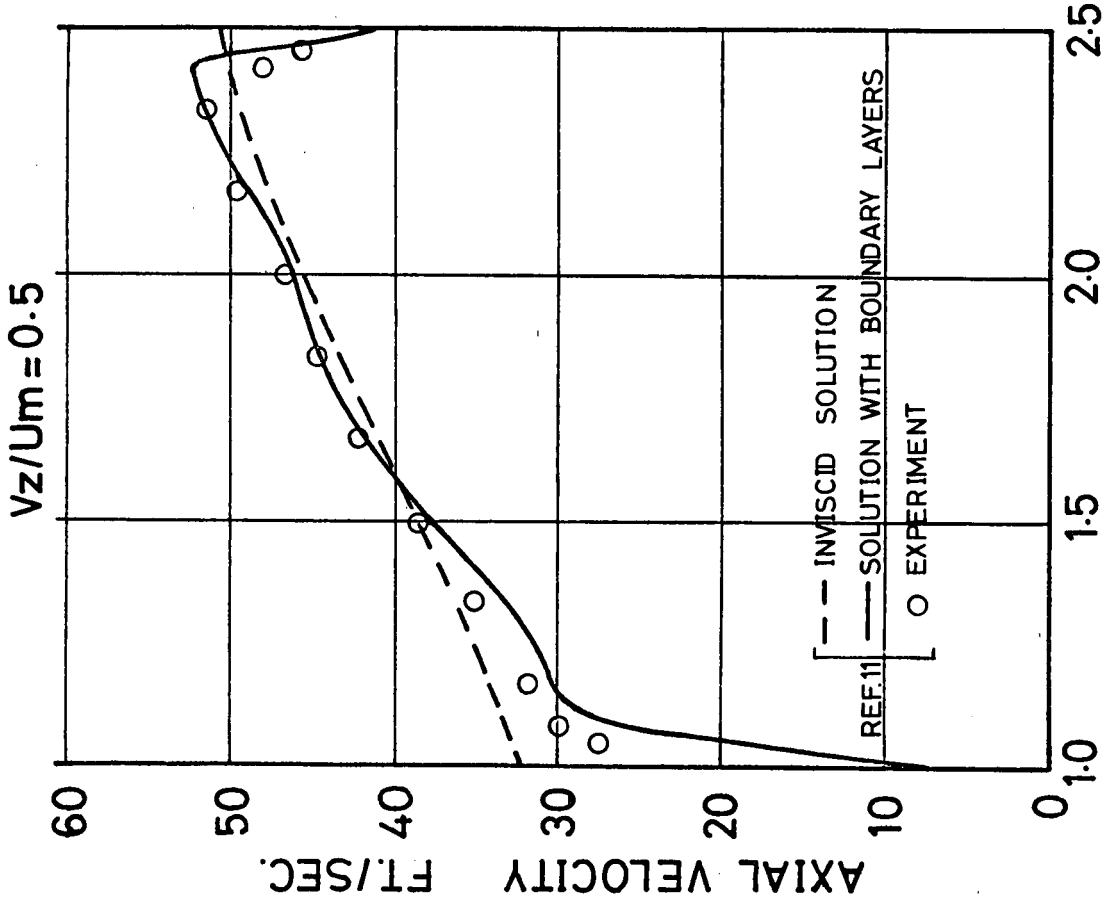

FIGURE 5 ISOLATED ROTOR
COMPLETE FLOW 15.8IN. DOWNSTREAM

MASS FLOW LIMITATION IN SUPERSONIC COMPRESSORS

by Jean FABRI

Office National d'Etudes et de Recherches Aérospatiales
92 - CHATILLON - France

SUMMARY

Accurate prediction of supersonic compressor mass flows is the main condition of progress for these machines. As in the case of supersonic aircraft air-inlets, different types of flow patterns may appear. The choked (or unstarted) regime corresponds to high subsonic or low supersonic rotor speeds. The sonic choking of the blade channel throats limitates the mass flow. The supersonic (or started) regime appears for higher supersonic rotor Mach numbers. The periodicity of the shock and expansion wave pattern, that extends upstream of the rotor inlet, imposes the mass flow. The corresponding unique incidence, function of rotor speed, can be calculated. For even higher supersonic rotor speeds, the shock waves are swallowed by the rotor: the inlet velocity in absolute reference frames becomes sonic and mass flow is independent of rotor speed.

The range of validity of these regimes is given. Values of limit mass flows are calculated. Experimental results are compared to theoretical evaluations .

SOMMAIRE

Le problème de la prévision précise du débit des compresseurs supersoniques constitue la pierre d'achoppement du développement de ces machines. Comme dans les prises d'air de turbomachines d'aviation en vol supersonique, des régimes différents de fonctionnement peuvent apparaître. Le régime mixte ou désamorcé correspond aux vitesses de rotation faiblement supersoniques. Il est caractérisé par un blocage sonique en mouvement relatif de la section de passage minimale des canaux interaubes. Le régime supersonique ou amorcé prend le dessus lorsque la vitesse de rotation est plus élevée. Il correspond à un fonctionnement avec une configuration périodique d'ondes de choc ou de faisceaux de détente remontant en amont de la grille. L'incidence, fonction du nombre de Mach de rotation, est définie par la périodicité de l'écoulement. Un troisième régime apparaît pour les vitesses de rotation encore plus élevées et correspond au blocage sonique du canal d'amenée.

Les conditions d'existence et les débits limite correspondant à chacun de ces régimes sont analysés. Une comparaison avec des résultats expérimentaux est effectuée.

1. - INTRODUCTION

Accurate prediction of the mass flow of supersonic compressors is one of the main problems in supersonic compressor design. The role of compressibility in axial compressor mass flow limitation is visualized on Figure 1 . When , at a given speed of rotation, the downstream throttle is progressively closed, the flow through the com - pressor decreases and the pressure increases until the surge line is attained (curve -a-). As the speed of rotation increases, compressibility effects appear. The slope of the pressure vs mass flow curve increases, i.e. the range of mass flow becomes narrower (curve -b-). For transonic operation the pressure rise curve may even be reduced to a vertical, constant mass flow, line. There would then be just a small variation of mass flow near the surge line (curve -c-).

Many of the aerodynamical problems encountered in the early supersonic compressor research [1] are due to this constant mass flow operation,at a mass flow a few percent lower than the expected design mass flow. The corresponding off-design losses, due to wrong angles of attack, reduced the compressor efficiency. It seems therefore very important to estimate correctly this unavoidably constant mass flow that depends only on rotational speed of the rotor. When flow angles willbe known correctly, it will be possible to set the compressor blades at a low loss angle of attack.

2.- BLADE SHAPES FOR SUPERSONIC COMPRESSORS

Most of the early designs of supersonic bladings for compressors [2] [3] [4] were based on low drag shock wave patterns derived from the BUSEMANN biplane [5] in which both compression and expansion waves are confined between two symmetrical airfoils (Fig.2).

An example of a low drag cascade designed for a supersonic compressor [2] is given on figure 3 . Internal compression is achieved by means of compression waves issued from the upper surface of a blade and focusing on the angular point of the next blade. Unfortunately, experimental results did not confirm the theoretical predictions. This can be easily understood, since an improved theory of supersonic compressor cascades[3] shows that the incident velocity is always parallel to the blade upper surface and not the lower surface.

A shock wave pattern such as the one of figure 4 may be more satisfactory. Inlet flow is parallel to the blade upper surface and the leading edge shock wave

is confined in the blade channel.At design operation, the trailing edge shock wave deflects the flow to a direction parallel to the downstream part of the blade lower surface. This shock pattern is strictly reduced to two shock waves.

Though these flow configurations seemed very attractive, experimental results on compressors were disappointing. One is then very naturally led to assume that there could be a different type of flow that takes place in actual compressors, at least at moderate supersonic rotational speeds.

Cascade wind tunnel experimentation shows that there exists actually two different flow regimes [6]. The started and the choked operation of a supersonic cascade made of trapezoidal blades is shown on figure 5 . The strong normal shock waves shown in the choked case gives the indication that there may exist a sonic section inside the blade channel.

Analysis of mass flow limitation in supersonic compressors intends to determine what are the conditions for choked and started operations.

3. - STARTED BLADE PASSAGES OR SUPERSONIC REGIME

Started blade passages, i.e. supersonic throughflow of the blade channels impose a "unique incidence" [3] [7]. Analysis of the supersonic operation of cascades made of more and more elaborate profils will define the laws of such a regime.

3.1. - Wind tunnel testing of compressor blade cascades in the supersonic regime

Consider first the supersonic wind tunnel testing of a cascade of blades with zero thickness and zero camber (Fig. 6) . In this semi- infinite cascade the most upstream blade induces a shock wave that gives for all the other blades (excepted the one near the wind tunnel upper wall submitted to shock wave wall reflexion) a flow parallel to the blades. If the cascade is set in such a way as to induce an expansion fan, the blades are again submitted to a flow parallel to them (Fig.7). Changing the blade setting or the inlet flow incidence angle results only in a change of Mach number in front of the cascade. Behind a shock wave Mach number is decreased, behind an expansion fan it is increased.

It has to be noted that the shock wave or the expansion fan extends upstream of the cascade inlet line only if the component of the Mach number normal to the cascade inlet is subsonic. In the other case, i.e. when the undisturbed wind tunnel velocity has a supersonic component normal to the cascade inlet, the shock waves or expansion fans enter the blade channels (Fig.8). In that case the cascade does not interfere with the upstream flow.

3.2.- Supersonic regimes of compressor rotors

One must be very careful in extending results obtained in supersonic wind tunnel testing to actual supersonic compressors. The difference between cascade and rotor operation is mainly the following :

a) In wind tunnel testing the undisturbed upstream velocity is fixed by wind tunnel geometry; the cascade controls the actual inlet velocity and "unique incidence" is the rule as long as the blade passages are started (supersonic regime). In rotor tests the mass flow is induced by the motion of the rotating blades and adjusts itself in order to satisfy all boundary conditions.

b) In wind tunnel testing semi-infinite cascades only are represented [3], whereas in rotors the blade cascade has neither a beginning nor an end.

The unique incidence case found for wind tunnel testing remains valid for the determination of the mass flow in started blade channel conditions.

3.2.1. - Consider first the ideal case of a rotor of heigth dr small compared to its radius r . The rotor has n blades of zero thickness and zero camber. They are set to an angle β with the axial direction. Supersonic motion relative to axes moving with the rotor is assumed.

In order to achieve flow periodicity, i.e. such that the flow in each blade channel be identically the same, the mass flow attains a value for which the relative velocity is parallel to the blades (Fig.9).

This mass flow is then given by

(1) $$d\dot{m} = 2\pi r \rho V_x dr$$

with , for the axial velocity,

(2) $$V_x = U \cot an \beta , \qquad U = \omega r$$

ω being the angular speed of the rotor.

3.2.2. - The next case to be considered is that of a rotor that has blades with a straight upper surface. Again flow periodicity requires such an axial velocity that relative velocity be parallel to these straight blade upper surfaces. In this case, shock waves can be generated, but near the blade leading edge, from the lower surface only. These shock waves are always confined in the blade channels. (Fig. 10) . The mass flow is still given by equation (1), where β represents the angle of the straight blade upper surface with the axial direction.

3.2.3. - Consider then the case of blades the upper surface of which is made of straight lines, the change of slope being close to the leading edge. The shock pattern is made up of a leading edge shock wave that extends upstream of the cascade and an expansion fan, induced by the change of slope, that extends also upstream and cancels the deflection given by the shock wave (Fig. 11) .

Though this is the simplest case of a shock pattern that extends upstream of the cascade, no uniform upstream flow can be defined and the mean mass flow has to be deduced from equation

$$d\dot{m} = 2\pi r \bar{\rho} \bar{V}_x dr = n \int_0^t \rho(y) V_x(y) dy\, dr \qquad (3)$$

where the y axis is parallel to the cascade inlet front, $\rho(y)$ and $V_x(y)$ are the local density and axial velocity, $\bar{\rho}$ and $\bar{V}_x$ their mean value, t is the spacing of the n blades ($t = 2\pi r/n$).

Since behind the last wave of the expansion fan the flow becomes uniform again and parallel to the blade upper surface, the mass flow is the most easier derived from equation

$$d\dot{m} = n \overline{A'A_1}\, \rho_1 W_1 dr \qquad (4)$$

where ρ_1 and W_1 are the density and velocity downstream of this last wave, β_1 the corresponding angle and $\overline{A'A_1}$ the distance from the leading edge to the upper surface of the next blade.

3.2.4. - The most complicated case considered here corresponds to blades with sharp leading edge and curved upper surface (*) . The leading edge of each blade is situated then inside of the expansion fan issued from the adjacent blade (Fig. 12).

Flow periodicity requires such a shock wave and expansion fan combination that the flow becomes at the outlet of the shock pattern as it was at the inlet. Calculation of such a periodical shock and expansion pattern is not too complicated if entropy losses can be neglected, i.e. whenever the leading edge shock wave is not too strong. In this case, the streamlines terminating at the leading edges cross only weak waves.

The mass flow corresponding to such a flow pattern is obtained in the following way (Fig. 12) : A'B is the Mach line issued from blade AC that attains blade A'C' at its leading edge A'. Therefore the angle of AB with the tangent to the upper surface of blade AC at point B is the Mach angle Ω , i.e. :

$$\tan\Omega = \frac{1}{\sqrt{M_B^2 - 1}} \qquad (5)$$

If entropy changes along the Mach line A'B can be neglected, this line is a straight line the equation of which is

$$\frac{t\cos\beta_0 - Y}{t\sin\beta_0 - X} = \frac{\tan\Omega + \frac{dY}{dX}}{1 - \frac{dY}{dX}\tan\Omega} \qquad (6)$$

where (X,Y) are the coordinates of point B, the axis AX being taken along the chord

---

(*) The case of blunt leading edges or that of leading edges with finite curvature will not be discussed here.

AC of the blade and axis AY normal to it; angle β_o is the angle of blade chord AC with the axial direction.

Choice of any point $B(X,Y)$ as initial point of the Mach line A'B defines by means of equations(5) and (6) the local Mach number M_B .The corresponding flow angle β_B is defined by

$$(7) \qquad \begin{cases} \beta_B = \beta_o + \varepsilon \\ \tan\varepsilon = \dfrac{dY}{dX} \end{cases}$$

For this flow pattern, where conditions are uniform along the Mach line terminating at the blade leading edge, the mass flow is given by

$$(8) \qquad d\dot{m} = n \rho_B W_B \left(t^2 - 2t(X\sin\beta_o + Y\cos\beta_o) + X^2 + Y^2\right)^{\frac{1}{2}} \sin\bar{m}\,\Omega\, dr$$

The mass flow conservation and the energy conservation equations give

$$(9) \qquad \rho_B W_B = M_B \left(\frac{2 + U^2/C_p T_o}{2 + (\gamma-1) M_B^2}\right)^{\frac{\gamma+1}{2(\gamma-1)}} \rho_o a_o$$

where a_o is the speed of sound in the stagnation conditions of the incoming flow (temperature T_o). The corresponding rotor speed , U , is given by the tangential momentum conservation equation

$$(10) \qquad \int_o^t \rho W \cos\beta \left(W \sin\beta - U\right) dy = 0$$

similar to the mass conservation equation (3) and where density ρ , relative velocity W and flow angle β along the rotor inlet are related by means of the characteristics theory of supersonic flows, to the corresponding values on the blade upper surface. Flow pattern determination is slightly more complicated when due to shock wave strength entropy changes have to be considered. This gives however, second order corrections only.

3.3. - Flow pattern with expansion waves

It was sometimes suggested to use compressor blades that have concave instead of convex upper surfaces near the leading edges (Fig. 13). The wave pattern begins then with an expansion fan followed either by continuous compression waves or discrete shock waves. As long as entropy change can be neglected, determination of the mean mass flow is made as in the case of blades of figure 12 .

3.4. - Saturated supersonic regime

Mass flows calculated in the above cases cannot exceed the critical mass flow

$$(11) \qquad d\dot{m}_* = 2\pi \left(\frac{2}{\gamma+1}\right)^{\frac{\gamma+1}{2(\gamma-1)}} \rho_o a_o r\, dr$$

corresponding to sonic axial velocity at cascade inlet. When rotor velocity takes high supersonic values, the compressor inlet is choked and mass flow given by equation (11)

corresponds to the condition

(12) $$M_x = 1$$

The shock and Mach waves are confined in the blade channels and do not extend in front of the rotor. In this saturated supersonic regime, the mass flow is independent of the rotor speed.

4. - CHOKED OR UNSTARTED OPERATION OF SUPERSONIC COMPRESSORS

The above calculations give the design mass flow expected from supersonic compressors. Testing of these machines showed that the mass flow was actually smaller than the one predicted. This mass flow limitation may be due to early choking of the blade passages at low supersonic velocities. The same phenomenon is responsible of mass flow limitation in transonic compressors. High subsonic and low supersonic velocities will be considered.

Consider again a cylindrical section of a compressor blading (Fig. 14). V_x is the axial velocity and $U = \omega r$ the rotational velocity of the rotor. Angle of attack of the flow, relative to axes moving with the rotor, β , is defined by equation

(13) $$\tan\beta = \frac{U}{V_x}$$

If the upstream stagnation conditions in absolute frames of references are P_0, T_0 , the compressor inlet conditions are given by the following relations

(14)

absolute Mach number $$M_x = \frac{V_x}{\sqrt{(\gamma-1)c_p T}}$$

relative Mach number $$M_W = \frac{W}{\sqrt{(\gamma-1)c_p T}} = \sqrt{\frac{V_x^2 + U^2}{(\gamma-1)c_p T}}$$

temperature $$T = \frac{2T_0}{2+(\gamma-1)M_x^2}$$

pressure $$p = P_0 \left(\frac{2}{2+(\gamma-1)M_x^2}\right)^{\frac{\gamma}{\gamma-1}}$$

where W is the velocity in the moving frames of references.

4.1.- Mass flow limitation due to choking of blade passages

4.1.1.- Isentropic choking. - If the relative Mach number is in the high subsonic range, the blade throat section, s , can be choked after an isentropic expansion of the flow. The mass conservation law

(15) $$\frac{s}{t\cos\beta} = M_W \left(\frac{\gamma+1}{2+(\gamma-1)M_W^2}\right)^{\frac{\gamma+1}{2(\gamma-1)}}$$

defines the relation between the flow angle and relative inlet Mach number. Axial Mach number is given by

(16) $$M_x = M_W \cos\beta$$

and mass flow by

$$(17) \qquad d\dot{m} = 2\pi z M_x \left(\frac{2}{2+(\gamma-1)M_x^2}\right)^{\frac{\gamma+1}{2(\gamma-1)}} \rho_0 a_0 dz$$

These last two equations will held all along the further caloulations.

4.1.2. - Choking with shock wave normal to inlet relative velocity - As relative velocity becomes supersonic, shock waves may appear and move with the blades. In the low supersonic range, only normal shock waves appear. It is not fundamentally important to describe exactly the shock pattern, that quite probably is similar to the choked configuration shown on figure 5, in order to determine the critical mass flow.

As a first approximation, the shock waves can be considered normal to the inlet relative velocity (Fig.15). The Mach number downstream of the shock wave is given by

$$(18) \qquad M'_w = \sqrt{\frac{2+(\gamma-1)M_w^2}{2\gamma M_w^2 - \gamma + 1}}$$

From the choking condition, similar to equation (15), that relates Mach number M'_w to the flow contraction the following relation is obtained

$$(19) \qquad \frac{s}{t\cos\beta} = \frac{1}{M_w^{\frac{\gamma+1}{\gamma-1}}} \left[\frac{2\gamma M_w^2 - \gamma + 1}{\gamma+1}\right]^{\frac{1}{\gamma-1}} \left[\frac{2+(\gamma-1)M_w^2}{\gamma+1}\right]^{\frac{1}{2}}$$

that gives inlet angle as a function of relative Mach number. Both equations (15) and (19) give the same result when inlet relative velocity is sonic ($M_w = 1$).

4.1.3. - Shock normal to the mean passage direction - It is quite hard to say whether the flow at the entrance of the blade channel is deflected before or after going through the shock wave. Therefore an other theoretical flow pattern is analyzed, where the shock wave is normal to the mean passage direction (Fig. 16). An isentropic expansion relates inlet conditions (M_w, β) to the conditions in front of the shock (M_{w_1}, β_1) where angle β_1 gives the mean channel direction. Mass flow conservation during this expansion is expressed by means of

$$(20) \qquad M_w \left(\frac{2}{2+(\gamma-1)M_w^2}\right)^{\frac{\gamma+1}{2(\gamma-1)}} \cos\beta = M_{w_1} \left(\frac{2}{2+(\gamma-1)M_{w_1}^2}\right)^{\frac{\gamma+1}{2(\gamma-1)}} \cos\beta_1$$

and again between the downstream face of the shock wave and the blade channel throat by means of

$$(21) \qquad \frac{s}{t\cos\beta_1} = \frac{1}{M_{w_1}^{\frac{\gamma+1}{\gamma-1}}} \left[\frac{2\gamma M_{w_1}^2 - \gamma + 1}{\gamma+1}\right]^{\frac{\gamma+1}{2(\gamma-1)}} \left[\frac{2+(\gamma-1)M_{w_1}^2}{\gamma+1}\right]^{\frac{1}{2}}$$

4.1.4. - Shock deflection - A thoroughly different representation [8] is obtained when momentum losses due to body forces are also taken into account [9]. The method generalizes to compressible flows the equations of hydraulic losses, more or less empirically used for the off-design studies of compressors [10] [11].

In this theoretical representation the flow deflection takes place with momentum conservation in the zero lift direction of the blade row . If momentum equation is projected on this direction, for a control surface that takes an integer number of blade passages, one obtains (subscript 1 for the zero lift direction)

$$(22) \qquad (p_1 + \rho_1 W_1^2)\cos\beta_1 = p\cos\beta_1 + \rho W^2 \cos\beta\cos(\beta-\beta_1)$$

Mass flow conservation gives

$$(23) \qquad \rho_1 W_1 \cos\beta_1 = \rho W \cos\beta$$

and energy conservation

$$(24) \qquad C_p T + \frac{W^2}{2} = C_p T_1 + \frac{W_1^2}{2}$$

Since pressure p is related to temperature T and density ρ by means of the gas state equation

$$(25) \qquad p = \frac{\gamma-1}{\gamma}\rho C_p T$$

there follows

$$(26) \qquad \frac{\cos\beta_1}{\cos\beta} = \frac{M_W}{M_{W_1}}\left\{(1+\gamma M_{W_1}^2)\left(\frac{2+(\gamma-1)M_W^2}{2+(\gamma-1)M_{W_1}^2}\right)^{\frac{1}{2}} - \gamma M_W M_{W_1}\cos(\beta-\beta_1)\right\}$$

where the Mach number M_{W_1} of the flow having gone through the shock-deflection is given by the contraction ratio equation

$$(27) \qquad \frac{s}{t\cos\beta_1} = M_{W_1}\left(\frac{\gamma+1}{2+(\gamma-1)M_{W_1}^2}\right)^{\frac{\gamma+1}{2(\gamma-1)}}$$

It has to be noted that :

a) in the direction normal to the zero lift direction the change of momentum gives the body forces acting on the fluid;

b) in the no-deflection case ($\beta = \beta_1$), shock-deflection is equivalent to isentropic flow when M_{W_1} is subsonic and to a normal shock wave when M_{W_1} is supersonic.

4.2.- Choice of the model describing actual choked flow

In order to compare the above described four theoretical models, application of the theory will be made to a rotor made of trianguàar blades (Table I). The inlet relative flow angles β and axial Mach numbers M_x calculated as functions of the rotor Mach number are presented in figure 17 .

The isentropic evolution (4.1.1.) is valid in the subsonic relative Mach number range only ($M_W < 1$). The corresponding curves are continued by those

obtained with the shock normal to inlet velocity model (4.1.2.) . Angles higher than the blade upper surface angle only are considered, $\beta > \beta_o$, since for $\beta = \beta_o$ the supersonic regime takes over (see § 5 , below).

TABLE I

Characteristics of a supersonic compressor cascade (theory)

Radius	r = 227 mm
Number of blades	n = 44
Blade spacing	t = 32,4 mm
Blade chord	c = 60 mm
Blade channel throat section	s = 14.1 mm
Blade leading edge angle	α = 4 °
Blade setting angle	β_o = 60 °
- - - - - - -	
Working gas	Air

The choice between these different models is quite difficult. The experimental results are not accurate enough to help efficiently in this choice. However it can be said that at low Mach numbers experiment shows [11] that shock deflection type losses are in good agreement with experimental results. Therefore this model seems to be the most appropriate.

4.3. - Pressure losses due to choking of the blade passages

Due to early choking of the blade passages pressure losses appear as a result of the off- design attack of the blades.

4.3.1. - For isentropic turning of the flow (4.1.1.) there are of course no losses. This is a reason why this model does not seem realistic.

4.3.2. - For a shock normal to inlet velocity the pressure losses are the conventional shock wave total pressure losses

$$\frac{\Delta P_w}{P_w} = 1 - \left[\frac{(\gamma+1) M_w^2}{2 + (\gamma-1) M_w^2} \right]^{\frac{\gamma}{\gamma-1}} \left[\frac{\gamma+1}{2\gamma M_w^2 - \gamma + 1} \right]^{\frac{1}{\gamma-1}} \tag{28}$$

and do not take into account the off-design attack of the blades.

4.3.3. - For a shock normal to deflected velocity (4.1.3.) the turning is isentropic and the losses independent of the speed of rotation, since Mach number in front of the shock wave depends on section contraction ratio only.

4.3.4. - In the shock-deflection model (4.1.4.) the compression ratio is given [8] by

$$(29) \qquad \frac{p_1}{p} = \frac{M_W}{M_{W_1}} \left(\frac{2 + (\gamma-1) M_W^2}{2 + (\gamma-1) M_{W_1}^2} \right)^{\frac{1}{2}} \frac{\cos\beta}{\cos\beta_1}$$

and the pressure losses by

$$(30) \qquad \frac{\Delta P_w}{P_W} = 1 - \frac{M_W}{M_{W_1}} \left(\frac{2 + (\gamma-1) M_{W_1}^2}{2 + (\gamma-1) M_W^2} \right)^{\frac{\gamma+1}{2(\gamma-1)}} \frac{\cos\beta}{\cos\beta_1}$$

4.3.5. - The total pressure losses corresponding to the four models are represented on figure 18. From the loss viewpoint also, the shock-deflection model seems the more adequate.

5. - MASS FLOW LIMITATION IN AXIAL FLOW COMPRESSORS

Since there is an overlapping of the range of validity of the three regimes, choked, supersonic and saturated regimes, a further condition has to be fixed in order to discriminate among these regimes.

It can be said, and experiment seems to verify this assumption, that among the three regimes the one will actually take place that gives the smallest mass flow for the same speed of rotation.

As an example of such a rule, figure 19 shows the variation of axial Mach number M_x as a function of rotor Mach number for the compressor defined by Table I.

For high subsonic or low supersonic operation the choked model controls the mass flow . Transition from this regime to the supersonic is obtained when relative inlet angle is the same for both regimes. This corresponds for the rotor considered to the somewhat high Mach number 1.48 . Then the supersonic regime is maintained until the inlet is choked. Sonic axial velocity is obtained for $M_U = 1.73$.

6.- ANALYSIS OF EXPERIMENTAL RESULTS ON MASS FLOW LIMITATION IN COMPRESSORS

Most of the experimental results published on supersonic compressors show evidence of unstarted operation . There exists however some results published by NACA [12] [13] [14] for which transition from the choked to the supersonic regime can be shown.

The compressor is a single stage, constant section, axial flow compressor. Freon - 12 was used as working gas. The main interest of this work comes from the shadowgraphs of the flow in the rotor.

Table II gives the main data of this compressor, the mean section of which is analyzed. The blading of this section is represented on figure 20 and figure 21 compares the axial Mach number vs rotor Mach number diagram obtained experimentally to the theoretical calculations based on Table II.

The satisfactory correspondance between theory and experiment is confirmed by the shadographs shown on the same figure.[14] .The normal shock that appears at blade entrance for rotor speeds lower than 9000 r.p.m. disappears at higher speeds.

TABLE II

NACA supersonic compressor for flow visualization [12]

Tip diameter	405 mm
Hub-tip ratio	0.75
Number of blades	46
Chord of blade at mean section	58 mm
Throat to spacing ratio	0.475
Angle of tangent to blade upper surface at leading edge	60 °

- - - - -

Working gas	Freon - 12
Isentropic constant	1.125

7. - CONCLUSION

Analysis of theoretical and experimental mass flow performances of supersonic compressors shows that at a given speed of rotation the compressor operates with constant mass flow over the most part of the pressure vs mass flow characteristic. The axial velocity of the incoming flow depends on the speed of rotation only :

- for high subsonic or low supersonic speeds, a choked regime appears and mass flow is limited by the choking of blade channels ; losses corresponding to the off-design angle of attack have to be taken into account if correct values of the mass flow have to be calculated;
- at higher supersonic speeds the blade channels are started; flow periodicity controls the mass flow; axial Mach number is usually proportional to rotor Mach number;
- at very high rotor speeds, the inlet channel is choked; the compressor mass flow is independent of the rotor speed.

Further experimental investigations are necessary to confirm the validity of the assumptions made.

- - - - -

REFERENCES

[1] G.K. SEROVY

Recent progress in aerodynamic design of axial flow compressors in the United States.

Trans ASME Journal of Engineering for Power, July 1966

[2] A.WEISE

Überschallaxialverdichter.

Lilienthal Gesellschaft Bericht 171, 1943

[3] J.R. ERWIN & A. FERRI

The Supersonic Compressor.

In W.R. HAWTHORNE - Aerodynamics of Turbines and Compressors - High Speed Aerodynamics and Jet Propulsion, vol X, Princeton University press,1964

[4] J. CALMON

Le fonctionnement des grilles de compression dans le domaine transsonique.

L'Aéronautique et l'Astronautique, vol. 17, n° 1, 1970

[5] A. BUSEMANN

Atti del V Convegno Volta

Accad. Nagl Lincei - Roma, 1935

[6] J. FABRI, J. PAULON, G. JANSSENS

Use of supersonic cascades made of blades of simple geometric shapes for cascade wind tunnel performance evaluation.

ASME - Bruxelles meeting 1970

[7] J. CHAUVIN, F. BREUGELMANS & A. JANIGRO

Supersonic Compressors.

Von Kármán Institute for Fluid Mechanics, CR 7, 1967

[8] J. FABRI, R. SIESTRUNCK

La limitation du débit dans les compresseurs supersoniques

Entropie n° 11, Sept-Oct. 1966

[9] M.H. VAVRA

Aerothermodynamics and flow in turbomachines.

John Wiley & sons, New-York, 1960

[10] B. ECKERT

Axial und Radialkomspressoren.

Springer Verlag, Berlin 1953

[11] Y. LE BOT, J. PAULON, P. BELAYGUE

Theoretical and experimental determination of pressure losses in a single stage axial flow compressor.

ASME Bruxelles meeting 1970

[12] Th.J. GOLDBERG, E. BOXER & P.T. BERNOT

Experimental investigation of an axial flow Supersonic Compressor having rounded leading edge blades wich an 8-percent mean thickness - chord ratio.

NACA RM L 53 G 16,1953

[13] Th.J.GOLDBERG

Experimental investigation of an axial flow supersonic compressor having sharp leading edge blades with an 8-percent thickness - chord ratio.

NACA RM L 54 K 16, 1955

[14] Th.J. GOLDBERG & J.R.STERRET

Use of shadow-graph technique in the analysis of the performance of two supersonic axial flow compressor rotors operating over a mean radius relative inlet Mach number range of 0.85 to 1.7

NACA RM L 56 A05, 1958

SYMBOLS

a_o velocity of sound, upstream stagnation conditions
A blade leading edge
B origin of the Mach line attaining the leading edge of adjacent blade
c blade chord
C blade trailing edge
C_p constant pressure specific heat
dm mass flow between cylindrical surfaces of radius r and r + dr
$d\mathring{m}$ critical mass flow between cylindrical surfaces of radius r and r + dr
dr height of compressor between cylindrical surfaces of radius r and r + dr
M_B Mach number at point B
M_W Mach number corresponding to velocity in rotor coordinates
M'_W Mach number corresponding to M_W after a normal shock wave
M_x axial Mach number at rotor inlet
$\overline{M}_x$ mean Mach number of the incoming absolute flow
n number of rotor blades
p pressure at rotor inlet
p_1 pressure in section (1) of the blade channel
P_o stagnation pressure of the incoming flow
P_W stagnation pressure of flow in rotor coordinates
s throat section of blade channel
t blade spacing
T gas temperature at rotor inlet
T_o stagnation temperature of incoming flow
T_1 gas temperature in section (1) of the blade channel
U rotor velocity
V_x axial velocity at rotor inlet
$\overline{V}_x$ mean axial velocity at rotor inlet
W velocity in rotor coordinates
W_B velocity at point B , rotor coordinates
W_1 velocity in section (1) of the blade channel ,rotor coordinates
x abscissa measured along axial direction
X abscissa measured along blade chord AC
y ordinate measured along rotor inlet
Y ordinate measured along axis Ay normal to chord AC

α blade leading edge angle
β angle of velocity W (rotor coordinates) with axial direction
β_o angle of blade reference direction with axial direction
β_B angle of tangent to blade upper surface at point B with axial direction
β_1 angle of velocity at section (1) with axial direction
γ isentropic constant
ξ angle of tangent to blade upper surface with the chord blade
ΔP_W stagnation pressure loss (rotor coordinates)
ρ density at rotor inlet
$\overline{\rho}$ mean density at rotor inlet
ρ_B density at point B
ρ_o density of incoming flow in stagnation conditions
ω rotor angular speed
Ω Mach angle

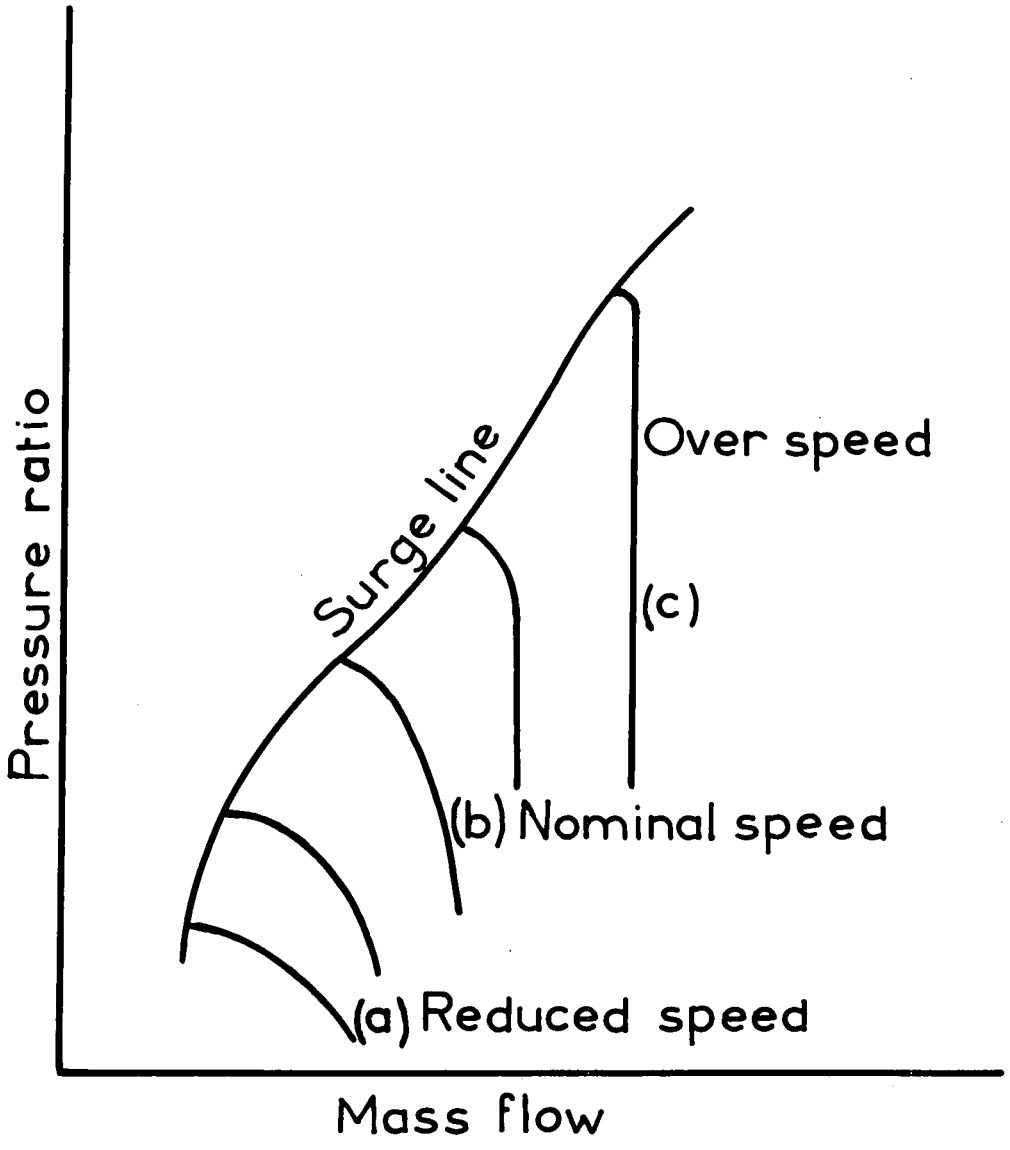

Fig. 1 Characteristics of a conventional axial compressor

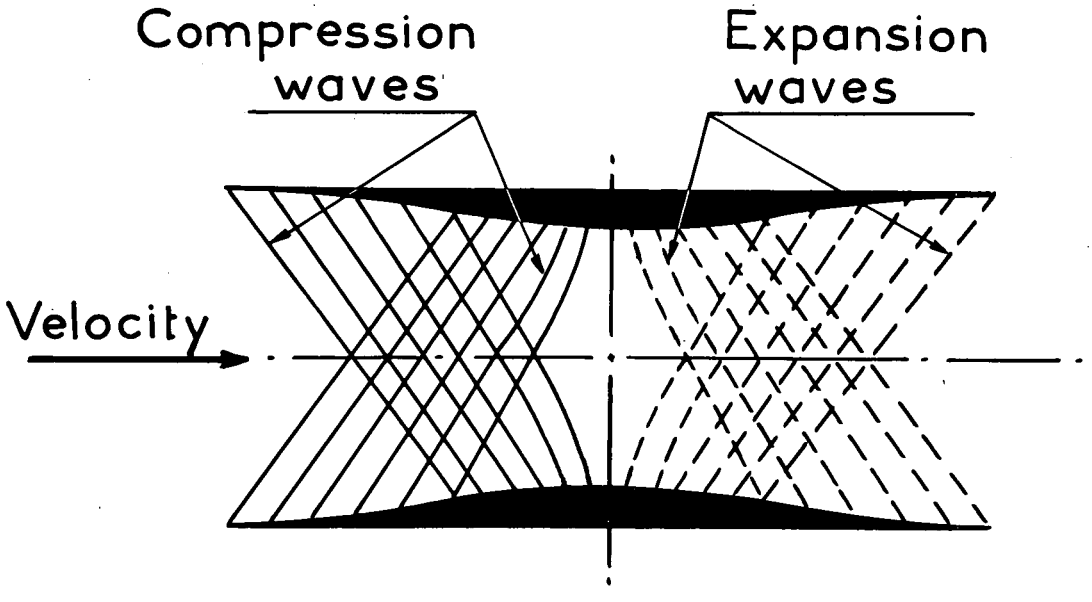

Fig. 2 Busemann biplane (Ref. 5)

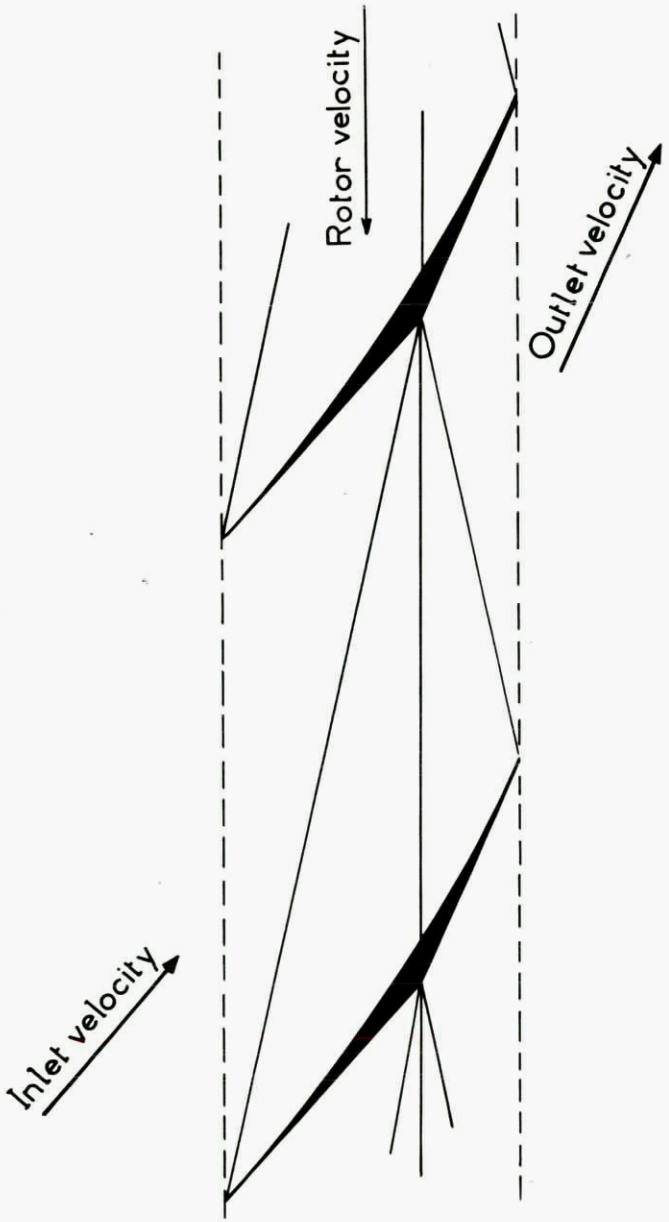

Fig. 3 Low drag supersonic blading (Ref. 2)

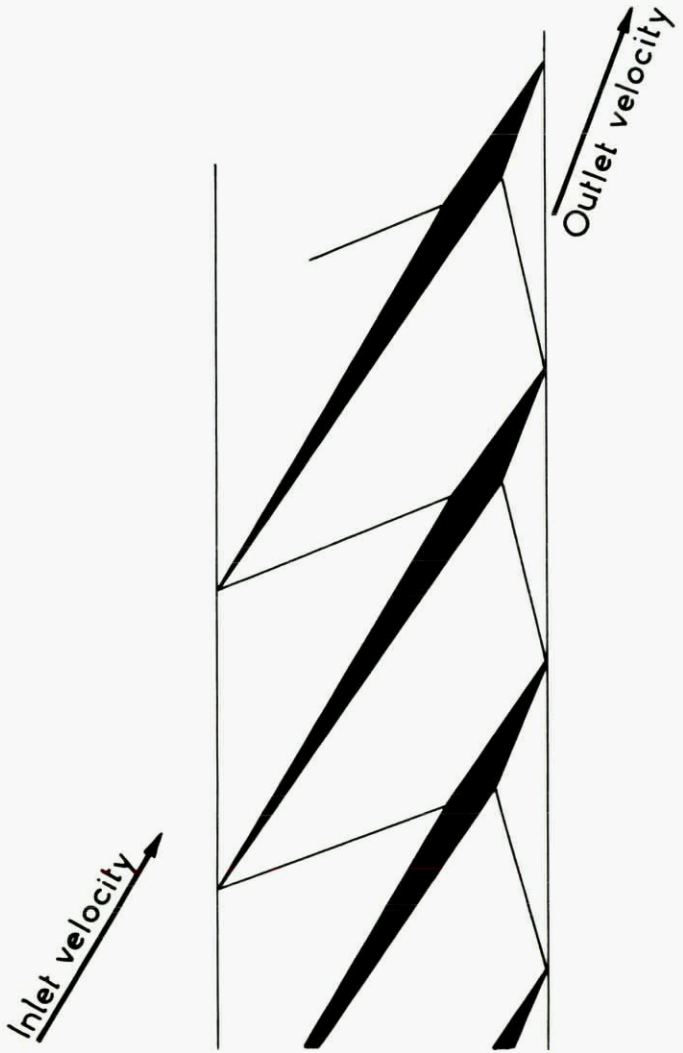

Fig. 4 Low drag blading with inlet velocity parallel to blade upper surface

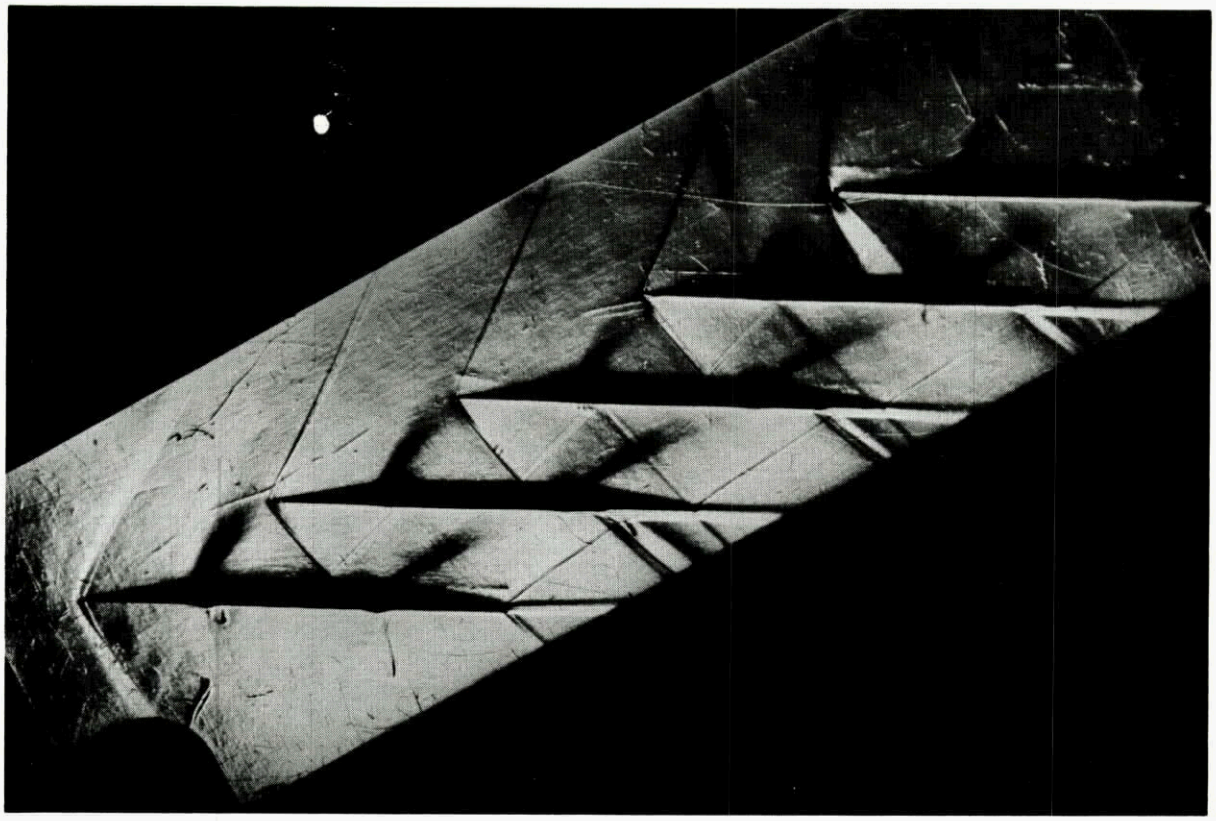

Supersonic regime

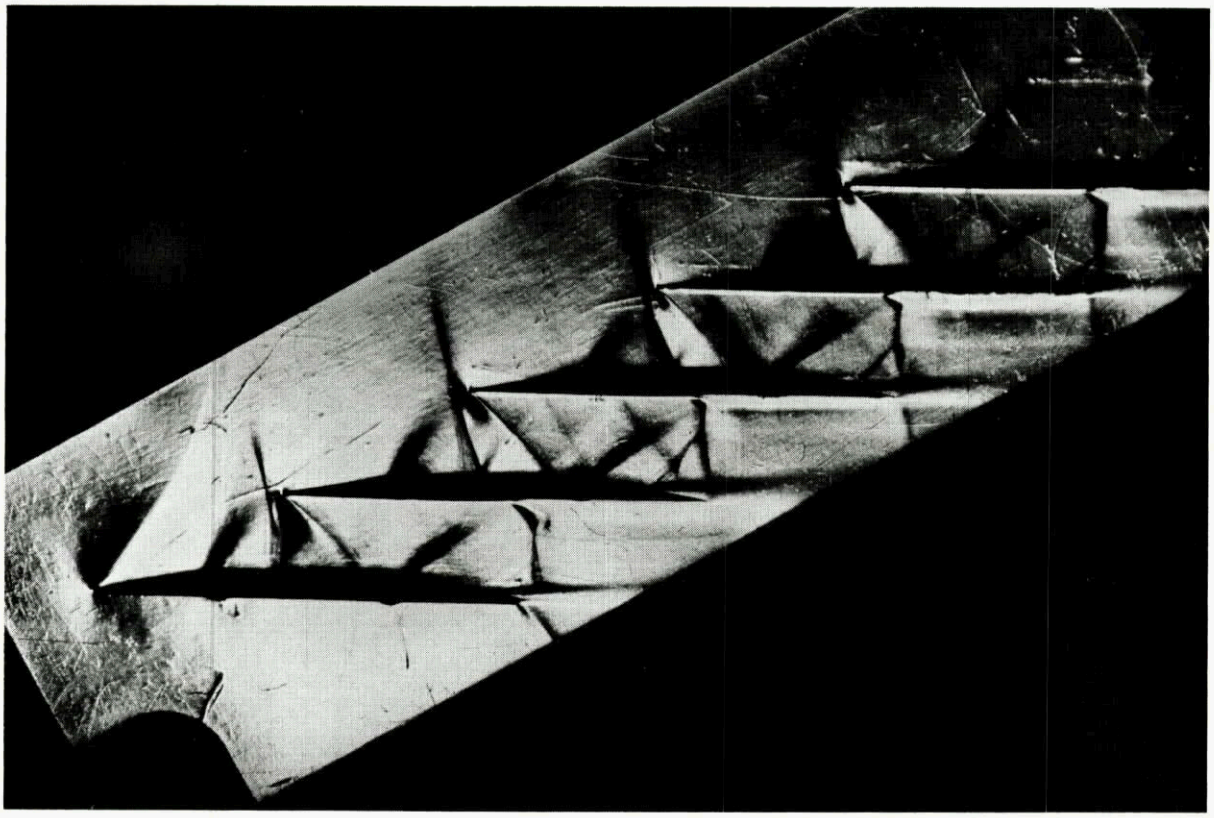

Choked regime

Fig. 5 Wind tunnel testing of supersonic compressor cascade

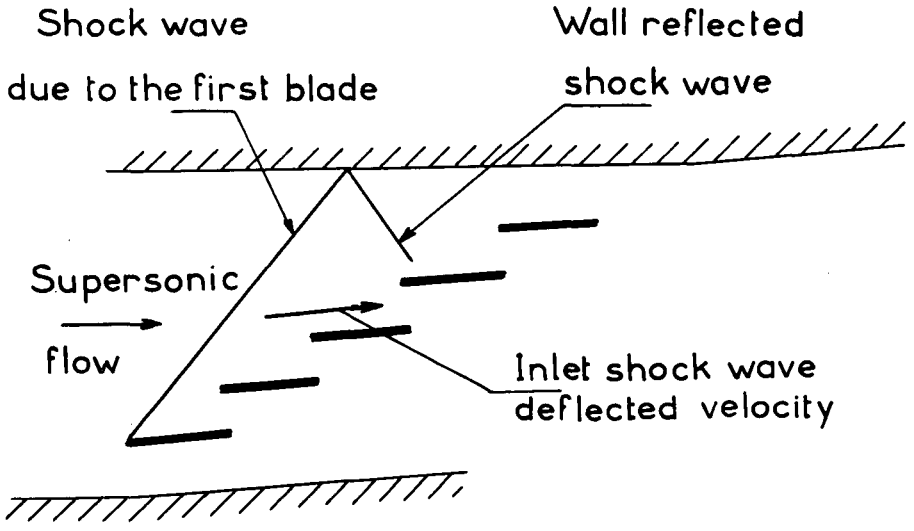

Fig. 6 Wind tunnel testing of a cascade of straight blades

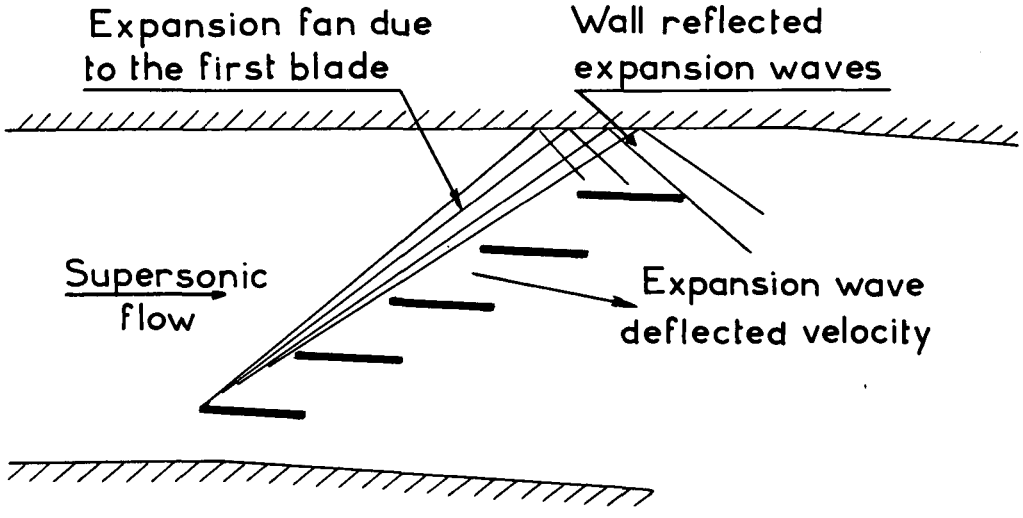

Fig. 7 Wind tunnel testing of a cascade of straight blades with flow expansion

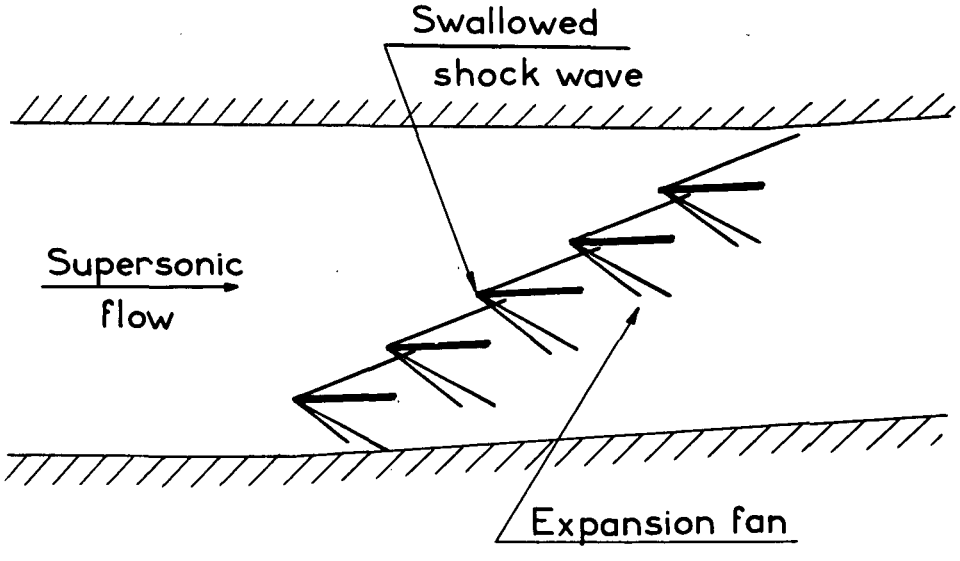

Fig. 8 Wind tunnel testing of a cascade of straight blades at high Mach number

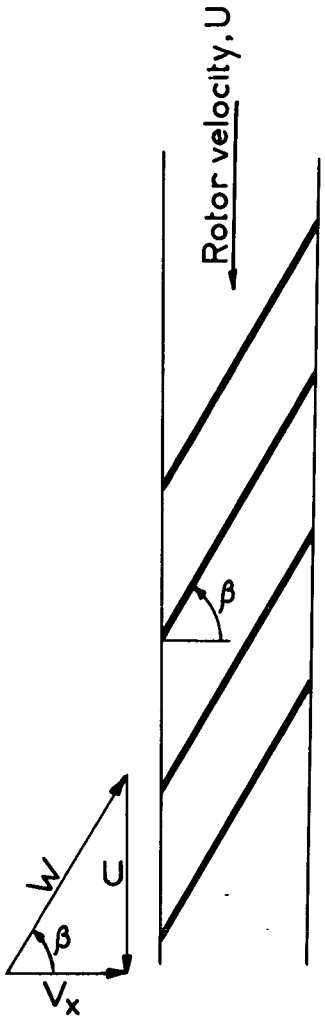

Fig. 9 Supersonic rotor with straight blades

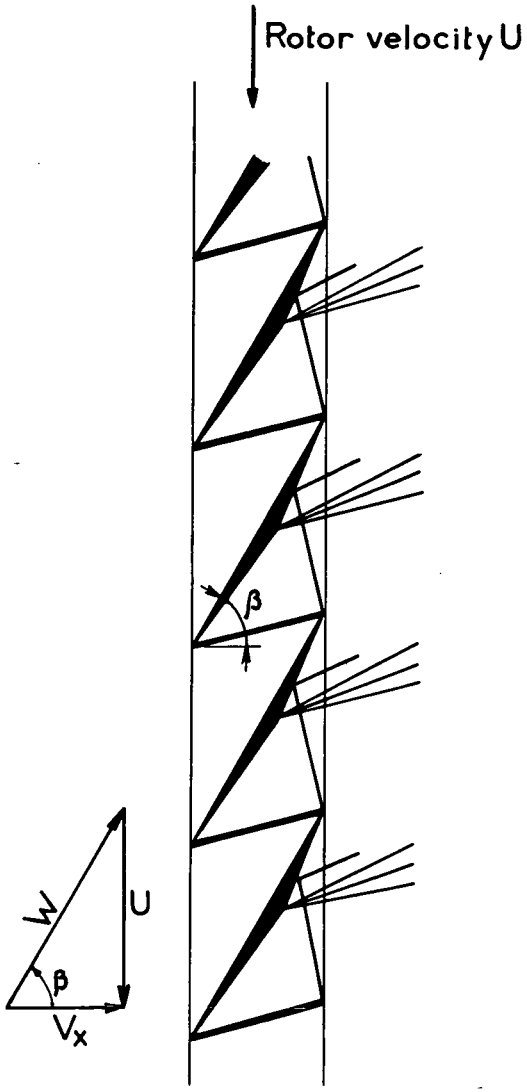

Fig. 10 Supersonic blading with flat upper surfaces

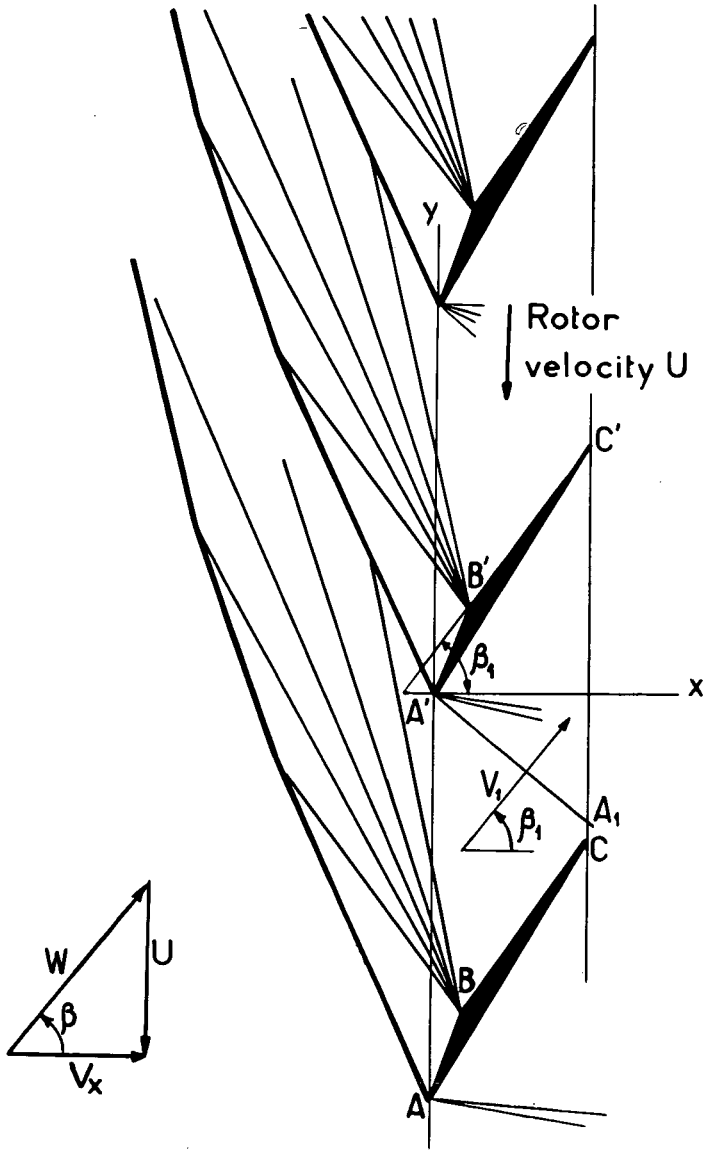

Fig. 11 Shock pattern with uniform flow at cascade inlet

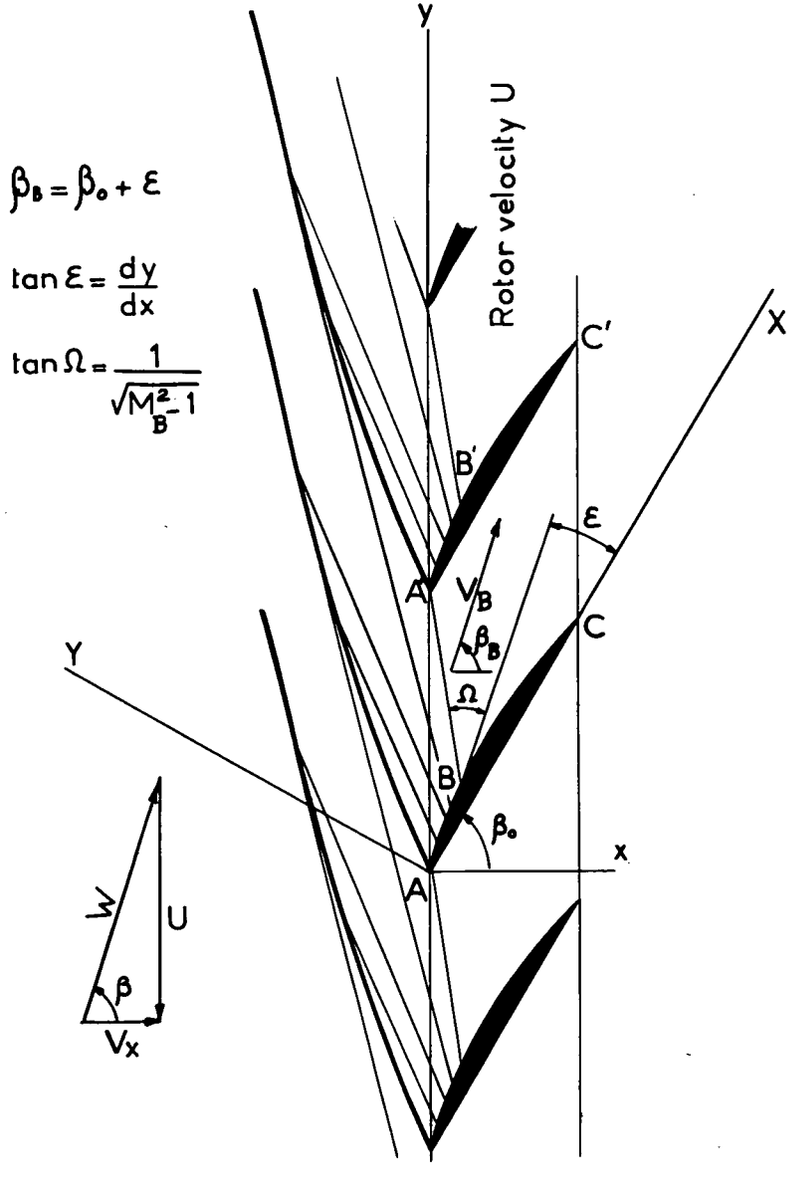

Fig. 12 Cascade with leading edge in the expansion fan

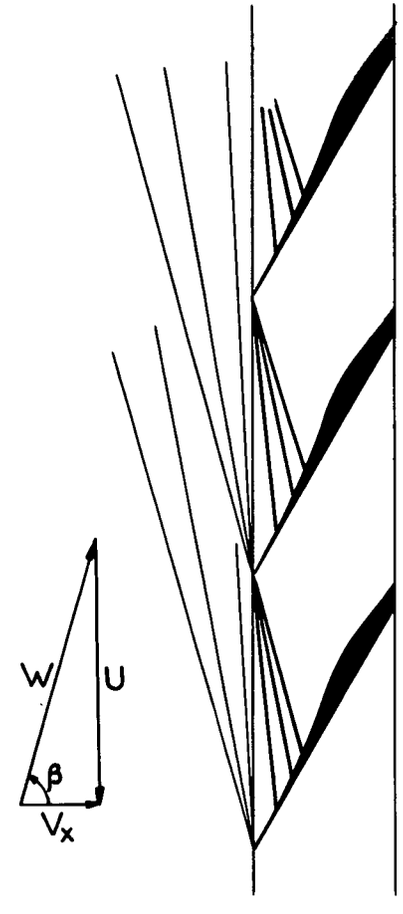

Fig. 13 Blunt trailing edge blades with concave upper surface

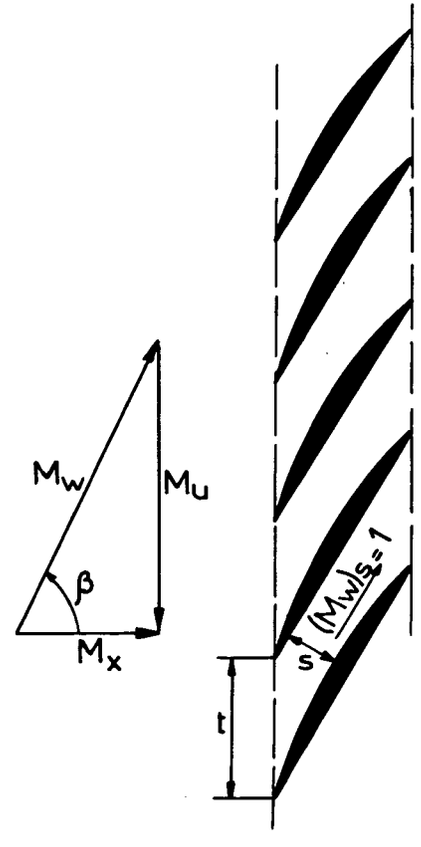

Fig. 14 Choked isentropic flow

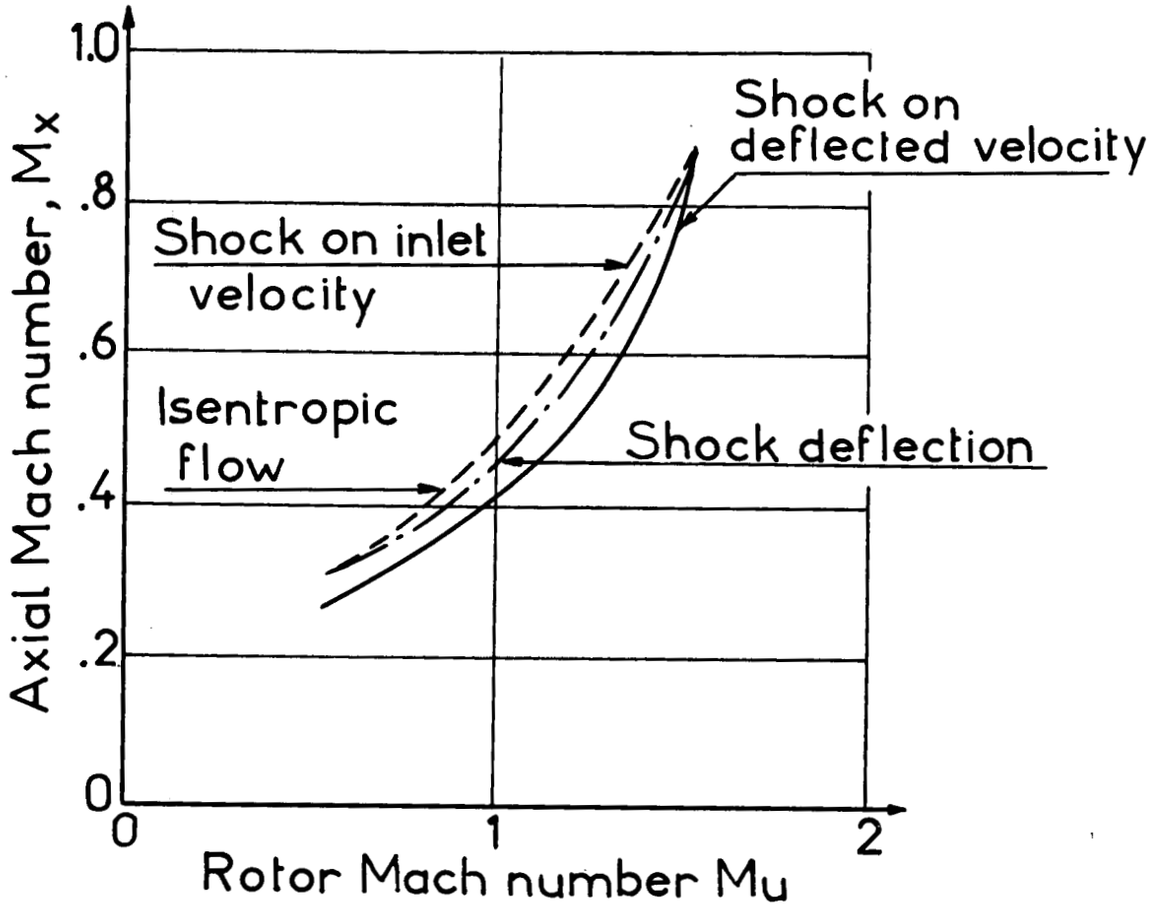

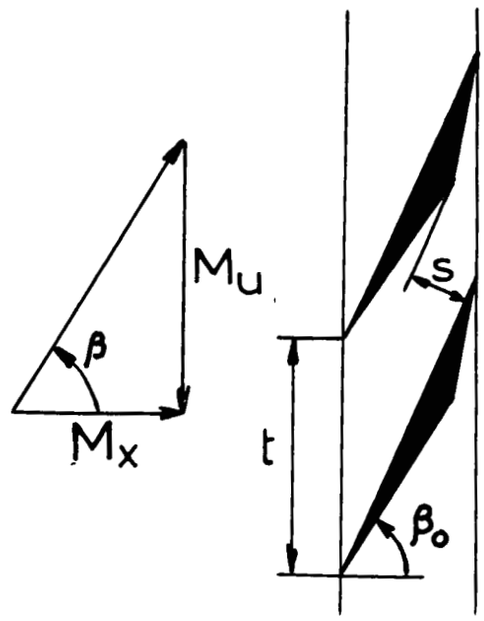

Fig. 17(b) Comparison of axial Mach numbers corresponding to the various flow patterns

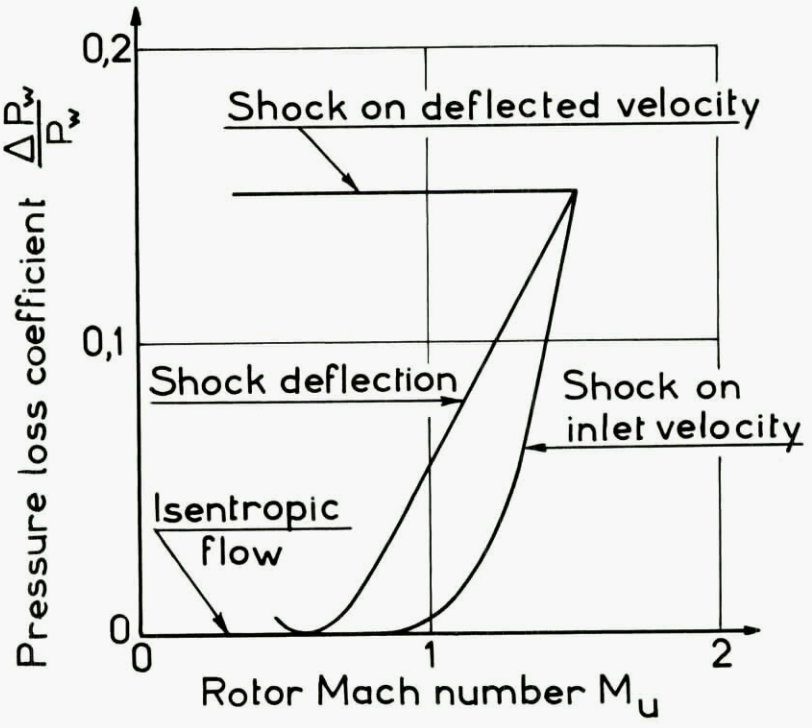

Fig. 18 Comparison of pressure losses corresponding to the various flow patterns

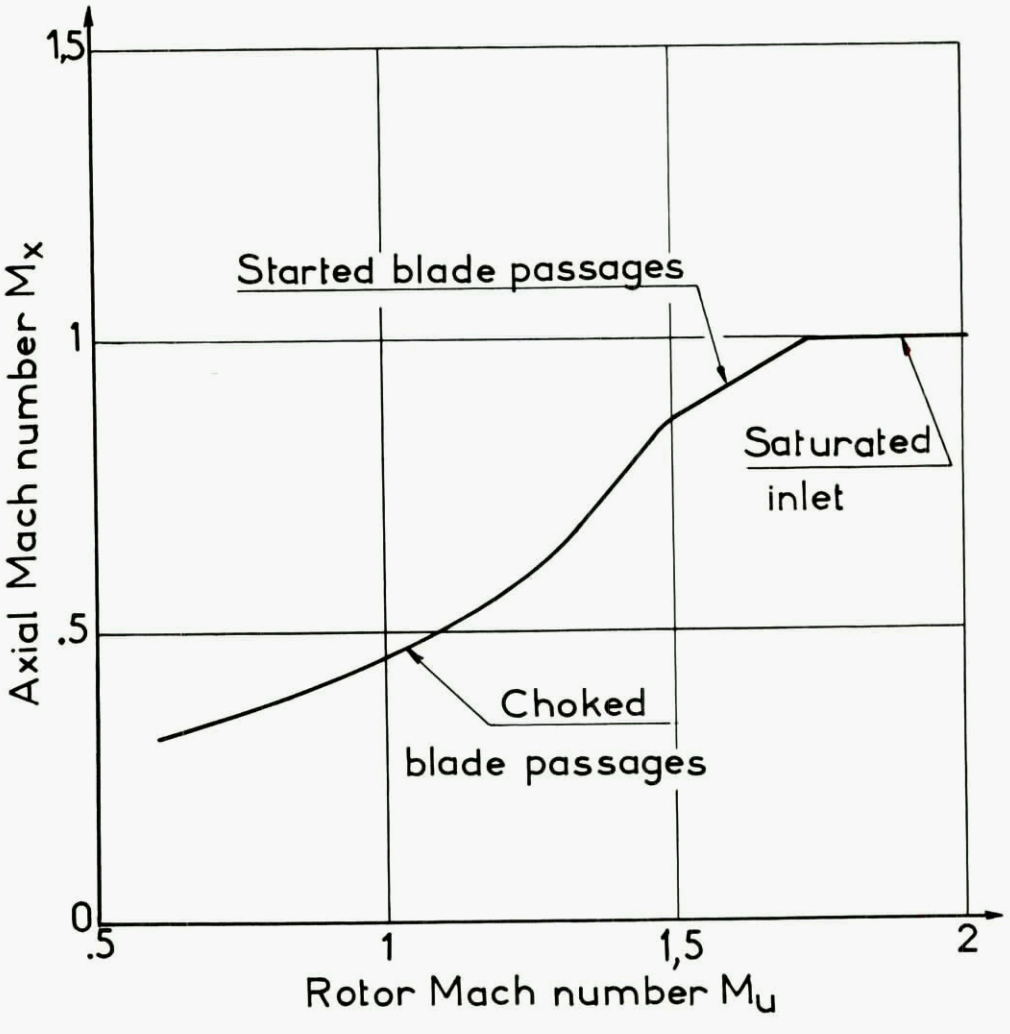

Fig. 19 Mass flow limitation in a supersonic compressor

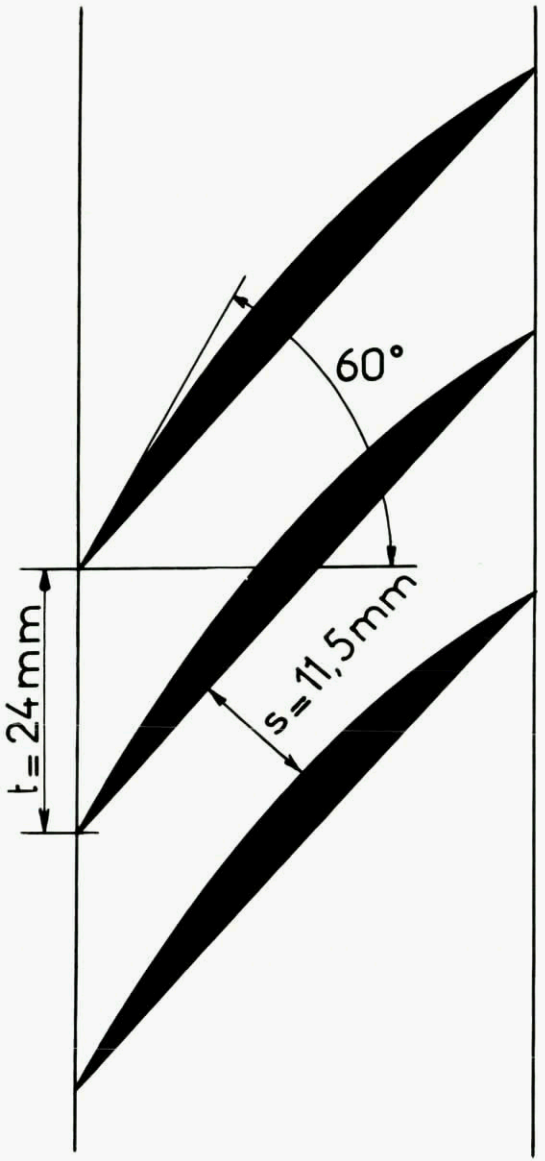

Fig. 20 Mean section blading of NACA supersonic compressor for flow visualization

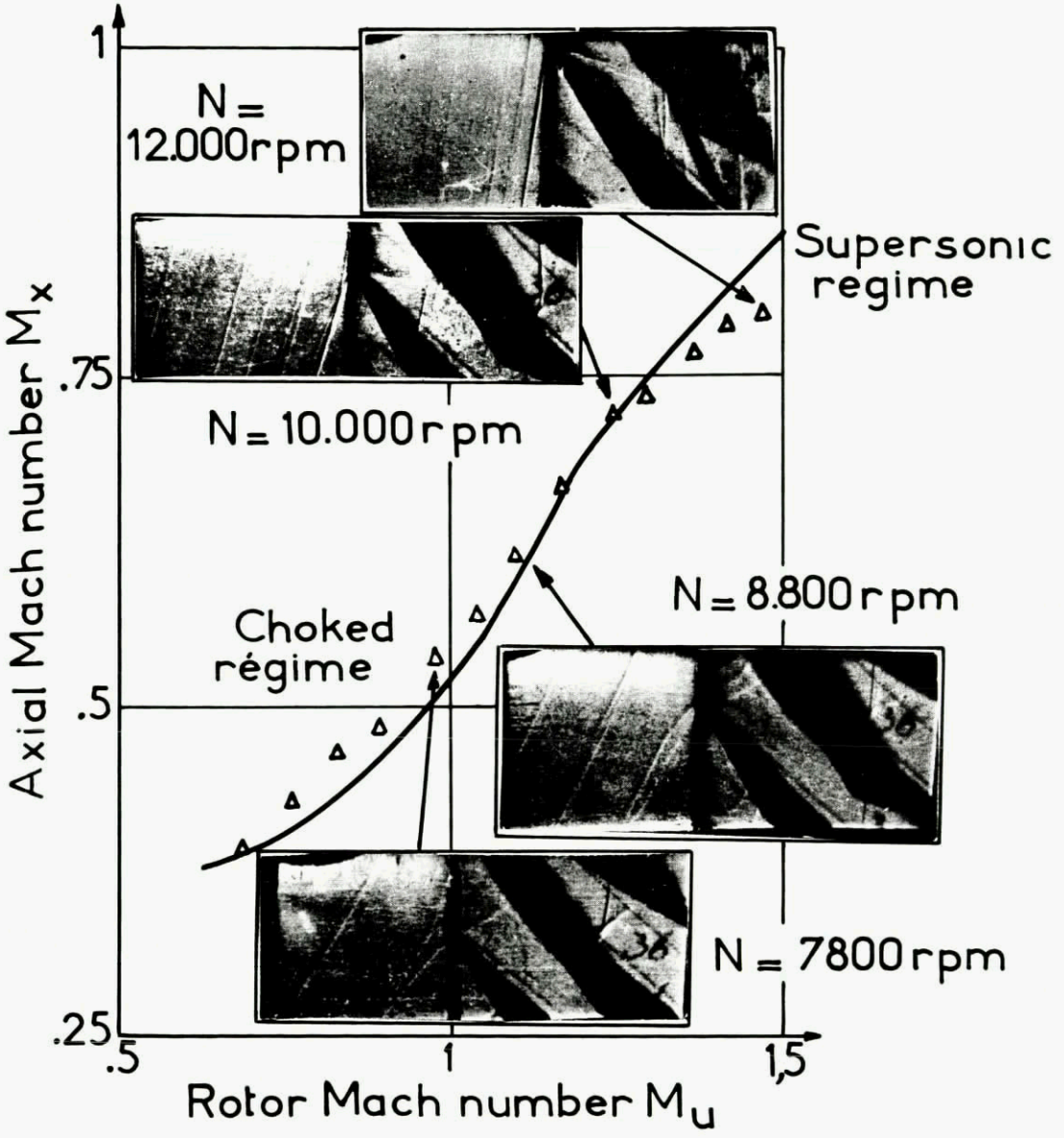

Fig. 21 Comparison of theoretical and experimental axial vs rotor Mach numbers in NACA supersonic compressor (Ref. 12)

T R A N S O N I C C O M P R E S S O R C A S C A D E S

H. GRIEPENTROG †

Gutehoffnungshütte Sterkrade A.G.

† formerly Project Engineer, von Karman Institute, Rhode Saint Genese, Belgium

S U M M A R Y

Bladings with inlet and outlet subsonic flows, but presenting a local supersonic region are used in all of the advanced axial compressors today. Prediction of their performance and performance optimisation are therefore a must.

The general features of the compressible flow effects in cascade are discussed, together with the influence of compressibility on the performance of compressor cascade. The notions of critical and choking Mach number are introduced, together with a physical description of the flow in the blade passage, where four distinct regions can be distinguished (subsonic inlet and outlet flow field, supersonic flow field, sonic line region and shock-boundary layer interaction region).

The evaluation of the critical and choking Mach number is then treated, as well as the effects of compressibility on losses, turning and static pressure rise. Some remarks are made on the design of transonic cascades.

The four regions of flow detailed above are then dealt with independently. A review is made of the existing theories and experimental correlations, and their limit of application for cascade flows is defined. A semi-empirical model, valid for cascade flows, is presented for the shock-boundary layer interaction region.

A particular method of calculation, developed by the author at VKI, and based on the analysis of the flow regions is then presented. This method starts from the incompressible flow field, in a blading, obtained theoretically or experimentally, and enables to calculate the compressible flow field, with a local supersonic region, taking fully into account the shock-interaction region. The validity of the method is limited to high solidity cascades, of any deflection. Comparison with experimental results shows the method to be satisfactory.

a	speed of sound
A	area
b	streamtube width
c	blade chord
c_p	static pressure rise coefficient $\frac{p_2-p_1}{p_{01}-p_1}$
g	pitch
h	blade height
H_{32}	form factor
i	incidence angle with respect to camber line
M	Mach number
p	static pressure
p_0	total pressure
r	recovery factor
s	distance
s_{th}	throat of blading
t	thickness
u,v	velocity components in x,y direction
w	relative velocity
x,y	cartesian coordinates
α	absolute flow angle
β	relative flow angle
γ	ratio of specific heat or stagger angle
δ_2	momentum loss thickness of boundary layer
Δ	"del" operator
θ	hodograph coordinate
θ	air turning angle $\beta_1-\beta_2$
ρ	mass density
σ	solidity
ϕ	camber angle
Φ	potential
ψ	stream function
ξ,η,ζ	coordinates for sink-source distribution
ω	total pressure loss coefficient $\frac{p_{01}-p_{02}}{p_{01}-p_1}$

Subscripts

o	total conditions
1	upstream of cascade
2	downstream of cascade
∞	free stream conditions
c	compressible
CH	choking conditions
CR	critical conditions
i	incompressible
ℓ	local
MAX	maximum value
MIN	minimum value
PS	pressure side
SS	suction side

Superscripts

$\hat{}$	conditions downstream of shock
*	sonic conditions
'	perturbation value

LIST OF FIGURES

TRANSONIC COMPRESSOR CASCADES

H. Griepentrog

1. INTRODUCTION

The appearance of high duty materials for the axial compressor construction allows the design of machines with high rotational speeds, resulting also in high velocities relative to the bladings. Following the classical law of Euler, an increase of the circumferential speed raises also the energy input per stage, leading to smaller and more compact machines.

The extreme of this design trend is the supersonic axial compressor with either subsonic or supersonic axial velocities. But due to the unfavorable operating characteristics (no off design operation possibility for the first type), this extreme can only be used very seldom for a practical application. The designer will be forced to use the flow field with subsonic inlet and outlet Mach numbers and local supersonic regions inside of the cascade to combine high energy input into the fluid and a wide marge of operation for the compressor. A cascade working in this particular flow field is called 'transonic cascade'.

We find also this transonic flow field in the supersonic axial compressor of the shock-in-rotor type - the supersonic compressor type giving, up to now, the best results - for the stator blading, which has to accept inlet Mach numbers of the order of $M_1 = 0.80 \div 0.90$.

The aim of this note is the description of the physical flow behaviour in transonic cascades. A discussion will be included on the theoretical methods available for the prediction of the local velocity distribution on the blade surface.

2. COMPRESSOR CASCADE IN COMPRESSIBLE FLOW FIELD

In this chapter some general features of compressible flow effects in cascade are discussed together with the influence of the compressibility on the performance of compressor cascades.

An increase of the inlet velocity of a cascade in the incompressible flow field results in a similar increase of the local velocities on the blade surface following Eulers equation. If the inlet velocity is raised to higher values exceeding the incompressible flow range, the local overvelocities on the blade contour are increased more than proportional to Eulers equation while the local undervelocities increase less than proportional. This behavior results from the satisfying of the continuity equation $\rho_\ell \cdot v_\ell = \text{const.}$

The inlet Mach number determining the limit between the incompressible flow range where a change of ρ can be neglected and the compressible flow range is a function of every particular cascade. Principally, this limit Mach number depends particularly on the shape of the leading edge, on the curvature of the suction side and the incidence flow angle.

A further increase of the inlet velocity will lead to a characteristic limit value of the cascade, defined as the critical Mach number M_{CR}, where sonic velocity exists at one point on the blade contour. With a continuing raise of the inlet Mach number supersonic regions will be forced, embedded in the subsonic flow field thru the cascade. These supersonic flow pockets will grow with an increase of inlet Mach number and finally merge into a flow region extending from the suction side to the pressure side of the two neighbouring blades forming a passage. This region is limited to the upstream subsonic flow field by the sonic line, which is positioned at the effective throat of the blade passage. The smallest inlet Mach number causing a sonic line in the cascade is called the choking Mach number, M_{CH}, of the cascade determining also the maximum mass flow which can pass the cascade, for given pressure and density of the inlet flow field.

The supersonic region or pockets are closed downstream by a quasi-normal shock. This general statement can be made here regarding the purpose of this note although theoretically the problem is not yet solved for potential flows whether a non-isentropic (with shocks) diffusion from supersonic to subsonic flow is possible or necessary or not. Considering also this viscous effects on the blade surface, a shock will probably always perform the diffusion. For the case of $M_1 \geq M_{CH}$ the shock spans the whole blade passage which will give some interesting applications.

In figure 1 the above described process is sketched schematically. This sketch is illustrated with Schlieren pictures of a rather conventional NACA 65(11.3 A2I8b)09 blading for a slightly negative incidence angle. For a Mach number of $M_1 = .736$ local supersonic pockets are indicated on the suction side near the trailing edge and more pronounced at the leading edge on the pressure side. An increase of the inlet velocity to $M_1 = .767$ shows the point where the supersonic pockets are close to merge. This condition is obtained at $M_1 = .824 \geq M_{CH}$. A small non periodicity in the three passages shown in fig. 2c

indicates an influence of the inlet stream field of the two upper cascades by the local supersonic flow field formed on the suction side of the lowest blade.

Figure 3 shows the measurements of local static pressure on the surface of a high deflection blade extremely well suited for the use in the transonic flow region. The local static pressure ratio p_2/p_{01} is plotted in function of the nondimensionalized chord distance x/c. The parameter of the set of curves is the inlet Mach number. Local sonic velocities are reached first at an inlet Mach number between $M_1 = .70$ and $M_1 = .80$.

For the coordinate position x/c = .35 on the suction side of the blade, the local M number (calculated with the data of fig. 3) is presented in function of the inlet Mach number M_1 in fig. 4. This plot indicates the linear variation of the local Mach number with the inlet Mach number in the flow range not influenced by compressibility effects. The 'incompressible' flow range extends up to $M_1 \leq .525$ which is an extremely high value. For Mach numbers $M_1 > .525$ the local Mach number grows over linearly $(\frac{x}{c} < (\frac{x}{c})_{crest})$.

From these rather general considerations of compressible flows in cascade it can be deduced that two limit inlet Mach numbers will determine the behavior of a cascade in transonic flows:

a) the critical Mach number indicating that a small rise of the inlet velocity will create shocks on the blade surface;
b) the choking Mach number indicating the maximum mass flow.

Furthermore, for the calculation of the flow field in the blade passage four regions have to be considered:

a) subsonic inlet and outlet flow field ($M < 1$);
b) supersonic flow field ($M > 1$);
c) sonic line ($M = 1$);
d) shock-boundary layer interaction.

Following this partition, the prediction methods will be discussed.

Formulae for a rough estimation of the critical and the choking Mach number are presented in the following. The knowledge of these values is of extreme necessity for the first choice of a suitable transonic compressor cascade.

2.1 Critical Mach number

The critical Mach number for the inlet flow field is obtained, if at one position of the blade contour the velocity is sonic. This position is also the point for the minimum local static pressure rise coefficient $c_{p_{MIN}}$. Hence, using the classical gas dynamic relations, the critical inlet Mach number in function of $c_{p_{MIN}}$ is:

$$M_{CR} = \sqrt{\frac{2}{\gamma-1}\left[\left(\frac{1 - c_{p_{MIN}}}{\left(\frac{2}{\gamma+1}\right)^{\frac{\gamma}{\gamma-1}} - c_{p_{MIN}}}\right)^{\frac{\gamma-1}{\gamma}} - 1\right]} \qquad (1)$$

with $c_{p_{MIN}} = \frac{p_{MIN}-p_1}{p_{01}-p_1}$ and $p_{MIN} = p^*$.

The equation (1) can be used directly for the determination of M_{1CR} with the help of incompressible flow results. For this application it has to be supposed that the compressibility effects will not change the position of the minimum static pressure. The relation (1) is plotted in fig. 5 and can be used for a first estimation of the critical Mach number of a cascade.

Scholz (ref. 1) proposed two limit values for the estimation of the critical Mach number with incompressible data. A maximum limit value of the critical Mach number will be obtained with the assumption that the velocity ratio w_2/w_1 is not influenced by compressibility effects. Hence, the peak velocity on the blade surface will be sonic for an inlet Mach number higher than in reality and it can be written

$$\frac{a^*}{w_{1CR}} = \left(\frac{w_{2MAX}}{w_1}\right)_i \qquad (2)$$

and resulting

$$M_{1CR} < \sqrt{\frac{1}{1 - \frac{\gamma+1}{2} c_{p_{MIN_i}}}} \qquad (2a)$$

or

$$M^*_{1CR} < \sqrt{\frac{1}{1 - c_{p_{MIN_i}}}} \qquad (2b)$$

The limit value indicating the critical Mach number smaller than in reality is obtained with the assumption that the streamline form will not change in incompressible flows. Hence,

$$\frac{\rho_1 \cdot a_1}{\rho^* \cdot a^*} > \left(\frac{w_1}{w_{2MAX}}\right)_i = \frac{1}{\sqrt{1-c_{p_{MIN_i}}}}$$

and

$$M^*_{1CR}\left(1-\frac{1}{\gamma+1} M^{*2}_{1CR}\right)^{\frac{1}{\gamma-1}} > \left(\frac{2}{\gamma-1}\right)^{\frac{1}{\gamma-1}} \frac{1}{\sqrt{1-c_{p_{MIN_i}}}} \qquad (3)$$

This is an implicit relation for M^*_1. Scholz (ref. 1) gives an approximate solution :

$$M^*_{1CR} > \approx \frac{2}{\pi} \sin\left(\sqrt{\frac{1}{1-c_{p_{MIN_i}}}}\right) \qquad (3a)$$

The relations (2b) and (3a) are plotted in fig. 6. Cascades with higher solidities will be closer to equation (3a), while cascades with small solidities will be better represented by relation (2b), supposing that for both cases the same blading is used.

These equations can only give a first estimation of the critical Mach number. A more sound result can only be obtained with one of the procedures of prediction of local velocity distribution, presented in chapters 4 and 5.

2.2 Choking Mach number

The choking Mach number determines, together with the throat length of the cascade, the maximum mass flow rate which can pass the cascade. Using the one dimensional continuity equation, the choking Mach number can be predicted by

$$\frac{s_{th}}{g\cos\beta_1} = \frac{\rho_1 \cdot w_1}{\rho^* \cdot a^*} \qquad (4)$$

and

$$M_{1CH} \simeq \sqrt{1-\sqrt{1-\frac{s_{th}}{g\cos\beta_1}}} \qquad (4a)$$

In figure 7 the function (4a) is shown. This figure indicates that the cascade in real flow will always be choked for inlet Mach numbers smaller than indicated by the isentropic equation (4a) due to viscous flow effects and local supersonic regions at the profile leading edge with downstream shocks changing the potential flow into a nonisentropic type.

2.3 Total pressure loss

The compressibility effects on the total pressure loss is mainly due to the shock-boundary layer interaction for $M_1 > M_{1CR}$. In addition, the local pressure gradients on the blade surface increase with the inlet Mach number (see fig. 3) which results in a higher loading of the boundary layer coupled with increased total pressure loss.

A compensating effect exists due to the favorable influence of compressibility on the momentum loss thickness of the boundary layer. Taking the relation given by Rotta (ref. 2), the ratio of the incompressible and compressible momentum loss thickness for turbulent boundary layers is:

$$\frac{\delta_{2_i}}{\delta_{2_c}} = 1 + r\left(\frac{\gamma-1}{2}\right) M^2_\infty \cdot H_{32}(2-H_{32})(1-.043M_\infty) \qquad (5)$$

Hence, the total pressure loss will be independent of the inlet Mach number from the optimum point of operation, up to the critical inlet Mach number. This statement is verified with the measurements on a double circular arc blading with the parameters

camber angle	$\phi = 11.2°$
maximum thickness	$(t/c)_{max} = 6\%$
pitch/chord ratio	$s/c = .924$
stagger angle	$\gamma = 45°$

presented in ref. 3. The total pressure loss coefficient is plotted in function of the incidence angle in fig. 8 for this blading.

Up to an inlet Mach number of $M_1 = .78$, there is practically no change in total pressure loss coefficient between $i = 1°$ and $i = 5°$ like it could be expected from the foregoing qualitative discussion. For incidence angles smaller or larger than these limits,

the total pressure loss increases considerably due to local supersonic regions on the suction side for positive incidence angle and on the pressure side for negative incidence angles with shock-boundary layer interaction losses. A further increase of the inlet Mach number to $M_1 = .90$ will diminish further the operation range, while for $i = 5°$ there is no change in the total pressure loss value .For Mach numbers $M_1 > M_{1CR}$ also at the optimum point a sharp increase of total pressure loss occurs.

It can be stated that the influence of the compressibility on the performance of the cascade manifests itself mainly by a reduction of the operating range with a shift of the optimum incidence angle to higher values.

The operating range of a cascade will reduce with an increase of M_1. For the extreme $M_1 \geq 1$, the cascade will operate at one incidence angle only which is a unique function of the inlet Mach number of the particular cascade.

2.4 Turning angle

The effective turning angle of a cascade is very closely related to the boundary layer behavior on the blade. Hence, the general trend valid for the compressibility influence on the total pressure loss is also valid for the turning angle. In figure 9 the turning angle in function of the incidence angle is shown for the cascade discussed above. Up to $M_1 = .78$ the effective turning is practically not altered. A drop in turning angle occurs for $M_1 > M_{1CR}$ due to the shock induced separated boundary layer.

2.5 Static pressure rise

The static pressure rise in a cascade is determined by the turning angle and the total pressure loss. In fig. 10 the development of these three parameters is presented in function of the inlet Mach number for an incidence angle $i = 5°$. The static pressure rise coefficient drops only slightly for $M_1 > M_{1CR}$. This effect is more pronounced for measurements shown in fig. 11 on a cascade with NACA 65 blades (ref. 4).

2.6 Some remarks on the design of transonic cascades

The adaptability of a compressor cascade for its use in the high subsonic flow field is determined by the critical Mach number M_{1CR} and the choking Mach number M_{1CH}, which should attain the highest value possible. Both characteristic Mach numbers are unique functions of the cascade configuration, i.e., the blade shape, the stagger angle and the solidity. These cascade parameters influence also the boundary layer conditions on the blade surface and end walls, which determine the effective flow section in the cascade.

The critical Mach number is characterized by a significant increase in total pressure loss due to shock boundary layer interaction effects. The magnitude of the interaction depends primarily on the local Mach number ahead of the shock. The value of this Mach number is a function of the blade contour curvature upstream of the shock. A minimization of this convex curvature results also in a decrease of the shock boundary layer interaction loss or in a higher critical Mach number of the cascade. This philosophy has been applied by NASA (ref. 5) in the development of the Multiple Circular Arc blade. For this blading the suction side is constructed of two circles, reparting the total curvature into a small curvature for the forward blade part and a high curvature for the back part of the blade. The pressure side consists of a constant curvature contour. The choice of the repartition has to be performed in such a way to get an optimum of overall profile losses - low shock boundary layer interaction losses in the front part and no separation in the subsonic back part of the blade. The gain in total pressure loss due to small interaction losses can easily be offset by high separation losses. Obviously, a cascade with a high critical Mach number has also a high choking Mach number.

The exact determination of the choking Mach number is of particular importance for the design of a blade row for a given mass flow. A maladjustment of the stator to the mass flow required can force the rotor to stall. For the case of a supersonic compressor of the shock-in-rotor type, this danger is extremely pronounced, because the supersonic rotor has practically no marge in mass flow, indeed.

The typical flow conditions, a stator for a supersonic compressor has to accept, are an inlet Mach number in the range of $M_1 = .80$ and a required turning of the order $\theta = 60°$. These values are valid for the shock-in-rotor type and subsonic stator configuration.

In fig. 12 an example for a blading suitable for these extreme conditions is shown (This blading has been designed and tested at the von Karman Institute in the development program of a supersonic axial compressor - ref. 6). The geometrical throat is placed near the leading edge followed by a continuous divergent channel. The resulting blade consists of a straight entrance section followed by a constant curvature contour. The trailing edge is blunted. In fig. 7 the critical Mach number for this blading is compared with classical ones. An unusual high limit Mach number is obtained for this blading, due to the application of the design criteria mentioned above by forming the entrance section with a straight part (low local Mach number) and placing the throat close to the inlet section (high choking Mach number). The theoretical choking Mach number $M_{1CH} = 1$ for this design has not been achieved due to a small displacement of the geometrical throat down-

stream from the leading edge plane. Also the correct estimation of the boundary layer thickness diminishing the effective flow section plays an important role in the region $M_1 = 1$, where a tiny change of flow section produces a large variation of the Mach number.

With this blading an interesting feature has been found for changing the back pressure when the cascade is operated at choked conditions (ref. 2). An increase of the back pressure, hence an increase of the static pressure rise, decreases the total pressure loss of the cascade. The application of back pressure is possible due to the existence of a sonic line separating the upstream and the downstream field. In fig. 13 the total pressure loss coefficient is plotted in function of the static pressure rise coefficient. An approximately linear relation exists between these two parameters. This phenomenon can be explained physically with the upstream movement of the shock terminating the supersonic region in the blade passage with an increase of the back pressure. The upstream movement of the shock results in a reduction of the local Mach number upstream of the shock. Hence, the shock boundary layer interaction losses are smaller. The maximum back pressure, close to spillage of the cascade, is given with the position of the shock close to the sonic line.

Very recently, the use of choked bladings was proposed as inlet guide vanes (ref.8). For this application use was made of the supersonic region in the blade passage, preventing any upstream influence of a downstream perturbation, like the noise radiated forward from the fan or first compressor stage.

But in general a choked blading at the design point should always be avoided. This demand asks for precise prediction methods of local velocity distribution on the blade surface.

3. MATHEMATICAL SOLUTIONS FOR COMPRESSIBLE FLOWS IN GENERAL AERODYNAMICS

In this chapter, we shall give only a very brief survey on the classical methods for the calculation of compressible nonviscous subsonic flows, necessary to understand the calculation methods for compressible potential flows in cascades.

The potential flow equation is a non linear partial differential equation of the elliptic type for the subsonic flow in a plane x,y:

$$\Delta\phi = \frac{1}{2}\left(\phi_x^2\phi_{xx}+\phi_y^2\phi_{yy}+2\phi_x\phi_y\phi_{xy}\right) \tag{6}$$

For this type of equation general solutions can be found only for special cases. Particularly, because of the non linearity, solutions cannot be superposed as for the incompressible flow. Hence, the possibility of producing additional solutions by simple algebra is eliminated.

In general, three different approaches are used for the solution of equation (6):
1) linearization of the potential flow equations;
2) development in power series of the potential flow equation;
3) hodograph method.

3.1 Linearization methods

For the linearization of the compressible potential flow equation, the potential ϕ is replaced by

$$\phi = \phi_\infty + \phi' = w_\infty \cdot x + \phi' \tag{7}$$

where ϕ_∞ is the potential of the basic flow and ϕ' is a small perturbation potential. Nelgecting the second and higher order terms in the derivatives of ϕ', the potential equation (6) is simplified to

$$(1-M_\infty^2)\,\phi_{xx} + \phi_{yy} = 0 \tag{8}$$

Obviously, this equation is valid for the total potential ϕ and for the perturbation potential $\phi' = \phi - w_\infty \cdot x$ with w_∞ = constant. Hence, eq. (8) can be written as

$$\beta^2(\phi'_{xx})_c + (\phi'_{yy})_c = 0 \tag{9}$$

with

$$\beta^2 = 1 - M_\infty^2$$

The subscript c indicates that this equation is valid for compressible flow. With the affine transformation

$$x_i = x_c \qquad y_i = \beta y_c \qquad \phi'_i = \lambda\phi'_c \tag{10}$$

the elliptical equation ($M_\infty < 1$) can be converted into the Laplace equation

$$(\Phi'_{xx})_i + (\Phi'_{yy})_i = 0 \tag{11}$$

for an incompressible perturbation potential $\Phi'_i(yy)$. The factor λ has still to be determined.

Using this transformation, the perturbation velocities u' and v' are

$$u'_i = \Phi_{ix} = \lambda \Phi'_{cx} = \lambda u'_c$$
$$v'_i = \Phi_{iy} = \lambda \Phi'_{cy} \frac{dy_c}{dy_i} = \frac{\lambda}{\beta} v'_c \tag{12}$$

Hence, with eq. (11) and (12) results of the incompressible flow field, which are relatively easy to obtain, can be transformed into the compressible flow field. The magnitude of M_∞ determines the influence of the compressibility. With the choice of the parameter λ different types of transformations can be performed. Three of those are discussed in the following.

The transformation with $\lambda = 1-M_\infty^2$ will give for an incompressible flow field around a slender body the compressible flow by distortion of the body and the angle of attack with:

$$\frac{\alpha_c}{\alpha_i} = \frac{\theta_c}{\theta_i} = \frac{t_c}{t_i} = \sqrt{1-M_\infty^2}$$

Th static pressure p' distribution around a profile can be determined by using the Bernoulli equation (ref. 9)

$$p' = p - p_\infty = \Delta p = -\int_{w_\infty}^{w} \rho \cdot w \cdot dw = -\rho_\infty w_\infty (w-w_\infty) = -\rho_\infty \cdot w_\infty - u'$$

and

$$c_p = \frac{\Delta p}{p_{01}-p_1} = -2\frac{u'}{w_\infty} \tag{13}$$

Hence, with eq. (12)

$$\frac{c_{p_c}}{c_{p_i}} = \frac{u'_c}{u'_i} = \frac{1}{\lambda} = \frac{1}{1-M_\infty^2} \tag{14}$$

This relation is normally named the 'Goethert rule'.

The <u>first</u> rule of Prandtl-Glauert assumes equal bodies for the treatment in compressible and incompressible flow

$$\frac{\alpha_c}{\alpha_i} = \frac{\theta_c}{\theta_i} = \frac{t_c}{t_i} = 1$$

and with

$$\lambda = \sqrt{1-M_\infty^2}$$

$$\frac{c_{p_c}}{c_{p_i}} = \frac{1}{\sqrt{1-M_\infty^2}} \tag{15}$$

The <u>second</u> rule of Prandtl-Glauert assumes the same pressure distribution on the blade surface for the compressible and incompressible flow field:

$$\frac{c_{p_c}}{c_{p_i}} = 1 \tag{16}$$

This relation gives the transformation for the blade contour:

$$\frac{\alpha_c}{\alpha_i} = \frac{\theta_c}{\theta_i} = \frac{t_c}{t_i} = \frac{1}{\sqrt{1-M_\infty^2}}$$

The first of the two Prantl-Glauert rules is of interest to study the behavior of a given blading over a range of different Mach numbers, while the second can help to find a profile which has the same lift coefficient for different Mach numbers.

A difficulty for a practical application exists always due to the assumptions made for the linearization:

$$M_\infty^2 \left(\frac{u'}{w_\infty}\right)^2 << 1 \qquad M_\infty^2 \left(\frac{v'}{w_\infty}\right)^2 << 1 \qquad M_\infty^2 \left(\frac{u'v'}{w_\infty^2}\right) << 1$$

$$\frac{M_\infty^2}{1-M_\infty^2}\frac{u'}{w_\infty} \ll 1 \qquad\qquad M_\infty^2 \frac{v'}{w_\infty} \ll 1$$

The first three assumptions are included in the last two ones. Normally, these assumptions cannot be fulfilled with the type of blading used in compressor cascades.

3.2 Power series

We consider in this note only the development in power series of the Mach number. Another possibility is the expansion in series of a parameter describing the tangent of the profile contour against the main flow direction. The last procedure is of particular interest for slender bodies. But we are looking here for a procedure to be useful for thick bodies in opposition to the small perturbation method discussed in the preceding chapter.

Let us consider again a two dimensional flow in the plane x,y for which the potential equations can be written as

$$\phi_{xx} + \phi_{yy} = \frac{1}{a^2}\left(\phi_{xx}\phi_x+\phi_{yy}^2\phi_y+2\phi_{xy}\phi_x\phi_y\right) \equiv 2\pi\tau \qquad (17)$$

where a^2 is a function of $w^2 = \phi_x^2+\phi_y^2$ determined with the compressible gas flow conditions as

$$a^2 = \frac{1}{M_\infty^2} w_\infty^2 \left(1+ \frac{\gamma-1}{2} M_\infty^2\left(1- \frac{w^2}{w_\infty^2}\right)\right)$$

Knowing that an incompressible flow around a body is qualitatively not too different from the subsonic compressible flow, the solution of the left hand side of eq. (17), the Laplace equation $\phi_{xx}+\phi_{yy} = 0$, can be taken as a first appproximation for the potential flow equation. The solution for $\phi(x,y)$ of this first approximation is taken as the first factor of an expansion in series of eq.(17) (ref. 9) :

$$\phi(x,y) = \phi_0(x,y) + \phi_1(x,y)M_\infty^2 + \phi_2 M_\infty^4 + \ldots \qquad (18)$$

Equation (18) is introduced into eq. (17). After an arrangement with the powers of M_∞^2, a system of linear differential equations is obtained for the functions $\phi_k(x,y)$

$$\begin{aligned}
&(\phi_0)_{xx} + (\phi_0)_{yy} = 0\\
&(\phi_1)_{xx} + (\phi_1)_{yy} = 2\pi\tau_1(x,y)\\
&\cdots\cdots\cdots\cdots\cdots\\
&(\phi_k)_{xx} + (\phi_k)_{yy} = 2\pi\tau_k(x,y)
\end{aligned} \qquad (19)$$

The right hand sides of the system of Poisson's equation (19) $2\pi\tau_k(x,y)$ incorporate only the approximations $\phi_0, \phi_1, \ldots, \phi_{k-1}$.

Inserting the appropriate boundary conditions

$$\frac{\partial\phi_0}{\partial x} = u_\infty \qquad \frac{\partial\phi_0}{\partial y} = 0 \qquad \text{at } x=\infty,\ y=\infty$$

$$\frac{\partial\phi}{\partial n} = 0 \qquad \text{at solid boundary (n is normal to the boundary)}$$

$$\frac{\partial\phi_1}{\partial x} = \frac{\partial\phi_2}{\partial x} = \ldots = \frac{\partial\phi_k}{\partial x} = 0$$

$$\frac{\partial\phi_1}{\partial y} = \frac{\partial\phi_2}{\partial y} = \ldots = \frac{\partial\phi_k}{\partial y} = 0 \qquad \text{at } x=\infty,\ y=\infty$$

$$\frac{\partial\phi_1}{\partial n} = \frac{\partial\phi_2}{\partial n} = \ldots = \frac{\partial\phi_k}{\partial n} = 0 \qquad \text{at solid boundary}$$

the solutions of the system (19) are determined.

Sauer (ref. 9) proposes to consider not only the solution $\phi_0(x,y)$ as an incompressible one, but also the following approximations $\phi_k(x,y)$. For the latter case additional

sources and sinks are distributed in the flow field with the strength $\tau_k(x,y)$. This means that also the interior of the profile has to include sources and sinks to fulfill the boundary condition at the blade contour. Hence, the approximations are

$$\Phi_k(x,y) = \iint \tau_k(\xi,\eta) \ln \sqrt{(x-\xi)^2+(y-\eta)^2}\, d\xi d\eta \qquad (20)$$

Now the functions $\Phi_k(x,y)$ are not any longer considered as factors of the series expansion (18), but as successive approximations for eq. (17). The approximation $\Phi_{k-1}(x,y)$ is introduced into the right hand side of eq. (17) to obtain $\Phi_k(x,y)$ and following from (20) $\Phi_k(x,y)$. A practical application of this procedure has been found for the calculation of compressible flows in cascades.

The procedure to develop the compressible potential flow equation in a series of Mach number has the advantage of not to be restricted to slender bodies. But unfortunately, there is no evidence that the method converges.

3.3 Hodograph method

In chapter E.1 the compressible flow equations have been linearized by neglecting some higher order terms, Hence, the resulting linear differential equations are valid only approximately for stream fields close to the main parallel stream field.

Another type of linearization is the use of a hodograph method, the transformation of the Φ or Ψ functions from the x,y plane into the velocity plane u,v or w,θ. The linear differential equations obtained in this way are exact. They are also valid for high perturbation stream fields and in the range $M \approx 1$.

Two types of transformation are possible for a plane and irrotational flow

1) the Molenbroek transformation, which converts only the independent variables and not the functions Φ and Ψ, giving the streamfunction in the w,θ plane with θ = arc cos(u/w):

$$w^2\Psi_{ww} + w\left(1+\frac{w^2}{a^2}\right)\Psi_w + \left(1-\frac{w^2}{a^2}\right)\Psi_{\theta\theta} = 0 \qquad (21)$$

2) the Legendre transformation which converts not only the velocity components but also the Φ and Ψ functions:

$$\left(1-\frac{v^2}{a^2}\right)\Phi_{uu} + 2\frac{uv}{a^2}\Phi_{uv} + \left(1-\frac{u^2}{a^2}\right)\Phi_{vv} = 0 \qquad (22)$$

with $\Phi = x\phi_x + y\phi_y - \phi$.

The difficulty for the practical application of the hodograph method is that the problem of flow past given boundaries is susceptible to a direct treatment.

A significant simplification for the application of the hodograph method has been obtained with an approximation of the pressure-density relation $p = p(\rho)$ by a hypothetical relation for a limited range of velocity, like the well known <u>tangent-gas</u> relation leading to the Karman-Tsien correction formula.

For the tangent gas relation the isentropic relation $p\cdot\rho^{1/\gamma} = \text{const.}$ is approached by a straight line in the plane $p = p(1/\rho)$ (fig. 19) :

$$p - p_\infty = a_\infty^2 \rho_\infty^2 \left(\frac{1}{\rho_\infty} - \frac{1}{\rho}\right) \qquad (23)$$

Introducing (23) into the Bernoulli equation, we get

$$w^2 - w_\infty^2 = a_\infty^2 \rho_\infty^2 \left(\frac{1}{\rho^2} - \frac{1}{\rho_\infty^2}\right) \qquad (24)$$

With $\rho^2\cdot a^2 = \rho_\infty^2\cdot a^2 = \rho_0^2\cdot a_0^2$ which is valid because of

$$-\left(\frac{dp}{d(\frac{1}{\rho})}\right) = -\left(\frac{dp}{d(\frac{1}{\rho})}\right)_\infty = -\left(\frac{dp}{d(\frac{1}{\rho})}\right)_0 = \text{const.}$$

we obtain from eq.(24)

$$w^2 - a^2 = w_\infty^2 - a_\infty^2 \qquad w^2 = a^2 - a_0^2$$

$$\left(\frac{\rho}{\rho_0}\right)^2 = 1 - \frac{w^2}{a^2} = 1 - M^2 \qquad \frac{\rho_0}{\rho} = 1 + \frac{w^2}{a_0^2} \qquad (25)$$

Using these relations, the eq. (21) can be written as (ref. 10) :

$$\frac{w}{\sqrt{1-M^2}}\frac{\partial}{\partial w}\left(\frac{w}{\sqrt{1-M^2}}\psi_w\right) + \psi_{\theta\theta} = 0 \qquad (26)$$

This equation can be reduced into that of an incompressible flow by defining a new variable w_i with the relation

$$\frac{dw_i}{w_i} = \sqrt{1-M^2}\,\frac{dw}{w} \tag{27}$$

Introducing this unique relation between w_i and w_1 the equation (26) is transformed into

$$w_i \frac{\partial}{\partial w_i}(w_i \psi_{w_i}) + \psi_{\theta\theta} = 0$$

Comparing eqs (26) and (28) it is evident that for M = 0 in eq. (26) both the relations are identical. Hence, eq. (28) is the differential equation for an incompressible fluid in the hodograph plane w_i,θ.

The importance of this result is that it is possible now to obtain more easily results in the physical plane for given boundaries. Knowing the incompressible results for a given profile $\psi_i = \psi_i(x_i,y_i)$, the velocity components u_i and v_i can be determined to give $\psi_i = \psi_i(w_i,\theta)$. This function has the same form like $\psi = \psi(w,\theta)$, due to the transformation (27) used. The compressible solution, found by replacing w_i and w, will give the body shape in the physical plane, by integrating :

$$dx = \left(\frac{\cos\theta}{w}\phi_w - \frac{\rho_0}{\rho}\frac{\sin\theta}{w}\psi_w\right)dw + \left(\frac{\cos\theta}{w}\phi_\theta - \frac{\rho_0}{\rho}\frac{\sin\theta}{w}\psi_\phi\right)d\theta$$

$$dy = \left(\frac{\sin\theta}{w}\phi_w + \frac{\rho_0}{\rho}\frac{\cos\theta}{w}\psi_w\right)dw + \left(\frac{\sin\theta}{w}\phi_\theta + \frac{\rho_0}{\rho}\frac{\cos^0\theta}{w}\psi_\phi\right)d\theta$$

The body form will be slightly different from the incompressible one.

To perform this procedure, we have to solve two steps. First, a relation between the corresponding velocities in the compressible and incompressible flow field has to be established. Second, a relation between the corresponding profile shapes has to be formulated.

3.3.1 Corresponding velocities

A relation between the corresponding velocities is obtained using the eqs (25) and (27) :

$$\frac{w}{w_\infty} = \frac{\frac{w_i}{w_{i_\infty}}(1-\lambda)}{1-\lambda\left(\frac{w_i}{w}\right)^2} \tag{29}$$

with

$$\lambda = \frac{M_\infty^2}{\left(1+\sqrt{1-M_\infty^2}\right)^2} \tag{30}$$

The detailed derivation which is purely mathematical can be found in ref. 10.

Similar to the Prandtl-Glauert rule, we can also construct a static pressure rise coefficient correction formula with eq. (29) :

$$c_{p_c} = \frac{c_{p_i}}{\sqrt{1-M_\infty^2} + \frac{M_\infty^2}{1+\sqrt{1-M_\infty^2}}\frac{c_{p_i}}{2}} \tag{31}$$

This formula is th so-called Karman-Tsien pressure correction formula. In fig. 15 the eq. (31) is plotted in form of a graph.

The eq. (31) of course does not represent exactly the influence of the compressibility on the pressure distribution of an airfoil, because the profiles for which the c_p values are compared are slightly different.

For the practical application of eq. (31) it is useful to know that counteracting errors exist, which seem to nearly cancel each other. The linear pressure density relation overestimates the compressibility effects. On the other hand, the compressibility correction of the profile coordinates will produce a thicker profile. Hence, using the thinner incompressible profile, we shall be closer to reality.

3.3.2 Profile coordinate correction

The detailed derivation of the correction parameter can be found in ref. 10. Here this procedure is outlined only very briefly.

The corresponding points in the x,y plane are best represented by complex quantities:

$$z = x + iy, \quad z_i = x_i + iy_i$$

and

$$F(z_i) = \phi_i + i\psi_i \qquad \tilde{F}(z_i) = \phi_i - i\psi_i \tag{32}$$

These relations give the connection between z and z_i:

$$z = z_i - \lambda \int \left(\frac{1}{w_{i_\infty}} \frac{d\tilde{F}}{dz_i}\right) dz_i \tag{33}$$

with

$$\lambda = \frac{w_{i_\infty}}{2a_0^2}$$

The influence of the correction term on z_i is small, specially for moderate Mach numbers. For $M \to 0$, it approaches zero, the incompressible contour $z = z_i$.

3.3.3 Conclusions

For the application of the Karman-Tsien rule it should be held in mind that this rule is also restricted to small perturbations due to the linear pressure density relation. But the rule is not like the one of Prandtl-Glauert limited to small Mach numbers shown in fig. 16.

4. MATHEMATICAL SOLUTIONS FOR SUBSONIC COMPRESSIBLE FLOW IN CASCADES

Based on the relations developed for isolated airfoils, we shall discuss their application for cascades in the following chapter, outlining their main assumptions and restrictions.

4.1 Prandtl-Glauert rule for cascades

For the application of the Prandtl-Glauert rules developed in chapter 3.1 for single airfoils to compressor cascades, we have to consider the influence of the transformation factors on the cascade parameters and the profile contour.

The transformation of the incompressible flow field into the compressible one demands a shortening of the y-coordinate with the factor $\beta = \sqrt{1-M_\infty^2}$. The result is a cascade with a smaller pitch chord ratio s/g and a high stagger angle γ (fig. 17) :

$$\frac{tg\gamma_i}{tg\gamma} = \frac{y}{y_i} = \frac{1}{\sqrt{1-M_\infty^2}} \tag{34}$$

The subscript i indicates here, and in the following, the dimensions in the incompressible flow field of a cascade working in the compressible flow.

The pitch chord ratio is

$$\frac{\left(\frac{s}{g}\right)_i}{\frac{s}{g}} = \left(\sin^2\gamma + (1-M_\infty^2)\cos^2\gamma\right)^{0.5} \tag{35}$$

For the determination of the profile contour in the incompressible flow field, we can use either the condition of equivalent static pressure distribution or equivalent profile contours. For $c_{p_i} = c_{p_c}$ the profile contour has to be changed according to

$$\frac{dy_{\ell i}}{dy_{\ell c}} = \frac{1}{\sqrt{1-M_\infty^2}} \tag{36}$$

Hence, the profile is thicker and more cambered in the incompressible flow field. Also the relative inlet and outlet flow angles are changed at infinity upstream and downstream of the cascade (ref. 1) :

$$ctg(90°-\beta_{1,2i}+\gamma_i) = \frac{v_{1,2i}}{u_{1,2}} = \frac{1}{\sqrt{1-M_\infty^2}}\, ctg(90°-\beta_{1,2}+\gamma) \tag{37}$$

wi h $u_{1,2} = u_{1,2_i}$ because in the x-direction there is no influence of compressibility.

In first approximation it can be stated that the deflection will be higher for the compressible flow due to the same lift per blade but a smaller pitch chord ratio.

For the practical application it is more suitable to use the second case, the profile form constant with the Mach number. Now, the perturbation velocity component v is constant, while the component u has to be changed according to

$$u = \frac{u_i}{\sqrt{1-M_\infty^2}} \; ; \qquad v = v_i \tag{38}$$

The axial velocity components have to be equal in the incompressible case upstream and downstream of the cascade :

$$\frac{u_\infty \cos\gamma}{(u_{1,2})_i \cos\beta_{1,2_i}} = 1 \tag{39}$$

This relation results in the following function for the flow angle velocity at cascade inlet and outlet plane :

$$ctg\beta_{1\ 2_i} = \frac{\sqrt{1-M_\infty^2}\ tg(90°-\beta_{1,2}+\gamma) - \frac{tg\gamma}{\sqrt{1-M_\infty^2}}}{1 + tg(90°-\beta_{1,2}+\gamma)tg\gamma - (1-\sqrt{1-M_\infty^2})(1+\frac{tg^2\gamma}{1-M_\infty^2})} \tag{40}$$

To conclude, the following steps are necessary to use the above outlined methods:

1) the cascade parameters γ,σ have to be changed according to eq. (34) and (eq. (25);
2) the inlet angle has to be transformed following eq. (40);
3) the static pressure distribution can be calculated with eq. (15) and the outlet angle with eq. (40).

For the application of the Prandtl-Glauert transformations it should always be held in mind that the small perturbation theory is the basic assumption. Hence, only for small cambered and thin profiles sufficient results will be obtained. For transonic compressor cascades designed for the tip sections of a rotor these conditions are mostly satisfied. Another rather annoying parameter is the Mach number M_∞ determining the influence of the compressibility. This Mach number is changing through the blade passage and not constant like for isolated airfoils. Normally, the inlet Mach number is taken as M_∞. But a slight improvement could be obtained by using an average Mach number of outlet and inlet streamfield.

In fig. 18 some experimental results are compared with measurements. A comparison of the incompressible and compressible theoretical calculations shows tha good improvement of the latter. A direct comparison with the measurements is not possible, due to viscous flow and three dimensional flow effects not considered in the theoretical calculation. But in general, it seems that the transformation does not take sufficiently into account the higher local Mach number regions.

To diminish this difference of prediction and measurement of the suction peak velocity, it has been proposed by different authors (ref. 11, 12) to take into account also higher order terms for the solution of the potential flow equation instead of only the first one for the linearized solution.

Spreiter and Alksne (ref. 11) have shown for single airfoils that the compressible flow equation, taking into account second and first order terms, can be written as

$$(1-M_\infty^2-C\phi_x)\phi_{xx} + \phi_{xx} = 0 \tag{41}$$

with

$$C = M_\infty^2 \frac{\gamma+1}{w_\infty}$$

The factor $(1-M_\infty^2-C\phi_x)$ can be kept constant within small steps and the eq. (41) can be considered as a locally linearized differential equation.

For cascade flow, Fottner (ref. 12) performed the local linearization based on the Prandtl-Glauert rule and obtain for the velocity distribution :

$$\frac{w_c}{u_\infty} = \left[1 + \frac{1}{\sqrt{1-M_\infty^2}}\left(\frac{w_{f_i}}{u_\infty} - 1\right) 1 + \frac{1}{8} C \left\{1+ \frac{1}{3} C \left[1+ \frac{7}{16} C \left(1+ \frac{1}{2} C\right)\right]\right\}\right] \cdot \frac{1}{R} \tag{42}$$

with

$$C = \frac{M_\infty^2(\gamma+1)}{(1-M_\infty^2)^{3\ 2}} \cdot 2\left(\frac{w_{f_i}}{u_\infty} - 1\right) \qquad R = \sqrt{1 + \left(\frac{dy_t}{dx}\right)}$$

w_f = relative velocity at the camber line

y_t = coordinate of the thickness distribution.

In figure 19 the pressure coefficient distribution on the suction side is compared for:

1) The incompressible pressure distribution;
2) The calculations of the Prandtl-Glauert rule for the determination of the equivalent cascade geometry (eq. 34, 35, 40);
3) Calculation of the local variable cascade geometry with the Prandtl-Glauert rule;
4) Local linearization for the determination of the locally variable equivalent cascade geometry (eq. 42).

A considerable improvement is obtained with the use of the additional terms specially for the high excess speeds. The influence of local shocks cannot be predicted with this method, of course.

4.2 Expansion in series

Two methods only are mentioned here using the approximative procedures described in chapter 3.2. The application of these methods is normally restricted to thick profiles due to their basic assumptions. They are not valid for supersonic regions.

4.2.1 Method of Price (ref. 13)

Price extends the Martensen method (ref. 14) - originally for incompressible flows - to compressible flows by successively approximating to the compressible potential equation by a Poisson equation like it has been described in chapter 3.2. The incompressible solution is used for the first approximation of the flow potential.

In Martensen's method, the blade is represented by a set of vortices on the blade contour. The method is only valid for blade contours having no discontinuity, i.e., the second derivative. Pal (ref. 15) has changed the method to allow for one discontinuity, the trailing edge.

In chapter 3.2 we have seen that the compressible potential flow equation can be written as :

$$\phi_{xx} + \phi_{yy} = 2\pi\, F(x,y) \tag{43}$$

where $F(x,y)$ can be considered as the strength of a plane source-sink distribution over the whole flow field according to the change of volume flow due to local compressibility effects in the flow field.

On the boundaries of the flow field, the blade contours, additional sources or sinks have to be distributed to reduce the normal velocity induced by the flow field sources and sinks to zero. The potential, due to the incompressible solution (ϕ_0 in chapter 3.2), the source and sink distribution in the flow field and on the blade contours are used to calculate the right hand side of eq. (43). This will be continued iteratively until the process converges.

The source and sink strength in the flow field required is, following ref. 13 :

$$F(\xi,\eta) = \frac{\phi_\xi^2\,\phi_{\xi\xi} + \phi_\xi^2\,\phi_{\eta\eta} + 2\phi_\xi\,\phi_\eta\,\phi_{\xi\eta}}{2\pi\left(\frac{w_1^2}{M_1^2} - \frac{\gamma-1}{2}\left(\phi_\xi^2+\phi_\eta^2-w_1^2\right)\right)} \tag{44}$$

This source and sink strength induces at the profile boundary a normal velocity $w_n(\lambda)$ with λ a coordinate describing the profile by increasing from $0 - 2\pi$:

$$w_n(\lambda)\sqrt{\left(\frac{dx(\lambda)}{d\lambda}\right)^2+\left(\frac{dy(\lambda)}{d\lambda}\right)^2} = \int_0^d\int_{-\infty}^{+\infty} \frac{F(\xi,\eta)\,\frac{dx(\lambda)}{d\lambda}\,\sin\frac{2\pi}{d}(\eta-y(\lambda)) - \frac{dy(\lambda)}{d\lambda}\,\mathrm{sh}\,\frac{2\pi}{d}(\xi-x(\lambda))}{\mathrm{ch}\,\frac{2\pi}{d}(\xi-x(\lambda)) - \cos\frac{2\pi}{d}(\eta-y(\lambda))}\,d\xi\,d\eta \tag{45}$$

The line source distribution on the blade is given with eq. (45) :

$$m(\lambda)\sqrt{\left(\frac{dx(\lambda)}{d\lambda}\right)^2+\left(\frac{dy(\lambda)}{d\lambda}\right)^2} + \frac{1}{2\pi}\int_0^{2\pi} m(\mu)\cdot\sqrt{\left(\frac{dx(\mu)}{d\mu}\right)^2+\left(\frac{dy(\mu)}{d\mu}\right)^2}\cdot k(\lambda,\mu)\,d\mu =$$

$$= 2w_n(\lambda)\cdot\sqrt{\left(\frac{dx(\lambda)}{d\lambda}\right)^2+\left(\frac{dy(\lambda)}{d\lambda}\right)^2} \tag{46}$$

with

$$k(\lambda,\mu) = \frac{2\pi}{d}\,\frac{\frac{dy(\lambda)}{d\lambda}\,\mathrm{sh}\,\frac{2\pi}{d}(x(\lambda)-x(\mu)) - \frac{dx(\lambda)}{d\lambda}\,\sin\frac{2\pi}{d}(y(\lambda)-y(\mu))}{\mathrm{ch}\,\frac{2\pi}{d}(x(\lambda)-x(\mu)) - \cos\frac{2\pi}{d}(y(\lambda)-y(\mu))}$$

$m(\lambda)$ strength of line source.

With the results of the equations (44, 45, 46) the derivations of the potential $\phi(\xi,\eta)$ are recalculated and introduced into eq. (44) to give a new $F_1(\xi,\eta)$. The process

is repeated until $F_k(\xi,\eta) - F_{k-1}(\xi,\eta)$ is sufficiently small.

The main difficulties for the practical application is the integration of the equations giving the derivatives of ϕ. In general, the continuous vortex and source-sink distribution is replaced by a set of point vortices and sources. But there is a general difference in the behavior of a line vortex and a point vortex which gets important for thin profiles, we consider in this note.

Close to a point vortex the induced velocity tends to infinity, while close to a line vortex, the velocity tends to $\pm \gamma/2$.

Hence the use of this method to the application of compressor cascades is very restricted, due to the use of point vortices and Martensen's incompressible solution. Up to now, no published results are available of this procedure.

4.2.2 Method of Imbach (ref. 16)

The method of Imbach is presented in this chapter of "expansion in series" due to its close resemblance with the method of Price, although it is better suited for a presentation with the flux analysis methods.

Imbach is using the classical solution for the Laplace equation by superposition also in the compressible case. The flow through the cascade is constructed by a parallel main flow $\tg\beta_\infty = \frac{\tg\beta_1+\tg\beta_2}{2}$ and a circulation flow around the profile. The last one is produced by a vortex distribution on the blade contour, which is corrected for the compressibility effects represented with a source-sink distribution in the passage flow violating the boundary conditions on the blade ($w_n = 0$) due to an additional induced velocity component.

The source-sink distribution is calculated according to a change of volume flow along a stream line. Hence, for the first approximation the streamline for the incompressible flow will be used. The difference between the volume flow of two flow sections of a streamtube with the width $\Delta y \cdot \cos\beta$ is :

$$w \cdot \Delta y \cos\beta - w_1 \cdot \Delta y \cdot \cos\beta_1 = \int_0^{F'} q(\xi,\eta)\, dF'_q \qquad (47)$$

with F' equal to the passage section in which the sources and sinks are distributed.

Using the relations for compressible flows, the equation (47) can be expressed as

$$\frac{\Delta y}{\Delta y_1} \cdot \frac{\cos\beta}{\cos\beta_1} \left(\frac{2+(\gamma-1)M_1^2}{\gamma+1}\right)^{\frac{1}{2}} \frac{M}{M_1} - 1 = \int_0^{F'} \frac{q(\xi,\eta)}{w_1 \cdot \Delta y \cdot \cos\beta_1}\, dF'_q \qquad (48)$$

relating the source-sink strength in the field F' with the inlet Mach number M_1.

The additional velocity induced by this source-sink distribution is

$$u_q + iv_q = \frac{1}{2g} \int_0^{F'_q} q(\xi,\eta)\left(f_y(z,\zeta) + if_x(z,\zeta)\right) dF'_q \qquad (49)$$

with

$$-f_x = \frac{\sin\frac{\pi(y-\eta)}{g} \quad \cos\frac{\pi(y-\eta)}{g}}{\sh^2\frac{\pi(y-\eta)}{g} + \sin^2\frac{\pi(y-\eta)}{g}} \quad \text{and} \quad f_y = \frac{\sh\frac{\pi(x-\xi)}{g} \quad \ch\frac{\pi(x-\xi)}{g}}{\sh^2\frac{\pi(y-\eta)}{g} + \sin^2\frac{\pi(y-\eta)}{g}}$$

Hence, the local velocity components are the sum of the terms due to the main flow, the vortex distribution on the blade contour and the source-sink distribution in the flow field :

$$v(z) = v_\infty + v_\gamma(z) + v_q(z)$$

$$u(z) = u_\infty + u_\gamma(z) + u_q(z)$$

The vortex distribution on the profile contour is determined with the fulfillment of :
1) the conditions at infinity upstream : $u(-\infty) = w(-\infty)\cos\beta_1$

$$v(-\infty) = w(-\infty)\sin\beta_1$$

2) the velocity component normal to the blade contour has to be zero
3) the Kutta condition.

Knowing the corrected velocities it is possible to trace a new set of streamlines, which again will determine a new sink-source distribution.

Results for a turbine cascade are represented in fig. 20 for $M_1 = .20$ and $M_2 = .60$. The agreement between calculated and experimental values is sufficient. A slight overestimation of the high suction side velocities is shown.

4.3 Flux analysis

The flux analysis method considers the cascade built up of an infinite number of channels instead of an infinite number of isolated airfoils. Hence, this approach is particularly suitable for high solidity low stagger cascades. Also, there is no restriction on the maximum value of the camber angle for the blades.

4.3.1 Method of Traupel (ref. 17)

The method proposed by Traupel consists of the construction of the ψ,ϕ net through a blade channel using the continuity relation to get a unique function between the inlet Mach number, the local Mach number and the local flow section :

$$\frac{A}{A_1} = \frac{M_1^*}{M^*} \left(\frac{\gamma+1-(\gamma-1)M_1^{*2}}{\gamma+1-(\gamma-1)M^{*2}}\right)^{\frac{1}{\gamma-1}} \qquad (50)$$

With fig. 21 a potential line is drawn in the smallest section of the blade channel from A to B. This line is divided into two parts - in the first assumption the two parts are equal which is only true if the velocity is constant along $\overline{AB}$ - following the relation :

$$\Delta\psi = w_1 \cdot F_1 = w \cdot F \qquad (51)$$

with $F_1 = \Delta b_1 \cdot h$, $F = \Delta b \cdot h$

A mean streamline is drawn upstream and downstream of the line $\overline{AB}$ determining at each point the ratio $\Delta b/\Delta b_1$ and with eq.(50) the velocity ratio $w/w_1 = M^*/M_1^*$. For a quadrature net of streamlines and potential lines, then it is valid

$$\Delta\psi = \Delta\phi = w \cdot \Delta s$$

and with eq. (51)

$$\Delta s = \frac{\Delta b_1}{w/w_1} \qquad (52)$$

In this manner potential lines are obtained for one of the two streamtubes. The potential lines can be extended over the second streamtube which allows also a calculation of w/w_1 at any place on this tube with $w/w_1 = \frac{\Delta\phi}{w_1 \cdot \Delta s} = \frac{\Delta b_1}{\Delta s}$ for $\Delta\psi = \Delta\phi$. On the other hand, w/w_1 can be determined with the function (50) at this place. The resulting value will probably be different from the first one. A correction of the first guessed streamline is necessary until an agreement is obtained.

This procedure can be continued by cutting into halves the first two streamtubes and applying the same process like above. For regimes with high velocity gradients on the contour, it is advisable to diminish further the net size.

This method can be applied also for supersonic flows if the influence of shock waves are neglected. Some difficulties can arise in the inlet or outlet section where the position of the stagnation streamline is not known a priori.

4.3.2 Method of Uchida (ref. 18)

Uchida is using the same procedure like Traupel (ref. 17), but more adapted to the numerical treatment with a digital computer due to the use of the potential flow equation in curvi linear coordinates. Some difficulties will occur for the convergence of the solutions in the neighbourhood of $M_2 = 1$.

In fig. 22 some calculated results are shown for a turbine cascade indicating the Mach number effect. The cascade parameters are mentioned in the diagram.

4.3.3 Transformation method based on flux analysis

In ref. 19 a method has been developed based on the proposal of Oswatitsch and Ryhming (ref. 20). For high solidity cascades with small stagger angles it can be supposed that the streamline curvature is given by the blade or channel form. The influence of the compressibility on the streamline form can be neglected. Hence, for the known incompressible streamline field the potential lines for constant potential difference $\Delta\phi$ change the position for the compressible flow field compared to the incompressible one.

The two governing flow equations, the continuity equation and the condition of irrotationality are written in curvilinear coordinates ψ_i, ϕ_i (fig. 23) for incompressible flow

$$\frac{1}{w_i}\frac{\partial w_i}{\partial \phi_i} + \frac{\partial \beta}{\partial \psi_i} = 0 \qquad (53a)$$

$$\frac{1}{w_i}\frac{\partial w_i}{\partial \psi_i} - \frac{\partial \beta}{\partial \phi_i} = 0 \qquad (53b)$$

with $\beta = \beta_i$ the angle of the slope of the incompressible streamline. For the compressible case with the assumption of $\beta_c = \beta_i = \beta$:

$$\frac{1}{\rho w_c}\frac{\partial(\rho \cdot w_c)}{\partial \phi_i} + \frac{\partial \beta}{\partial \psi_i} = 0 \qquad (54a)$$

$$\frac{1}{w_c}\frac{\partial w_c}{\partial \phi_i} - \frac{\partial \beta}{\partial \psi_i} = 0 \qquad (54b)$$

The first one of these two systems of equations is correct, while the second one is only an approximation due to $\beta_c = \beta_i$.

The following procedure is developed with the assumption that the incompressible solution is known. This solution can be obtained either from experimental results or theoretical ones. This freedom is of extreme importance for the treatment of high deflection blades where the influence of viscous effects is predominant and no valid method is actually at hand for a theoretical calculation of the viscous effects (normally separated turbulent boundary layer).

To get a connection between the incompressible and compressible flow field there can be used either the continuity equations (53a)(54a) or the conditions of the irrotationality (53b) (54b). The first approach results in an integration along a streamline which will be rather inaccurate due to the long integration distance with an approximate solution. More appropriate is an integration along a potential line using the conditions (53b) and (54b)

$$\int_{w_{c_{SS}}}^{w_{c_{PS}}} \frac{1}{w_c}\, dw_c = \int_{w_{i_{SS}}}^{w_{i_{PS}}} \frac{1}{w_i}\, dw_i \quad \text{or} \quad \frac{w_{c_{PS}}}{w_{c_{SS}}} = \frac{w_{i_{PS}}}{w_{i_{SS}}} \qquad (55)$$

The connection between the local velocity and the inlet Mach number is established with the continuity equation applied between the inlet section and the potential line for which the eq. (55) is used.

The local flow section $A = n \cdot h$ is determined for a known blade height h and the length of the potential line between the suction and pressure side of the blade.

It is assumed a second order polynomial for the velocity distribution along the potential line :

$$w(\psi_i) = a\psi_i^2 + b\psi_i + d \qquad (56)$$

The validity of this assumption has been verified by a finite difference calculation of the incompressible flow field in ref. 21. An example is shown in fig. 24. The constants a, b and d are determined with the boundary conditions

$$w_i(\psi_i = 0) = w_{i_{SS}} \qquad w_i(\psi_i = n) = w_{i_{PS}}$$

and the condition of irrotationality

$$\left(\frac{1}{w_i}\frac{\partial w_i}{\partial \psi_i}\right)_{PS} = \left(\frac{\partial \beta}{\partial \phi_i}\right)_{PS}$$

The solution of the continuity equation

$$\rho \cdot w_{i_1} \cdot g \cdot \cos\beta_1 = \int_{\psi_i=0}^{\psi_i=n} \rho \cdot w_i(\psi_i)\, d\psi_i \qquad (57)$$

will give the length n.

For the compressible solution also a second order polynomial can represent the velocity distribution along a streamline, nondimensionalized with a^* :

$$M^{*}(\psi_i) = M_{SS}^{**} (A\psi_i^2 + B\psi_i + 1) \qquad (58)$$

The constants A and B are determined similar to the incompressible solution. An introduction of eq. (58) with the known length n and mass flow $\rho_1 \cdot w_{c_1} \cdot g \cdot \cos\beta_1$ into the compressible continuity equation will give an implicit equation for M_{SS}^{**}. The corresponding Mach number at the pressure side on the same potential line is found with eq. (55).

Some results obtained with this method, which is also valid in the supersonic flow range, if the total pressure losses due to shocks are neglected, are presented in chapter 7.

5. SUPERSONIC FLOW RANGE

With the methods presented above, the flow field upstream of the sonic line and downstream of the local shock can be described. Downstream of the sonic line, a supersonic expansion develops forming supersonic flow pockets which can extend rather long into the direction of chord for highly staggered and high pitch chord ratio cascades. For high solidity cascades critical and choking Mach numbers are very close; a supersonic flow field extends over the whole blade passage.

The methods of flux analysis are valid also in the supersonic flow field due to the double solution of the continuity equation. Hence, a special treatment for the supersonic flow calculation is not necessary.

In the supersonic flow pockets embedded in the subsonic flow, a Prandtl-Meyer expansion exists on which a compression process is superposed due to the expansion lines reflected as compression lines from the sonic line (fig. 25).

Instead of having to perform the rather tedious and complex work of determining the velocity distribution on the blade profile in such a supersonic flow pocket, which can only be executed with an iterative process, because the sonic line is not known, Fottner (ref. 12) established an empirical rule for the prediction of the pressure ratio p/p_{01} in this range (fig. 26). Measurements of p/p_{01} in function of the slope variation $\Delta\alpha_c$ can be approximated with a straight line :

$$\frac{p}{p_{01}} = 0.5283 - 0.8611\ \Delta\alpha_c \qquad (59)$$

Of course, this relation should be considered as a tentative one because the use of some additional measurements (ref. 4) in cascades with NACA blades indicated a higher difference between the Prandtl-Meyer expansion and the experimental results than predicted by ref. 12. Also the difference of Prandtl-Meyer calculation and measurements is not only due to the reflected compressible waves but also to the boundary layer which decreases the effective slope variation on the blade contour.

6. SHOCK-BOUNDARY LAYER INTERACTION

A great number of theoretical and analytical results are published for the problems of shock-boundary layer interaction. But most of these investigations treat the case of a normal shock on a flat plate or the interaction effects due to shocks created by compression corners or forward facing steps. A use of their results for the treatment of shocks on profiles is extremely restricted due to the important difference between these cases.

In fig. 27 a schematic model of the interaction process is shown. The case with separation is presented, because it is the usual one for cascades. The pressure rise in the free stream through a nearly normal shock produces a separation of the boundary layer connected with an increase in boundary layer thickness. The increase of the boundary layer thickness forms a wedge shaped contour which generates a weak oblique shock, the upstream leg of the bifurcated normal shock. The second leg of this shock is perpendicular to the flow direction or under a small angle to form a supersonic downstream tongue, confirmed by measurements of Seddon (ref. 22).

With the actual state of knowledge the flow conditions in the interaction region cannot be treated purely theoretically. Empirical solutions have to be used.

The interaction process can be described with three parameters, sketched in fig. 28 :
1) shock intensity $\hat{p}/p$
2) displacement phase κ
3) boundary layer thickness growth.

The shock intensity is found empirically by plotting the pressure ratio $\hat{p}/p_{01}$ in function of the ratio p/p_{01}. This correlation is shown in fig. 29 for conditions on different curvatures together with the theoretical normal shock solution and a separation criterion of Pearcey (ref. 23).

For a pressure ratio $p_1/p_{01} > .45$ the static pressure downstream of the shock follows the trend of the normal shock and no separation of the boundary layer below the shock has to be expected. The small difference existing is mainly due to the boundary layer effect and the reacceleration or rediffusion of the static pressure immediately downstream of the shock for a convex or concave surface (see fig. 30). This is shown theoretically for a nonviscous flow by Zierep (ref. 24). For values $p_1/p_{01} < .45$ separation is indicated because the growth of the separation bubble prevents a further compression downstream of the shock due to a diminishing of the flow section. The separation criteria of Pearcey, established with measurements on single airfoils :

$$\frac{p_s}{p_{01}} = 1.4 \frac{p}{p_{01}} \qquad (60)$$

gives the slope of the curves for cascades rather good, although the flow separates in cascades already for smaller shock upstream Mach number than for isolated airfoils due to the higher pressure gradient downstream of the shock for cascades.

The extension of the displacement phase κ is mainly a function of the initial boundary layer momentum loss thickness, confirmed by measurements in an axisymmetrical nozzle by Little (ref. 25), and the shock intensity. A correlation between these parameters is presented in fig. 31. A cross plot of these results is shown in fig. 32 to give a nomogram for the determination of κ in function of δ_2 and $\hat{p}/p$.

The increase in boundary layer thickness in the displacement phase can be calculated with any integral method, by assuming a linear increase of the static pressure from p to $\hat{p}$ which is justified by experimental data.

With these three parameters determined it is possible to describe the static pressure distribution in the shock boundary layer interaction region. Also, it is justified for a first approximation to suppose that the boundary layer downstream of the shock thickens by the constant value of boundary layer increase in the displacement phase.

7. EXAMPLE FOR TRANSONIC CASCADE

For a high deflection blade suitable for the operation as a stator blading for a supersonic axial compressor of the shock-in-rotor type, the predicted pressure distributions are compared with experimental results. Also, this allows us to establish a prediction method constructed of the foregoing procedures.

The parameters of the cascade are (fig. 12):

equivalent camber angle	$\phi_{eq} = 50°7$
stagger angle	$\gamma = 30°$
solidity	$\sigma = 3$
geometric inlet angle	$\beta'_{1SS} = 58°$
geometric outlet angle	$\beta'_2 = 0°$

Due to the high loading of this cascade, we shall start with experimental incompressible results to consider also a part of the viscous effects. The transformation into the compressible range is performed with the method of chapter 4.2.3 particularly suited for this type of blading. This transformation will always give a subsonic and supersonic solution along the blade (values a and b in fig. 33). If sonic conditions exist on the blade surface, the two lines a and b will cross, while in the leading edge region and the outlet plane the respective subsonic solution is valid, the two solutions a and b can only be connected by a normal shock downstream of the sonic point.

In the following the two solutions a and b will be corrected for the influence of the compressibility on the boundary layer momentum loss thickness with eq. (5). Applying this procedure, it is assumed that the pressure gradient on the blade will not change its influence on the boundary layer with the Mach number. With this correction the solutions a' and b' are obtained in fig. 33.

The position of the shock is found iteratively. For a choosen point x/c on the curve a', the pressure $\hat{p}$ downstream of the shock, the displacement phase κ and the boundary layer thickness increase is determined with the procedure outlined in chapter 6. For the new boundary layer thickness downstream of the shock, the solution b' is recalculated. The pressure $\hat{p}$ should be equal with this solution at $\frac{(x+\kappa)}{c}$. If not, the procedure has to be repeated.

In figure 34 the theoretical results obtained in the above outlined way are compared with experimental results.

8. CONCLUSIONS

This note has presented, in an introductory way, some aspects of compressor cascades working in the transonic flow range.

The discussion of the performance behavior of a cascade with increasing inlet Mach number has shown the decrease of operation range. Hence, an exact inverse or direct method is necessary for a satisfactory design.

Direct methods are, with the actual knowledge, not available for compressible flows in compressor cascades. For the indirect procedures, i.e., the prediction of the pressure distribution for a given blading, there are two principal groups of methods available for the potential flow calculation, supersonic as well as subsonic. The first one can be applied to high pitch-chord ratio, high stagger cascades with thin small cambered blades, typical for the tip section of a rotor. The methods of the second group are valid for high solidity, low stagger angle cascades. The type of blading is normally not restricted. A method for an intermediate type of cascade is still missing.

For shock boundary layer interaction regions an approach for an empirical solution has been presented, although this one has to be considered as a tentative one. Some further investigation is necessary to completely understand the interaction of a nearly normal shock with a turbulent boundary layer.

9. LIST OF REFERENCES

1. SCHOLZ, N.: Aerodynamik der Schaufelgitter, Band I.
Verlag G. Braun, Karlsruhe, 1965.

2. ROTTA, J.C.: Introduction to turbulent boundary layer calculations.
VKI Lecture Series 5, 1968.

3. KONDO, H., MINOTA, M., YAMAZAKI, N., FURUKAWA, N.: High speed tests of compressor cascades with double circular arc blade sections.
National Aerospace Lab., TR 152, 1968.

4. VAN DEN BRAEMBUSSCHE, R.: Theoretical and experimental study of choking in cascades in the Mach number range .6 to 1.2.
VKI PR 69-250, 1969.

5. MONSARRAT, N.T. & KEENAN, M.J.: Experimental evaluation of transonic stators; preliminary analysis and design report.
NASA CR 54620, 1967.

6. CHAUVIN, J. & BREUGELMANS, F.: Research on the use of blunt trailing edge blades in supersonic compressor stages.
Scientific Report N° 1, Grant AF EOAR 65-65, VKI, 1965.

7. BREUGELMANS, F. & SIEVERDING, C.: Cascade data for high camber blunt trailing edge blades. VKI IN 17, 1966.

8. CHESTNITT, D.: Noise reduction by means of inlet guide vanes choking in axial flow compressors. NASA TN D 4682, July 1968.

9. SAUER, R.: Einführung in die theoretische Gasdynamik, 3. Aufl.
Berlin, 1960.

10. SHAPIRO, A.H.: The dynamics and thermodynamics of compressible fluid flow.
The Ronald Press Company, 1954.

11. SPREITER, J.R. & ALKSNE, A.Y.: Thin airfoil theory based on approximate solution of the tran sonic flow equation.
NACA R 1359, 1958.

12. FOTTNER, L.: A semi-empirical approach of the transonic flow past cascades including shock and viscous effects.
AGARD CP 34, 1968.

13. PRICE, D.: Two dimensional compressible flow around profiles in cascade.
Proc.Seminar on Adv.Problems in Turbomachinery, VKI, March 29-30, 1965, Part I.

14. MARTENSEN, E.: Berechnung der Druckverteilung an Gitterprofilen in ebener Potentialströmung mit einer Fredholmschen Integralgleichung.
Arc. Rat.Mech.Anal., 3, 1959, pp 235-270.

15. PAL, P. Untersuchungen über den Interferenzinfluss bei Strömungen durch Tandem-Schaufelgitter. Ingenieur-Archiv, Bd 34, 1965.

16. IMBACH, H.E.: Die Berechnung der kompressiblen, reibungsfreien Unterschallströmung durch räumliche Gitter aus Schaufeln auch grosser Dicke und starker Wölbung.
Mitt.Inst.für theoretische Turbomashcinen an der E.T.H., Zürich, nr 8, 196[illegible].

17. TRAUPEL, W.: Thermische Turbomaschinen, Bd I.
Springer Verlag 1962.

18. UCHIDA, S.: Calculation of compressible cascade flow by the method of flux analysis.
J.Aeron. Sc., 1954.

19. GRIEPENTROG, H.: Prédictions des performances des grilles d'aubes transsoniques à haute déflexion et faible allongement.
Ph.D. Thesis, Univ. Liège - VKI, 1969; VKI TN 59, 1969.

20. OSWATITSCH, K. & RYHMING, I.: Über den Kompressibilitäteinfluss bei ebenen Schaufelgittern starker Umlenkung.
DVL Bericht 28, 1957.

21. ROTTIERS, H.: Optimization of blunt trailing edge blades at low speed (potential flow calculation).
VKI PR 69-237, 1969.

22. SEDDON, J.: The flow produced by interaction of a turbulent boundary layer with a normal shock wave of strength sufficient to cause separation.
ARC R & M 3502, 1960.

23. PEARCEY, H.H.: Some effects of shock induced separation of turbulent boundary layers in transonic flow past aerofoils.
ARC R & M 3108, 1959.

24. ZIEREP, J.: Der senkrechte Verdichtungsstoss am gekrümmten Profil.
DVL Bericht 51, 1963.

25. LITTLE, B.H., Jr: Effects of initial turbulent boundary layer on shock induced separation in transonic flow.
VKI TN 39, 1967.

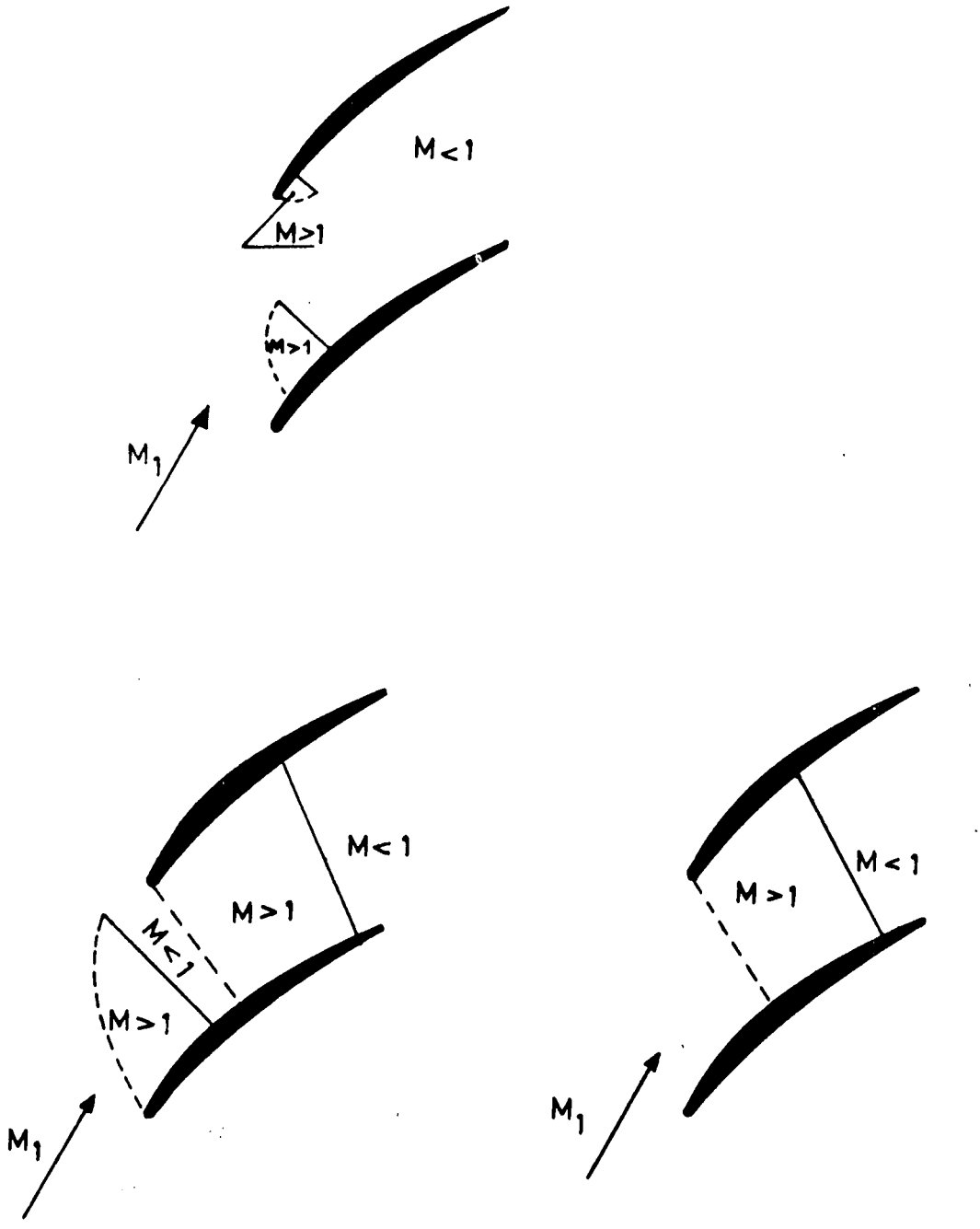

Fig. 1 Flow region in transonic cascade

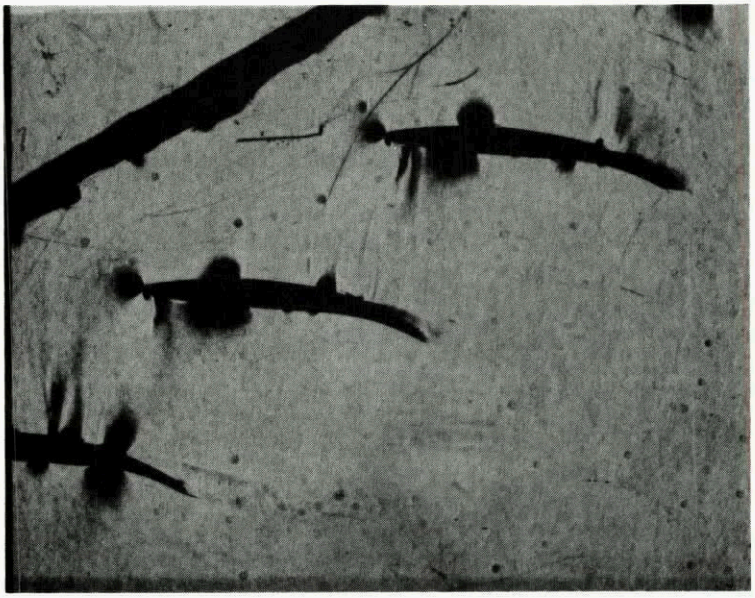

M1 = 0.736

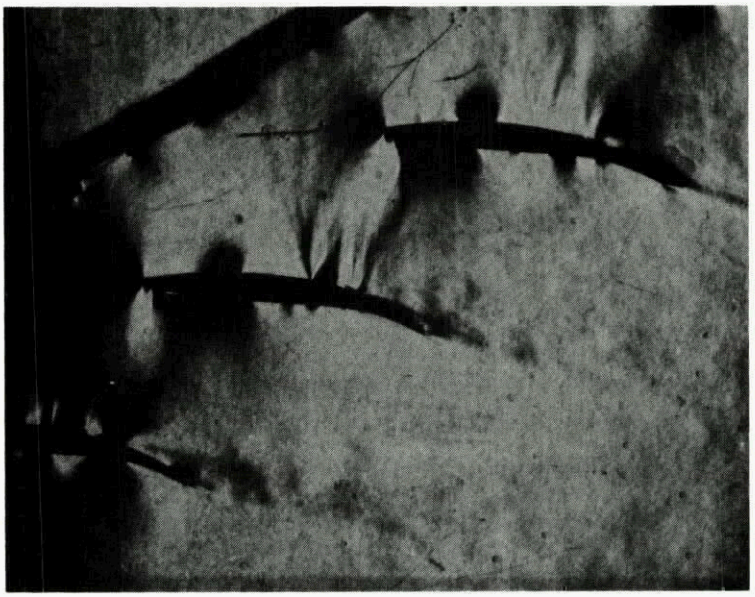

M1 = 0.767

Fig. 2(a) $\gamma = 47.2^{o}$ $\sigma = 1$ $\beta_1 = 57.2^{o}$

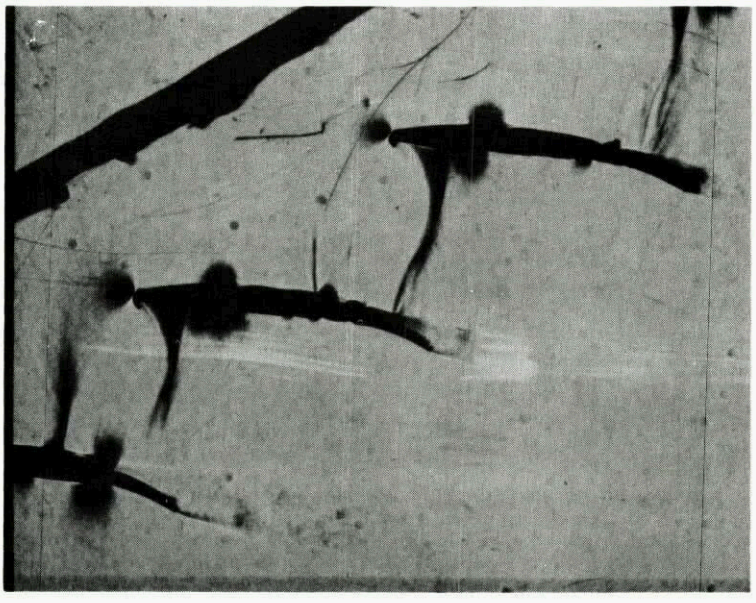

M1 = 0.824

M1 = 0.835

Fig. 2(b) $\gamma = 47.2^{o}$ $\sigma = 1$ $\beta_1 = 57.2^{o}$

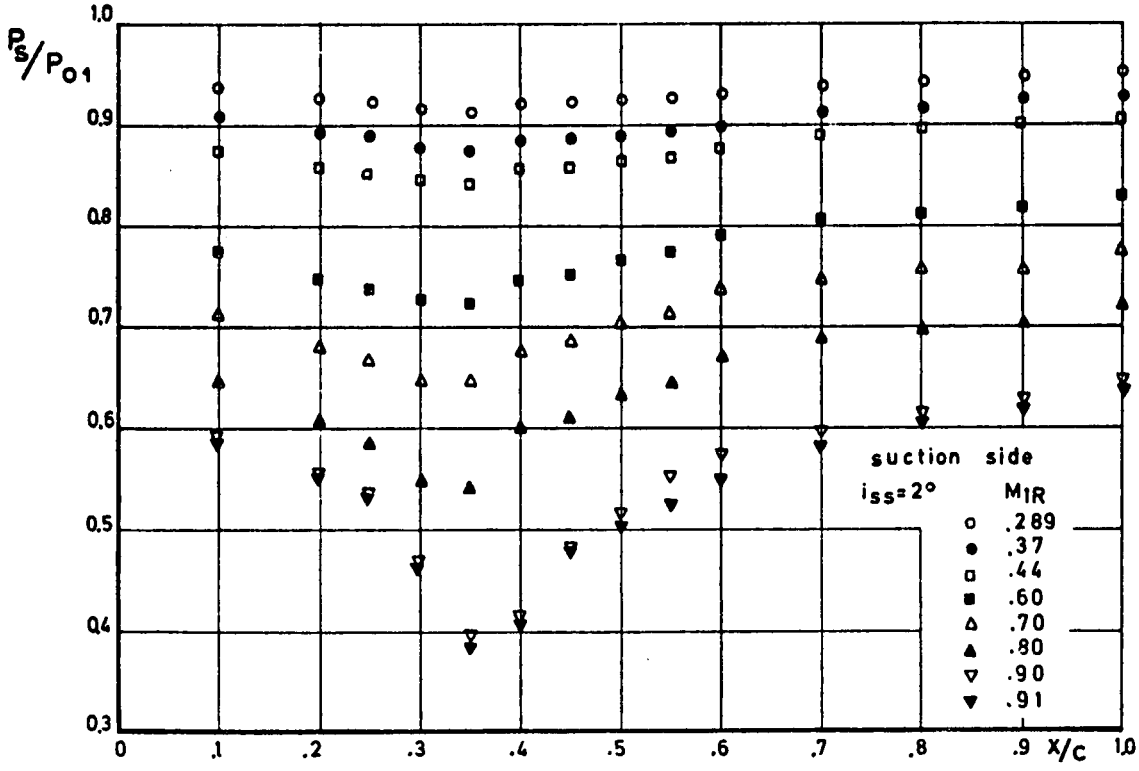

Fig. 3(a) Blade local static pressure distribution

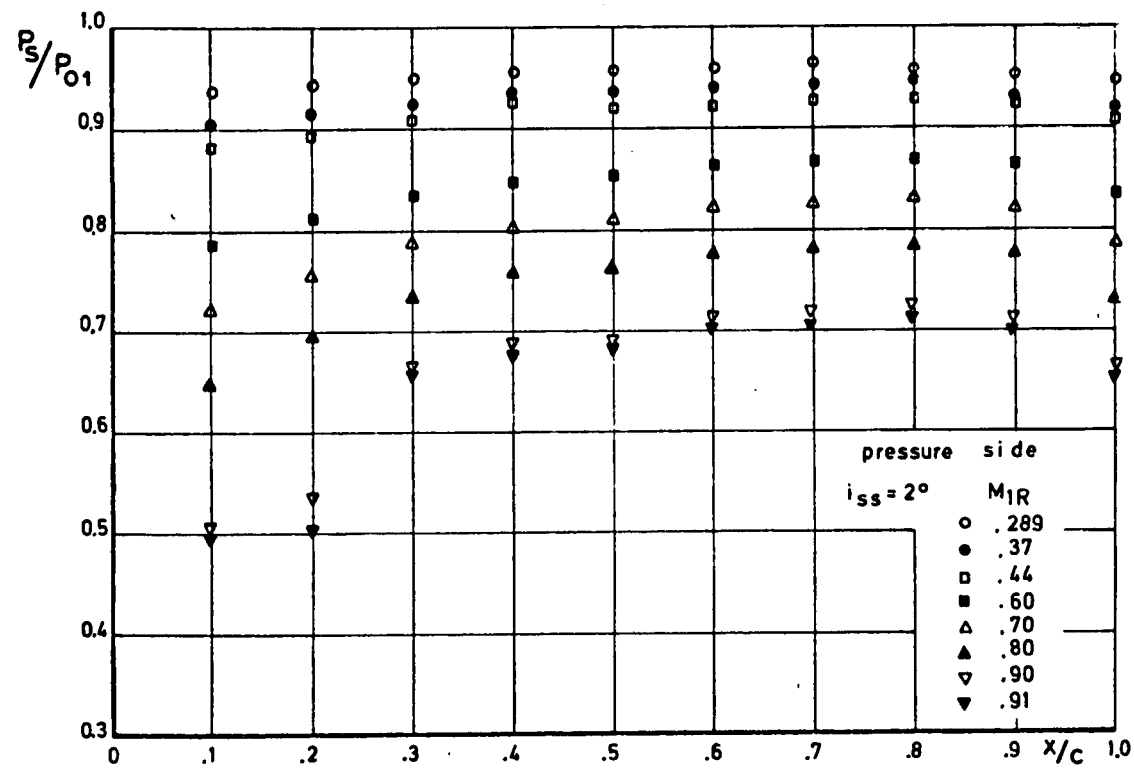

Fig. 3(b) Blade local static pressure distribution

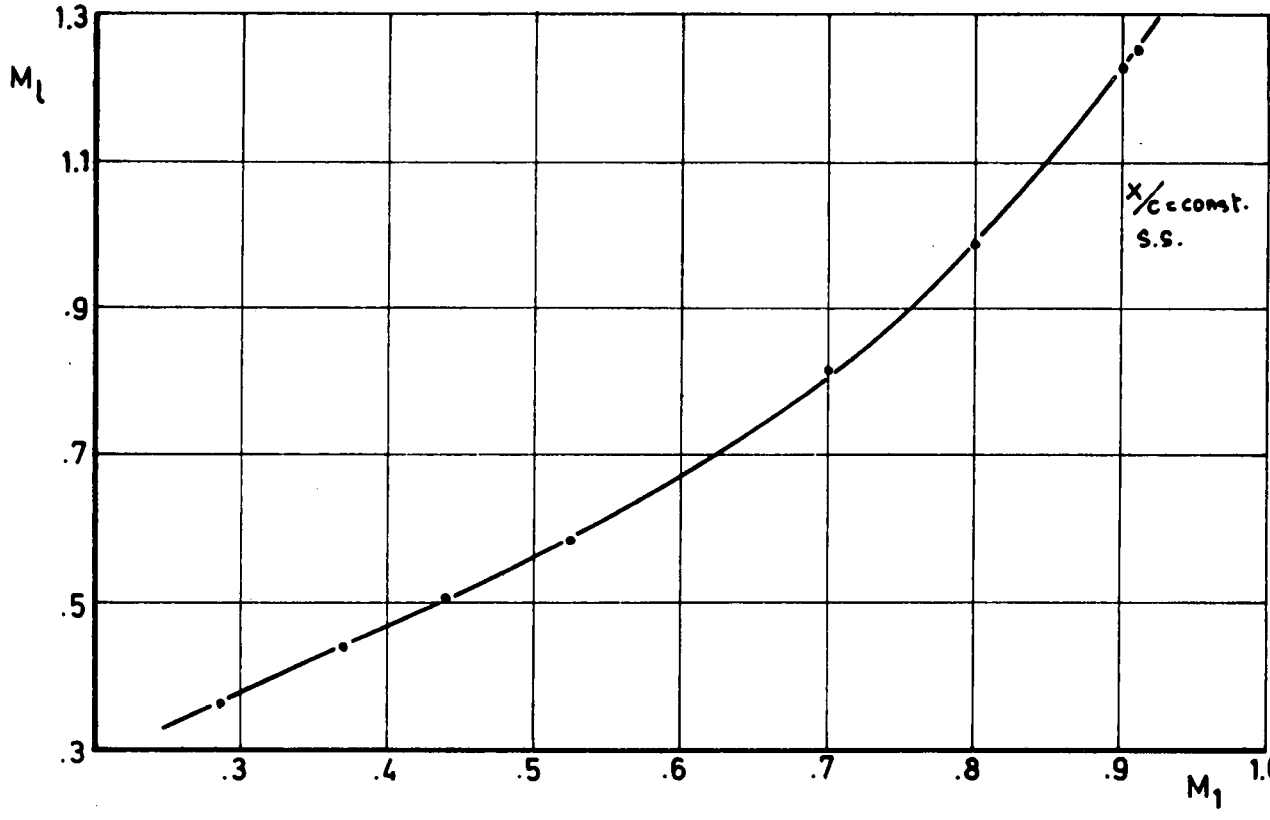

Figure 4

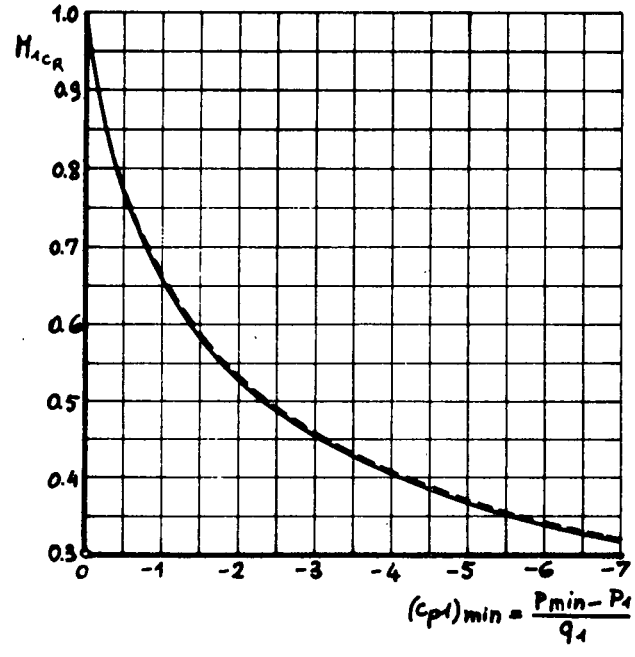

Figure 5

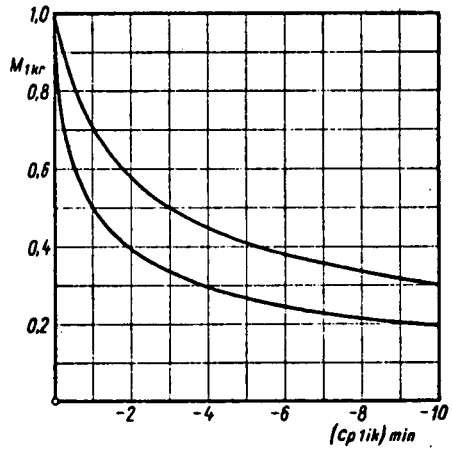

Figure 6

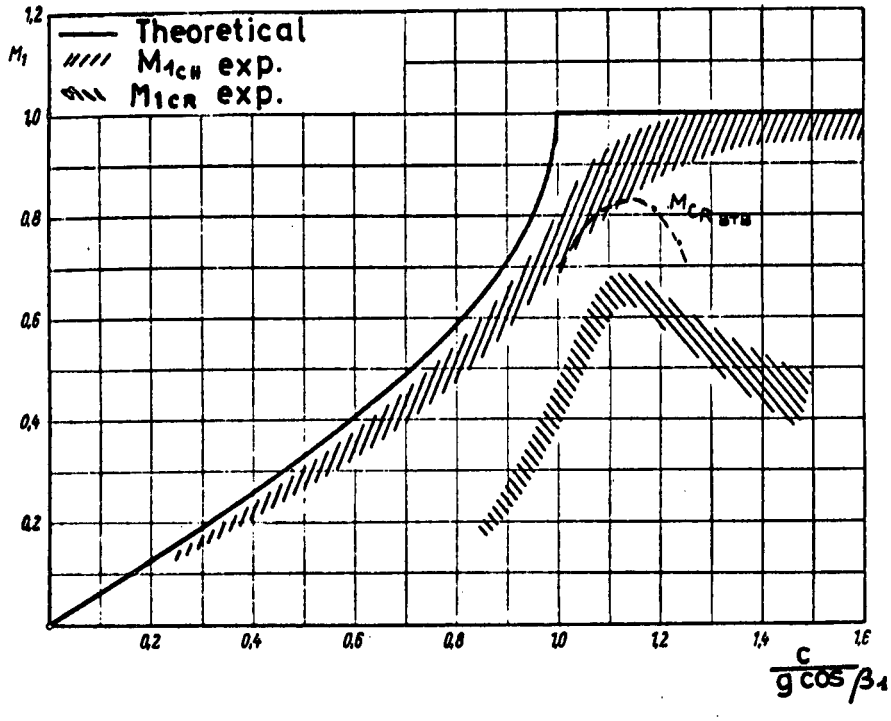

Figure 7

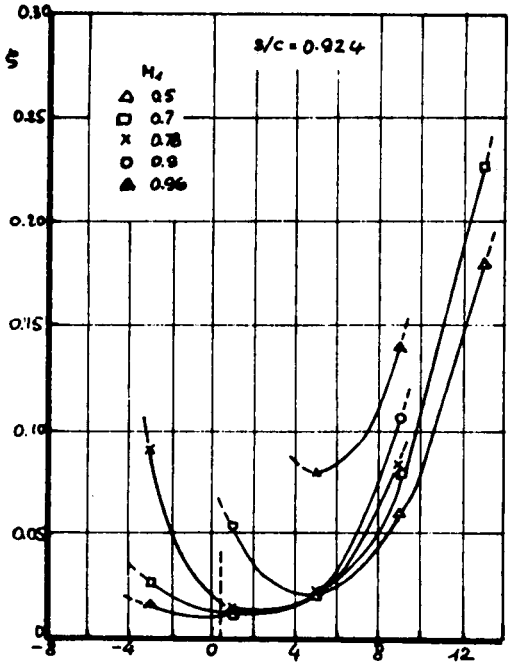

Figure 8

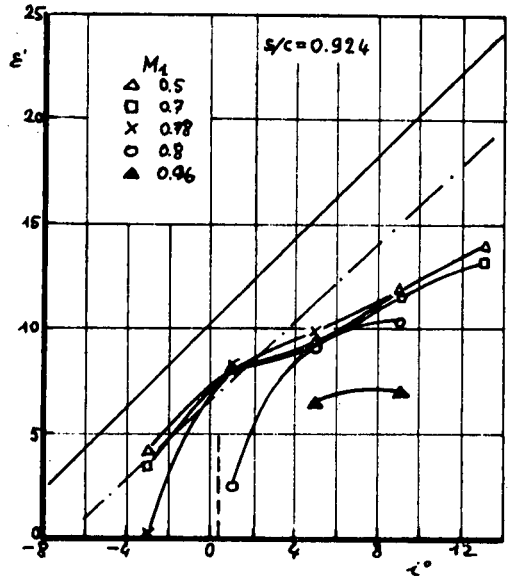

Figure 9

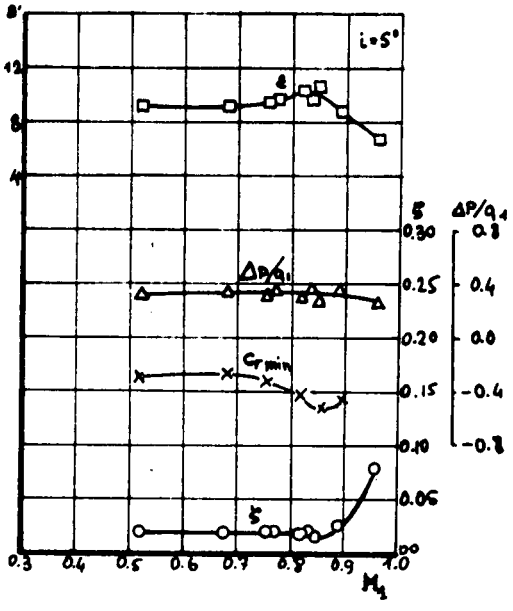

Figure 10

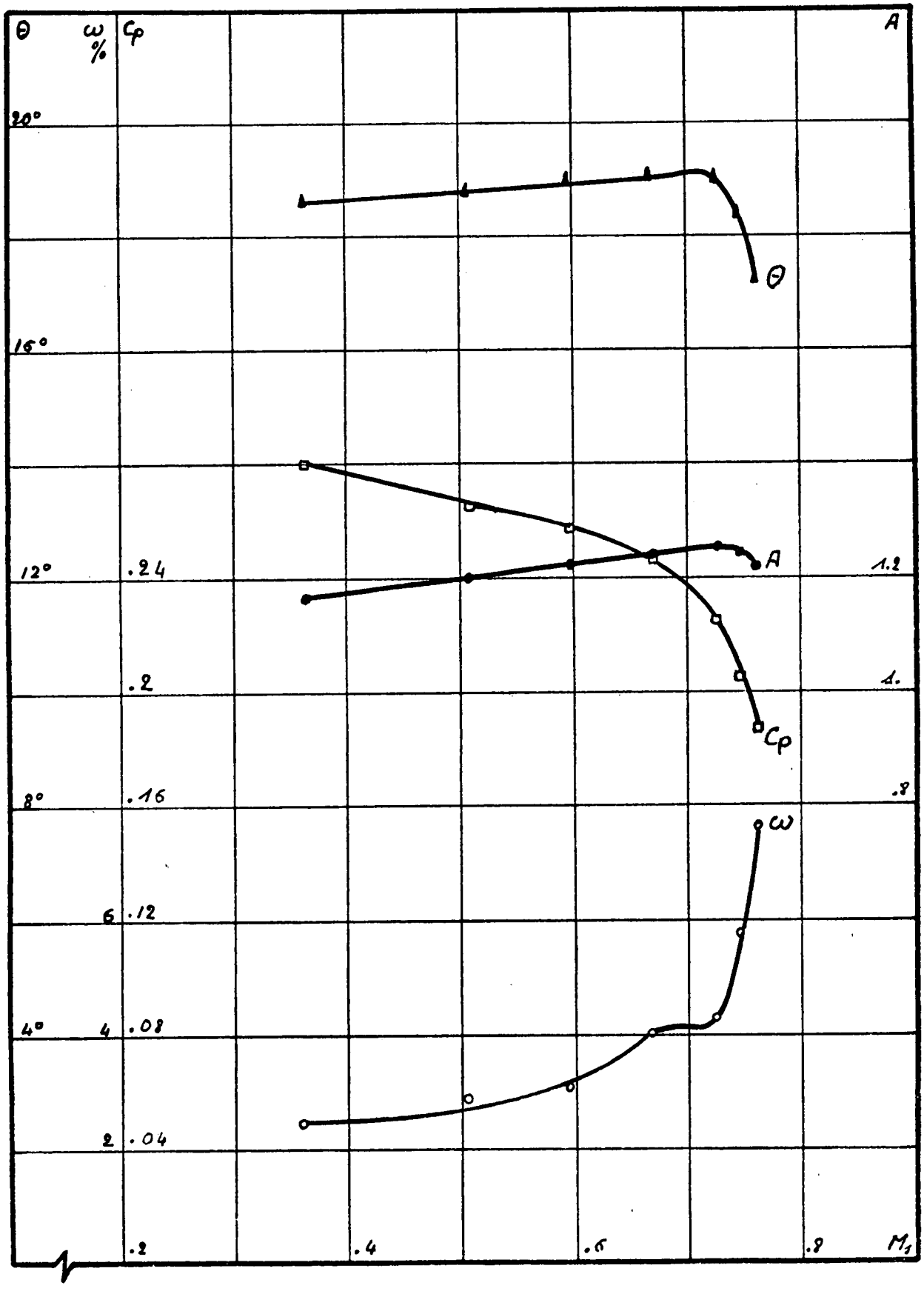

Fig. 11 General cascade performances $\alpha_1 = 70$

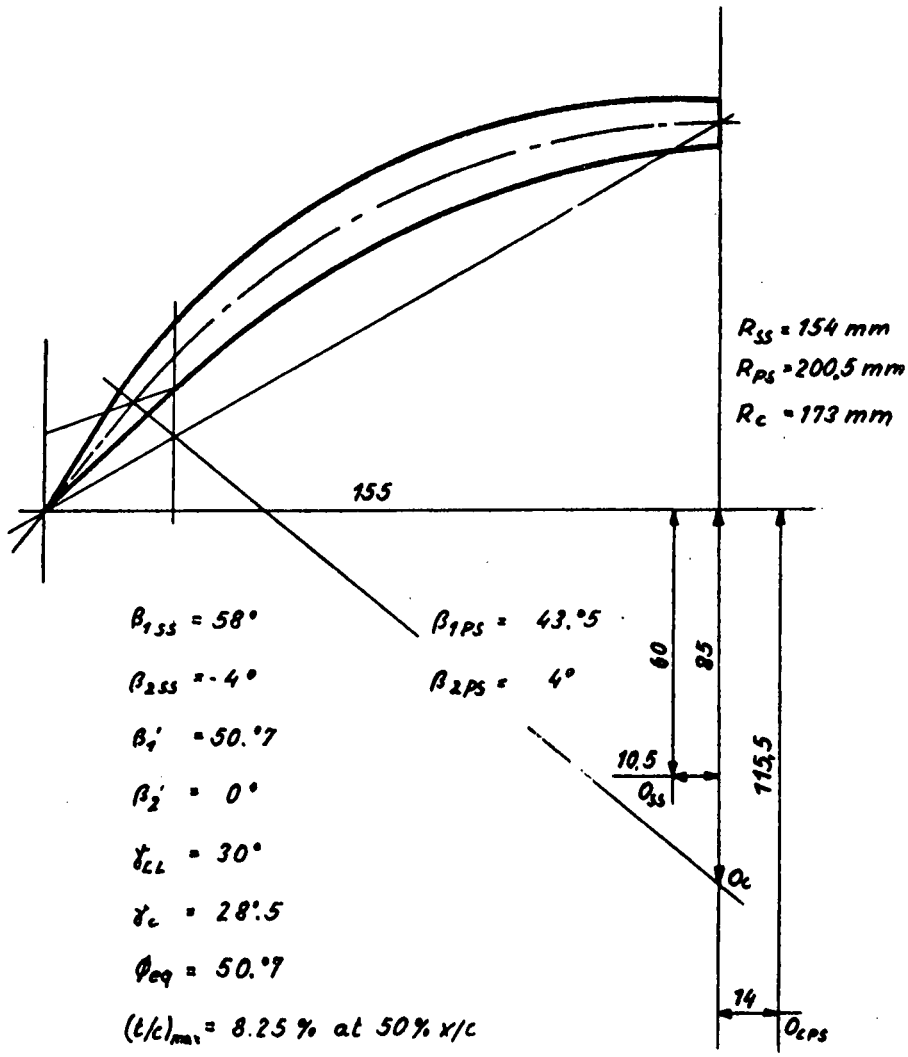

ss suction side
cl camberline
c chord

Fig. 12 Stator blading configuration

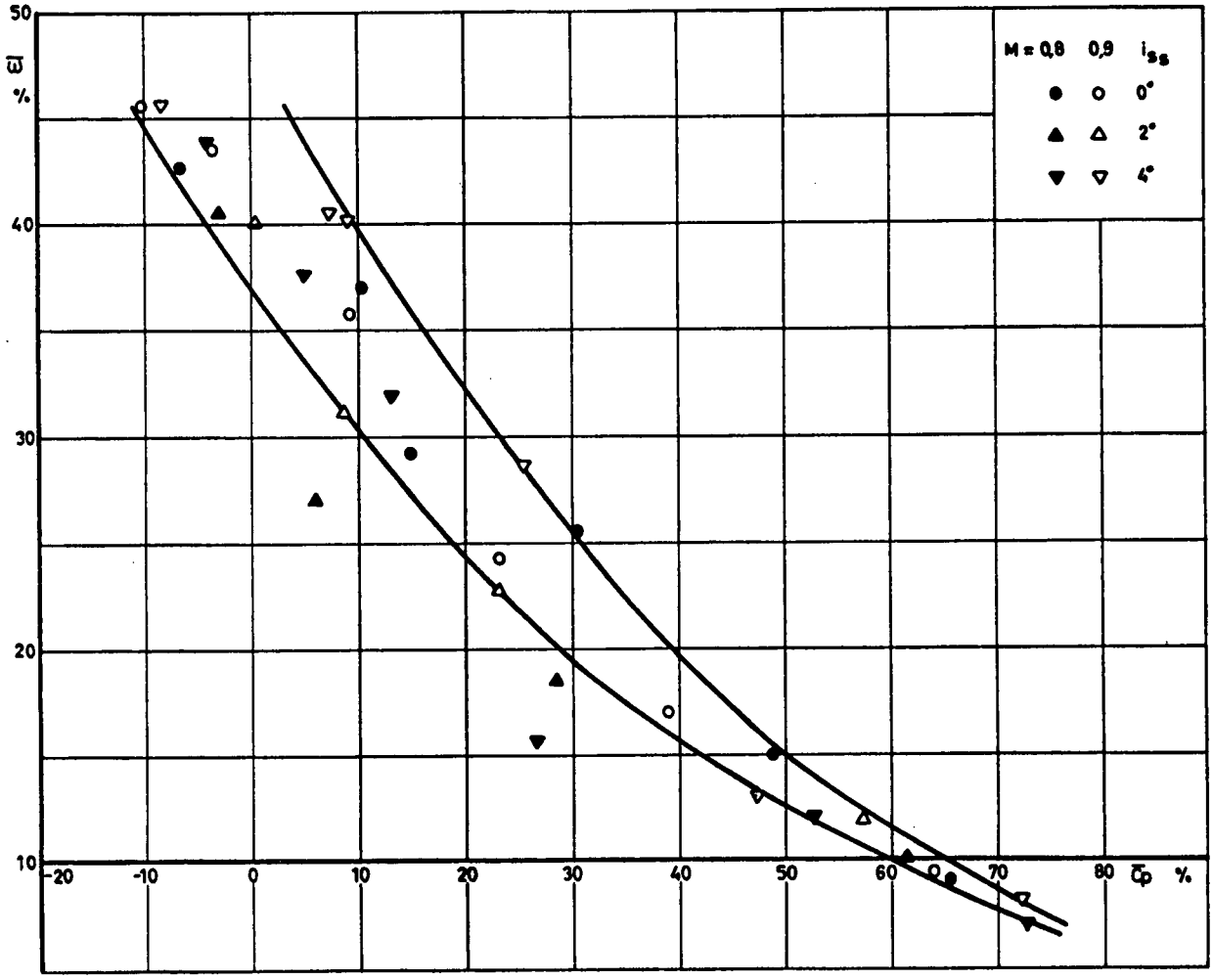

Fig. 13 BTB Cascade II $\sigma = 2$

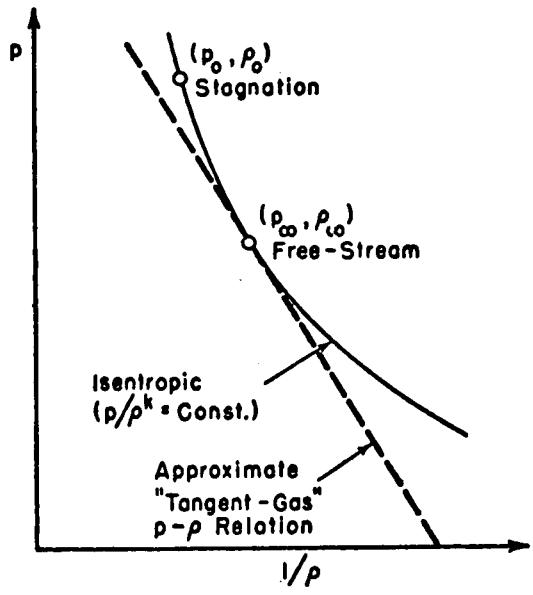

Figure 14

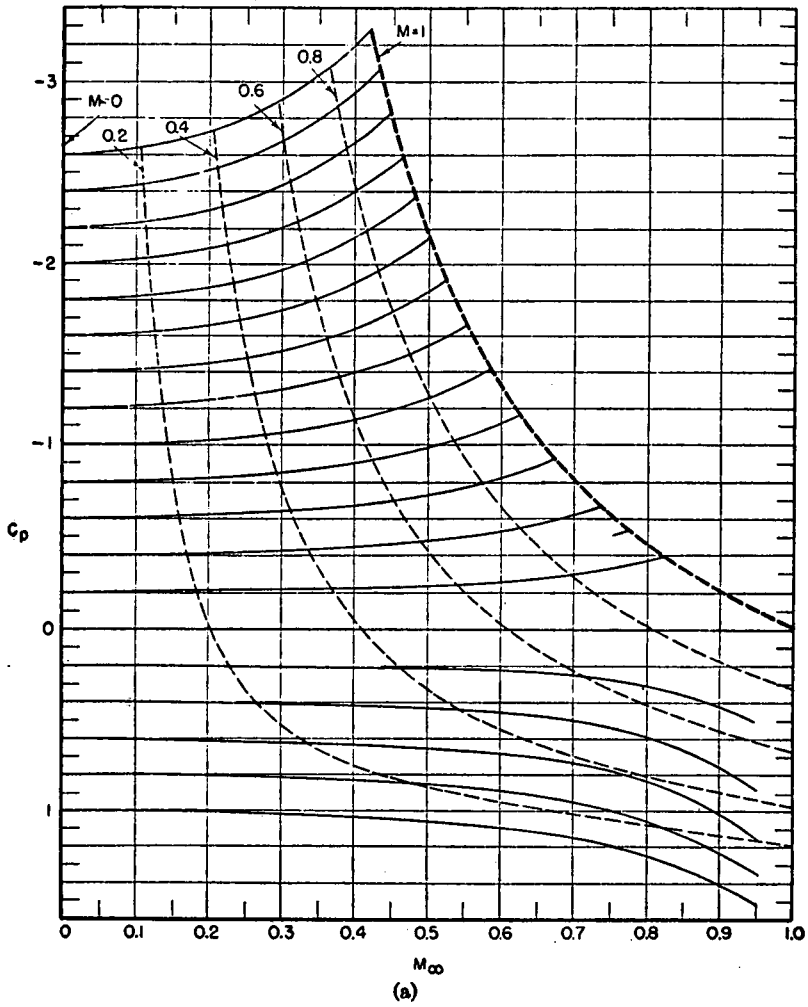

Figure 15

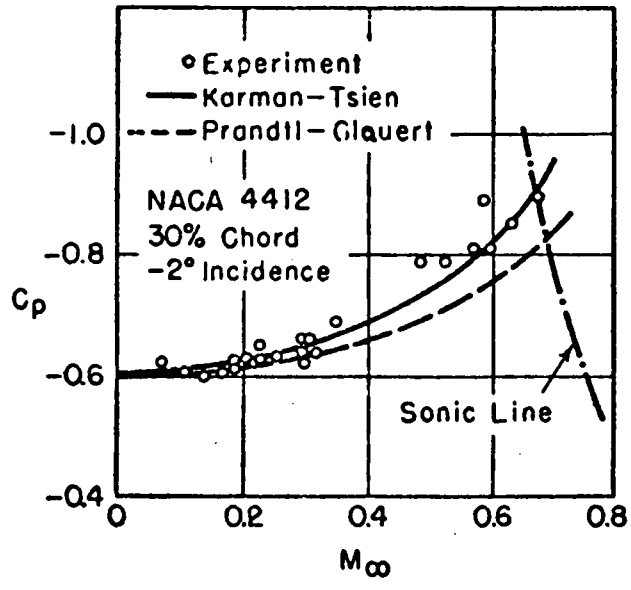

Figure 16

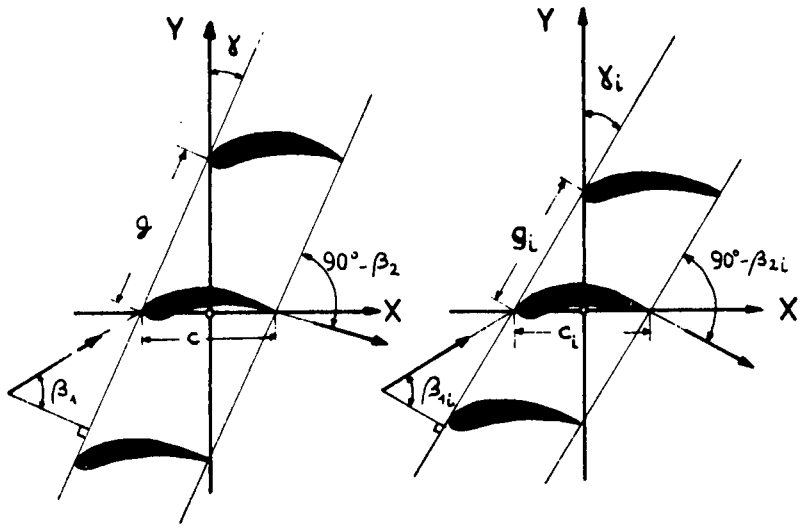

Figure 17

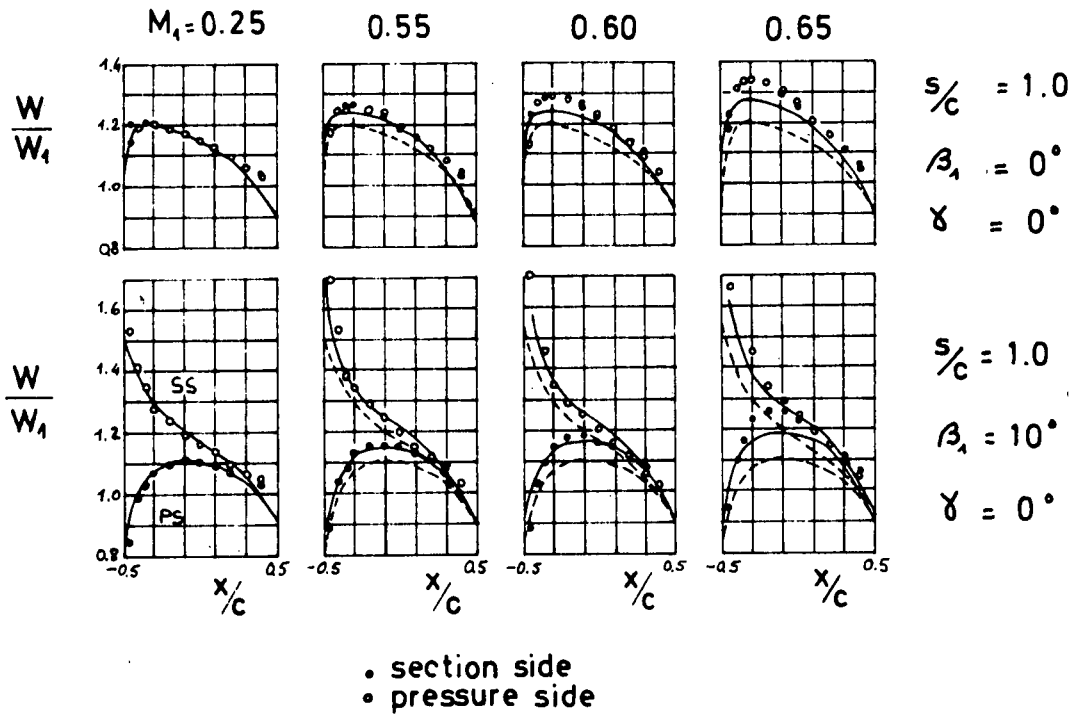

Figure 18

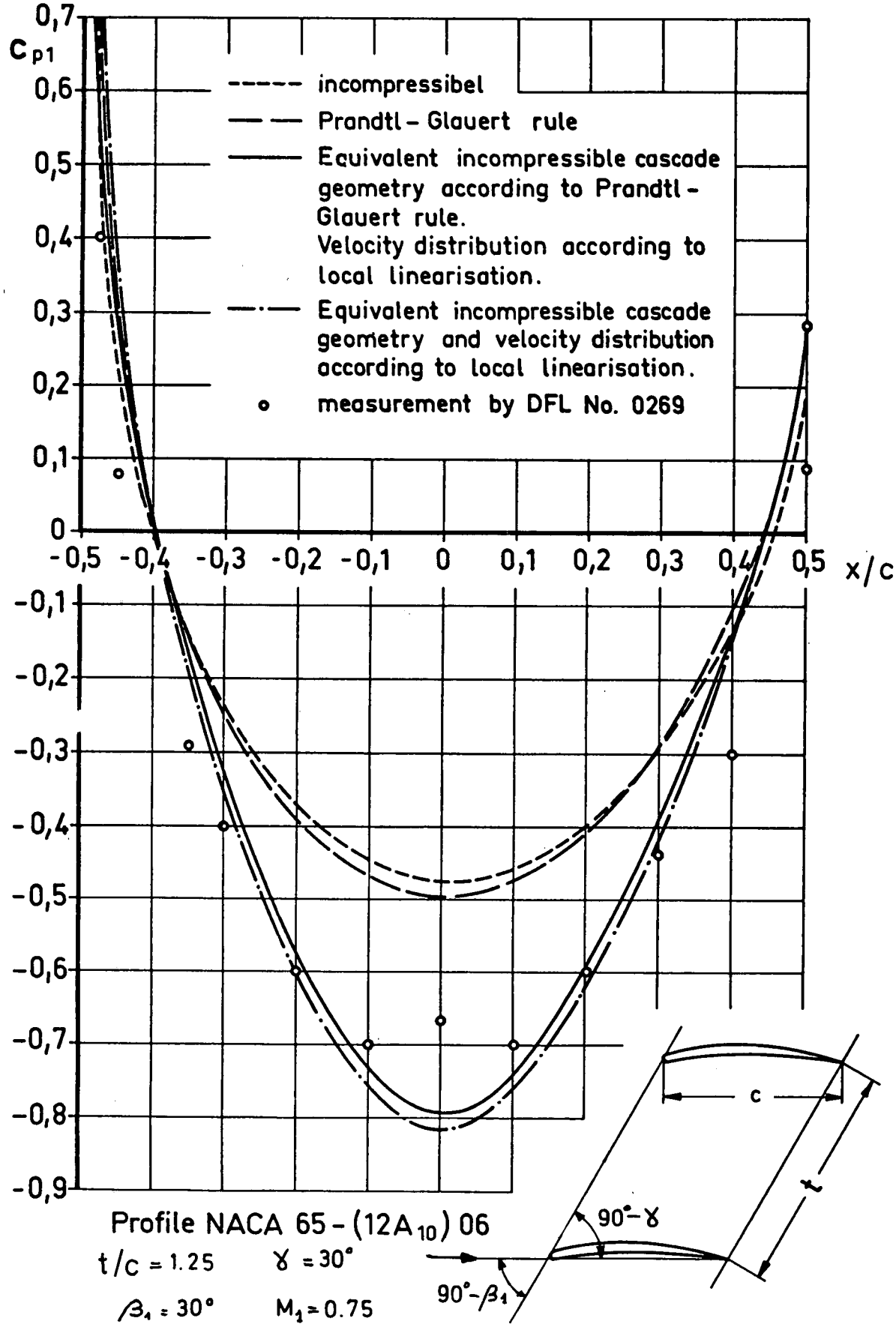

Fig. 19 Pressure distribution calculated by improved linearisation and by Prandtl-Glauert rule in comparison with measurements

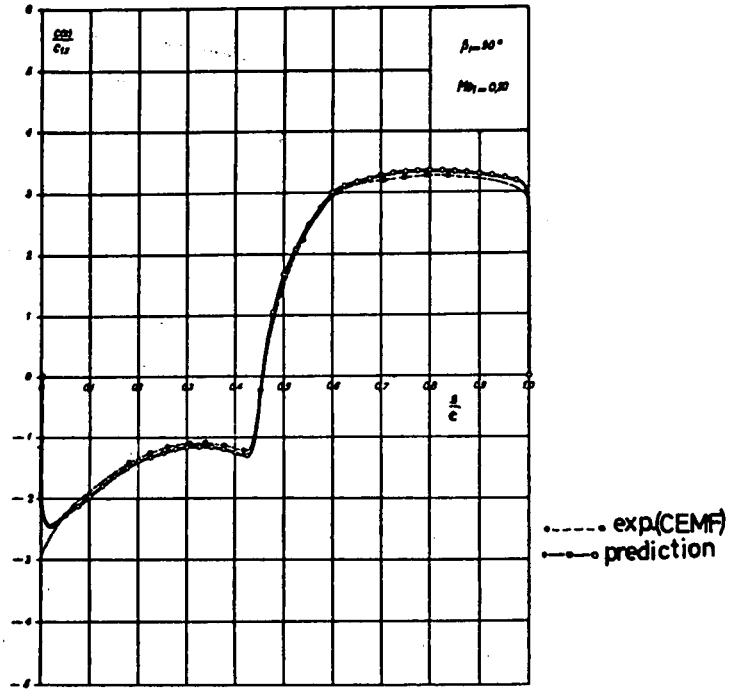

Figure 20

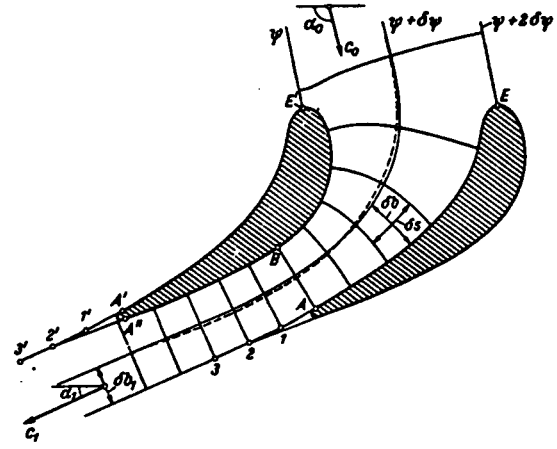

Figure 21

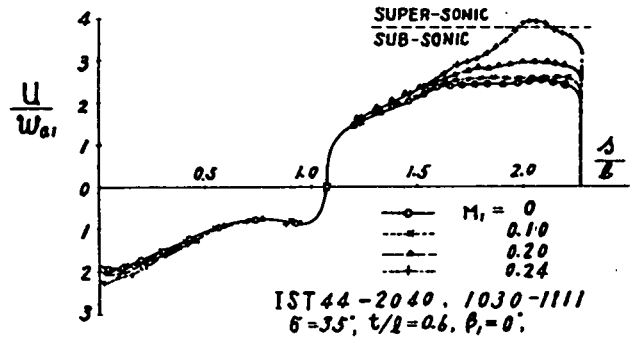

Fig. 22 Velocity Distributions

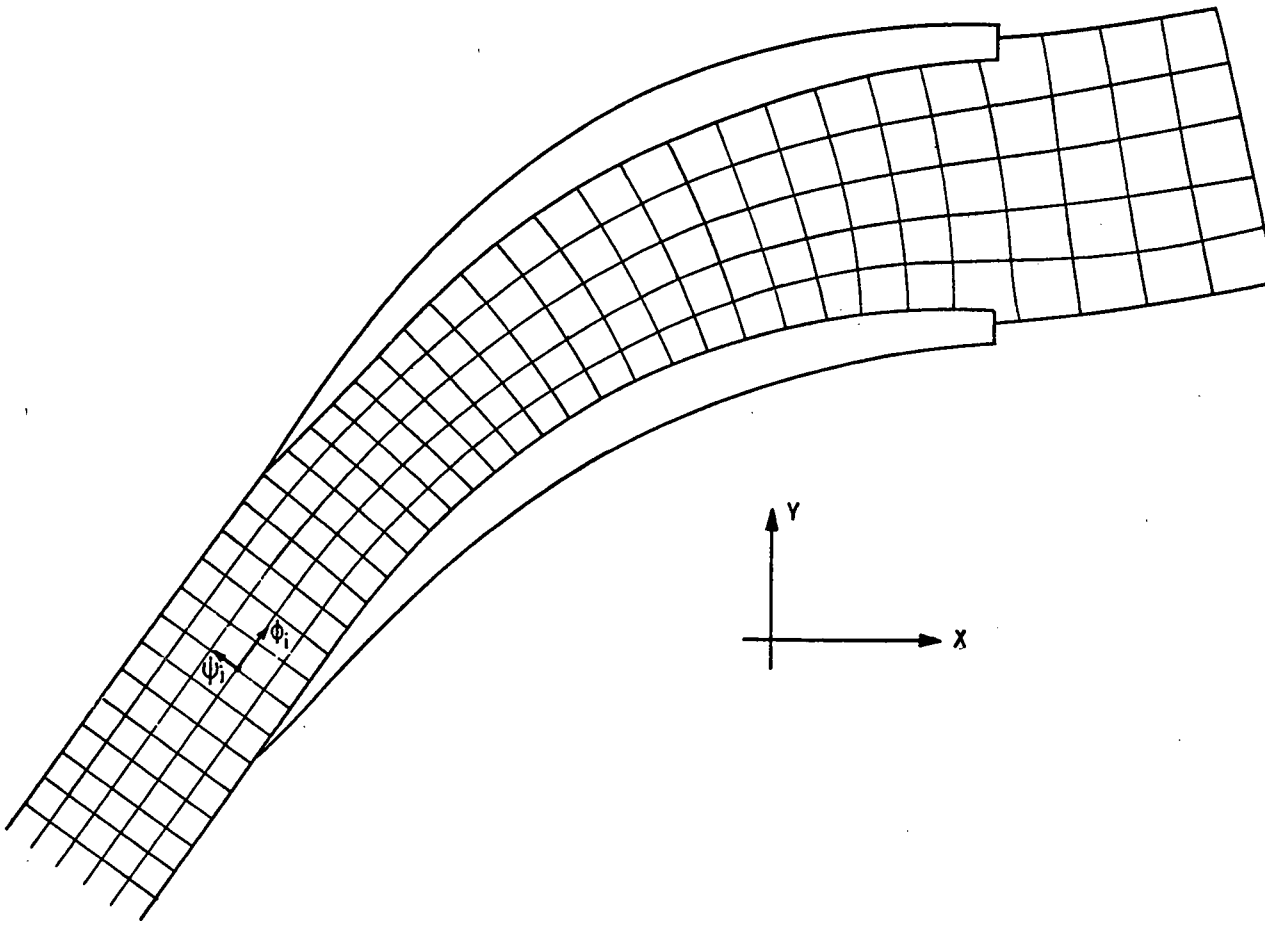

Fig. 23 Streamlines net in a cascade

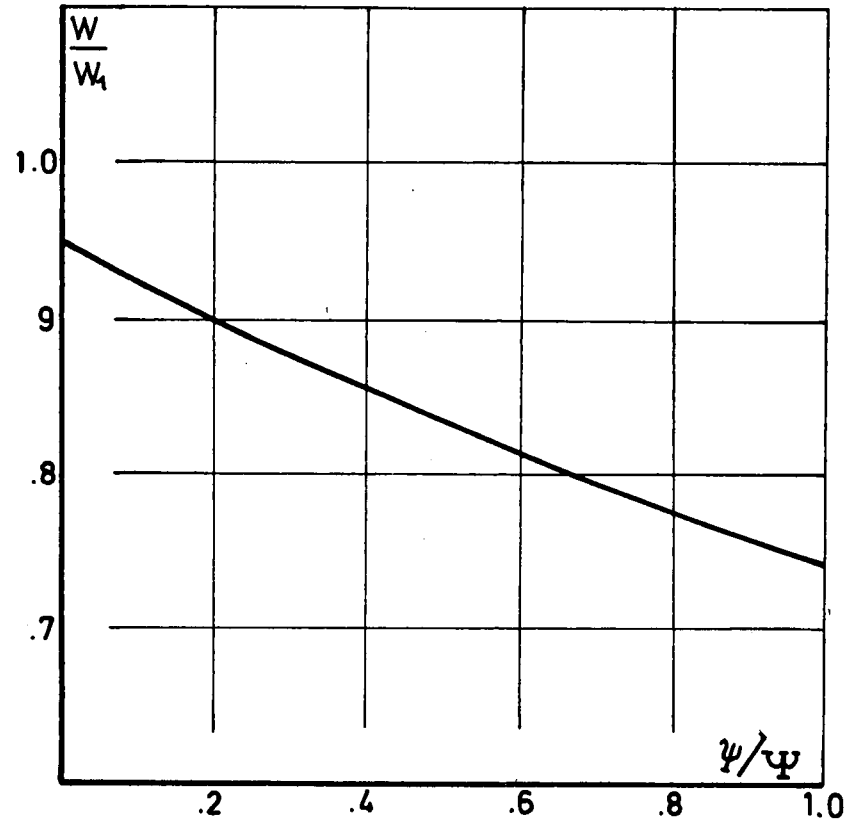

Figure 24

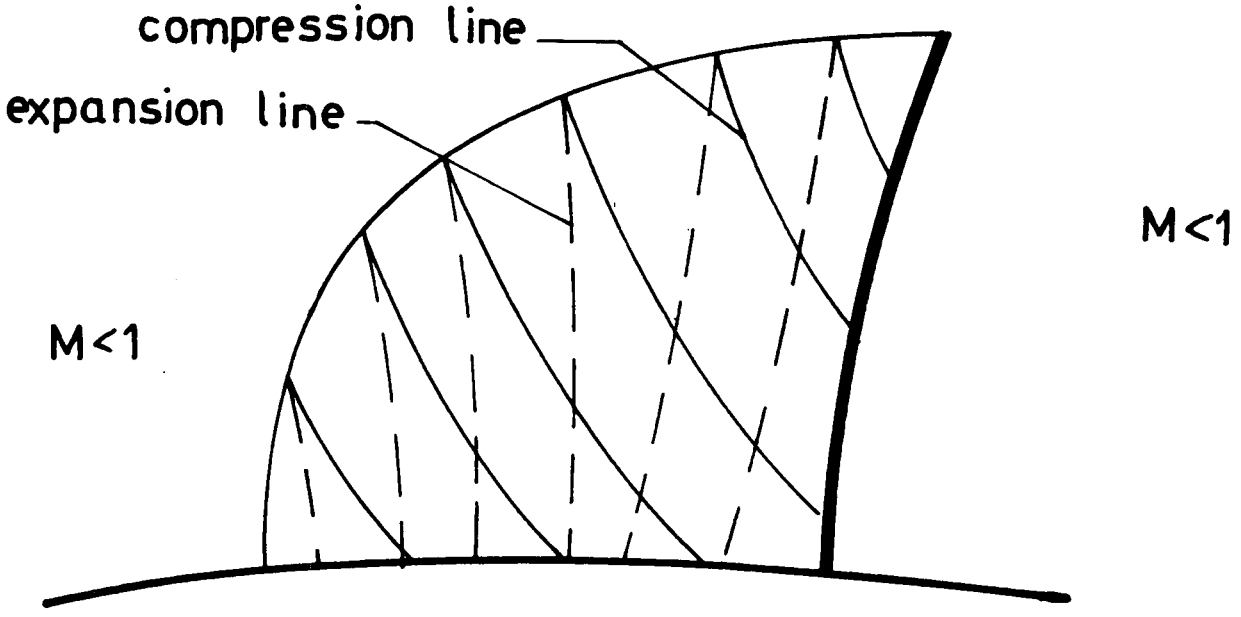

Figure 25

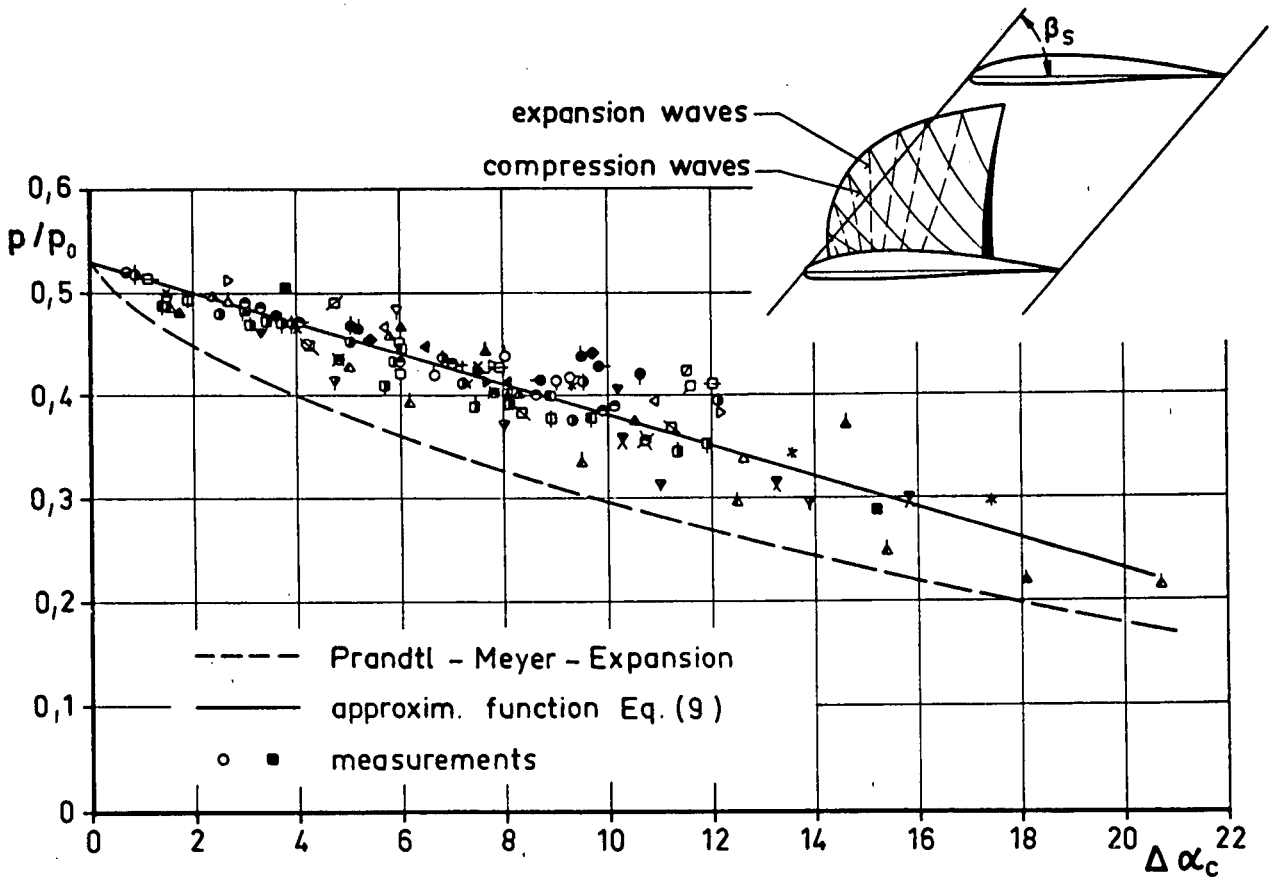

Fig. 26 Measured supersonic expansion along the profile contour in cascades

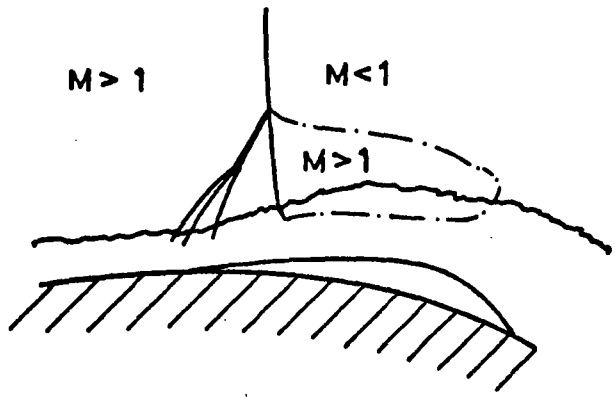

Fig. 27 Sketch of shock boundary layer interaction region

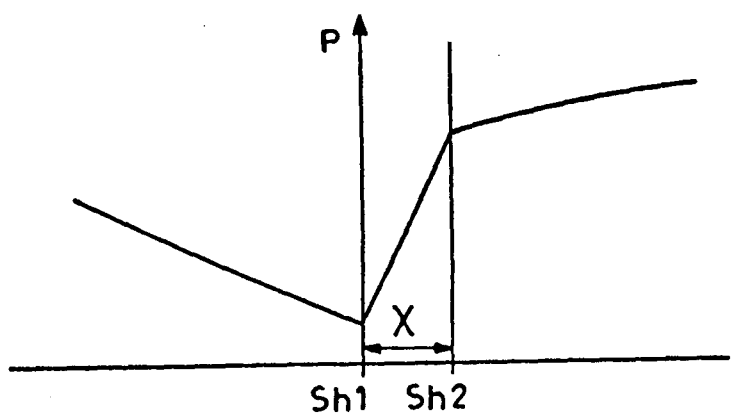

Fig. 28 Model of shock boundary layer interaction region

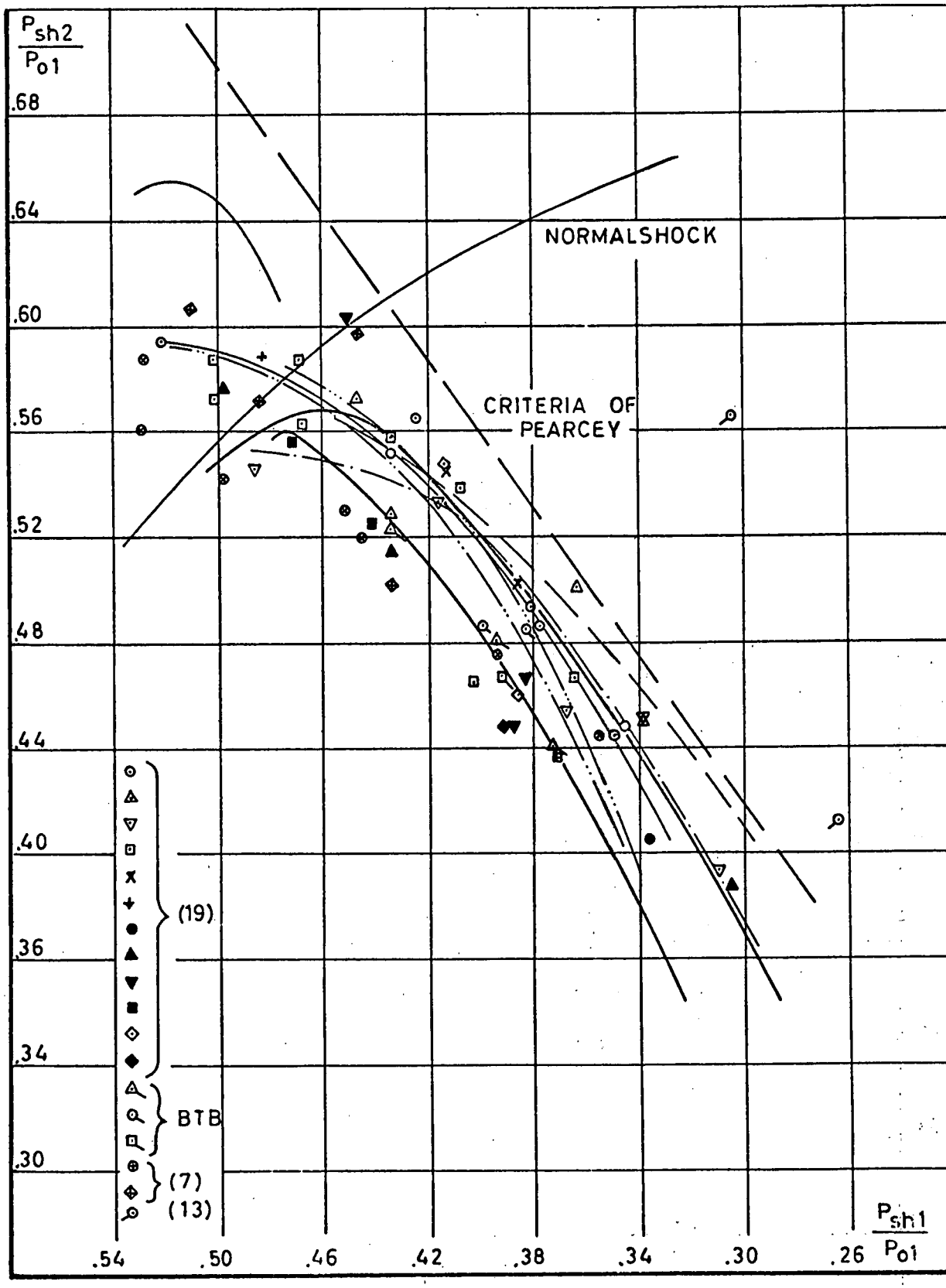

Fig. 29 Shock intensity correlation

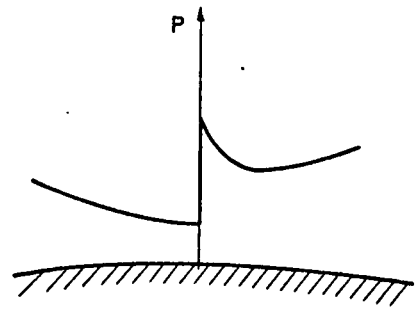

Figure 30(a)

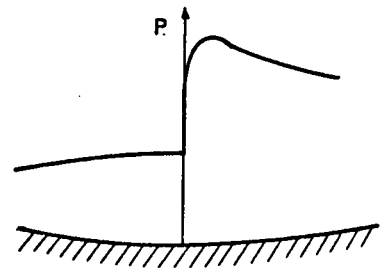

Figure 30(b)

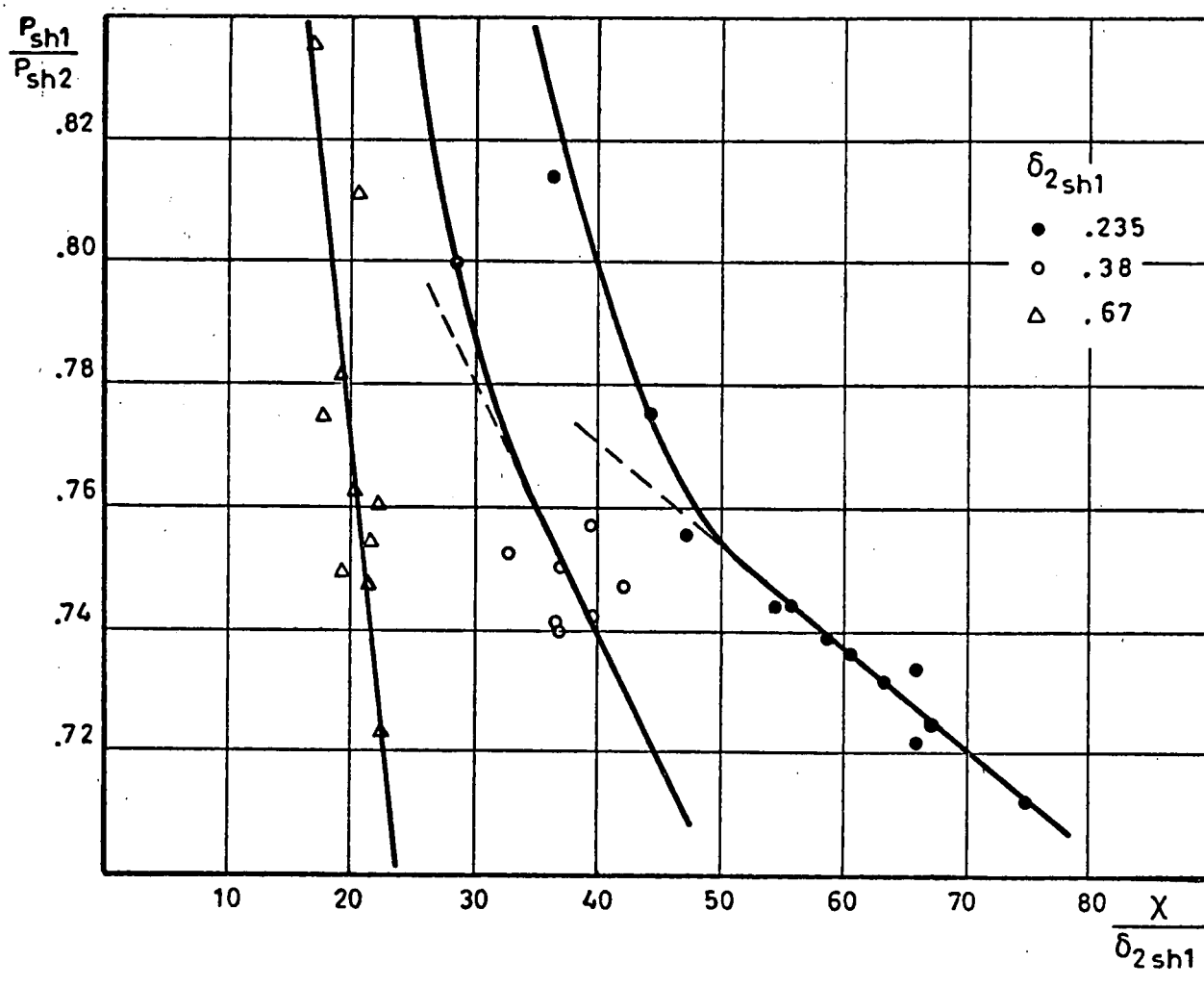

Fig. 31 Shock intensity versus displacement phase

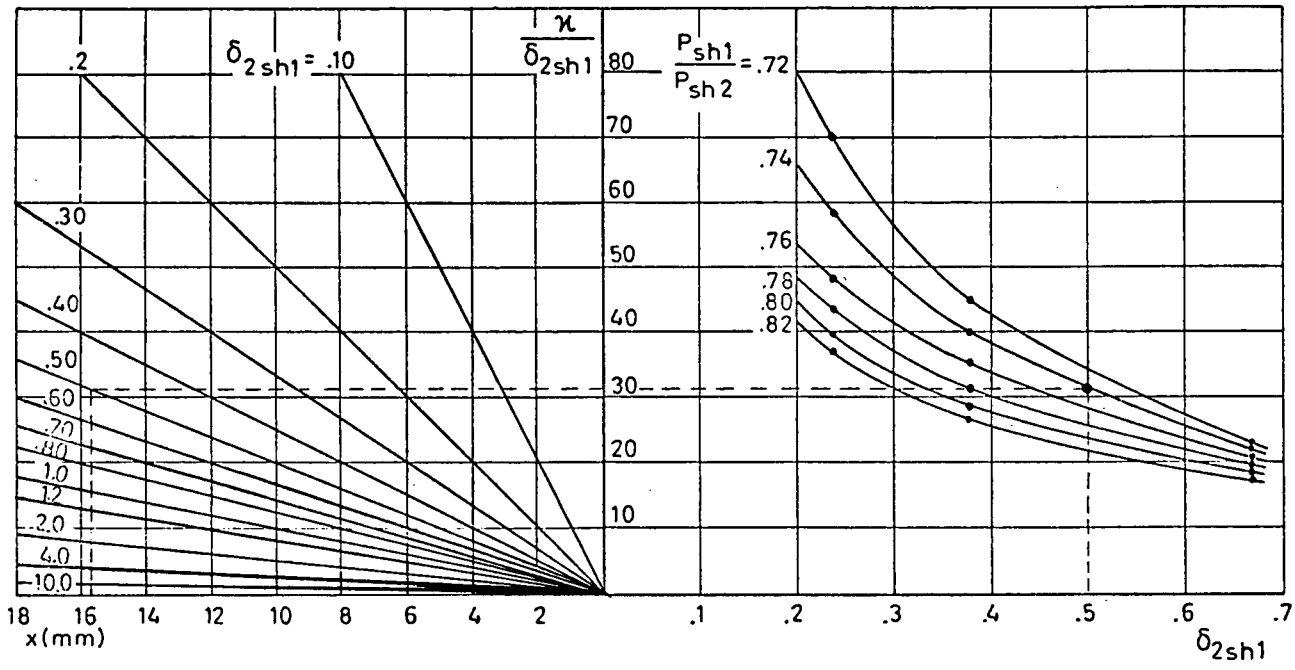

Fig. 32 Displacement phase correlation

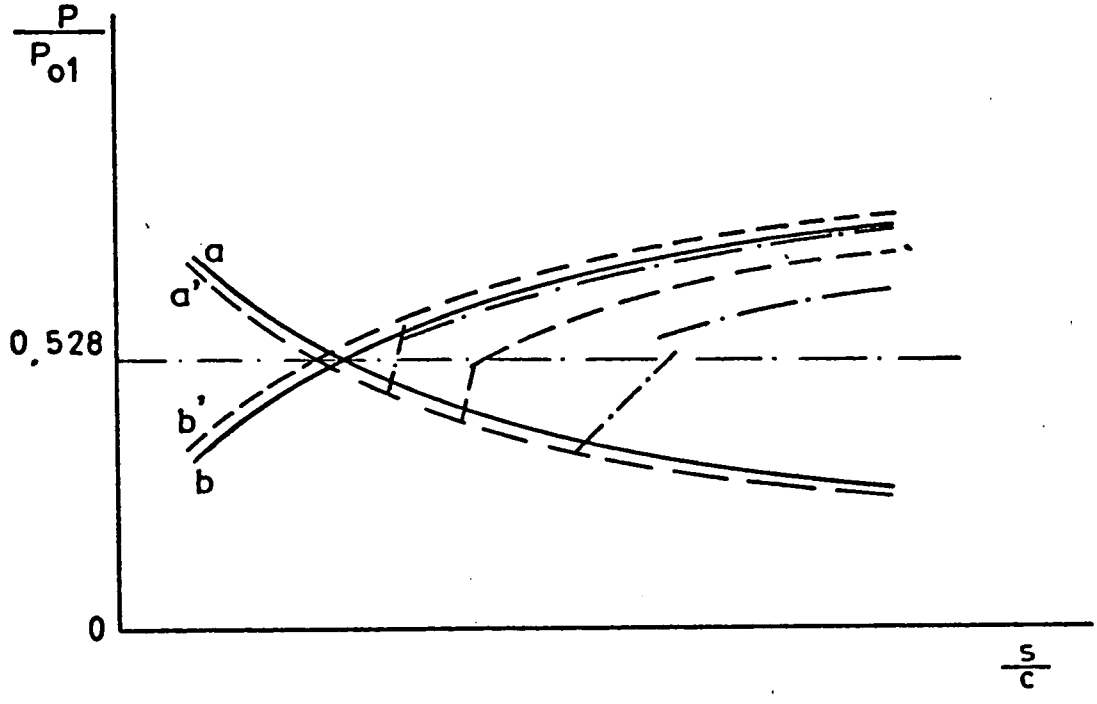

Fig. 33 Sketch for the application of the prediction method

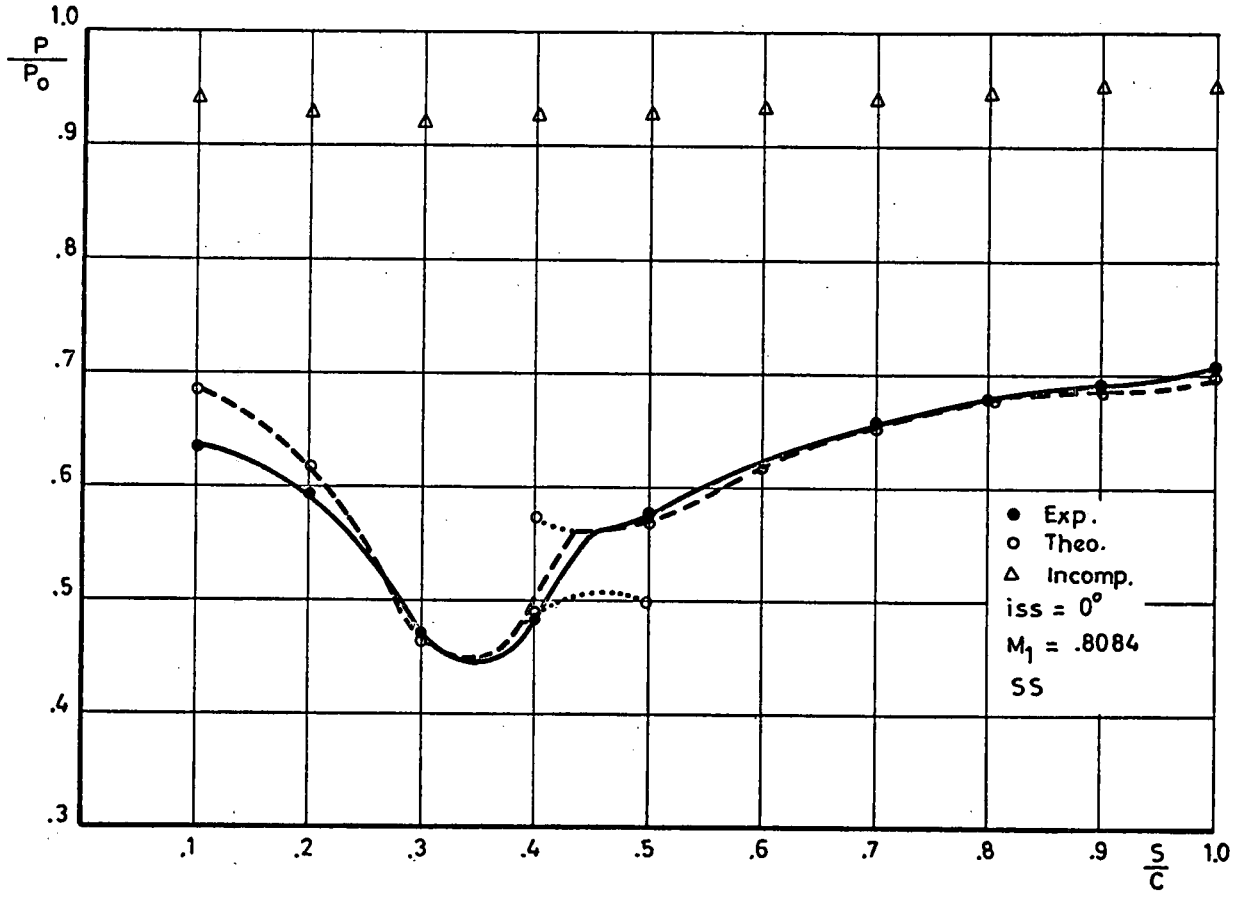

Fig. 34(a) Comparison between calculated and measured velocity distribution

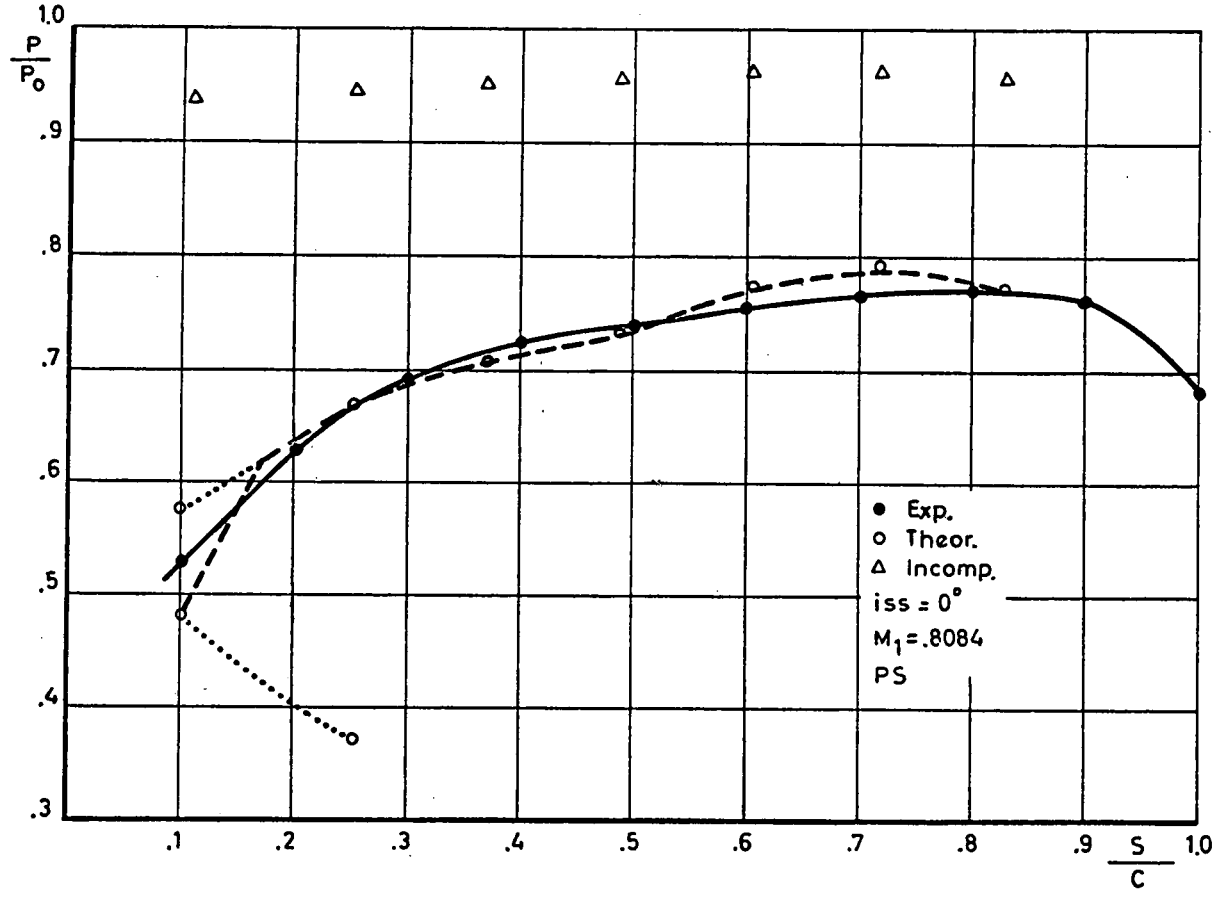

Fig. 34(b) Comparison between calculated and measured velocity distribution

S E C O N D A R Y F L O W L O S S E S
I N A X I A L C O M P R E S S O R S

H. GRIEPENTROG †
Gutehoffnungshütte Sterkrade A.G.

† formerly Project Engineer, von Karman Institute, Rhode Saint Genèse, Belgium

S U M M A R Y

The importance of secondary flows and losses in highly loaded compressor is stressed. The various types of possible secondary flows are described, and the three most usual models, representing those flows are presented, together with their limitations. The sources of the losses induced by the secondary flows are then identified, with the relevant cascade parameters, and the classical semi-empirical formula of loss evaluation (Howell, Vavra, Ehrich and Detra, etc.) are presented. Comparing the predictions made with those formulas with actual data on highly loaded compressor blading, it can be concluded that they fail in predicting correctly the losses for high camber and/or low aspect ratio bladings. A new model for secondary flow is introduced, based on boundary layer growth on the hub or casing and a horse-shoe vortex model (as suggested by Carter and Cohen) and a formula is derived, which appears to be valid for a larger range of blading configuration. Effects of secondary flow on outlet flow direction are then treated. Finally, the methods available to reduce secondary flow losses are discussed and then the range of application is defined.

LIST OF SYMBOLS

A	aspect ratio
c	chord
C_L	lift coefficient
C_D	drag coefficient
h	blade height
h'	blade height of replacement blade
p	pressure
q	dynamic pressure
s	pitch
x,y,z	cartesian coordinate system
u,v,w,	velocity components
β	relative flow angle
δ	boundary layer thickness
ω	total pressure loss coefficient
ρ	density
σ	solidity
θ	camber angle
ξ,η,ζ	vorticity components

Subscripts

o	stagnation point conditions
i	induced
m	meridional
s	secondary flow effect
1	upstream
2	downstream

LIST OF FIGURES

SECONDARY FLOW LOSSES IN AXIAL COMPRESSORS

H. Griepentrog

1. INTRODUCTION

In relation with the design of high specific energy turbomachines, the secondary flow effects are of considerable importance. In figure 1, the total pressure loss distribution along the blade height is shown for the rotor blading of a supersonic compressor of the type shock-in-rotor, which is characteristic for the new generation of small axial compressors. For the construction of this distribution, which has to be known for the application of any three dimensional or quasi-three dimensional flow calculation method in an axial machine, one must take into account the shock losses, profile losses, mixing losses due to the blunted trailing edge of this blading and the secondary loss. In figure 1b, the measured total pressure loss distribution indicates, for different values of back pressure, the high amount of secondary loss for this type of blading, which has, actually, an aspect ratio far below unity.

In the following, we shall sketch the physical behaviour of secondary flow and the possibility is discussed of using some theoretical and empirical methods for the prediction of the secondary loss for high cambered bladings with low aspect ratios.

2. PHYSICAL PICTURE OF SECONDARY FLOW

'Secondary flow' in the turbomachinery domain is normally described as the difference between the real flow and the two dimensional flow in a cascade or the difference between the real flow and the hypothetical flow through a stage constructed by dividing the flow section into a number of streamtubes with axisymmetric two dimensional flow. Hence, the secondary flow is due to the interaction of the side wall or casing boundary layer with the main through flow.

The different flow features represented by the designation 'secondary flow' can be split down, using figure 2 :

1) cascade secondary flow,
2) trailing vortices,
3) tip leakage flow in unshrouded bladings,
4) radial flows,
5) scraping flow effects in unshrouded bladings.

Two pairs of vortices are formed in the downstream flow field of a blade row. A pair of corner vortices placed in the corner formed by the suction side of the blading and the casing and a pair of bulk vortices in the main stream.

The bulk vortices or cascade secondary vortices are due to the boundary layer upstream of the cascade. A relatively sound representation of this flow can be obtained using the model of a gyroscope. The boundary layer upstream of the cascade can be represented with a vortex sheet. A turning of these vortex filaments around an axis parallel to the blade span results in a vortex pair parallel to the flow direction downstream of the cascade.

The vortex sheet attached to the trailing ed e of the cascade blading originates from a variable distribution of circulation along the blade span due to a variable camber of the blading or a non-uniform inlet velocity distribution. A vortex sheet is unstable in real flow and rolls up into a single vortex. In our case, a vortex pair is formed in opposite direction of rotation. In real flow measurements, it is impossible to distinguish the trailing edge vortex from the corner vortex formed by the interaction of the boundary layer accumulated in the corner of the suction side of the blade and end wall.

The tip leakage flow is due to two effects. The slot between casing or shaft and blades allows for a part of the mass flow not to participate at the energy exchange. In addition, a tip vortex is formed due to the pressure difference on the suction and pressure side of the blade.

The scraping flow vortex is formed by the relative motion between the casing and the blades. Ths effect is of a certain importance only for high circumferential speeds.

In a similar way to the overturning in the side wall boundary layer, low energy material is transported along the blade span, mainly in the rear part of the blade. The direction and amount of radial flow depends on the type of blade design (free vortex or forced vortex, stator or rotor).

Secondary flow models

The complex mechanism of secondary flows is not completely understood up to now, because it is principally a three dimensional boundary layer problem. This boundary layer separates and rolls up into a vortex, a problem which cannot be solved with the actual knowledge.

The research in secondary flow has made considerable progress thanks to the use of two different models: the inviscid model and the viscous model, sketched in figs. 3 and 4. Recently, it has been found out that these two models fail to describe the secondary flow for highly loaded bladings with a low aspect ratio. A third model should be used based on the analogy with a rectangular bend (ref. 2).

The inviscid model neglects the viscous effects in the blade passage. Only the influence of the nonuniformity of the flow upstream of the cascade is considered on the downstream flow. The two cascade secondary vortices,parallel to the downstream flow direction, are formed. An analytical treatment is possible as shown by the classical papers of Squire and Winter and Hawthorne (refs 1 and 3). Squire and Winter found a relation between the vorticity downstream of the cascade, the camber angle of the blade and the velocity gradient in direction z :

$$\xi_z = - 2\theta \frac{\partial U}{\partial z} \qquad (1)$$

with the assumption that the vorticity is zero in direction of the upstream flow.

Due to the very restrictive assumptions necessary to arrive at eq. (1), the inviscid model can only be used for the description of the flow in high aspect ratio and small cambered bladings. The model cannot be used for the blading necessary for small high specific energy turbomachines.

The viscous model takes into account the viscous effects inside of the cascade. The development of the corner vortices (fig. 4) which are determined with this model, can be described physically using the condition of equilibrium between the centrifugal forces created by the curvature of the streamlines and the static pressure gradient between two neighbouring blades. The boundary layer fluid on the end walls has to support the same pressure gradient as the main flow, but the kinetic energy is smaller. Hence, the boundary layer material is deflected from the pressure side to the suction of a blade channel. In the corner formed by the suction side and the end wall, the boundary layer material accumulates and the corner vortex is formed by the interaction with the main flow. The creation of the corner vortex can be described by representing the boundary layer on the end wall by a vortex sheet. The deflection of this vortex sheet in the corner between end wall and blade results in a self-induced roll up of the vortex sheet.

This description is confirmed by the flow visualization with titaniumdioxyde presented in figure 5.

An analytical treatment of the flow described by the viscous model is not possible in the actual state of knowledge.

3. SECONDARY FLOW LOSS

The cascade secondary models treated in the preceding chapter can a give a physical description of the secondary flow, but not of the secondary losses in which the turbomachine desginer is interested in. Most probably, the following factors will have a certain influence on the magnitude of the secondary loss:

1) the cascade secondary vortices and corner vortices,
2) the interaction of the corner vortices with the main flow,
3) the separation on the side wall.

Detra (ref. 4) has shown that the energy bounded in the vortices can be neglected in comparison to the other total pressure losses occuring in the blade passage.

Louis (ref. 5) could show experimentally that only the interaction of the corner vortices with the main flow has to be considered or the determination of the total pressure loss. The influence of the cascade vortex pair can be neglected.

Hence, it can be assumed that most of the secondary losses are originating of two factors, whose fluid mechanics cannot be described theoretically with actual knowledge. We are forced to use empirical or, at the best, semi-empirical relations.

A comprehensive résumé of the classical empirical relations can be found in ref. 1.

With the inviscid model of Squire and Winter, we know that the vorticity downstream of the cascade is proportional to the deflection angle of the cascade. Hence, the total pressure losses are proportional to θ^2.

Also, the camber angle of a blade can be considered as an indication of the loading of the blading and the end walls.

Using this condition, Howell (ref. 6) has established the relation for the induced drag due to secondary flow :

$$C_{D_{is}} = .018\ C_L^2 \qquad (2)$$

with measurements of classical compressor cascades.

Following Scholz (ref. 7), it can be supposed in first approximation that the secondary losses are a unique function of the blade turning. That means, the ratio of secondary losses to total losses increases with a decrease of the blade height. Generally, the blade height is not used as characteristic parameter, but the ratio h/c, the aspect ratio. This ratio also takes into account the length of the flow path on which the particles of the end wall boundary layer are travelling to form the corner vortex.

Vavra (ref. 8) gives the following relation using the influence of the aspect ratio and the camber angle on the secondary drag coefficient :

$$C_{D_{is}} = .04\ C_L^2 \cdot \frac{c}{h} \qquad (3)$$

A third parameter, the solidity σ of the cascade, can influence the secondary losses, although the experimental ev dence of its influence is contradictory. Ehrich and Detra (ref. 9) are using this parameter in the form : A.R. = A·σ = h/s. The following relation is proposed :

$$C_{D_{is}} = \frac{.1178\ \theta^2}{A.R.(1-.2/A.R.)^3} \qquad (4)$$

Relations (3) and (4) are also established with experimental results of classical compressor blades, i.e., with aspect ratios h/c > 1 and camber angles $\theta < 30°$.

At the von Karman Institute a method to predict the secondary flow loss in function of the turning angle and aspect ratio was developed (ref. 10) using a model that can be placed between the viscous and the inviscid model. This intermediate position occurs due to the consideration of the boundary layer thickness build up in the cascade passage, but not of the interaction between the end wall and the suction side boundary layer.

The calculation of the end wall boundary layer is based on the assumption that a mean loading of the pressure and suction side loading at midspan exists on the end walls, due to the assumption of a constant static pressure gradient over the span. The boundary layer thickness is determined at the trailing edge, using the diffusion factor relation with Buri's separation criterion as determination of the blade loading.

The important influence of the boundary layer thickness on the size and position of the corner vortex has been proved amongst other by measurements of Senoo (ref. 11). He could show that the size of the vortex and the distance between the center of the vortex and the endwalls rises with the boundary layer thickness (fig. 6).

Assuming a linear variation of the velocity distribution in the boundary layer at the blade outlet plane, the circulation along the blade span can be approximated by the model of a horse-shoe vortex (fig. 7). The distance between the two trailing vortices is fixed in function of the boundary layer thickness with the condition that the lift of the original blade and the replacing blade using the horse-shoe model, is the same. The following relation is obtained for the ratio of replacement blade height and real blade height

$$\frac{h'}{h} = 1 - \frac{4}{3}\frac{\delta}{h} \qquad (5)$$

In figure 8 the calculated values of the vortex centers are compared with the measurements. A satisfactory correspondence is obtained.

Using a proposal of Carter and Cohen (ref. 12) the whole cascade system is replaced by the model blades as shown in fig. 9. The induced drag due to the trailing edge vortices and their images is calculated in ref. 10 with less restrictions than in ref. 12.

$$C_{D_{is}} = \frac{1}{4} C_L^2\ \sigma \frac{1-h'/h}{\sqrt{1-(1-h'/h)^2}} \qquad (6)$$

The secondary flow loss coefficient, ω_s, can be calculated using the formula

$$\omega_s = \frac{\sigma \cdot C_{D_{is}}}{\cos\beta_m} \qquad (7)$$

With the above briefly outlined method, the secondary loss has been calculated for different cascades. A sufficient agreement has been obtained between calculated values and measured ones.

In figure 10, the ratio of secondary loss to the total cascade loss is shown in function of the main parameters influencing the secondary flow : θ and c/h. The secondary loss is calculated with the above described method using the measurements obtained at midspan, or taken directly from measurements if a sure distinction between profile loss and secondary loss could be made. The curve shows for small values of $\theta(c/h)$ an increase of the secondary loss of parabolic type. For higher values of $\theta(c/h)$, this ratio tends to approach a constant value. The blade forms used in the investigations up to now for compressor blades were all in the range of $\theta = 30°$, $c/h \leq .5$, that means, $\theta(c/h) \leq .25$ rad. Hence, the approach to a constant value could not be predicted.

The formulae (2), (3) and (4) roughly give the same results for classical blades. In figure 11, the equations of Vavra and Detra and Ehrich are compared. Almost identical results are obtained for the two relations for small to moderate loadings of the blade. Also, at high C_L values the difference is only small between the results of the two equations.

For very highly loaded blades, these classical relations and the VKI method are compared with measurements in fig. 12, where the secondary loss coefficient is plotted in function of the aspect ratio. None of the classical methods is able to predict the secondary loss for this type of blading sufficiently exact.

4. OUTLET FLOW ANGLE

The change of deflection due to secondary flows can be approached in two different ways :

1) the trailing edge vortices are taken as principal origin of secondary loss by inducing a deflection at the lifting line;
2) the change of outlet angle over the span is determined due to the influence of the cascade secondary flow using the stream function for the secondary flow in the cascade outlet plane. Normally, an underturning at the center of the vortex and an overturning at the side wall is indicated.

At the side wall, the influence of the cascade secondary vortex is predominant and causes an overturning of the flow. Moving to the center of the blade the influence of the corner vortex diminishes this overturning until the core of this vortex is passed where the highest deviation angle exists. Now the corner vortex and the secondary vortex causes an increase of the turning which weaks off to the midspan of the blade.

Some analytical results are published by Horlock (ref. 13) and Hawthorne based on the theory of the latter. But due to the restriction of the validity of this method, the range of applications is also very limited for the outlet angle distribution.

A comparison between calculated and measured values is shown in fig. 13 for a compressor cascade with blades of 30° camber angle and an aspect ratio of unity. A spanwise variation of 7° is shown.

In figure 14 the outlet flow angle distribution for a 50° camber compressor blade is presented, indicating even a variation of higher than 10°, which makes the design task for the following blade row extremely difficult.

5. MINIMIZATION OF SECONDARY FLOW LOSS

Many attempts have been made to reduce the secondary flow loss. This can be achieved using the following possibilities :

1) to reduce the end wall boundary layer thickness;
2) to reduce the radial pressure gradient;
3) to reduce the pressure difference between suction and pressure side of the blade;
4) to use an optimum tip clearance.

The end wall boundary layer can be reduced using small chord blades, what is often impossible to obtain due to mechanical reasons. Another possibility is the suction of the end wall boundary layer material upstream of the blade row and inside of the blade passage.

A further means to reduce the end wall boundary layer was suggested by Burrows (ref. 14). In the nozzle design for small gas turbines with high inlet temperature the necessity arises of side wall cooling. The cooling air can be injected in such a way that side wall flow separation is prevented due to reenergizing the boundary layer with the injected air.

The difference in pressure between the concave and the convex side of the flow channel, one of the main factors to create secondary flows, can be diminished using a meridional constriction (fig. 15).

A different twisting (ref. 15) of the blade or a long chord in the annulus boundary layer section can reduce the corner vortices, due to creating a uniform distribution of circulation along the blade. Together with the prolongation of the blade chord, a higher camber angle in the leading edge part should be used, to take the higher (measured against axial direction) flow angle in the boundary layer into account.

Some investigators propose a twisting of the blade in such a way to produce a uniform outlet angle, which is advantageous for the adaptation of the following blade row.

Todd (ref. 16) used some flow fences on the blade to reduce the cross flow on the suction side of the blade. The total pressure loss could be decreased by this means, but for the whole blade passage the total pressure loss was increased due to :
1) additional viscous losses on the fence, and
2) additional losses produced by a maladaptation of the streamlines on the blade surface and the fence.

At the von Karman Institute, partial slotting of the blades has been applied rather successfully (ref. 10). A decrease of 20% of the total pressure loss coefficient of the whole blade passage has been obtained, which corresponds to an increase of 15% of the efficiency of a compressor stage.

6. CONCLUSIONS

The influence of secondary flow effects has to be taken into account to be able to establish a sound design of high specific power turbomachines.

Only the viscous and the channel model give a sufficient prediction of the secondary loss. The use of the inviscid model has to be restricted to the design of inlet guide vanes.

With the actual knowledge the viscous and the channel model cannot be treated mathematically. Hence, it is necessary to develop semi-empirical rules based on measurements of the type of blades necessary for the new generation of turbomachines.

LIST OF REFERENCES

1. LAKSHMINARAYANA, B. & HORLOCK, J.H.: Secondary flows and losses in cascades and axial flow turbomachines. Int. Jnl Mech. Sc., vol. 5, 1963.

2. GRIEPENTROG, H.: Ecoulements secondaires dans les grilles d'aubes de compresseurs à forte déflexion et faible allongement. Conférence donnée au 9e Congrès Int. Aéron. Paris, juin 1969; also VKI IN 30, 1969.

3. SQUIRE, H.B. & WINTER, K.G.: The secondary flow in a cascade of airfoils in a non-uniform stream. J.A.S., April 1951.

4. DETRA, R.W.: The secondary flow in curved pipes. Ph.D. Thesis, ETH Zürich, 1953.

5. LOUIS, J.F.: Secondary flow and losses in a compressor cascade. ARC R&M 3136, 1960.

6. CARTER, A.D.S.: The axial compressor. Section 5 'Gas Turbine Principles and Practice', edited by Sir H.A. Lex, 1955.

7. High speed and jet propulsion, vol. X - Aerodynamics of turbines and compressors. Princeton University Press, 1964.

8. VAVRA, M.H.: Aero-thermodynamics and flow in turbomachines. Wiley, 1960.

9. EHRICH, F.W. & DETRA, R.W.: Transport of the boundary layer in secondary flow. J.A.S., 1954.

10. GRIEPENTROG, H.: Prédiction des performances des grilles d'aubes transsoniques à haute déflexion et faible allongement. Ph.D. Thesis, Université de Liège, 1969. also VKI TN 59, 1969.

11. SENOO, J.: The boundary layer on the end wall of a turbine nozzle cascade. ASME Transact. 1958.

12. CARTER, A.D.S. & COHEN, E.M.: Preliminary investigation into the three dimensional flow through a cascade of aerofoils. ARC R&M 2339, 1949.

13. HORLOCK, J.H., et al.: Wall stall in compressor cascades. ASME Transact., Jnl Basic Engrg, 1966.

14. BURROWS, L.: Investigation of the design and performance of small axial flow turbines. VKI PR 68-211, 1968.

15. DEICH, M.E.: A new method of profiling the guide cascades of stages with small ratios of diameter to length. AIE Ltd, Transl. No 3277, 18 July, 1963.

16. TODD,K.W.: Flow characteristics in steamturbines. Reprint of Paper given at the Conf. on Reheat Steam Turbines of great output, Inst. of FLuid-Flow Machinery of the Polish Academy of Sciences, Gdansk, 1962.

17. CHAUVIN, J., BREUGELMANS, F.A.E., JANIGRO, A.: Supersonic compressors. VKI CN 67, 1967.

18. SHALAAN, M.R.A.: A wind tunnel investigation of the stalling performance of two compressor cascades of different aspect ratio at low speed. ULME/B26

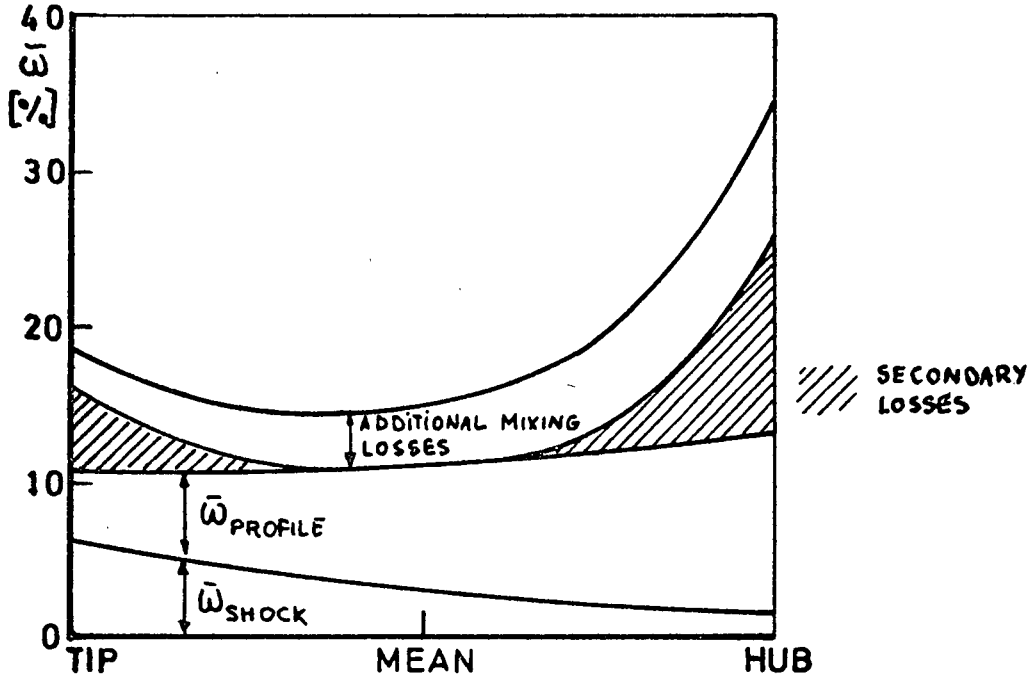

Fig. 1(a) Loss distribution (Ref. 17)

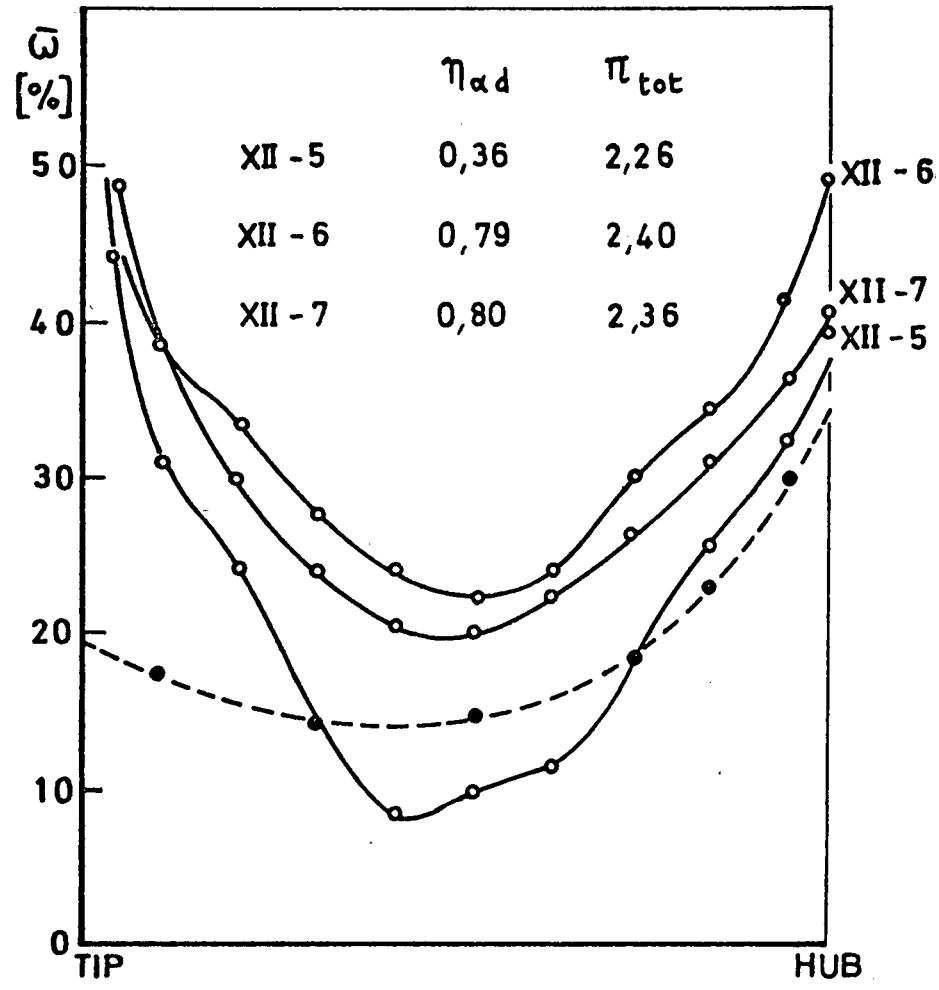

Fig. 1(b) Comparison with measurements (Ref. 17)

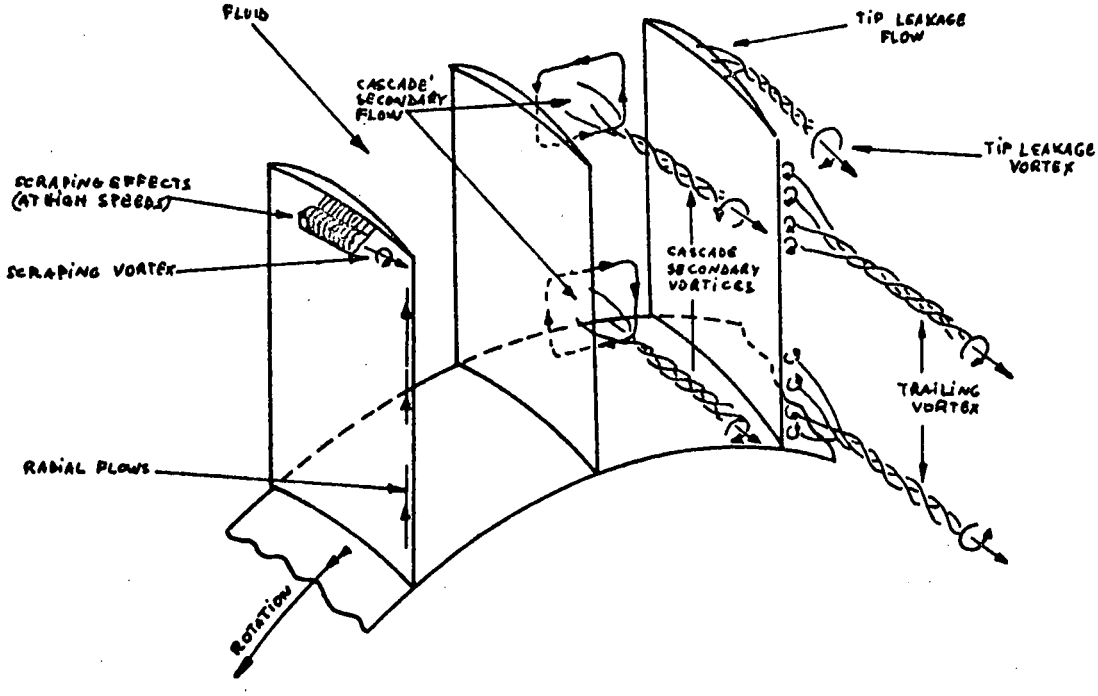

Fig. 2 Secondary flow elements (Ref. 1)

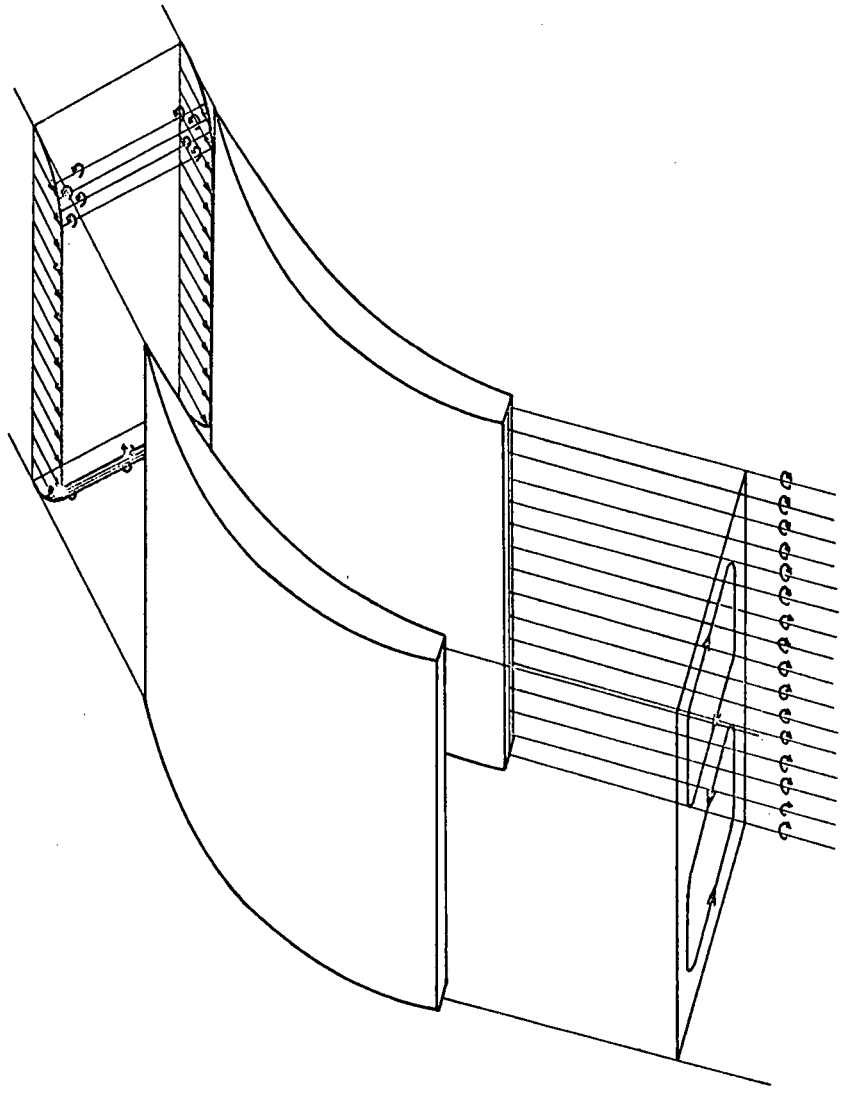

Fig. 3 Inviscid model

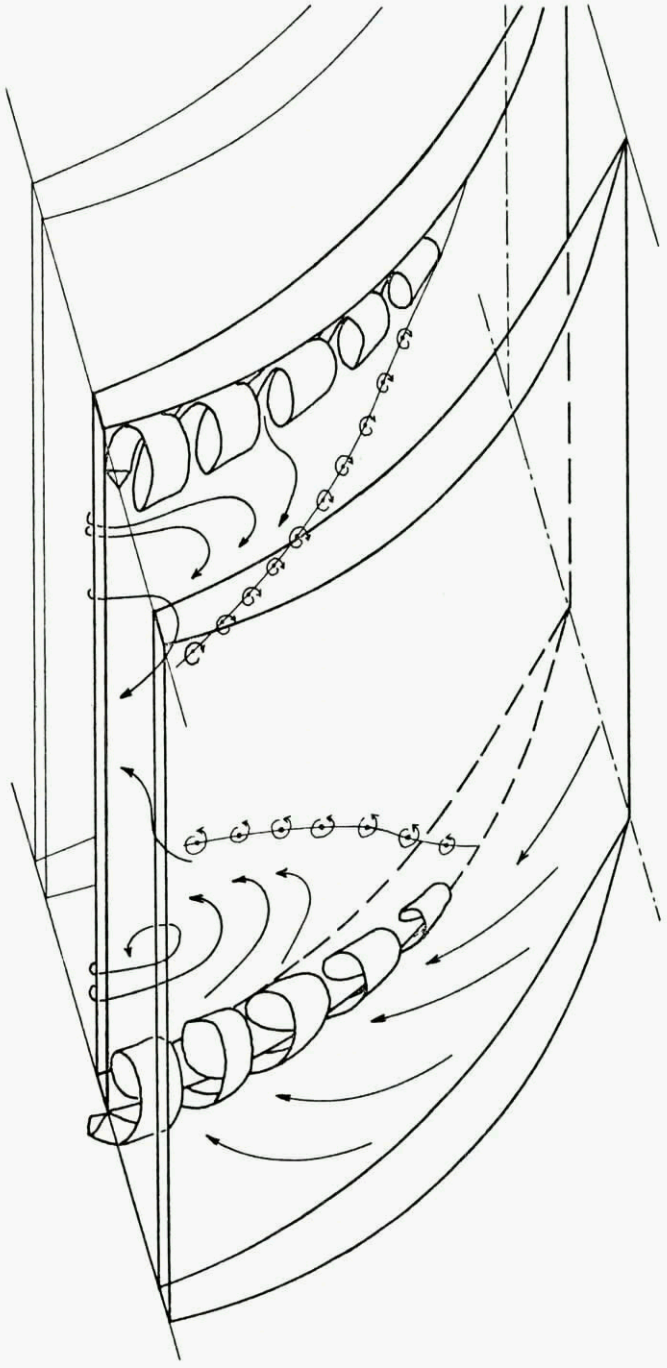

Fig. 4 Viscous model

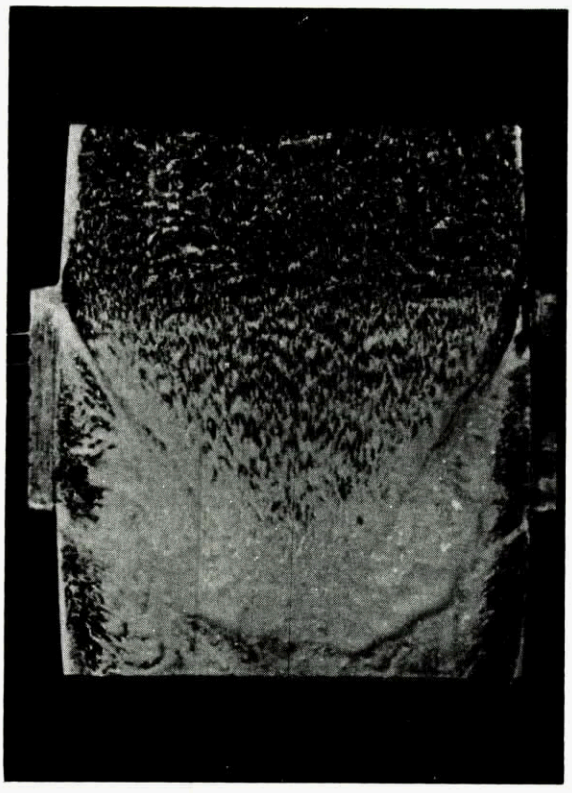

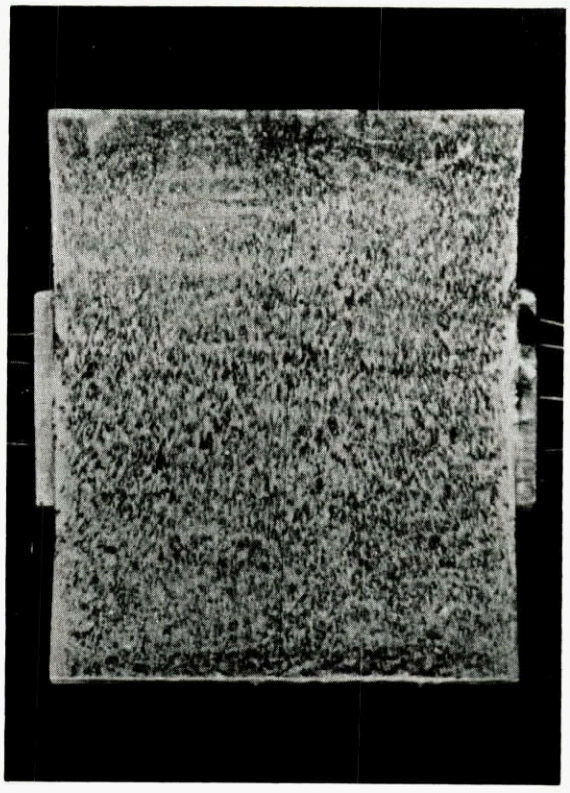

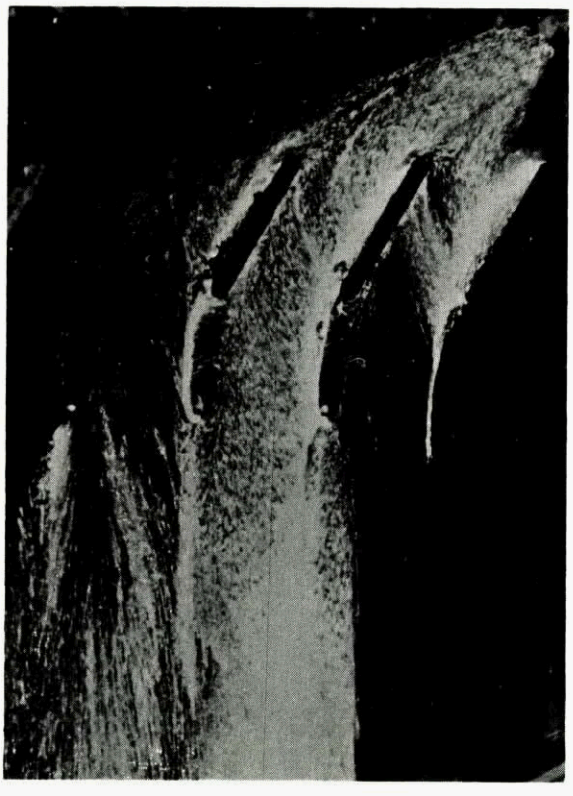

BTB_o
$i_{ss} = 2°$

Figure 5

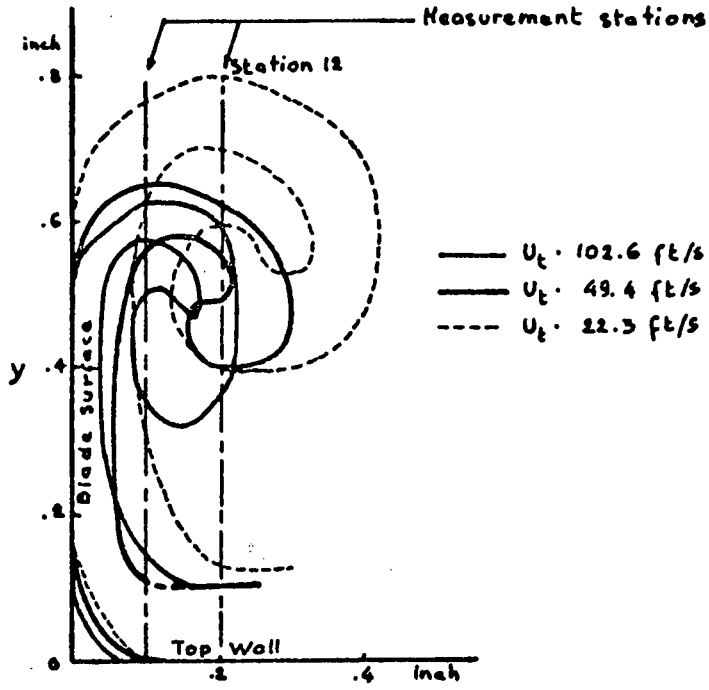

Fig. 6 Corner vortex (Ref. 11)

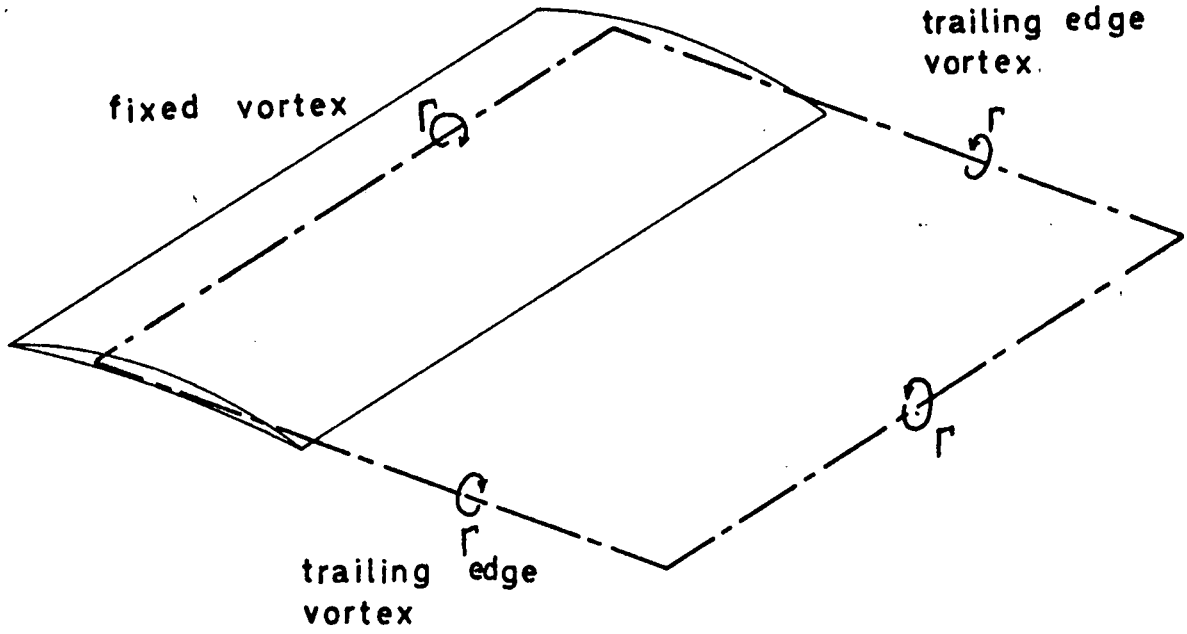

Fig. 7 Horse shoe vortex

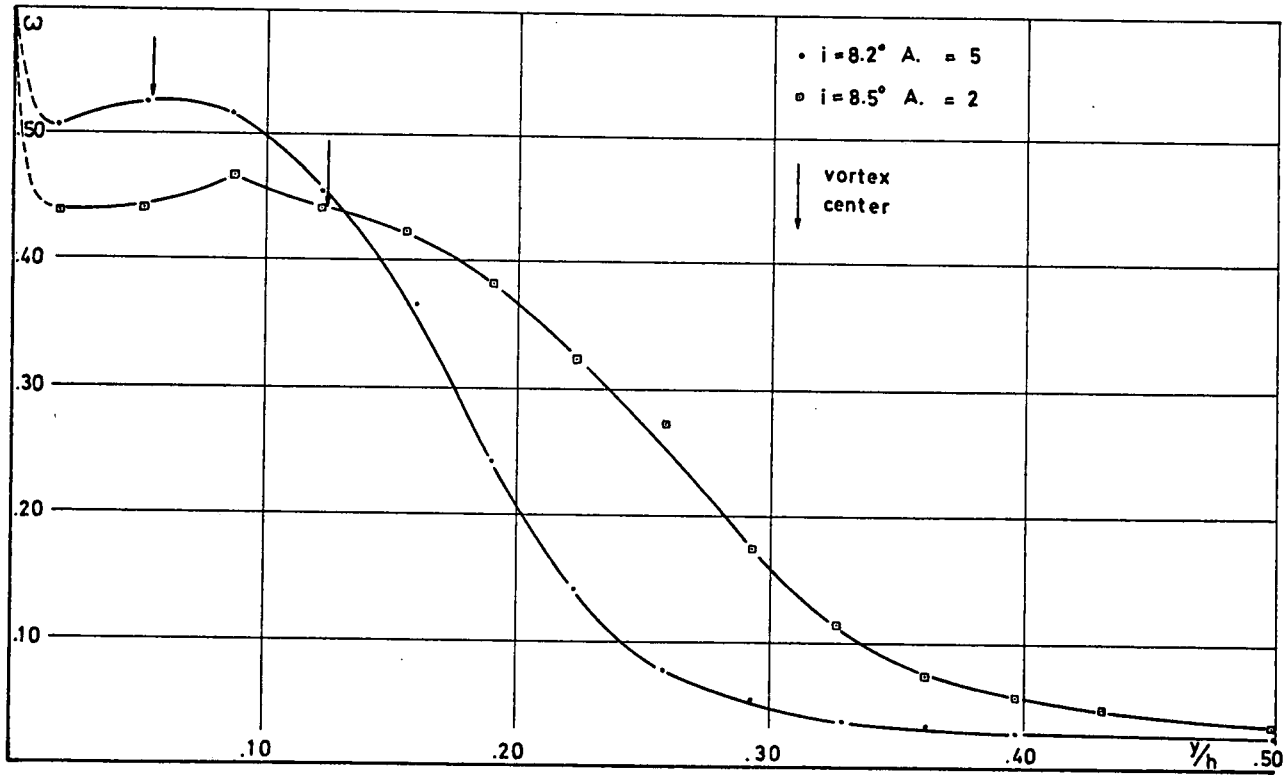

Fig. 8 Spanwise total loss pressure coefficient distribution

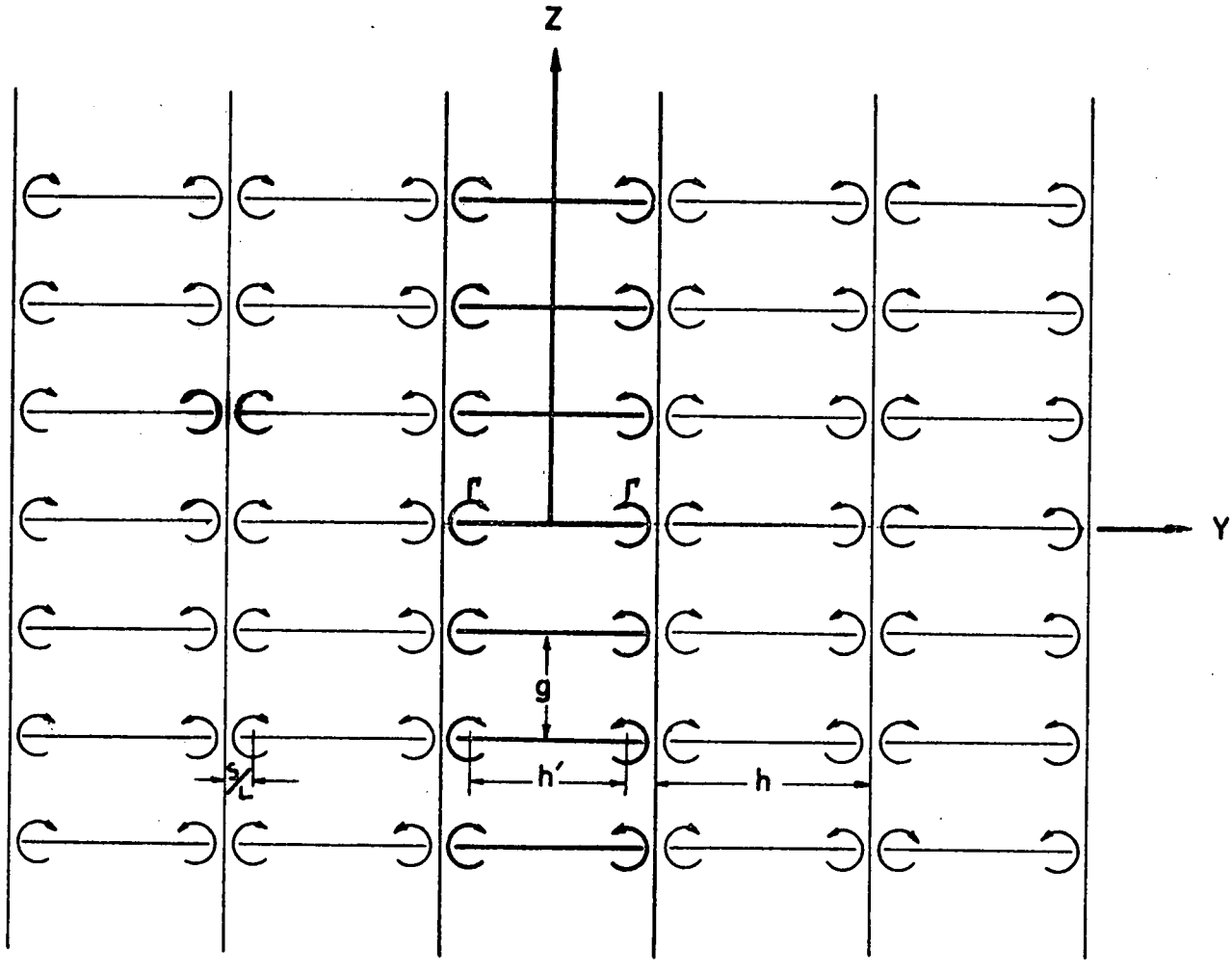

Fig. 9 Cascade model system

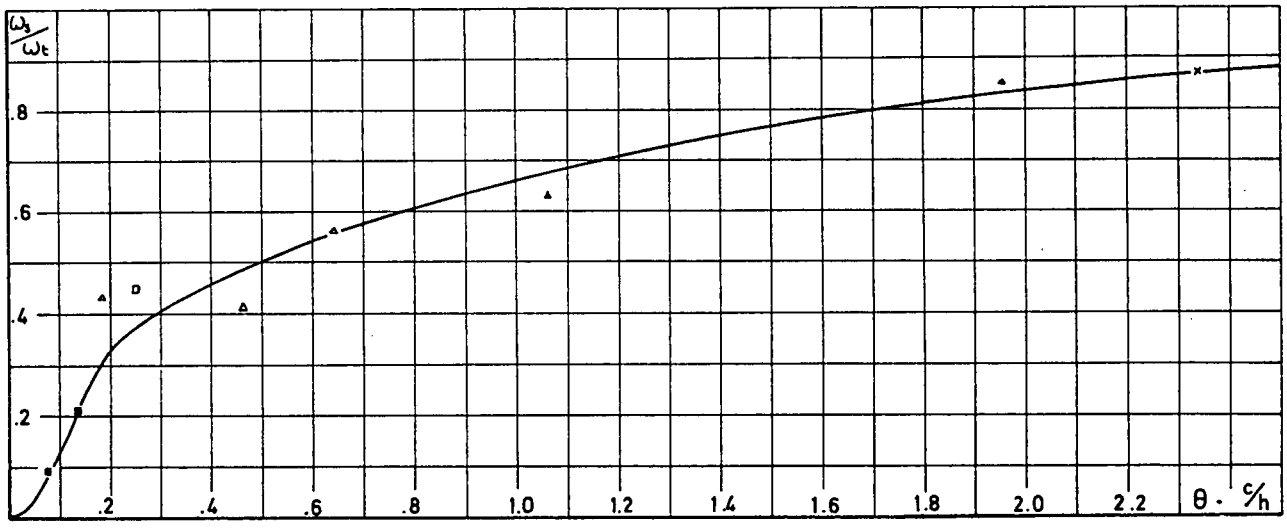

Fig. 10 $\omega_s/\omega_t = f\left(\theta \frac{c}{h}\right)$

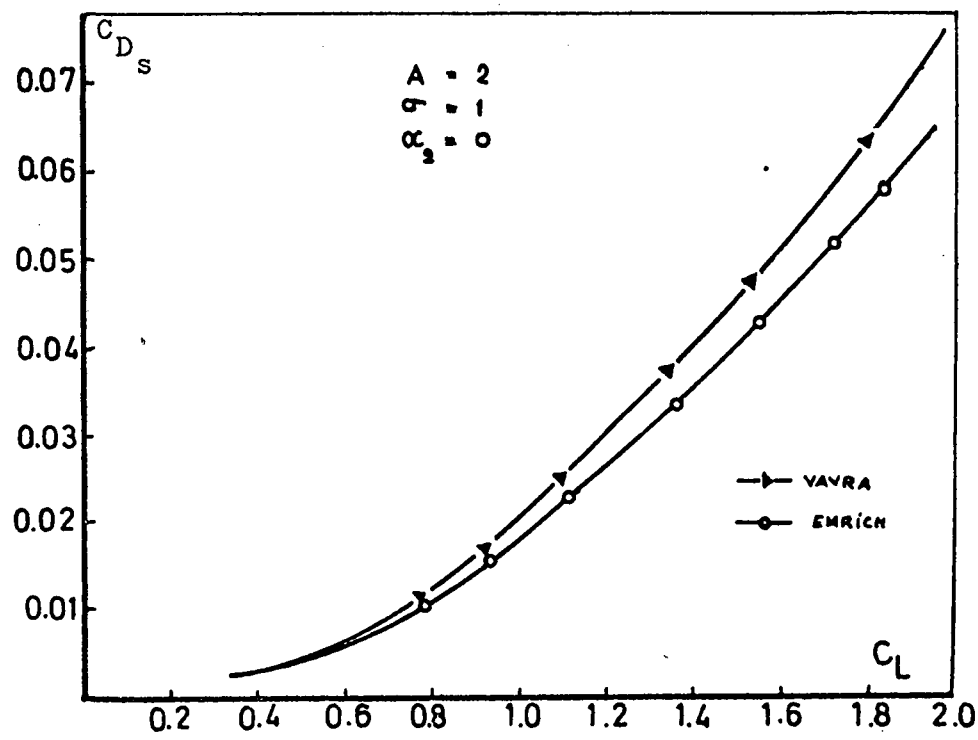

Fig. 11 Comparison of empirical formulae for secondary flow drag coefficient in cascade

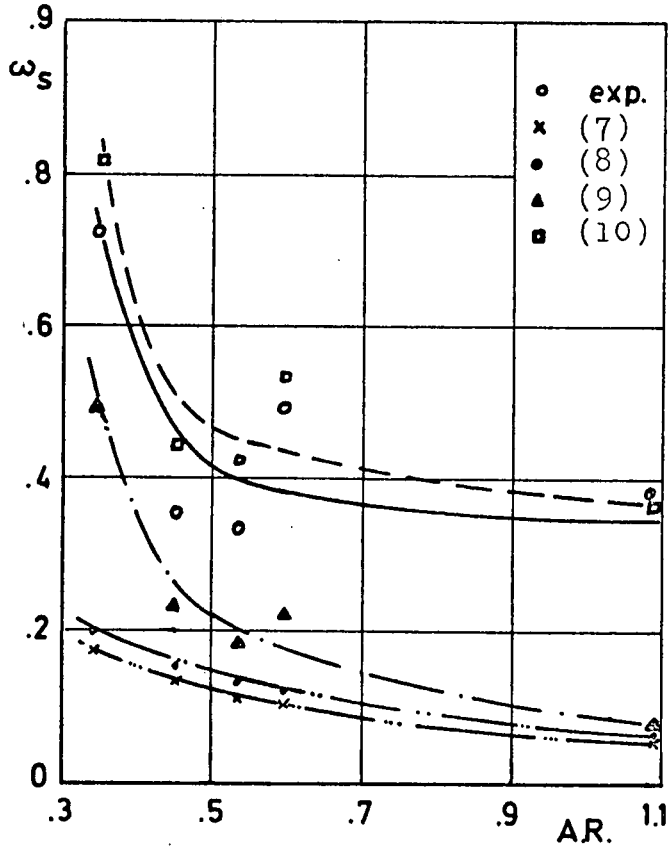

Fig. 12 Comparison of measured and predicted secondary flow

Cascade outlet angle distribution

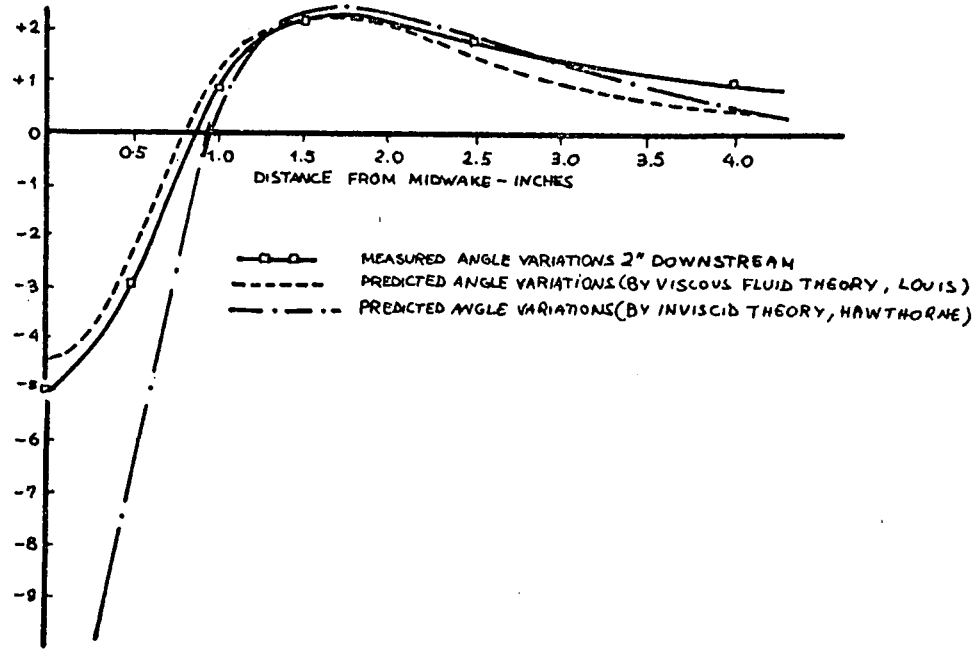

Fig. 13 Comparison of measured and predicted spanwise outlet flow angle distribution (Ref. 13)

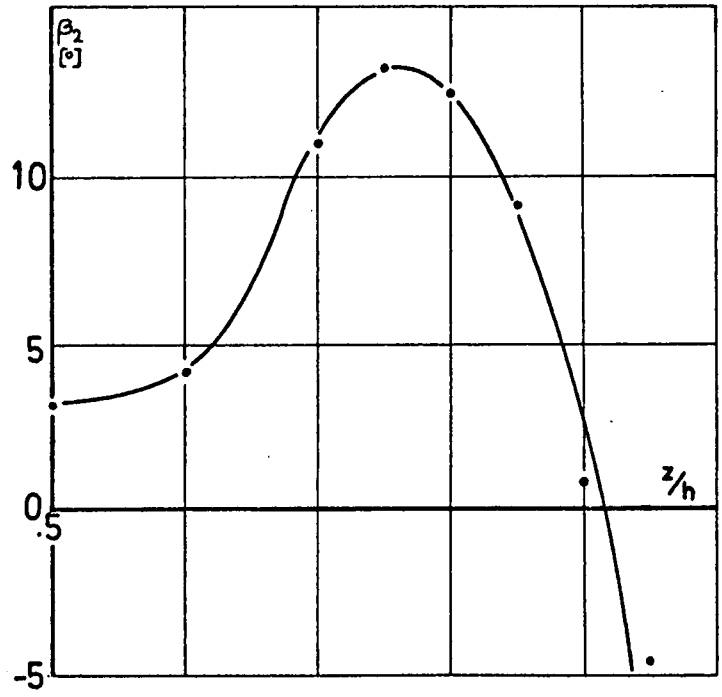

Fig. 14 Measured spanwise outlet flow angle distribution for a highly louded compressor cascade

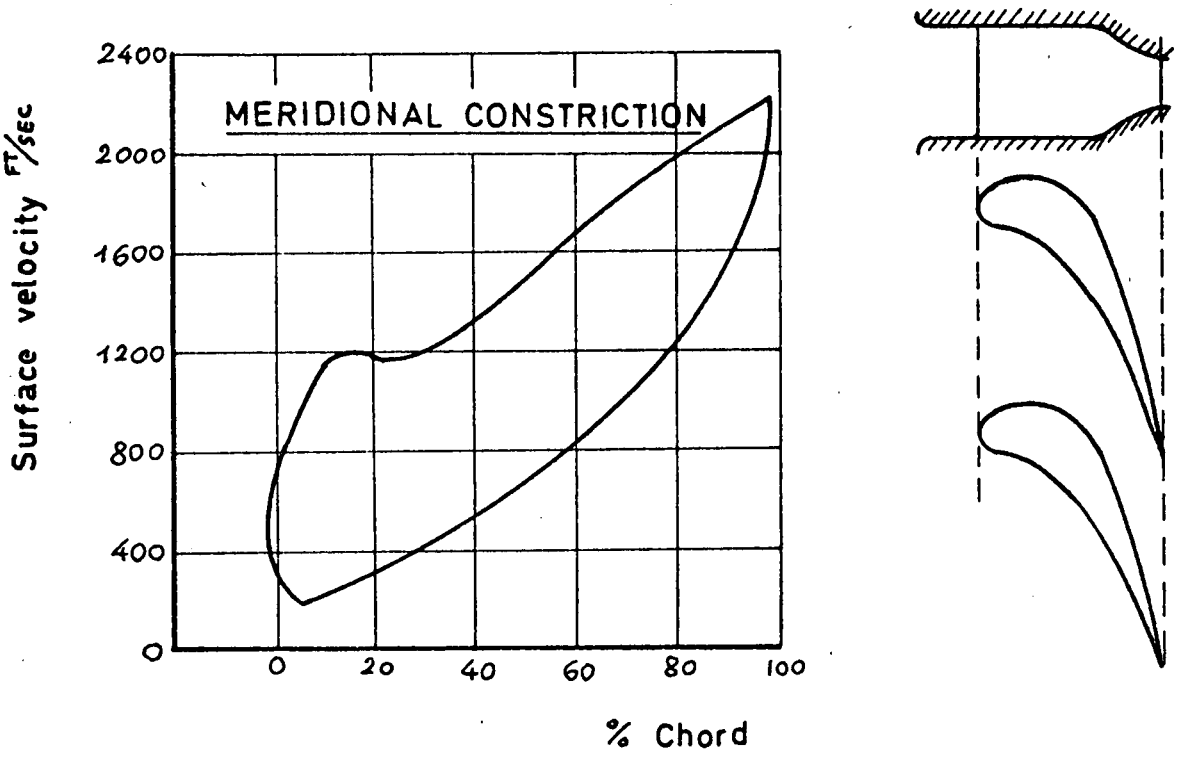

Fig. 15 Influence of meridional contraction (Ref. 14)

BASIC ELEMENTS FOR ADVANCED DESIGNS OF RADIAL-FLOW COMPRESSORS

by

M. H. Vavra

Naval Postgraduate School
Monterey, California 93940

SUMMARY

Dimensionless parameters are presented for the design of compressors with axial inlet velocities and radial blades at the rotor discharge. These parameters take account of the compressibility of the flow and hold for arbitrary fluids. They permit to evaluate the effect of changes of the design variables on the conditions of state of the fluid at different locations, and on the geometry of the design. Loss relationships are discussed and their effects on performance are shown. The design parameters are compared with the so-called specific speed criteria to show that the latter do not satisfy the laws of similarity if compressibility effects are taken into account.

BASIC ELEMENTS FOR ADVANCED DESIGN OF RADIAL-FLOW COMPRESSORS

M. H. Vavra

1. INTRODUCTION

Under consideration are high-speed centrifugal compressors with rotors of the type shown in Fig. 1 that have radial blades at the discharge and where the absolute inlet velocities are in axial direction. With a straight annular inlet duct these inlet velocities will be uniform between the radii R_{1i} and R_{1o} of the impeller eye. For a particular relative flow angle β_{1o} and the relative velocity W_{1o} at R_{1o}, there is then known the peripheral speed U_{1o}, which, for chosen radius ratios R_2/R_{1o}, establishes the peripheral rotor speed U_2 at R_2. The average relative velocity W_2 at the discharge of a rotor with radial blades is not radial, but has an average angle β_2. With the slip factor μ there is

$$\beta_2 = \tan^{-1} \frac{(1-\mu)\, U_2}{V_{m2}} \tag{1}$$

where V_{m2} is the average meridional velocity at the rotor discharge. Equation 1 is a consequence of the definition of the slip factor

$$\mu = \frac{V_{u2}}{U_2} \tag{2}$$

For a simplified analysis of the compressor performance that assumes uniform conditions at the rotor discharge not only in peripheral but also in axial direction, across the blade width b_2, and for axial absolute velocities V_1 at the rotor inlet, the specific work ΔH_w necessary to drive the compressor is from moment of momentum consideration, for an assumed adiabatic process,

$$\Delta H_w = \mu\, U_2^2 \qquad \left(\frac{\text{ft-lb}}{\text{slug}}\right) \tag{3}$$

For a perfect gas with $\gamma = c_p/c_v$ = constant, the actual rise in total temperature ΔT_w in the rotor is

$$\Delta T_w = \frac{\Delta H_w}{c_p} = \frac{\mu\, U_2^2}{c_p}$$

With the gas constant R_G there is

$$c_p = R_G\, \frac{\gamma}{\gamma-1} \tag{4}$$

Let

$$a_0 = \sqrt{\gamma\, R_G\, T_{t1}} \quad = \sqrt{\gamma\, R_G\, T_0} \tag{5}$$

be the velocity of sound at the total inlet temperature $T_{t1} = T_0$. Then

$$\frac{\Delta T_w}{T_0} = \mu\, (\gamma-1)\, \left(\frac{U_2}{a_0}\right)^2 \tag{6}$$

For an isentropic compression process from the total inlet pressure $P_0 = P_{t0} = P_{t1}$ to the discharge pressure P_{t4}, the necessary work required would be $c_p\, \Delta\, T_{is}$, where

$$\Delta T_{is} = T_0 \left[\left(\frac{P_{t4}}{P_0}\right)^{\frac{\gamma-1}{\gamma}} - 1 \right] \tag{7}$$

The compressor efficiency η_c is defined by

$$\eta_c = \frac{\Delta T_{is}}{\Delta T_w} = \frac{\left(\frac{P_{t4}}{P_0}\right)^{\frac{\gamma-1}{\gamma}} - 1}{\mu(\gamma-1)\left(\frac{U_2}{a_0}\right)^2} \tag{8}$$

For a particular design the following data are usually prescribed:

$\dot{m}$ - mass flow rate (slug/s)

P_0 - total inlet pressure (psia)

T_0 - total inlet temperature (^oR)

P_{t4} - discharge pressure (psia)

γ - ratio of specific heats c_p and c_v

R_G - gas constant ($\frac{ft\text{-}lb}{slug,\,^oR}$)

With the indicated units, which are frequently used for engineering purposes, a quantity of mass is in slugs which is derived from the chosen units of force, length, and time. However, the relations which are going to be established hold for any consistent system of units, hence also for one where the primary units are mass, length and time, and where forces are in derived units.

For the given conditions there are to be found the following data for an optimum design:

U_2 - peripheral rotor speed at R_2

b_2/R_2 - $\frac{\text{ratio of axial impeller width at discharge}}{\text{outer radius of impeller}}$

R_{1o}/R_2 - $\frac{\text{outer radius at rotor inlet}}{\text{outer radius of impeller}}$

R_{1i}/R_{1o} - $\frac{\text{inner radius at rotor inlet}}{\text{outer radius at rotor inlet}}$

ω - angular velocity of impeller (radians/s)

β_{1o} - relative flow angle at R_{1o}

α_2 - absolute flow angle at R_2

R_3/R_2 - $\frac{\text{radius at inlet lip of diffusor blades}}{\text{outer radius of impeller}}$

R_4/R_2 - $\frac{\text{radius at discharge of diffusor}}{\text{outer radius of impeller}}$

Important design criteria are also:

$M_{W1} = \frac{W_{1o}}{a_1}$ - Mach number of relative velocity W_{1o} at outer radius R_{1o} at impeller inlet

$M_{V2} = \frac{V_2}{a_2}$ - Mach number of absolute velocity V_2 at impeller discharge

Mechanical and fluid dynamics considerations impose design limits of:

a) U_2, because of permissible rotor stresses
b) R_{1o}/R_2, which cannot exceed about 0.70 to 0.75 to obtain an outer rotor contour with acceptably small curvatures in the meridinal plane
c) R_{1i}/R_{1o}, which, if too small, does not permit the arrangement of a sufficiently large number of rotor blades Z_R with reasonable thickness
d) β_{1o}, which cannot be larger than about 70^o for manufacturing reasons
e) b_2/R_2, which cannot be smaller than certain limits to obtain good efficiencies
f) α_2, which cannot exceed 70^o to 80^o because of manufacturing reasons and because of poor diffusor performance, especially if M_{V2} is larger than unity.

2. COMPRESSION PROCESS

Figure 2 is a temperature-entropy diagram showing the thermodynamic process in the compressor of Fig. 1. The temperature differences in Fig. 2 correspond roughly to the velocities of the triangles of Fig. 1 to obtain a realistic representation. Since by Eq. 6 the work input ΔT_w is also $\Delta T_w = \mu\,(U_2^2/c_p)$, the temperature rise $T_2 - T_1$ in the rotor is roughly one-half of ΔT_w. Later on the so-called degree of reaction r* will be introduced to determine this ratio more precisely.

Station (1) in Fig. 2 corresponds to the static condition at the rotor inlet, given by the static pressure p_1 and the static temperature T_1. The total pressure and total temperature at this station are $P_{t1} = P_0$ and $T_{t1} = T_0$. For the isentropic process between (0) and (1).

$$\frac{T_{t1}}{T_1} = \frac{T_0}{T_1} = 1 + \frac{\gamma-1}{2} M_{V1}^2 \qquad (9)$$

and

$$\frac{P_{t1}}{p_1} = \frac{P_0}{p_1} = \left(\frac{T_0}{T_1}\right)^{\frac{\gamma}{\gamma-1}}$$

where

$$M_{V1} = \frac{V_1}{a_1} = \frac{V_1}{[\gamma R_G T_1]^{\frac{1}{2}}}$$

is the Mach number of the absolute velocity V_1 at the rotor inlet.

The conditions of state at all locations can be expressed with the parameters U_2/a_0, R_{1o}/R_2, M_{W1}, β_{1o}, α_2, μ, and loss coefficients that establish the entropy increments between the different stations, if it is assumed that the flow process along the outer contour of the rotor between the radii R_{1o} and R_2 is representative of the rotor flow in general. The later assumption is made because the relative velocity W_1 and the relative flow angle β_1 are higher at R_{1o} than at other radii R_1. Hence along the outer rotor contour from R_{1o} to R_2 there occur the highest deceleration ratio W_{1o}/W_2 and the largest flow deflection $\Delta\beta = \beta_{1o} + \beta_2$. Moreover since the path travelled by a fluid particle along the outer rotor contour is shorter than that travelled by a particle entering at other radii R_1, the conditions along the outer rotor contour will establish design limitations and have a critical influence on the rotor losses.

With the chosen parameters, Eq. 9 can be rewritten

$$\frac{T_1}{T_0} = \frac{1}{1 + \frac{\gamma-1}{2} M_{W1}^2 \cos^2\beta_{1o}}$$

This formula is also given by Eq. I(5) of Table I. This table has been arranged to list the pertinent relations for the determination of the flow properties in the compressor for ready reference. In the following only the main steps will be indicated that led to these formulas without going into the details of their derivations. Some of the equations, for instance Eq. I(6), can be obtained directly from Fig. 2. It can be noted that all temperatures are given as multiples of the total inlet temperature $T_0 = T_{t1}$, and pressures are listed as ratios with respect to $P_0 = P_{t1}$. The static temperature T_2 of the rotor discharge [Eq. I(7)] is equal to the difference of the total temperature T_{t2} at the rotor exit and $V_2^2/2c_p$, where V_2 is given by Eq. I(3). The temperature T_2' is necessary to calculate the pressure ratio p_2/P_0 by Eq. I(20). Evidently T_2' depends on the entropy increase $s_2 - s_1$ in the rotor.

The process between stations (1) and (2) from the rotor inlet to its discharge can be formulated by

$$T_1 - \frac{W_{1o}^2}{2c_p} - \frac{U_{1o}^2}{2c_p} = T_2 + \frac{W_2^2}{2c_p} - \frac{U_2^2}{2c_p} \qquad (10)$$

which is a fundamental relation obtained from the energy equation for steady, adiabatic flows along streamlines in rotors, as shown in Art. 7.5 of Ref. 1.

The following discussion uses a relation which is obtained from Eq. 10 for incompressible flows (See Eq. 7(44) of Ref. 1). At a particular radius R along the outer rotor contour where the peripheral and relative velocities are U and W, respectively, the static pressure p is

$$p = p_1 + \frac{\rho}{2}(U^2 - U_{1o}^2) + \frac{\rho}{2}(W_{1o}^2 - W)^2 - \Delta p_f \qquad (11)$$

where ρ is the constant mass density of the fluid, and Δp_f the pressure loss due to frictional effects in the rotor. At the rotor inlet, where $U = U_{1o}$ and $W = W_{1o}$, the static pressure is evidently equal to p_1, the static pressure in the absolute flow just ahead of the rotor at R_{1o}. Equation 11 shows that, independently of the values of W and Δp_f, there will always occur a pressure increase $\rho/2(U^2-U_{1o}^2)$ if a fluid particle moves from R_{1o} to R. An additional pressure rise is produced by decelerating the relative velocity from W_{1o} to W. A flow that moves in a direction where the static pressure increases is more susceptible to separations than an accelerated flow, but the frictional pressure loss between neighboring stations is proportional to the dynamic head $(\rho/2)\ W^2$ in both flows. In view of Eq. 11 however there exist differences between flows that pass through stationary channels and those in rotating impellers. If a relative flow is decelerated in a rotating channel, whose distance from the axis of rotation increases in flow direction, it will not necessarily separate even though it moves against rapidly increasing static pressures, provided these pressure gradients are produced by the centrifugal force field and not by large reductions in relative velocity. If the same static pressure rise would have to be produced in a stationary channel of the same length as the rotating one, the deceleration of the flow per unit length would very likely become excessive and could be associated with considerably increased losses because of flow separations. On the other hand, if it were possible to ignore the effects due to Coriolis accelerations, it could be stated that the pressure losses in a stationary and in a rotating channel of equal length and shape would have to be equal for the same velocity heads and equal flow decelerations, except for influences due to Reynolds number differences. Moreover, for different velocity heads the pressure losses would be directly proportional to the velocity heads at corresponding locations in the two channels. However if the respective performance of the two channels were evaluated by a loss coefficient ζ_R that relates the frictional pressure drop Δp_f to the actual static pressure rise in the channel, its value would be lower for the rotating channel than for the stationary one because of the additional pressure rise $(\rho/2)(U^2 - U_{1o}^2)$. The performance of the channels can be compared only by means of a loss coefficient ζ_W that is defined as the ratio of the pressure drop Δp_f and

the pressure rise $(\rho/2)(W_{1o}^2 - W_1^2)$ due to the flow deceleration, irrespective of whether additional pressure rise is produced by the centrifugal force field or not.

These elementary considerations have not been presented here to imply that the loss coefficients ζ_W in a rotating and in a stationary channel of the same geometry are equal. In Ref. 1, Art. 8.5, it is shown that flows in stationary and rotating channels have fundamental differences as far as their rotational characteristics are concerned, and consequences of these conditions are described in Arts. 10.5 and 12.2 of Ref. 1. The intent of the above discussion is to draw attention to the fact that frequently used formulations for the efficiency of impellers for centrifugal turbines and compressors cannot serve as a measure for the performance of these rotors, and that some of the separation criteria applied to flows in centrifugal rotors have no physical meaning.

A commonly used definition for the efficiency of a centrifugal compressor rotor is

$$\eta_R = \frac{T_2' - T_1}{T_2 - T_1} \tag{12}$$

The significance of the temperatures is evident from Fig. 2. Equation 12 holds for the compressible flow of fluids with a constant value of $\gamma = c_p/c_v$. Similar to the preceding discussion that delt with incompressible flows, part of the temperature rise in the rotor is due to the increase in peripheral speed from station (1) to station (2). Equation 10, rewritten as

$$T_2 - T_1 = \frac{U_2^2 - U_{1o}^2}{2c_p} + \frac{W_{1o}^2 - W_2^2}{2c_p} = T_u - T_1 + \frac{W_{1o}^2 - W_2^2}{2c_p} \tag{13}$$

shows that the static temperature rise $T_u - T_1$ due to the centrifugal force field is equal to the first term on the right-hand side of Eq. 13. It occurs in rotors with and without flow losses, hence it is independent of the entropy increase $s_2 - s_1$. Thus the compression corresponding to $(U_2^2 - U_{1o})^2/2\,c_p$ occurs along the isentropic line s_1 = constant from T_1 to T_u, from station (1) to station (u) in Fig. 2, producing the static pressure rise $p_u - p_1$, where

$$\frac{p_u}{p_1} = \left(\frac{T_u}{T_1}\right)^{\frac{\gamma}{\gamma-1}} = \left(1 + \frac{(U_2^2 - U_{1o}^2)}{2\,c_p\,T_1}\right)^{\frac{\gamma}{\gamma-1}} = \left(1 + \frac{\gamma-1}{2}\,\frac{U_2^2 - U_{1o}^2}{\gamma\,R_G\,T_1}\right)^{\frac{\gamma}{\gamma-1}}$$

The deceleration of the relative velocity from W_{1o} to W_2 produces the temperature rise

$$T_2 - T_u = \frac{W_{1o}^2 - W_2^2}{2\,c_p} \tag{14}$$

with an entropy increase from s_1 to s_2, due to the flow losses, which in turn affect the pressure rise $p_2 - p_u$. The efficiency of the process from (u) to (2) can be defined by the so-called wheel efficiency η_W

$$\eta_W = \frac{T_2' - T_u}{T_2 - T_u} = \frac{T_2' - T_u}{(W_{1o}^2 - W_2^2)/2\,c_p} \tag{15}$$

giving

$$\frac{T_2'}{T_u} = \eta_W\,\frac{T_2}{T_u} + 1 - \eta_W$$

and

$$\frac{p_2}{p_u} = \left(\frac{T_2'}{T_u}\right)^{\frac{\gamma}{\gamma-1}}$$

From a fluid dynamics view point only the efficiency η_W is a measure for the quality of the rotor performance. In particular, low measured values of η_W are indications for the existence of flow separations, although η_W will be affected also by the tip clearance losses, the so-called scrubbing losses produced by the rotating blades in the wall boundary layer at the fixed shroud, and the mixing losses after the rotor. However, low efficiencies η_W are only partly reflected in the rotor efficiency η_R of Eq 12 because of the temperature rise $T_u - T_1$ which is produced without entropy increases. If the entropy diagram of Fig. 2 were to represent the actual conditions in the compressor of Fig. 1, there would be, by measuring the temperature differences in Fig. 2,

$$\eta_R = 0.84$$

and

$$\eta_W = 0.57$$

Although the value of $\eta_R = 0.84$ seems to indicate that the flow in the rotor is reasonably good, the low value of $\eta_W = 0.57$ shows clearly that it should be possible to improve the rotor considerably with a redesign. Such improvement should be undertaken not only to increase the overall efficienty of the compressor by reducing the entropy rise $s_2 - s_1$ in the rotor, but also to produce more uniform flow conditions at the

rotor discharge since it might then be possible to reduce the diffusor losses also.

The process in the rotor that involves the relative velocity changes can be considered also from a different view point. Equation 10 may be written as

$$T_E = T_1 + \frac{W_{1o}^2}{2\,c_p} + \frac{U_2^2 - U_{1o}^2}{2\,c_p} = T_u + \frac{W_{1o}^2}{2\,c_p} = T_2 + \frac{W_2^2}{2\,c_p} \tag{16}$$

where T_E is the so-called equivalent total temperature of the rotor flow. Equation 16 has the same form as the energy equation for an adiabatic process of an absolute flow if T_E is replaced by the constant absolute total temperature T_t and W_2 by the absolute velocity V. The temperature T_E is constant for a process in a particular rotor having a fixed radius ratio R_{1o}/R_2 and turning at a specified speed. Thus, for given inlet conditions, Eq. 16 can be used also for an isentropic process along s_1 = constant from (u) to (2') to give, in accordance with Fig. 2,

$$T_E = T_2' + \frac{W_{2is}^2}{2\,c_p} \tag{17}$$

for the same pressure rise $p_2 - p_u$ as produced by the process with friction, and W_{2is} is the theoretical velocity available at the pressure p_2. In turbine calculations it is customary to express the rotor losses by so-called velocity coefficients ψ

$$\psi = \frac{W_2}{W_{2is}} \tag{18}$$

If this formulation is used for compressors also, there is from Eq. 17,

$$T_2' = T_E - \frac{1}{\psi^2}\frac{W_2^2}{2\,c_p} \tag{19}$$

Introduced into Eq. 15

$$\eta_W = \frac{W_{1o}^2 - W_2^2/\psi^2}{W_{1o}^2 - W_2^2} = \frac{1 - \frac{1}{\psi^2}\left(\frac{W_2}{W_{1o}}\right)^2}{1 - \left(\frac{W_2}{W_{1o}}\right)^2} \tag{20}$$

or

$$\psi = \frac{W_2/W_{1o}}{\left[1 - \eta_W + \eta_W \left(\frac{W_2}{W_{1o}}\right)^2\right]^{\frac{1}{2}}} \tag{21}$$

The reason for introducing ψ as an alternate for η_W is that η_W equals - ∞ for the special condition where $W_2 = W_{1o}$, or $T_2 = T_u$. In this case, and if W_2 is larger than W_{1o}, the velocity coefficient ψ can however still be applied. On the other hand, for usual designs where W_2 is smaller than W_{1o}, the velocity coefficient is not a good measure for the rotor performance since ψ can be increased by simply making the velocity W_2 smaller, and it is then more appropriate to use the wheel efficiency η_W for the loss evaluation. Since the same difficulties in expressing the losses occur in turbines also, an additional formulation is sometimes used which establishes the drop in total pressure that is associated with the entropy increase $s_2 - s_1$. For radial compressor rotors these formulation are either

$$Y_1 = \frac{P_{E1} - P_{E2}}{P_{E1} - p_u} \tag{22}$$

or

$$Y_2 = \frac{P_{E1} - P_{E2}}{P_{E2} - p_2} \tag{23}$$

depending on whether the pressure drop $P_{E1} - P_{E2}$ is referred to the inlet or the exit conditions. Although these total pressure loss coefficients are useful at small Mach numbers, or for incompressible flows where $P_{E1} - p_u = (\rho/2)\,W_{1o}^2$ and $P_{E2} - p_2 = (\rho/2)W_2$, it can be shown that the corresponding coefficients which relate the losses to the kinetic energy of the flow (in the same manner as η_W of Eq. 15, or ψ of Eq. 18) become smaller for constant values of Y_1 or Y_2 if the Mach number of the inlet or discharge flow increases.[2] Although the actual energy losses tend to increase with increasing flow Mach numbers, an indiscriminate application of Eqs. 22 or 23 with values of Y from low-speed tests can be used as a wrong argument that the opposite is true.

To simplify the relations for the determination of the conditions of state in the compressor the velocity coefficients ψ will be used in the equations of Table I. To compare two rotors with different radius ratios and different deceleration ratios W_2/W_{1o}, the efficiency η_W of Eq. 15 should be used as a

measure for their performance. Equations 20 and 21 relate ψ and η_W to each other. Paragraph 5 contains a discussion that deals with the magnitudes of η_W. With the formulas of Table I it is possible also to establish a relation for the determination of η_W for known values of η_R of Eq. 12, or vice versa. From

$$\eta_R = \frac{\eta_W \left[\left(\frac{W_{1o}}{U_2}\right)^2 - \left(\frac{W_2}{U_2}\right)^2\right] + 1 - \left(\frac{R_{1o}}{R_2}\right)^2}{\left(\frac{W_{1o}}{U_2}\right)^2 - \left(\frac{W_2}{U_2}\right)^2 + 1 - \left(\frac{R_{1o}}{R_2}\right)^2} \tag{24}$$

and with

$$C = \frac{1 - \left(\frac{R_{1o}}{R_2}\right)^2}{\left(\frac{R_{1o}}{R_2}\right)^2 \cot^2\beta_{1o} + 2\mu \left(1 - \frac{\mu}{2\sin^2\alpha_2}\right)} \tag{25}$$

there are

$$\eta_R = \eta_W + C\,(1 - \eta_W) \tag{26}$$

and

$$\eta_W = \frac{\eta_R - C}{1 - C} \tag{27}$$

High performance compressors with high pressure ratios cannot be equipped with diffusors that are circular cascades with airfoil shaped blades. Figure 1 is a realistic sketch of a high speed compressor operating with an average discharge velocity V_2 that is supersonic. To obtain reasonably large axial blade widths b_2 as well as acceptable shapes of the meridinal rotor contours, it is necessary to resort to large angles α_2 at the rotor discharge. At large angles α_2, practical consideration dictate a limited number of diffusor channels, say, about 8 to 10 for angles α_2 of about 75°, and the permissible diffusion in these individual channels produces configurations similar to that depicted in Fig. 1. One of the most critical problem areas is the design of the flow passages from the rotor discharge to the entrance of the diffusor channels proper. The absolute flow leaving the rotor is not only non-uniform but also non-steady, because the relative velocity at the rotor discharge must by necessity vary between the suction and the pressure sides of the rotor blades at R_2. Designs where the radius R_3 is very much larger than the outer rotor radius R_2, or compressors with vaneless diffusor for large angles α_2, were found to be inferior to machines with small radial gaps $R_3 - R_2$, especially for high subsonic or supersonic velocities V_2. If it were not for the excessive noise the diffusor lips would preferably be arranged even closer to R_2 as shown in Fig. 1.

Theoretical attempts were made in Refs. 3 and 4 to evaluate the losses in the space between R_2 and R_3, and in vaneless diffusors, that are due to mixing and frictional effects. The results of these investigations do not agree with reality if M_{V2} and/or α_2 are large. These inconsistencies are due to the assumption that equal flow angles are supposed to occur across the axial width b_2 of the flow channel after the rotor, a condition which is created by assuming that the frictional forces along the walls act equally on all particles between them. In actuality the flow angles α (measured with respect to the radial direction) decrease radically in the wall boundary layers in the direction from the mid-section of the channel toward the wall. The particles inside the boundary layers then move more rapidly to larger radii into zones of higher pressure than those outside of the boundary layers and very easily cause flow separations from the walls, thereby impairing the effectiveness of such diffusors.

In the writer's opinion it is incorrect to state that in efficient diffusors the vanes must not be too close to the impeller, or that the velocity at their entrance must be subsonic in all cases. For the reason mentioned above, it is equally wrong to maintain that vaneless diffusors must be arranged for supersonic absolute velocities at the rotor discharge.

Because of the inability to separate the losses that exist between the radii R_2 and R_4 of Fig. 1 an overall diffusor efficiency η_D will be introduced. With the symbols of Fig. 2

$$\eta_D = \frac{T_4' - T_2}{T_4 - T_2} \tag{28}$$

where

$$T_4 - T_2 = \frac{V_2^2 - V_4^2}{2\,c_p} \tag{29}$$

The velocity V_4 exists at the diffusor discharge at the radius R_4, and is taken as

$$V_4 = \lambda\, V_2 \tag{30}$$

With small values of λ the radius ratios R_4/R_2 become large because of the limited amount of diffusion that is possible per unit length in flow direction to avoid separations in the diffusor channels. Values of λ of about 0.20 to 0.30 are common to limit R_4/R_2 to about 2. With designs of the type shown in Fig. 1 the kinetic energy $V_4/2\,c_p$ cannot be converted into pressure rise, since the flow from the individual diffusors is dumped into a receiver surrounding them. As indicated by station (d) in Fig. 2 the total pressure P_{t4} at the compressor discharge is then equal to the static pressure p_4 at the diffusor exit, and

the total temperature at the compressor discharge is $T_{t4} = T_{t2}$ for adiabatic processes. The dumping of the kinetic energy $V_4^2/2\,c_p$ is reflected in the overall diffusor efficiency η_D^* between rotor and compressor discharge

$$\eta_D^* = \eta_D\,(1 - \lambda^2) \tag{40}$$

Diffusor design criteria and approximate methods to evaluate the diffusor losses are given in paragraph 5.

Since

$$T_4 = T_{t2} - \frac{V_4^2}{2\,c_p} = T_{t4} - \lambda^2\,\frac{V_2^2}{2\,c_p}$$

and with Eq. 28 there is then obtained the temperature T_4, as given by Eq. I(11) of Table I. The pressure $p_4 = P_{t4}$ is determined from

$$\frac{p_4}{p_2} = \left(\frac{T_4'}{T_2}\right)^{\frac{\gamma}{\gamma-1}}$$

for the isentropic process along the line s_2 = constant. Because the isentropic temperature differences between lines of constant pressure are proportional to the initial temperatures of the processes, there is, with the symbols of Fig. 2,

$$\frac{T_4'' - T_2'}{T_4' - T_2} = \frac{T_2'}{T_2}$$

and

$$\frac{T_4''}{T_0} = \frac{(T_4'/T_0)(T_2'/T_0)}{T_2/T_0}$$

As shown in Table I the ratio T_4''/T_0 can be expressed by Eq. I(13) which has the form

$$\frac{T_4''}{T_0} = \frac{1 + A(X_1 + A\,X_2)}{1 + A\,B} \tag{41}$$

where X_1 and X_2 are given by Eqs. I(14) and I(15), and

$$A = (\gamma-1)\,\mu\,\left(\frac{U_2}{a_0}\right)^2 \tag{42}$$

$$B = 1 - \frac{\mu}{2\,\sin^2\alpha_2} \tag{43}$$

The temperature rise ΔT_{is} for an isentropic compression from the total conditions P_0, T_0 at the compressor inlet, to the discharge pressure P_{t4} is, with Eq. 41,

$$\frac{\Delta T_{is}}{T_0} = \frac{T_4''}{T_0} - 1 = \frac{A[X_1 - B + A\,X_2]}{1 + A\,B} \tag{44}$$

Eq. 44 is identical with Eq. I(16) of Table I.

As shown in Table I the pressures at the different stations can be determined from the established temperatures by using the pressure-temperature relation for isentropic processes of perfect gases.

3. PERFORMANCE AND DESIGN PARAMETERS

The overall compressor efficiency defined by Eq. 8 is, with Eqs. 6, 42, and 44,

$$\eta_c = \frac{\Delta T_{is}}{\Delta T_w} = \frac{X_1 - B + A\,X_2}{1 + A\,B}$$

With Eqs. 42 and 43 the above relation establishes Eq. II(1) of Table II. This table lists the equations necessary to determine the performance and the geometry of the compressor. Only the principal steps that led to the equations of Table II are described in the following, the details of the derivations are omitted. The symbols of Table II are those of Figs. 1 and 2, with additional ones that are defined in this paragraph.

The degree of reaction r* is defined as the ratio of the isentropic temperature rise $T_2' - T_0$ in the rotor to that corresponding to the pressure ratio P_{t4}/P_0. Equation II(2) of Table II shows that for $\eta_c = 1$ and $\psi = 1$, the degree of reaction is

$$r^* = r_o^* = \left[1 - \frac{\mu}{2 \sin^2 \alpha_2}\right]$$

For a slip factor $\mu = 0.85$, r_o^* changes from about 0.544 to 0.433 if the angle α_2 is reduced from 75° to 60°. For low degrees of reaction a large part of the overall pressure rise must be produced in the diffusor. Since this energy conversion is associated with greater losses than the pressure rise produced in the rotor, high degrees of reaction are desirable. This condition is used in hydraulic pumps which usually have backward-bent rotor blades to produce most, if not all, of the pressure rise in the rotor. However, if such rotors were employed for light gases, such as air, the pressure rise would be too small for most applications, not only because of the reduced specific work input but also because such rotors would not be able to operate at high speeds on account of the high bending stresses in the blades. In rotors with radial blades it seems beneficial to use large angles α_2 to increase r*. At a fixed peripheral speed U_2 the velocities V_2 decrease if α_2 is increased, but difficulties occur then because of the geometry of the passages from the wheel to the diffusor inlet. The deceleration ratio W_2/W_{1o} becomes smaller also, as shown by Eq. II(5), and the increased losses caused by larger flow decelerations in the rotor may off-set the gain that would be obtained from the increased degree of reaction if other conditions would remain unchanged. The choice of these design parameters to obtain the best possible solution must usually be based on experience because of the interactions between rotor and diffusor that are greatly influenced by their designs.

The slip factor μ appears in most of the equations of Tables I and II. More has been written on this subject than on any other in the field of radial pumps and compressors, primarily because it is of great importance to know exactly how much energy a wheel will absorb. If wrong values of μ are used in a design the desired pressure ratio will not be obtained even though the expected efficiency is reached. Reference 7 is a recent paper where tests obtained with one particular wheel are compared with data obtained from experiments, and with slip factor formulas, by other authors. As is frequently the case in many studies on the subject, test data from a single wheel obtained at off-design conditions are used to establish design point data for other impellers. Moreover, the highest ratio U_2/a_0 was only about 0.51 in the tests of Ref. 7. The bibliography of Ref. 7 fails to mention the investigations of Refs. 5 and 6 which were undertaken at Daimler-Benz A. G. by systematically testing ten high-performance impellers of different shapes up to values of U_2/a_0 of about 1.1. In the writer's opinion, the data published in Refs. 5 and 6 are extremely valuable to the designer and the original curves of the article have been replotted in Fig. 3 to give wider publicity to this important contribution to the state of the art.

With the slip factor known from Fig. 3 the compressor efficiency of a particular design can be determined from Eq. II(1) for known losses. Equation II(3) is plotted in Fig. 4 for $\gamma = 1.4$, and different values of $\mu\eta_c$, to show the magnitudes of U_2/a_0 necessary to produce particular pressure ratios. For advanced gas turbine applications it would be desirable to operate at pressure ratios of between 8 and 10. For $\eta_c = 0.8$ and $\mu = 0.875$, Fig. 3 shows that values of U_2/a_0 of about 1.8 are necessary to reach this goal. Thus, at an inlet temperature of 60°F, where $a_0 = 1120$ ft/s, the rotor of such a compressor has to operate with a peripheral speed U_2 of about 2000 ft/s, requiring special materials and careful rotor designs for the resulting high stresses.

By Eq. I(6) the rise of the total temperature in the compressor is $T_{t2} - T_0 = T_0(\gamma-1)\mu(U_2/a_0)^2 = 590°F$, or about 600°F, for $\mu = 0.875$ and $T_0 = 520°R$. Since the degree of reaction is around 0.5, the static temperature T_2 at the rotor discharge is then about 60 + 600/2 = 360°F. At this temperature, high-strength aluminum alloys have rupture stresses, and stresses for specified creep rates, which are less than one-half of the allowable stresses at room temperature. Hence it is necessary to use titanium alloys, for instance those with about 6 percent aluminum and 4 percent vanadium. At 360°F the design criterion for these materials is the yield stress since no appreciable creep effects occur even for operating times of 100,000 hours. Their 0.2 percent offset yield strength at 360°F is about 120 kpsi, with an ultimate strength of about 150 kpsi. As shown in chapter C of Ref. 8, the tangential stress in a non-supported ring of small radial thickness rotating with the peripheral speed U_2 is ρU_2^2. For titanium with a specific gravity of 4.43, this value is about 240 kpsi at $U_2 = 2000$ ft/s. Figures C.27 and C.29 of Ref. 8 show the so-called equivalent centrifugal stresses σ_e in rotors with radial blades as multiples of $\rho U2^2 = \rho\omega^2 R_2^2$, for a design where the disk extends to the outer tip of the blades at R_2, and another which has so-called scallops between the blades, similar to the rotor design shown in Fig. 1. Not counting the stress peaks at the central bore, which are more of the nature of stress concentrations that will be relieved by plastic deformations, because titanium has high ductility on account of its 20 percent elongation, the maximum stress ratios $\sigma_e/(\rho U_2^2)$ are about 0.25 and 0.16 for the rotors without and with scallops, respectively. Hence the maximum stresses at 2000 ft/s will be about 60 kpsi for one and about 40 kpsi for the other rotor. This discussion shows that compressor rotors operating at tip speeds of 2000 ft/s are feasible and that by arranging scallops, and using 75 percent of the 0.2 percent offset yield stress, or 90 kpsi, as design criterion, the maximum tip speed could be as high as 3000 ft/s or over 900 m/s. The latter speeds would give velocity ratios U_2/a_0 of about 2.68 at $T_0 = 60°F$ and $\gamma = 1.4$. For $U_2/a_0 = 2.68$, $\mu = 0.85$, $\eta_c = 0.80$, pressure ratios P_{t4}/P_0 of about 43 could be reached in a single stage for gases with $\gamma = 1.4$. The extreme difficulties that would be associated with such a design, in particular those arising because of the large volume flow reductions, will not be discussed here. The intent of the fore-going deliberations is to show that pressure ratios in centrifugal compressors for air are not restricted because of rotor stresses.

Important advances are being made in nuclear gas turbines with helium as working fluid, as described in a recent article by Bammert and Bohm[9]. The main difficulties in the design of the turbomachines for this plant are the low pressure ratios that can be produced with helium in a conventional compressor stage, since the molecular weight of helium is only about 4 and $\gamma = 1.659$. At 60°F the velocity of sound in helium is 3275 ft/s. For a rotor with $U_2 = 3000$ ft/s, a speed ratio $U_2/a_0 = 0.916$ would be obtained in a radial compressor. All velocities in the compressor would be subsonic and design point efficiencies of about $\eta_c = 0.85$ seem feasible. For μ=0.90, $\eta_c = 0.85$, $U_2/a_0 = 0.916$, at $\gamma = 1.659$, the resulting pressure ratio P_{t4}/P_0 would be 2.43 in accordance with Eq. 8.

In Ref. 9 a 25 MW_e closed-cycle helium gas turbine plant is described that operates with a turbine pressure ratio of 2.55. The pressure ratio of the compressors will have to be about 2.7 to overcome the pressure losses in the reactor and heat exchangers, of which no values are given in the paper. Reference 9 shows however that the plant has three axial compressors in series, each consisting of 9 stages. Since intercoolers are arranged between the three compressors each will produce a pressure ratio of about 1.4. If the three axial compressors were replaced by two single-stage radial compressors, of the type described with an intercooler between them, it would be possible to obtain an overall pressure ratio of about six which would be of advantage for the cycle. The writer does not want to minimize the difficulties that would be connected with the development of radial compressors and radial turbines for such applications, in addition to those connected with the bearings, seals and gear drives, but it is felt that they might be the ultimate solution for these highly interesting power plants.

Equation I(1) will be used in an example to show the influence of the diffusor losses on the compressor efficiency at different speed ratios U_2/a_0, for absolute flow angles α_2 of 60° and 75°. The velocity coefficients ψ will be determined by assuming a wheel efficiency η_W of Eq. 15 of 0.7 for both impellers. Equations 21 and 24 were used to establish Fig. 5. The deceleration ratios W_2/W_{1o} are 0.68 for $\alpha_2 = 60°$ and 0.366 for $\alpha_2 = 75°$ by Eq. I(5) for the data listed in Fig. 5. This difference makes the choice of equal efficiencies η_W for both cases somewhat dubious. It is seen from Fig. 5 that the rotor efficiencies η_R are 0.89 and 0.855 for $\alpha_2 = 60°$ and $\alpha_2 = 75°$, respectively. The corresponding values of ψ, which will be used in Eq. I(1), are 0.865 and 0.585. It is assumed further that the velocity V_4 at the diffusor discharge is 0.2 V_2, or $\lambda = 0.2$, so that $\eta_D{}^* = 0.96\ \eta_D$ by Eq. I(12). Figure 6 shows the large effect of the diffusor losses on the compressor efficiency. To obtain $\eta_c = 0.85$, the diffusor efficiency must be about 0.9 for all speed ratios U_2/a_0. If η_D were 0.7 instead of 0.9, the compressor efficiency would only be 0.75. At $U_2/a_0 = 1.6$, this decreased diffusor efficiency would reduce the pressure ratio of the compressor from about 7 to 5.8, which in a gas turbine plant would produce a mismatch between turbine and compressor, with additional adverse effects on the thermal efficiency of the plant. Figure 6 shows also that the diffusor has a larger influence on η_c at the higher flow angle α_2. On the other hand, the Mach number M_{V2} of the rotor discharge velocity will be lower at $\alpha_2 = 75°$ than at $\alpha_2 = 60°$. The respective values can be obtained from Eq. II(6) which has been represented in Fig. 7 for $\gamma = 1.4$. At $U_2/a_0 = 1.6$, the values of M_{V2} are 1.16 and 1.24 for α_2 of 75° and 60°, respectively, for the design parameters listed in Fig. 5.

Figure 7 shows that the Mach number M_{V2} becomes unity for values of U_2/a_0 between 1.1 and 1.3, depending on the choice of α_2. From Fig. 8, which is a representation of Eq. II(4), it can be noted that for a speed ratio $U_2/a_0 = 1.2$ and at a radius ratio R_{1o}/R_2 of about 0.67, which represents an average design value, the relative velocity W_{1o} at the rotor inlet has a Mach number M_{W1} of about 0.9 at an inlet angle β_{1o} of 65°. Figures 8 and 4 show that the Mach number M_{W1} for air compressors will not have to be larger than about 1.3 to produce pressure ratios up to about ten. Some sources state that no efficient inducers can be built for values of M_{W1} larger than 0.8 because of "shock losses". It seems to the writer that such statements are not different from those made some years ago, which predicted that it would be impossible for an airplane to break the "sonic barrier", or others which maintained that an axial compressor has to operate at subsonic velocities to be efficient. Advances in transonic axial-flow compressor stages have shown that human ingenuity can overcome these so-called barriers. Reference 10 is cited as an example, where a transonic boost stage ahead of the inlet of a centrifugal compressor is described, which produces a pressure ratio of 1.43 for air at an efficiency of 90 percent with a tip Mach number of 1.05.

The flow in an inducer of an impeller with radial blades is different from that in an axial-flow rotor. In the latter, particles that have been moving along the suction and the pressure sides of the blades are mixed at essentially constant static pressure after the trailing edges at the discharge, whereas no such mixing occurs in the flow channels where the inducer joins the radial blades of the impeller. Hence the pressure distributions along the walls of the inducer blades must be radically different from those along the surfaces of an axial rotor blade, and separation criteria that are based on the diffusion factor of axial cascades cannot be applied. Similar to the conditions in transonic axial stages the supersonic relative velocity at the tip of an inducer becomes sonic at a particular radius R_{1c}, and subsonic at radii R_{1x} smaller than R_{1c}. Denoting the Mach number of W_1 at R_{1x} by M_{1x}, and that at R_{1o} by M_{W1} as previously defined, there is

$$\frac{R_{1x}}{R_{1o}} = \frac{1}{\sin\beta_{1o}}\left[\left(\frac{M_{1x}}{M_{W1}}\right)^2 + \sin^2\beta_{1o} - 1\right]^{\frac{1}{2}} \qquad (45)$$

Figure 10 shows the values of R_{1x}/R_{1o} obtained from Eq. 45 for $M_{W1} = 1.3$, at different relative flow angles β_{1o} at the inducer tip, and for particular values of the Mach number M_{1x}. This graph is presented to show that it is non-sensical to state that M_{W1} cannot exceed particular values without specifying at what angle β_{1o} and at what ratio R_{1i}/R_{1o} this limitation holds. Whereas at $\beta_{1o} = 75°$ a Mach number of unity occurs at $R_{1x}/R_{1o} = 0.75$, the whole inlet annulus will have supersonic relative velocities at $\beta_{1o} = 50°$, for the same Mach number $M_{W1} = 1.3$ at the tip. Moreover, if at $\beta_{1o} = 75°$ the hub/tip ratio R_{1i}/R_{1o} of the inlet eye is 0.75 in one machine and, say, 0.3 in another the losses due to compressibility effects will certainly be different. Figure 10 also shows the Mach numbers M_{V1} of the absolute velocity V_1 ahead of the impeller which, as indicated earlier, has been assumed to remain constant in radial direction. They have values of 0.336 and 0.919, respectively, for $\beta_{1o} = 75°$ and $\beta_{1o} = 55°$ at $M_{W1} = 1.3$, and it is inconceivable to the writer that the losses will remain constant independent of M_{V1}. Clearly, if M_{V1} becomes larger than unity very special conditions occur since the flow in the annulus becomes choked at $M_{V1} = 1$ as has been discussed in Art. 9.9 of Ref. 1. Some of the peculiarities associated with cascades at supersonic inlet velocities are mentioned in Art. 9.10 of the same reference.

The writer believes that the, by now, almost classical view points of flows through turbomachines have outlived their usefulness. They may even be a hindrance for future developments and if accepted without questioning, may prevent original thinking and could make people believe that all problems have been or will be solved by their use. This classical method assumes that the fluid particles in a turbomachine move on axisymmetric stream surfaces of shapes which are either assumed a priori, or obtained

by simplified theoretical methods. Further, it is assumed that the flow through a turbomachine can be replaced by the flows through a multiplicity of annular channels bounded by neighboring stream surfaces, which are closely spaced between the meridional contours of the flow channel of the machine at hub and tip. The stream surfaces are actually considered to be thin, solid walls that do not create disturbances, and it is assumed that the flows in these individual channels do not interact with each other. In each one of the channels there exists then a so-called quasi two-dimensional flow of the type described in Art. 12 of Ref. 1. The performances of the different cascades, which are now arranged in the various flow channels to produce the specified flow deflection, are taken to be those of two-dimensional cascades obtained either in cascade test rigs or by theoretical methods. With the latter, one can at best attempt a solution for the special relative flows W in rotors that satisfy the condition $\nabla \times \vec{W} = -2\vec{\omega}$; that is, where the curl of the velocity function is a constant, since $\vec{\omega}$ is the angular velocity vector of the rotor. Such flows are isentropic but can be compressible. However, disturbances due to shocks cannot occur. This condition limits the theoretical evaluation to flows where the local Mach numbers must be less than or, at the most, equal to unity. More general solutions of the so-called blade-to-blade problem on axisymmetric stream surfaces have not yet been obtained and are very difficult to formulate.

So-called quasi two-dimensional flows with $\nabla \times \vec{W} = -2\vec{\omega}$ are discussed in Art. 12 of Ref. 1. By introducing a stream function ψ there is obtained a second order partial differential equation of the form (see Eq. 12(9), p. 307, Ref. 1)

$$\frac{1}{R^2}\psi_{,,\theta} + \psi_{,,m} - \frac{1}{R^2}\left[(\ln\rho)_{,\theta}\right]\psi_{,\theta}$$

$$+ \left[(\ln R)_{,m} - [\ln(\Delta h\rho)]_{,m}\right]\psi_{,m} = -2(\Delta h)\,\rho\omega\sin\lambda \qquad (46)$$

The commas denote partial differentions with respect to the coordinates listed after them, where θ is the angle in peripheral direction and m the length along the generatrix of the stream surface. The mass density is denoted by ρ, R is the radius from the axis, Δh is the varying distance between neighboring stream surfaces, ω is the angular rotor velocity, and λ is the angle of the tangent to the generatrix with the axis of rotation. For $\lambda = 0$ the particles move on cylindrical stream surfaces, and $\lambda = 90^\circ$ covers flows in radial compressor wheels with stream surfaces that are planes perpendicular to the axis. For the latter case, and for conical stream surfaces, Eq. 46 has been solved by Stanitz for thin blades.[3] For cascades with airfoil-shaped blades, that are arranged on an arbitrary surface of revolution, computer programs are described in Ref. 11 for solutions with relaxation methods that need high-speed computers with large storage capacities. As interesting and useful these theoretical attempts are, one must be critical to evaluate what they really produce in form of results, and whether or how these data will help to improve present designs, and to create the turbomachinery which is to be built in the future.

The mere fact that modern computers can solve differential equations with complicated boundary conditions which, hitherto, could not be tackled by hand calculations is no assurance that the results must be correct from a physical point of view. Computers can only perform mathematical manipulations as they are told to do, and no result is better than the assumptions that were used to formulate the problem that is solved by these apparently sophisticated, but inherently stupid, machines.

Two of the necessary boundary conditions for solving Eq. 46 with the programs of Ref. 11 require that the flows upstream and downstream of the blades are uniform, and that the flow angles at these stations be specified. These conditions imply that the tangential deflection through the cascade is known a priori, whereas in actuality the possible deflection depends on the attitude of the blades in the cascade and the upstream conditions only. Whereas in turbine cascades it is possible to calculate the discharge angle from the geometry of the cascade with approximate methods, such predictions are not possible in axial compressor cascades, in fact one of the major problems is to find out what the discharge angles are for imposed incidence angles. Actually then, Ref. 11 produces pressure distributions about blades for specified locations of the rear stagnation points, and if they have been chosen wrongly the pressure pattern will be wrong also. As in most theoretical cascade flow investigations the effects of upstream or downstream cascades cannot be taken into account; the row investigated constitutes in actuality a disturbance located between two flow fields that extend to infinity far upstream and far downstream without being disturbed by other cascades.

A major drawback of all methods that are based on Eq. 46 is however that the right-hand side of this relation becomes zero if either ω is zero, or if λ is zero. If the angular velocity is zero the cascade is stationary and instead of the pattern of the relative velocity W one deals with the absolute velocity V in a stator whose curl $\nabla \times \vec{V}$ is now zero because of the initial condition that $\nabla \times \vec{W} = -2\vec{\omega}$. The velocities V of such flows must be gradients of a potential function φ, and Eq. 46 can be modified to

$$\nabla^2\varphi = \frac{\nabla\varphi}{a^2} \cdot \nabla\left(\frac{V^2}{2}\right) \qquad (47)$$

where "a" is the variable velocity of sound at the different locations in the flow field. As before it is necessary that $M = V/a$ is everywhere smaller than unity. For incompressible flows, where the velocity of sound "a" is tending toward infinity, Eq. 47 reduces to Laplace's equation $\nabla^2\varphi = 0$. Equation 47 is a partial differential equation of the Poisson type and the term on its right-hand side can be interpreted mathematically to be the result of sources in the flow field. Expressed differently, the curl of $\vec{V}$ is zero, but its divergence $\nabla \cdot \vec{V}$ is not; which means that flow must be generated somewhere in the field, and sources judiciously arranged therein can take care of this situation. Reference 12 develops calculating methods that are based on this idea by using the principles of superposition, but again for assumed axisymmetric stream surfaces, namely, cones in particular.

It can be noticed also, that Eq. 46 changes into Eq. 47 if $\lambda = 0$; that is, if cylindrical stream surfaces are assumed to exist. Thus, as far as axial machines with cylindrical stream surfaces are concerned, the flow through a rotor is not different from the flow through a stator, if the cascades have the same geometries and if the flow angles of the relative and absolute flows are equal. On the other hand it can be proved without a shadow of a doubt, e.g., by Art. 8.5 of Ref. 1, that even isentropic relative flows in rotors must be fundamentally different in character from absolute flows. From Eq. 8(23) of Ref. 1 it can be seen clearly that the simplest relative flow must have $\nabla \times \vec{W} = -2\vec{\omega}$, and if Kelvin's theorem is extended to relative flows (Eq. 8 (22) of Ref. 1), and applied to isentropic conditions, one sees that the change of the circulation Γ_R around a moving fluid curve C in a relative flow is not zero but equal to

$$\frac{D\Gamma_R}{dt} = -2 \oint_{(C)} d\vec{r}_R \cdot \vec{\omega} \times \vec{W} \tag{48}$$

In an absolute isentropic flow, however, the change of the circulation around a moving fluid is indeed zero. Equation 48 indicates that $D\Gamma_R/dt$ is zero only if the relative flow vectors $\vec{W}$ are everywhere parallel with $\vec{\omega}$, hence parallel with the axis of rotation. Rotors of this type are not capable of changing the energy of fluids and have no practical interest. That the condition $\nabla \times \vec{W} = -2\vec{\omega}$ is not in conflict with Eq. 48 can be proved with simple means.

It can be stated therefore that the stream surfaces in a rotating cascade must differ from those that would occur if the same cascade were stationary. More precisely, the stream surface in a stationary cascade, whose flow satisfies $\nabla \times \vec{V} = 0$, must change to a pattern that satisfies $\nabla \times \vec{W} = -2\vec{\omega}$, and it is not possible that the relative flow in the rotating cascade has the same stream surfaces as the absolute flow. In particular, the relative stream surfaces cannot be axisymmetric, if those of the absolute have this character. More about these conditions has been described in Art. 10.5 of Ref. 1, but it is evident from the above discussion that results obtained by solving Eqs. 46 and 47 must be of approximate nature even for the idealized flows that are investigated, and they must be interpreted in the proper perspective of their initial assumptions.

Such results, or data from stationary cascade test rigs which basically are obtained with the same assumptions as those of the above-mentioned theories, are now used to establish the blading elements in the individual flow channels between the solid stream surfaces. The classical method consists in designing the actual blade surfaces through the profiles of these blade elements. The "solid" stream surfaces are then, so to say, removed and it is assumed that the originally calculated or assumed stream surfaces will also exist for the flow about these three-dimensional blades. It is quite clear that there are many possibilities of arranging an actual blading with the profile sections that are obtained from the flows through the individual flow channels, depending, for instance, on how the leading edge of the blade is arranged. In the inducer of Fig. 1 the leading edge of the blade could be pulled forward in flow direction to obtain a blade surface that is leaning more away from a meridional plane than if the leading edge were to slant backward, although at the different radii the blade angles would be exactly equal. Without a doubt these two blades would exert different forces on the flow, one could tend to push the flow toward the tip, the other toward the hub, and it is inconceivable that the flow pattern in the meridian channel would remain unchanged. In Ref. 2 (Table C-2, p. 26) an investigation dealing with the blading of an axial-flow machine has been carried out to check whether it is possible to build a rotor with a very large number of thin blades that produces the idealized relative flow with $\nabla \times \vec{W} = -2\vec{\omega}$ near its cylindrical hub. This flow condition establishes a particular change of the flow angle in radial direction, and requires that the blade surface consists of radial lines. Since for a large number of blades the flow and the blade angles must be identical, the last mentioned requirement establishes the change of the flow angle along the radius by itself. It can be seen that the two values differ, primarily because from $\nabla \times \vec{W} = -2\vec{\omega}$ the necessary blade angle change depends on the ratio of ω and the axial component of $\vec{W}$, whereas this is not the case for the other. Hence, it is evident that the condition $\nabla \times \vec{W} = -2\vec{\omega}$ cannot be maintained in a blading with a finite axial length, and that the actual blade shapes as a whole will have an influence on the flow through them. These examples show that the flow patterns in a machine can be influenced by particular arrangements of the profiles in direction of the blade height and that they will have a bearing on the meridional flow. The classical approach, so to say, linearizes the problem, and does not take account of the interactions that occur between the flows through the different elementary channels from the hub to the tip. It further tries to explain all phenomena with a two-dimensional model, at best with one on stream surfaces that are surfaces of revolution, and looses sight of the actual three-dimensional effects that occur in reality. These limiting view points seem to be particularly harmful if supersonic flows occur in a relative flow field where, as discussed earlier in connection with the inducer inlet, the absolute flow is subsonic. Stationary cascade test data cannot give a true picture of the conditions since they replace again the relative flows by an absolute flow between "solid" stream surfaces, where in particular the condition that the flow component perpendicular to the cascade axis, which is in reality the actual absolute flow, has no special significance. In a supersonic cascade test rig it will hardly be possible to determine cascade performance at different incidence angles nor establish design data for blades where only parts of the blades have supersonic velocities. For inducers of radial compressors which are followed by radial blades it does not seem possible to use cascade data with any degree of realism, and only experimental work with actual rotating wheels will show what detrimental effects high relative flow Mach numbers have on the performance.

There seem to exist a number of design variables that should be examined for supersonic inducers. The possibility of influencing the flow pattern near the tip by appropriate blade shapes to produce, say, greater mass flow rates per unit area near the hub, has been mentioned. These designs could be extended to produce swept-wing effects, similar to what has become the standard design of wings for high-speed airplanes. It is well known that in supersonic flows the velocity parallel with the leading edge of a swept-back wing with infinite span cannot produce variations in pressure, hence only the component of velocity perpendicular to the leading edge can create losses that are caused by compressibility effects. Peculiar conditions could however occur at the outer wall, if this principle were applied to the design of the inducer inlet edges, but it might be possible to obtain considerable improvements. The writer is surprised that such designs

have not been tried for axial compressor stages, especially for those with large blade heights. Swept-back blades would not necessarily have greatly increased bending stresses, since the maximum section modulus of an airfoil profile is a large multiple of the minimum modulus about the outer principal axis. If the centers of gravity of the profiles along the blade height were displaced backward along this axis of the hub profile, it should be possible to minimize the stresses that are caused by the additional bending moment about the other principal axis.

The writer believes that it is possible to build inducers at supersonic relative inlet velocities for absolute inlet Mach numbers M_{V1} of about 0.5 to 0.6 with good efficiency and minimum flow disturbances. Converging-diverging passages in the inducer seem unnecessary, especially if only part of the rotating channel has supersonic velocities. Leading edge radii must be as small as possible, but large enough to avoid damage by flutter, and great care must be taken to properly design the suction side of the blade to provide a good transition into the actual blade channel. It is not believed however that the blades must be designed for incidence angles if the proper blockage factor is used for the flow area calculations at the inlet. This statement contradicts the data of Ref. 13, where the optimum rotor efficiency η_R is shown to occur at positive incidence angles of about 10° at R_{1o} for blade angles of 57°. The inlet channel ahead of the eye of the wheel that was tested, has curved meridinal contours, hence the inlet velocity V_1 is not uniform from R_{1i} to R_{1o}. Although it is stated in Ref. 13 that the distribution of V_1 was determined by probes, slight inaccuracies of the measurements, or a location of the probe at some distance forward of the leading edges of the rotor could easily be responsible for these unusually large incidence angles. By means of theoretical methods, which are not described in detail, the velocity distributions along the inducer were determined also in Ref. 13 to verify the test data. However, as shown by Fig. 5 of Ref. 13, the inducer has simply been replaced by a cascade, since at its discharge the velocities on either sides of the blade are shown to be equal, a situation which cannot exist in reality, and which gives questionable value to the argumentation based on it.

Design criteria for the whole rotor passages from the inlet to the discharge are often given in terms of the deceleration ratio W_2/W_{1o} of the relative rotor velocities. From earlier discussions with regard to rotor losses it is evident that not all losses in a rotating impeller depend exclusively on this ratio. They will also be greatly influenced by the performance of the inducer, in particular, on the velocity distribution that exists at the station where the inducer blades join the radial impeller blades. It is necessary to have a good appreciation of the complexities of flows in rotating impellers to avoid over-simplifications and the setting up of design criteria that are based on wrong models. An invaluable contribution to investigating the real flow phenomena in rotating impellers has been made by Fowler[14], who actually measured the velocity distribution in the passages of a large compressor with probes from a platform inside the hub that was rotating with the wheel. Figure 11 has been adapted from a personal communication of Mr. Fowler to the writer. It shows the velocity profiles at seven cross sections of the rotor flow channel of an unshrouded wheel with radial blades at the discharge, when operating at a peripheral speed U_2 = 17 ft/s. The meridional flow channel has the smoothly changing contours used for modern designs. Plane 1 of Fig. 11 is at the inlet section of the inducer blades, extending from the leading edge of one blade to the back of a neighboring one, and the blades become radial near plane 3. The zones with reduced velocities at the blade tips that are due to the blade gap and the scrubbing effects along the outside wall, remain almost equal from plane 3 to the discharge plane 7. It is of interest to compare these measured velocity distributions with the theoretical solutions of Eq. 47 for radial blades and incompressible flows. The pattern of the streamlines obtained by Stanitz for a radial impeller with 20 blades is shown in Fig. 3.5.2 of Ref. 3. The velocities are inversely proportional to the distance between neighboring streamlines. The leading surface of a blade will be called the pressure side, the trailing surface of the same blade is its suction side. Hence the direction in a blade channel from the pressure side of one blade to the suction side of the neighboring one, is in direction of rotation of the wheel.

At the outer radius of the wheel (R = 1 in Fig. 3.5.2 of Ref. 3) the theoretical analysis predicts that the velocity in a blade channel increases in direction of rotation, whereas exactly the opposite trend is seen to occur in plane 7 of Fig. 11. However in planes 3 and 4, and to a lesser degree in plane 5, the measured velocity changes agree in the main with the theoretical ones which predict a velocity increase in direction of rotation at all radii. This situation occurs because the theoretical method shows, or is based on the assumption, that at radii smaller than about 70 percent of R_2 the relative velocities are everywhere radial. Then, as determined in Art. 10.6 of Ref. 1, and as shown in Fig. 10(5a), they will increase linearly with the angle along the periphery in direction of rotation. The measured reversal of this behavior, starting from plane 5 to the discharge plane 7, cannot be due to viscous effects only, which are neglected in the theoretical treatment, but must occur because of flow peculiarities that a simplified theory cannot take into account. In his personal communication to the writer, Mr. Fowler also remarked that the directions of the relative velocities at the discharge did not have as large a deviation from the radial direction as Fig. 3.5.3 of Ref. 3 shows. The measured flow distributions suggest that considerable mixing of the different flow strata must occur while they pass through the compressor and it is very unlikely that there exist axisymmetric surfaces. Reference 15 describes tests of single, straight diffusors that were arranged radially and rotated in the test rig of Ref. 14, to examine the effects of centrifugal and Coriolis forces on decelerated flows that move radially outward. Diffusors with different divergence angles where investigated, first while stationary and then while rotating. It was found that considerable differences occur if a diffusor is rotated. Static tests with a two-dimensional diffusor with an included angle of 10° showed the well-known peaked velocity distributions that occur for these angles. If rotating, the peaks flatten out and the flow becomes more stable. These results agree with the conclusions reached earlier about the beneficial effects of a centrifugal force field on decelerated flows, but they show also that boundary layers along rotating walls, where the fluid particles are also affected by Coriolis forces, exhibit different characteristics than those along stationary walls. Similar results have been obtained in Ref. 16 which describes tests of flows through a channel with constant cross section that is rotated about an axis. Because of these conditions, different separation criteria for boundary layers must be applied if they occur on stationary walls or on surfaces that rotate about an axis.

For this reason it is not possible to use conventional boundary layer theories as a means to find permissible deceleration ratio W_2/W_{1o} for the relative flows in impellers, nor can attempts be successful that try to relate this ratio to the NASA diffusion factor, which has proved to be a satisfactory separation criterion for axial compressor bladings which have small flow deflections, hence, where the changes of the

Coriolis forces are small if the blading rotates. Much more fundamental work dealing with boundary layers on rotating walls and investigations with modern flow visualization methods must be carried out before it is possible to establish satisfactory design limits for flows in radial impellers. Recent endeavors that use holography with Pulse-Lasers for investigations of flows in rotating wheels might open entirely new ways to study actual flows in high-speed machines where the effects of centrifugal and Coriolos forces are large.

If the above-mentioned peculiarities of rotor flows are not taken into account one might come to the conclusion, as some sources do, that flow separations will occur in an impeller if W_2/W_{1o} equals 0.6, and that a ratio of 0.62 should be used for design purposes to avoid excessive losses. Such values are obtained from analogies with stationary diffusors or oversimplified boundary layer considerations for, say, linearly changing velocities along a surface, as is the case on the suction side of a blade in an axial compressor cascade. Figure 9 is a diagram for the determination of the deceleration ratio W_2/W_{1o} in accordance with Eq. II(5) of Table II. If, for instance, the limit for this ratio were set at 0.65, the discharge angle α_2 could not be larger than about 60° for a radius ratio R_{1o}/R_2 of 0.7 and $\beta_{1o} = 60°$. For larger discharge angle α_2 the radius ratio R_{1o}/R_2 would have to be decreased. Figure 12 is presented to show these conditions more precisely if the lower limit of W_2/W_{1o} is assumed to equal 0.6 and if the slip factor μ is 0.85. For these conditions and at $\alpha_2 = 75°$, the maximum radius ratio R_{1o}/R_2 could not exceed 0.42 at a relative flow angle $\beta_{1o} = 70°$. Experience with high performance compressors shows however that impellers with radius ratio in accordance with the dashed curve have operated successfully. At $\alpha_2 = 75°$, for instance, and at a radius ratio R_{1o}/R_2 of 0.68 the deceleration ratio is of the order of 0.35 to 0.3, depending on β_{1o}, as shown in Fig. 9 by following path "b" in the diagram. Therefore, if the deceleration ratio W_2/W_{1o} is used as a preliminary design criterion it is permissible to apply minimum values of about 0.3 or even somewhat lower, say, about 0.26. A unique relationship between W_2/W_{1o} and the wheel efficiency η_W cannot be established because of lack of test data but in Paragraph 5 some test results are plotted to show the order of magnitude of η_W. A correlation between W_2/W_{1o} and η_W can probably never be obtained because of the additional rotor losses that depend on a number of additional factors.

For known values of M_{W1}, β_{1o}, and U_2/a_o it is possible to calculate the wheel radius R_2 with Eq. II(9) of Table II, if the ratio R_{1i}/R_{1o} were known. The quantity k_{B1} is a blockage factor which is primarily depending on the number of inducer blades and their thickness at the inlet throat, although excessively thick boundary layers on the walls of the inlet annulus can affect k_{B1} also. Evidently if U_2/a_o is known the angular velocity ω is known also, if R_2 has been determined. However ω can be determined directly by Eq. II(10) of Table II, for known or chosen quantities M_{W1} and β_{1o}. Eq. II(10) is useful to establish the necessary rotative speed to handle particular flow rates. If ω is given, because of the prime mover that drives the compressor, Eq. II(10) makes it possible to verify whether a particular flow rate can be handled at this speed. The ratio of axial blade width b_2 and R_2 is obtained by Eq. II(11). The blockage factor k_{B2} is the ratio of the actual flow area at the wheel discharge and the area $2\pi R_2 b_2$, multiplied by an experience factor that depends on the boundary layer thickness on the side walls.

The necessary diffusor exit area A_4 at the radius R_4 is obtained from Eq. II(14) for specified values $\lambda = V_4/V_2$ and known efficiencies η_c. A blockage factor k_{B4} takes account of the displacement thickness of the boundary layers which reduce the actual flow area at the discharge of the diffusor. Section x-x of Fig. 1 is taken to be either the throat of the diffusor where the flow is choked if the absolute velocity V_2 after the rotor is supersonic, or the entrance section of the actual diffusor if V_2 is subsonic. The necessary total flow area of all diffusor channels is denoted by A_x, and k_{Bx} is again an area blockage factor. The area A_x can be determined for both cases if the ratio of the total pressures P_{tx} at station x and P_{t2} at the rotor discharge is known. Although P_{t2}/P_o could be expressed by Eq. I(19) of Table I and then introduced into Eqs. II(13) and II(14), it is better to use these relations as listed, since it is possible to judge approximately what values the ratio P_{tx}/P_{t2} will have for particular diffusor designs. If V_2 is supersonic the throat area is obtained with the dimensionless critical flow function Φ_c of Eq. II(14) which has a value $\Phi_c = 0.6847$ for $\gamma = 1.4$. For subsonic velocities V_2 the diffusor inlet area can be determined only if the velocity V_x at station x is specified, by assuming a value $\xi = V_x/V_2$. Usually this ratio is taken to be about 1.02 to 1.05 because a slight acceleration between stations (2) and (x) will produce more uniform flow conditions at the diffusor inlet. For a chosen number of diffusor flow channels, usually arranged between parallel walls, the diffusor widths at inlet and discharge can be determined from A_x and A_4, and the methods described in Paragraph 5 establish the necessary length of the diffusor channels. With this length and the chosen diffusor arrangement it is possible to establish the outer radius R_4 of the diffusor.

4. SIMILARITY CONSIDERATIONS

If effects due to gravity, surface tension, and heat conductivity can be ignored, which is permissible for most flows in turbomachines, the laws of dynamic similarity establish that flow processes of perfect gases in geometrically similar channels are equal in performance if the Reynolds numbers R_e and the velocity ratios $V/\sqrt{R_G T}$ are respectively equal at corresponding stations in the channels. As derived for instance by Ackeret et. al., in Ref. 17, the latter condition can be expressed in terms of equal Mach numbers M, with the additional requirement that the fluids passing through the geometrically similar channels have equal specific heat ratios γ. Reference 17 shows also that the effects of different values of γ are small only if the Mach numbers are less than about 0.6. The reason is that gases with different heat ratios γ produce different relative changes in density if passing through a channel with particular area ratios. Hence the values $V/\sqrt{R_G T}$ cannot remain equal in geometrically similar channels.

Assuming then that gases with equal values of γ are considered only, and that the Reynolds numbers of the flows in the compressors to be compared are in a range where they can vary considerably without largely changing the frictional coefficients; that is, if they are moderately large and if the flow surfaces are rough, dynamic similarity is achieved in geometrically similar machines at equal Mach numbers.

In hydraulic machines, similarity considerations that are based on the so-called specific speed have been used with success and it will now be examined whether it is possible to apply this method also to the compressors considered here that operate at high speed ratios U_2/a_o. Attempts to obtain design limits and to establish the optimum operating range of radial compressors with this means are described in Refs.

18 and 19. In both reference there is used the specific speed N_S (see Eq. III(1) of Table III)

$$N_S = \frac{N\, Q^{\frac{1}{2}}}{H_{is}^{3/4}}$$

similar to the practice in hydraulic pump design. In the latter application, Q, which is the volume flow rate through the machine, is everywhere constant. In a compressor for gases however, where the volume flow rate will change considerably from inlet to discharge, a choice must be made whether Q at station (1), or at, say, station (2) is to be used in Eq. 50. In both references the quantity Q is taken to be the inlet flow rate Q_1 without giving reasons for this choice. As in Refs. 18 and 19, and as shown in Table III by Eq. III(1), the value of N_S depends on the system of units which is used. In the two cited references N_S has the dimension rpm $ft^{3/4}$ $sec^{-1/2}$, which is awkward for purposes of comparison with similar coefficients in other systems of units, and such formulations are not in keeping with the general and very desirable tendency to use dimensionless quantities throughout. For this reason it is more appropriate to use the dimensionless speed n_S, with units as defined by Eq. III(3) of Table III, which for particular conditions has the same value in all consistent systems of units. The quantity n_S is obtained by dividing the value of N_S in the given English units by 129.

Whereas Ref. 18 (Fig. 2.8) simply presents a graph showing a direct correlation of the efficiency of different compressor types with N_S, Ref. 19 uses the so-called specific diameter D_S as an additional parameter, which is defined by (see Eq. III(2) of Table III)

$$D_S = \frac{D\, H_{is}^{1/4}}{Q_1^{1/2}}$$

This quantity is also not dimensionless. However Eq. III(4) defines a dimensionless specific diameter d_S that is obtained from D_S in English units by division with 0.42.

The coefficient ξ_1 of Eq. III(5) represents the ratio of the area of the flow annulus at the compressor inlet and the area πR_{1o}^2, where R_{1o} is the outer radius of the rotor inlet eye. As shown in Table III the quantities n_S and d_S can be expressed also with the chosen parameters of Tables I and II, to obtain Eqs. III(6) and III(7). Both contain ξ_1, so that this ratio can be obtained from either of these relations as shown by Eqs. III(8) and III(9). By equating these expressions there is obtained Eq. III(10), or

$$n_S\, d_S = \frac{2}{(\mu\, \eta_c)^{1/2}}$$

where μ is the slip factor and η_c the compressor efficiency. Since μ is a known quantity for a particular compressor design, and because η_c can be determined with Eq. II(1), the specific diameter d_S is directly related to n_S and there is no reason why both n_S and d_S should be specified for a design with radial blades. Equation III(11) shows that by specifying n_S there can be obtained the radius ratio R_{1i}/R_{1o} for particular values of β_{1o} and R_{1o}/R_2 which are usually chosen on the basis of other considerations, as explained earlier, Equations II(9) and II(10) of Table II, with the known ratios R_{1i}/R_{1o}, would then give directly the necessary radius R_2 or the angular velocity ω for given operating conditions. If the optimum efficiency of a compressor were a unique function of n_S, and if R_{1i}/R_{1o} and/or the other parameters could be adjusted to meet the optimum value, the designer would have a simple criterion for the optimization of compressors.

From Ref. 18 (Fig. 2.8, p. 38) it appears that radial compressors should have the best efficiency for values of N_S between 75 and 85, or for n_S between 0.58 and 0.66. Table III gives an example for design parameters that have been used successfully. In one case, a radius ratio R_{1o}/R_2 of 0.56, in another a ratio $R_{1o}/R_2 = 0.7$ was chosen. For the smaller value of R_{1o}/R_2 it is not possible to design for $N_S = 80$, since the hub/tip ratio at the inlet becomes zero at $N_S = 71$. In an actual design of a compressor that had efficiencies higher than 80 percent, the hub/tip ratio at the inlet was about 0.46 for $R_{1o}/R_2 = 0.56$, hence it operated at $N_S = 60$ and did not have the much lower efficiency predicted by Ref. 18. For the example in Table III with the higher ratio $R_{1o}/R_2 = 0.7$ the ratio R_{1i}/R_{1o} becomes zero at $N_S = 99.4$, and an actual high-performance machine is known to the writer that has an inlet hub/tip ratio of 0.34, hence it operates at $n_S = 0.725$ or $N_S = 93.5$. Thus, the sharp optimum for N_S in Ref. 18 does not occur in reality and $N_S = 80$ or $n_S = 0.62$ is not a design criterion.

It is obvious from Eq. III(6) that all radial compressors have values of N_S between, say, 60 and 110. Lower and higher values would lead to impossible designs which would never be built anyway. The only merit of the specific speed is to find out whether a radial compressor can be built at all for given values of N, Q_1, and H_{is}. If N_S is outside the range of 60 to 110, and if the above-mentioned design conditions cannot be changed, another type of compressor has to be chosen. However, if the relations of Table II were applied, the same conclusions would also be reached immediately even if the specific speed concept had never been invented. In fact its use can also be dangerous if, as might be the case for the example of Table III with $R_{1o}/R_2 = 0.56$, the designer would try to reach the highest possible N_S by making the radius ratio R_{1i}/R_o excessively small or choosing too high a value of R_{1i}/R_o to reduce N_S for $R_{1o}/R_2 = 0.7$. The example also shows that large changes of R_{1i}/R_{1o} have a small influence of N_S except, near the maximum possible value of N_S where R_{1i}/R_o tends toward zero. Further, if $N_S = 80$ would be considered necessary, a large number of high-performance radial compressors would never have been built, much to the detriment of the development of these promising machines, where a better physical understanding of the complicated flow phenomena can still lead to considerably improved performance.

Unfortunately there always exists the tendency in engineering to try to set up simple rules or criteria which make it possible to judge whether or not a design is feasible, without having to go through the strenuous mental processes to try to understand the phenomena that actually occur and to relate them to the fundamental laws of nature. If our only task were to build the same machines over and over again, sometimes

a little smaller, all would be well with this kind of handbook engineering. However, if an engineer believes that improvements are possible,aand if he reflects on what has happened during the past years he cannot doubt that this will be the case, he must not accept the barriers that have been set up by past experience, and be impressed by the achievements that have been made. With a critical mind he has to evaluate what is true and what is false with accepted methods, and his aim must be to try to understand, to search, and to improve. Too often engineers are handlers of formulas or recipes, and there is the tendency to accept their results as correct without much questioning, especially if they are ground out by a computer, without finding out what sort of basic principles and assumptions led to the numbers. In the near future our modern computers may well be the biggest obstacle to imaginative original thinking and the use of new concepts, since for every problem there will very soon exist some sort of a program that can show that everything is known, and that nothing new needs to be added. All one has to know is the necessary format for the input to obtain the desired result, in print, in graphs, even in drawings. The inventive and critical engineer however must take the trouble to find out how the program was established and what basic principles and assumption were made, and must then evaluate the obtained numbers in the light of these conditions.

The biggest objection to the specific speed criteria is however that they do not satisfy the laws of dynamic similarity, even not for the limiting conditions that were assumed earlier. Equation III(6) shows that n_S is independent of the pressure ratio that is produced by a compressor. If all factors in Eq. III(6) are equal for two compressors, they can have different values of U_2/a_0 and therefore widely different blade width b_2 at the rotor discharge. One compressor could operate with subsonic, the other with supersonic velocities at the diffusor inlet. Figure 13 is an adaptation of Fig. 4 of Ref. 19. The curves of constant efficiency $\eta_c = 0.7$ and $\eta_c = 0.8$ and the curves labeled $N_{W1} = 1.0$ and $N_{W1} = 1.2$ for P_{t4}/P_0 were taken from Ref. 19 and redrawn in a bigger scale. Although labeled as lines of constant Mach number in Ref. 19 the curves for N_{W1} = constant are for constant ratios of relative inlet and critical velocity for the total inlet temperature. Equation III(14) of Table III shows how these ratios are related to the actual Mach numbers M_{W1}. Although the differences between N_{W1} and M_{W1} are small at low Mach numbers, the values of M_{W1} vary from 0.94 to 1.01 for $N_{w1} = 1.0$ if β_{1o} changes from 50° to 75°. According to the author of Ref. 19 the curves for $N_{W1} = 1.0$ and 1.2 represent design limits for higher pressure ratios. It is stated that maximum efficiencies will occur for impellers with backward bent blades operating at specific speeds N_S between 90 and 130, and specific diameters D_S between 1.3 and 1.7. The straight lines labeled $\mu\eta_c$ = constant which the present writer drew into the original diagram of Ref. 19 represent Eq. III(10), and relate D_S to N_S for wheels with radial blades at the discharge. Average values for $\mu\eta_c$ for such impellers are 0.7, hence all radial compressor of this type must lie in the vicinity of this curve for $\mu\eta_c$ in Fig. 13. The points labeled (1) to (7) in Fig. 13 represent design points for some actual compressors known to the writer, operating with U_2/a_0 of about unity, and inlet Mach numbers of 0.9 and higher. It is of interest to note that all these points lie on the curve $\eta_c = 0.70$ of Ref. 19 whereas all compressors, even those having N_S-values between 60 and 70, have efficiencies of 80 percent and higher. This situation shows again that the specific speed concept is a highly unsatisfactory design criterion, especially for radially-bladed compressor wheels, since it is impossible to design such machines with operating points that fall inside the closed curve, labeled $\eta = 0.8$ in Fig. 13. It is pointed out in Ref. 19 that the data presented in its Fig. 4 were calculated on the basis of loss considerations. It can be concluded therefore that this loss evaluation is in error or unsuitable for compressors with rotors that have radial blades at the discharge.

What seems more crucial to the writer is the fact that on the basis of Fig. 4 of Ref. 19 (or Fig. 13 of the present article) one might come to the conclusion that it is not possible to build high-speed compressors of the type discussed here with high efficiencies, for instance, as required for gas turbines, and that further developments of these machines might not be undertaken because of "proof" that improvements are not possible. This is again a case which shows that an analysis is no better than its assumption. Since the specific speed has no real physical meaning, unlike the actual similarity parameters such as Reynolds number, Mach number and others, the writer deplores the tendency to express everything in flow machines with N_S, also phenomena on which N_S has really no primary influence. Because of the definition of N_S it is always possible to do so because either rotative speeds and flow velocities, or lengths, can be related to it, and since in all these expressions there then appears N_S in one form or another, depending on what simplifying assumptions were made, the reader is given to believe that N_S has a governing influence on the performance, and that manipulating N_S is all that needs to be done to create an optimum design. Everyone who has observed actual flows in turbomachines in test rigs, and has tried to understand the complexities of these processes will agree that nature just is not so simple that it can be explained by a set of convenient numbers.

5. LOSSES IN RADIAL COMPRESSORS

It has been stated earlier that the wheel efficiency η_W of Eq. 15 is the best measure for the quality of a rotor wheel. As indicated, a number of factors influence η_W, but it will be examined now whether the deceleration ratio W_2/W_{1o} has an overriding effect on η_W, as has been suggested by some sources which state that W_2/W_{1o} should not be smaller than about 0.6 to avoid flow separations. It has already been shown in Fig. 12 that such a limit cannot be used for compressors that operate at high speed ratios U_2/a_0 because the radius ratios R_{1o}/R_2 become too small, and it is then not possible to handle the large changes in volume flow rate from rotor inlet to rotor discharge, that occur at high pressure ratios, with acceptable ratios of axial blade width b_2 and R_2. The example of paragraph 6 demonstrates this condition clearly. If $W_2/W_{1o} \geqq 0.6$ were a realistic criterion, the losses in rotors with high speed ratios would be large and it would be difficult to obtain high efficiencies. Figure 14 is presented to show that many compressors have deceleration ratios that are smaller than 0.6 without a drastic decrease in η_W. The circles in Fig. 14 represent design point data of some of the compressors of Ref. 6, and others that are known to the writer. The points indicated by × and + were calculated from the data given in Ref. 13, and the curves drawn through them represent the change of η_W with operating conditions of a particular wheel at values of U_2/a_0 of 0.83 and 1.02, respectively. All data points are for impellers with radial blades at the rotor discharge, and all compressors operate at high speed ratios, having overall efficiencies in excess of 80 percent.

In contrast to the expected trend that η_W decreases with decreasing values of W_2/W_{1o}, the opposite

could be deduced from Fig. 14, since wheel No. 1 with $W_2/W_{1o} = 0.265$ has the highest efficiency $\eta_W = 0.77$. For each data point in Fig. 14 are also given the ratios R_{1o}/R_2, R_{1i}/R_{1o}, b_2/R_2 and $\Delta x/\Delta R$ of the rotor. The latter ratio establishes the general shape of the meridional channel and the values show that the contours of the meridional flow paths of all compressors must have small curvatures with the exception, maybe, of wheel No. 11. Definite reasons for the higher values of η_W in some designs cannot be given, probably because of the effect of the design of the inducers on the wheel performance. However, it is recognizable from Fig. 14 that high efficiencies η_W are reached either for high ratios R_{1i}/R_{1o} or high values of b_2/R_2. The influence of R_{1o}/R_2 seems small, although most good wheels have values of R_{1o}/R_2 between 0.6 and 0.7. Large ratios R_{1i}/R_{1o} require high relative Mach numbers M_{W1} to pass the flow rate through the eye of the impeller, and high ratios b_2/R_2 are obtained if the absolute flow angles α_2 are large. For high values of M_{W1} the inducer becomes critical, and with large angles α_2 the design of the diffusor, especially the transition between wheel and diffusor throat, becomes a difficult task. It is felt that high performance compressors can be developed if more attention is given to these two problem areas.

From the curves in Fig. 14 it is quite evident that the range in which η_W remains constant for off-design operation becomes smaller the higher the speed ratio U_2/a_0 is, a condition which is, at least in part, responsible for the steeper characteristics of compressors operating at high speed ratios.

The ratio of b_2/R_2 also has an effect on the disk friction loss of an impeller. Assuming that the disk extends to the outer radius R_2; that is, if no scallops are arranged, a frictional moment M_{DF} acts on the back side of the impeller which can be determined by [20]

$$M_{DF} = c_M \rho_2 D_2^3 U_2^2 \tag{49}$$

where c_M depends on the Reynolds number

$$Re = \frac{U_2 D_2}{\nu} \tag{50}$$

and the axial gap δ_a between the rotating disk and the stationary wall. The influence of the ratio δ_a/R_2, and the effect of disk roughness, which have been investigated by Refs. 21, 22, 23, and 24 are discussed in Ref. 8. Figure 15 has been established from the results of the quoted references, but experience has shown that the values of c_M can be a multiple of those of Fig. 15 if the flow in the region between the disk and the wall has radial velocity components pointing away from or toward the axis of the impeller. For compressors pumping ambient air the Reynolds number of Eq. 50 varies between about (10^6) and $3(10^7)$ for peripheral speeds between 1000 and 1600 ft/s, and rotor diameters between 3 and 20 inches. Although the average value of c_M from Fig. 15 is then about $1.5\ (10^{-4})$, it has been shown by experience that $c_M = 2.5(10^{-4})$ is more realistic for actual compressor wheels. For a mass flow rate $\dot{m}$ the power absorbed by an impeller is $\dot{m}\ \mu\ U_2^2$ in accordance with Eq. 3, which is also equal to $M\omega$, where M is the driving moment, and

$$M = \frac{\dot{m}\ \mu\ U_2^2}{\omega} = \dot{m}\ R_2\ \mu\ U_2$$

However

$$\dot{m} = 2\pi\ R_2\ b_2\ k_{B2}\ V_{m2}\ \rho_2$$

and, with the relations of Table I,

$$M = 2\pi\ R_2^3 \left(\frac{b_2}{R_2}\right) k_{B2}\ \mu^2\ U_2^3\ \rho_2\ \cot\alpha_2 \tag{51}$$

The total moment which has to be overcome by the driving source is then $M + M_{DF}$ and if the efficiency of the compressor is η_c, without taking the disk friction moment into account, the actual compressor efficiency η of the machine is $\xi_{DF}\ \eta_c$, and

$$\xi_{DF} = \frac{M}{M + M_{DF}} = \frac{1}{1 + (M_{DF}/M)}$$

Then by Eqs. 49 and 51

$$\xi_{DF} = \frac{1}{1 + \dfrac{(4/\pi)\ c_M \tan\alpha_2}{(b_2/R_2)\ \mu^2\ k_{B2}}} \tag{52}$$

It can be noted that ξ_{DF} is independent of the mass density ρ_2 and R_2 since both M and M_{DF} are proportional to these quantities. Hence Eq. 51 holds for all impellers with radial blades the outer radius R_2. Equation

52 is plotted in Fig. 16. This figure shows that with small ratios b_2/R_2 there can occur a considerable reduction in efficiency, which is the greater the larger the angle α_2 is. For $\alpha_2 = 75^o$ the ratio (b_2/R_2) $k_{B2}\ \mu^2$ should not be less than about 0.06 to limit ξ_{DF} to 0.98. Then, with $k_{B2} = 0.95$ and $\mu = 0.90$, the ratio of b_2/R_2 must not be smaller than 0.08 to avoid efficiency reductions because of disk friction moments.

Although the above limit for b_2/R_2 has been obtained by considering the frictional moment at the back side of the impeller, it is very probably that the so-called scrubbing loss of the blade tips at the outer contour of the meridional flow path produces frictional moments which are of similar nature and of the same order of magnitude as the disk friction moments. Moreover, as shown in Fig. 15 for the latter, these moments will also not be greatly influenced by the ratio of tip clearance and R_2 if it is of the order of 0.05, which constitutes a normal to lower limit for most designs. The scrubbing loss is similar to the loss due to disk friction because the boundary layer along the stationary outer wall is rotated by the blade tips. If the losses at the blade tip would be taken to be those due to the flow of the fluid from the pressure side to the pressure side of the blade across the blade clearance, it would be inconceivable that the reductions in compressor efficiency with increased tip clearance are as small as shown by the measurements of Ref. 25. The same behavior has been found in radial turbines[8] where an increase of the ratio of tip clearance and axial blade width b from 4 percent to 10 percent produced practically no drop in efficiency, but if 10 percent was exceeded there occured a radical efficiency reduction. The sudden drop beyond the 10 percent clearance ratio could occur because of massively increased leakage flows across the blade tips once they are outside the wall boundary layer.

Experience has also shown that the ratio of blade width b_2/R_2 should not be less than 8 percent. The value of c_M in Eq. 51 for the representation in Fig. 16 has actually been increased from the average value for disk friction ($\sim 1.5\ (10^{-4})$) to $2.5(10^{-4})$ to demonstrate that this limit is very likely due to the combined effects of disk friction and scrubbing loss. For this ratio of b_2/R_2 and for properly designed inducer sections of an impeller, with meridional contours having small and smoothly changing curvatures, it should be possible to obtain wheel efficiencies η_W of between 0.75 and 0.80 for $b_2/R_2 = 0.08$ if the ratios R_{1i}/R_{1o} are not less than about 0.5.

A large portion of the total losses in radial compressors occurs between the discharge of the wheel and the diffusor throat. The non-uniform distribution of the relative velocities at the rotor discharge produces a non-steady and greatly irregular absolute flow at this station which must be directed toward the diffusor inlet, preferably in a manner that provides uniform flow conditions at this station. If this uniformity is not achieved it is very unlikely that the diffusor proper can perform its function with minimum losses. Very limited data are available for the design of and the losses in these transition sections. Figure 17 shows a typical distribution of the static pressures along the side walls of such a diffusor inlet for a machine that has a value of M_{V2} of about 1.18. Firstly it is clear that the absolute flow is irregular, judging from the change of the pressures in peripheral direction at the wheel discharge. Secondly, the design of the diffusor inlet is not as good as it is desirable because fluid particles undergo compressions and expansions before they reach the diffusor throat. Moreover, Fig. 17 also shows the futility of trying to apply simplified calculating method for this part of the process in the compressor.

Of particular importance is the design of the leading edge of the diffusor blade since the slightest misorientation will produce major disturbances usually with the effect that the flow rate at which the compressor surges is too close to its design flow rate. This condition occurs if the mean angle of the lip section with respect to the radial direction is too large or too small, and since the optimum angle depends on the performance of the rotor, it is not possible to indicate exactly how the transition section must be designed. Experiences have made it obvious, however, that theoretical methods which prescribe a logarithmic spiral or other shapes for the curved part of the transition section overlook the fact that the flows to be handled are so far from being uniform that is almost impossible to obtain optimum solutions without extensive experimental work that investigate the performance of different shapes, not only with respect to optimum efficiency but also to obtain the necessary surge margin. One of the major problems with experiments however is the accurate measurement of the static pressures in these irregular flows. In most cases it is found that Pitot-static pressure probes with even the smallest possible tube diameters are sufficient to change the flow pattern, in fact they usually throw the compressor into surge if it is operating near the design point, so that one has to rely on static wall pressure taps to investigate the effectiveness of different designs. Schlieren pictures for supersonic conditions do also not give information that can be interpreted with ease because of the three-dimensional character of the flow, not to mention the difficulties associated with the arrangement of the necessary optical system. It is therefore quite difficult to measure the true average static pressure after a compressor wheel, and because of the uncertainties that arise if the average static wall pressures at R_2 is identified with it, the separation of the losses into those originating in the wheel, and those occuring in the transition section to the diffusor, is equally difficult. For this reason the evaluation of the actual wheel efficiency η_W may be associated with errors and this could be the reason why it is often impossible to correlate experimental data from different sources. Laser systems were mentioned earlier as an experimental tool to investigate flows in turbomachines, and if the so-called velocimeter, using two laser beams for the determination of the actual magnitude and direction of the velocity in the vicinity of a particular station has been perfected, this instrumentation would be the best possible means to observe the true flow patterns in machines, not only qualitatively but also quantitatively.

In accordance with a limited amount of test data with a compressor operating at $U_2/a_0 = 1.4$, with $M_{V2} = 1.18$, the approximate ratio of the total pressure P_{t2} at the rotor discharge and P_{tx} at the throat of the diffusor was found to be about 1.14, giving an efficiency of the transition section of 0.63. This efficiency is defined as the ratio of the actual static temperature rise to obtain sonic velocity at the throat to that of an isentropic compression for the same pressure ratio. The average discharge flow angle α_2 was about 75°. It seems however that the transition section of the compressor in question could be improved, so that the numbers given above represent only orders of magnitude and not values that cannot improved.

Although a large number of tests have been carried out with subsonic diffusors by many sources, these data cannot be applied directly to the diffusors of compressors with high speed ratios, especially if the

Mach numbers at the diffusor inlet are close to unity. Moreover, it has almost become standard procedure to apply the so-called equivalent cone angle of straight, round diffusors to decelerating flow channels with other cross sections. This procedure converts the inlet and discharge flow areas of a diffusor with arbitrary cross sections into circular ones, either with equal areas or by means of the hydraulic diameter, and then determines the equivalent cone angle with these diameters and the actual length of the diffusor. Either of the two methods for the determination of the equivalent cone angle breaks down for particular designs, or gives results that are in disagreement with actual test data.

An attempt to establish a more rigorous calculating method for arbitrary channels has been made by Traupel[26], primarily for incompressible flows and approximations for the compressible case, but it is then suggested that the equivalent cone angle be used again as a criterion for the permissible deceleration. A different approach is possible, however, which has a minimum of simplifying assumption and has proved to be valid for diffusors of arbitrary geometry, even axisymmetric ones with curved meridian channels and annular cross sections, for instance those arranged after turbomachines to deflect the flow from the axial to the radial direction. The derivation and the use of the equations are given in Table IV. From the laws of conservation of momentum, mass, and energy, combined with the first law of thermodynamics, there is obtained Eq. IV(10) which relates the frictional heat $T\,ds$ to the work necessary to overcome the action of the shear stresses along the channel walls. With the so-called referred mass flow rate $\dot{m}_{r3}$ at the diffusor inlet, which is a dimensionless quantity defined by Eq. IV(14), there is then obtained the principal equation IV(15). This equation is of the form $dX_1 = dX_2$, where dX_1 contains the properties of state ρ, p, and s, at the stations along the channel length, and dX_2 is depending only on the channel geometry and the skin friction coefficient c_f. Actually, for a given diffusor the variables in dX_1 are not independent of the changes of the channel geometry along its length L that occur in dX_2. However, if one were to adjust the flow areas A and the wetted perimeter C of the sections between the inlet and the exit in such a manner that the thermodynamic process of the fluid in the channel would follow a polytropic law, it would be possible to integrate dX_1 independently from dX_2 since s, and ρ are then unique functions of the pressure p for a constant polytropic efficiency η_p or a constant loss coefficient $\zeta = 1 - \eta_p$. Conversely, if an average skin friction coefficient $\bar{c}_f$ is introduced, the value of X_2 is obtained by integrating the quantity $d\Omega$ from diffusor inlet to diffusor discharge, establishing the so-called diffusor shape factor Ω which is identical with the value Φ of Ref. 26. The diffusor shape factor is a dimensionless quantity which depends only on the area and perimeter changes along the length L of the diffusor.

From the integration of dX_1 there is obtained the quantity X_1 as a unique function of the static pressure ratio in the diffusor, γ, and the polytropic loss coefficient ζ. For $\gamma = 1.4$ the function X_1 is plotted in Fig. 18 for different values of ζ, as function of the pressure ratio p_4/p_3. Obviously the conditions of state change monotonously during the polytropic process from p_3 to p_4 in Fig. IV(2), and the function X_1 only holds for such changes. Hence if the area changes in the diffusor would be such that compressions in one part would be followed by expansions in another part, the function X_1 could not take care of the situation, since for an expansion the polytropic law established by Eq. IV(7) would produce an entropy decrease in violation of the second law of thermodynamics. However, even for smoothly changing areas in the diffusor, which it will have in any case, the thermodynamic process in the T-s diagram of Fig. IV(2) might not follow the isentropic line which is shown there, but one which curves either upward or downward from it. It must be recognized however that the value of the function X_1 will not be greatly changed by different distribution of p along L, similar to the integral of Tds which is about equal to $(T_3 + T_4)\,(s_4 - s_3)/2$ almost independent of how the process proceeds from station (3) to station (4), provided it goes along a smooth and fairly regular curve in the T-s diagram.

Moreover, the polytropic loss coefficient ζ is not assumed a priori, but adjusted to satisfy the equation of continuity at the diffusor discharge for a specified average skin friction coefficient. The necessary iteration to solve this problem is explained in Table IV. The method employs the dimensionless flow function Φ which is plotted in Fig. 18 also, with the ratio of total and static pressure that correspond to an isentropic process as variable. Blockage factors for the diffusor areas are introduced to take account of the boundary layer thickness.

For small pressure ratios p_4/p_3; that is, for low Mach numbers at the diffusor inlet, the method leads to relations that are identical with those commonly applied for the loss evaluation for incompressible diffusor flows. In particular, the average skin friction coefficient is equal to

$$\bar{c}_f = \frac{C_{PRi} - C_{PR}}{\Omega} \tag{53}$$

where C_{PRi} and C_{PR} are the so-called ideal and actual recovery factors, which express the increase in static pressure as percentage of the kinetic energy of the flow at the diffusor inlet. The quantity Ω is the diffusor shape factor defined by Eq. IV(19).

Figure 19 shows the skin friction coefficients $\bar{c}_f$ obtained with Eq. 53 from the experimental data of Ref. 27 for two-dimensional diffusors. Except for the diffusor with $L_o/a_i = 48$, which is unduly long, the data lie within a relatively small band, with the test data for a thin displacement thickness of the boundary layer at the inlet near its lower boundary. It is of interest to note that for large values of Ω the skin friction coefficients are very nearly equal to those of fully developed turbulent flows along moderately rough surfaces in pipes or along plates, as shown by Ref. 20 (p. 587, and p. 611). The results of Ref. 28 which were obtained, in part, at high subsonic speeds give values of $\bar{c}_f$ that lie in the same band as in Fig. 19, indicating that the skin friction coefficients $\bar{c}_f$ are directly related to Ω for different types of cross sections, and at speeds where compressibility effects cannot be disregarded.

This product is shown in Fig. 20

From Eq. IV(18) of Table IV it is seen that X_2 is directly proportional to $\bar{c}_f\,\Omega$, for the same data points of Ref. 27 as plotted in Fig. 19. Hence it appears that a diffusor with a shape factor Ω equal to 10 represents an optimum solution. If Ω is smaller the efficiency decreases radically and for values of Ω larger than 10 a diffusor does not make full use of the possible adverse pressure gradient that a boundary layer can sustain without flow separations. The criterion $\Omega = 10$ has been used by the writer with

success for a number of diffusor designs, and a variety of different diffusor shapes is now being tested at NPGS to verify the validity of the criterion at high inlet velocities and with inlet flow distortions.

As shown also in Ref. 26, the shape factor of a round conical diffusor with inlet radius R_i, length L, and the half-angle ϵ of its divergence is

$$\Omega = \frac{1}{2 \tan \epsilon} \left[1 - \frac{1}{(1 + 2(L/R_i) \tan \epsilon)^4} \right] \qquad (54)$$

For conical diffusors where L is large with respect to R_i, Eq. 54 gives a divergence angle of $2\epsilon = 5^o45'$. The influence of the ratio L/R_i is small if L/R_i is larger than about 10. Two-dimensional straight diffusors with constant depth b, and widths a_i at the inlet and a_d at the discharge, determined by $a_d = a_i + 2\ L \tan \epsilon$, where ϵ is again the half-angle of the channel, have shape factors

$$\Omega = \frac{L/a_i}{1 + 2(L/a_i) \tan \epsilon} \left[1 + \frac{1}{1 + 2(L/a_i \tan \epsilon} + \frac{2\ a_i}{b} \right] \qquad (55)$$

If the diffusor of Fig. 17 had a ratio $a_i/b = 2.4$, the value of Ω for $\epsilon = 5^o$ and $L/a_i = 10$, is about equal 22.4, which appears to be excessive. Hence the diffusor should have a divergence perpendicular to the plane of drawing also to increase b_i at the inlet to b_d at the discharge. For shapes of this type the expression of Eq. IV(19) for Ω leads to complicated integrals. However with a simple graphical integration for a half-angle of divergence of about 2^o that produces a ratio $b_d/b_i = 2.4$ with the widths a_i and a_d remaining unchanged, the diffusor form factor is reduced to about 11.2. A diffusor channel for this value of Ω for compressors is very likely very close to the optimum possible solution because of then non-uniform flow conditions that exist at its inlet.

Because of these disturbances, the values of $\Omega\ \bar{c}_f$ presented in Fig. 20 should also be increased, say, from 0.10 to about 0.15, or 0.20, for Ω of about 10. How these values affect the diffusor efficiency will be shown with a simplified approach of the diffusor design method of Table IV. It is assumed that the Mach number M_{V3} at the throat is unity, but the method is not restricted to this value. The flow function Φ_3 of Eq. IV(22) is then equal to 0.6847 in accordance with Fig. 18, and $P_{t3}/p_3 = 1.8929$. From Eq. IV(28) for for $M_{V3} = 1$, $\gamma = 1.4$,

$$\dot{m}_{r3} = (0.6847)\ (1.2)^3 = 1.1832$$

From Eq. IV(18)

$$X_2 = \frac{1.1832^2}{2}\ \bar{c}_f\ \Omega = 0.7\ \bar{c}_f\ \Omega$$

Hence, $X_2 = 0.07$ for $\bar{c}_f\ \Omega = 0.1$, $X_2 = 0.14$ for $\bar{c}_f\ \Omega = 0.2$, and these values are equal to the values of the function X_1 which is plotted in Fig. 18. It will now be assumed that the area ratio A_3/A_4 of the diffusor is $1/6.6 = 0.151$ as is the case for the design of Fig. 17 with a half-angle of divergence of 2^o to increase the depth b also. With blockage factors $k_{B3} = 0.96$ and $k_{B4} = 0.90$, by Eq. IV(29)

$$\Phi_4 = (0.6847)\ (0.151)\ (0.96/0.9)\ (P_{t3}/P_{t4}) = 0.11\ (P_{t3}/P_{t4})$$

Assuming that P_{t3}/P_{t4} is about 1.05, the value of Φ_4 is 0.115. From the plot of Φ vs P_t/p_t it can be seen that for $\Phi_4 = 0.115$, or slight changes of it on account of a wrongly chosen value of P_{t3}/P_{t4}, the value of P_{t4}/p_4 will not be higher than 1.02 because of the large change of Φ with P_t/p_t close to unity. Then,

$$\frac{p_4}{p_3} = \frac{P_{t3}/p_3}{P_{t4}/p_4} \frac{P_{t4}}{P_{t3}} = \frac{1.8929}{1.02} \left(\frac{1}{1.05}\right) = 1.77$$

The approximate values of ζ can then be read from Fig. 18 at the intersection of the lines for the known values of X_1 and for $p_4/p_3 = 1.77$. For $\bar{c}_f\ \Omega = 0.1$, or $X_1 = 0.07$, there is $\zeta = 0.070$, and for $\bar{c}_f\ \Omega = 0.2$, or $X_1 = 0.14$, one finds $\zeta = 0.130$, giving approximate values of the diffusor efficiency of 0.93 and 0.87, respectively, without taking account of the reheat effects that are reflected in Eq. IV(35). The values of ζ thus obtained can then be used to determine the pressure ratio p_4/p_3 more precisely, by taking the pressure ratio P_{t3}/P_{t4} to be that obtained from Eq. IV(33) with the approximate pressure ratio $p_4/p_3 = 1.77$.

6. SAMPLE CALCULATIONS

To demonstrate the effectiveness of the developed performance parameters, and the help of the figures, the dimensions of an impeller for an air compressor with a pressure ratio of eight will be established for the following conditions:

$$\dot{m} = 2.5 \text{ lbm/s} = (2.5/32.174) \text{ slug/s}$$

$$P_0 = 14.7 \text{ psia};\ T_0 = 520^o\text{R}$$

$$P_{t4}/P_0 = 8$$

$$R_G = 1716.48 \frac{\text{ft-lb}}{\text{slug, }^\circ R}\ ;\ \gamma = 1.4$$

From Eq. 5

$$a_0 = 1117.8 \text{ ft/s}$$

Assuming $\mu = 0.9$; $\eta_c = 0.82$, from Eq. II(3), or Fig. 4,

$$U_2/a_0 = 1.658$$

hence

$$U_2 = 1853.4 \text{ ft/s}$$

Figure 8 clearly shows that for this U_2/a_0 and reasonable ratios R_{1o}/R_2 the relative inlet velocity M_{W1} must be supersonic. For $M_{W1} = 1.15$ and $\beta_{1o} = 70^\circ$ there is from Fig. 8, or Eq. II(4),

$$\frac{R_{1o}}{R_2} = 0.642$$

Judging from Fig. 4 it is necessary to choose $\alpha_2 = 74^\circ$ to obtain a value of W_2/W_{1o} of about 0.4. More precisely from Eq. II(5)

$$\frac{W_2}{W_{1o}} = 0.405$$

For a chosen value of the wheel efficiency η_W of 0.7, there are from Eq. 21

$$\Psi = 0.629;\ \Psi^2 = 0,394$$

and the usual rotor efficiency η_R defined by Eq. 12, in accordance with Eq. 24, is

$$\eta_R = 0.88$$

With these values by Eq. II(9)

$$[1 - (\frac{R_{1i}}{R_{1o}})^2]\ k_{B1} = \frac{\dot{m}\sqrt{R_G\ T_0}}{\pi\ R_2^{\ 2}\ P_0} \quad (5.7138)$$

and from Eq. II(11)

$$\frac{b_2}{R_2}\ k_{B2} = \frac{\dot{m}\sqrt{R_G\ T_0}}{\pi\ R_2^{\ 2}\ P_0} \quad (0.4127)$$

and, for approximate values $k_{B1} = 0.85$, $k_{B2} = 0.95$, by division of two above-listed relations,

$$\frac{b_2/R_2}{1 - (R_{1i}/R_{1o})^2} = 0.0646$$

Evidently this ratio holds for all compressors for the chosen conditions, irrespective of the flow rate and the inlet pressure. For chosen radius ratios R_{1i}/R_{1o} there are:

R_{1i}/R_{1o} =	0.2	0.3	0.4	0.5
b_2/R_2 =	0.062	0.059	0.054	0.048

All these ratios are too small to obtain the desired efficiency. They were obtained because R_{1o}/R_2 was chosen too small and the angle β_{1o} is too large, and both these values were taken to maintain a low Mach number M_{W1}. For a second try, let:

$$R_{1o}/R_2 = 0.7;\ \beta_{1o} = 60^\circ;\ \alpha_2 = 75^\circ$$

Then, from the inverse of Eq. II(4), expressing M_{W1} as function of R_{1o}/R_2 and β_{1o},

$$M_{W1} = 1.3198$$

From Eq. II(5)

$$\frac{W_2}{W_{1o}} = 0.360$$

The latter value seems acceptable in view of Fig. 14, and by proper rotor dimensioning a wheel efficiency $\eta_W = 0.7$ should still be reached. By Eq. 21.

$$\Psi = 0.576; \quad \Psi^2 = 0.332$$

By Eq. II(9)

$$\left[1 - \left(\frac{R_{1i}}{R_{1o}}\right)^2\right] k_{B1} = \frac{\dot{m}\sqrt{R_G T_0}}{\pi R_2^2 P_0} \quad (3.7063)$$

and, from Eq. II(11)

$$\frac{b_2}{R_2} k_{B2} = \frac{m\sqrt{R_G T_0}}{\pi R_2^2 P_0} \quad (0.4494)$$

With $k_{B1} = 0.85$, $k_{B2} = 0.95$

$$\frac{b_2/R_2}{1 - (R_{1i}/R_{1o})^2} = 0.1074$$

For the chosen value $b_2/R_2 = 0.08$ the radius ratio R_{1o}/R_2 can be 0.5, which makes it possible to design a meridional flow path that has an acceptable shape.

From the inlet conditions and the design flow rate:

$$\frac{m\sqrt{R_G T_0}}{P_0} = \frac{\frac{2.5}{32.174}\sqrt{(1716.48)(520)}}{14.7} = 4.994 \text{ in.}^2$$

because the pressure P_0 was introduced in pound per sq. in.. Then, from the previous data,

$$\pi R_2^2 = \frac{(4.994)(3.7063)}{(1 - 0.25)(0.85)} = 29.034 \text{ in.}^2$$

Hence

$$R_2 = 3.04 \text{ in.} \; ; \; D_2 = 6.08 \text{ in.}$$

$$R_{1o} = 2.125 \text{ in.} \; ; \; D_{1o} = 4.25 \text{ in.}$$

$$R_{1i} = 1.062 \text{ in.} \; ; \; D_{1i} = 2.125 \text{ in.}$$

$$b_2 = 0.243 \text{ in.}$$

For the chosen data, from Eq. II(6),

$$M_{V2} = 1.256$$

The rotative speed N can be determined from Eq. II(10), or directly from

$$N = \frac{30}{\pi} \omega = \frac{30}{\pi} \frac{U_2}{R_2} = \frac{(30)(1853.4)}{\pi(3.04/12)} = 69{,}860 \text{ rpm}$$

REFERENCES

1. Vavra, M. H. — Aerothermodynamics and Flow in Turbomachines, Wiley Bros, New York, 1960.

2. Vavra, M. H. — Axial Flow Turbines, Von Karman Institute for Fluid Dynamics, Lecture Series 15, pp. 99/100, April 1969.

3. Traupel, W. — Die Theorie der Stroemung durch Radialmaschinen, Braun, Karlsruhe, 1962.

4. Johnston, J. P.; Dean, R. C., Jr. — J. Engg. for Power, Trans. ASME, pp. 49-62, January 1966.

5. Stiefel, W. — "Experimental Investigations on Radial Compressors ...", Course Note 53b, Von Karman Institute, March 1965.

6. Stiefel, W. — "Undersuchung an Radialen Verdichterlauefern," AVA Forschungsbericht 63-01, Triebwerksaerodynamik der Turbomaschinen, Teil II, Goettingen, 1963.

7. Sakai, T.; Watanabe, I., et al. — "On the Slip Factor of Centrifugal and Mixed-Flow Impellers", ASME Paper 67-WA/GT-10.

8. Vavra, M. H. — "Radial Turbines", Part 4 of AGARD-VKI Lecture Series 6 on "Flow in Turbines", Von Karman Institute, March 1968.

9. Bammert, K.; Bohm, E. — "Nuclear Plants with High-Temperature Reactor and Helium Turbine," ASME Paper 69-GT-43, March 1969.

10. Groh, F. W.; Robb, W. L. — "High Efficiency Can Be Achieved in Small Size Transonic Compressor Rotors," SAE Paper 820C, January 1964.

11. Katsanis, T.; McNally, W. D. — "Programs for Computation of Velocities and Streamlines on a Blade-to-Blade Surface of a Turbomachine" ASME Paper 69-GT-48, March 1969.

12. Jmbach, H. E. — "Die Berechnung der kompressiblen, reibungsfreien Unterschallstroemung durch rauemliche Gitter aus Schaufeln auch grosser Dicke und starker Woelbung" Mittlg No 8, Inst. Thermische Turbomaschinen, ETH, Juris Verlag, Zurich, 1964.

13. Linsi, U. — Brown Boveri Review, Vol. 53, No. 3, p. 161, March 1965.

14. Fowler, H. S. — "Some Measurements of the Flow Patterns in a Centrifugal Compressor Impeller," ASME Paper 65-WA/FTP-7, April 1965.

15. Fowler, H. S. — "The Distribution and Stability of Flow in a Rotating Channel," ASME Paper 68-GT-1, March 1968.

16. Halleen, R. M.; Johnson, J. P. — "The Influence of Rotation on Flow in a Long Rectangular Channel" Stanford University, Report MD-18, May 1967.

17. Ackeret, J.; Keller, C.; Salzmann, F. — Schweizer Bauzeitung, No. 23, December 1934.

18. Shepherd, D. G. — "Principles of Turbomachinery", Macmillan; New York, 1956.

19. Baljé, O. E. — J. Engg for Power, Trans. ASME Series A, Vol. 84, No. 1, pp. 83-114, Jan 1962.

20. Schlichting, H. — Boundary-Layer Theory, 6th ed., p. 606, McGraw-Hill, N. Y., 1968.

21. Daily, J. W.; Nece, R. E. — J. of Basic Engg., Trans. ASME, p. 217, March 1960.

22. Nece, R. E.; Daily, J. R. — J. of Basic Engg., Trans. ASME, p. 553, Sept. 1960.

23. Pantel, K. — Forschung, Vol. 16, p. 97, 1950.

24. Maroti, L. A.; Deak, G.; Kreith, F. — J. of Basic Engg., Trans. ASME, p. 539, Sept. 1960.

25. Schmidt-Theuner, P.; Mattern, J. — Brown Boveri Review, Vol. 55, No. 8, p. 453, 1968.

26. Traupel, W. — Thermische Turbomaschinen, Bd. I., p. 308, Springer, Berlin, 1962.

27. Waitman, B. A.
Reneau, L. R.
Kline, S. J. — J. of Basic Engg., Trans. ASME, Vol. 83, Series D., No. 3, p. 349, Sept. 1961.

28. Sovran, G.
Klomp, E. D. — "Experimentally Determined Optimum Geometries for Rectinlinear Diffusors with Rectangular, Conical or Annular Cross Sections," Symposium on Fluid Mechanics of Internal Flow, General Motors Research Laboratories, Sept. 1965.

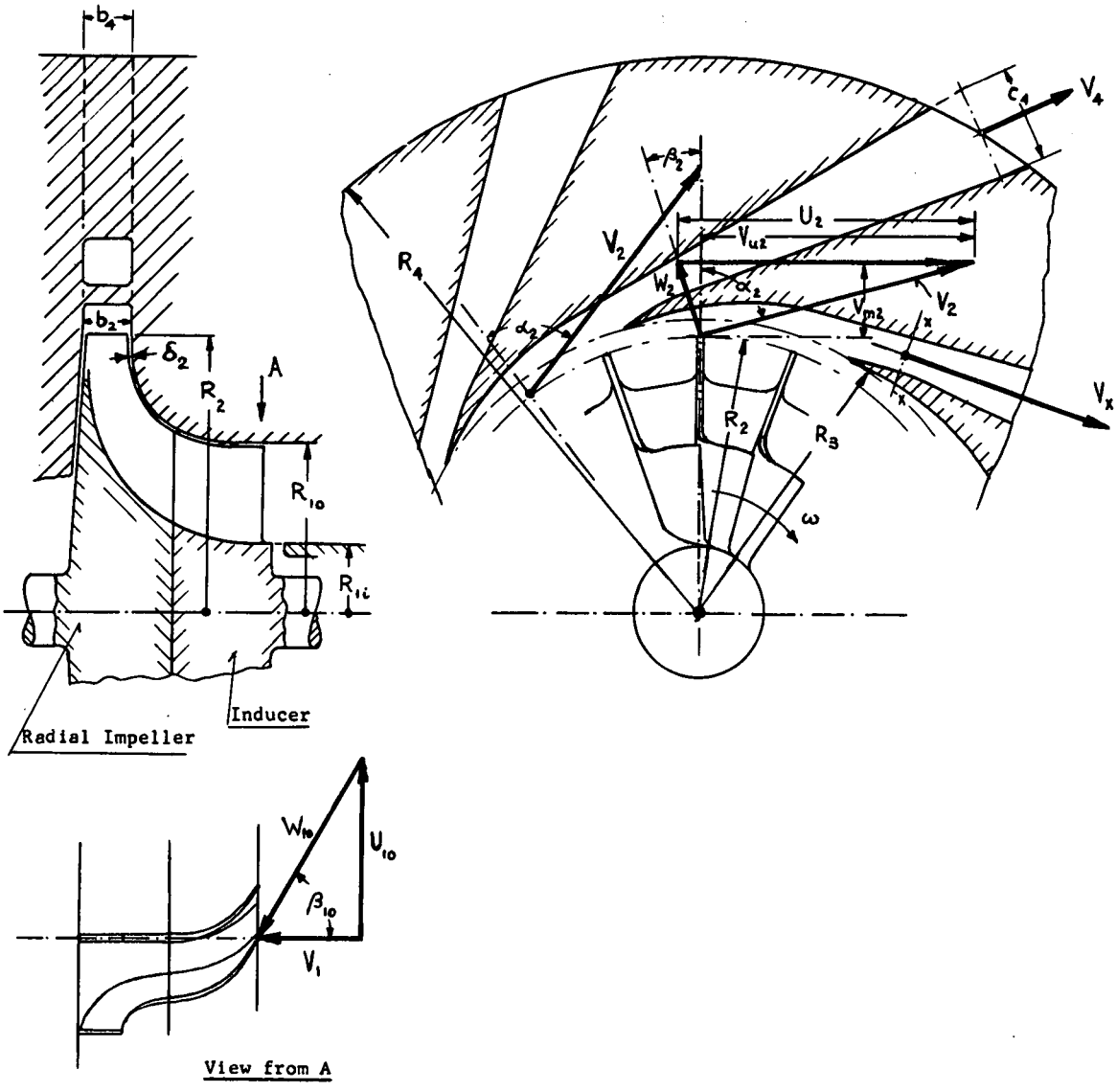

FIG. 1 RADIAL - FLOW COMPRESSOR

R - Radius
V - Absolute Velocity
W - Relative Velocity
U - Peripheral Speed
α - Absolute Flow Angle
β - Relative Flow Angle
b - Axial Channel Width
c - Height of Diffusor Channel

Subscripts:

1 - refers to rotor inlet
2 - refers to rotor discharge
3 - refers to inlet lip of diffusor blades
x - refers to throat of diffusor channel
4 - refers to discharge of diffusor channel

m - refers to meridional direction
u - refers to peripheral direction
i - refers to inner radius at compressor inlet
o - refers to outer radius at compressor inlet

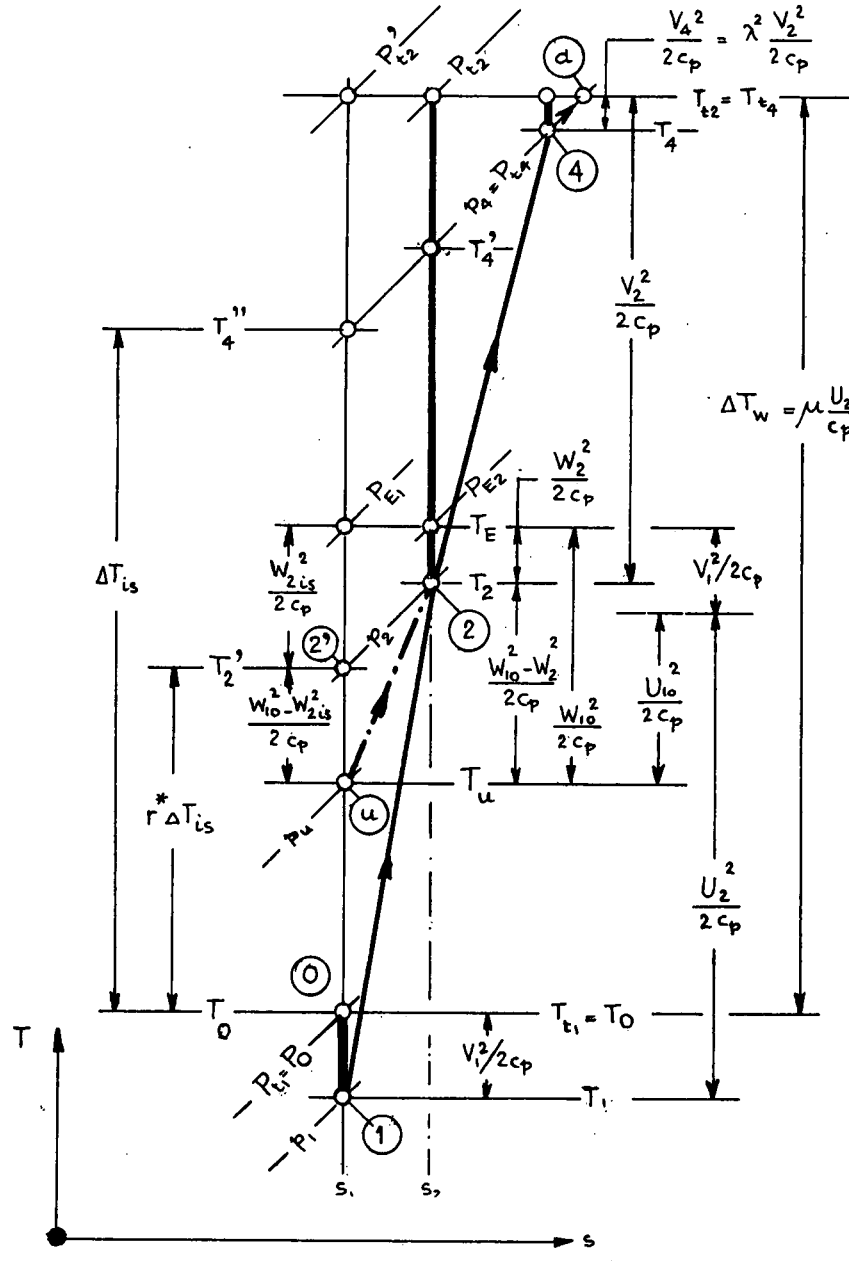

FIG.2 TEMPERATURE-ENTROPY DIAGRAM OF COMPRESSION PROCESS IN COMPRESSOR OF FIG. 1

- c_p - Specific Heat at constant Pressure
- p - Static Pressure
- P_t - Total Pressure
- T - Static Temperature
- T_t - Total Temperature
- s - Entropy
- $\lambda = V_4 / V_2$.

(For other symbols and station designation see Fig.1)

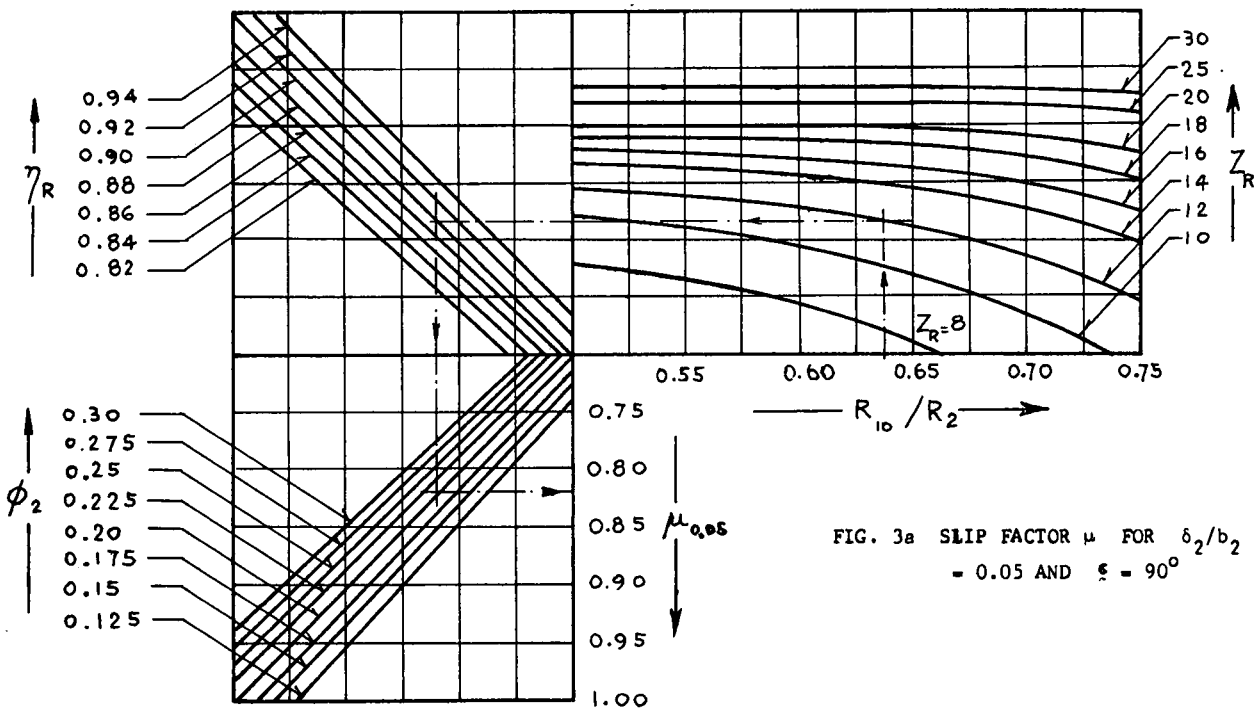

FIG. 3a SLIP FACTOR μ FOR $\delta_2/b_2 = 0.05$ AND $\varepsilon = 90^\circ$

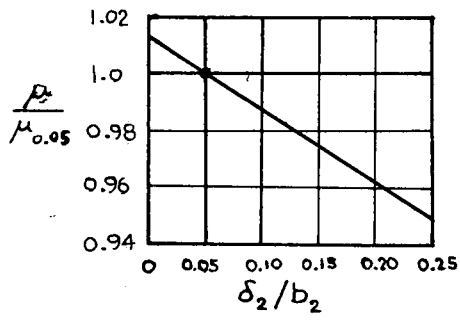

FIG. 3b CORRECTION FACTOR FOR RATIOS OF TIP CLEARANCE δ_2 AND AXIAL BLADE WIDTH b_2 DIFFERENT FROM 0.05

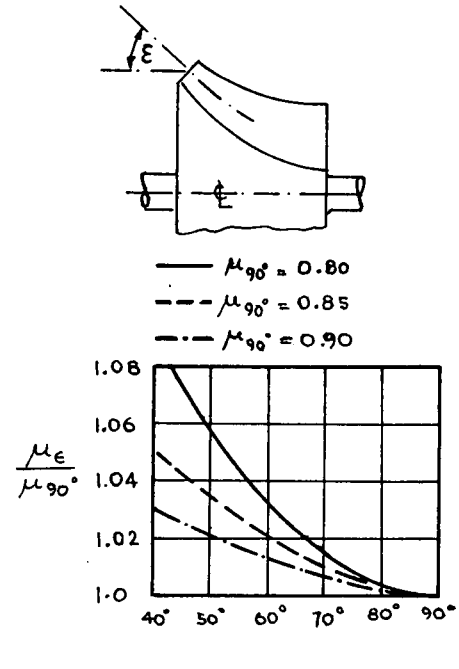

FIG. 3c CORRECTION FACTOR FOR MIXED-FLOW IMPELLERS

FIG. 3 SLIP FACTOR FOR RADIAL COMPRESSOR IMPELLERS WITH RADIAL BLADES AT DISCHARGE

(Figures were adapted from Refs. 5 and 6)

$\phi_2 = \frac{V_{m2}}{U_2}$ (see Eq. II(8) of Table II)

η_R - Rotor Efficiency (see Eq. 12)

Z_R - Number of Rotor Blades

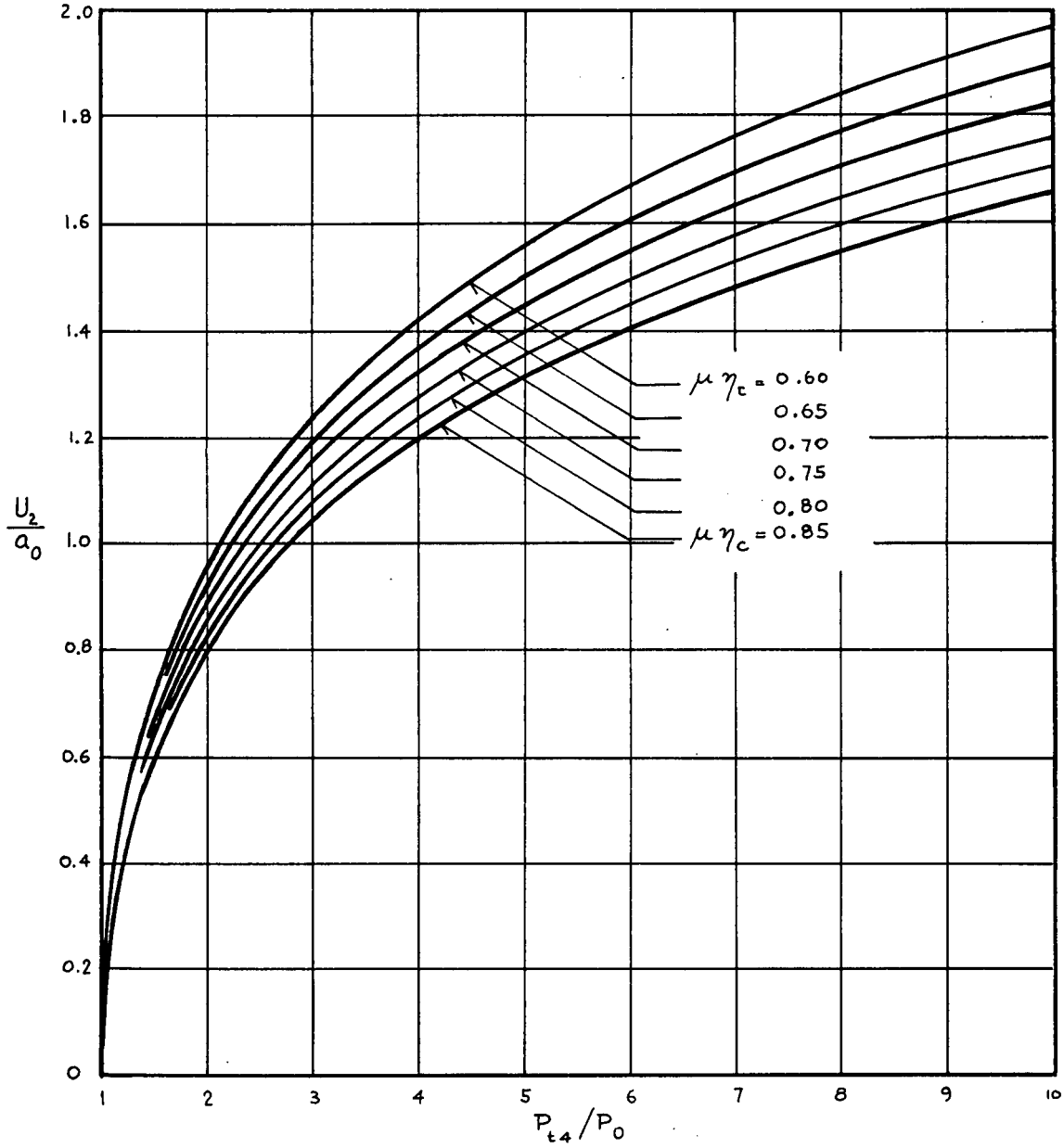

FIG. 4 RELATION BETWEEN PRESSURE RATIO AND U_2/a_0 FOR $\nu = 1.4$ (Eq. II(3))

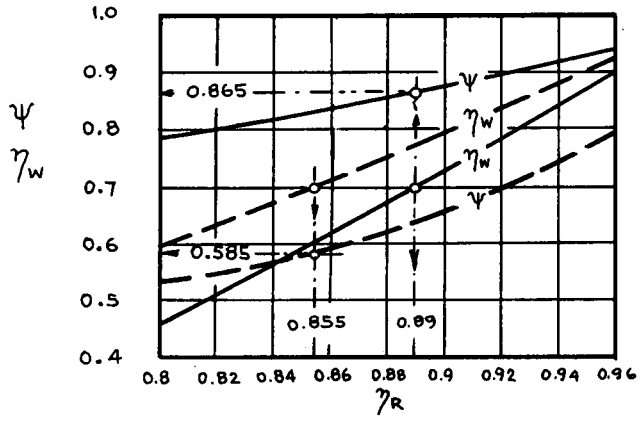

FIG. 5 RELATION BETWEEN ROTOR LOSS FORMULATIONS WITH η_R, η_W AND ψ(Eqs. 22 and 24)

——— $\alpha_2 = 60^\circ$
– – – $\alpha_2 = 75^\circ$
} $\beta_{1o} = 70^\circ$, $R_{1o}/R_2 = 0.7$, $\mu = 0.85$

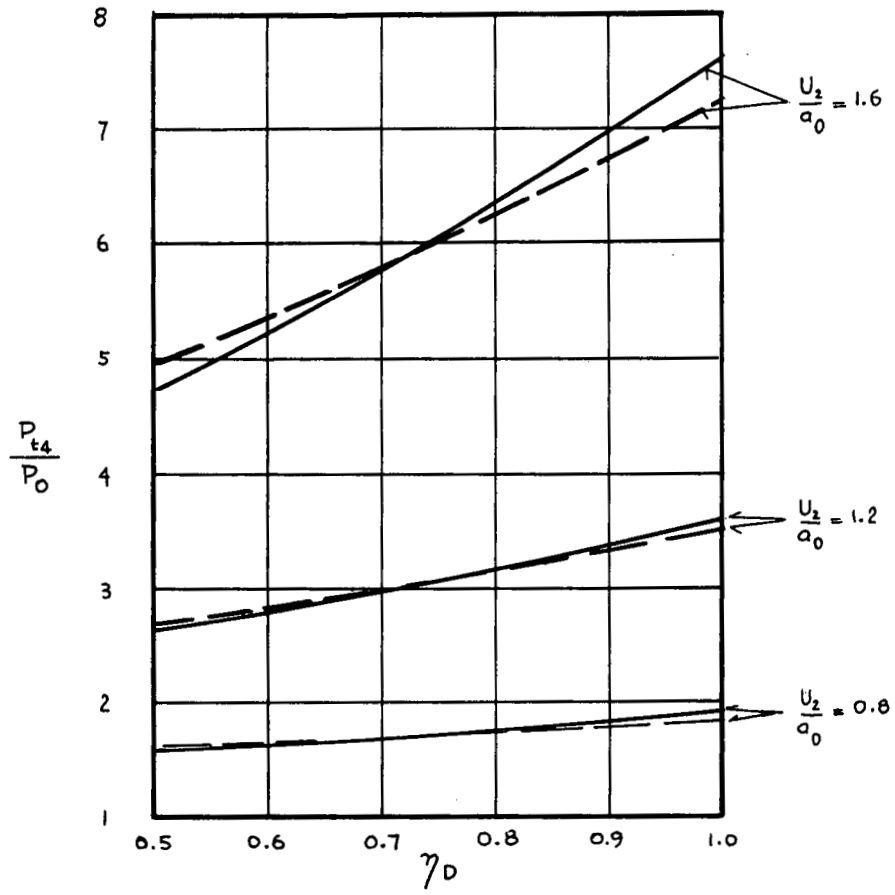

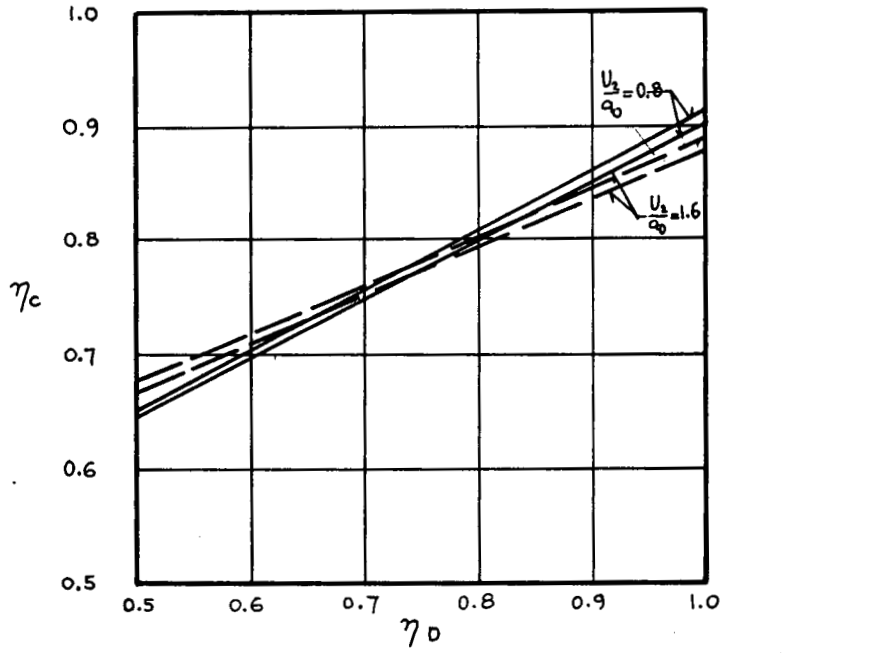

FIG.6 INFLUENCE OF DIFFUSOR EFFICIENCY η_D ON EFFICIENCY η_c AND PRESSURE RATIO P_{t4}/P_0 OF COMPRESSORS AT DIFFERENT SPEED RATIOS U_2/a_0

$\beta_{1o} = 70^\circ$; $R_{1o}/R_2 = 0.7$; $\lambda = V_4/V_2 = 0.2$

——— $\alpha_2 = 60^\circ$; $\eta_W = 0.7$; $\eta_R = 0.89$; $\psi = 0.865$

— — — $\alpha_2 = 75^\circ$; $\eta_W = 0.7$; $\eta_R = 0.855$; $\psi = 0.585$

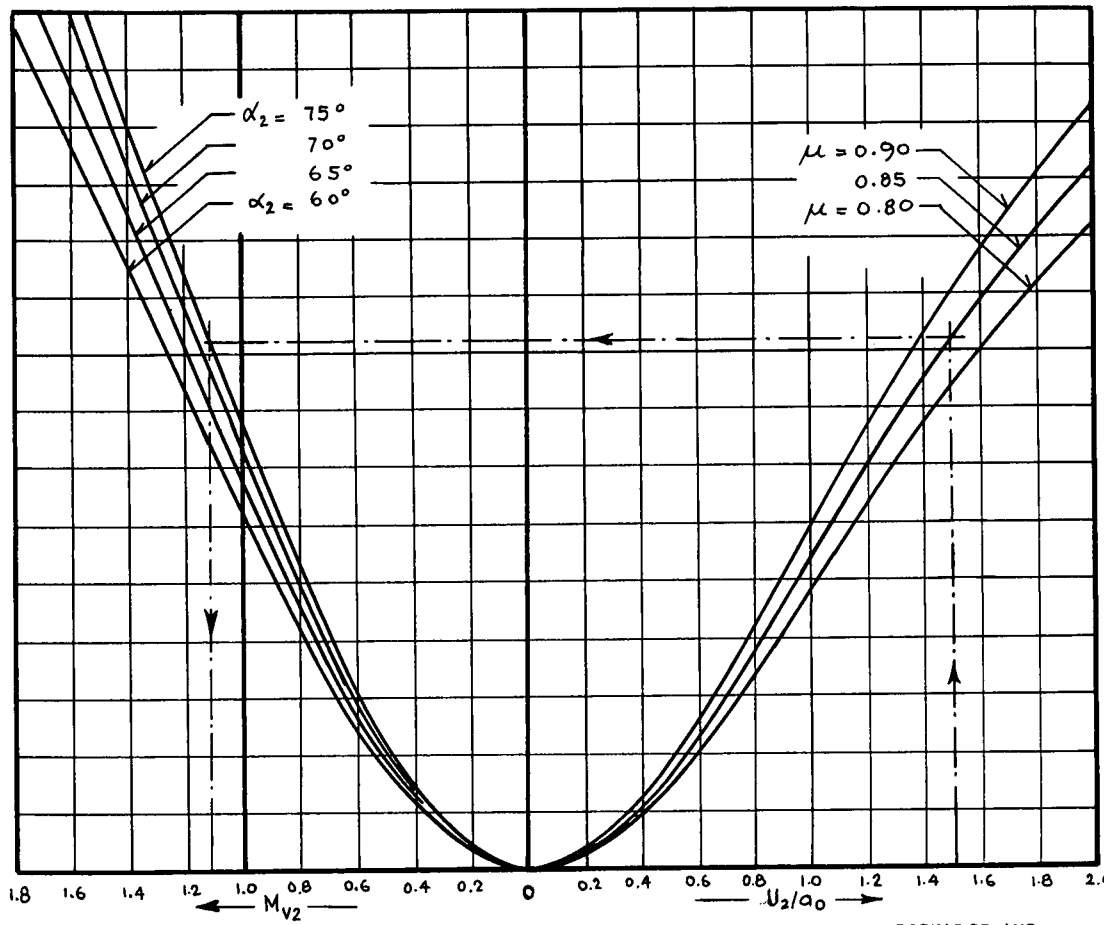

FIG.7 RELATION BETWEEN MACH NUMBER M_{V2} OF ABSOLUTE VELOCITY AT ROTOR DISCHARGE AND SPEED RATIO U_2/a_0 , FOR $\gamma = 1.4$ (Eq. II(6) of Table II)

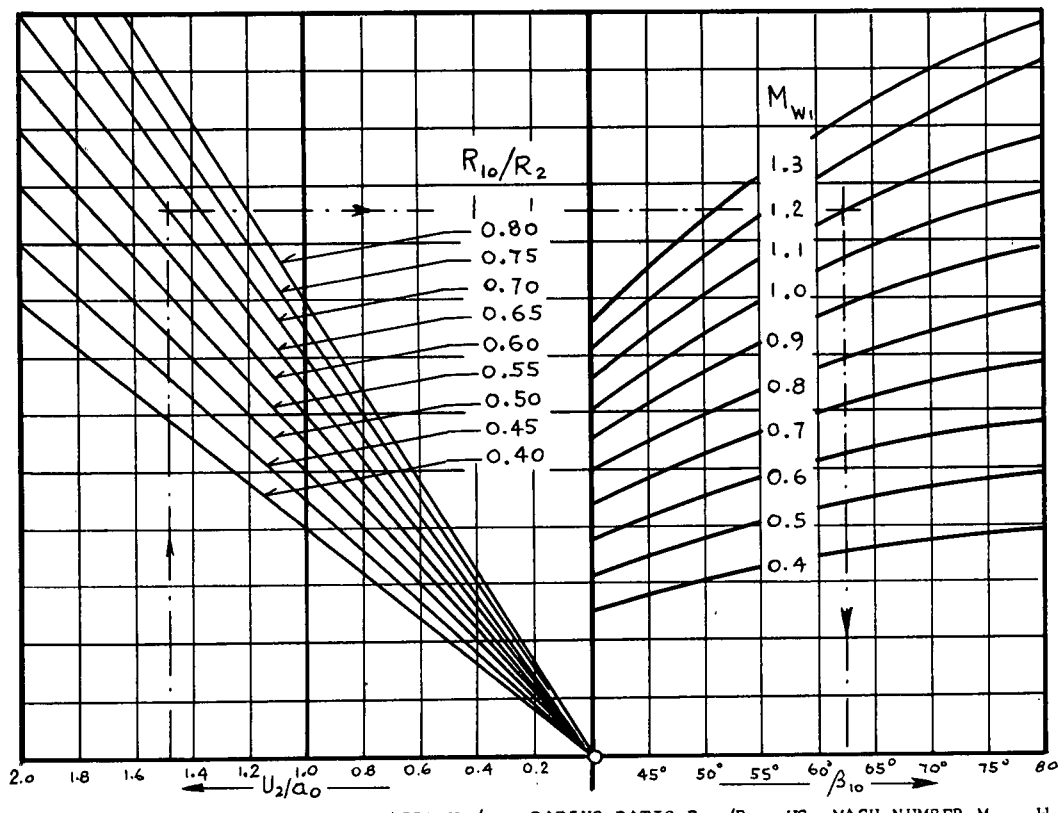

FIG.8 RELATION BETWEEN SPEED RATIO U_2/a_0 ,RADIUS RATIO R_{1o}/R_2, VS. MACH NUMBER $M_{W1} = W_{1o}/a_1$ AND RELATIVE FLOW ANGLE β_{1o} AT OUTER RADIUS R_{1o} OF COMPRESSOR INLET, FOR $\gamma = 1.4$.
(Eq. II(4) of Table II)

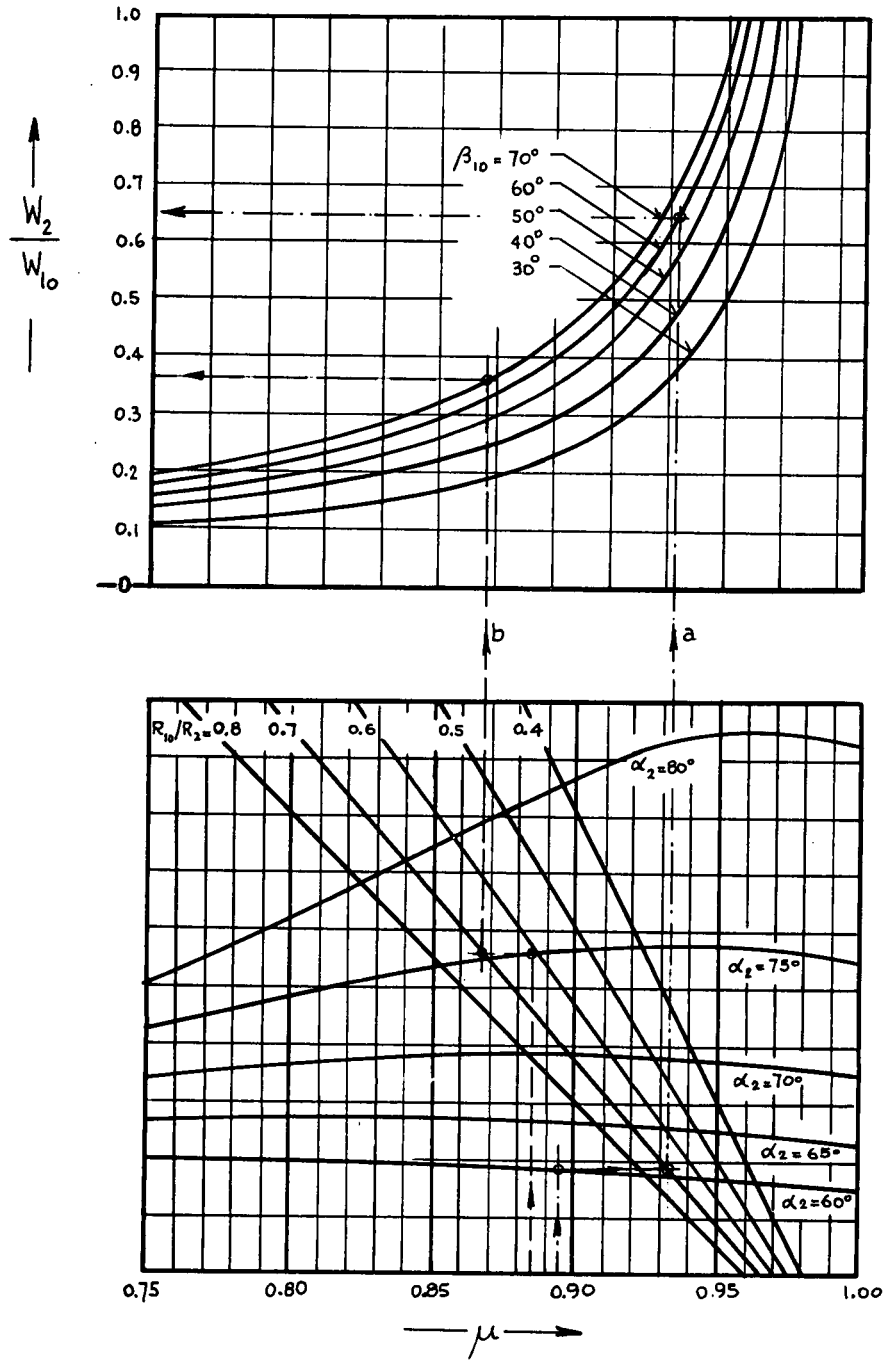

FIG.9 DIAGRAM REPRESENTING EQUATION II(5) OF TABLE II, SHOWING RELATIONSHIP BETWEEN DECELERATION RATIO W_2/W_{1o} OF RELATIVE ROTOR VELOCITIES, RADIUS RATIO R_{1o}/R_2, RELATIVE INLET FLOW ANGLE β_{1o}, ABSOLUTE ROTOR DISCHARGE ANGLE α_2, AND SLIP FACTOR μ.

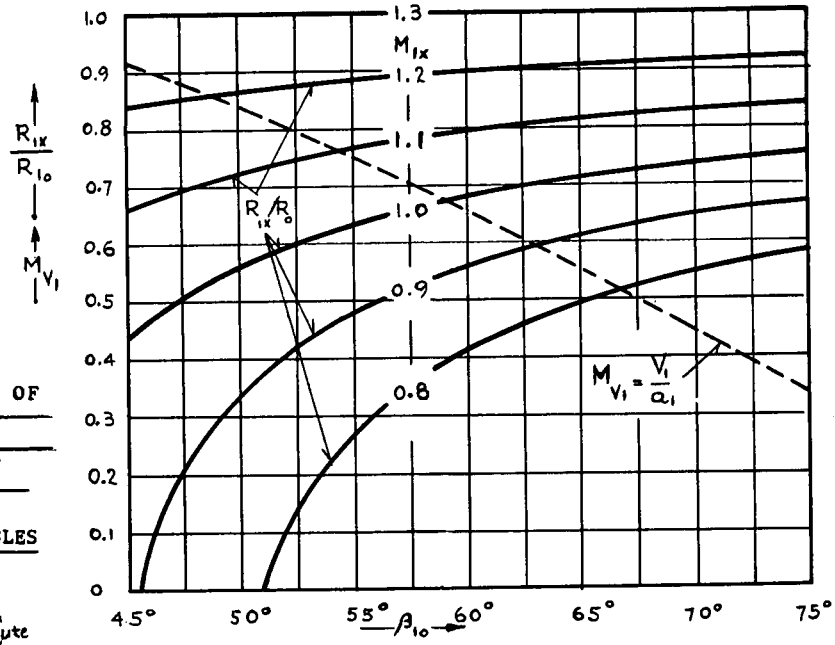

FIG. 10 MACH NUMBER M_{1x} OF RELATIVE INLET VELOCITY AT RADIUS R_{1x} FOR M_{W1} = 1.3 AT OUTER RADIUS R_{1o} OF WHEEL INLET, AT DIFFERENT FLOW ANGLES β_{1o} AT R_{1o}

M_{V1} = Mach number of Absolute Velocity V_1 at Inlet

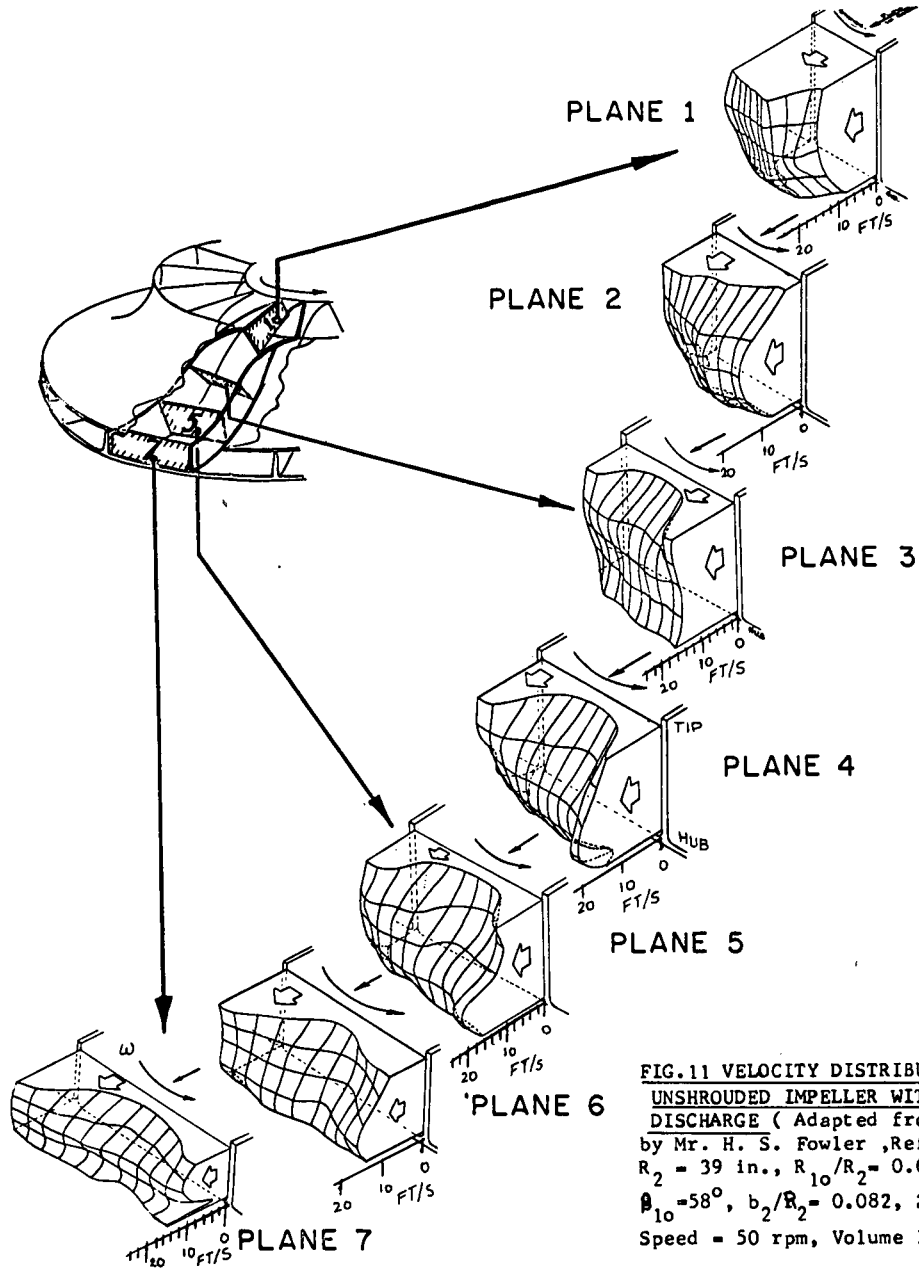

FIG.11 VELOCITY DISTRIBUTIONS MEASURED IN UNSHROUDED IMPELLER WITH RADIAL BLADES AT THE DISCHARGE (Adapted from Personal Communication by Mr. H. S. Fowler ,Refs.14 and 15)
R_2 = 39 in., R_{1o}/R_2 = 0.629, R_{1i}/R_{1o} = 0.752
β_{1o} =58°, b_2/R_2 = 0.082, Z_R = 26, δ_2/R_2 = 0.005
Speed = 50 rpm, Volume Flow = 64.2 ft^3/s

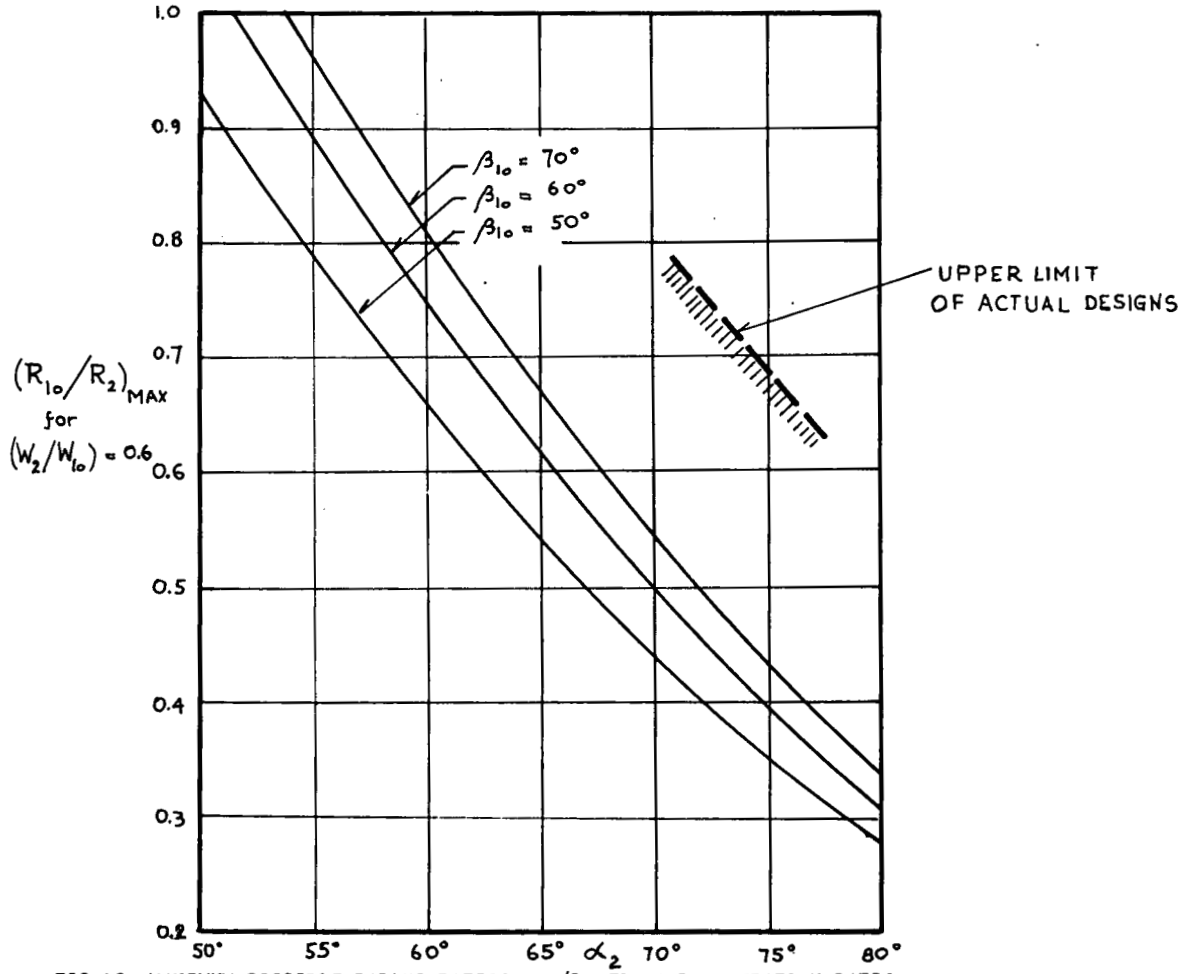

FIG.12 MAXIMUM POSSIBLE RADIUS RATIOS R_{1o}/R_2 FOR A DECELERATION RATIO $W_2/W_{1o} = 0.6$ FOR A SLIP FACTOR $\mu = 0.85$

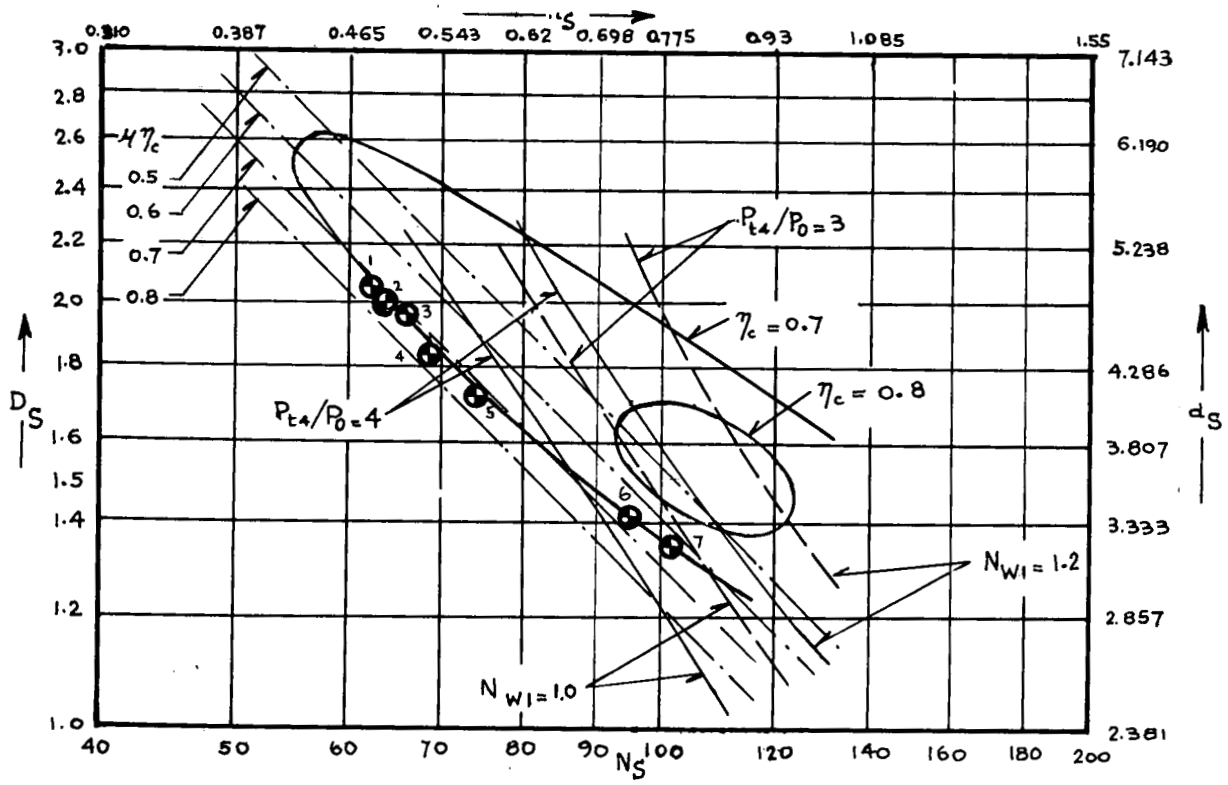

FIG.13 REPRESENTATION OF EQUATION $n_S d_S = 2/(\mu \eta_c)^{\frac{1}{2}}$ OF EQ. III(10) WITH DESIGN DATA POINTS OF ACTUAL COMPRESSORS

(Other Curves adapted from Fig. 4 of Ref. 19)

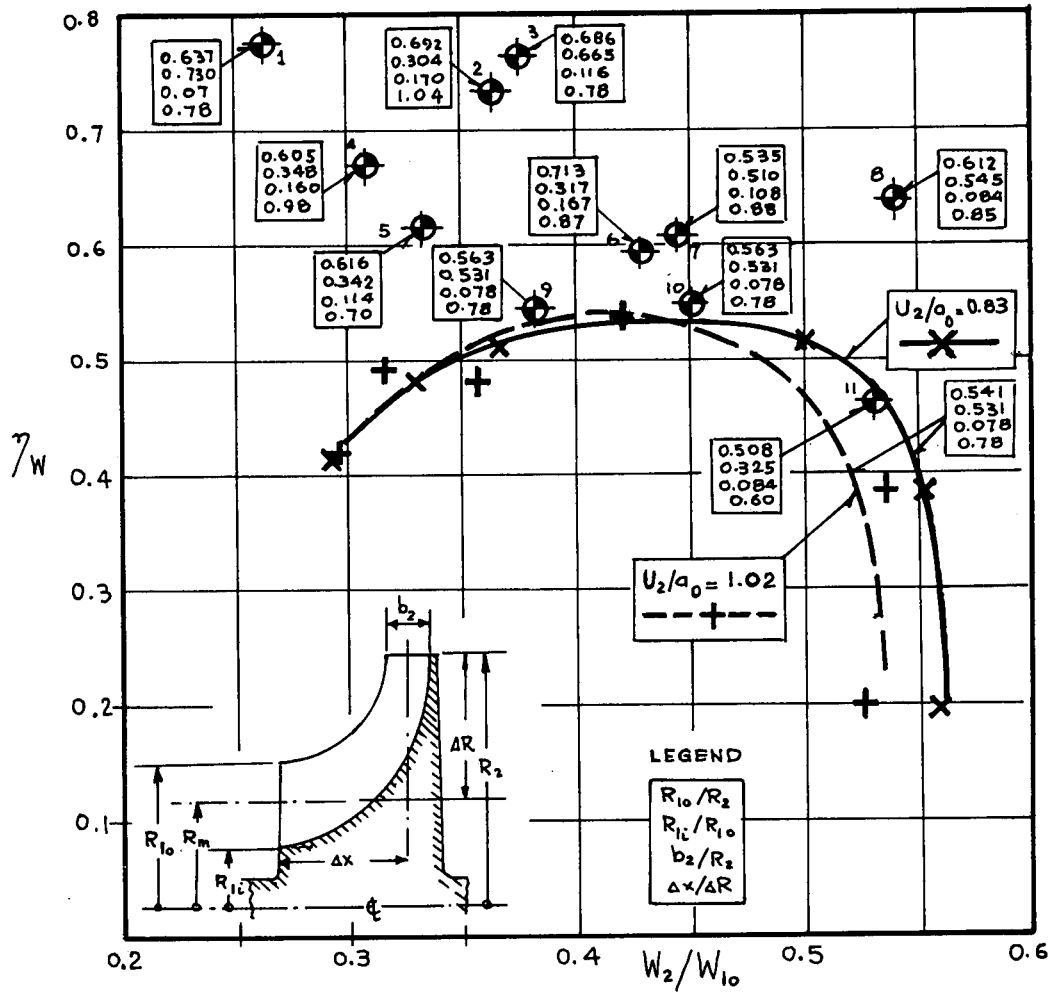

FIG. 14 WHEEL EFFICIENY η_W AS FUNCTION OF THE DECELERATION RATIO W_2/W_{1o} OF DIFFERENT RADIAL IMPELLERS

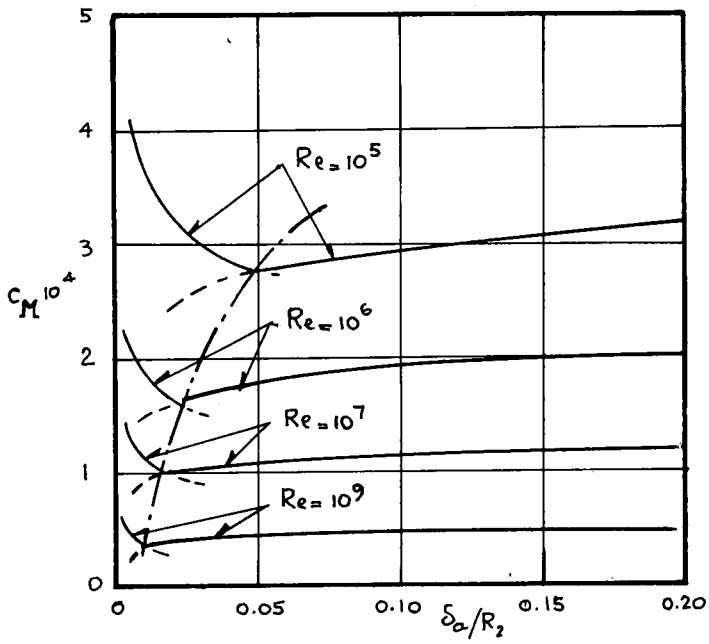

FIG. 15 DISK FRICTION MOMENT COEFFICIENT AS FUNCTION OF CLEARANCE AND REYNOLDS NUMBER

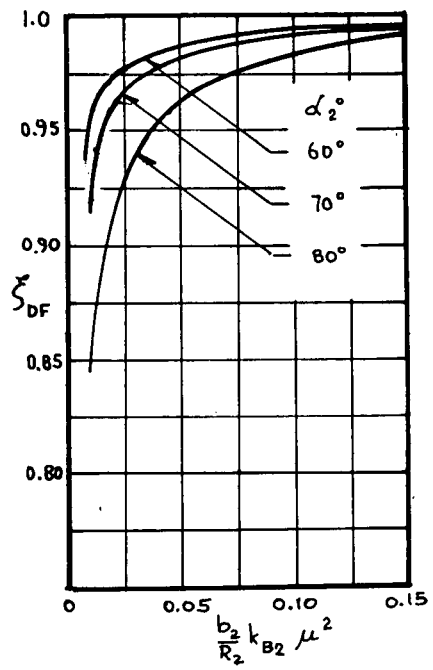

FIG. 16 INFLUENCE OF DISK FRICTION MOMENT ON COMPRESSOR EFFICIENCY

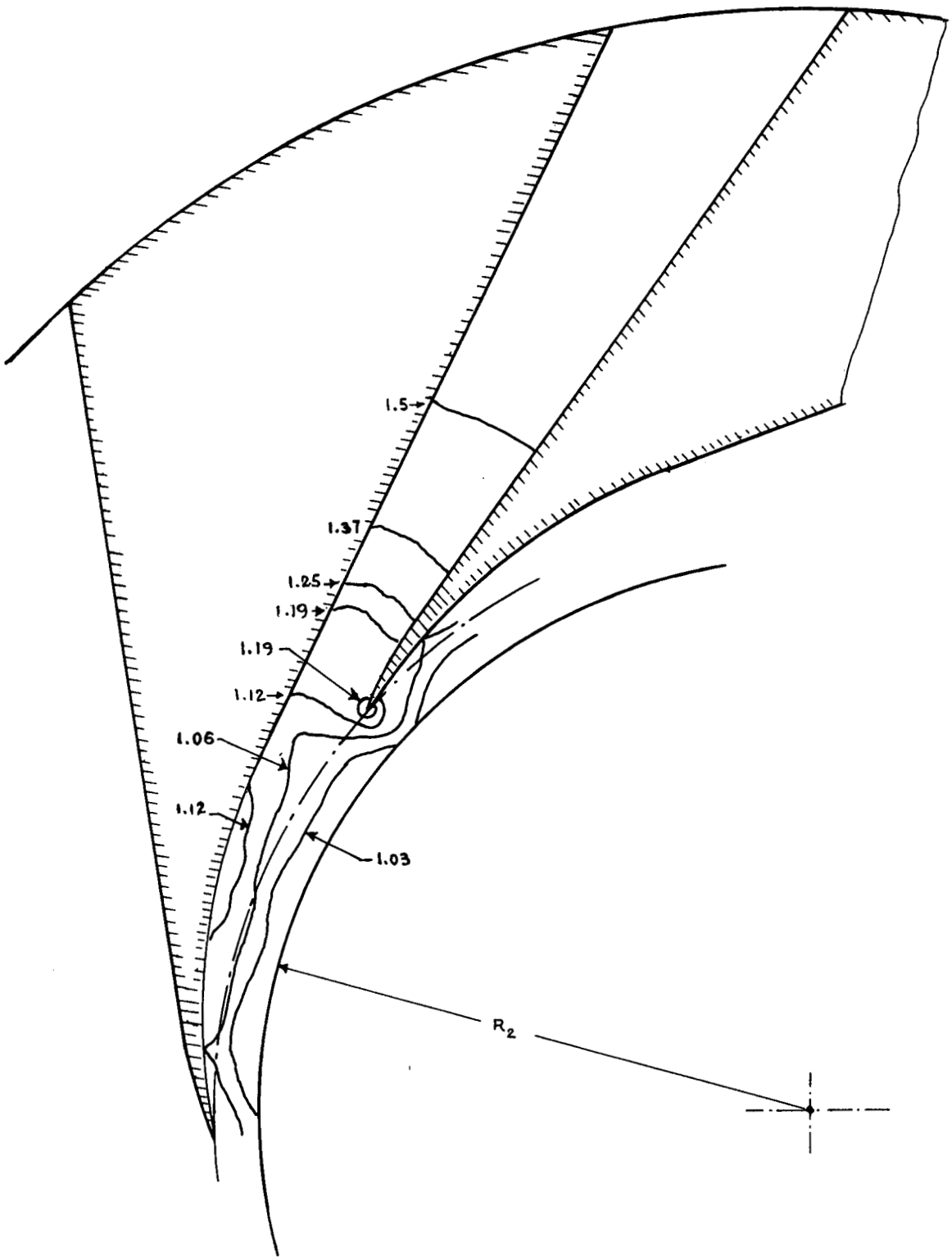

FIG. 17 TYPICAL DISTRIBUTION OF STATIC PRESSURES IN TRANSITION SECTION AND DIFFUSOR OF HIGH SPEED COMPRESSOR

(Numbers represent approximate ratios of static pressures and average pressure p_2)

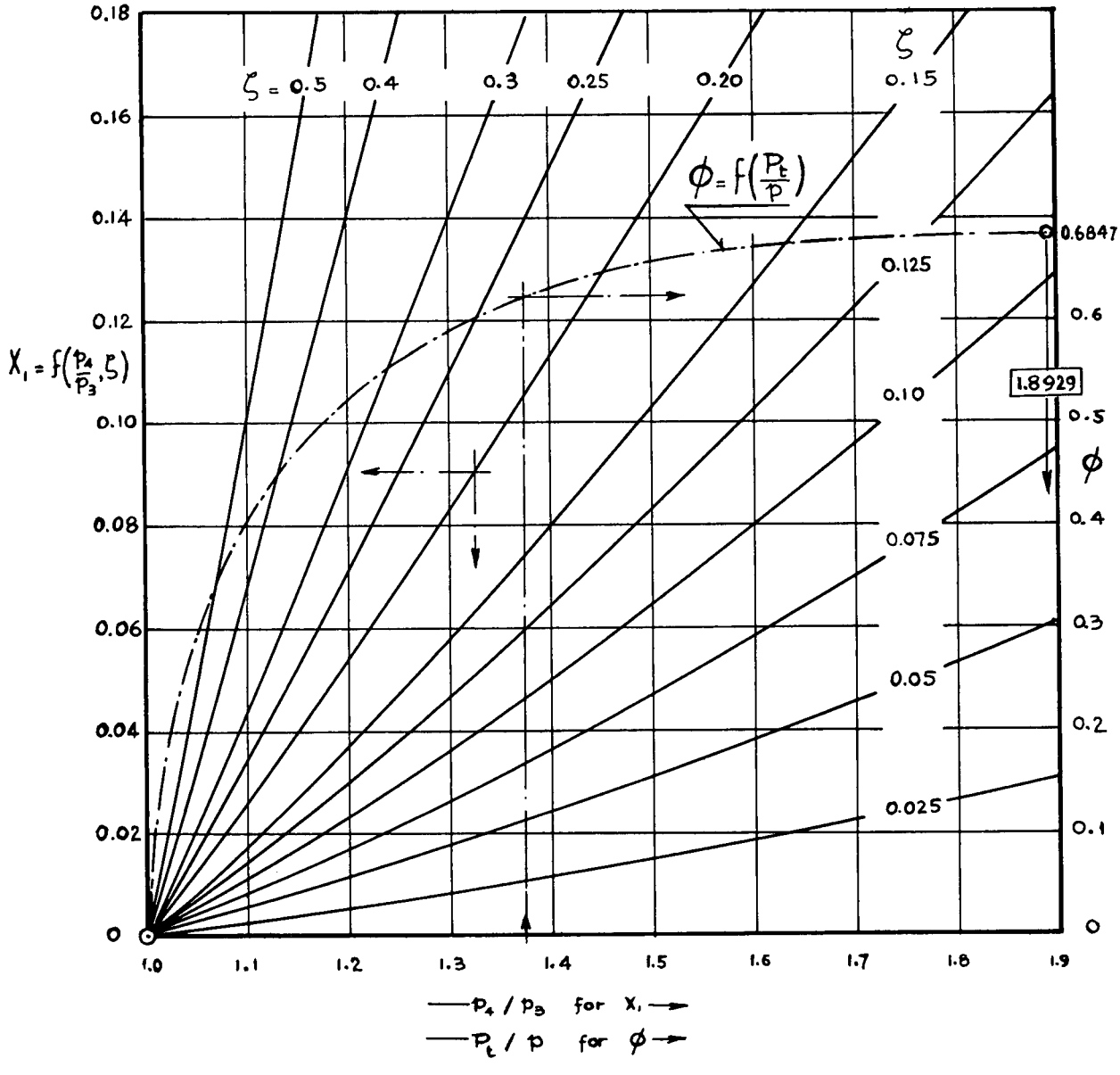

FIG.18 FUNCTION X_1 OF EQ.IV(16) OF TABLE IV FOR DIFFUSOR CALCULATION AND DIMENSIONLESS FLOW FUNCTION OF EQ.IV(22) AND IV(29) OF TABLE IV

$(\gamma = 1.4)$

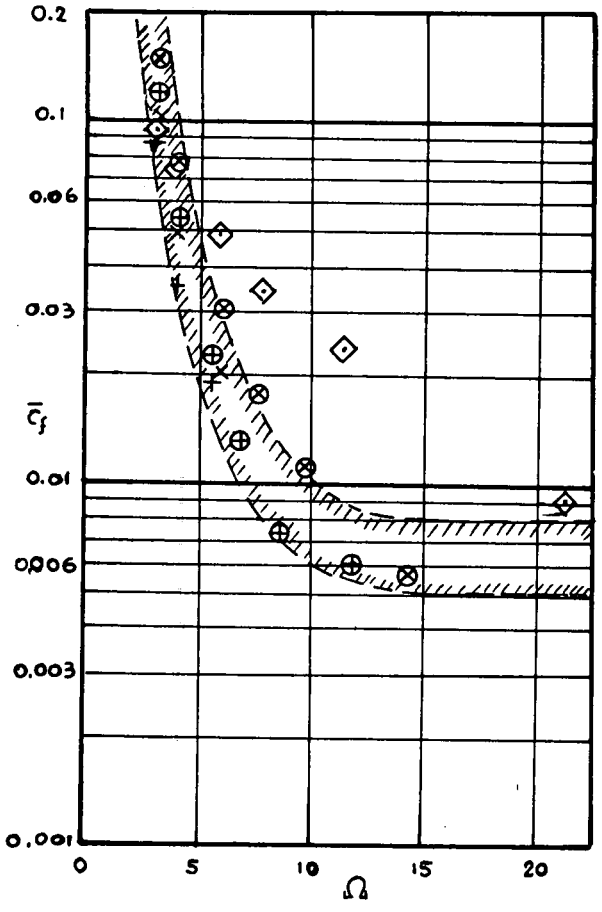

FIG.19 AVERAGE SKIN FRICTION COEFFICIENTS $\bar{c}_f$ OBTAINED FROM TWO-DIMENSIONAL DIFFUSOR TEST DATA OF REF.27 AS FUNCTION OF THE DIFFUSOR SHAPE FACTOR Ω

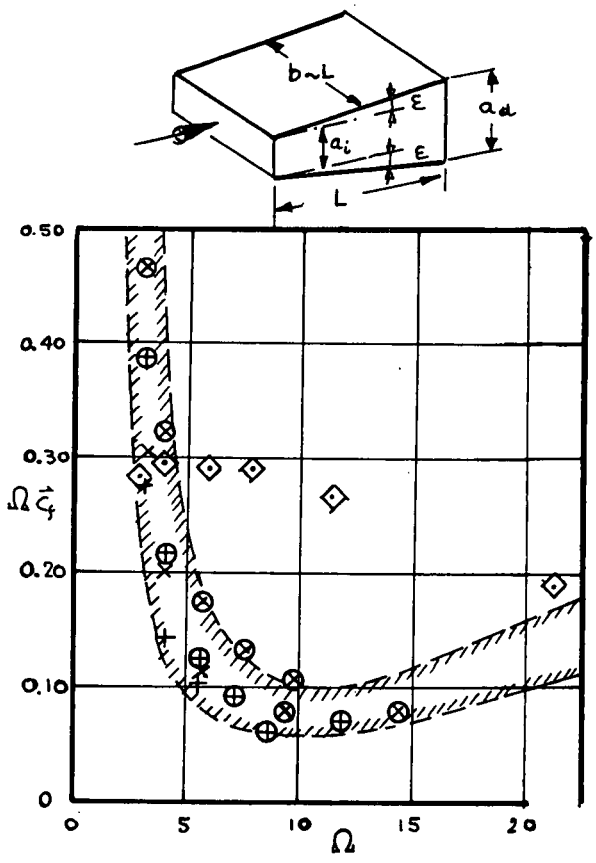

FIG.20 VALUES OF Ω $\bar{c}_f$ FROM FIG.19 AS FUNCTION OF Ω

SYMBOLS IN FIGS. 19 AND 20:

- ⊕ $L/a_i = 8$, $2\delta^*/a_i \cong 0.017$
- ⊗ $L/a_i = 12$, $2\delta^*/a_i \cong 0.025$
- ◇ $L/a_i = 48$, $2\delta^*/a_i \cong 0.018$
- \+ $L/a_i = 8$, $\delta^*/a_i \cong 0$
- × $L/a_i = 12$, $\delta^*/a_i \cong 0$

δ^* = Displacement Thickness of Boundary Layer on Top and Bottom Wall

TABLE I FLOW PROPERTIES IN COMPRESSOR

(For Symbols see Figs. 1 and 2)

VELOCITIES

$$\frac{V_1}{U_2} = \frac{R_{1o}}{R_2}\cot\beta_{1o} \quad I(1) \qquad \frac{W_{1o}}{U_2} = \frac{R_{1o}}{R_2}\frac{1}{\sin\beta_{1o}} \quad I(2)$$

$$\frac{V_2}{U_2} = \frac{\mu}{\sin\alpha_2} \quad I(3) \qquad \frac{W_2}{U_2} = \left[1 - 2\mu\left(1 - \frac{\mu}{2\sin^2\alpha_2}\right)\right]^{\frac{1}{2}} \quad I(4)$$

$$\frac{V_{u2}}{U_2} = \mu \qquad \frac{W_{u2}}{U_2} = 1-\mu$$

$$\frac{V_{m2}}{U_2} = \mu\cot\alpha_2$$

$$V_4 = \lambda V_2 \qquad W_2 = \psi W_{2is}$$

TEMPERATURES

$$\frac{T_{t1}}{T_0} = 1$$

$$\frac{T_1}{T_0} = \frac{1}{1 + \frac{\gamma-1}{2}M_{w1}^2\cos^2\beta_{1o}} = \frac{1 + \frac{\gamma-1}{2}\left(\frac{U_2}{a_0}\right)^2\left(\frac{R_{1o}}{R_2}\right)^2}{1 + \frac{\gamma-1}{2}M_{w1}^2} \quad I(5)$$

$$\frac{T_{t2}}{T_0} = 1 + (\gamma-1)\mu\left(\frac{U_2}{a_0}\right)^2 \quad I(6) \qquad \frac{T_2}{T_0} = 1 + (\gamma-1)\mu\left(\frac{U_2}{a_0}\right)^2\left[1 - \frac{\mu}{2\sin^2\alpha_2}\right] \quad I(7)$$

$$\frac{T_{t4}}{T_0} = \frac{T_{t2}}{T_0} \qquad \frac{T_2'}{T_0} = 1 + (\gamma-1)\mu\left(\frac{U_2}{a_0}\right)^2\left[\frac{1}{\psi^2}\left(1 - \frac{\mu}{2\sin^2\alpha_2}\right) - \frac{1}{2\mu}\left(\frac{1}{\psi^2}-1\right)\right] \quad I(8)$$

$$a_0 = \left[\gamma R_G T_0\right]^{\frac{1}{2}} \qquad \frac{T_4}{T_0} = 1 + (\gamma-1)\mu\left(\frac{U_2}{a_0}\right)^2\left[1 - \frac{\lambda^2\mu}{2\sin^2\alpha_2}\right] \quad I(9)$$

$$\frac{T_E}{T_0} = 1 + \frac{\gamma-1}{2}\left(\frac{U_2}{a_0}\right)^2 \quad I(10) \qquad \frac{T_4'}{T_0} = 1 + (\gamma-1)\mu\left(\frac{U_2}{a_0}\right)^2\left[1 - \frac{\mu}{2\sin^2\alpha_2}\left(1 - \eta_D^*\right)\right] \quad I(11)$$

$$\eta_D^* = \eta_D\left(1 - \lambda^2\right) \quad I(12)$$

$$\frac{T_4''}{T_0} = \frac{(T_4'/T_0)(T_2'/T_0)}{T_2/T_0} = \frac{1 + (\gamma-1)\mu\left(\frac{U_2}{a_0}\right)^2\left[X_1 + (\gamma-1)\mu\left(\frac{U_2}{a_0}\right)^2 X_2\right]}{1 + (\gamma-1)\mu\left(\frac{U_2}{a_0}\right)^2\left[1 - \frac{\mu}{2\sin^2\alpha_2}\right]} \quad I(13)$$

$$X_1 = \eta_D^* - \frac{1}{2\mu}\left(\frac{1}{\psi^2}-1\right) + \left(1 - \frac{\mu}{2\sin^2\alpha_2}\right)\left(1 + \frac{1}{\psi^2} - \eta_D^*\right) \quad I(14)$$

$$X_2 = \frac{\eta_D^*}{2\mu}\left(1 - \frac{1}{\psi^2}\right) + \left(1 - \frac{\mu}{2\sin^2\alpha_2}\right)\left(\frac{\eta_D^*}{\psi^2} - \frac{\left[1-\eta_D^*\right]}{2\mu}\left[\frac{1}{\psi^2}-1\right]\right) + \left(1 - \frac{\mu}{2\sin^2\alpha_2}\right)^2\left(\frac{1-\eta_D^*}{\psi^2}\right) \quad I(15)$$

$$\frac{\Delta T_{is}}{T_0} = \frac{T_4'' - T_0}{T_0} = \frac{(\gamma-1)\mu\left(\frac{U_2}{a_0}\right)^2\left[X_1 - \left(1 - \frac{\mu}{2\sin^2\alpha_2}\right) + (\gamma-1)\mu\left(\frac{U_2}{a_0}\right)^2 X_2\right]}{1 + (\gamma-1)\mu\left(\frac{U_2}{a_0}\right)^2\left[1 - \frac{\mu}{2\sin^2\alpha_2}\right]} \quad I(16)$$

PRESSURES

$$\frac{P_{t2}'}{P_0} = \left(T_{t2}/T_0\right)^{\frac{\gamma}{\gamma-1}} \quad I(17) \qquad \frac{P_1}{P_0} = \left(T_1/T_0\right)^{\frac{\gamma}{\gamma-1}} \quad I(18)$$

$$\frac{P_{t2}}{P_0} = \frac{p_2}{P_0}\frac{P_{t2}}{p_2} = \left[\frac{(T_2'/T_0)(T_{t2}/T_0)}{T_2/T_0}\right]^{\frac{\gamma}{\gamma-1}} \quad I(19) \qquad \frac{p_2}{P_0} = \left(T_2'/T_0\right)^{\frac{\gamma}{\gamma-1}} \quad I(20)$$

$$\frac{P_{t4}}{P_0} = \frac{p_4}{P_0} = \left(T_4''/T_0\right)^{\frac{\gamma}{\gamma-1}} \quad I(21) \qquad \frac{p_4}{p_2} = \left(T_4'/T_2\right)^{\frac{\gamma}{\gamma-1}} = \left(\frac{T_4'/T_0}{T_2/T_0}\right)^{\frac{\gamma}{\gamma-1}} \quad I(22)$$

$$\frac{P_{E1}}{P_0} = \left(T_E/T_0\right)^{\frac{\gamma}{\gamma-1}} \quad I(23) \qquad \frac{P_{E2}}{P_0} = \frac{p_2}{P_0}\frac{P_{E2}}{p_2} = \left[\frac{(T_2'/T_0)(T_E/T_0)}{T_2/T_0}\right]^{\frac{\gamma}{\gamma-1}} \quad I(24)$$

TABLE II PERFORMANCE AND DESIGN PARAMETERS

$$\eta_c = \frac{\Delta T_{is}}{\Delta T_w} = \frac{X_1 - \left(1 - \frac{\mu}{2\sin^2\alpha_2}\right) + (\gamma-1)\mu\left(\frac{U_2}{a_0}\right)^2 X_2}{1 + (\gamma-1)\mu\left(\frac{U_2}{a_0}\right)^2\left[1 - \frac{\mu}{2\sin^2\alpha_2}\right]} \qquad \text{II(1)}$$

(X_1 and X_2 are given by Eqs. I(14) and I(15) of Table I)

$$r^* = \frac{T_2' - T_0}{\Delta T_{is}} = \frac{\frac{1}{\psi^2}\left(1 - \frac{\mu}{2\sin^2\alpha_2}\right) - \frac{1}{2\mu}\left(\frac{1}{\psi^2} - 1\right)}{\eta_c} \qquad \text{II(2)}$$

$$\frac{U_2}{a_0} = \left[\frac{\left(P_{t4}/P_0\right)^{\frac{\gamma-1}{\gamma}} - 1}{(\gamma-1)\mu\,\eta_c}\right]^{\frac{1}{2}} \qquad \text{II(3)}$$

$$\frac{R_{10}}{R_2} = \frac{M_{W1}\sin\beta_{10}}{\frac{U_2}{a_0}\left[1 + \frac{\gamma-1}{2}M_{W1}^2\cos^2\beta_{10}\right]^{\frac{1}{2}}} \qquad \text{II(4)}$$

$$\frac{W_2}{W_{10}} = \frac{\left[1 - 2\mu\left(1 - \frac{\mu}{2\sin^2\alpha_2}\right)\right]^{\frac{1}{2}}\sin\beta_{10}}{(R_{10}/R_2)} \qquad \text{II(5)}$$

$$M_{V2} = \frac{V_2}{a_2} = \frac{\mu\frac{U_2}{a_0}}{\sin\alpha_2\left[1 + (\gamma-1)\mu\left(\frac{U_2}{a_0}\right)^2\left(1 - \frac{\mu}{2\sin^2\alpha_2}\right)\right]^{\frac{1}{2}}} \qquad \text{II(6)}$$

$$\phi_1 = \frac{V_1}{U_2} = \frac{M_{W1}\cos\beta_{10}}{\frac{U_2}{a_0}\left[1 + \frac{\gamma-1}{2}M_{W1}^2\cos^2\beta_{10}\right]^{\frac{1}{2}}} \qquad \text{II(7)}$$

$$\phi_2 = \frac{V_{m2}}{U_2} = \mu\cot\alpha_2 \qquad \text{II(8)}$$

$$\pi R_2^2\left[1 - \left(\frac{R_{1i}}{R_{10}}\right)^2\right]k_{B1} = \left(\frac{\dot m\sqrt{R_G T_0}}{P_0}\right)\left(\frac{U_2}{a_0}\right)^2\frac{\left[1 + \frac{\gamma-1}{2}M_{W1}^2\cos^2\beta_{10}\right]^{\frac{3\gamma-1}{2(\gamma-1)}}}{\sqrt{\gamma}\,M_{W1}^2\cos\beta_{10}\sin^2\beta_{10}} \qquad \text{II(9)}$$

$$\frac{\omega}{\left[1 - \left(\frac{R_{1i}}{R_{10}}\right)^2\right]k_{B1}} = \left[\frac{a_0 P_0}{\dot m}\right]^{\frac{1}{2}}\frac{\sin\beta_{10}\left[\pi\gamma\cos\beta_{10}\right]^{\frac{1}{2}}}{\left[1 + \frac{\gamma-1}{2}M_{W1}^2\cos^2\beta_{10}\right]^{\frac{3\gamma-1}{4(\gamma-1)}}} \qquad \text{II(10)}$$

$$\left(\frac{b_2}{R_2}\right)k_{B2} = \left(\frac{\dot m\sqrt{R_G T_0}}{\pi R_2^2 P_0}\right)\frac{1 + (\gamma-1)\mu\left(\frac{U_2}{a_0}\right)^2\left(1 - \frac{\mu}{2\sin^2\alpha_2}\right)}{2\mu\sqrt{\gamma}\cot\alpha_2\left(\frac{U_2}{a_0}\right)\left\{1 + (\gamma-1)\mu\left(\frac{U_2}{a_0}\right)^2\left[\frac{1}{\psi^2}\left(1 - \frac{\mu}{2\sin^2\alpha_2}\right) - \frac{1}{2\mu}\left(\frac{1}{\psi^2} - 1\right)\right]\right\}^{\frac{\gamma}{\gamma-1}}} \qquad \text{II(11)}$$

Diffusor Exit Area A_4:

$$A_4 k_{B4} = \left(\frac{\dot m\sqrt{R_G T_0}}{P_0}\right)\frac{\sin\alpha_2}{\lambda\mu\sqrt{\gamma}\left(\frac{U_2}{a_0}\right)}\frac{\left[1 + (\gamma-1)\mu\left(\frac{U_2}{a_0}\right)^2\left(1 - \frac{\lambda^2\mu}{2\sin^2\alpha_2}\right)\right]}{\left[1 + \eta_c(\gamma-1)\mu\left(\frac{U_2}{a_0}\right)^2\right]^{\frac{\gamma}{\gamma-1}}} \qquad \text{II(12)}$$

Diffusor Throat Area A_x if $M_{V2} > 1$:

$$A_x k_{Bx} = \frac{\left(\frac{\dot m\sqrt{R_G T_0}}{P_0}\right)}{\phi_c\left(\frac{P_{tx}}{P_{t2}}\right)\left[1 + (\gamma-1)\mu\left(\frac{U_2}{a_0}\right)^2\right]^{\frac{\gamma+1}{2(\gamma-1)}}}\,Y^{\frac{\gamma}{\gamma-1}} \qquad \text{II(13)}$$

where

$$\phi_c = \left\{\frac{2\gamma}{\gamma-1}\left[\left(\frac{2}{\gamma+1}\right)^{\frac{2}{\gamma-1}} - \left(\frac{2}{\gamma+1}\right)^{\frac{\gamma+1}{\gamma-1}}\right]\right\}^{\frac{1}{2}} \qquad \text{II(14)}$$

and

$$Y = \frac{T_2/T_0}{T_2'/T_0} = \frac{1 + (\gamma-1)\mu\left(\frac{U_2}{a_0}\right)^2\left[1 - \frac{\mu}{2\sin^2\alpha_2}\right]}{1 + (\gamma-1)\mu\left(\frac{U_2}{a_0}\right)^2\left[\frac{1}{\psi^2}\left(1 - \frac{\mu}{2\sin^2\alpha_2}\right) - \frac{1}{2\mu}\left(\frac{1}{\psi^2} - 1\right)\right]} \qquad \text{II(15)}$$

Diffusor Throat Area A_x if $M_{V2} \leqq 1$, and $V_x = \xi V_2$:

$$A_x k_{Bx} = \frac{\sin\alpha_2\left(\frac{\dot m\sqrt{R_G T_0}}{P_0}\right)}{\xi\mu\sqrt{\gamma}\left(\frac{U_2}{a_0}\right)\left(\frac{P_{tx}}{P_{t2}}\right)\left[1 + (\gamma-1)\mu\left(\frac{U_2}{a_0}\right)^2\left(1 - \frac{\xi^2\mu}{2\sin^2\alpha_2}\right)\right]^{\frac{1}{\gamma-1}}}\,Y^{\frac{\gamma}{\gamma-1}} \qquad \text{II(16)}$$

TABLE III SPECIFIC SPEED RELATIONS

DEFINITIONS WITH ENGLISCH UNITS

(see Refs. 18 and 19)

SPECIFIC SPEED

$$N_S = \frac{N\ Q_1^{1/2}}{H_{is}^{3/4}} \qquad \text{III(1)}$$

SPECIFIC DIAMETER

$$D_S = \frac{D\ H_{is}^{1/4}}{Q_1^{1/2}} \qquad \text{III(2)}$$

DEFINITIONS IN DIMENSIONLESS FORM

$$n_S = \frac{N_S}{129} = \frac{\omega\ Q_1^{1/2}}{(c_p\ \Delta T_{is})^{3/4}} \qquad \text{III(3)}$$

$$d_S = \frac{D_S}{0.42} = \frac{D\ (c_p\ \Delta T_{is})^{1/4}}{Q_1^{1/2}} \qquad \text{III(4)}$$

N - Rotative Speed (rpm)
ω - Angular Velocity (radians/s)
Q_1 - Inlet Volume Flow Rate (cuft/s)
$H_{is} = g_o\ c_p\ \Delta T_{is}$ - Isentropic Head (ft-lb/lbm)
g_o - Gravitational Constant = 32.174 ft/s^2
c_p - Specific Heat at Constant Pressure (ft-lb / slug, deg.R)
ΔT_{is} - Isentropic Temperature Rise in Compressor (deg. R)
D - Rotor Diameter (ft)

RELATIONS WITH SYMBOLS OF TABLES I AND II

$$\xi_1 = 1 - \left(\frac{R_{1i}}{R_{1o}}\right)^2 \qquad \text{III(5)}$$

$$Q_1 = \pi R_{1o}^2\ \xi_1\ k_{B1}\ V_1$$
$$V_1 = U_{1o}\ \cot \beta_{1o}$$
$$c_p\ \Delta T_{is} = \mu\ \eta_c\ U_2^2$$
$$\omega = U_2/R_2$$
$$D = 2\ R_2 = 2\ U_2/\omega$$

$$n_S^2 = \pi\left(\frac{R_{1o}}{R_2}\right)^3 k_{B1}\ \frac{\cot \beta_{1o}\ \xi_1}{(\mu\ \eta_c)^{3/2}} \qquad \text{III(6)}$$

$$d_S^2 = \frac{4}{\pi}\ \frac{(\mu\ \eta_c)^{1/2}}{(R_{1o}/R_2)^3\ k_{B1}\ \cot \beta_{1o}\ \xi_1} \qquad \text{III(7)}$$

and

$$\xi_1 = \frac{n_S^2}{\pi}\ \frac{(\mu\ \eta_c)^{3/2}\ \tan \beta_{1o}}{k_{B1}\ (R_{1o}/R_2)^3} \qquad \text{III(8)}$$

$$\xi_1 = \frac{4}{\pi\ d_S^2}\ \frac{(\mu\ \eta_c)^{1/2}\ \tan \beta_{1o}}{k_{B1}\ (R_{1o}/R_2)^3} \qquad \text{III(9)}$$

Equating Eqs. 8 and 9:

$$n_S\ d_S = \frac{2}{(\mu\ \eta_c)^{1/2}} \qquad \text{III(10)}$$

From Eq.8

$$\frac{R_{1i}}{R_{1o}} = \left[1 - \frac{n_S^2}{\pi}\ \frac{(\mu\ \eta_c)^{3/2}\ \tan \beta_{1o}}{k_{B1}\ (R_{1o}/R_2)^3}\right]^{1/2} \qquad \text{III(11)}$$

EXAMPLE: For μ= 0.88 , η_c= 0.83 , k_{B1}= 0.85 , and β_{1o}= 68° , find R_{1i}/R_{1o} for different values of N_s for the two radius ratios R_{1o}/R_2 = 0.56 and R_{1o}/R_2 = 0.70

For R_{1o}/R_2 = 0.56; from Eq.11

$$\frac{R_{1i}}{R_{1o}} = \left[1 - n_S^2(3.288)\right]^{1/2} \qquad \text{III(12)}$$

R_{1i}/R_{1o} is zero for $n_{S\ max}$=0.552, or N_{Smax}=71
For values of N_S lower than 71:

N_S	60	65	70
n_S	0.465	0.504	0.543
R_{1i}/R_{1o}	0.537	0.406	0.178

For R_{1o}/R_2 = 0.70; from Eq.11

$$\frac{R_{1i}}{R_{1o}} = \left[1 - n_S^2(1.683)\right]^{1/2} \qquad \text{III(13)}$$

R_{1i}/R_{1o} is zero for n_{Smax} = 0.771, or N_{Smax}=99.4
For values of N_S lower than 99.4:

N_S	70	80	90	98
n_S	0.543	0.620	0.698	0.760
R_{1i}/R_{1o}	0.710	0.594	0.424	0.169

Relation between so-called Mach Number $N_{W1} = W_{1o} / \sqrt{\frac{2\gamma}{\gamma+1} R_G T_0}$ and actual Mach Number $M_{W1} = W_{1o}/a_1$:

$$N_{W1}^2 = \left[\frac{\gamma+1}{2}\ M_{W1}^2\right] \Big/ \left[1 + \frac{\gamma-1}{2} M_{W1}^2 \cos^2 \beta_{1o}\right] \qquad \text{III(14)}$$

TABLE IV ANALYSIS OF FLOWS IN DIFFUSORS

ONE-DIMENSIONAL FLOW IN CHANNEL

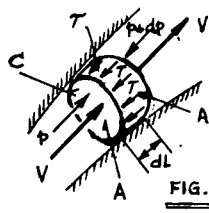

FIG. IV(1)

A - Flow Area
C - Wetted Perimeter
L - Channel Length
$\dot{m}$ - Mass Flow Rate
p - Static Pressure
τ - Wall Shear Stresses
ρ - Mass Density

From Momentum Theorem:

$$\frac{1}{\rho}\,dp + d\left(\frac{V^2}{2}\right) = -\frac{\tau}{\rho}\frac{C}{A}\,dL \qquad \text{IV (1)}$$

From Equation of Continuity:

$$\dot{m} = A\,\rho\,V \qquad \text{IV (2)}$$

Derivation:

Eq. IV(4) into Eq. IV(1)

$$c_p\,dT - T\,ds + d\left(\frac{V^2}{2}\right) = -\frac{\tau}{\rho}\frac{C}{A}\,dL$$

$$d\left(c_p\,dT + \frac{V^2}{2}\right) - T\,ds = -\frac{\tau}{\rho}\frac{C}{A}\,dL$$

From Eq. 3

$$dT_t = 0 = d\left(T + \frac{V^2}{2c_p}\right)$$

$$T\,ds = \frac{\tau}{\rho}\frac{C}{A}\,dL \qquad \text{IV (10)}$$

From Frictional Law with Eq. 2:

$$\tau = c_f\frac{\rho}{2}V^2 = \frac{c_f}{2}\frac{\dot{m}^2}{\rho A^2} \qquad \text{IV (12)}$$

Into Eq. 10

$$T\,ds = \frac{c_f}{2}\frac{\dot{m}^2}{\rho^2 A^3}\,C\,dL \qquad \text{IV (13)}$$

THERMODYNAMIC CONDITIONS

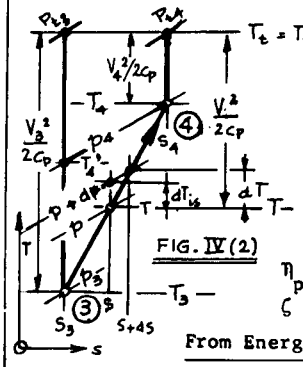

FIG. IV(2)

P_t - Total Pressure
T_t - Total Temperature
T - Static Temperature
s - Entropy

η_p - Polytropic Efficiency
$\zeta = 1-\eta_p$ - Loss Coefficient

From Energy Equation:

$$T_t = T_{t3} = T_{t4} = T + \frac{V^2}{2c_p} = T_3 + \frac{V_3^2}{2c_p} = T_4 + \frac{V_4^2}{2c_p} \qquad \text{IV (3)}$$

From First Law of Thermodynamics:

$$T\,ds = c_p\,dT - \frac{1}{\rho}\,dp = R_G\frac{\gamma}{\gamma-1}\,dT - \frac{1}{\rho}\,dp \qquad \text{IV (4)}$$

$$ds = R_G\left[\frac{\gamma}{\gamma-1}\frac{dT}{T} - \frac{dp}{p}\right] \qquad \text{IV (5)}$$

For Adiabatic Polytropic Process

$$\eta_p = \frac{dT_{is}}{dT} = \frac{T\left[\left(\frac{p+dp}{p}\right)^{\frac{\gamma-1}{\gamma}} - 1\right]}{dT} = \frac{T}{dT}\,\frac{\gamma-1}{\gamma}\,\frac{dp}{p} \qquad \text{IV (6)}$$

$$\frac{dT}{T} = \frac{\gamma-1}{\eta_p\,\gamma}\,\frac{dp}{p} \qquad \text{IV (7)}$$

$$T = \text{constant}\;\; p^{\frac{\gamma-1}{\eta_p\gamma}} \qquad \text{IV (8)}$$

$$\rho = \text{constant}\;\; p^{1-\frac{\gamma-1}{\eta_p\gamma}} \qquad \text{IV (9)}$$

From Eqs. 5 and 7

$$\frac{ds}{R_G} = \left(\frac{1}{\eta_p} - 1\right)\frac{dp}{p} = \frac{\zeta}{1-\zeta}\,\frac{dp}{p} \qquad \text{IV (11)}$$

Dimensionless Referred Mass Flow Rate

$$\dot{m}_{r3} = \frac{\dot{m}\sqrt{R_G\,T_3}}{p_3\,A_3} \qquad \text{IV (14)}$$

PRINCIPAL EQUATION obtained from Eqs. 13 and 14, and $\rho = \frac{p}{R_G\,T}$

$$dX_1 = \frac{\rho}{\rho_3}\frac{p}{p_3}\,d\left(\frac{s}{R_G}\right) = \frac{c_f}{2}\left(\dot{m}_{r3}\right)^2\left(\frac{A_3}{A}\right)^3\frac{C\,dL}{A_3} = \frac{c_f}{2}\left(\dot{m}_{r3}\right)^2 d\Omega = dX_2 \qquad \text{IV (15)}$$

$$X_1 = \int_3^4 dX_1 = \int_3^4 \frac{\rho}{\rho_3}\frac{p}{p_3}\,d\left(\frac{s}{R_G}\right) \qquad \text{IV (16)}$$

With Eqs. 11 and 9

$$dX_1 = \left(\frac{1}{\eta_p} - 1\right)\frac{\rho}{\rho_3}\frac{p}{p_3}\frac{dp}{p} = \left(\frac{1}{\eta_p} - 1\right)\frac{\rho}{\rho_3}\,d\left(\frac{p}{p_3}\right)$$

$$dX_1 = \left(\frac{1}{\eta_p} - 1\right)\left(\frac{p}{p_3}\right)^{1-\frac{\gamma-1}{\eta_p\gamma}}\,d\left(\frac{p}{p_3}\right)$$

$$X_1 = \int_1^{(p_3/p_4)} dX_1 = \frac{\frac{1}{\eta_p} - 1}{2 - \frac{\gamma-1}{\eta_p\gamma}}\left[\left(\frac{p_4}{p_3}\right)^{2-\frac{\gamma-1}{\eta_p\gamma}} - 1\right]$$

and

$$X_1 = \frac{\zeta\,\gamma}{\gamma+1-2\zeta\,\gamma}\left[\left(\frac{p_4}{p_3}\right)^{\frac{\gamma+1-2\zeta\gamma}{(1-\zeta)\gamma}} - 1\right] \qquad \text{IV (20)}$$

$$X_2 = \frac{1}{2}\left(\dot{m}_{r3}\right)^2\int_0^L c_f\,d\Omega = \frac{\bar{c}_f}{2}\left(\dot{m}_{r3}\right)^2\int_0^L d\Omega \qquad \text{IV (17)}$$

$$X_2 = \frac{\bar{c}_f}{2}\left(\dot{m}_{r3}\right)^2\Omega \qquad \text{IV (18)}$$

$$\Omega = \int_0^L\left(\frac{A_3}{A}\right)^3\frac{C\,dL}{A_3} \qquad \text{IV (19)}$$

Ω will be denoted as Diffusor Shape Factor

From Eq. 20

$$\frac{p_4}{p_3} = \left[\frac{X_1(\gamma+1-2\zeta\gamma)}{\zeta\,\gamma} + 1\right]^{\frac{(1-\zeta)\gamma}{\gamma+1-2\zeta\gamma}} \qquad \text{IV (21)}$$

TABLE IV (CONTD.) METHODS OF SOLUTION

For Effective Flow Area $A_3^* = k_{B3} A_3$ (k_{B3} = Blockage Factor, A_3 = Actual Area at Diffusor Inlet)

$$\frac{\dot m \sqrt{R_G T_{t3}}}{A_3^* P_{t3}} = \sqrt{\frac{2\gamma}{\gamma-1}\left[\left(\frac{p_3}{P_{t3}}\right)^{\frac{2}{\gamma}} - \left(\frac{p_3}{P_{t3}}\right)^{\frac{\gamma+1}{\gamma}}\right]} = \phi_3 = f\left(\frac{P_{t3}}{p_3}, \gamma\right) \qquad \text{IV (22)}$$

From Eq.14

$$\dot m_{r3} = \frac{\dot m \sqrt{R_G T_3}}{A_3^* p_3} = \phi_3 \frac{\sqrt{(T_3/T_{t3})}}{p_3/P_{t3}} \qquad \text{IV (23)}$$

If p_3 is known,

$$\frac{T_3}{T_{t3}} = \left(\frac{p_3}{P_{t3}}\right)^{\frac{\gamma-1}{\gamma}} \qquad \text{IV (25)}$$

Into Eq.23

$$\dot m_{r3} = \phi_3 \left(\frac{P_{t3}}{p_3}\right)^{\frac{\gamma+1}{2\gamma}} \qquad \text{IV (27)}$$

If $M_{V3} = V_3/\sqrt{\gamma R_G T_3}$ is known, with $c_p = R_G \frac{\gamma}{\gamma-1}$,

$$\frac{T_{t3}}{T_3} = 1 + \frac{V_3^2}{2 c_p T_3} = 1 + \frac{\gamma-1}{2}\frac{V_3^2}{\gamma R_G T_3} = 1 + \frac{\gamma-1}{2} M_{V3}^2 \qquad \text{IV (24)}$$

$$\frac{P_{t3}}{p_3} = \left[1 + \frac{\gamma-1}{2} M_{V3}^2\right]^{\frac{\gamma}{\gamma-1}} \qquad \text{IV (26)}$$

Into Eq.23

$$\dot m_{r3} = \phi_3 \left[1 + \frac{\gamma-1}{2} M_{V3}^2\right]^{\frac{\gamma+1}{2(\gamma-1)}} \qquad \text{IV (28)}$$

For known Ω and $\bar c_f$, i.e. X_2 from Eq.18, and $X_1 = X_2$, the Loss Coefficient ζ must be obtained with an iteration to satisfy the Equation of Continuity at Diffusor Discharge. For Effective Flow Area $A_4^* = k_{B4} A_4$ (k_{B4} = Blockage Factor, A_4 = Actual Diffusor Discharge Area), since $T_{t4} = T_{t3}$,

$$\frac{\dot m \sqrt{R_G T_{t3}}}{A_4^* P_{t4}} = \sqrt{\frac{2\gamma}{\gamma-1}\left[\left(\frac{p_4}{P_{t4}}\right)^{\frac{2}{\gamma}} - \left(\frac{p_4}{P_{t4}}\right)^{\frac{\gamma+1}{\gamma}}\right]} = \phi_4 = f\left(\frac{P_{t4}}{p_4}, \gamma\right) = \phi_3 \frac{A_3^*}{A_4^*} \frac{P_{t3}}{P_{t4}} \qquad \text{IV (29)}$$

Since P_{t3}/P_{t4} is as yet unknown, it is not possible to determine P_{t4}/p_4 from function ϕ_4 to obtain $p_4/p_3 = (P_{t3}/p_3)/(P_{t4}/p_4)$. Additional relation is obtained by calculating entropy increase $\Delta s = s_4 - s_3$ for polytropic process from p_3 to p_4 with Eq.11, and for T_t = constant from P_{t3} to P_{t4} with Eq.5.

For Polytropic Process:

$$\frac{\Delta s}{R_G} = \frac{\zeta}{1-\zeta} \ln\left(\frac{p_4}{p_3}\right) = \ln\left[\left(\frac{p_4}{p_3}\right)^{\frac{\zeta}{1-\zeta}}\right] \qquad \text{IV (30)}$$

Equating Eqs.30 and 31

$$\frac{p_4}{p_3} = \left(\frac{P_{t3}}{P_{t4}}\right)^{\frac{1-\zeta}{\zeta}} \qquad \text{IV (32)}$$

Along Line $T_{t3} = T_{t4}$ = Constant:

$$\frac{\Delta s}{R_G} = -\ln\left[\frac{P_{t4}}{P_{t3}}\right] = \ln\left[\frac{P_{t3}}{P_{t4}}\right] \qquad \text{IV (31)}$$

$$\frac{P_{t3}}{P_{t4}} = \left(\frac{p_4}{p_3}\right)^{\frac{\zeta}{1-\zeta}} \qquad \text{IV (33)}$$

With Eq.33

$$\frac{P_{t4}}{p_4} = \left(\frac{P_{t4}}{P_{t3}}\right)\left(\frac{P_{t3}}{p_3}\right)\left(\frac{p_3}{p_4}\right) = \frac{(P_{t3}/p_3)}{(P_{t3}/P_{t4})(p_4/p_3)} = \frac{(P_{t3}/p_3)}{\left(\frac{p_4}{p_3}\right)^{\frac{1}{1-\zeta}}} \qquad \text{IV (34)}$$

ITERATION PROCEDURE

(1) For given values of Ω and $\bar c_f$ calculate X_2 from Eq.18 with Eq.27 or 28. $X_1 = X_2$

(2) Choose initial value of ζ

(3) Calculate $p_4/p_3 = p_4'/p_3$ by Eq.21 for X_1 and ζ

(4) Calculate $P_{t3}/P_{t4} = P_{t3}/P_{t4}'$ from Eq.33 for p_4'/p_3

(5) Calculate $\phi_4' = \phi_3 (A_3^*/A_4^*)(P_{t3}/P_{t4}')$ (Eq.29)

(6) Calculate P_{t4}'/p_4' from Eq.34 for p_4'/p_3

(7) Calculate $\phi_4 = \phi_4''$ from Flow Function (Eq. 29) for $P_{t4}/p_4 = P_{t4}'/p_4'$

$\phi_4'' = \phi_4'$?

No → Change Value of ζ → (3)

Yes → $\zeta_j (p_4/p_3) = (p_4'/p_3)_j (P_{t4}/P_{t3}) = P_{t4}'/P_{t3}$

Diffusor Efficiency η_{D3-4} between Stations (3) and (4)

$$\eta_{D3-4} = \frac{T_4' - T_3}{T_4 - T_3} = \frac{T_4'/T_3 - 1}{T_4/T_3 - 1} = \frac{(p_4/p_3)^{\frac{\gamma-1}{\gamma}} - 1}{T_4/T_3 - 1}$$

With Eq.8

$$\eta_{D3-4} = \frac{(p_4/p_3)^{\frac{\gamma-1}{\gamma}} - 1}{(p_4/p_3)^{\frac{\gamma-1}{\gamma(1-\zeta)}} - 1} < (1-\zeta) \qquad \text{IV (35)}$$

SUPERSONIC RADIAL DIFFUSERS

D.P. KENNY

Supervisor,
Compressor Research,
United Aircraft of Canada, Limited,
Ville Jacques Cartier,
P.Q., Canada.

LIST OF SYMBOLS

ROMAN

AR	area ratio
AS	aspect ratio of diffuser throat = width (hub to shroud)/height
B^*	throat blockage = $(1 - C_D^*)$
C_D^*	throat discharge coefficient = $\text{Flow}/\rho_{CORE}\, V_{CORE}\, A$
d*, D*	throat diameter
L*	parallel throat length
M	Mach number
p	static pressure
PR	total pressure ratio
$q = \frac{\gamma}{2} p M^2$	dynamic head
Re	Reynolds' number
U	wheel speed
W	weight flow

GREEK

α	flow angle
θ	temperature correction factor for standard day = $\frac{T}{519^\circ R}$; included angle for two dimensional and conical diffuser
δ	pressure correction factor for standard day = $\frac{P}{14.7}$ psia
Δ	increment
γ	ratio of specific heats
η	adiabatic efficiency = $(PR^{\frac{\gamma-1}{\gamma}} - 1)/\Delta T/T_{ENTRY}$
η^*	static pressure effectiveness = $\frac{\text{actual static pressure rise}}{\text{ideal static pressure rise}}$

SUBSCRIPTS

H	hydraulic
LE	leading edge
*	throat
T	tangential

SUPERSCRIPTS

*	throat

A DISCUSSION OF SUPERSONIC DIFFUSERS for centrifugal compressors implies a general discussion of diffusers for centrifugal compressors, since for pressure ratios greater than 3.8 the diffuser entry Mach number exceeds 1.0. This is indicated in Fig. 1 where diffuser entry Mach number is plotted vs. stage pressure ratio for zero prewhirl rotors with radial exit blading. The limiting asymptotic value of $\simeq$ 2.3 for infinite pressure ratio is indicated. It is commonly accepted that for Mach number exceeding 1.25 shock/boundary layer interaction effects lead to separation. In Fig. 1 this corresponds to PR = 12 which suggests an upper limiting target for contemporary state of the art without special devices for reducing the adverse effect of shock/boundary layer interaction. In Fig. 1 is also plotted normalized tip speed vs. stage pressure ratio. At present, maximum safe operating tip speeds are about 2800 fps corresponding to a stage PR = 28:1 and entry Mach number = 1.405.

To date the maximum pressure ratio of centrifugal compressors in an operating engine is 7:1 in the UACL JT15D corresponding to an entry Mach number of $\simeq$ 1.20. Many other operating engines with centrifugal compressors are in the 4 - 6:1 pressure ratio range with entry Mach numbers down to 1.0. Recently, research stages have demonstrated an operating pressure ratio up to 12:1 with an overspeed maximum of 14:1.

Since the pressure ratio requirement of centrifugal compressors has increased with time, the entry Mach number capability has evolved in a natural chronological order.

Therefore the various diffuser concepts for centrifugal compressors are discussed initially with regard to overall performance in the chronological order; vaneless, vaned, passage, multiple cascade and pipe. Then each type is discussed individually with regard to its basic mechanism, design technique, performance evaluation and possible improvements. Finally, general conclusions are drawn with regard to the capability of the various types and possible ultimate performance.

OVERALL PERFORMANCE OF VARIOUS DIFFUSER CONCEPTS

In their earlier applications, centrifugal compressors for air were designed for the 2:1 pressure ratio level with vaneless diffusers which had an exceptionally wide operating range from rotor choke to vaneless space stall with acceptable efficiency = 75%, while retaining the utmost mechanical and aerodynamic simplicity. The major drawback of such diffusers is the large frontal area required to attain a useful diffusion, typically four times the rotor frontal area.

As pressure ratio requirements increased up to 3 and 4:1 vaned diffusers (cambered and flat plate) were introduced to reduce frontal area and improve range at higher pressure ratio. However, diffuser entry Mach numbers were now becoming supersonic and a large vaneless space was retained to obtain diffusion to subsonic Mach number at cascade entry. Thus the vaneless diffuser was still the only diffuser for supersonic flow. When pressure ratios of 5 - 6:1 were attempted, the vaneless space required for subsonic leading edge Mach number was prohibitive and improved diffuser types were introduced namely, passages with a low loading uncovered suction surface and multiple cascade. Typical performance is shown in Fig. 2 for the passage type. In Ref. 1 a 4.2 pressure ratio cambered vane stage at 74% was improved to 4.6 pressure ratio at 84% efficiency for a 20 lb/sec. compressor by converting to a multiple cascade diffuser.

At this time the swept leading edge, unloaded vaned diffuser concept, was introduced by Dallenbach and Van Le at 4 - 6:1 pressure ratio. This proved effective as shown in Fig. 3 but performance was still in the 75% efficiency range.

Recently, both UACL and Boeing/AVLABS demonstrated the high pressure ratio capability of single centrifugal stages. (UACL - 10:1 pressure ratio at 74% and Boeing - 10:1 pressure ratio at 72%) in Refs. 2 and 3. UACL used the pipe diffuser concept of Ref. 4 with a medium specific speed rotor of Ns = 70 (Fig. 4).

Boeing used the rectangular channel concept with spiral leading edge and a low specific speed rotor of Ns = 50 (Fig. 5). By refining the downstream channels they were able to improve on the basic early 5 - 6:1 capability of Fig. 2.

This recent Boeing and UACL work demonstrates that centrifugal compressor diffusers can be operated up to entry Mach numbers of 1.4.

VANELESS DIFFUSERS

The vaneless diffusers accomplish diffusion primarily by the inverse reduction of swirl with radius for conservation of angular momentum. Typically centrifugal impeller exit flow angles are $\simeq$ 20° from tangential, so that the tangential velocity is 94% of the total, while the radial velocity is $\simeq$ 34%. Thus a 2:1 radius ratio will reduce the tangential velocity by 50% and the total by 42% for constant radial velocity, while also halving the radial velocity only reduces the total velocity another 8%. Even reducing the radial velocity to zero only decreases the total velocity another 3%. Thus the diffusion capability of a vaneless diffuser is primarily dependent on the radius ratio.

The vaneless diffuser would seem to be the most effective for supersonic flow, having no obstructions. However, as it turns out, it is the worst. Primarily both the range and effectiveness of the vaneless diffuser are severely limited by the invariable instability of the radial velocity profile at exit from the impeller particularly for PR $>$ 2.

STABILITY AND RANGE In Fig. 6 is presented the map for a vaneless diffuser of radius ratio 2 feeding a scroll collector with a doubling of the width at about radius ratio 1.5 Choking is due to the rotor and surge due to the vaneless diffuser. Range essentially disappears above 3.5 pressure ratio with overall efficiency about 20 points less than for other diffuser types at 4:1 pressure ratio.

At PR = 2 and less the vaneless diffuser is far superior in range but poorer in overall effectiveness than the other types. Jansen (Ref. 5) has shown that the vaneless diffuser has ranges of inherent stability and instability defined by a plot radius ratio vs. inlet swirl for constant rotor tip Reynolds' number as shown in Fig. 7.

In Fig. 8 the stability limit of the diffuser of Fig. 6 is plotted as entry swirl angle vs. entry Mach number as estimated from Ref. 5. Also plotted in Fig. 8 is the locus of overall surge for the map of Fig. 6. This shows that the surge line is within the unstable range. On the overall compressor map of Fig. 6 is located the locus of Jansen's stability limit which falls at about mid range. At high speeds the overall surge occurs adjacent to rotor choke which provides a stabilizing effect.

Also shown on the vaneless diffuser stability map of Fig. 8 is the limit for radius ratio = 1.07 as estimated from Jansen's data. It is evident that for this extent of vaneless space, which is typical of that used with vaned or passage diffusers, the vaneless region is unlikely to ever contribute to the stalling limit of the overall diffuser, since the maximum swirl at 1.3 Mach number = 3.5°, while rotor exit average flow angles are rarely less than 10°.

Generally, the instigating mechanism for instability is the radial boundary layer profile. For most impellers the exit radial and tangential profiles are as shown in Fig. 9. The tangential profile is a typical flat plate turbulent power law on the shroud and hub, being much thicker on the shroud due to the development of a tangential boundary layer along the open shroud of the impeller. The radial profile, having been subjected to the diffusion in the impeller, has typically a shape factor, $H = 3$, and $C_f = .0001$ and is quite close to separation. Further diffusion in the vaneless diffuser can only result in a three dimensional separation which is often observed even in the vaneless space of a vaned diffuser. Thus the vaneless diffuser is generally poor on performance above 2:1 pressure ratio due to the deteriorating exit radial velocity profile from the rotor with increasing pressure ratio.

In addition, vaneless diffusers require an excessive frontal area for any significant diffusion. Since velocity ratio $\propto$ Radius Ratio at constant width, for a typical 5:1 area ratio about 3 times the frontal radius is required over a vaned system.

Thus vaneless diffusers are always severely limited by the unstable nature of the radial profile occurring at exit from the rotor due to the internal diffusion. However, a vaned or passage diffuser can operate moderately well under such conditions since it is governed by the <u>total</u> velocity profile at rotor exit which, in turn, is dominated by the tangential profile due to the tangential nature of the flow. This tangential profile is highly stable having been through a zero pressure gradient. Therefore, vaned and passage diffusers always have an inherent advantage over the vaneless diffuser. In addition, the stalling range of vaned or passage diffusers is not limited by the stability of the <u>radial</u> profile.

VANED DIFFUSERS

The principle of a vaned or cascade diffuser (Fig. 10) is to provide additional reduction of the swirl over the vaneless concept by reducing the angular momentum. Typically 50% of the inlet angular momentum may be removed which effectively halves the radial extent required for a given reduction in swirl compared to the vaneless diffusers. In addition, vaned diffusers are not primarily limited by the stability of the rotor exit radial velocity profile, since they "see" the total velocity which, due to the highly tangential nature of the rotor exit flow, is governed by the very stable tangential profile.

Vaned or cascade diffusers have been successfully applied up to 6:1 pressure ratio and $M_{LE} = 1.15$, where typical stage efficiencies of 75% are common, with excellent range. Fig. 11 shows a peak efficiency of 78% at 5:1 for a UACL research compressor with a cambered vane diffuser at 1.0 lb/sec.

There are two general classes of vaned diffusers; cambered vane and flat plate as shown in Figs. 10 and 15. Generally, the cambered vane diffuser retains a normal static pressure loading across the vane passage, while the flat plate, being a symmetrical, straight passage, exhibits no loading normally across the passage. However, the diffusion rates of flat plate cascades are generally higher than the cambered vane because of their higher turning to radial. In our (UACL) experience, cambered vanes are superior to flat plate as shown in Table I where at 5:1 pressure ratio the cambered vane is 4 points better.

CAMBERED VANE DIFFUSER Although analogous to axial stator cascades, centrifugal compressor vaned diffusers have not been based on the same design philosophy. The design techniques have been very two dimensional, assuming a uniform flow in the spanwise direction and accounting for mainstream and normal flow property variations. Various techniques for specifying the blade profile of cambered vanes have been developed. Faulders (Ref. 6) recommends, for low inlet Mach numbers, transforming rectilinear cascades and presents a detailed study of such a diffuser fed by a static air supply. Dallenbach and Van Le in Ref. 7 describe a blade loading/momentum analysis assuming velocity and angle variation across the blade passage. Such a technique is effective within a channel in the absence of three dimensional effects, but is poor for determining the leading edge suction peak and any local supersonic effects which strongly influence the initial diffusion on the suction surface and hence the boundary layer conditions.

Dallenbach and Van Le in Ref. 7 also recommend a technique for handling the supersonic leading edge Mach number with a swept leading edge concept to minimize shock effects in the transition from supersonic to subsonic flow combined with a lightly loaded (angular momentum change) cascade.

On a full compressor test, only state of the art performance was attained as indicated in Fig. 3. Since the cascade has some turning to radial, the long V-notch swept effect may have contributed more to improved matching of the flow angle variation in the spanwise direction at rotor exit.

At UACL an attempt was made to improve on the momentum/loading technique for a supersonic diffuser entry Mach number of 1.05 as described in Ref. 4. A simplified bow wave configuration was constructed and a simple momentum/loading analysis was applied through the leading edge mixed (supersonic-subsonic) flow region. Supersonic and subsonic regions were treated as simple lump sum quantities and an attempt was made to maintain a constant suction surface Mach number to minimize shock/boundary layer interaction effects. A long, thin, low turning vane was obtained and is shown with the resultant loading diagram in Fig. 13. The leading edge suction peak was estimated using static pressure data for circular cylinders. The effect of the passage shock intersecting the suction surface is shown as a rapid drop in loading. The remainder of the loading was specified to avoid the recurrence of supersonic flow. The map of Fig. 11 with 5:1 at 78% was attained with this diffuser, although the good performance is not all attributable to the diffuser. At higher Mach numbers the performance of this diffuser deteriorates rapidly as seen in Fig. 14 where a loss map is presented.

FLAT PLATE DIFFUSER At UACL we did extensive research on flat plate diffusers using three basic developments; a blunt leading edge, a chamferred leading edge and a scalloped leading edge of the configurations shown in Fig. 15 and reported in Ref. 4. As for the cambered vane diffuser, $M_{LE} = 1.05$ at 5:1 pressure ratio.

The following table shows a comparison of overall efficiency at 5:1 pressure ratio.

TABLE 1

Comparative Overall Performance of
A Stage with Various Flat Plate
Diffuser Configurations

Leading Edge Type	Pressure Ratio	η	Flow
Blunt	5:1	65	1 lb/sec.
Chamferred	5:1	72	"
Chamferred and scalloped	4.85	73	1 lb/sec.

There is a general improvement of efficiency through blunt leading edge, chamferred and chamferred and scalloped. The basic flat plate cascade was defined to have 36 vanes which gives the optimum 10° included angle of the conventional two dimensional diffuser. The chamferred case includes a chamfer angle of 4° giving an initial included angle of 6° for AR = 1.3. Finally the scallop defined by a hollow grind gives the shape shown in Fig. 15.

It is felt that the leading edge scallop has an ameliorating effect because it peels the wall boundary layers away from the cascade corners. The same concept reduced the loss of a UACL cambered vane diffuser by about 10%.

The ideal flow pattern approaching a supersonic flat plate cascade for an entry Mach number = 1.31 is shown in Fig. 16. This was obtained by a supersonic characteristic analysis assuming a uniform limit circle source/vortex flow with sharp leading edge vanes. The local leading edge Mach number upstream of the leading edge shock is 1.443 and downstream is 1.27 which re-accelerates to 1.46 at the passage shock along the flat suction surface. This example demonstrates the general effect of the uncovered suction surfaces of the vanes of two dimensional radial cascades in supersonic flow. Turning towards radial (reducing angular momentum) gives acceleration and turning towards tangential (adding angular momentum) gives diffusion. This is analogous to rectilinear cascades, where a flat surface (no turning) gives constant velocity, turning towards axial gives acceleration and turning towards tangential gives diffusion. However, the turning is relative to the local tangential and radial directions for the radial cascade so that a flat surface gives an effective turning to radial and hence acceleration. This indicates that at least zero loading type uncovered suction surface profiles should be used from leading edge to throat to minimize shock effects and even a negative loading profile might be desirable. Of course, the lack of loading from leading edge to throat must be made up downstream of the throat.

LOSSES AND STATIC PRESSURE EFFECTIVENESS From an axial cascade view, the radial cambered vane and flat plate diffuser represent low aspect ratio, high solidity, thick sidewall boundary layer cases with high de Haller number velocity ratio (high diffusion). Unfortunately, for many years only the angular momentum loading aspect of the cascade loading was recognized. A typical number used by

UACL is the coefficient $C_n = \frac{\Delta H}{\bar{q} A_T \bar{R}}$ = 0.4 maximum. I say unfortunately because equivalent NACA D factors for such diffuser cascades are ≈ 0.8 with 80% of it due to streamwise diffusion. Thus the single greatest source of loss in radial cascades had been ignored. In Fig. 17 is presented a comparison of measured losses for the cambered vane and flat plate diffusers discussed previously on the NACA axial cascade D factor basis. It is interesting that the data correlate quite well with an extrapolation of the NACA loss correlation fitting the NACA data band quite well. Leading edge Mach numbers up to 1.15 are noted in Fig. 17. The higher D factor level of the flat plate over cambered vane diffuser is noteworthy. It is quite satisfying that, in spite of the gross variation of incidence over the blade span, the cambered vane and flat plate diffuser losses correlate with axial stators which (the latter) generally operate at much more uniform incidence distributions.

Referring to the strongly varying distributions of radial and tangential velocity obtained at exit from a centrifugal impeller, Fig. 9, the combined effect is shown as a typical absolute flow angle profile in Fig. 18. When compared with the conventional constant two dimensional leading edge metal angle of a cascade diffuser, which would be about the mean of this profile, incidence would vary from +12° at the sidewalls to -12° at midchannel. An attempt to scallop a vaned diffuser and reprofile to match this flow angle distribution should result in an improvement in performance. The form of the scallop is shown in Fig. 19. Note that a large area of the vane has been removed or altered in the carefully designed supersonic region. The results of this are shown in Fig. 20 as a curve of peak efficiency vs. pressure ratio over the map, as much as four points in efficiency were gained at 5:1 pressure ratio. In addition the flow range, as also shown, improved about 50%. In Fig. 20 the diffuser losses are also plotted vs. M_{LE}. Minimum loss at M_{LE} = 1.03 decreased by 30%. This suggests that rather than being highly concerned with the leading edge Mach number effects, one should take more account of the three dimensional nature of the rotor exit flow (which is likely to be more effective in reducing losses). For, in spite of the effective gouging of a large portion of the vane in the supposedly highly critical area along the suction surface from leading edge to throat, a large gain in performance has been obtained.

It has been demonstrated in the literature by Dean and Runstadler (Ref. 8) and Sprenger (Ref. 9) that the static pressure effectiveness (defined as actual static pressure rise/ideal static pressure rise from the throat to exit) correlates well with throat blockage (defined as $1-C_D^*$) for a wide range of throat Mach numbers and geometry with both rectangular and conical diffusers. In Fig. 21 data for the UACL cambered vane diffuser has been plotted on this basis for the whole range of the map, where entry Mach number varies from 0.7 to 1.15. The correlation is quite good indicating relatively high throat blockage levels of ≃ .25 at high speed. Note the low value of the throat Reynolds' number ($1.0 - 1.8 \times 10^5$). A comparison of this data with Dean and Runstadler's data for $Re_{\delta_H^*}$ to 9×10^5 (Ref. 8) is also shown in Fig. 21. The throat Reynolds' number correlation would give a 1/5th power law of $Re_{\delta_H^*}$ vs. $(1 - \eta^*)$ which is consistent with the turbulent friction law for straight pipes in this range as shown in Fig. 22. The shape of the effectiveness vs. throat blockage correlation is also quite consistent with that of Dean and Runstadler. The configuration of the diffuser for the Ref. 8 data was a straight two dimensional 8° included angle with throat AS = 1 for M^* = 0.2 to 1.0. The UACL cambered vane data is for throat AS = .92 with a curved centerline and a 13° included angle with M^* = 0.7 to 1.0. This correlating of effectiveness with throat blockage for diffuser elements would appear to be superior to the D factor concept in that the former covers the whole range of operation from surge to choke, while the latter applies to the optimum leading edge incidence match point.

THROAT BLOCKAGE To determine the source of the high throat blockage levels for the cambered vane diffuser, a correlation of throat blockage with nondimensional leading edge to throat static pressure rise was formulated. This is shown in Fig. 23. There tend to be separate correlations for entry Mach numbers > 1 and < 1. It is to be expected that throat blockage would correlate with leading edge to throat static pressure rise, since the wall boundary layers will grow under the adverse pressure gradient and become more defected. The step increase in blockage on reaching supersonic entry Mach numbers is consistent with the fact that for entry Mach number > 1 the static pressure rise occurs more abruptly through a shock system. From Fig. 23 it is evident that due to the losses which occur in the diffusing system $\frac{\Delta p^*}{q_{LE}}$ = .35 corresponds to ≃ half the overall diffusion required to M = .1 occurring from leading edge to throat. As entry Mach number increases beyond 1.0 this becomes increasingly severe so that at entry Mach number = 1.25 for surge M^* = .8, $\frac{\Delta p^*}{q_{LE}}$ = 0.65 would be required. With the throat blockage levels of Fig. 23 little diffusion would be accomplished after the throat. This would seem to be the major problem with supersonic diffuser for centrifugal compressors; the leading edge to throat diffusion required, while still minimizing throat blockage to maximize downstream effectiveness. The leading edge scallop test quoted above indicates that simply matching the leading edge flow angle profile makes large improvements in performance, presumably because of a considerable reduction in throat blockage and a consequent improvement in recovery.

Further evidence to indicate the importance of matching the spanwise incidence correctly is shown in Fig. 24 where choking throat discharge coefficient is plotted vs. entry Mach number for the two dimensional and scalloped leading edge cambered vane and a pipe diffuser. The pipe diffuser retains considerably lower throat blockage levels and the scalloped leading edge cambered vane is midway between pipe and two dimensional leading edge cambered vane. The pipe diffuser characteristics will be discussed further in a later section.

STALL LIMIT In Fig. 25 is presented a stalling correlation for the two dimensional leading edge cambered vane diffuser compared to a pipe. Here, leading edge to throat nondimensional static pressure rise at surge is plotted vs. entry Mach number. Up to entry Mach number = 1.0 it is almost constant for both cases. Beyond entry Mach number = 1.0 it rises for both cases. For comparison, the static pressure rise across a normal shock is plotted. For the two diffuser types, the leading edge to throat static pressure rise seems to approach the normal shock curve for entry Mach number exceeding 1.0 but eventually rise more slowly. Actually, the diffuser $\frac{\Delta p^*}{q_{in}}$ stall curves would not be expected to rise for M entry = 1 until the normal shock level had exceeded this level which occurs above M entry = 1. Since the M entry scale corresponds to the mass average value and not the peak, the normal shock static pressure rise curve for the peak is also plotted. For both diffuser types the stalling limit curves commence rising when they intersect the peak entry Mach number shock rise curves. The pipe diffuser has about 60% better stalling static pressure rise. This all indicates that supersonic diffusers can have good stall capability, in fact, even better than subsonic with the stalling limit increasing with entry Mach number. However, the higher rate of increase of throat blockage from Fig. 24 suggests that choking blockage may remove much of the mass flow range advantage of the superior stall capability over subsonic diffusers.

MULTIPLE CASCADE DIFFUSERS

Multiple cascade diffusers (Fig. 26) comprise multiple succeeding rows of cascade or vaned diffusers. Usually there are two, sometimes three rows. The basic advantage of this concept over the single row vaned is the subdividing of the loading which results. Thus a two row multiple cascade system may accomplish the same diffusion as a single cambered vane but with half the D factor per row, i.e. 0.4 vs. 0.8. A value of 0.4 is generally accepted as a useful maximum for axial stator cascades with low loss. In addition, the adjacent cascades may be relatively indexed to optimize the blade surface boundary layer entry condition for the following row.

Very little published data are available for such diffusers. However, Continental have published a map with up to 4.8:1 pressure ratio for a multiple cascade single stage centrifugal compressor at 20 lbs/sec. compared with a corresponding vaned diffuser. At the maximum speed (PR = 4.2 to 4.8) efficiency increased from 74% to 84% from the vaned to the multiple cascade diffuser with an improved surge range. No data on the geometry of this case is available, however, from Fig. 1 for a conventional vaneless space gap of 7% the diffuser entry Mach number would be expected to be supersonic for PR = 4.8.

Another published case of a multiple cascade diffuser in a centrifugal stage is Ref. 10 at 2.7 pressure ratio and 2 lbs/sec. Here a direct comparison was made with pipe diffuser operation with the same rotor. Generally the pipe diffuser stage is over 1 point better on efficiency. However, no attempt was made to match the spanwise leading edge angle distribution of the first row cascade to the flow angle distribution at rotor exit. The entry Mach number at design point for this case is 0.8 with double circular arc and NACA 400 series for the first and second rows. Gap/chord ratios were 0.8 and 0.43, respectively, compared with the 0.34 for the UACL cambered vane diffuser. The predicted loss for this multiple cascade diffuser is $\frac{\Delta P}{P_{t_a}}$ = .02, while the measured was 0.04. This difference of 0.02 would correspond to the 1 point efficiency difference between pipe and cascade. Again, this accentuates the importance of matching the inlet flow angle profile to maximize the performance of centrifugal compressor diffusers.

PASSAGE DIFFUSERS

The passage diffuser as shown in Fig. 27 is a concept which ignores the angular momentum reduction principle of the cascades and relies on capturing the flow with a cambered leading edge and directing it through an enclosed passage, whence it is fed to a collector after diffusion to some low Mach number. As in other diffuser concepts, it is the leading edge to throat region which is important for supersonic entry Mach number. In most cases (applications to 6:1 pressure ratio) a compressible log spiral or some type of low loading suction surface is applied and the pressure surface is faired to give a desired throat. After the throat some moderate diffusion rate, straight channel is applied; with either circular or rectangular cross section. Boeing, G.M. and Chrysler have published information on such application at pressure ratios of 6:1 and 3:1 and 4:1, respectively, in Ref. 11.

Performance similar to or better than cascade diffusers is possible. In Fig. 2 Boeing obtained 6:1 pressure ratio at 80%. Generally, these diffusers are bulky and have a relatively large frontal area.

Recently Boeing/AVLABS has demonstrated an efficiency level of 72% at 10:1 pressure ratio (Fig. 5) with this diffuser concept indicating an entry Mach number level of 1.3. Detailed analysis of the diffusion performance from throat to exit as effectiveness vs. throat blockage from Ref. 3 is as shown in Fig. 28 (AS = .45, 2θ = 10° and AR = 4:1, Re_{D_H} = 4 x 10^5). A comparison with the static straight rectangular section data of Ref. 8 by Dean and Runstadler is shown. This result is consistent with the correlation of UACL cambered vane diffuser effectiveness with throat blockage.

In both Refs. 8 and 3 for the static channel tests and the 10:1 pressure ratio compressor tests a significant effect of aspect ratio was determined. Fig. 29 shows the results from Ref. 8 for the static channel tests indicating an optimum aspect ratio of 0.75 = depth/width with a critical dependence on the 0 - .75 side of the curve. Throat parallel length was also found to be critical, the important condition to satisfy, being to avoid re-accelerating the throat flow to supersonic Mach numbers. A parallel throat length = 0.33 of throat hydraulic diameter was found to be satisfactory.

In the following section on the pipe diffuser, all of these parameters will be compared. In Ref. 3 on the 10:1 pressure ratio compressor work, the same trend of increasing throat blockage towards surge was determined as for the UACL cambered vane, although insufficient data to form a leading edge to throat static pressure rise correlation is available. The same reasoning, as presented previously in the vaned diffuser section, is presented for this characteristic in Ref. 3. In fact, schlieren photos are presented in Ref. 3 which indicate that a "zone of rapid readjustment" occurs at the diffuser leading edge. So that rather than a continuous free vortex flow field occurring from rotor exit to diffuser leading edge, a rapid readjustment of the swirling flow with radial static pressure gradient at rotor exit to a constant static pressure flow at diffuser throat occurs through leading edge normal shock. The strength of this shock then adjusts itself to match continuity in the diffuser throat with an increase of strength towards surge due to the decreasing throat Mach number in this direction.

Just as for the vaned diffuser, these passage diffusers will suffer from the same leading edge incidence mismatching for two dimensional straight leading edges.

PIPE DIFFUSER

This novel concept, Fig. 30, is based upon an array of drillings arranged symmetrically in a radial plane with their center lines all tangent to the same circle. The geometry is such that, when these drillings mutually intersect, a pseudo vaneless space is formed between the tangency circle and an outer circle called the leading edge circle. Since the intersection of two coplanar cylinders is an ellipse, this pseudo vaneless space is composed of an array of symmetrically located elliptic ridges at the intersection of each drilling. When this drilling array is arranged around a centrifugal impeller, the flow will exit into the tangency circle plane, flow through the pseudo vaneless space, and enter the discrete pipes formed by the drillings. A conical diffuser may then be arranged downstream of each discrete pipe to diffuse the flow and feed any type of passage such as the trumpet in Fig. 31 which, in turn, feeds an axially directed annulus.

The merits of this diffuser concept are both economic and aerodynamic. Economic because of the leading edge region is easily defined by a series of simple drillings and comes out extremely accurately for relatively little effort. The major aerodynamic advantages lie with the leading edge ridge or scallop. As seen in Fig. 30 the ridge is inclined at 0° from tangential at its own tangency circle (slightly greater in radius than the passage centerline tangency circle) and builds up to a maximum inclination at the leading edge circle. The three dimensional shape of this leading edge allows it to accommodate the type of flow angle distribution usually found at the exit of centrifugal compressors due to fairly thick hub/shroud boundary layers.

The swept shape of the leading edge is conducive to the "normal Mach number $<$ 1" concept of the swept wing at incidence. This vortex has been found to be conducive to the stability of the flow in the passages and is considered to suppress the separation tendencies of the wall boundary layer in the downstream diffuser. In particular, it suppresses the separation of the flow over the apex, Fig. 30, of the scallop in the leading edge plane.

The circular cross section of the drillings is considered to allow these diffusers to "swallow" a highly non uniform flow much better than the two dimensional cascade type; particularly where the rolled vortices mix the flow. It would at first appear that the swept leading edge should allow the supersonic leading edge flow to enter the diffuser channel supersonically. However, this is only possible for one throughflow at a given speed for a fixed geometry diffuser, since the leading edge Mach number is very nearly constant along a speed line and the throat Mach number is largely a function of flow.

The simplest pipe diffuser cross section, circular, has a natural aspect ratio of 1.0 which is just over the optimum of $\simeq$ .75 determined for rectangular section passage diffusers in Ref. 8.

The effect of parallel throat length on pipe diffuser performance has been demonstrated in Ref. 4. This is repeated in Fig. 32 where the wall static pressure distribution of short and long throat pipe diffusers is plotted. In both cases, just upstream of the apex of the leading edge scallop, a normal shock occurs which automatically adjusts itself to suit continuity in the diffuser throat. This is the same finding as for Ref. 3 on the Boeing/AVLABS 10:1 pressure ratio centrifugal program where schlieren photographs show the same leading edge normal shock. In the throat, for the short case, a continuous static pressure rise occurs merging into the static pressure rise of the downstream cone. For the long throat case, an initial static pressure rise occurs in the throat followed by a drop, possibly to supersonic Mach number, with a relatively slow static pressure recovery in the downstream cone. The overall static pressure rise of the short throat case is 19% greater than that of the long throat combined with a 0.5 percentage point improvement in overall efficiency. The corresponding throat dimensions for the two cases are $L^*/d^* = 1.84$ and 0.5.

STATIC PRESSURE EFFECTIVENESS As for the vaned and passage diffusers, the throat to exit effectiveness of the pipe diffuser cones may be correlated with throat blockage. Fig. 33 shows such a correlation for a UACL 6:1 and 10:1 pressure ratio match pipe diffuser. The maximum entry Mach number of the 6:1 and 10:1 pressure ratio data are 1.2 and 1.42. The latter is likely one of the highest Mach number levels of which a radial diffuser has ever been operated. For comparison, Sprenger's (Ref. 9) straight conical diffuser throat blockage correlation is also shown. The shapes of the curves are quite similar. Due to the throat Reynolds' number difference, the curves are relatively displaced. However, they do correspond on a $1/5^{th}$ power law at $B^* = .1$ as indicated in Fig. 22. Sprenger's data correspond to low throat Mach number, while the UACL data are for $M^* = 0.6 - 1.0$. However, the data from Ref. 8 show that effectiveness is very weakly dependent on M^* as

indicated in Fig. 33. Again, the throat to exit effectiveness of a centrifugal compressor diffuser has been shown to correlate with static, single channel on the throat blockage/effectiveness base.

In Fig. 34 the throat to exit effectiveness is plotted vs. throat Mach number and shock Mach number for a 6:1 pressure ratio speedline. On the left is a scale of throat Mach number up to 1.0. On the right is a scale of diffuser passage upstream shock Mach number. Just as for the Boeing/AVLABS work, a continuous set of data is obtained even above M* = 1.0 with only a slight fall off in effectiveness up to 1.1 Mach number. Note that the throat Reynolds' number of the UACL pipe diffuser is about 1/4 of the Boeing/AVLABS. The increase in effectiveness with increasing M* is due to the corresponding reduction in throat blockage. The core or maximum throat total pressure used to calculate the throat Mach number for the UACL cambered vane and pipe diffuser data was obtained from impeller tip static and temperature rise with flow factor and shroud friction temperature rise determined from numerous tip traverses of total pressure and flow angle. The throat total pressure includes a correction for leading edge shock loss. Invariably at all speeds, verge of choke (maximum flow) corresponds to M* = 1.0 which suggests that very little core total pressure loss occurs from leading edge to throat.

Comparing the pipe diffuser effectiveness vs. throat blockage data with the UACL cambered vane data as in Fig. 35 shows that they both follow the same type of correlation (same throat Reynolds' number) but that the cambered vane data falls lower on effectiveness and is at a higher level for the same speed. In fact, the cambered vane diffuser at the 6:1 pressure ratio speed operates at the same B* (= .25) level as the 12:1 pipe diffuser. This brings out one of the principle advantages of the pipe diffuser leading edge concept. The superior matching of the leading edge flow angle profile and the swept shape reduce the resultant throat blockage levels and raise the effectiveness. Although the matching is not perfect, it certainly is much superior to a straight two dimensional leading edge. In Fig. 36 the incidence distribution is plotted vs. fraction of flow. About 70% of the flow is operating at an incidence level of $\pm$ 6° vs. the $\pm$ 12° of a two dimensional leading edge.

THROAT BLOCKAGE The same leading edge to throat static pressure rise concept as for the vaned diffuser has been found to correlate the throat blockage of a pipe diffuser. The data are shown in Fig. 37, both for 6:1 and 10:1 pressure ratio stages. Only high speed (10:1 to 14:1 pressure ratio) data are available for the 10:1 pressure ratio stage. A general increase of blockage occurs with increasing static pressure rise with two curves for entry Mach number $>$ 1 and $<$ 1. As discussed previously for the cambered vane diffuser, a general increase of throat blockage with increasing static pressure rise leading edge to throat is to be expected, since more diffusion is required of the boundary layer resulting in a thicker, more defected boundary layer. The higher level curve for $M_{LE} > 1$ is a result of requiring that most of the diffusion (leading edge to throat) be accomplished abruptly through a normal shock. Although the 10:1 pressure ratio data approach the 6:1 pressure ratio data at lower blockage (.13) for $M_{LE} > 1$, they follow a steeper trend for increasing blockage than the 6:1 pressure ratio data. Possibly, for higher entry Mach number levels ($>$ 1.29) the curves of B^* vs. $\frac{\Delta p^*}{q_{LE}}$ increase in level or the different rotor for the 10:1 pressure ratio case feeds a different incidence profile to the pipe diffuser leading edge resulting in a somewhat different throat blockage characteristic. In fact, it might be expected that different diffuser leading edge incidence distributions result in different throat blockage characteristics, i.e. the difference between two dimensional leading edge cambered vane and pipe diffuser. In any case, it appears that throat blockage levels for a simple throat at the leading edge of a pipe diffuser can be rising rapidly for entry Mach numbers approaching 1.4. The equivalent trend of a two dimensional leading edge diffuser would likely be disastrous. In Fig. 38 a comparison of the correlations for the two diffuser types is plotted. For entry Mach number $<$ 1, the curves tend to coincide at high static pressure drop to the throat with an increasing divergence for increasing static pressure rise (or decreasing static pressure drop) with the cambered vane blockage levels considerably exceeding those of the pipe diffuser. For instance, at $\frac{\Delta p^*}{q_{LE}}$ = 0.225 the cambered vane diffuser exhibits minimum loss at the 6:1 pressure ratio speed for the pipe diffuser, while the same point for the pipe diffuser is at $\frac{\Delta p^*}{q_{LE}} \approx 0.2$. These correspond to B* = 0.21 and 0.1, respectively, with $M_{LE} > 1$ on Fig. 38. This gives η^* = 0.51 and .65, respectively, in Fig. 35 with $\Delta\eta^*$ = 0.14. The result is a difference of about 5 points in overall efficiency. Therefore, much of the poor performance of diffuser types other than the pipe is due to the higher throat blockage levels which they incur. The scalloped vaned diffuser leading edge test quoted previously demonstrates this.

Other evidence of the superiority of the pipe diffuser is demonstrated by the throat blockage at choke correlation of Fig. 24 discussed previously with regard to vaned diffuser. The pipe diffuser is far superior to the vaned at supersonic entry Mach number while at subsonic Mach numbers its correlation approaches the vaned, whence the two curves merge at M_{LE} = .8. For the high pressure ratio (10:1) case of the pipe diffuser throat blockage levels as high as 0.25 are encountered at 1.4 entry Mach number but this data do tend to fair into the 6:1 pressure ratio pipe data. In addition, rate of drop of C_D^* more than doubles from M_{LE} = 1.2 to 1.4 which is considerable. In fact, the trend of the curve suggests that, for entry Mach number approaching 1.5, C_D^* drops vertically with M_{LE}. The lower throat blockage of the pipe diffuser allows a smaller geometric throat for the same flow and consequently a more compact diffusing system as well as higher effectiveness.

STALL LIMIT The stalling correlation of the two diffuser forms is presented in Fig. 25. The limiting leading edge to throat static pressure rise has been plotted vs. entry Mach number. Since stall is likely a breakdown of sidewall boundary layers in traversing the static pressure gradient from leading edge to throat, it would seem likely that the above correlation is relevant. As explained in the previous section on vaned diffusers, a nearly constant value of $\Delta p^*/q_{LE}$ is obtained up to MIE = 1 with the pipe diffuser level about 60% higher. Above entry Mach number = 1, both curves rise coinciding with the intersection of the curve of $\Delta p^*/q_{LE}$ for the peak entry Mach number normal shock. This might be expected since, when a leading edge normal shock occurs, the flow would try to follow the abrupt static pressure rise of the shock until sidewall boundary layer separation became

predominant. Data for both 6:1 pressure ratio and 10:1 pressure ratio pipe diffuser stages are presented. Unfortunately, only a few high speed points were obtained for the 10:1 pressure ratio case as indicated at $\simeq$ 1.4 entry Mach number. These data correspond to choking of the diffuser as shown by the line of $\frac{\Delta p^*}{q_{LE}}$ vs. M_{LE} for a choked throat which passes through the data. The remainder of the stall limit $\frac{\Delta p^*}{q_{LE}}$ curve for the 10:1 pressure ratio case is shown estimated from the data of Fig. 37. At about 1.33 entry Mach number, the stall locus breaks off from the choked throat curve and traverses linearly across to the 6:1 pressure curve at entry Mach number = 1.135. This indicates that increasing from entry Mach number 1.33, the diffuser has lost its stall capability and is only sustained by the choked throat condition and that around entry Mach number = 1.15 a maximum stall capability occurs with $\frac{\Delta p^*}{q_{LE}} \simeq 0.50$ or more. Presumably, with entry Mach number exceeding $\simeq$ 1.15, the abrupt static pressure rise required through a normal shock results in an excessive static pressure gradient for the sidewall boundary layers. It should be considered as indicated in Fig. 25 that for all these UACL small centrifugal data with absolute flow = 1 lb/sec., the resulting low Reynolds' numbers give fully developed boundary layers. With thinner wall boundary layers and higher Reynolds' number diffuser throat blockage, stall limit and effectiveness will all improve.

It is interesting to note that the superior stalling and choking limits of the pipe diffuser do not necessarily lead to a wider mass flow range at a given speed. In fact, the higher rate of increase of blockage of the vaned diffuser with increasing static pressure rise leading edge to throat allows it to reach a lower relative mass flow at surge than the pipe diffuser so that the loss of choke flow capacity is just balanced. The mass flow range at supersonic Mach numbers is about equal for the two diffuser types and is superior for the cambered vane at low Mach numbers, i.e. .8. This suggests that diffusers with low throat blockage characteristic and good effectiveness will tend to have inferior flow range.

GENERAL CONCLUSIONS

The overall loss levels at minimum loss for constant entry Mach number (constant rotor speed) of radial cascade diffusers have been shown to fit the NACA D factor correlation for axial cascade stators up to entry Mach numbers of 1.15 (axial cascade stator entry Mach number $\simeq$ .8). This radial diffuser data provides D factor concept data up to levels of 0.9. Mainstream diffusion accounts for 80% of the D factor loading of radial cascades. Leading edge scalloping of cascade diffusers to match the entry flow angle profile has reduced the loss levels by 30% up to entry Mach number = 1.10.

The correlation of cascade diffuser performance as throat to exit static pressure effectiveness with throat blockage compares well with single passage static measurements for the whole range of the compressor map and is superior to the D factor concept, since it covers the whole range of operation (not just minimum loss).

Some available published data have demonstrated that multiple cascade diffusers are superior to single cascade vaned up to 5:1 pressure ratio (Ref. 1), while other such data show that the pipe diffuser is superior to a multiple cascade for a 2.7 pressure ratio stage (Ref. 11).

The performance of both rectangular passage and pipe diffusers may be successfully correlated with single passage static tests on the throat to exit effectiveness vs. throat blockage concept considering Reynolds' number to the 1/5th power.

Similar correlation of effectiveness with throat blockage is obtained over the whole compressor map for both a cambered vane up to 5:1 pressure ratio and pipe diffuser up to 12:1 pressure ratio with a single line fitting the whole range of data from surge to choke on every speedline.

Throat blockage has been found to be a prime function of leading edge to throat static pressure rise with separate correlations for supersonic and subsonic entry Mach numbers. The single greatest problem with supersonic radial diffusers is that for entry Mach number exceeding 1.2 nearly 1/2 the total required static pressure rise of the diffuser must occur from leading edge to throat in about 10% of the total diffusion path length mostly through a normal shock.

To improve the performance of higher pressure ratio centrifugal compressors, some method of reducing the throat blockage is required. The entry Mach number itself may be reduced by using rotors with exit blading sweepback which raises prohibitive stress problems or by increasing the extent of vaneless space which usually leads to increased vaneless space losses and increased frontal area with little improvement in overall performance. Some method of reducing the effect of the leading edge shock on throat blockage is likely most promising.

The following overall centrifugal stage performance levels have been obtained with radial supersonic diffuser types.

Manufacturer	Type	Entry Mach No.	PR	Stage Efficiency	Flow (lb/sec.)
UACL	Cambered Vane	1.05	5	78 %	1
Continental	Multiple Cascade		4.8	84	20
Boeing	Passage	1.2	6	80	6
Boeing	Passage	1.3	10	72	2
UACL	Pipe	1.3	10	74.5	1

REFERENCES

(1) "Heavy-Lift Tip Turbojet Rotor System"
Vol. XI, Engine Design
U.S. AVLABS, October 1965.

(2) Morris, R.E. and Kenny, D.P. "High Pressure Ratio Centrifugal Compressor for Small Gas Turbine Engines"
Prepared for the 31st Meeting of the Propulsion and Energetics Panel of AGARD "Helicopter and Propulsion Systems"
June 1968, Ottawa, Canada.

(3) Schorr, P.G., Welliver, A.D. and Winslow, L.J. "Design and Development of Small High Pressure Ratio, Single Stage Centrifugal Compressor"
Presented on March 1969 at the ASME Cleveland Conference.

(4) Kenny, D.P. "A Novel Low Cost Diffuser for High Performance Centrifugal Compressors"
A.S.M.E. Paper No. 68/GT-38.

(5) Jansen, W. "Rotating Stall in a Radial Vaneless Diffuser"
A.S.M.E. Paper No. 64-FE-6.

(6) Faulders, C.R. "Aerodynamic Design of Vaned Diffusers for Centrifugal Compressors"
A.S.M.E. Paper No. 56-A-213.

(7) Dallenbach, F. and Van Le, N. "Supersonic Diffuser for Radial and Mixed Flow Compressors"
A.S.M.E. Paper No. 60-Hyd.-11.

(8) Runstadler, P.W. Jr. and Dean, R.C. Jr. "Straight Channel Diffuser Performance at High Inlet Mach Numbers"
A.S.M.E. Paper No. 63-WA/FE-19.

(9) Sprenger, H. "Experimental Investigations of Straight and Curved Diffusers"
Mitt. Inst. Aerodyn., Zurich, (27), 1959, Switzerland.

(10) Groh, F.G., Wood, G.M., Kulp, R.S. and Kenny, D.P. "Evaluation of a High Hub/Tip Ratio Centrifugal Compressor"
A.S.M.E. Paper No. 69-WA/FE-28.

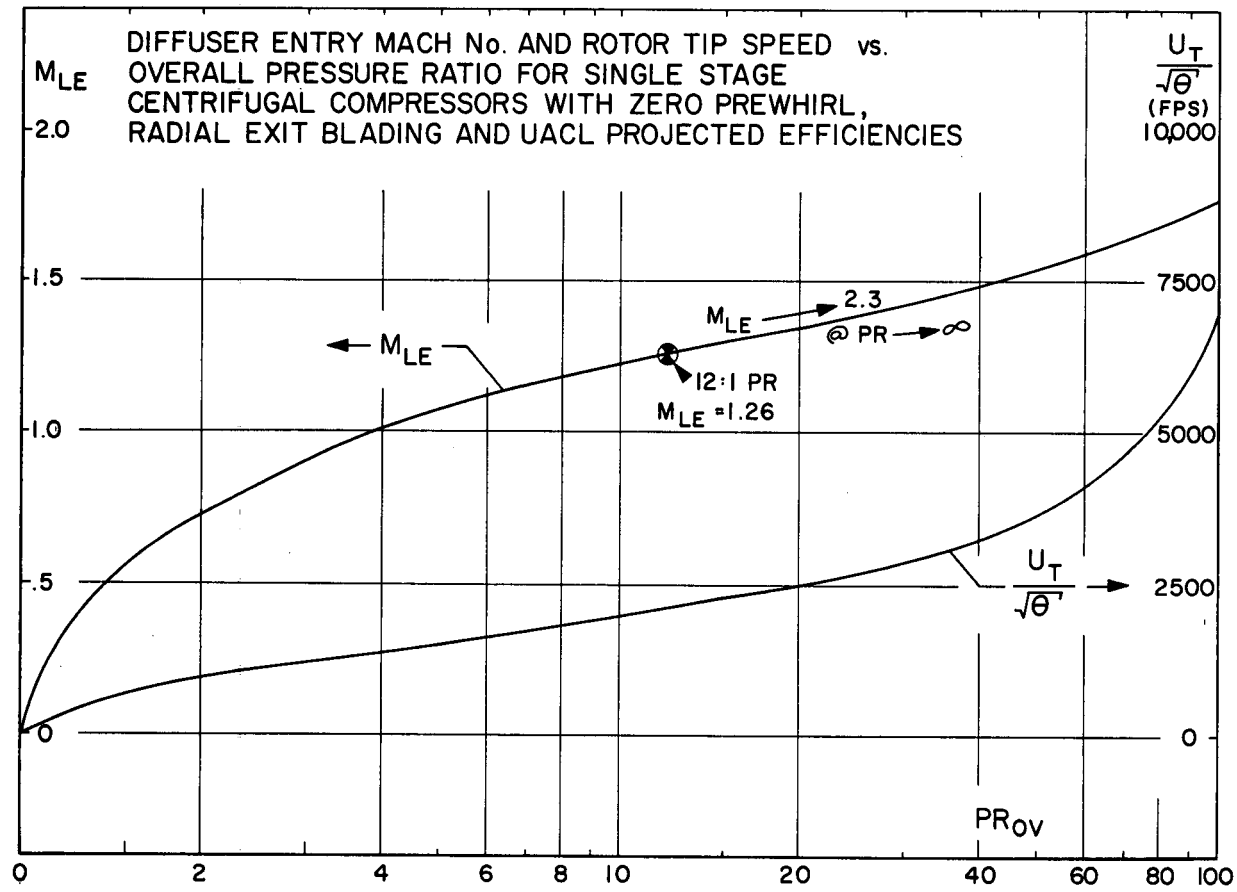

Fig. 1 Diffuser entry Mach number and rotor tip speed vs overall PR

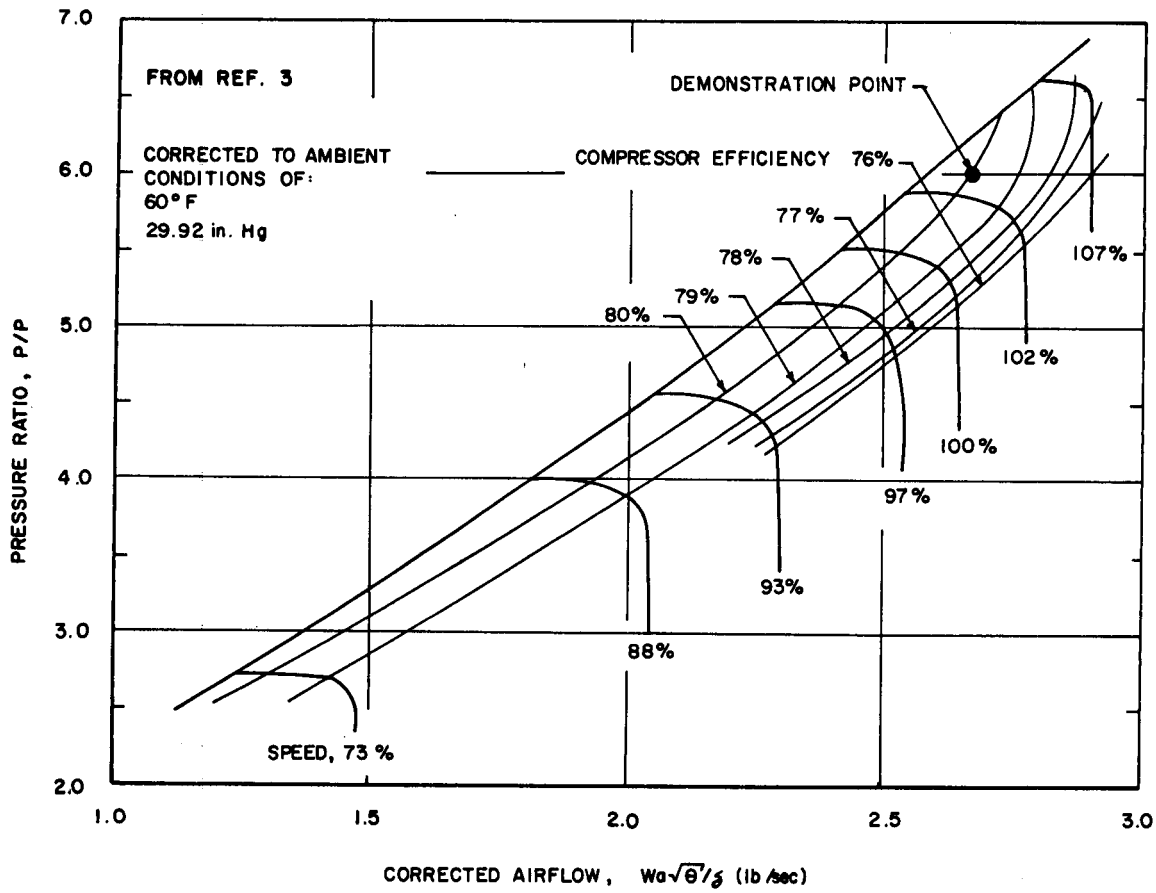

Fig. 2 Boeing 6:1 PR single stage centrifugal

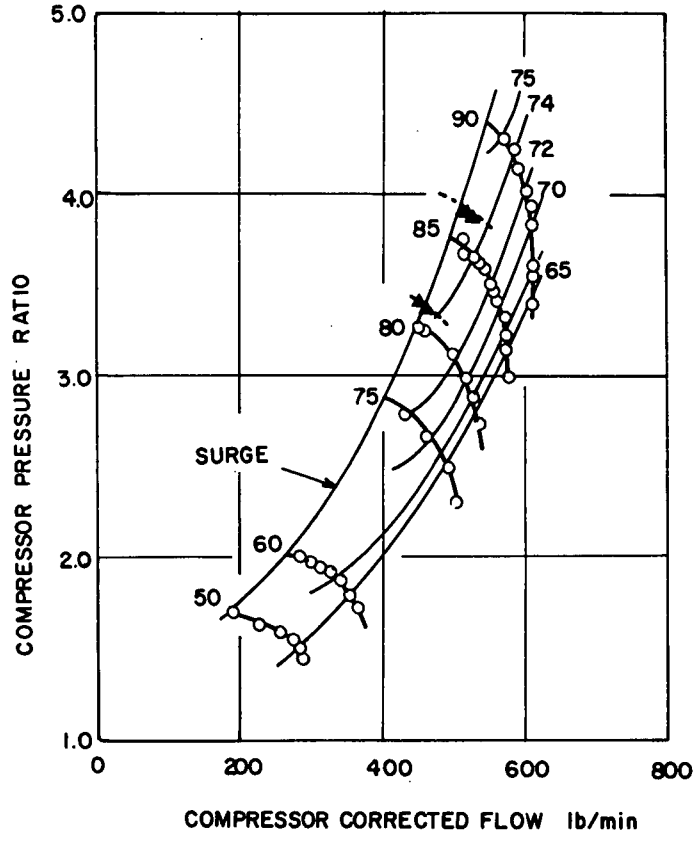

Fig. 3 Airesearch single stage centrifugal with V-notch LE vaned diffuser

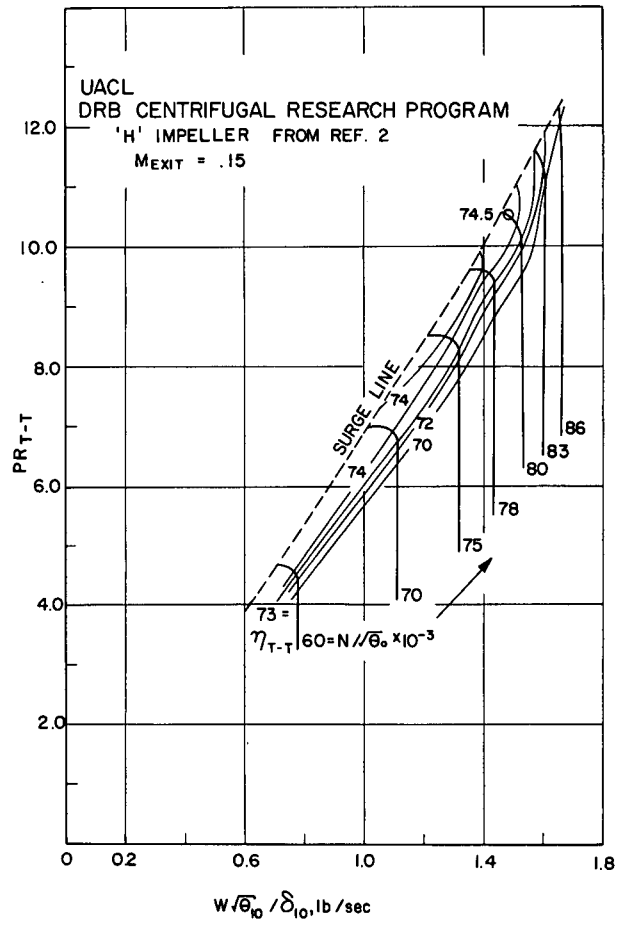

Fig. 4 UACL DRB centrifugal research program 10:1 PR

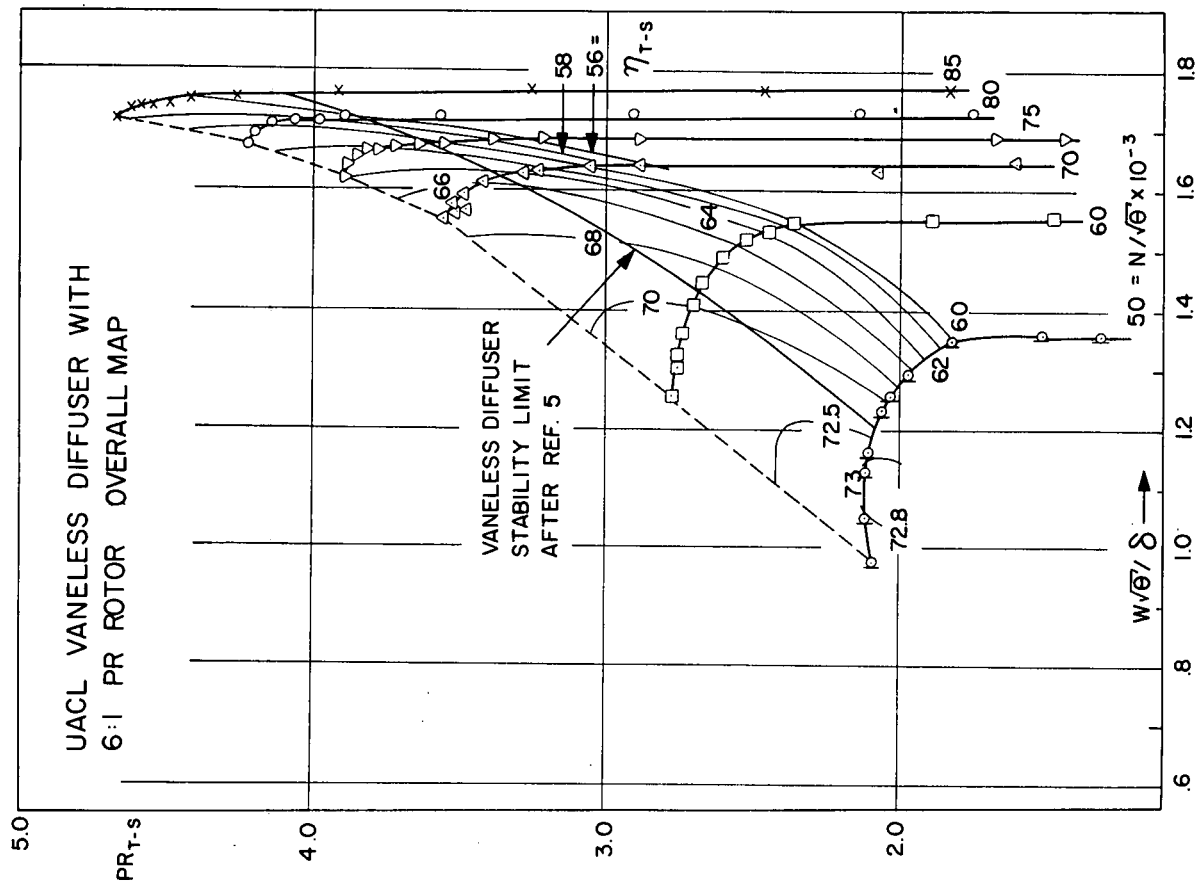

Fig. 6 UACL vaneless diffuser with 6:1 PR rotor overall map

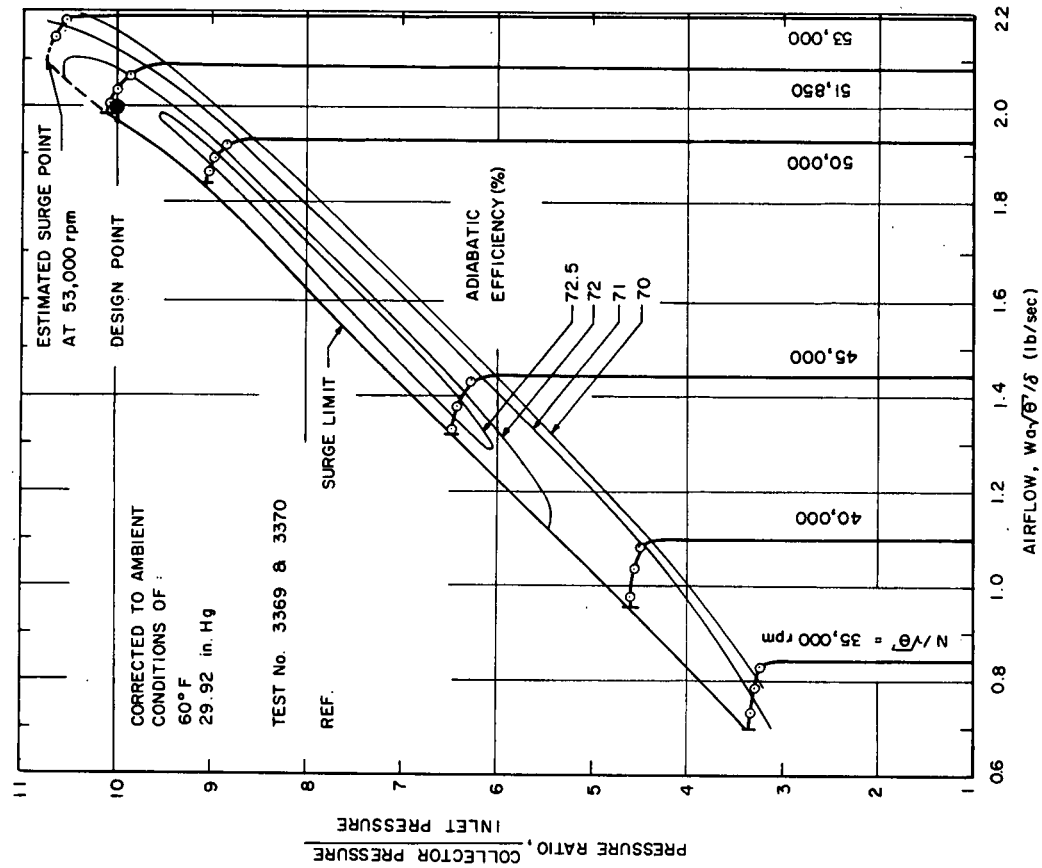

Fig. 5 Boeing/AVLABS 10:1 PR single centrifugal research

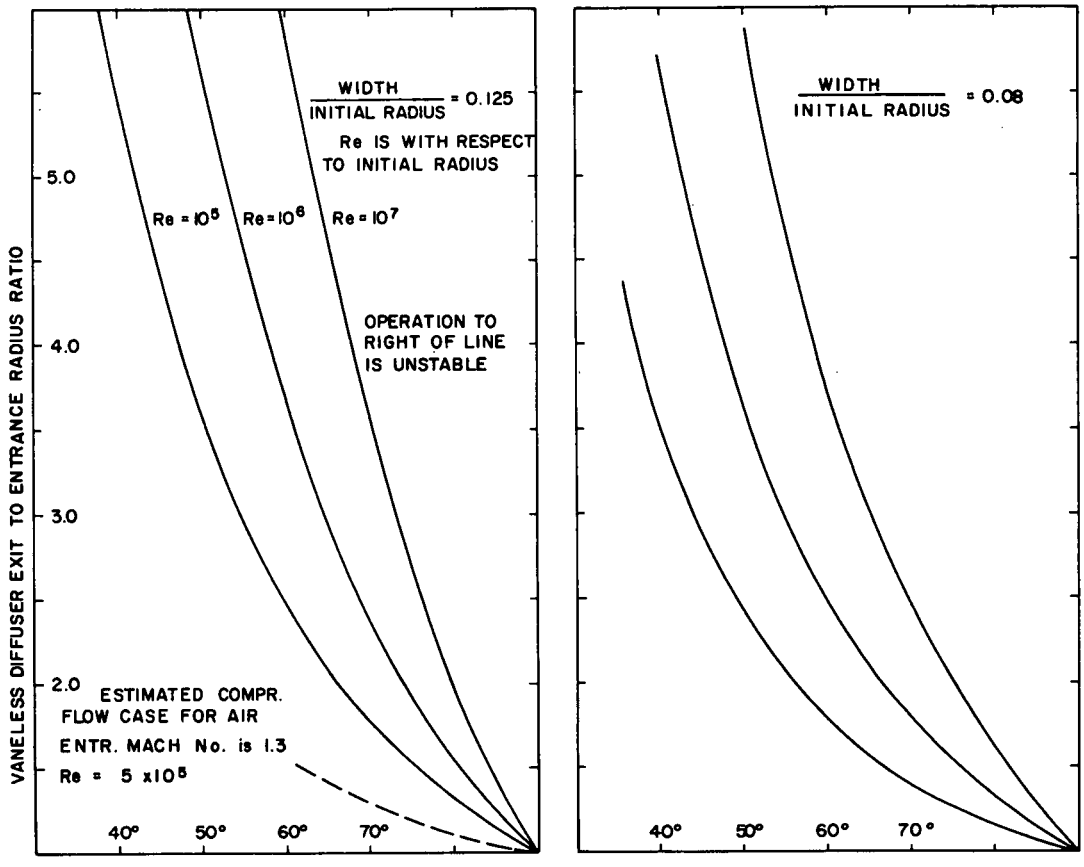

Fig.7 Stable operating range of vaneless diffusers after Reference 5

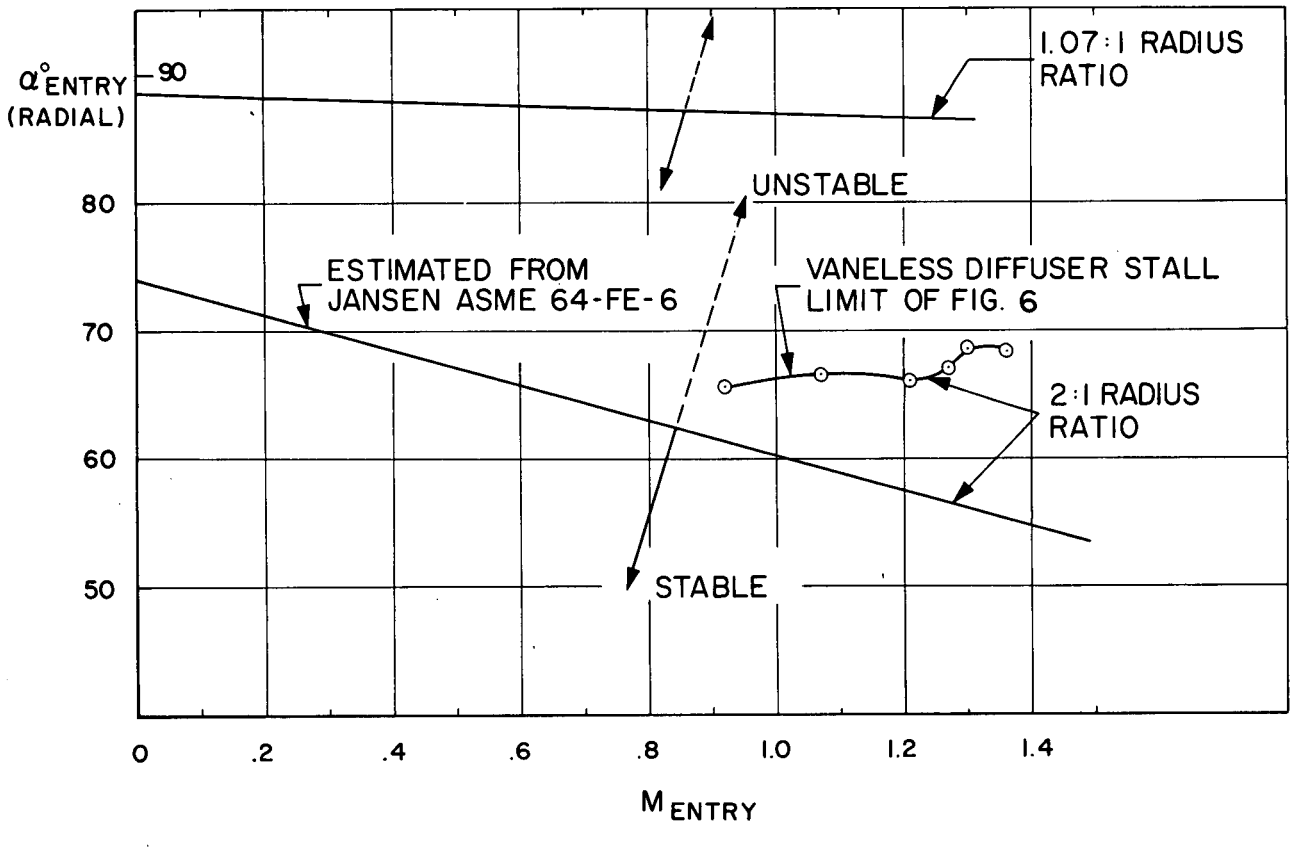

Fig.8 Stability limit for vaneless diffuser of 2:1 radius ratio with 6:1 PR rotor

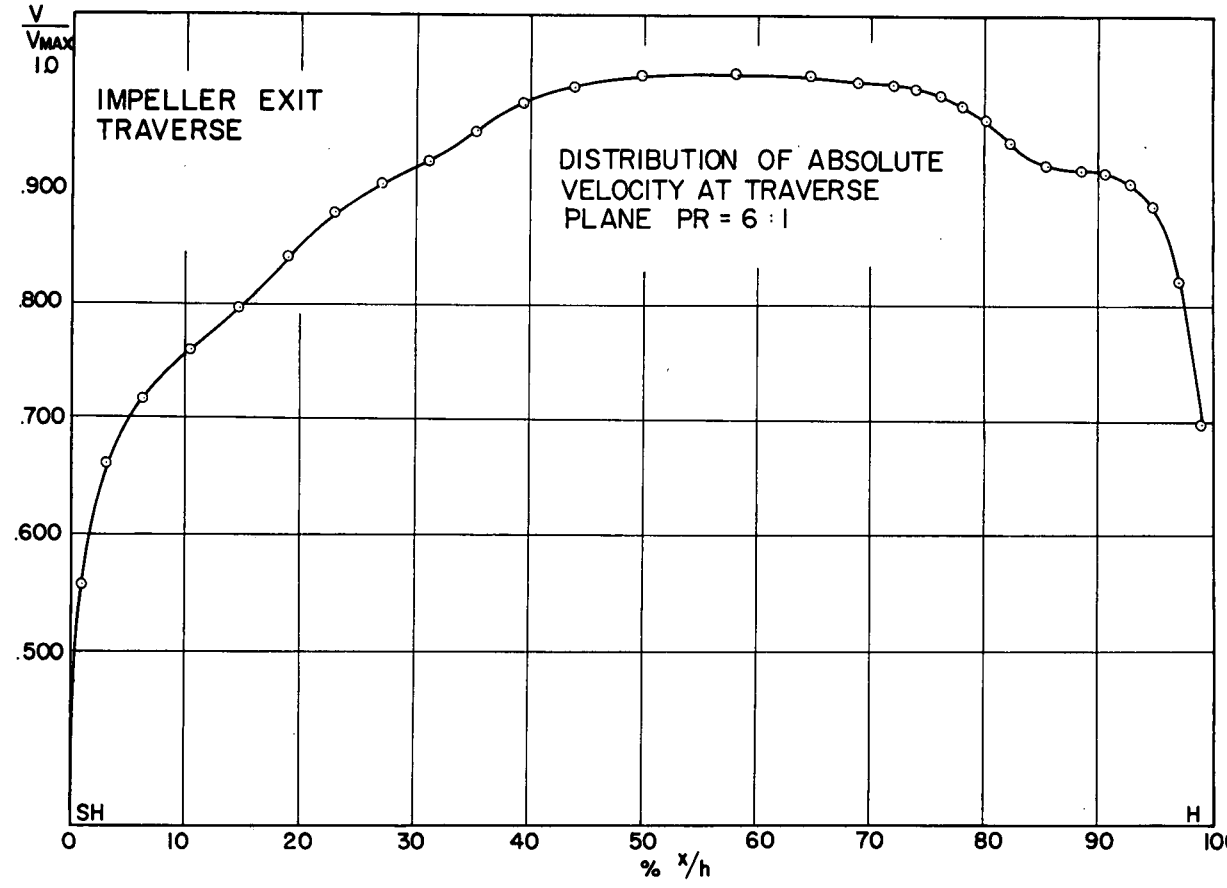

Fig.9(a) Impeller exit traverse distribution of absolute velocity at traverse plane PR = 6:1

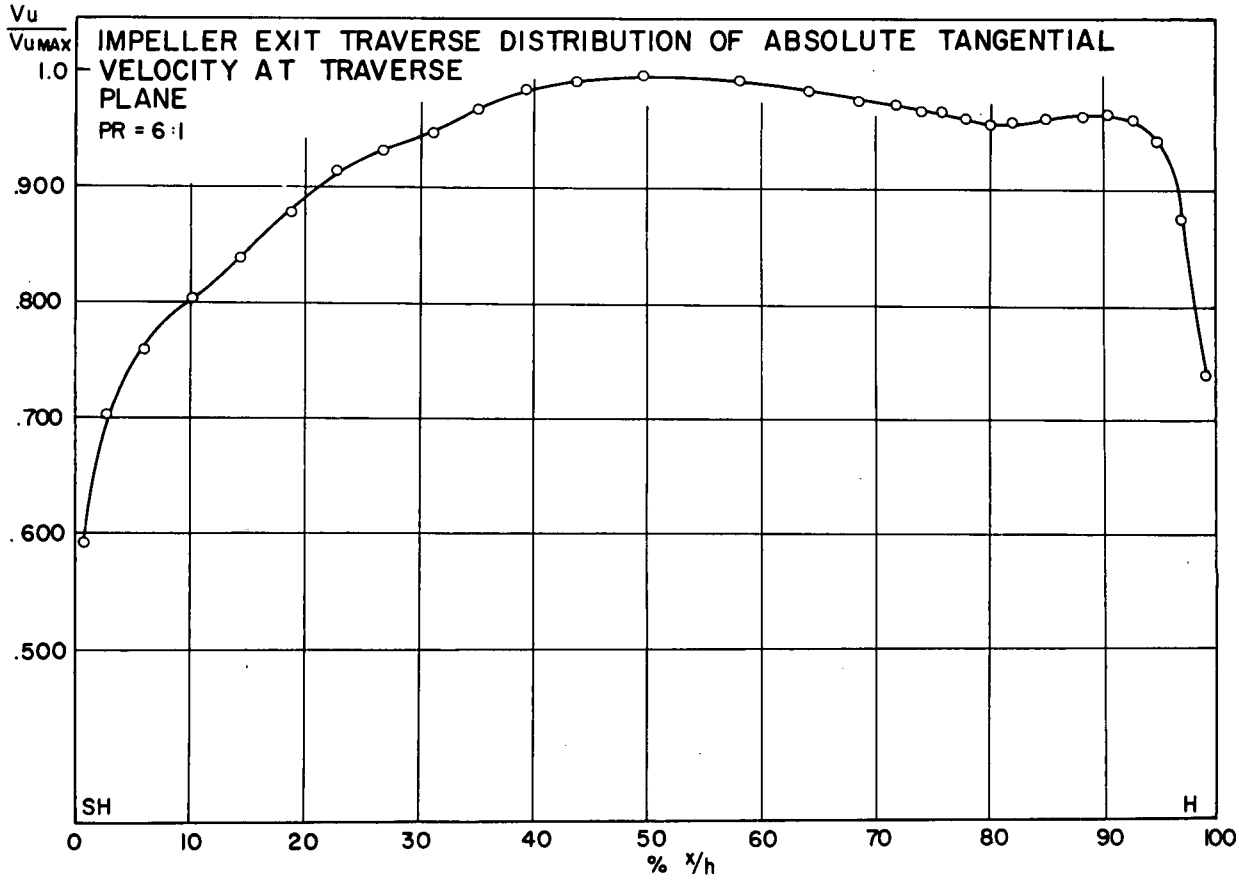

Fig.9(b) Tangential velocity

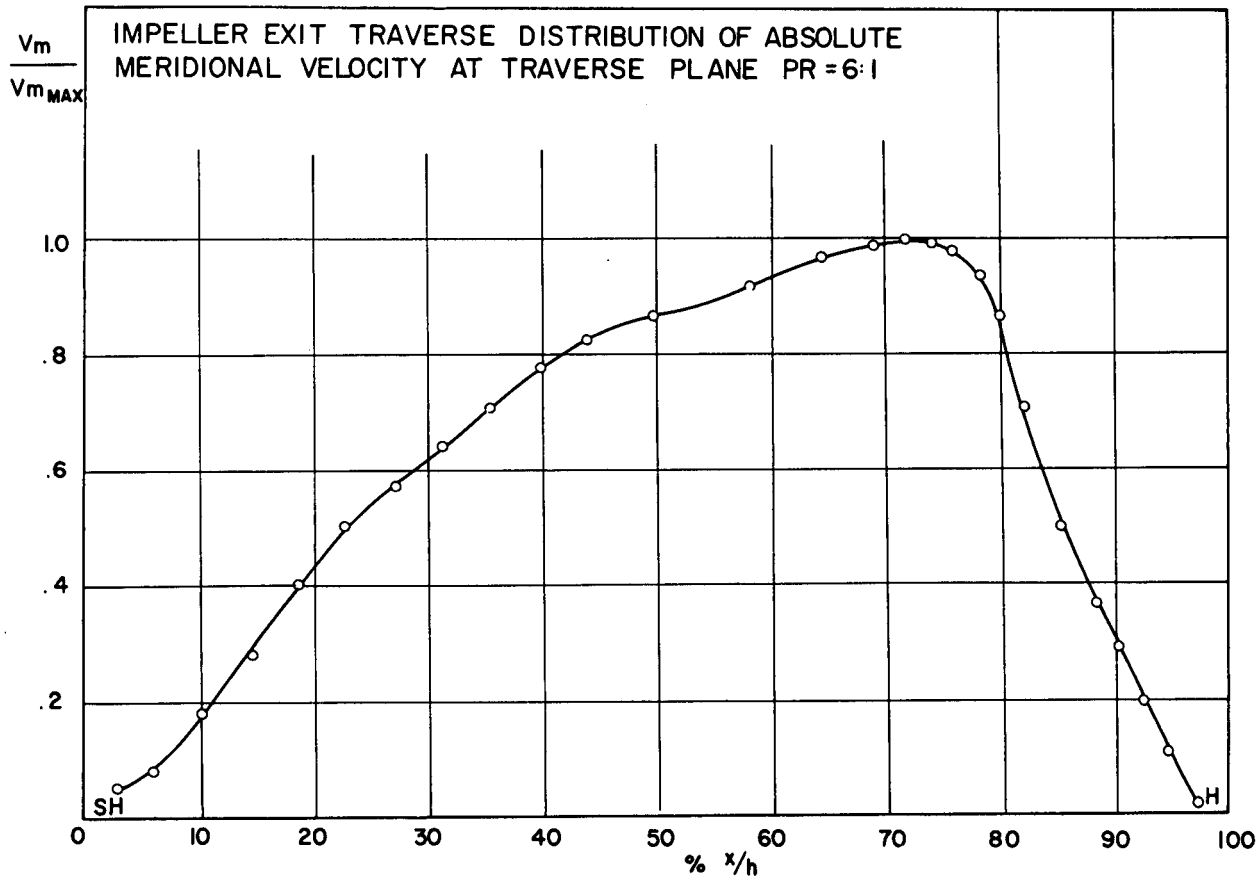

Fig. 9(c) Meridional velocity

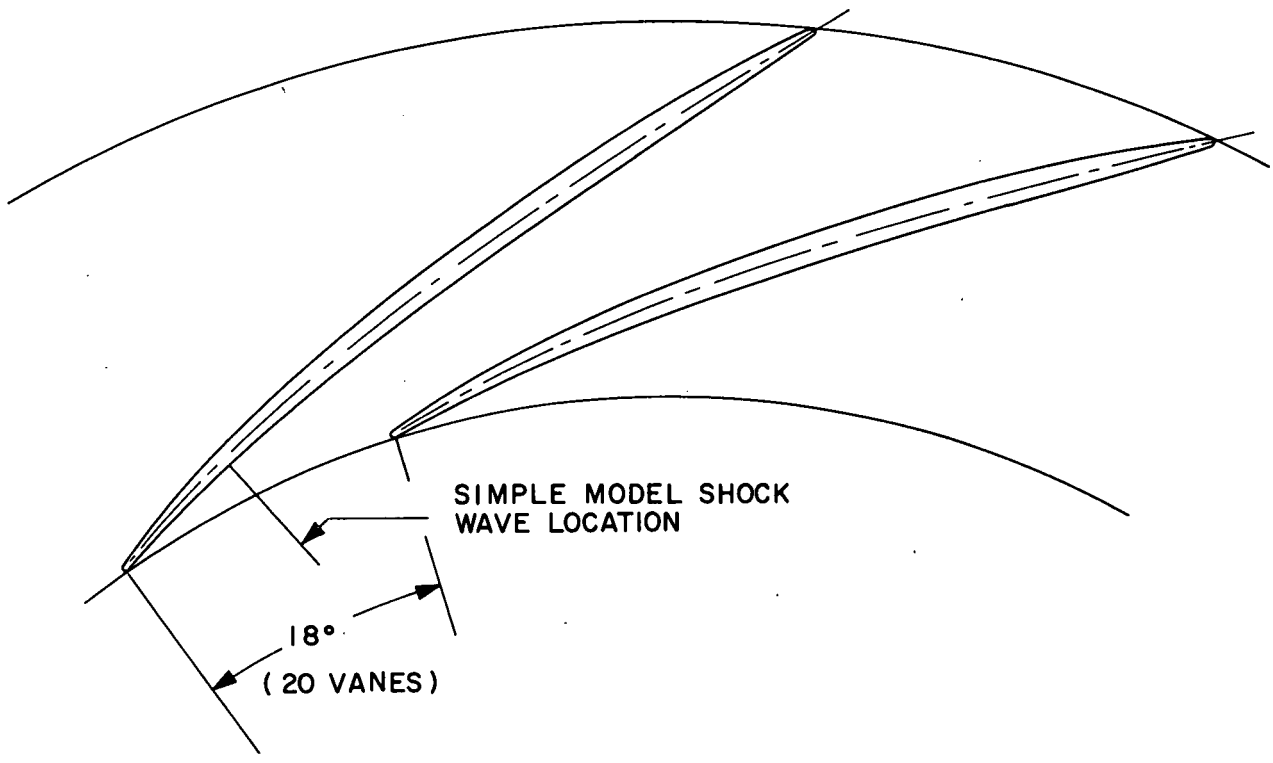

Fig. 10 UACL vanes diffuser design profile

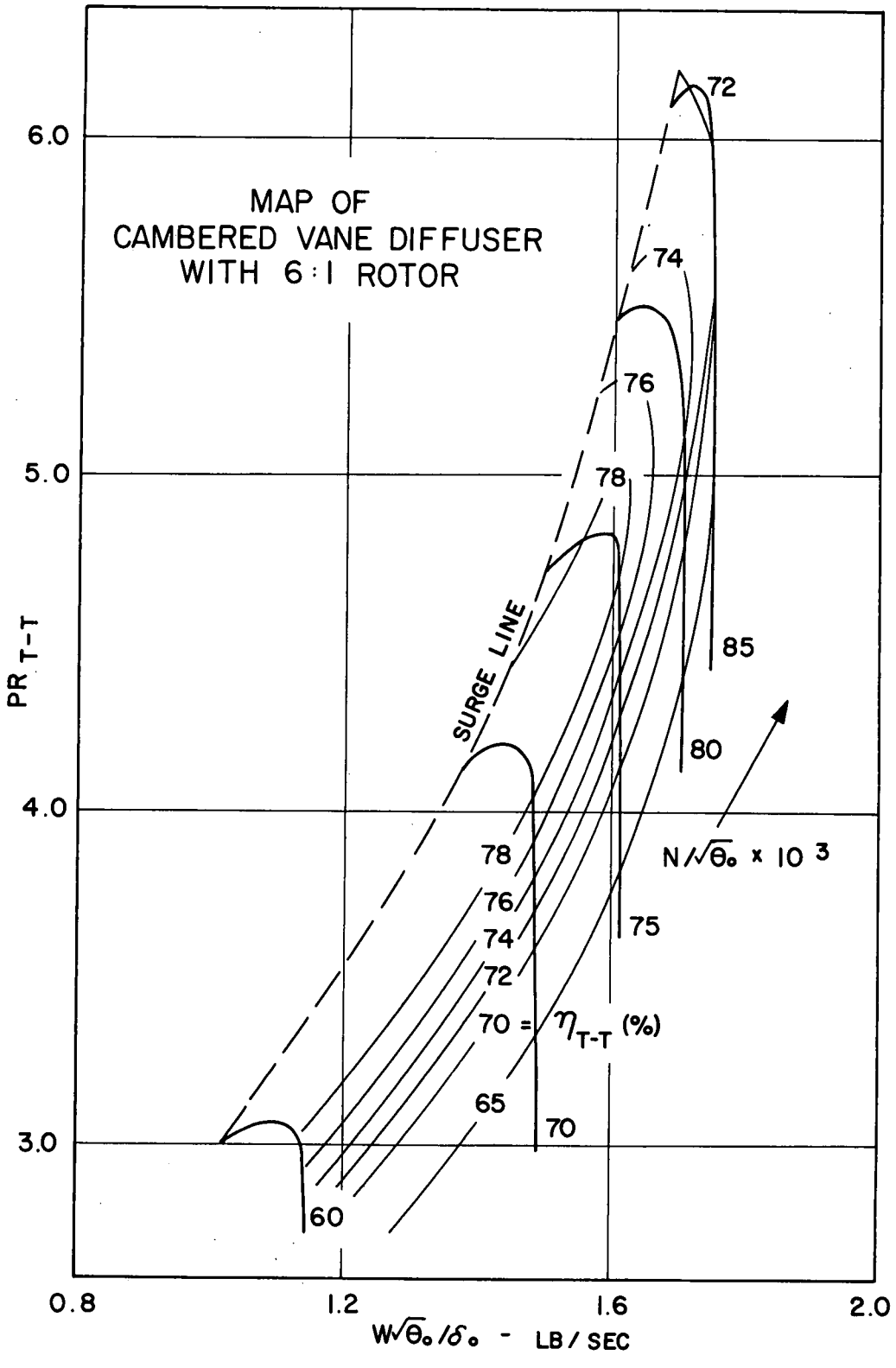

Fig. 11 Map of cambered vane diffuser with 6:1 rotor

There is no Figure 12

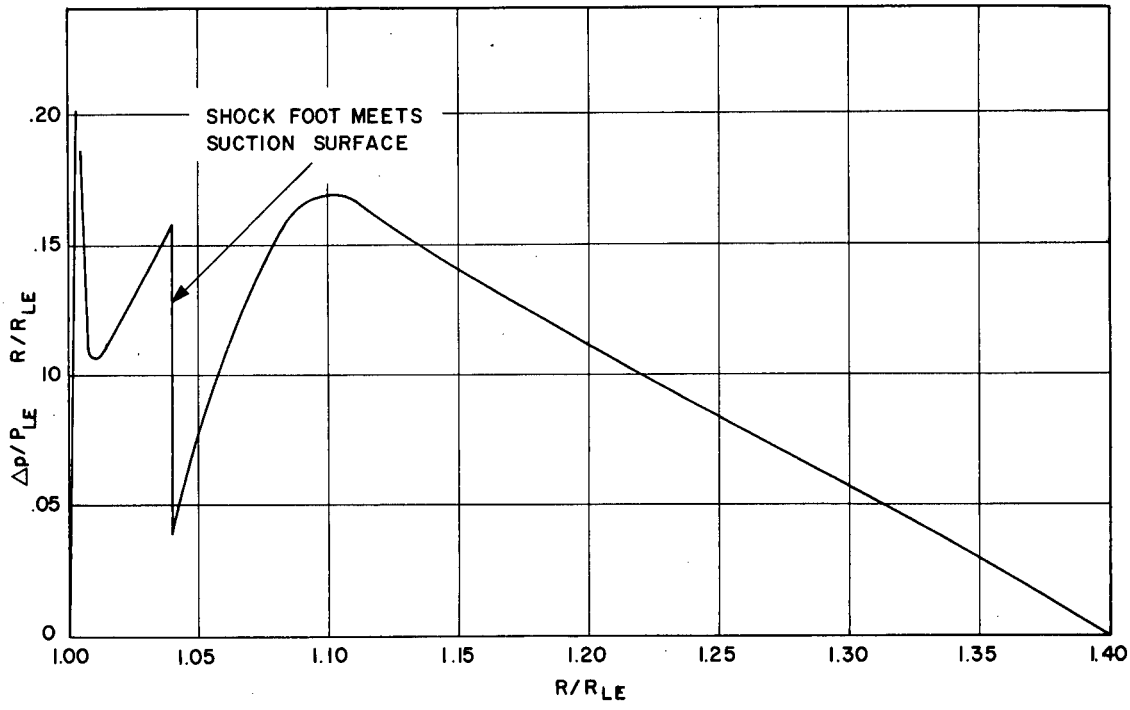

Fig. 13 UACL vaned diffuser static pressure loading

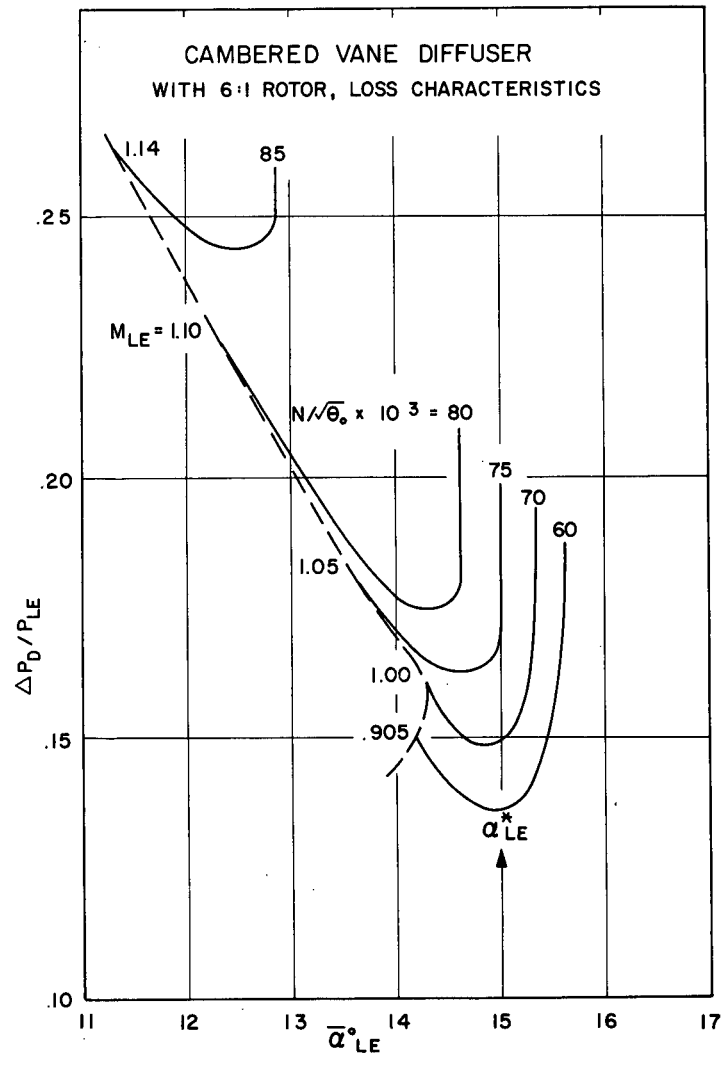

Fig. 14 Cambered vane diffuser with 6:1 rotor, loss characteristic

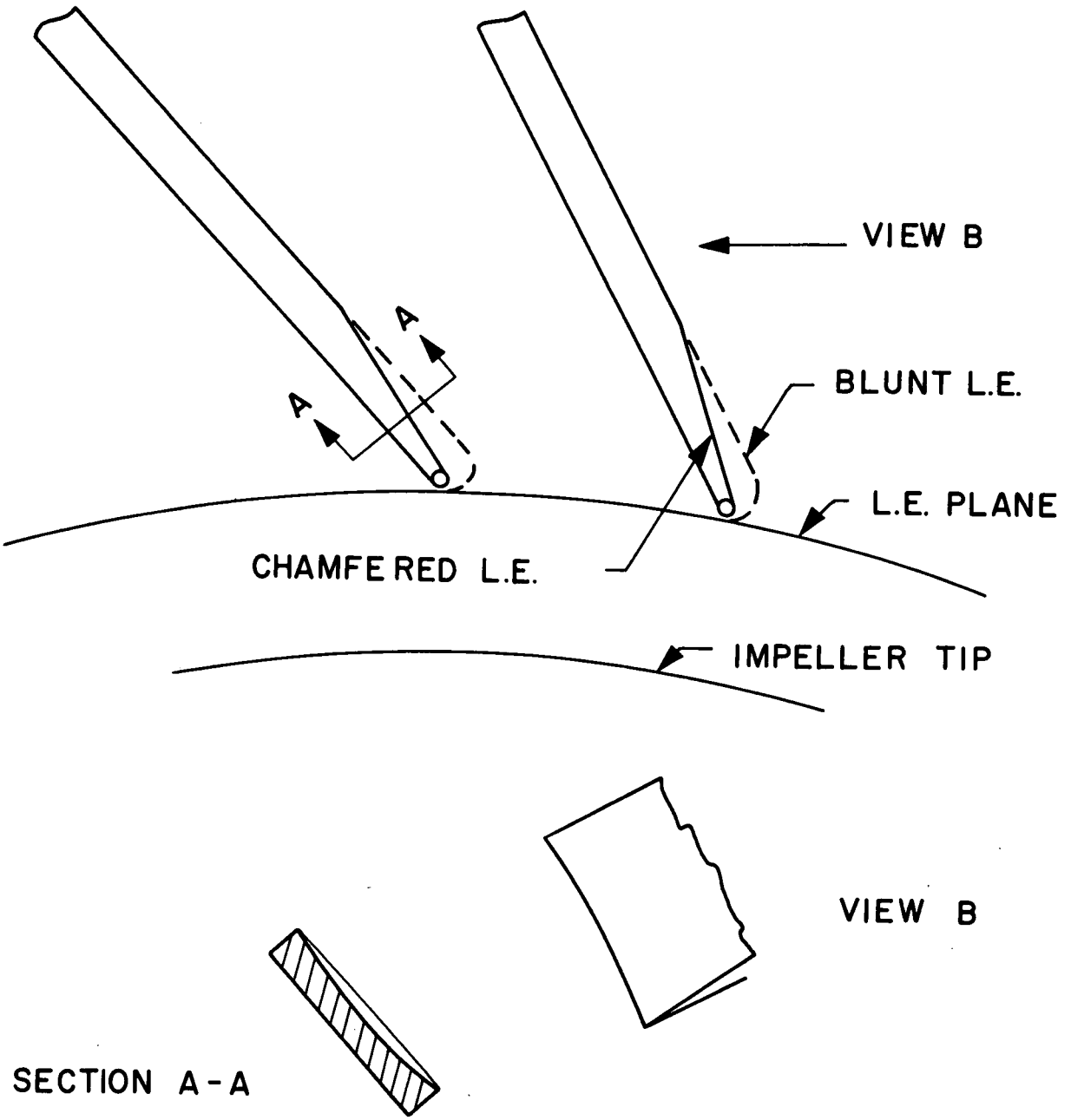

Fig. 15 UACL flat plate diffuser LE types

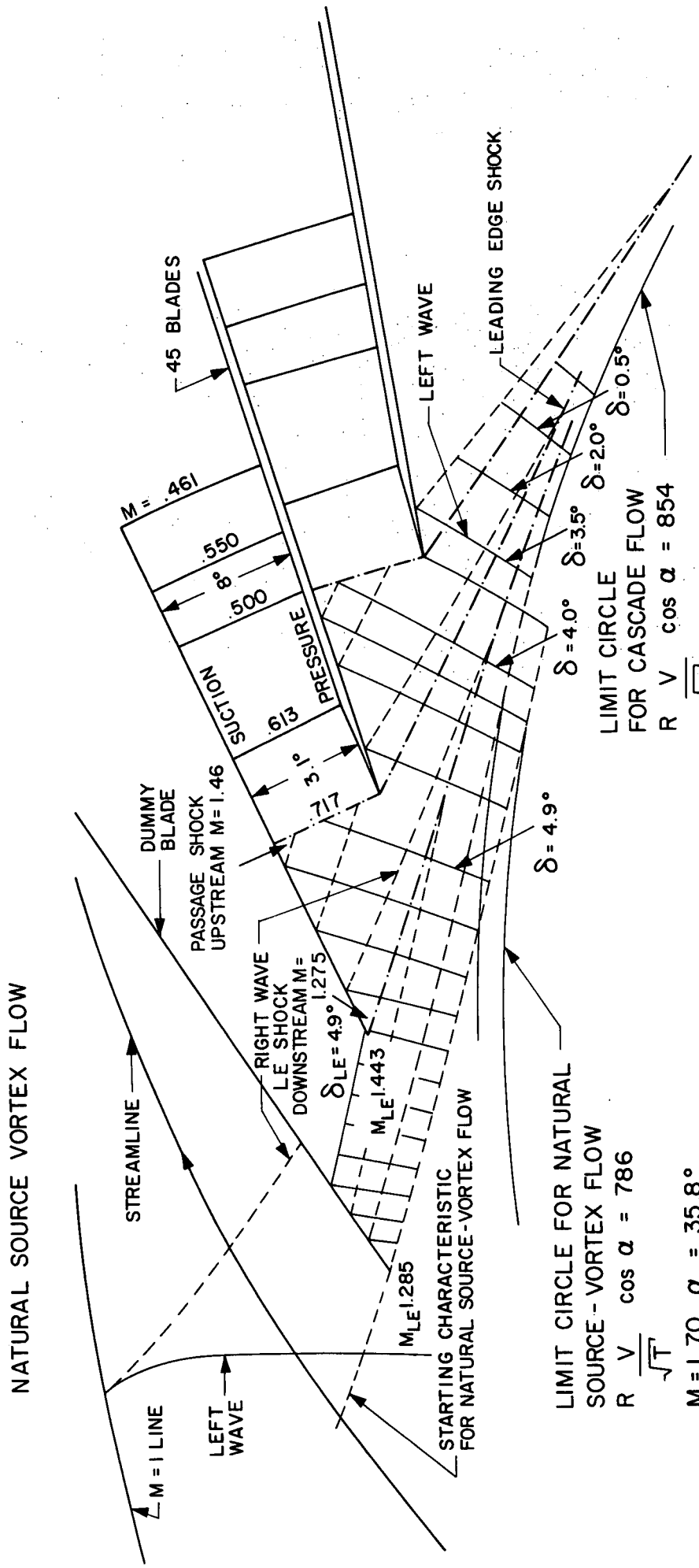

Fig. 16 LE characteristic pattern for a two-dimensional radial cascade with a supersonic approach flow, but but $M_R < 1$

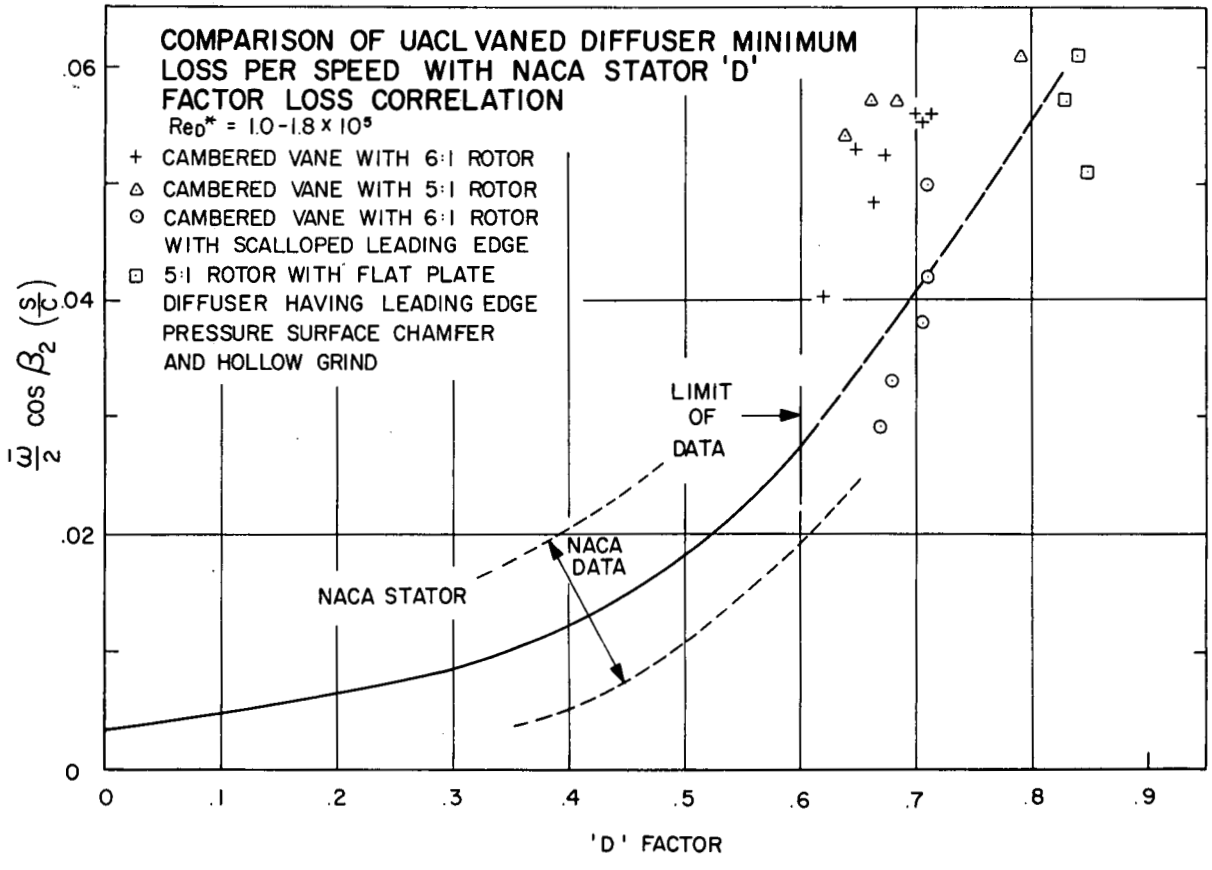

Fig. 17 Comparison of UACL vaned diffuser minimum loss per speed with NACA stator "D" factor loss correlation

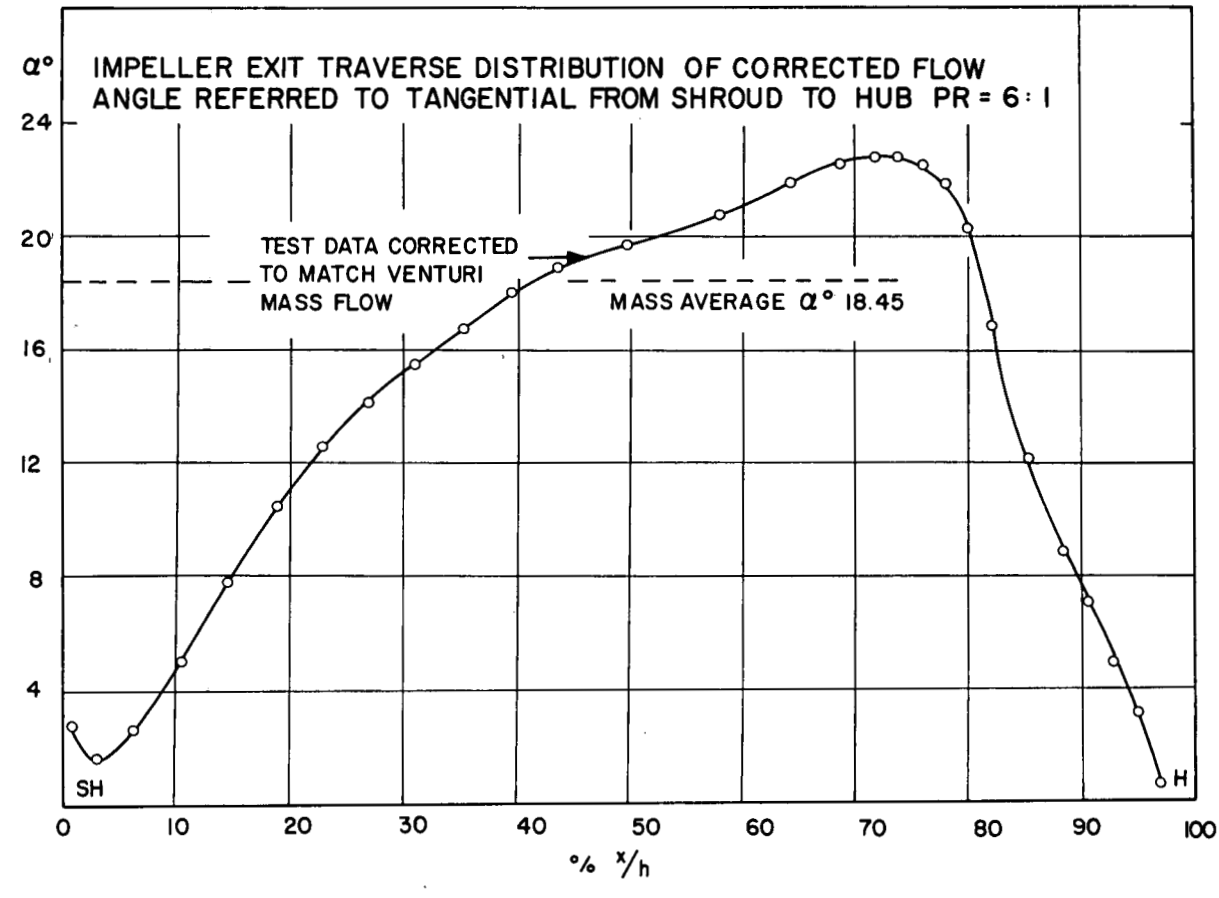

Fig. 18 Impeller exit traverse distribution of corrected flow angle

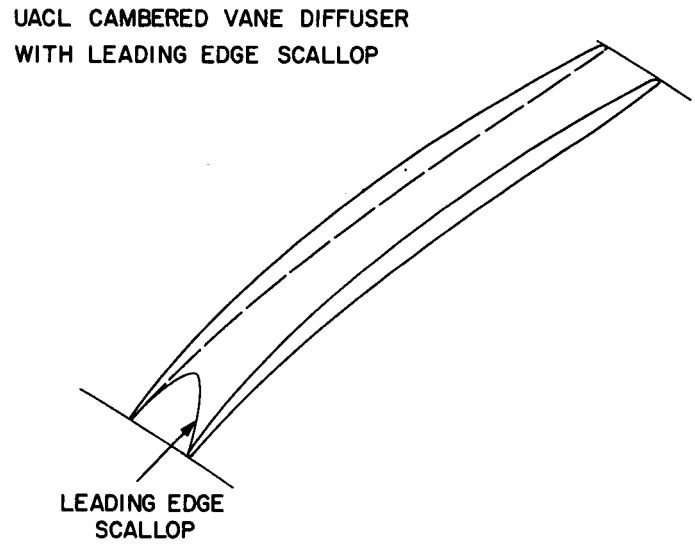

Fig. 19 UACL cambered vane diffuser with LE scallop

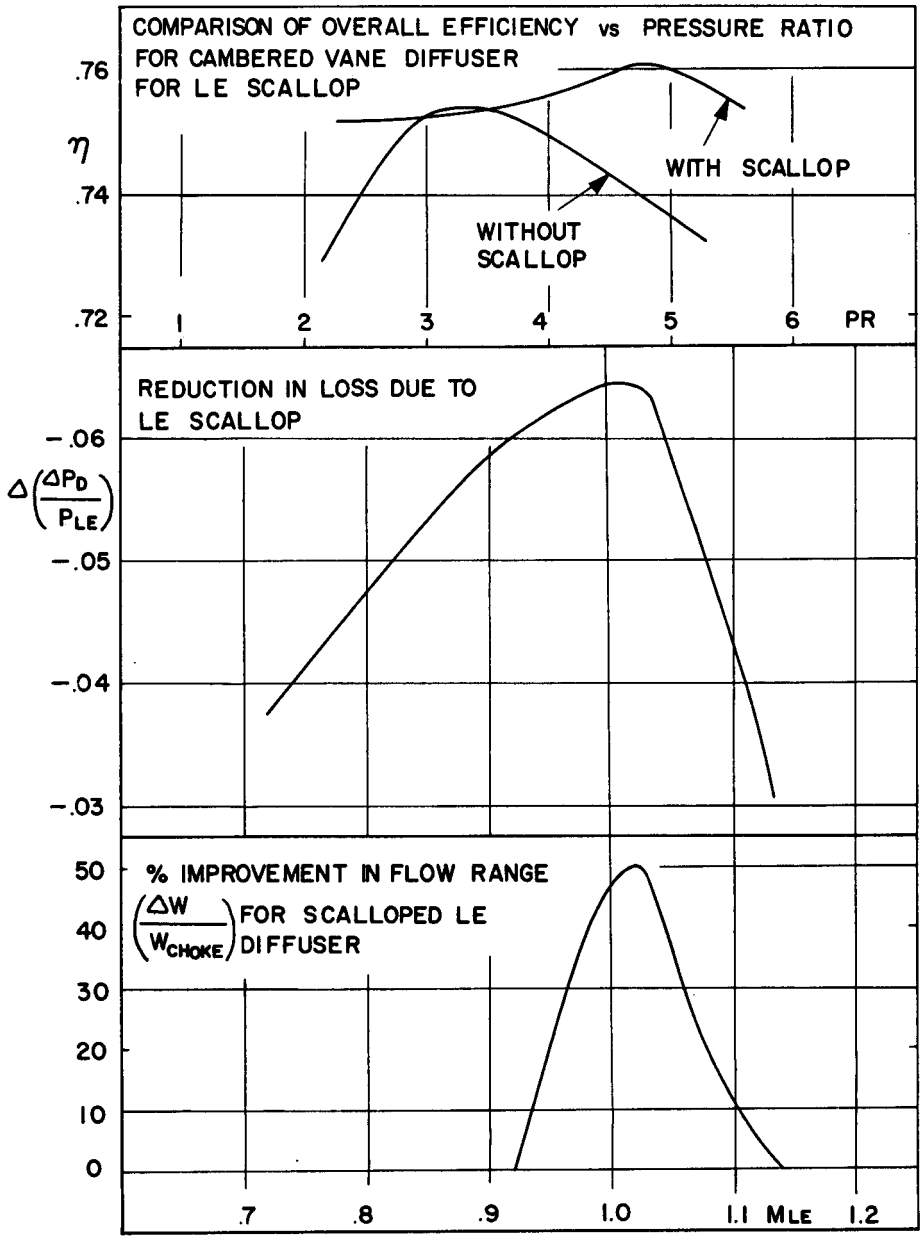

Fig. 20 Comparison of overall efficiency vs PR for cambered vane diffuser for LE scallop

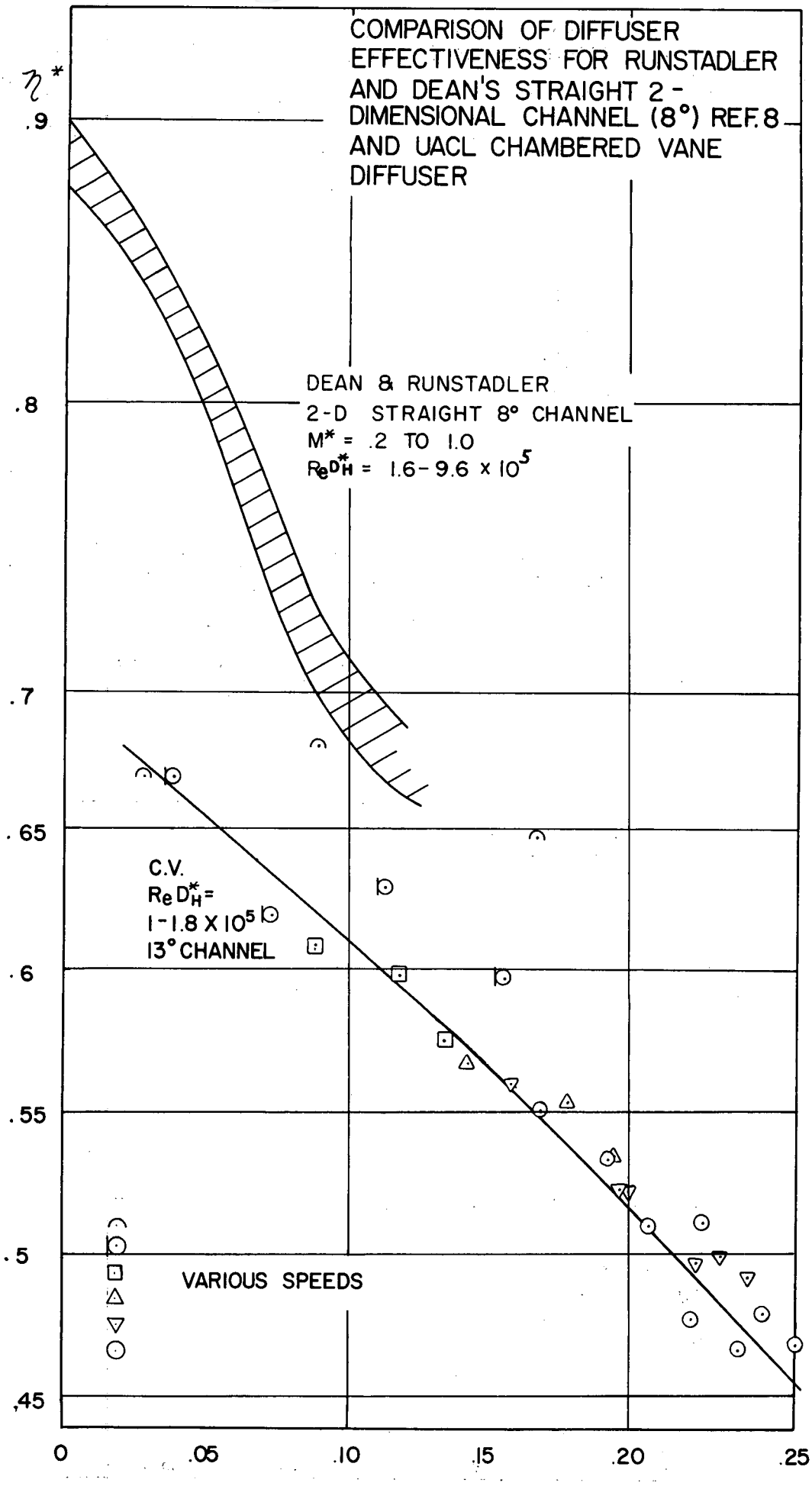

Fig. 21 Comparison of diffuser effectiveness for Runstadler and Dean's straight 2-D channel – Reference 8 and UACL cambered vane diffuser

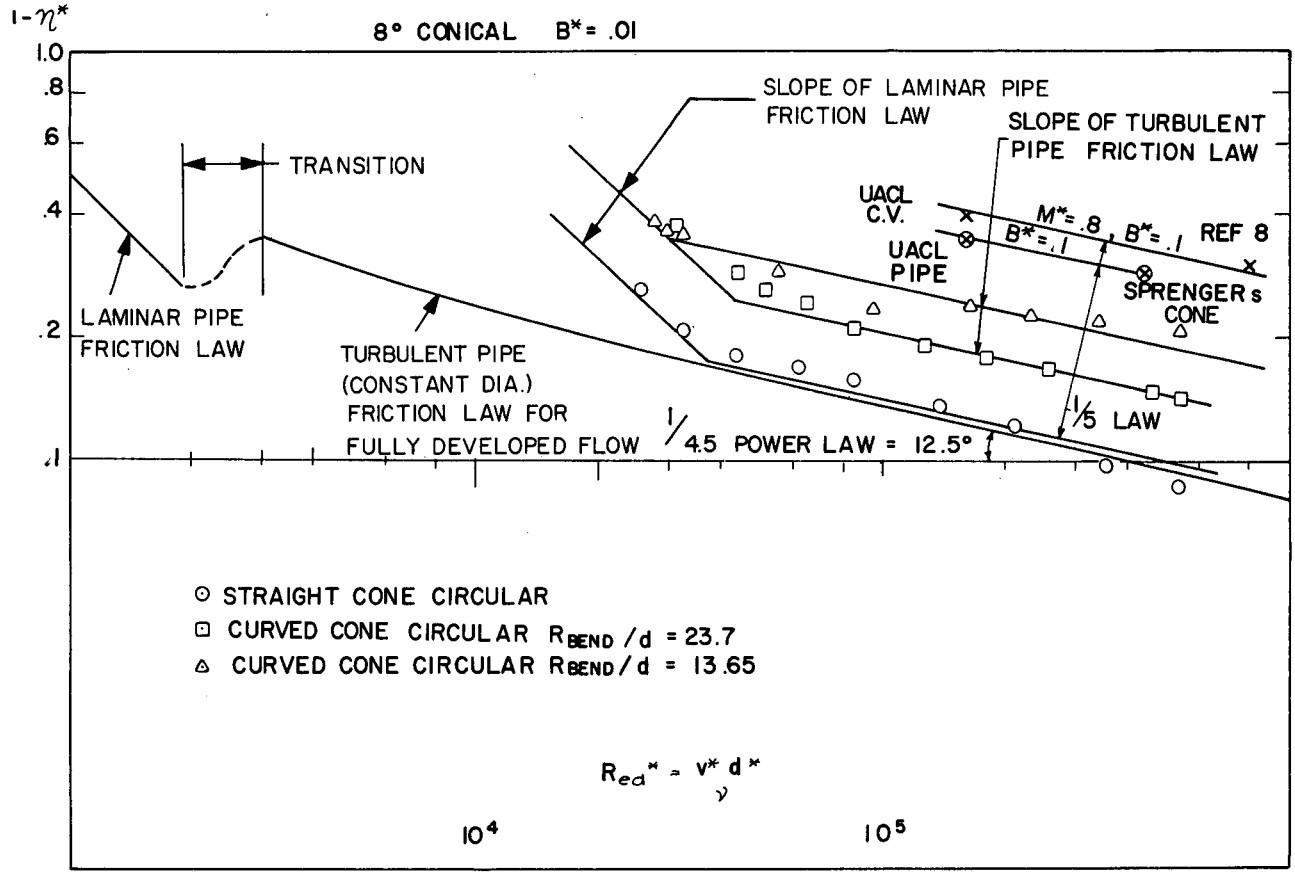

Fig. 22 Sprenger's incompressible diffuser Reynolds' number data comparison

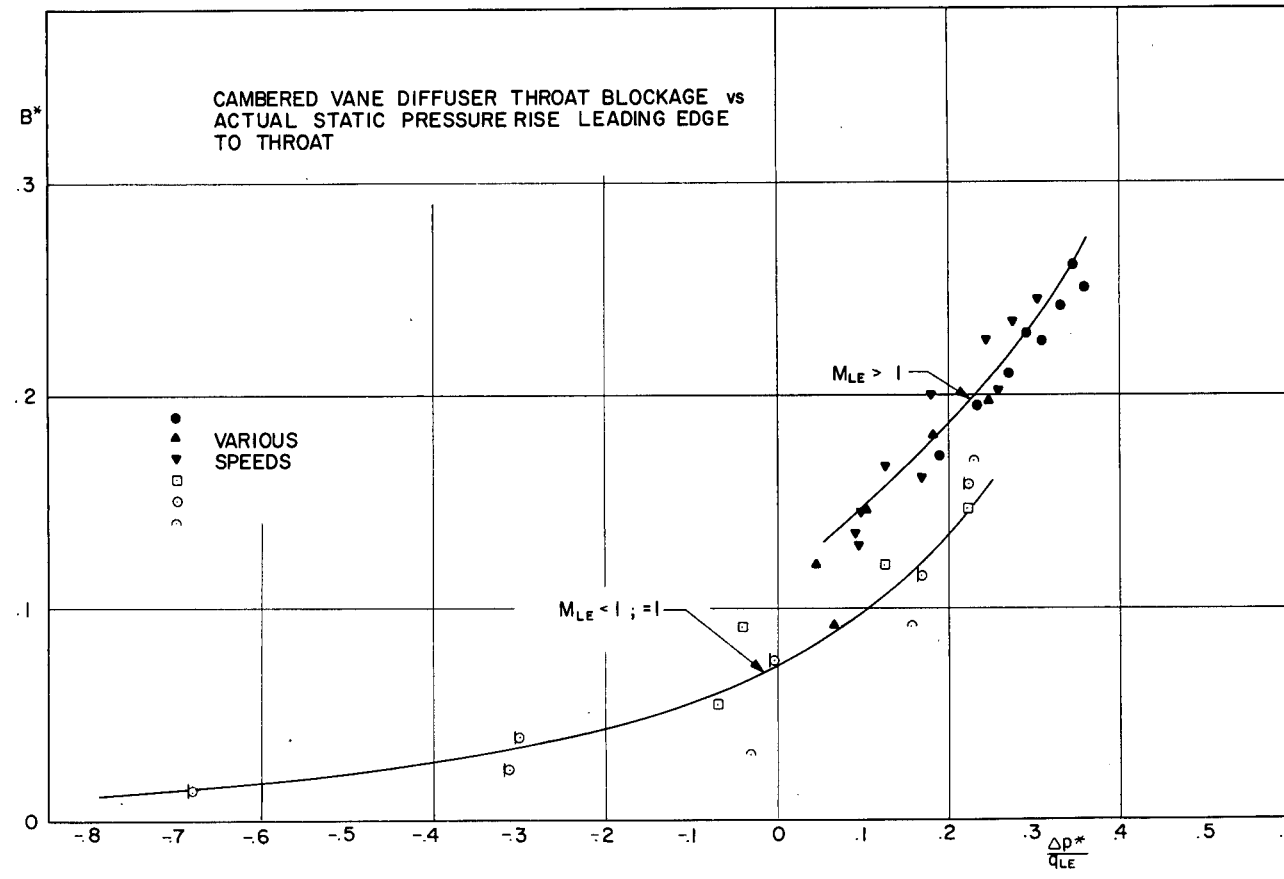

Fig. 23 Cambered vane diffuser throat blockage

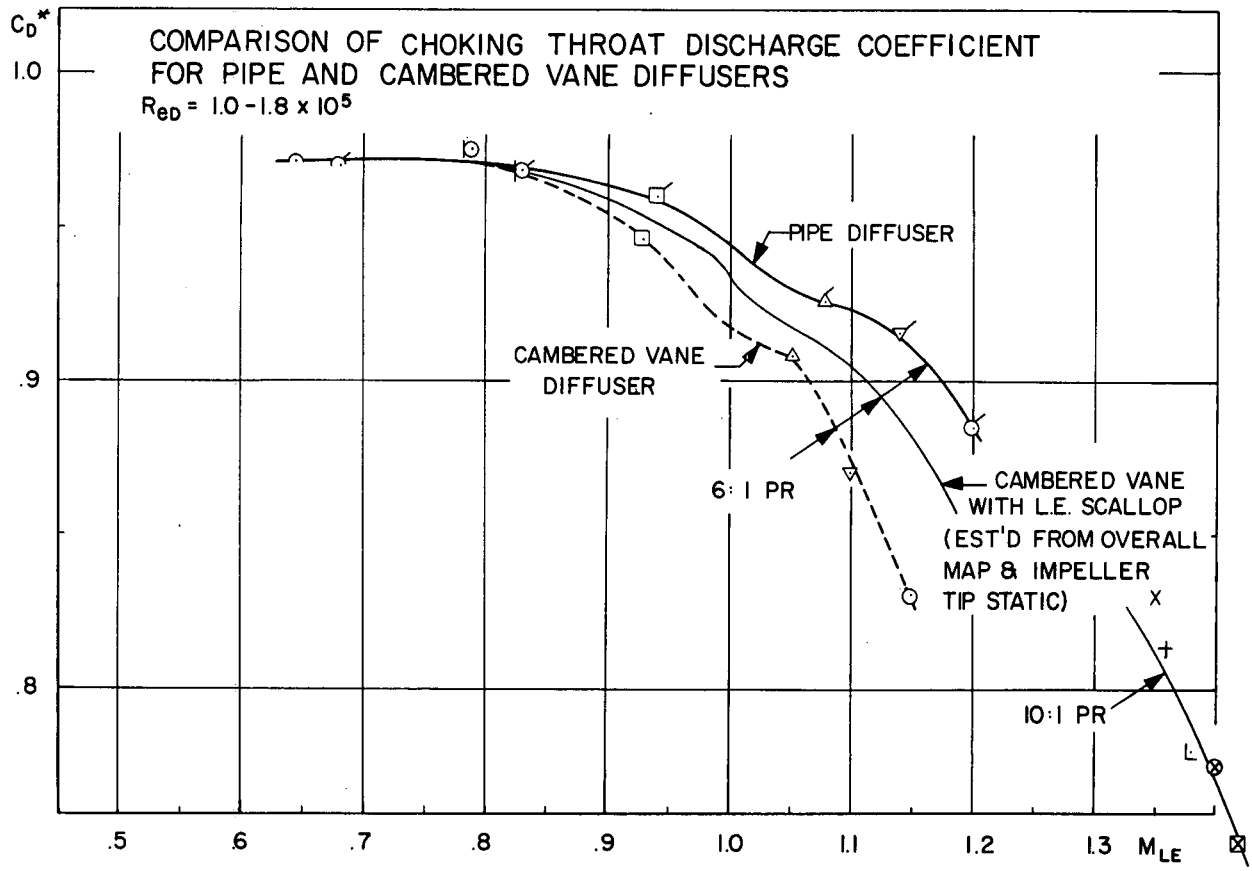

Fig. 24 Comparison of choking throat discharge coefficient for pipe and cambered vane diffusers

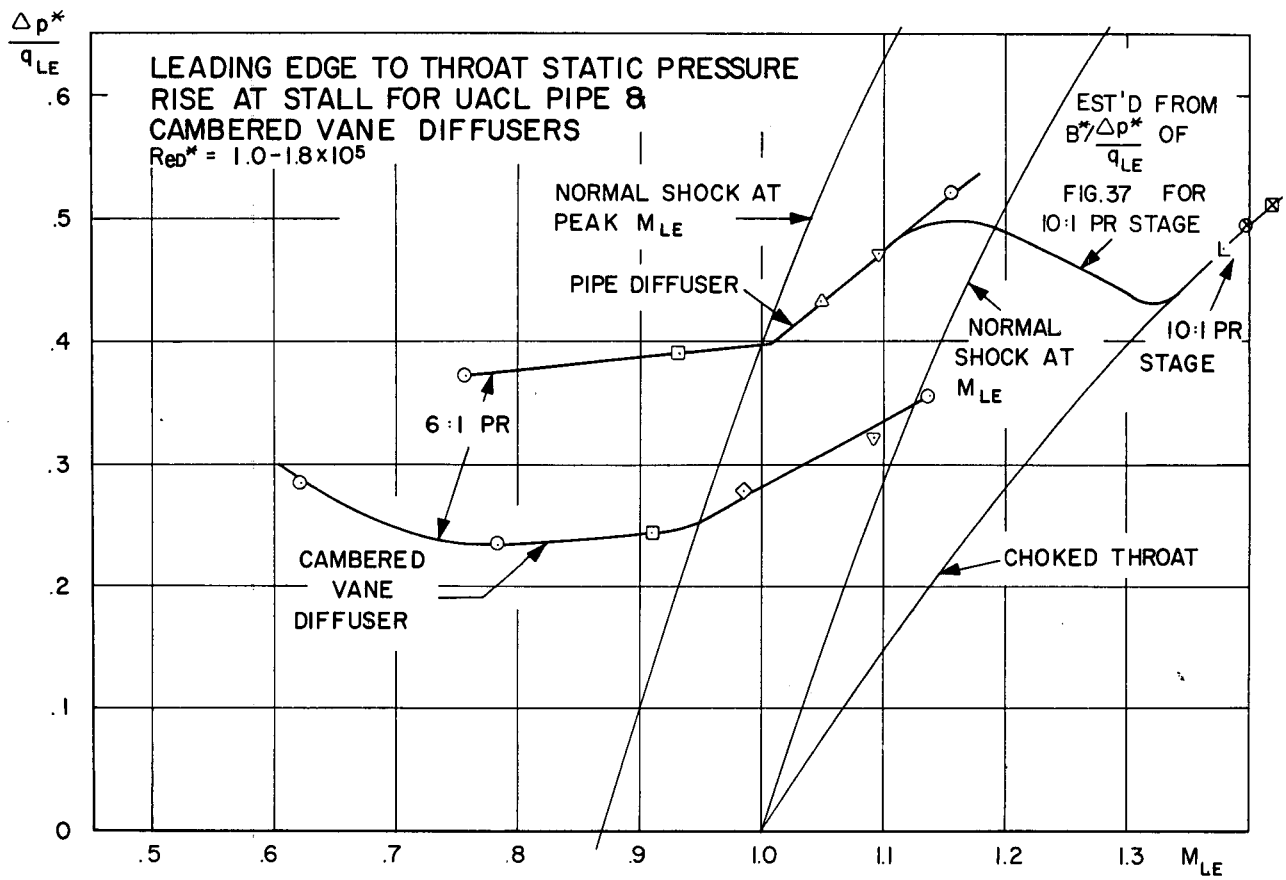

Fig. 25 LE to throat static pressure rise at stall for UACL pipe and cambered vane diffusers

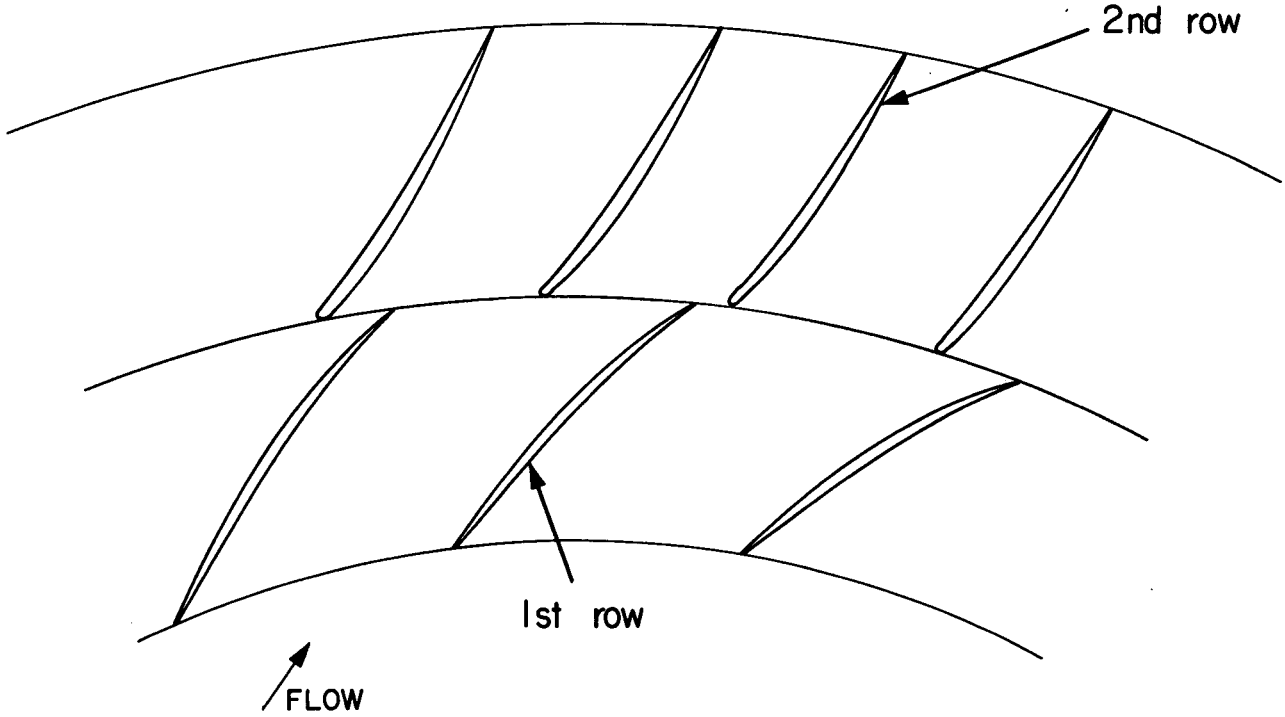

Fig. 26 Typical multiple cascade diffuser

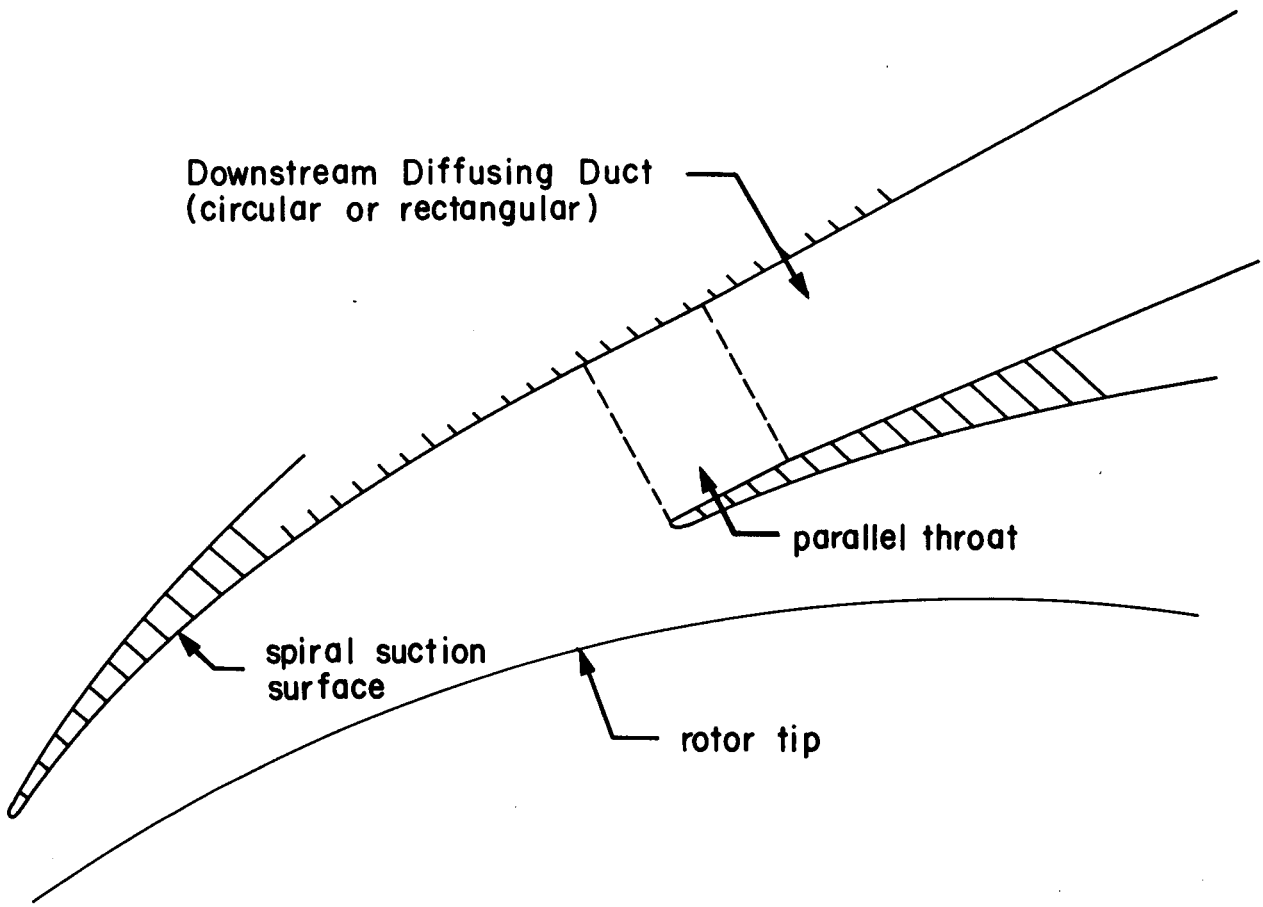

Fig. 27 Typical passage diffuser

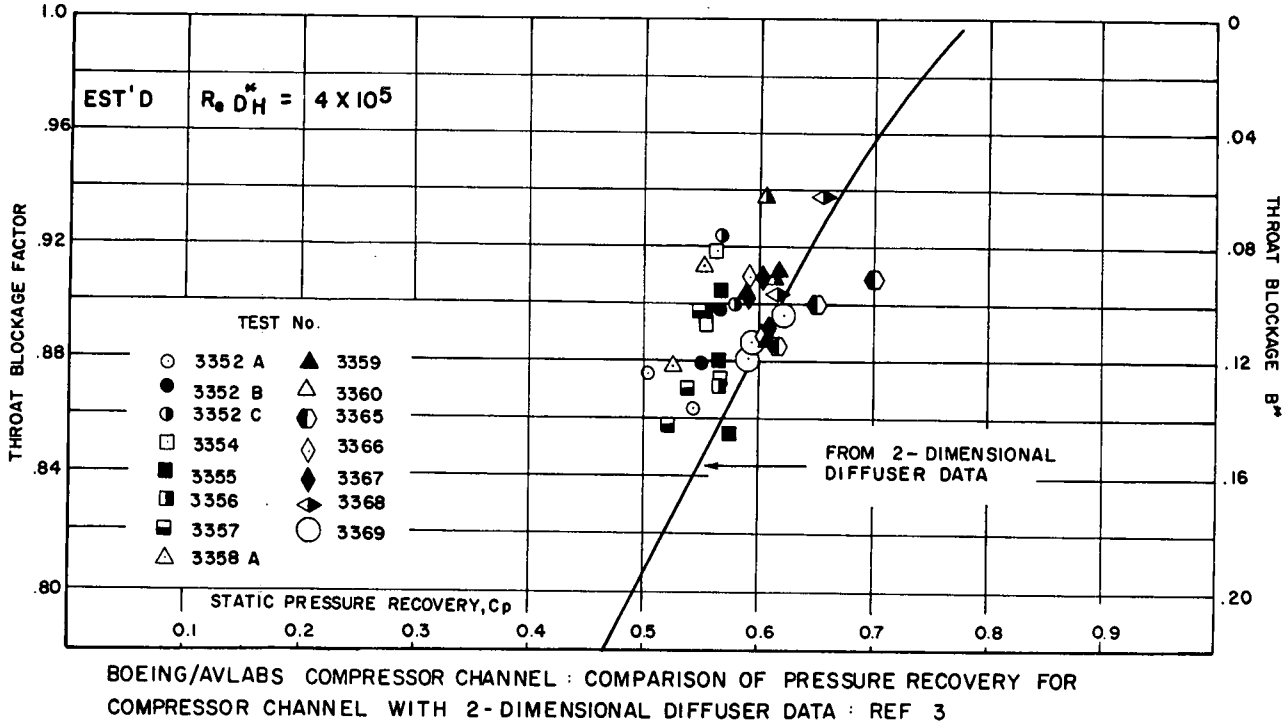

Fig. 28 Boeing/AVLABS compressor channel: comparison of pressure recovery

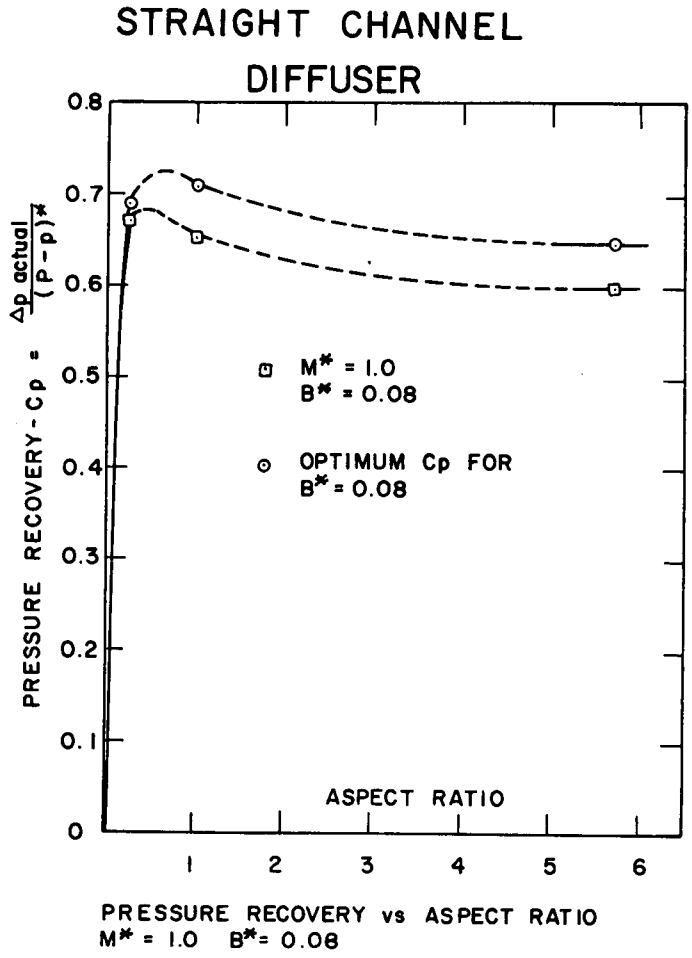

Fig. 29 Pressure recovery vs aspect ratio after Reference 8

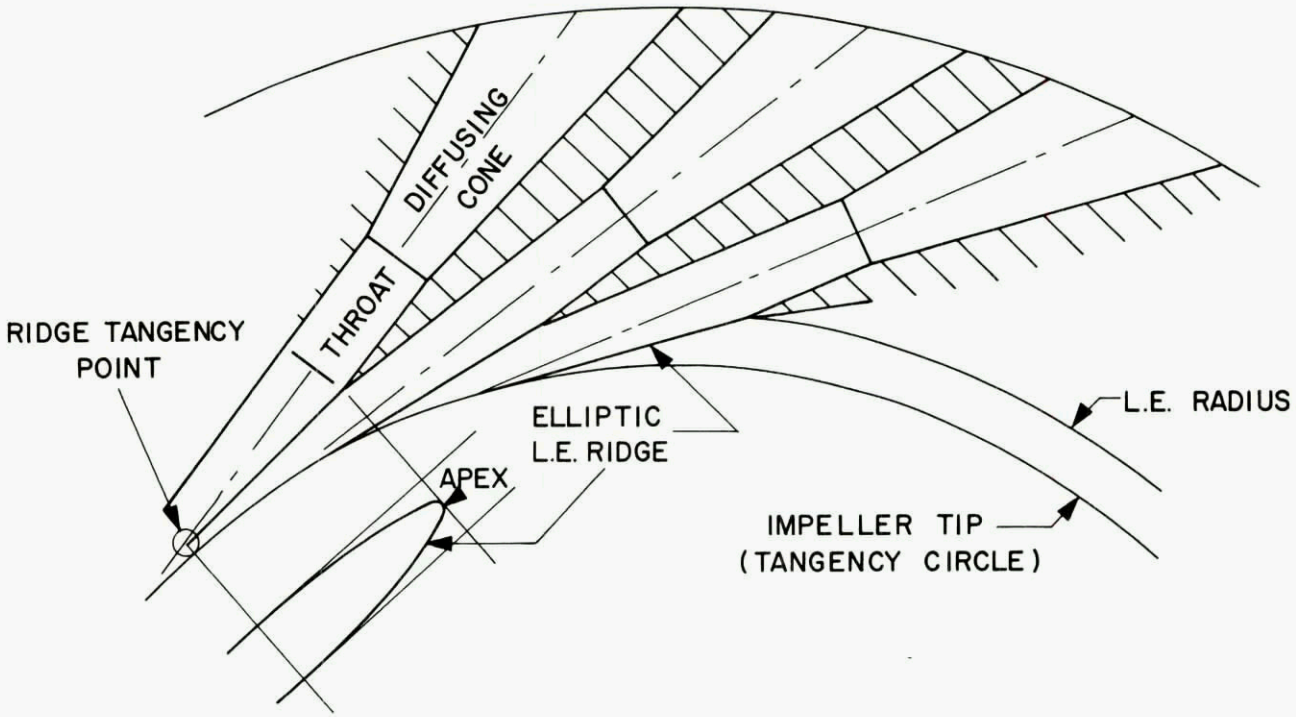

Fig. 30 Pipe diffuser

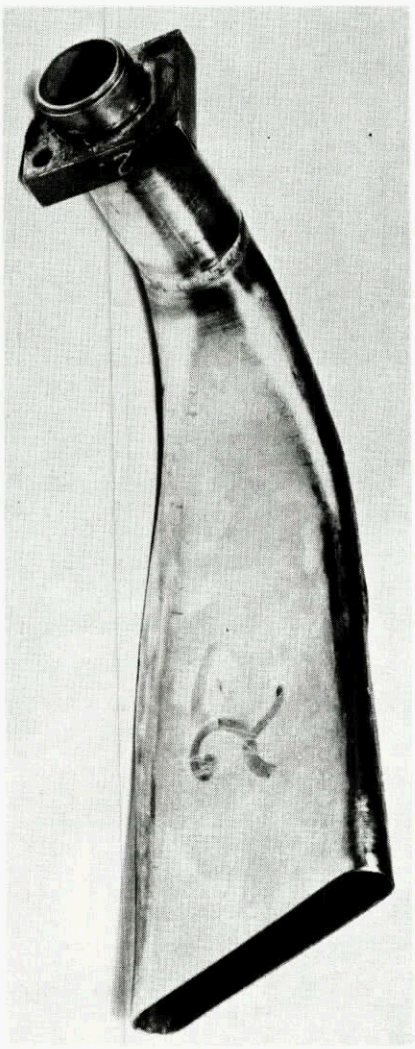

Fig. 31 Pipe diffuser trumpet

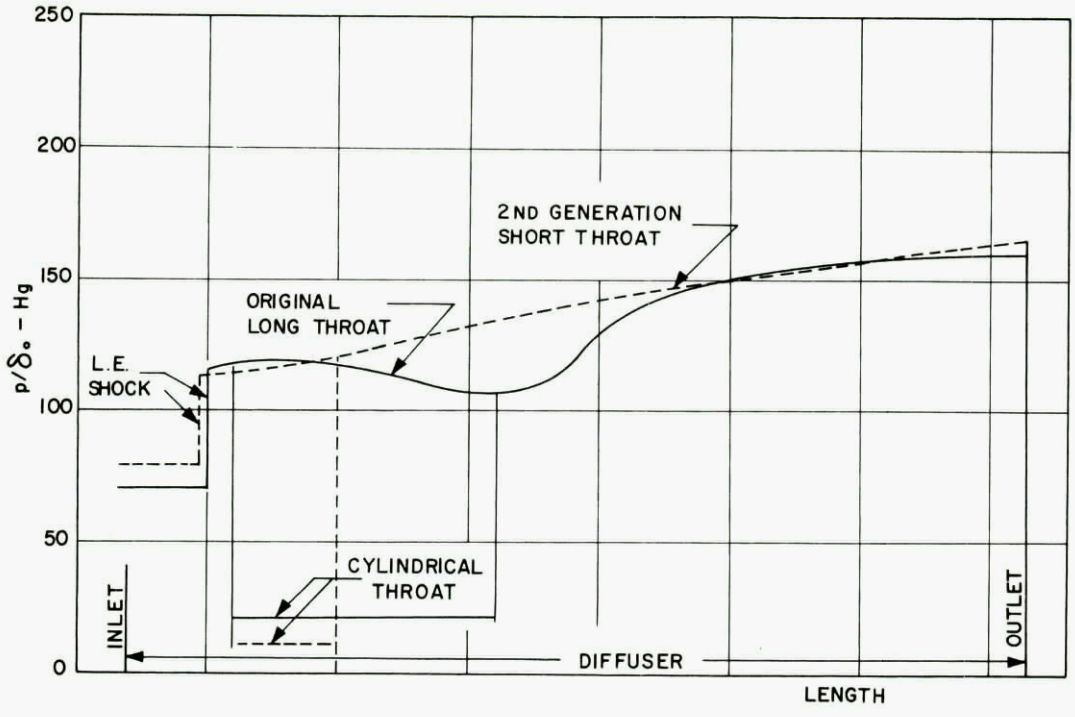

Fig. 32 Comparison of static pressure distributions along the pipes

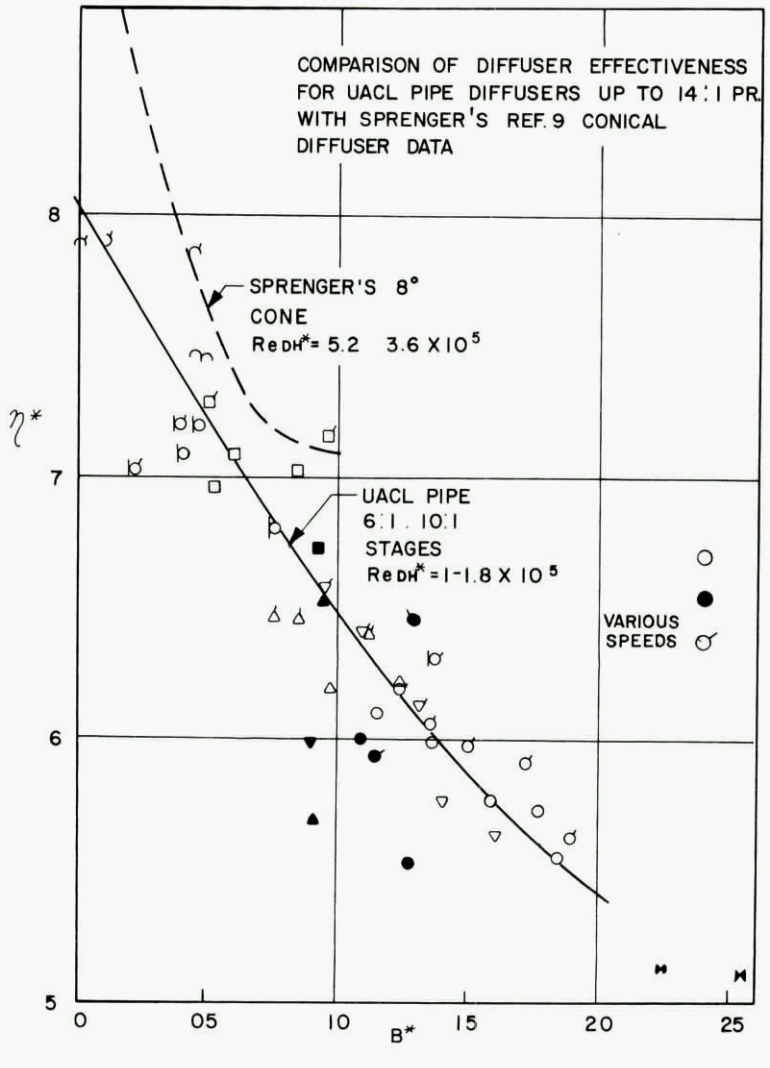

Fig. 33 Pipe diffuser effectiveness vs throat blockage

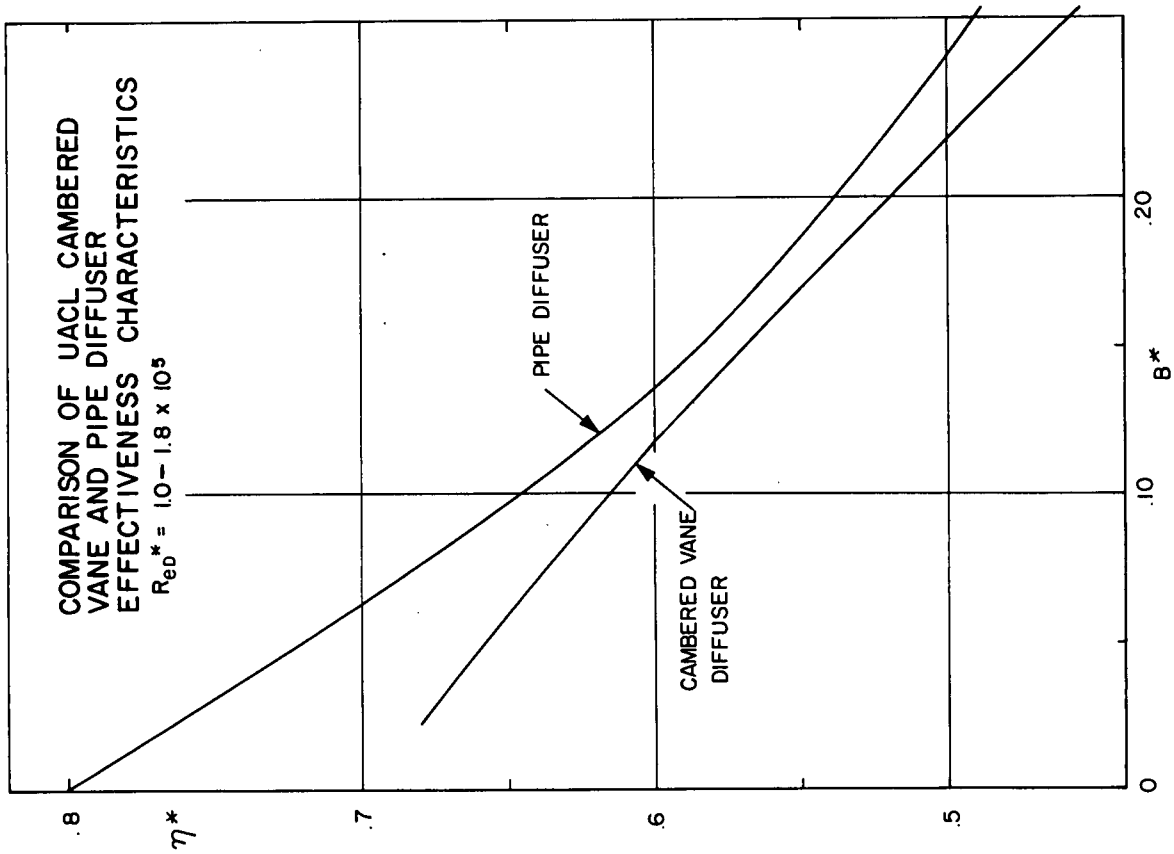

Fig. 35 Comparison of UACL cambered vane and pipe diffuser effectiveness characteristics

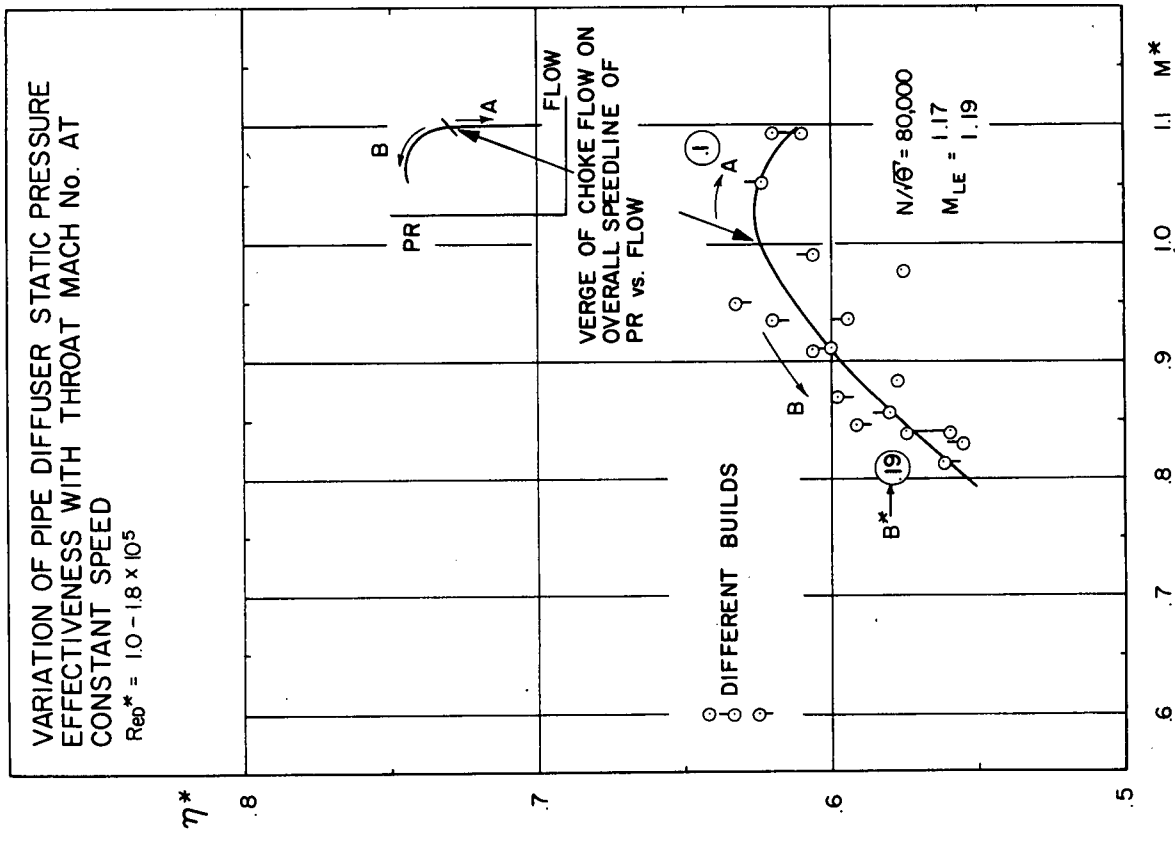

Fig. 34 Variation of pipe diffuser static pressure effectiveness with throat Mach number at constant speed

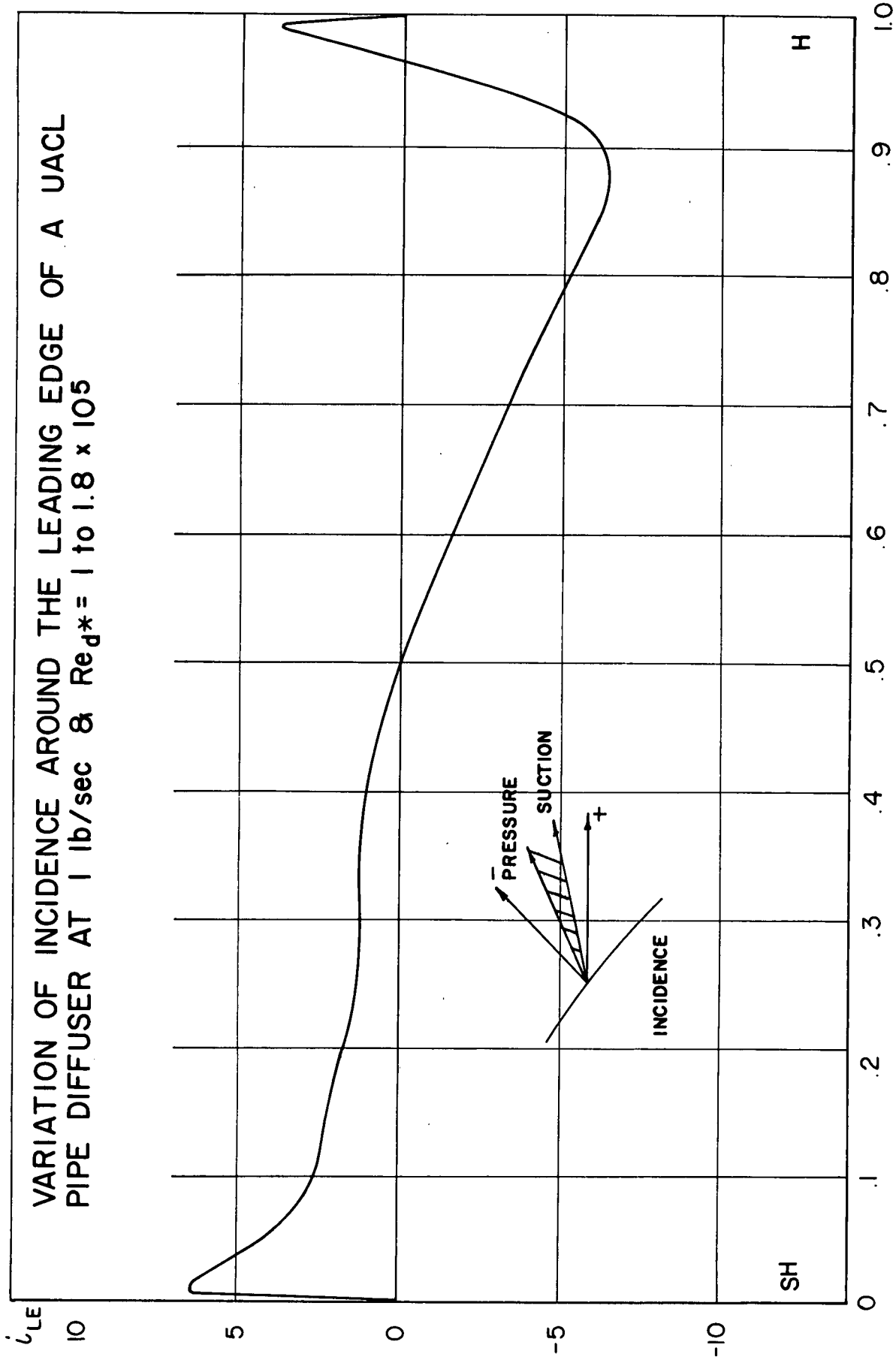

Fig. 36 Variation of incidence around the LE of a UACL pipe diffuser

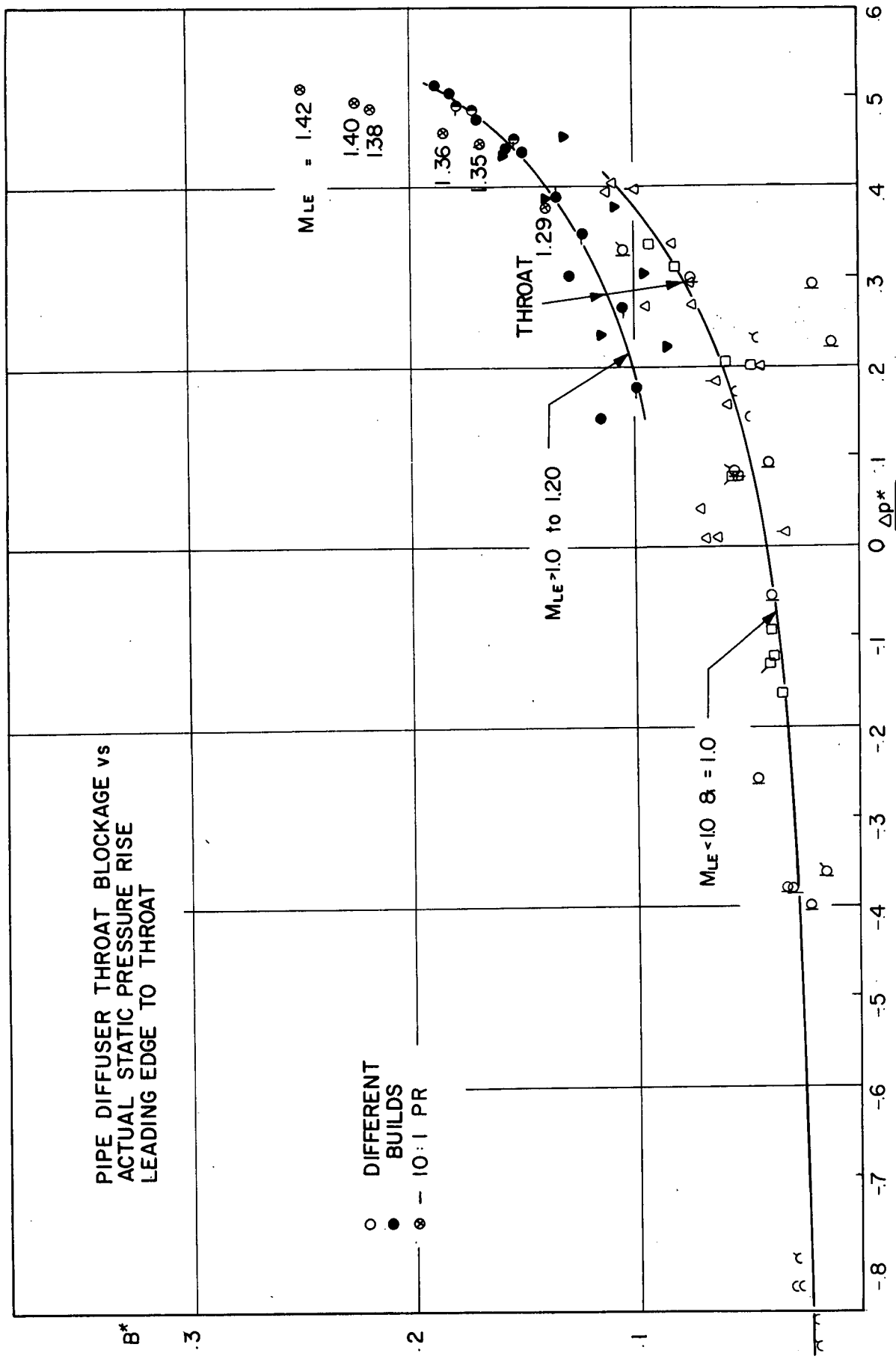

Fig. 37 Pipe diffuser throat blockage vs actual static pressure rise LE to throat

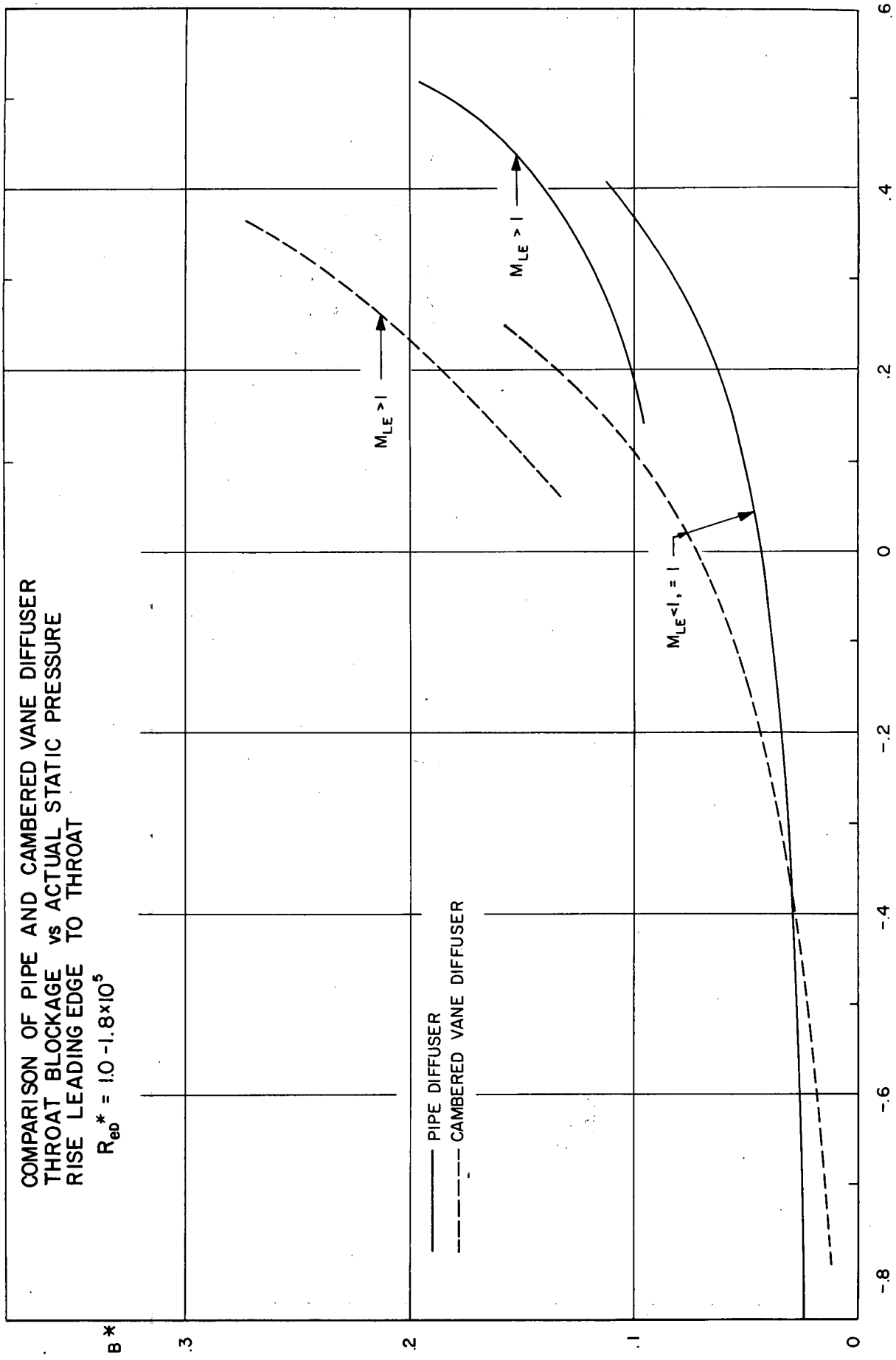

Fig. 38 Comparison of pipe and cambered vane diffuser throat blockage vs actual static pressure rise LE to throat

S U P E R S O N I C C A S C A D E P E R F O R M A N C E

BY

H. STARKEN
H.J. LICHTFUß

DEUTSCHE FORSCHUNGS- UND VERSUCHSANSTALT
FÜR LUFT- UND RAUMFAHRT E.V.
INSTITUT FÜR LUFTSTRAHLANTRIEBE
GERMANY

SUMMARY

An introduction to the fundamentals of supersonic flow through cascades is presented. The effect of back pressure and the starting conditions are described using simplified flow models.

Different design methods proposed in the literature are discussed. In detail, the inflow conditions at design and off-design operations of a supersonic cascade are presented. Finally, approximate methods are described for calculating shock losses and the dependency of total pressure losses from static pressure rise and axial-velocity-density ratio.

NOMENCLATURE

A	flow area
A_T	cross section area of throttle behind the cascade
e	length of the left running characteristic through E
h	energy per unit mass flow
l	chord length
M	Mach number
M^*	critical Mach number
$\Delta M^*_{t_{abs}}$	difference of tangential components of absolute critical Mach numbers.
p	pressure
T	temperature
t	spacing
w	velocity
β	flow angle (wit respect to cascade front)
β_s	stagger angle
$\Theta = \beta_2 - \beta_\infty$	turning
κ	ratio of specific heats
μ	Mach angle
ν	Prandtl-Meyer angle
ρ	density
$\Omega = \frac{\rho_2 w_2 \sin\beta_2}{\rho_\infty w_\infty \sin\beta_\infty}$	axial velocity density ratio
$\bar{\omega} = \frac{(p_{tot\ 2} - p_{tot\ \infty})}{(p_{tot\ \infty} - p_\infty)}$	total pressure loss coefficient
$\bar{\omega}_s$	shock loss coefficient
$\bar{\omega}_p$	profile loss coefficient

SUFFIXES

abs	absolute values (in a rotor)
ax	axial component (normal to cascade front)
C	value at point C (fig.4.15)
E	value at point E (fig.4.10 and 4.15)
I	neutral characteristic of a cascade (fig.4.9)
L	value at point L (fig.4.9)
max	maximum value
N	neutral characteristic of a single profile (fig.4.14).
P	value at point P on the profile surface (fig.4.17)
S	sonic point on the bow wave (fig.4.15)
SP	sonic point on the surface (fig.4.15)
t	component in tangential direction (parallel to cascade front)

tot	total value
*	value at the critical point (where M = 1)
^	value behind shock
0	value at the exit of the Laval nozzle in a cascade wind tunnel
I	first throat of a Laval nozzle (with two throats)
II	second throat of a Laval nozzle (with two throats)
2	values far downstream of the cascade
∞	conditions at infinity upstream.

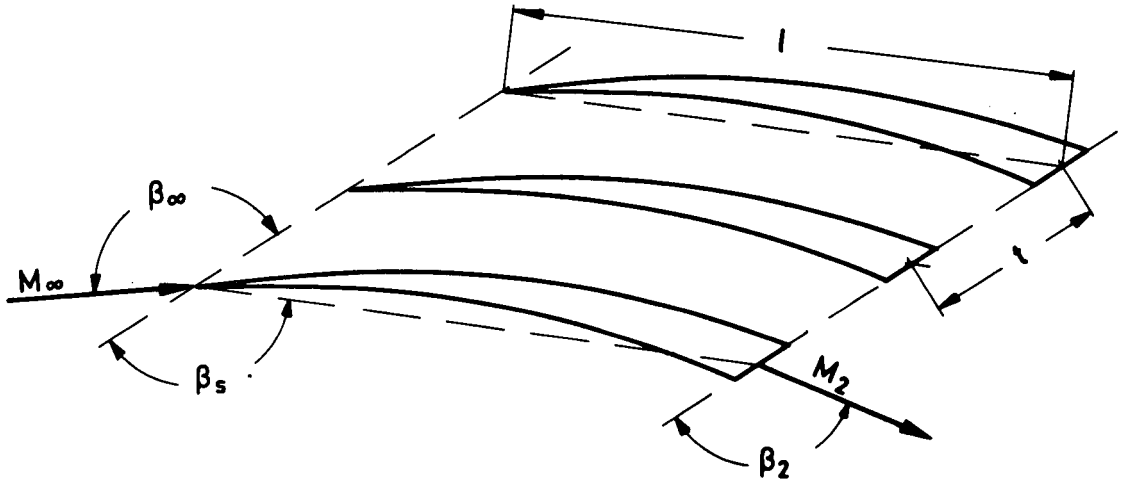

Cascade notation.

1. INTRODUCTION

The basic philosophy of the design and development of a modern compressor is directed towards the birth of an efficient, light and compact machine with large flow capacity and high compression ratio.

A compressor is a pressure producing mechanism involving geometrical and aerodynamical problems. The increase in pressure across a row of blades of an axial flow compressor depends not only on flow turning, but also on the circumferential velocity of the rotor. The turning angle is limited to a definite value, and as such an increase in the energy transfer becomes possible only by increasing the rotational speed.

In order to handle maximum mass flow per unit frontal area, the axial velocity at inlet will have to be quite high and even up to the sonic speed. The relative flow velocities gets therefore considerably increased because of high circumferntial and axial velocities.

In the early stages of compressor development, it was felt that the relative flow velocities should be well within the sonic value. The research and development in the last decade indicates that this could even be supersonic without an appreciable sacrifice in the efficiency. The limitations on the relative inlet velocity of a modern compressor is dictated more by the mechanical strength of blade material, the required high efficiency and the very limited scope for the variation of mass flow.

Theoretically there is no limitation on the static pressure ratio across a rotor and is just dependent upon the inlet Mach number. It is possible to achieve this high pressure rise in an infinitesimaly small distance across a normal shock wave. But the inherent rise in entropy across a normal shock beats down the efficiency to a low value at high relative Mach numbers. In a finite distance, however, the same high static pressure rise could be accomplished by a partial isentropic compression.

Simulation of such flow conditions in an actual machine may give the desired high efficiency even at high Mach numbers.

The potentialities of a supersonic compressor were realized long back, and in fact such rotors have been built and tested by WEISE (1.1) and BETZ, ENCKE (as reported by DAVIDSON (1.2) and ERWIN (1.3)) in the middle of thirty's. After the second world war these investigations received impetus, and further continuation in this field was made by KANTROWITZ (1.4), REDDING (1.5), FERRI (1.6) and many others at NACA. Up to 1956, many experimental compressors of different designs were developed and tested - unfortunately none of them had even the minimum desired efficiency.

Some of these compressors showed a surprisingly good performance at reduced inlet velocities in the transonic regime. Added to this, rotors designed for high subsonic Mach numbers using circular-arc blade sections also showed encouraging results at transonic inlet Mach numbers (up to $M_\infty = 1.3$). At Mach numbers in excess of $M_\infty = 1.3$ a steep increase in the shock losses will be noticed for circular-arc blades, thus demanding the development of special profiles. Intensive work was discontinued around 1956 by NACA. Only a few years back the necessity of its continuence was felt and the work has been resumed.

A complete theoretical solution of the flow problem in a supersonic turbo-compressor including the effects of flow instability, strong shock waves, boundary layer effects and flow separation, together with their interactions, is far from being solved with

the existing knowledge.

In view of the complexity of the flow problem, comprehensive testing of blade profiles in two-dimensional annular cascade tunnel and model compressors is therefore strongly necessary. In order to obtain a better understanding of the flow in a supersonic compressor, it is advisible first to investigate simpler flow configurations in two-dimensional models. This would at least give a qualitative picture of the complex flow problem. A helpful and valuable tool for such investigations is a twodimensional cascade wind tunnel. The superiority of the two-dimensional cascade flow research lies in the low number of flow parameters, simplicity of testing and the overall economy, as compared with a three-dimensional rotating test rig.

The impact of the importance of two-dimensional testing is realized by way of several new test apparatus in operation, and under construction all over the world.

A single volume summerizing all the important events that have taken place in the field of supersonic compressors and cascades does'nt seem to exist. The current paper also restricts itself to some of the special flow problems in a supersonic blade row.

Some of the important publications attempting to sumerize the state of art are from HOTTNER (1.7), LIEBLEIN (1.8), SAVAGE (1.9), KLAPPROTH (1.10), JOHNSON (1.11), and CHAUVIN (1.12).

2. FUNDAMENTALS OF SUPERSONIC CASCADES

2.1 Flow Field at Different Inlet Flow Mach Numbers

In order to present the important flow problem in a cascade at high inlet Mach numbers, several Schlieren pictures and explanatory diagrams are shown (The dark lines and spots in the Schlieren pictures, which are not shown in the diagrams, are due to pressure tubes and stresses in the plexiglas side walls). Figs. 2.1 and 2.2 show a cascade with an inlet Mach number $M_\infty = 0.9$, in which the existence of a local supersonic velocity field on the suction surface could be seen, together with a normal shock downstream of the local supersonic flow field, which in turn forms the upstream of the next blade profile. With increasing inlet Mach number, the local supersonic velocity field also increases and to such a value wherein the shock wave ahead of the cascade reaches infinity ($M_\infty = 1$). Under these operating conditions the shock wave remains stable and stationary (fig.2.3 and 2.4). Further increase of the inlet Mach number results in a shift in the shock position nearer to the leading edge.

The continuous change over from subsonic to supersonic inlet Mach number is possible, only when the inlet flow angle β_∞ is large enough to accomodate the sonic line on the suction surface still in front of the following blades as shown in figs. 2.3 and 2.4. Choking occurs when the sonic line crosses the passage formed by two adjacent blade profiles, and thereafter no further increase in the inlet Mach number at a constant inlet flow angle is possible (figs.2.5 and 2.6).

Shown in fig.2.7 and fig.2.8 is the flow field at $M_\infty = 1.1$. The supersonic flow field ahead of the cascade gets itself increased, but the subsonic flow field in the passage reaches up to the passage shock at the leading edge. Further increase in the upstream Mach number results in a complete supersonic flow condition in the blade passage and downstream of the cascade (figs.2.9 and 2.10). In such an operating condition,only a small region of subsonic velocity flow field exists around the leading edge of the blade

profile. When the axial component of the upstream flow velocity reaches a sonic value, then the detached shock wave collides with the pressure surface of the following blade and gets itself reflected (figs.2.11 and 2.12). In this case there exists no influence between the cascade and the upstream flow field.

2.2 The Effect of Back Pressure

In the figures shown from 2.1 to 2.12, the static pressure behind the cascade is approximately of the same order of magnitude as in front of the cascade. As long as the flow in the blade passage remains supersonic (figs.2.9 and 2.11), it is possible to alter the static pressure rise of the cascade by throttling; this means that it is possible to obtain different downstream static pressure values but still maintain the same inlet flow condition.

It is shown in figs.2.9, 2.13 and 2.14 how the flow field in a cascade with different throttle settings change. These figures show respectively the flow fields corresponding to a low, a medium and maximum back pressure. Further increase of back pressure results in the movement of the passage shock till it reaches the detached shock at the leading edge. Occurence of this condition leads to a change in the upstream Mach number and the inlet flow angle. In chapter 4.5 more details about this particular phenomenon are discussed.

The effect of back pressure on the flow in a blade passage is synonymous to the flow in a Laval nozzle. This one-dimensional model is particularly very good to understand the mechanism by which the supersonic flow field changes, when the back pressure is altered.

The following discussions are based on ref.(2.1). In the forthcoming pictures the flow in a double-throat supersonic Laval nozzle is described, wherein the left part simulates the upstream flow conditions and as indicated the right part is analogous to the cascade flow region.

For back pressures lesser than the pressure corresponding to correct expansion, there results in an expansion at the nozzle exit (fig.2.15). This is of particular interest essentially for turbine cascades (see for instance DEICH (2.2) and LAWACZECK (2.3)). An increase in back pressure, over and above the back pressure corresponding to correct expansion, leads to a compression at the exit of the nozzle (fig.2.16).

Because the boundary layer at the exit of the nozzle can withstand only a definite pressure gradient, further increase in back pressure causes a separation to occur even before the nozzle exit (fig.2.17). This separation of the boundary layer is at the same time interconnected with the occurence of an oblique shock wave. The position of the point of separation is determined by the maximum pressure difference across the shock which the boundary layer can withstand, and by the downstream compression beyond the point of separation.

Further increase of the back pressure causes a change from oblique shock to normal shock in the nozzle, and hence results in higher compression. In a condition like this, pressure differences across the shock wave may be too high for the boundary layer to withstand, and therefore a pseudo-shock occurs (fig.2.18). In the other case there will be only one normal shock and just a local thickening of the boundary layer without separation (fig.2.19).

Finally, any further increase in the back pressure renders the flow just subsonic in front of the second throat (fig.2.20). This corresponds to an unstarted condition of the

cascade, which is involved with changes in the upstream flow field (see chapter 4.5).

2.3 Starting Conditions of Supersonic Flow

If the total properties and the relative flow angle upstream of a Subsonic Cascade are held constant, then the maximum flow conditions are reached wherein in the minimum passage area sonic condition is attached (choking).

For the case of Supersonic Operation, the upstream conditions will have to be so matched that sonic conditions are again obtained at the throat in order to get maximum flow. Before a complete supersonic flow field is established ahead of a cascade, there will be building up of a strong shock in front of the passage. This shock is associated with a loss in total pressure, which must be accounted for in the calculation of the minimum passage area.

Calculation of the flow areas in a one-dimensional frictionless Laval-nozzle model is well known (EGGINK (2.4), KANTROWITZ, DONALDSON (2.5)). The flow in a blade passage is essentially the same as in the Laval-nozzle, and hence this comparison is made use of in determining the flow through the blade passage. In fig.2.21 are shown the flow fields in a Laval-nozzle with supersonic diffusor. In the top picture the flow everywhere between the minimum area passages A_I^* and A_{II} is supersonic. Because there is no total pressure loss involved, the area of the second throat A_{II} could be reduced even up to A_I^*, before a complete break down of the supersonic flow occurs. In this case the flow in the second throat is also sonic $A_{II} = A_{II}^*$.

In the bottom picture of fig.2.21 is shown a normal shock wave in front of the second throat. In this case sonic conditions exist at A_{II} and therefore $A_{II} = A_{II}^*$. But due to losses in the normal shock A_{II}^* has to be greater than A_I^*. Using the continuity and the energy equations we have:

Continuity relationship:

$$\rho_I^* \cdot w_I^* \cdot A_I^* = \rho_{II}^* \cdot w_{II}^* \cdot A_{II}^* \tag{2.1}$$

Energy relationship:

$$T_{tot\ I} = T_{tot\ II} \tag{2.2}$$

From (2.1) and (2.2) we have,

$$\frac{A_{II}^*}{A_I^*} = \frac{P_{tot\ I}}{P_{tot\ II}} \tag{2.3}$$

And so it is seen that the area ratio between the first and the second throat is inversely proportional to the ratio of total pressures. The ratio of the total pressures is once again dependent upon the Mach number in front of the normal shock. Therefore the location of the normal shock is determined by the size of the second throat A_{II}^*. Increase in the area of the second throat renders the normal shock to move nearer to A_{II}^*, and it reaches its limiting position at A_{max}. Any further increase causes the normal shock to move completely downstream of the second throat, because there does not exist any stable condition between A_{max} and A_{II}^*. Now the nozzle flow is completely supersonic, with a Mach number greater than unity at A_{II}. It is now possible to reduce A_{II} to a value up to and including A_I^* and the same has been shown at the top in fig.2.21. This flow condition is called "Started" whereas the flow field in fig.2.21b is usually called "Unstarted".

The theoretical relationship between the Mach number and the corresponding area ratios for the started and the starting conditions are shown in fig.2.22.

Applicability of the above onedimensional model to a cascade flow problem demands accounting for a two-dimensional flow that exists in it. Unfortunately, till now there appears to exist no exact theoretical method by which a general two-dimensional flow field with strong shocks could be predicted. An acceptable and emperical estimate of the probable position and shape of the sonic line is therefore necessary to get an idea about the starting of a supersonic cascade.

The flow fields in a started and unstarted supersonic cascade are shown in figs.2.23 and 2.24, with Mach numbers $M_\infty = 1.1$ and $M_\infty = 1.24$ respectively.

3. DESIGN METHODS OF SUPERSONIC BLADING

The geometry of the supersonic blading depends essentially on the flow conditions required at the exit of the rotor. That means, the mode of energy transfer plays an important role. Typical supersonic cascades together with velocity triangles are shown in fig.3.1. Fig.3.1a shows a cascade of the impulse type, wherein the relative critical Machnumber M^* remains nearly unchanged and only high turning exists symmetrical to the axial flow direction. However, such a rotor cascade is inherent with strong acceleration in the absolute flow M^*_{abs} followed by large deflection. In other words, it means that the change in the absolute circumferential critical Machnumber $\Delta M^*_{t\,abs}$ is high. As the possible value of $\Delta M^*_{t\,abs}$ is high for a blading of this class, it is seen from the Euler-Turbine equation the energy transfer h is also quite high:

$$h = M^*_t \cdot \Delta M^*_{t\,abs} \tag{3.1}$$

In a symmetrical blading as shown in fig.3.1a, it is seen that the entire change in the static pressure has to take place completely in the following stator at a high supersonic velocity since the static pressure remains constant across the rotor.

The other type of blading as shown in fig.3.1b has a very small camber and hence the deflection of the relative flow is also small. The large turning in the absolute flow is due to the severe deceleration of the relative flow (pressure rise) and this is responsible for the energy transfer.

The design of the blading as such governs the absolute outlet velocity (identical to the inlet velocity of the stator), which may be subsonic or supersonic. Apart from the above said two limiting cases, a variety of configurations having different turnings and static pressure rises are possible and many of them have also been tested. Three different types of supersonic cascade can be thought off, taking into consideration the relative components of the flow.

a) Impulse type cascade.
   A cascade of this type is shown in fig.3.1a. To establish the flow of an impulse type rotor, a cascade with high turning and low pressure rise is required. The same geometry holds good for an accelerating and decelerating machine. Hence the knowledge available in the field of turbine blading becomes also useful for the design of supersonic compressors. For the same inlet and outlet conditions called for, there are different ways of getting the profile shape. SHAPIRO (3.1) has given a method and such a profile is shown in fig.3.2. The method consists in isentropically (simple wave) decelerating the flow in the inlet portion of the blades up to a parallel flow at the throat, and further accelerating it within the passage to the flow Mach number

at exit. Thus a deflection in the flow is obtained.

A second profile after STRATFORD (3.2) consists of two concentric circles to form the blade passage. Fig.3.3 shows an approximate profile of this type, together with some Characteristics and theoretically calculated zig zag-pressure distribution.

BOXER (3.3) and OSWATITSCH (3.4) have developed a third method, which has been made use of by STRATFORD (3.2), COLCLOUGH (3.5) and GOLDMAN (3.6, 3.7). The parallel upstream flow is transformed into a potential vortex flow and further changed over to a parallel flow at exit. To illustrate the method an example is presented in fig.3.4, together with a Schlieren picture obtained from NACA (unpublished work) in fig.3.5.

Another method proposed (LICCINI (3.8, 3.9), OSWATITSCH (3.10)) for the development of supersonic blade profiles consists in defining one portion of the profile and further determining the flow field by the method of Characteristics. A stream-line itself is selected to form the other half of the profile.

Although it is possible to prescribe the complete cascade itself, the basic and inherent compression waves and nonuniformity of downstream flow poses severe limitations. In effect, all the methods so far described necessitate a local acceleration and deceleration of the flow. Sometimes improper deceleration of the flow may lead to separation of the boundary layer. And therefore extreme care is necessary while constructing the profiles, so as to ensure minimum pressure rise on the blade surface.

The possibility of boundary layer separation and the associated difficulties makes the profile with zig zag pressure distribution rather unfavourable. Also for profiles designed by other design methods, a careful investigation of the boundary layer behaviour is absolutely necessary. A considerable reduction of the pressure gradients is found possible with blades of high solidity.

In the first method discussed, there is a limitation on the flow turning depending upon the upstream Mach number, since the minimum possible velocity at the throat is sonic. The maximum turning Θ_{max} has the form:

$$\Theta_{max} = \beta_\infty - \beta_2 = 2 \cdot \nu(M_\infty). \tag{3.2}$$

To satisfy the starting conditions, as already described in chapter 2.3 (fig.2.22), it becomes necessary to magnify the throat velocity, except in the case where a variable geometry of the blades is provided. This in turn reduces the flow deflection.

For vortex flow cascades there exists no limitation with regard to turning angle bearing in mind the possible starting difficulties.

b) Supersonic cascade with low flow turning.
To have a cascade of this type in operation (fig.3.1b), a blade row capable of producing high static pressure in spite of low turning would be necessary. Two possible methods of realizing this are:

a) Compression due to a shock front. The main part in pressure rise is accomplished in a normal shock in the blade passage.

b) Combining the design methods of obtaining subsonic and supersonic flows. Supersonic deceleration is associated with a reduction in flow area, that means a de-

flection in cascade flow, whereas deceleration in subsonic flow consists of an increase in area and a flow deflection of opposite sign. Combining these two principals it is possible to obtain a blade passage wherein the desired decelerated flow could be generated without appreciable turning.

Till now for shock compression, double circular arc blades (DCA) are essentially made use of. As shown in fig.3.6, both the suction and the pressure surfaces are made out of circular arcs. In such a profile the flow gets accelerated at the entrance region until a normal shock occurs at the entrance of the passage, and thereafter the flow gets decelerated to subsonic velocities. Further downstream of the passage the flow gets further decelerated depending on the contour of the passage. The main disadvantage of shock compression lies in the associated rise in entropy across the shock, which increases considerably at higher Mach numbers. This disadvantage led to the concept of multiple circular-arc blades (MCA), as shown in fig.3.7, where the suction surface is made out of two or more circular arcs of different curvature. This profile ensures reduced acceleration and shock losses of the flow in the entrance region because, the upstream suction surface arc is of lower camber (see chapter 5). This concept was first proposed by SEYLER and SMITH (3.11). Comparison of results obtained from rotor tests with MCA and DCA blades (GOSTELOW et al.(3.12)) indicates that definite advantage by way of efficiency and control behaviour exists when multiple-circular-arc profiles are used. A reduction in the curvature of the suction surface at the entrance region up to zero, leads to a new type of profile called the circular-wedge profile (CW_1,fig.3.8).

This type of profile was first investigated by EMERY (3.13). A cascade of this type is characterized by constancy of Mach number upstream and in front of the normal shock. Test results showing a reduction in total pressure losses of these profiles are published in (3.14) and (3.15).

Improvements in the performance realized by MCA and CW1 profiles will no longer be there when the flow Mach number M_∞ becomes large. At about $M_\infty = 1{,}6$ the rise in entropy will be high enough to reduce the efficiency considerably. It may be possible to obtain the desired compression with lower losses by decelerating the supersonic flow in several oblique shocks instead in one strong normal shock. Theoretically the shock losses could be altogether avoided by using isentropic compression. This was first proposed by OSWATITSCH (3.16) for inlets, and it has been succesfully applied in practice. However the results obtained in cascades up to now are not very encouraging.

Isentropic compression can further be subdivided into a) inner compression and b) outer compression, depending on whether the isentropic compression takes places within the passage or in the entrance region. In a cascade both the types of compression or combination of the two are possible, if the starting condition is taken into account.

External compression cascades, which have been essentially tested in rotors, were designed by GRAHAM (3.17), CREAGH (3.18), JAHNSEN (3.19), and FRÜHAUF (3.20). Schlieren pictures of such a lattice (3.20) are shown in fig.3.9. The principal flow condition at maximum back pressure is shown in fig.3.10, although it was not possible to establish a stable flow under this condition.

The instability may perhaps be due to the normal shock behind the passage throat. It can be avoided by reducing the back pressure, which results in a downstream movement of the passage shock.

The concept of internal compression was employed by KANTROWITZ (1.4), (fig.3.11), BEDER (3.21), (fig.3.12), LOWN (3.22), fig.(3.13), and FEJER (3.23), (fig.3.14). The high expectations of all these cascades remain yet to be fulfilled and is seen also from a

statistical investigation carried out by CONRAD (3.24).

The discrepancy may perhaps be due to shock-boundary layer interaction and lack of establishment of the required flow conditions in the rotor tests. A comprehensive and systematic investigation of two dimensional cascades with these profiles is not to be found at all.

c) High-turning supersonic compression cascade.
Stators to be used after an impulse type rotor demand a profile shape capable of ensuring high static pressure rise and flow turning, in order to reduce the flow moment of momentum after the rotor.

The blade contours can be classified under three headings depending on whether the flow is first decelerated through a shock and then deflected subsonic, or the flow is first deflected at supersonic speed and then decelerated, or the flow is compressed and deflected at supersonic as well as subsonic velocities.

Fig.3.15 shows a blade section of the first type (WILCOX (3.25)). A similar profile shape has been used by HARTMANN (3.26).

Fig.3.16a shows blades of the second type after SCHMALFUß (3.27). The division of compression and turning in the second type of blades is clearly shown in the tandem arrangement of ref.(3.27), (fig.3.16b). Figs. 3.17 and 3.18 show the profiles for simultanous deflection and deceleration, and were proposed by KLAPPROTH (3.28) and SHAPIRO (3.1).

Evidently, if starting is possible, all these profile forms could be made use of for the blading of compressor rotors, although they are proposed as stator bladings. The possibility of using the SHAPIRO profile with simultanous deflection and deceleration gets ruled out for lack of experimental data. The interpretation of experimental results of those stator blades, tested behind impulse type rotors is very difficult because it is not exactly known, if the design inlet flow conditions have been reached.

The tandem type cascade (3.27), when tested in a cascade wind tunnel, operates best if the normal shock is established at the entrance of the cascade. Under these conditions the turning and most of the pressure rise will be produced at subsonic speed and not at the design condition.

A new concept of supersonic compression was developped by JOHNSON (3.29), where he considered a blade passage of nearly constant cross section (fig.3.19) giving rise to pressure increase and turning in the channel, together with the establishment of pseudo shocks. The Schlieren picture in fig.3.20 illustrates this principle. It was expected from duct flow investigations (2.1) that the static pressure rise and total pressure loss coefficient would be of the same order of magnitude as that of a normal shock.

Exhaustive experimental investigations have been carried out on such blunt trailing edge cascades (BTE) and compressor stages at the VKI by CHAUVIN and BREUGELMANS (3.30, 3.31, 3.32, 3.33). Plane cascade measurements have been done by HEILMANN and WEYER (3.34) and on blunt trailing edge rotors by WENNERSTRÖM (3.35)and CARMAN (3.36). The value of the minimum measured total pressure losses is greater than that across a normal shock, and this may perhaps be due to finite thickness of the trailing edge. This led to a modification at the rear portion of blunt trailing edge blades at VKI.

Major difficulties of all supersonic flow investigations having pressure rise are due to the complex behaviour of boundary layer, particulary at the points of intersection of normal or oblique shocks with the wall boundary layer. Strong static pressure rise in these compression shocks lead to at least local flow separations. This problem is being attempted at different places to determine a suitable solution. In view of the existing state of art, only a simple separation criteria is presented here. When interaction between a normal shock wave and turbulent boundary layer takes place, separation generally occurs if the Mach number at the wall in front of the shock wave exceeds a value of M = 1.3 (3.37, 3.38). If separation takes place, the static pressure rise will have a value less than that of a normal shock wave. A theoretical relationship is shown in fig.3.21 (2.1).

4. RELATIONSHIP BETWEEN INLET FLOW ANGLE AND INLET MACH NUMBER

4.1 Straight Flat-Plate Cascade

Two possible cases, which have entirely different characteristics, are met with depending whether the axial component of the inlet velocity is greater or less than the sonic velocity. That is:

a) $M_{ax} = M_\infty \cdot \sin \beta_\infty \geq 1$ (supersonic axial velocity) and

b) $M_{ax} = M_\infty \cdot \sin \beta_\infty < 1$ (subsonic axial velocity).

In the first case, there will be no influence of the flow upstream of the cascade by the very existence of the cascade itself. This is shown in figs.4.1 and 4.2 for a flat-plate cascade.

Fig.4.1 shows that in the case where the inlet flow direction posesses an incidence which is negative with respect to the blade, than an oblique shock at the leading edge on the suction surface appears. The position of the shock is completely within the blade passage. In the second picture, the inlet flow angle is increased and in this case a centered Prandtl-Meyer expansion occurs well within the blade passage instead of the oblique shock wave.

Both the cases explain that the inlet flow direction is independent of the inlet Mach number, as long as the disturbances caused by the leading edges and the suction surfaces are enveloped by the blade passages. Therefore the flow in front of the following blades is not affected.

Incase where the axial component of the inlet velocity is rendered subsonic ($M_{ax\infty} < 1$) due to a decrease in inlet Mach number, than there exists an influence of the cascade into the flow upstream.

This flow can very well be explained by taking a semi-infinite flat-plate cascade (WEISE (1.1), KANTROWITZ (1.4)). Fig.4.3 shows such a semi-infinite cascade, wherein the constant flow upstream of the first blade is such as to give a centered Prandtl-Meyer expansion at the leading edge of the first blade and in front of the cascade. In turn, because of this expansion, the flow gets rotated so that it is parallel to all the other blades. In view of this fact there occur no further shocks or expansions in front of the following blades. Also when the incidence of the first blade is negative (fig.4.4), there will be an oblique shock at the leading edge of the first blade followed by true parallel flow for the rest of the blades. The direction remains the same for the shock free portion just in front of the cascade, for both positive and negative incidences of the semi-

infinite cascade.

In the case of an infinite flat-plate cascade there exists no "First Blade", and therefore one and only one inlet flow direction is possible and is parallel to the direction of the flat plates. This flow direction is sometimes referred to as "Unique Incidence" (CHAUVIN (1.12)).

A plot of the inlet flow angle β_∞ versus the inlet Mach number of an infinite flat-plate cascade exhibits a flat characteristics parallel to the M_∞-axis. This is shown in fig. 4.5 to the left of the point of branching, and in this region the axial velocity is subsonic. At the point of branching, the axial velocity is just sonic. Beyond this point the curve takes two limiting positions. The region bounded by these two curves determines the possible inlet flow direction for a given upstream Mach number. The top curve corresponds to an axial velocity which is just sonic, that is $M_\infty \cdot \sin\beta_\infty = 1$. A flow field with this configuration is shown in fig.4.6. In this figure a semi-infinite cascade with supersonic inlet Mach number M_0 in front of the first blade is shown. The axial component of M_0 is subsonic. This gets accelerated at the leading edge of the first blade in such a way that the axial component of the inlet velocity for the rest of the cascade is just sonic.

The bottom curve of fig.4.5 shows an axial inlet velocity which is supersonic. The oblique shock wave at the leading edge of each of the blades hit one another, and this gives rise to a continious oblique shock wave just in front of the cascade (fig.4.7).

Analytically, the bottom curve is determined by the relation:

$$M_\infty^2 = \left(\frac{\kappa+1}{2} \cdot \cos\beta_\infty \cdot \sin\beta_\infty \cdot \mathrm{tg}\beta_s - \frac{\kappa-1}{2} \cdot \sin^2 \beta_\infty\right)^{-1} \tag{4.1}$$

This relationship has a minimum value at:

$$\beta_\infty = \arctan\left(-\sqrt{\left(\frac{\kappa-1}{\kappa+1}\right)^2 \mathrm{ctg}^2\beta_s + 1} - \frac{\kappa-1}{\kappa+1} \mathrm{ctg}\,\beta_s\right) \tag{4.2}$$

To summerize for a cascade of flat plates, the region to the left of the point of branching (fig.4.5) determines only one inlet flow angle β_∞ possible for different inlet Mach numbers. To the right of the point of branching, within the upper and lower boundaries defined by the top and the bottom curves, a variety of M_∞ - β_∞ combinations become possible. Flow angles β_∞ in excess of β_∞ at the point of branching give rise to a flow field as shown already in fig.4.2. For all angles less than β_∞ at the point of branching, the flow field is as shown in fig.4.1.

The elegant way of Hodograph representation of this gasdynamic problems of fig.4.5 is presented in fig.4.8.

This analysis is valid not only for thin flat plate cascades, but also for cascades with finite thickness having a straight suction surface at the entrance region and very sharp leading edges. Near sonic inlet Mach numbers, some discrepancies may occur for real blades due to choking.

4.2 Cascade of Blades with Curvature

Constancy of inlet flow angle, which is valid for a flat-plate cascade at $M_\infty \cdot \sin\beta_\infty < 1$, no longer holds good when blade curvatures are involved. In this case the inlet flow angle β_∞ changes with different inlet Mach numbers M_∞. Further, there exists a definite functional interdependency between M_∞ and β_∞. This means that theoretically for every inlet Mach number M_∞ there will be one particular value of the inlet flow angle β_∞ (KANTROWITZ (1.4) and FERRI in (1.3)).

The curvature of the forward portion of the suction surface introduces flow disturbances in front of the cascade. Fig.4.9 shows the flow field of such a cascade. This profile has a pointed leading edge and a convex suction surface. This semi-infinite cascade has an inlet flow direction upstream of the first blade, which is chosen tangential to the blade leading edge. Assuming simple wave flow at the entrance region, the flow is accelerated to a higher Mach number due to the curvature of the convex surface, and hence the inclination of the Characteristics also gets reduced.

The flow direction along the characteristic EL', which passes through the leading edge of the following blade, runs parallel to the profile at the point E. Because the flow direction at E is something other than the direction of the profile contour at L', an oblique shock wave appears at L'.

The flow along L-I-E and L'-I'-E' (fig.4.9) is identical as long as the change of entropy is neglected. The logical conclusion of this is that the flow in the corresponding entrance region L-I-E of all the following blades is also the same. Because a special flow direction β_o has been chosen for the first blade of this semi-infinite cascade, the flow field ahead of this only one blade differs from the rest of the blades; however, the pressure distribution on the suction surface of the entrance region remains still identical.

Looking at the flow field in the region L'-I'-E', it is seen that:

a) The Characteristics which are generated between L' and I' meet the first bow wave emitted at the leading edge L'
and

b) Characteristics which are generated between I' and E' go and meet the bow wave of the leading edge L'' of the following blade. The bow waves at L', L'' ... are identical in all respects with a periodicity of one pitch length, and therefore the Characteristics at I', I'' ... are the limiting Characteristics of the bow waves at infinity upstream and are referred to as "Neutral Characteristics". It may also be mentioned that the flow is rendered periodic, because the interaction of the compression and the expansion waves of each of the blades nullify oneanother.

The Neutral Characteristic wholly represents the inlet flow conditions of the infinite cascade because, at infinity upstream the bow wave changes into a Characteristic which is parallel to the neutral one, and so we have:

$$M_{I'} = M_\infty$$

and

$$\beta_{I'} = \beta_\infty$$

The obvious conclusions are:

$$M_o \neq M_{I'} \neq M_{E'}$$

and

$$\beta_o \neq \beta_{I'} \neq \beta_{E'}$$

For the calculation of β_∞ and M_∞ of such a cascade, the Method of Characteristics is a helpful tool. The inherent drawback of this method is the cumbersomeness in drawing all the Characteristics up to infinity.

LEVINE (4.1, 4.2) suggests an analytical solution. The method consists in the determination of mass flow through the Characteristic EL (fig.4.10) for an arbitraryly chosen Mach number at L, which defines the position of the point E by the Mach angle μ_E. The

mass flow passing through one pitch of the cascade at infinity upstream must be the same as at EL. The two unknown quantities β_∞ and M_∞ are found by using the above said continuity relation and the Prandtl-Meyer equation as follows:

(4.3) $$t \cdot \rho_\infty \cdot w_\infty \cdot \sin \beta_\infty = e \cdot \rho_E \cdot w_E \cdot \sin \mu_E$$

and

(4.4) $$\beta_\infty + \nu_\infty = \beta_E + \nu_E$$

This method gives no clue whatsoever about the flow field in front of the cascade. This would necessitate the Characteristic construction, when the flow field is desired. YAMAGUCHI (4.3) has given a method by which the form of the bow wave could be determined.

For a special profile shape, having the suction surface with a kink made out of two straight lines at the entrance region, a method has been given by SCHWAAR (4.4) and STRATFORD (4.5).

In fig.4.11 a section of an infinite cascade with a convex suction surface is shown. LICHTFUß (4.7) has calculated this flow field using the analytical method of Characteristics after OSWATITSCH (4.6). In addition, the functional relation $\beta_\infty = f(M_\infty)$ after LEVINE, has also been presented in the same diagram.

The curve which limits the region of axial supersonic inflow condition below the branching point has been calculated for a flat plate cascade in the last chapter using the exact shock relations (see fig.4.5). In the case of a blade section with curved suction surface, this boundary can be derived under the assumptions of isentropic flow. It results as the second solution of the above described method of calculating the inflow conditions of a supersonic cascade at subsonic axial inlet velocity, with the aid of continuity and Prandtl-Meyer relations.

The flow in front of the cascade is everywhere constant with a supersonic axial component, and the curved oblique shock waves just meet the leading edges of the following blades.

This special flow configuration leads to considerable changes in flow direction at the cascade front, associated with increasing entropy and therefore the assumption of isentropic flow is only valid in a small range of inlet flow angles.

If the suction surface has a concave curvature instead of convex one, the corresponding flow field gets changed and for a semi-infinite cascade it is shown in fig.4.12. It is seen from this figure, the flow direction in front of the first blade is such that there occurs a centered Prandtl-Meyer expansion at the profile leading edge L. Downstream, the flow experiences a compression resulting in an increase in the inclination of the Characteristics. Again for the following blade there occurs the centered Prandtl-Meyer expansion at L' similar to the previous one, and from L' to E' the flow field repeats itself as from L to E.

In the process of this isentropic compression, the Characteristics gets bent also continuously resulting in an overlap of the different Characteristics. An oblique shock wave starts at the cusp of the envelop of Characteristics and is away from the blade surface (fig.4.12). This shock wave in an infinite cascade is again parallel to the neutral Characteristic at infinity. The position of this neutral Characteristic is at the leading edges of the blades, which means that I coincides with L.

For the calculation of the flow parameters M_∞ and β_∞, the methods already explained for

the convex suction surface profiles remain valid. Fig.4.13 shows the flow field for a typical infinite cascade, calculating procedure being based on ref. (4.7). In the same figure also included are the functional relation $\beta_\infty = f(M_\infty)$ after LEVINE and the limiting curve for axial supersonic flow.

4.3 Semi-Infinite Cascade

A two-dimensional cascade wind tunnel can only have finite dimensions. Hence, the flow field in such a tunnel can only be comparable to that of a semi-infinite cascade. The difference between an infinite and semi-infinite cascade is therefore exhaustively discussed.

Figs.4.14a to 4.14c presents the flow field in a semi-infinite cascade, wherein it is seen that the flow parameters M_∞ and β_∞ of an identical infinite cascade are the same. The difference between an infinite cascade and a semi-infinite cascade is essentially due to the "First Blade". The position of the neutral point I, I', I'' ... and the orientation of the Characteristic through it are the same.

The flow field ahead of the first blade, which refers to the flow prevailing just in front of the test section of a cascade wind tunnel, differs in all the three cases by way of flow direction β_o and the Mach number M_o. In the first two figures (4.14a and b) the nozzle exit angle β_o is greater than β_∞, and the nozzle exit Mach number M_o is lesser than M_∞. One of the possible condition is a shock-free expansion at the leading edge of the first blade, which is characterised by a centered Prandtl-Meyer expansion (fig.4.14a). The other possibility, as shown in fig.4.14b, is the occurence of a shock wave at the leading edge of the first blade. The strength of this shock is something different from that of the identical infinite cascade, and it is weaker than that of the following blades. At infinity upstream, the strength of the shock becomes zero for the infinite cascade, whereas for the first blade there will be still some residual shock strength as the flow has to turn from M_o at N to M_∞ at I. The first shock wave at infinity and the Characteristic through N, which is identical to that of a single isolated blade, are parallel. The position of the neutral Characteristic for an isolated blade profile (N) is displaced, and is in front of that of the infinite cascade (I).

In fig.4.14 c the flow ahead of the first blade (M_o, β_o) is such that the shock in front of it interferes with the detached shocks of the following blades. In this case the neutral Characteristic of the isolated blade profile lies downstream of the Characteristic through I.

A method other than that used for fig.4.14 consists in maintaining a constant flow condition (M_o) at the exit of the wind tunnel nozzle. Altering the position of the cascade (β_o) facilitates the achievement of the desired Mach number M_∞ in front of the infinite cascade.

4.4 Blade Profiles with Blunt Leading Edges

The cases so far handled consider the hypothetical and ideal flow past blade profiles with a sharp leading edge, which enables us to make the assumption that the shock waves are attached to it. In reality, finite thickness of the leading edges leads to a detachment of the shock waves. Calculation of the inlet flow condition (M_∞, β_∞) must account for this shock detachment. No exact solution for the calculation of the detached shock wave in front of the cascade profiles seems to have been published so far.

An approximate method for predicting the shock in front of a blunt leading edge isolated airfoil has been given by MOECKEL (4.9). With a fairly good agreement, this could also be

applied to a cascade for determining the inlet flow Parameters M_∞ and β_∞. STARKEN (4.10) and NOVÁK (4.11), around the same time, have established the use of this method for blunt leading edge cascades.

MOECKEL makes the following assumptions (fig.4.15):

a) The form of the detached bow wave follows a hyperbolic relation.
b) The sonic line is linear.
c) The stagnation stream line is normal to the detached shock and when extended, it passes through the center of the leading edge radius.

With the above mentioned assumptions and the condition that the mass flow passing through the shock between C and S should be identical to that crossing the sonic line S - SP, the detachment distance of the detached shock wave from the center of the leading edge could be evaluated. This in turn also enables to calculate approximately the rough form of the bow wave.

The flow upstream of a blade in a cascade is not constant, and so it differs from a corresponding isolated profile. Further, the flow in front of such a cascade has an inherent periodicity, which renders independent variation of β_∞ - M_∞ not possible at axial subsonic velocities (see chapter 4.2). As it has been said for the infinite cascade with attached bow waves, here also the mass flow crossing the Characteristic E-C must be identical to that at infinity upstream. Further the Prandtl-Meyer relation holds between E, SP and upstream infinity, if the shock losses are neglected. With these two conditions it becomes possible by iteration to calculate the upstream flow and the detached bow wave in front of the cascade.

Fig.4.16 shows the plot of such a calculation made for a double-circular-arc profile, compared with experimental results (4.10). For simplification the Mach number is assumed to be constant between the points C and S.

As direct measurements of the flow angle β_∞ in front of the cascade is not possible, the test points (fig.4.16) are derived making use of the Prandtl-Meyer relation:

$$\beta_\infty = \beta_p + \nu_p - \nu_\infty \tag{4.5}$$

In the above equation β_p refers to the contour angle at a point P on the profile (fig. 4.17). The Prandtl-Meyer angle ν_p is worked out from the measurements of the static pressure at P and the total pressure of the inlet flow. The Mach number M_∞ of the inlet flow is calculated by averaging the static pressure in front of the cascade (fig.4.17), and the value so obtained is in good agreement with the Mach number at infinity upstream (4.10). From the value of M_∞ so calculated, the Prandtl-Meyer angle ν_∞ is determined.

In spite of the simplifying assumptions, the agreement between the theoretical and the measured values is very good.

4.5 Unstarted Condition of the Cascade

In the chapters 4.1 to 4.4 the discussions were limited to the existance of different passage flow fields, which were never completely subsonic from trailing edge to leading edge at supersonic inlet velocities.

A similar blade passage with regions of different Mach numbers, seperated by a normal shock, is shown in fig.4.18a. This has its throat at entry of the blade passage. The position of the normal shock is solely dependent on the extent of downstream throttling,

because the flow in the throttled area A_T is assumed to be sonic. In the following discussion only the loss across the normal passage shock is accounted for. Hence, the throttled area A_T also represents the critical area behind the normal shock.

A decrease in A_T causes the normal shock to move nearer to the leading edge. The inlet flow field remains unaltered till the normal shock is just at the throat of the passage, and in this particular case it also happens to be at the leading edge of the blade profile (fig.4.18b). Any further throttling causes the flow within the blade passage to become completely subsonic.

Fig.4.18c shows such a completely subsonic flow passage and the following observations could be made:

a) The bow wave detaches itself from the leading edge.

b) There is a shift in the position of the stagnation stream-line, causing a reduction in the inlet mass flow into the blade passage

and

c) A decrease in the inlet Mach number M_∞ is followed by an increase in the inlet flow angle β_∞.

Theoretical calculation of the inlet flow condition (M_∞ - β_∞) for this case must account for the total pressure losses in the normal portion of the detached shock in front of the blade passage, and the mass flow as dictated by the choking at the throttled area. Different inlet flow angles β_∞ for a constant throttle position become possible for this unstarted case by an independent variation of the throttle position. In fig.4.19 the functional relationship $\beta_\infty = f(M_\infty)$ for a double-circular-arc profile is shown. At axial subsonic inlet velocity the bottom limiting curve corresponds to the started condition, which has been calculated with the method described in chapter 4.4. Some lines of constant critical area $\hat{A}^*/t$, which in frictionless flow are equal to the cross section $A_{T/t}$ of the downstream throttle, are added in this figure. They correspond to the unstarted operation of the cascade. An increase in the extent of throttling, that also means a decrease in the ratio A_T/t, accomodates higher inlet flow angles β_∞.

Experimental investigations in a two-dimensional cascade tunnel, (fig.4.20) as well as in three-dimensional compressor rotor test rigs (fig.4.21), clearly reflect upon the existence of a maximum inlet flow angle at the unstarted condition, which has not been so far theoretically well explained.

Even when the throat lies within the blade passage, the above arguments hold valid. As an example of this case the cascade shown in fig.4.19 has been modified. This modification creates a throat within the blade passage. Although essentially the theoretical characteristic of $\beta_\infty = f(M_\infty)$ with (A_T/t) as parameter remains the same, there is a maximum (A_T/t)-line below which the throttle has no effect to change the inlet angle (fig.4.22). The shaded area below this maximum (A_T/t) characteristic shows the region where no operation is possible.

Similar theoretical investigations have been made by GRAHAM (3.17) and MILLER (4.13). In both the papers the emphasis is placed on shock losses. In ref.(3.17) a simple case with straight suction surface at the inlet has been analysed, whereas in ref.(4.13) the interdependency of inlet Mach number and flow direction has not at all been taken care of.

5. SHOCK LOSSES IN SUPERSONIC CASCADES

What has been described in chapter 4 enables the calculation of supersonic flow field and

position of the normal and oblique shocks in front of a cascade, under the assumption that the inlet flow is isentropic. Using the well known shock relations, the total pressure losses due to shock waves can therefore be calculated for supersonic cascades having different geometries.

The inlet region of an infinite cascade, with the axial component of the inlet velocity subsonic, is associated with infinite number of shock waves. Evaluation of the total shock losses in front of a blade passage, that is also between two adjacent stagnation stream lines, consists in the summing up of all the shock losses along one shock wave up to infinity (5.1). Looking at figure 5.1 it is seen that the mesh of shock waves and stagnation stream lines resembles a matrix with identical diagonal bits, and each stagnation stream line intersects with an infinite number of shock waves of progressively decreasing shock strength.

The position of the passage shock, as already described earlier, is dependent on the extent of downstream throttling. Calculation of the supersonic flow within the blade passage for different passage shock position is possible as long as boundary layer seperation effects are not too large. It has not been possible up to now to calculate the exact position of the passage shock itself, although it is known to be dependent upon the back pressure.

A plot of calculated shock loss coefficients $\bar{\omega}_s$ as a function of M_∞ for double-circular-arc (DCA) and wedge type profiles (CW1) is presented in fig.5.2, with pitch-chord ratio t/l as parameter, based upon the assumption that the passage shock is just at the leading edge of the blade. In case the throat of the blade passage also happens to lie at the leading edge, this represents the optimum operating condition signified by minimum total pressure losses. KLAPPROTH (5.1) and YAMAGUCHI (4.3) have shown that the losses due to the bow waves are small and hence, they have been neglected for the purposes of calculation.

The wedge type profile CW1 with straight suction surface at entry is characterized by a flat β_∞ relation (see chapter 4.1), which is independent of the pitch chord ratio t/l (fig.5.3). Therefore, the shock loss coefficient $\bar{\omega}_s$ is also independent of t/l (fig.5.2). A considerable increase in the shock loss coefficient is noticed to be a function of the suction surface curvature at inlet, because the flow experiences a large acceleration in front of the shock in case of the DCA-cascade.

As a result of the above explained phenomenon, development of multiple-circular-arc (MCA) profiles (fig.3.7) with a relatively small suction surface curvature at the entrance region has received great emphasis (3.11).

A plot of profile losses $\bar{\omega}_p$, obtained by subtracting the calculated shock losses (fig. 5.2) from the measured total pressure losses, as a function of inlet Mach number M_∞ is shown in figure 5.4. The limited investigations indicate that $\bar{\omega}_p$ is almost independent of the inlet Mach number, the profile shape and the cascade configuration.

6. RELATION BETWEEN STATIC PRESSURE RISE AND TOTAL PRESSURE LOSSES IN A CASCADE

A cascade already started and operating under supersonic conditions, in contrary to the subsonic case, enable a change in the static pressure rise without affecting the inlet flow by varying the downstream pressure.

The variation in the flow field within the blade passage as a result of a change in the throttle position does'nt seem to have been theoretically calculated, because of the complicated and mixed subsonic-supersonic flow field existing together with a severe boundary layer seperation.

To get a better understanding of the flow mechanism of a supersonic cascade, in spite of the complexity of the flow, a simplified flow model has been indicated by DETTMERING (6.1), extended by STARKEN (3.15) for different axial velocity density ratios. This method places its complete emphasis on the flow conditions upstream and downstream of the cascade, without accounting for the probable and possible flow variations within the cascade.

The continuity equation between the inlet and outlet planes of the cascade can be written as:

$$\rho_\infty \, w_\infty \sin \beta_\infty = \rho_2 \, w_2 \sin \beta_2 . \tag{6.1}$$

To account for the contraction of the channel width due to the growth and possible separation of boundary layer on the side walls of the wind tunnel, the "Axial Velocity Density Ratio" Ω is introduced as a parameter into the continuity relation:

$$\Omega \cdot \rho_\infty \cdot w_\infty \sin \beta_\infty = \rho_2 \, w_2 \sin \beta_2 . \tag{6.2}$$

Rewriting in terms of total pressures, static pressures and total temperatures, the above equation can be transformed to get an expression for the total pressure loss coefficient $\bar{\omega}$ as follows:

$$\bar{\omega} = \frac{1}{1 - \frac{p_{tot\,\infty}}{p_\infty}} \cdot \left[\frac{p_2}{p_\infty} \left\{ \frac{1}{2} + \sqrt{\frac{1}{4} + \Omega^2 \cdot \left(\frac{p_{tot\,\infty}}{p_\infty}\right)^{\frac{\kappa-1}{\kappa}} \cdot \left[\left(\frac{p_{tot\,\infty}}{p_\infty}\right)^{\frac{\kappa-1}{\kappa}} - 1 \right] \cdot \left(\frac{\sin \beta_\infty}{\sin \beta_2}\right)^2 \cdot \left(\frac{p_\infty}{p_2}\right)^2 \cdot \frac{T_{tot\,2}}{T_{tot\,\infty}}} \right\}^{\frac{\kappa}{\kappa-1}} - \frac{p_{tot\,\infty}}{p_\infty} \right] \tag{6.3}$$

Under the assumption that the total temperature remains constant, that is

$$T_{tot\,\infty} = T_{tot\,2} \quad \text{(energy equation)}, \tag{6.4}$$

the total pressure loss coefficient $\bar{\omega}$ can be expressed as a functional relation in terms of the pressure ratio p_2/p_∞, the contraction coefficient Ω, the flow angles β_∞ and β_2 and the free stream Mach number M_∞ as follows:

$$\bar{\omega} = f_a \left(\frac{p_2}{p_\infty}, \; \Omega \cdot \frac{\sin \beta_\infty}{\sin \beta_2}, \; M_\infty \right) \tag{6.5}$$

Further simplification is possible for the case wherein the axial component of the inlet velocity is subsonic and M_∞ not too low ($M_\infty > 1{,}2$). For this case, as discussed in detail in chapter 4, the existence of a unique incidence holds valid and therefore $\bar{\omega}$ takes the form:

$$\bar{\omega} = f_b \left(\frac{p_2}{p_\infty}, \; \frac{\Omega}{\sin \beta_2}, \; M_\infty \right) \tag{6.6}$$

The axial velocity density ratio is therefore an independent parameter and can have any value.

Firstly when Ω is constant, the loss coefficient $\bar{\omega}$ is dependent only on the pressure ratio p_2/p_∞, the exit flow angle β_2 and the inlet Mach number M_∞.

To a first approximation, the exit flow angle β_2 is also assumed to be constant. If the value of β_2 is determined experimentally, from the functional relation (eqn.(6.6) derived from the continuity and energy relations) the loss coefficient $\bar{\omega}$ can be worked out in terms of p_2/p_∞.

Fig.6.1 shows a plot of the numerical results calculated on the above said basis for a wedge type profile. A family of curves for different inlet and exit Mach numbers, as shown in full and dotted lines respectively, are presented. The total pressure loss coefficient $\bar{\omega}$ reaches a maximum value when the exit flow Mach number M_2 is unity. The possible range of p_2/p_∞ operation continously becomes larger and larger with increasing M_∞.

The validity of this diagram depends on the existence of exact two-dimensional flow with no contraction of the stream. In a cascade wind tunnel inevitable contraction of the flow stream due to boundary layer effects makes the value of Ω different from unity. This is the reason for showing the curves of different Ω in fig.6.2. Increasing side contraction must result in decreasing pressure loss coefficient, if all the other flow parameters remain unaltered.

Both the diagrams 6.1 and 6.2 only give the common relationship existing between the inlet and the exit planes of a cascade, which have been essentially derived from the energy and continuity equations. Therefore it is impossible to get any insight into the really existing flow phenomena in a cascade.

Although a qualitative discussion of the trend in which the total pressure losses vary is possible, exact evaluation of it without an actual experiment still remains impossible. But an insight into the effect of axial velocity density ratio Ω on the overall performance of the cascade has become possible through this aproach.

To reflect the emphasis of this important parameter, test points of a high turning cascade have been superimposed on the theoretically determined $\bar{\omega}$-curves in fig.6.3 (ref. (3.15)). A strongdeviation from the expected trend, that is variation of Ω with back pressure from 1.0 to 1.7, stresses the great importance of this parameter. A sudden jump in the value of Ω from 1.0 to 1.5 occuring when the cascade changes from accelerating ($p_2/p_\infty < 1$) to decelerating ($p_2/p_\infty > 1$) flow, can be explained by a side wall boundary layer separation occuring in the case where p_2 is larger than p_∞. Further as throttling beyond a certain position causes no influence on (p_2/p_∞), it could be argued out that there must be naturally a contraction of the stream tube exhibited by an increase in Ω from 1.5 to 1.7.

From these test results it is strongly felt necessary that the axial-velocity-density ratio Ω has to be taken care off in all supersonic cascade measurements.

ACKNOWLEDGEMENTS

The authors wish to express her gratitude for the help given by M.R.Narasimha Swamy (National Aeronautical Laboratory, Bangalore) in the translation of this paper.

REFERENCES

Chapter 1

(1.1) WEISE, A. — Überschallaxialverdichter. Bericht 171 der Lilienthal-Gesellschaft, S.92 (1943).

(1.2) DAVIDSON, B. — Some Data Pertaining to the Supersonic Axial-Flow Compressor. ARC R&M No.2554 (1947).

(1.3) HAWTHORNE, W.R. (Editor) — High Speed Aerodynamics and Jet Propulsion, Volume X, Aerodynamics of Turbines and Compressors (1964).

(1.4) KANTROWITZ, A. — The Supersonic Axial-Flow Compressor. NACA Report 974 (1950).

(1.5) REDDING, A.H. — Superacoustic Compressor. US Patent 2, 435, 236 (1948).

(1.6) FERRI, A. — Preliminary Analysis of Axial-Flow Compressors Having Supersonic Velocity at the Entrance of the Stator. NACA RM L 9G06 (1949).

(1.7) HOTTNER, Th. — Amerikanische Versuche mit Überschallverdichtern. AVA-Bericht Nr. 59/A/25, (1959).

(1.8) LIEBLEIN, S., JOHNSEN, I.A. — Résumé of Transonic Compressor Research at NACA Lewis-Laboratory. Trans.ASME "Journal of Engineering for Power", 83 (1961), Series A, No.3.

(1.9) SAVAGE, M., BOXER, E., ERWIN, J.R. — Résumé of Compressor Research at the NACA Langley Laboratory. Trans.ASME "Journal of Engineering for Power", 83, (1961), Series A.

(1.10) KLAPPROTH, J.F. — A Review of Supersonic Compressor Development. Trans.ASME "Journal of Engineering for Power", Series A, 83 (1961), S.258.

(1.11) JOHNSON, E.G. — Introduction to Lectures on Supersonic Turbomachinery. AGARD Lecture Series, Varenna, May (1967).

(1.12) CHAUVIN, J., BREUGELMANS, F., JANIGRO, A. — Supersonic Compressors. AGARD Lecture Series, Varenna, May (1967), also: VKI CN 67.

Chapter 2

(2.1) EMMONS, H.W. (Editor) — Fundamentals of Gas Dynamics, High Speed Aerodynamics and Jet Propulsion Vol.III, (1958).

(2.2) DEICH, M.E. — Flow of Gas through Turbine Lattices. NACA TM 1393 (1956). Transl.of ch.7 from Tekhnickes Kaia Gazodinamika (1953).

(2.3) LAWACZECK, O. — Verfahren zur Ermittlung der Abströmgrößen transsonischer Turbinengitter. Diss.TU Braunschweig (1969).

(2.4) EGGINK — Strömungsaufbau und Druckrückgewinnung in Überschallkanälen. Deutsche Luftfahrtforschung. Forschungsbericht Nr.1756, (1943).

(2.5) KANTROWITZ, A., DONALDSON, C. — Preliminary Investigation of Supersonic Diffusers. NACA ACR No.L5D20, (1945).

Chapter 3

(3.1) SHAPIRO, A.H. — The Dynamics and Thermodynamics of Compressible Fluid Flow. Vol.I, The Ronald Press Corp., 1953, N.Y.

(3.2) STRATFORD, B.S., SANSOME, G.E. — Theory and Tunnel Tests of Rotor Blades for Supersonic Turbines. ARC R&M No.3275, 1962.

(3.3) BOXER, E., STERRET, J.R., WLODARSKI, J. — Application of Supersonic Vortex-Flow Theory to the Design of Supersonic Impulse Compressor or Turbine-Blade Sections. NACA RM L 52 B 06. April 1952.

(3.4) OSWATITSCH, K. — Potentialwirbel-Gitter für Überschallgeschwindigkeiten. ZfW 4, (1956), Heft 1/2, Seite 53.

(3.5) COLCLOUGH, C.D. Design of Turbine Blades Suitable for Supersonic Relative Inlet Velocities and the Investigation of their Performance in Cascades:
Part I - Theory and Design.
Journal Mechanical Engineering Science Vol.8, No.1,1966.
Part II - Experiments, Results and Discussion.
Journal Mechanical Engineering Science Vol.8, No.2, (1966).

(3.6) GOLDMAN, L.J., SCULLIN, V.J. Analytical Investigation of Supersonic Turbomachinery Blading.
I - Computer Program for Blading Design.
NASA TN D-4421, March 1968.

(3.7) GOLDMAN, L.J. Analytical Investigation of Supersonic Turbomachinery Blading.
II- Analysis of Impulse Turbine-Blade Sections.
NASA TN D - 4422, April 1968.

(3.8) LICCINI, L.L. Analytical and Experimental Investigation of 90° Supersonic Turning Passages Suitable for Supersonic Compressors or Turbines.
NACA RM L 9G07, 1949.

(3.9) LICCINI, L.L. Experimental Investigation of the Mixing Loss Behind the Trailing Edge of a Cascade of Three 90° Supersonic Turning Passages.
NACA RM L 50F21a, 1950.

(3.10) OSWATITSCH, K. Über die Strömung in einem Überschallgitter.
Allgemeine Wärmetechnik, Jahrgang 6, 1955.

(3.11) SEYLER, D.R., SMITH, L.H. Single Stage Experimental Evaluation of High Mach Number Compressor Rotor Blading,
Part 1, Design of Rotor Blading.
NASA CR-54581, April 1967.

(3.12) GOSTELOW, J.P., KRABACHER, K.W., SMITH, L.H.(Jr.) Performance Comparisons of High Mach Number Compressor Rotor Blading.
NASA CR-1256, 1968.

(3.13) EMERY, J.C., DUNAVANT, J.C., WESTPHAL, W.R. Experimental Investigation of a Transonic Compressor Cascade and Test Results for Four Blade Sections.
NASA TM X 197, Jan.1960.

(3.14) HEILMANN, W., STARKEN, H., WEYER, H. Cascade Wind Tunnel Tests on Blades Designed for Transonic and Supersonic Compressors.
in "Advanced Components for Turbojet Engines", Part 1,
AGARD CP No.34, 1968.

(3.15) STARKEN, H., LICHTFUß, H.J. Some Experimental Results of Two-Dimensional Compressor Cascades at Supersonic Inlet Velocities.
To be published in "Trans.of ASME", Journal of Engineering for Power.

(3.16) OSWATITSCH, K. Pressure Recovery for Missiles with Reaction Propulsion at High Supersonic Speeds.
NACA TM 1140, 1947.

(3.17) GRAHAM, C., KLAPPROTH, J.F., BARINA, F.J. Investigation of Off-Design Performance of Shock-In-Rotor Type Supersonic Blading.
NACA RM E51C22 (1951).

(3.18) CREAGH, J.W.R., KLAPPROTH, J.F. Utilization of External-Compression Diffusion Principle in Design of Shock-in-Rotor Supersonic Compressor Blading.
NACA RM E 53F18, 1953.

(3.19) JAHNSEN, L.J., HARTMANN, M.J. Investigation of Supersonic Compressor Rotors Designed with External Compression.
NACA RM E 54 G 27a, 1954.

(3.20) FRÜHAUF, H.H. DFVLR, unpublished.

(3.21) BEDER, E.D., BUHLER, R. A study of a Cascade System for Supersonic Flow Diffusion.
WADC TR-54-261, (1954).

(3.22) LOWN, H., HARTMANN, M.J. Investigation of a 24-Inch-Shock in Rotor Type Supersonic Compressor. Designed for Simple Radial Equilibrium Behind Normal Shock.
NACA RM E51H08, 1951.

(3.23) FEJER, A.A., WENZLAU, W.N. Supersonic Cascades Studies
TR No.AEI
Research Foundation, Univ.of Toledo (1951).

(3.24) CONRAD, O. — Statistische Untersuchung von Überschallverdichtern. WGLR-Jahrbuch 1965, Seite 374.

(3.25) WILCOX, W.W. — Investigation of Impulse-Type Supersonic Compressor with Hub-Tip Ratio of 0.6 and Turning to Axial Direction. II-Stage Performance with Three Different Sets of Stators. NACA RM E 55 F 28, 1955.

(3.26) HARTMANN, M.J., TYSL, E.R. — Investigation of a Supersonic-Compressor Rotor with Turning to Axial Direction. II-Rotor Component Off-Design and Stage Performance. NACA RM E 53L24, 1953.

(3.27) SCHMALFUß, H.G. — Experimentelle Untersuchungen an stark umlenkenden Überschall-verzögerungsgittern. Forschungsberichte des Landes Nordrhein-Westfalen Nr.1677 (1966).

(3.28) KLAPPROTH, J.F., ULLMAN, G.N., TYSL, E.R. — Performance of an Impulse-Type Supersonic Compressor with Stators. NACA RM E 52 B 22 (1952).

(3.29) JOHNSON, E.G., von OHAIN, H., LAWSON, M.O., CRAMER, K.R. — A Blunt Trailing Edge Supersonic Compressor Blading. WADC TN 59-269, (1959).

(3.30) CHAUVIN, J. — The Concept of Blunt Trailing Edge Blading for Use in Supersonic Compressors. Jahrbuch der WGLR, (1962), S.179.

(3.31) CHAUVIN, J. — Research on the Concept of Blunt Trailing Edge Blades. Part I - High Speed Range. AF EOAR GRANT 63-84, SR1(1964).

(3.32) CHAUVIN, J. — Research on the Concept of Blunt Trailing Edge Blades GRANT AF EOAR 64-4 (1965).

(3.33) CHAUVIN, J., BREUGELMANS, F. — Research on the Use of Blunt Trailing Edge Blades in Supersonic Compressor Stages. GRANT AF EOAR 65-65, SR 1 (1966).

(3.34) HEILMANN, W., WEYER, H. — Untersuchungen am Überschall-Gitterwindkanal. Aufbau der NACA-6-inch-Überschall-Meßstrecke in der DVL, Entwicklung des Meßsystems und erste Versuchsergebnisse. DLR FB 68-28, (1968).

(3.35) WENNERSTRÖM, A.J., JOHNSON, E.G., CARMAN, C.T. — Experimentally Determined Shock Configurations in a High-Solidity Supersonic Rotor. Advanced Components for Turbojet-Engines, Part 1., AGARD Conference Proceedings No.34, (1968).

(3.36) CARMAN, C.T., MYERS, J.R., WENNERSTRÖM, A.J., STEURER, J.W. — Experimental Investigation of Two-Blunt Trailing Edge Supersonic Compressor Rotors of Different Blade Thicknisses and with Circular Arc Camber Line. AEDC-TR-68-197 (1968).

(3.37) NUSSDORFER, T.J. — Some Observations of Shock-induced Turbulent Separation on Supersonic Diffusers. NACA RM E 51L26, 1951.

(3.38) PEARCEY, H.H. — Some Effects of Shock-induced Separation of Turbulent Boundary Layers in Transonic Flow past Aerofoils. ARC R&M No.3108, 1959.

Chapter 4

(4.1) LEVINE, P. — The Two Dimensional Inflow Conditions for a Supersonic Compressor with Curved Blades. WADC TR 55-387 (1956).

(4.2) LEVINE, P. — Two Dimensional Inflow Conditions for a Supersonic Compressor with Curved Blades. Journ.of Appl.Mech.Vol24, No.2, (1957).

(4.3) YAMAGUCHI, S. — On the Inlet-Flow Field for a Two-Dimensional Supersonic Cascade with Curved Entrance Regions. Bulletin of JSME Vol.7, No.25, (1964).

(4.4) SCHWAAR, P. — Determination of the Stationary Flow Field in Front of a Supersonic Cascade. Jorn.of Aeron.Sci., Vol.23, No.10 (1956).

(4.5) STRATFORD, B.S., SANSOME, G.E. — The Performance of Supersonic Turbine Nozzles. R&M No.3273 (1962).

(4.6) OSWATITSCH, K. — Das Ausbreiten von Wellen endlicher Amplitude. ZfW 10, Heft 4/5, (1962), S.130.

(4.7) LICHTFUß, H.J. — Die Berechnung der ebenen Überschallströmung, einschließlich schwacher Verdichtungsstöße, mit Hilfe des Analytischen Charakteristikenverfahrens. Erscheint als DLR-FB.

(4.8) COURANT, R., FRIEDRICHS, K.O. — Supersonic Flow and Shock Waves. Pure and Applied Mathematics Vol.1, N.Y.(1948).

(4.9) MOECKEL, W.E. — Approximate Method for Predicting Form and Location of Detached Shock Waves ahead of Plane or Axially Symmetric Bodies. NACA TN 1921, (1949).

(4.10) STARKEN, H. — Untersuchung der Strömung in geraden Überschallverzögerungsgittern. Erscheint als DLR-Forschungsbericht.

(4.11) NOVÁK, O. — Flow in the Entrance Region of a Supersonic Cascade. Strojnícky Časopis XIX, č.2-3, Seite 138 (1967), Vydavatel'stvo, Slovenskej Akadémie vied Bratislava.

(4.12) GOSTELOW, J.P., KRABACHER, K.W. — Single Stage Experimental Evaluation of High Mach Number Compressor Rotor Blading Part 5 - Performance of Rotor 2 B, NASA CR-54585, October 1967.

(4.13) MILLER, G.R., HARTMANN, M.J. — Experimental Shock Configurations and Shock Losses in a Transonic-Compressor Rotor at Design Speed. NACA RM E58A14b (1958).

Chapter 5

(5.1) KLAPPROTH, J.F. — Approximate Relative-Total-Pressure Losses of an Infinite Cascade of Supersonic Blades with Finite Leading-Edge Thickness. NACA RM E 9L21 (1950).

Chapter 6

(6.1) DETTMERING, W., BECKER, B. — Steps in the Development of a Supersonic Compressor Stage. Advanced Components for Turbojet Engines Part I AGARD CP No.34 (1968).

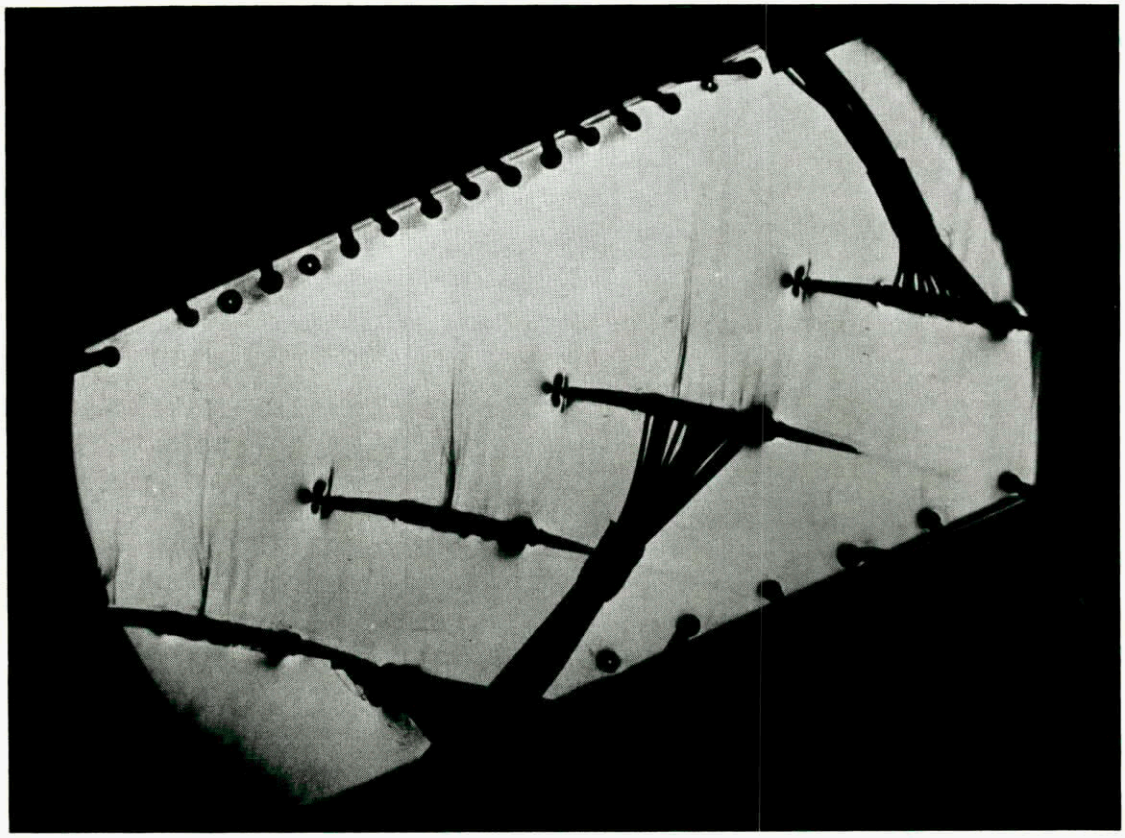

Fig.2.1: Schlieren picture of "Double circular Arc" (DCA)-cascade at subsonic inlet Mach number, M_∞ = 0.9.

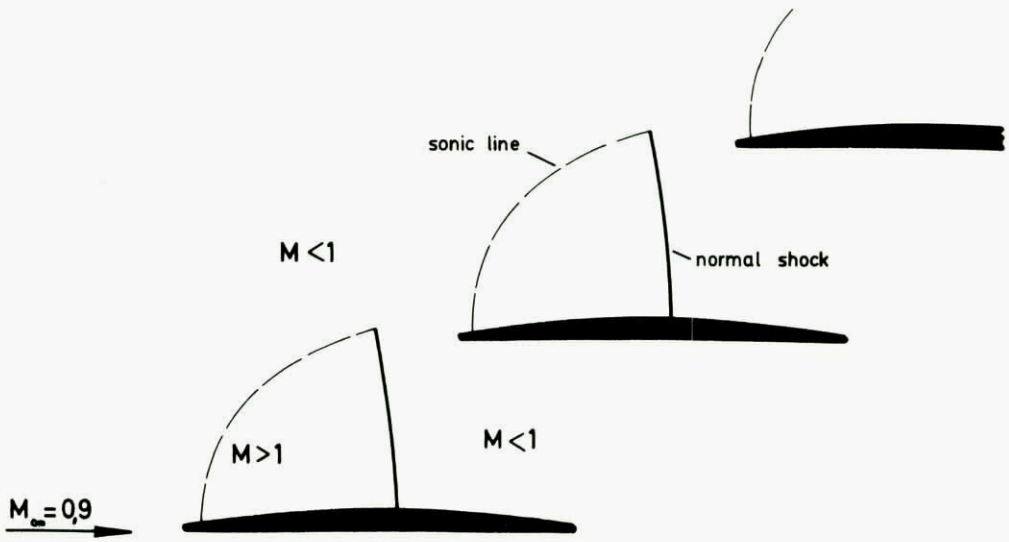

Fig.2.2: Diagrammatic view of Schlieren picture of fig.2.1.

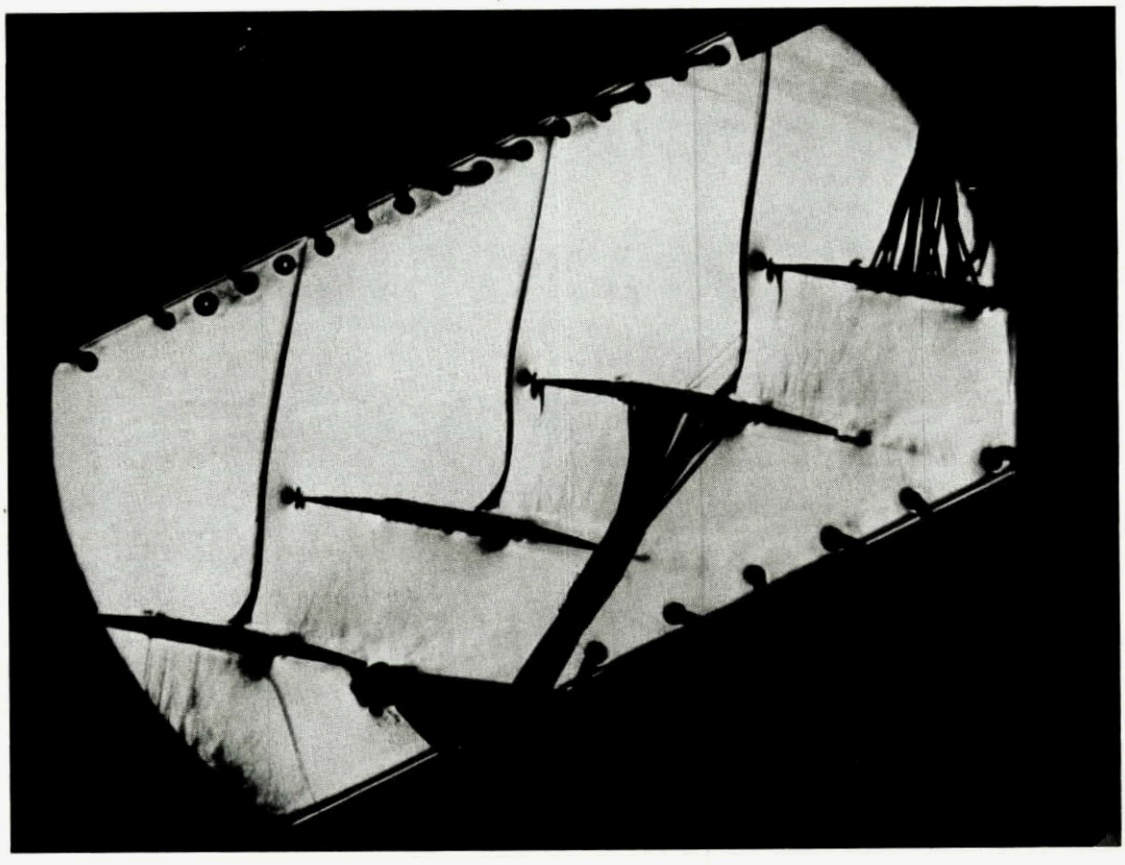

Fig.2.3: DCA-cascade at near sonic inlet velocity, M_∞ = 1.03.

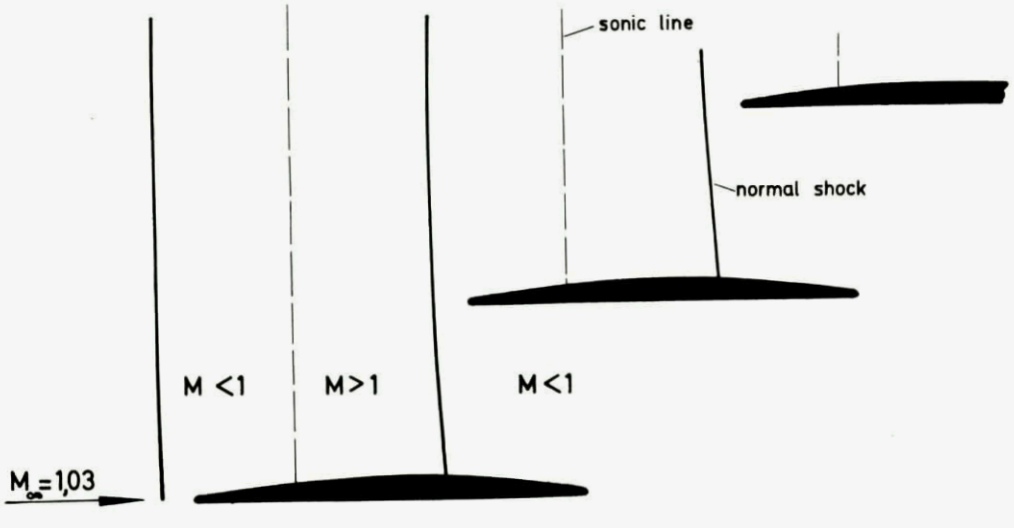

Fig.2.4 Diagrammatic view of fig.2.3.

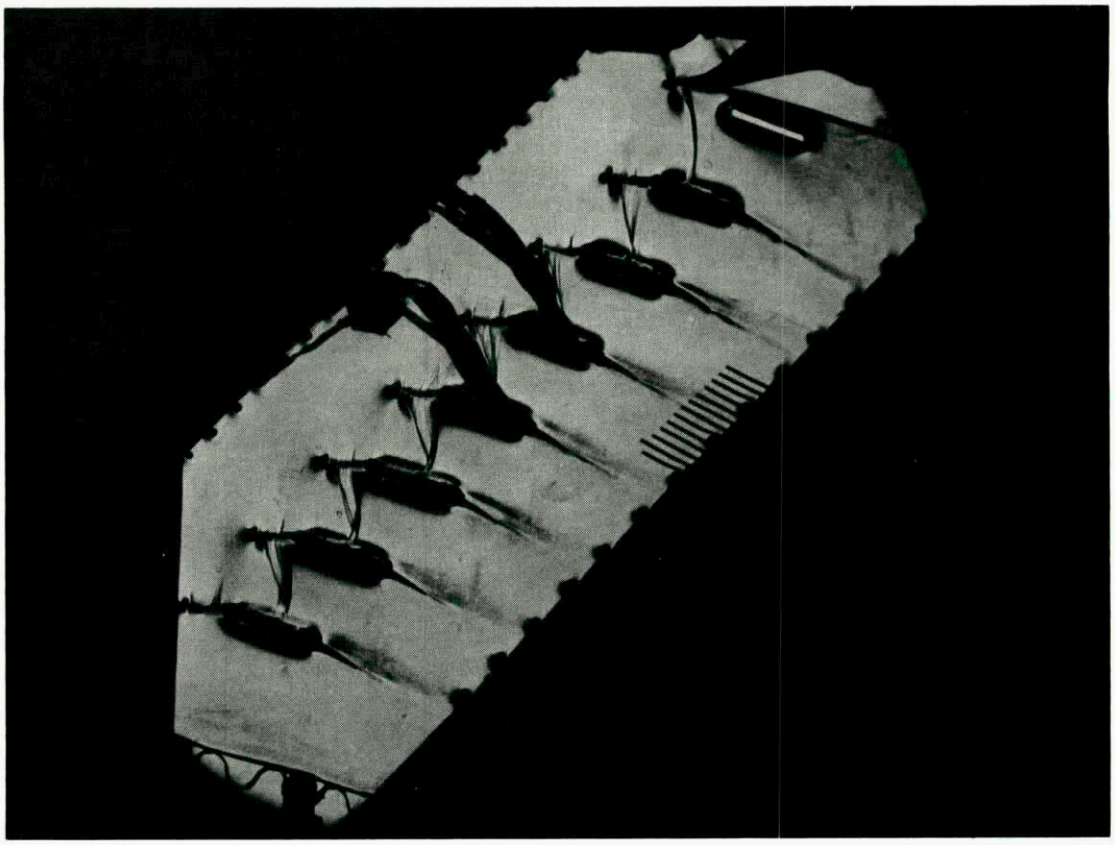

Fig.2.5: DCA-cascade at choked inlet.flow conditions, $M_\infty = 0.9$.

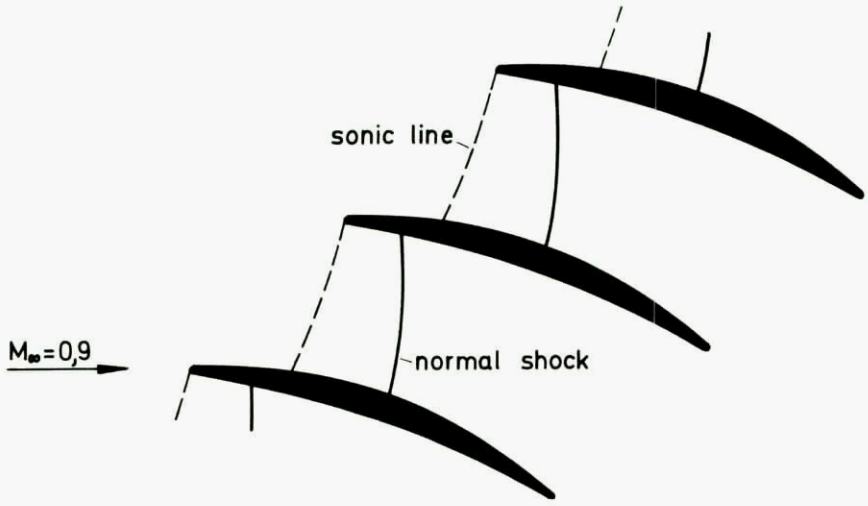

Fig.2.6: Diagrammatic view of fig.2.5.

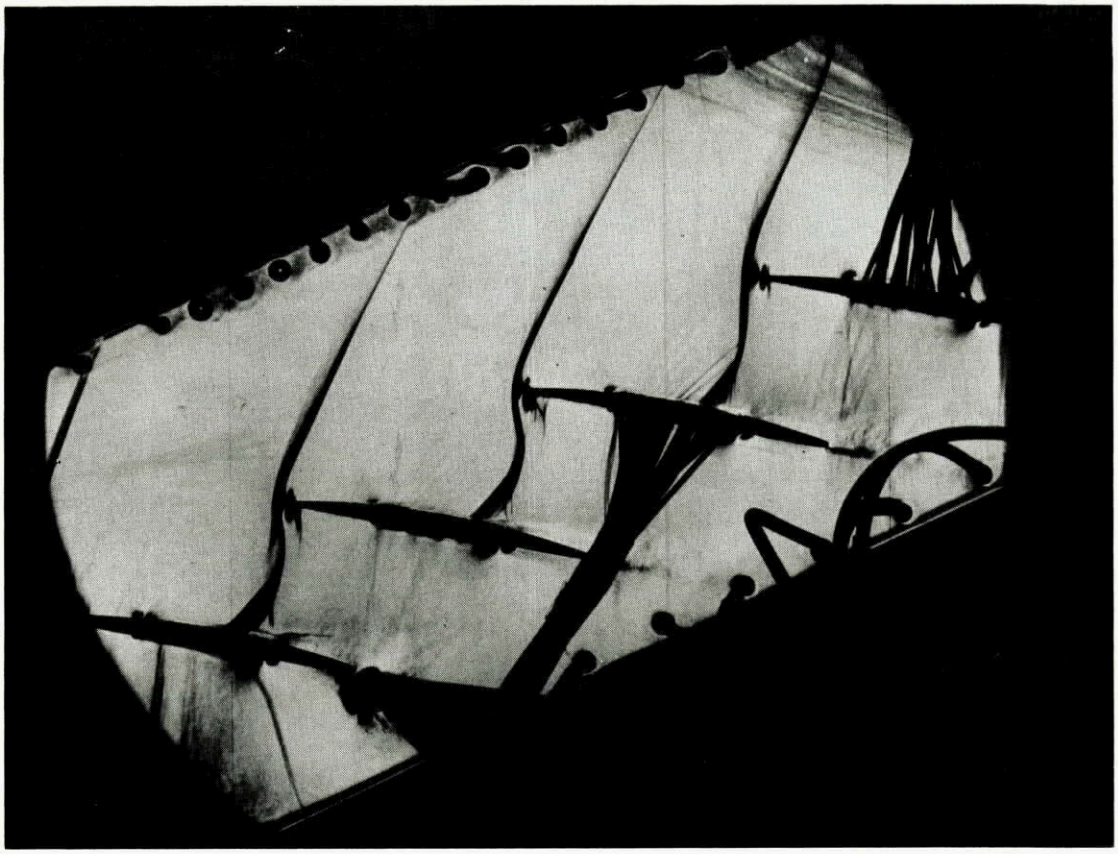

Fig.2.7: DCA-cascade at low supersonic inlet velocity, $M_\infty = 1.10$.

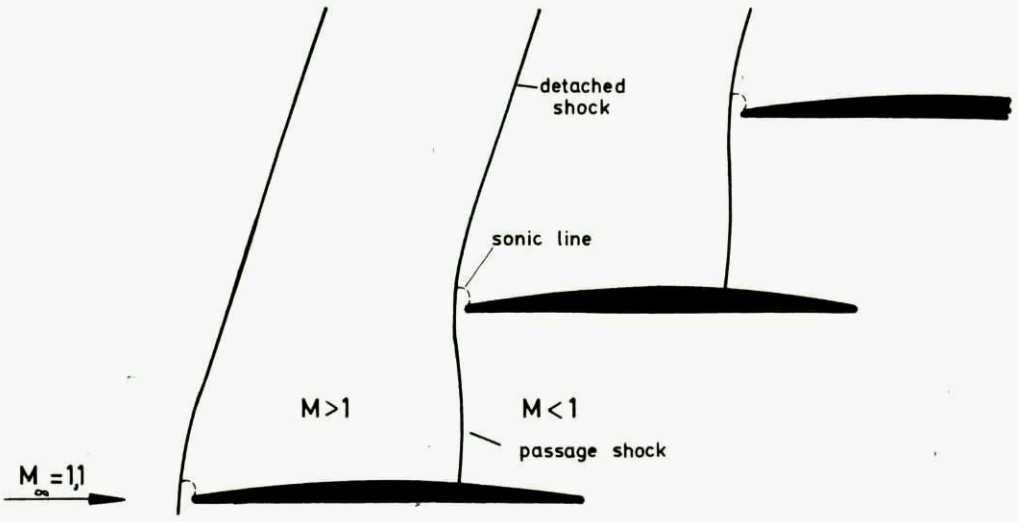

Fig.2.8: Diagrammatic view of fig.2.7.

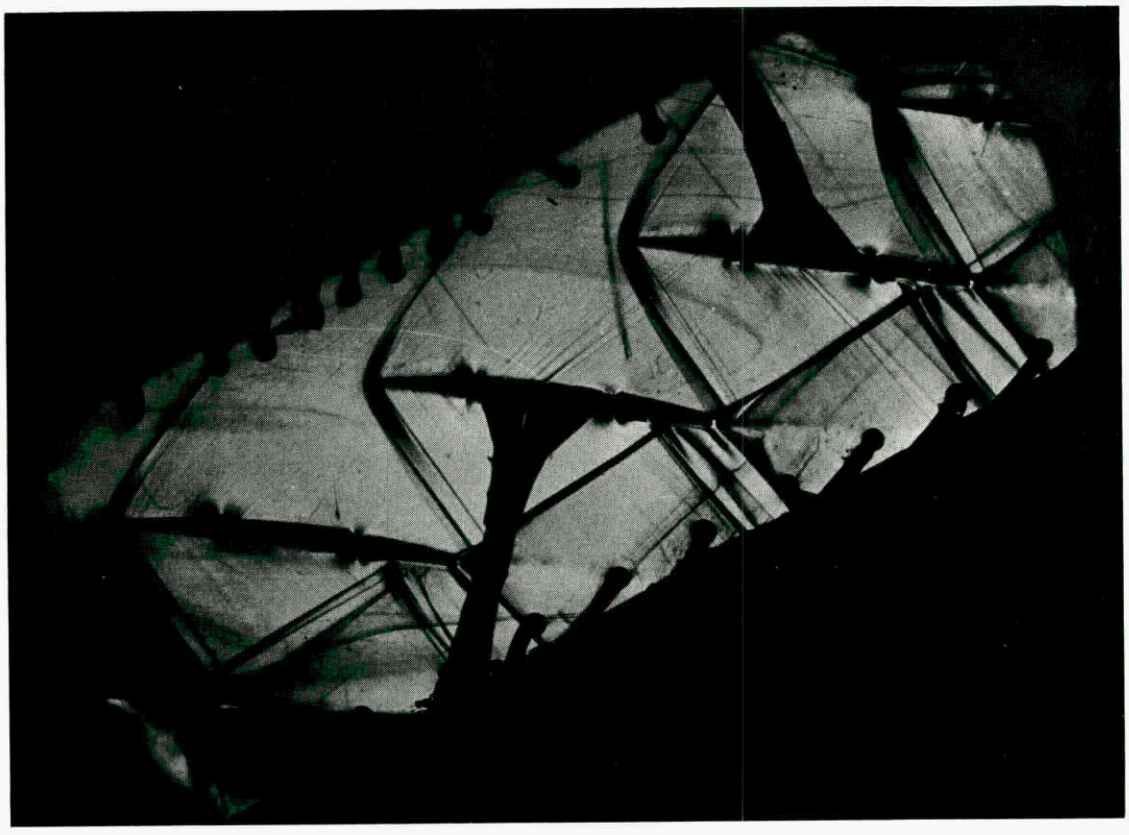

Fig.2.9: DCA-cascade at supersonic inlet velocity, $M_\infty = 1.30$.

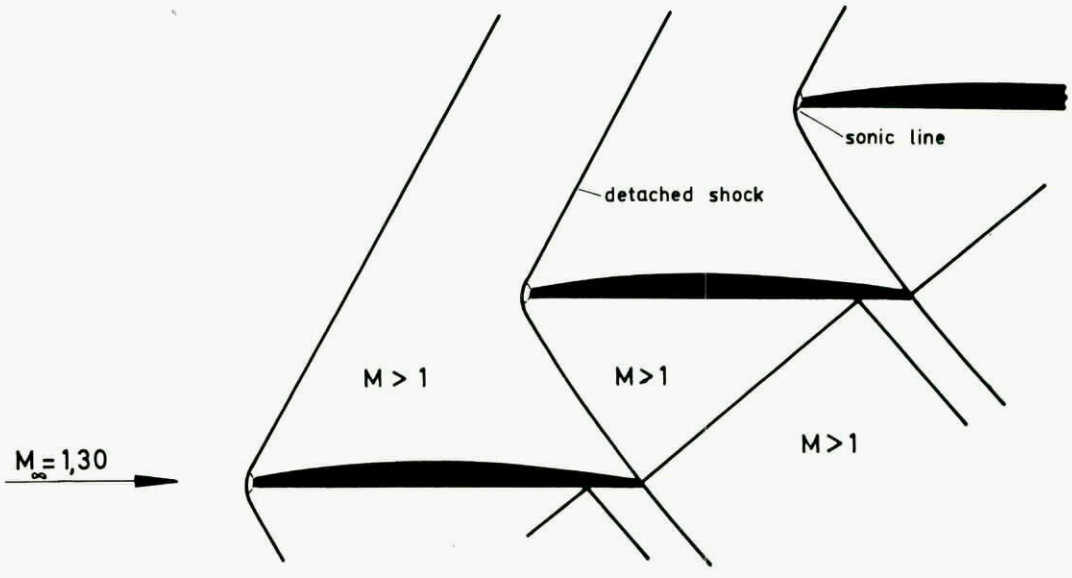

Fig.2.10: Diagrammatic view of fig.2.9.

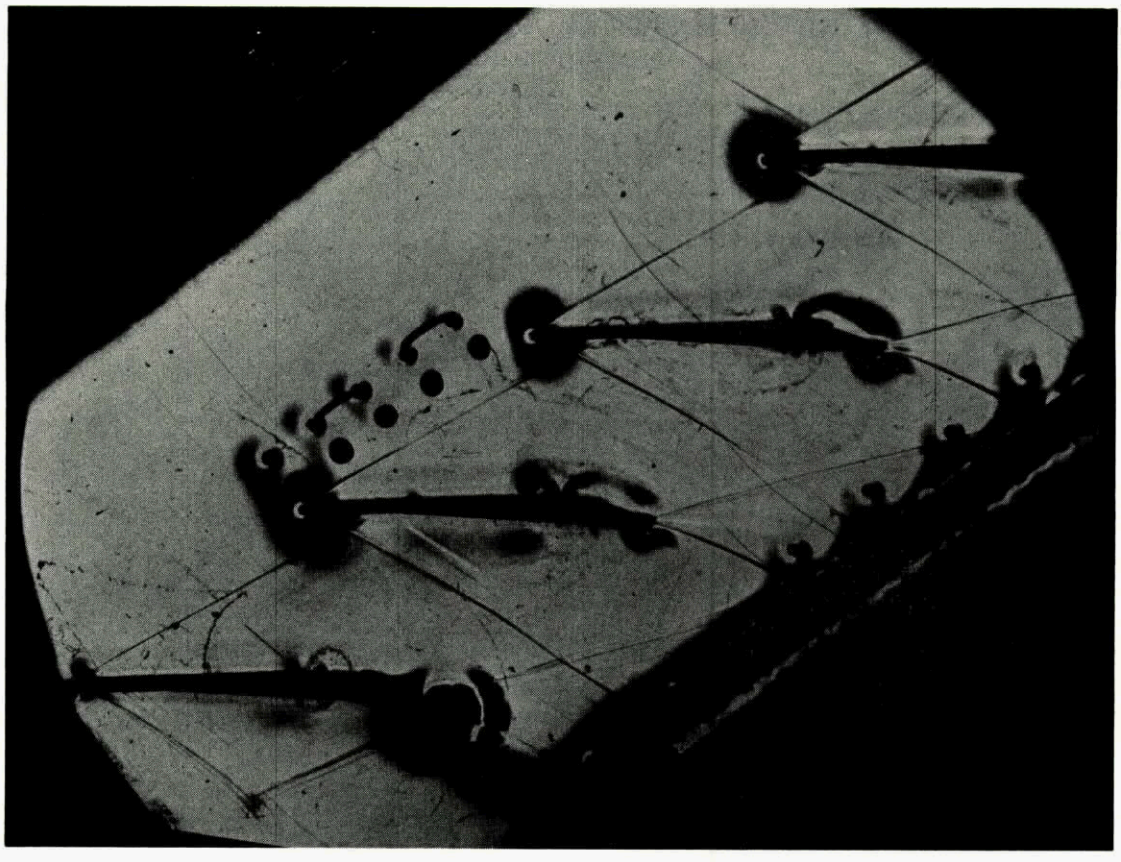

Fig.2.11: Schlieren picture of "Circular Wedge" (CW1) cascade at axial supersonic inlet Mach number, $M_\infty = 2.0$.

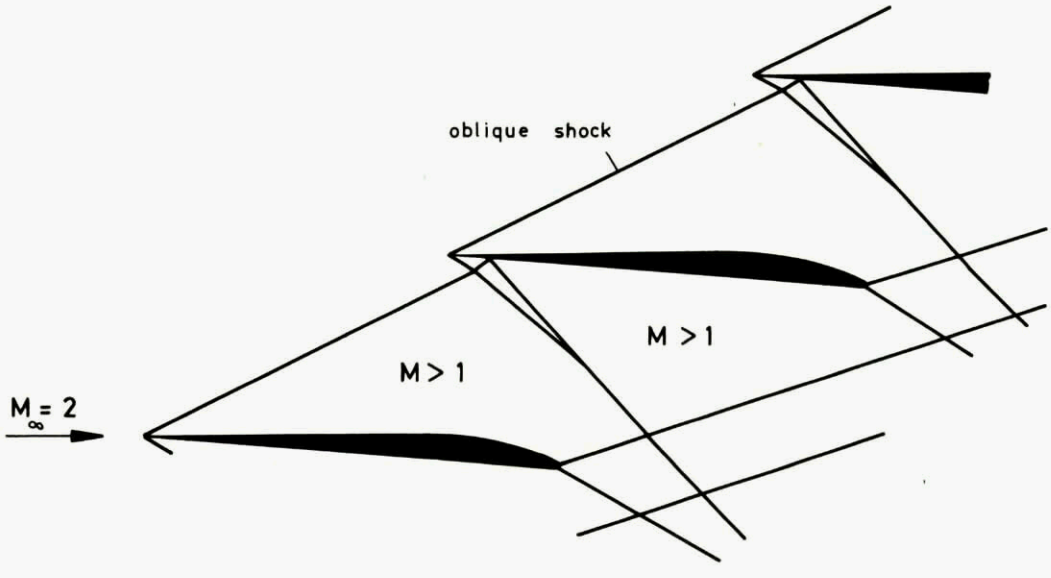

Fig.2.12: Diagrammatic view of Schlieren picture of fig.2.11.

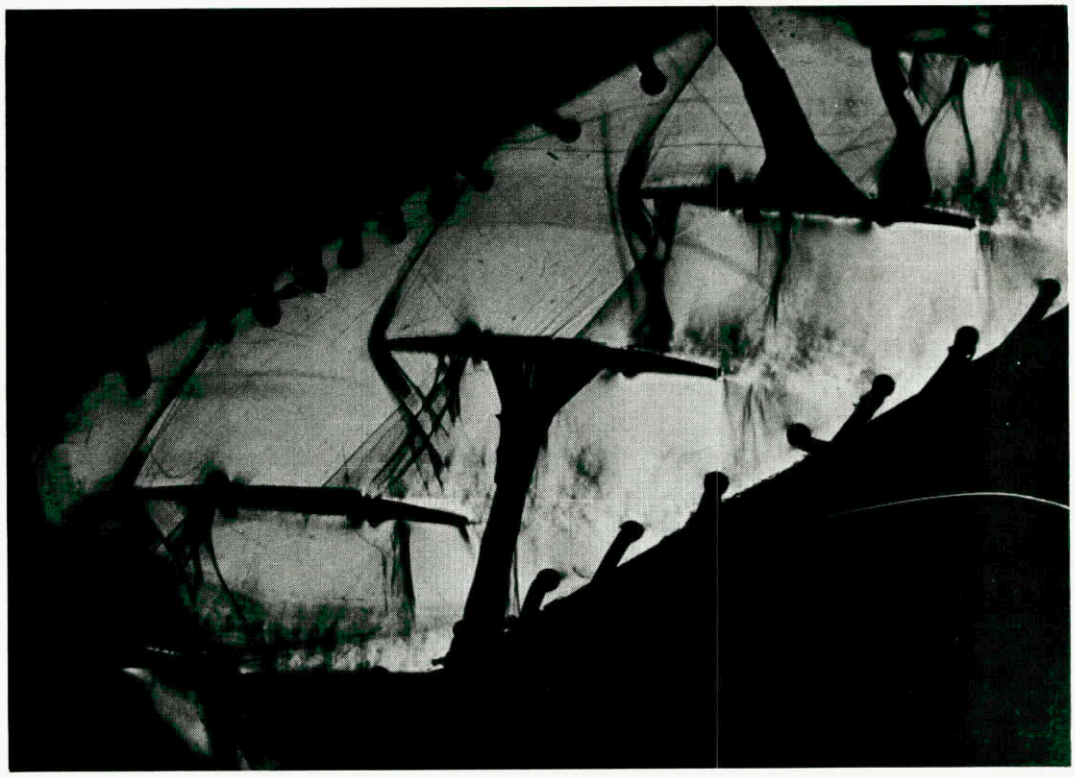

Fig.2.13: Schlieren picture of DCA-cascade at M_∞ = 1.3 and medium pressure ratio p_2/p_∞ = 1.52.

Fig.2.14: Schlieren picture of DCA-cascade at M_∞ = 1.27 and maximum pressure ratio p_2/p_∞ = 1.51.

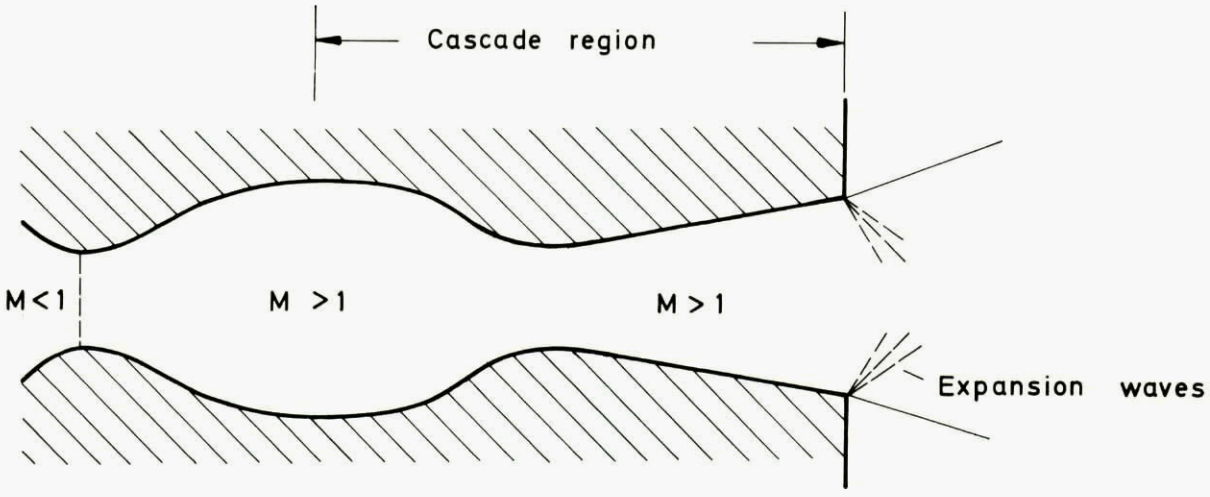

Fig.2.15

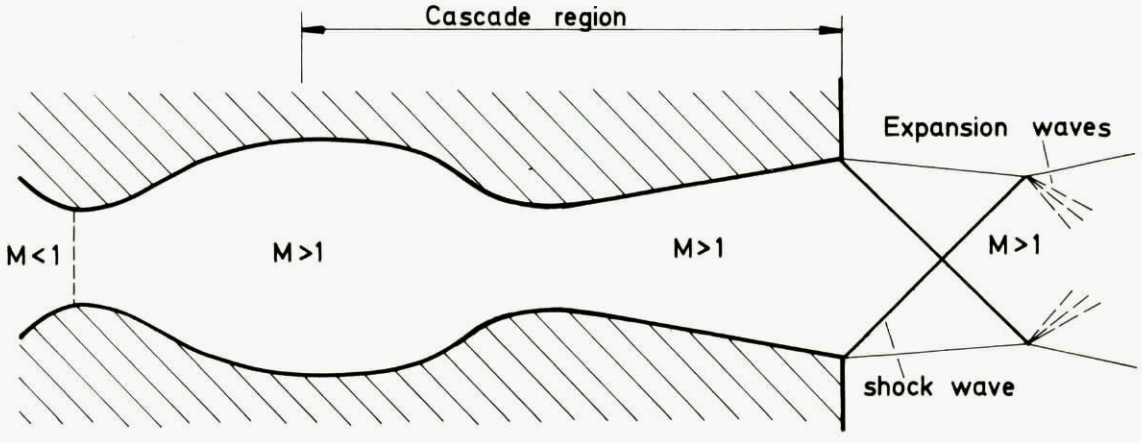

Fig.2.16

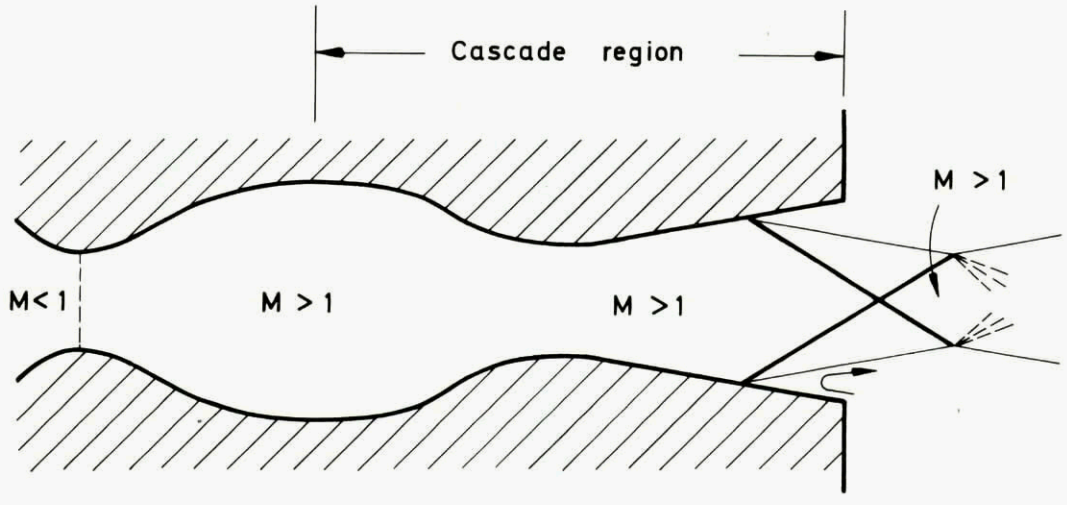

Fig.2.17: Flow patterns in a real Laval nozzle for varying back pressures.

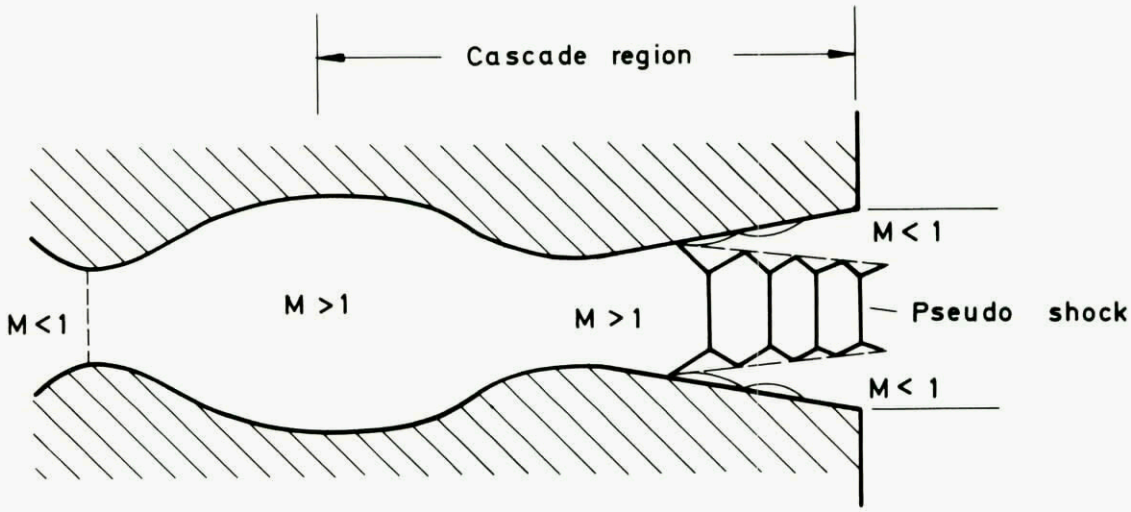

Fig.2.18

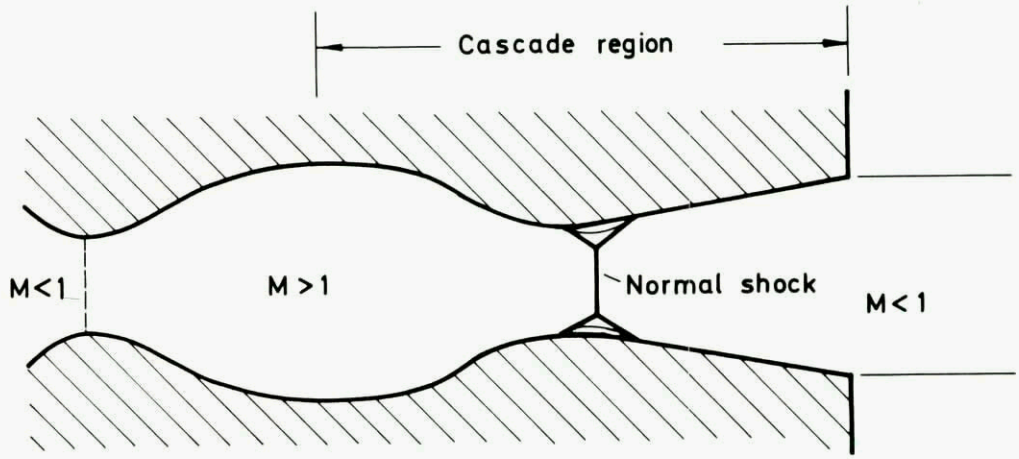

Fig.2.19

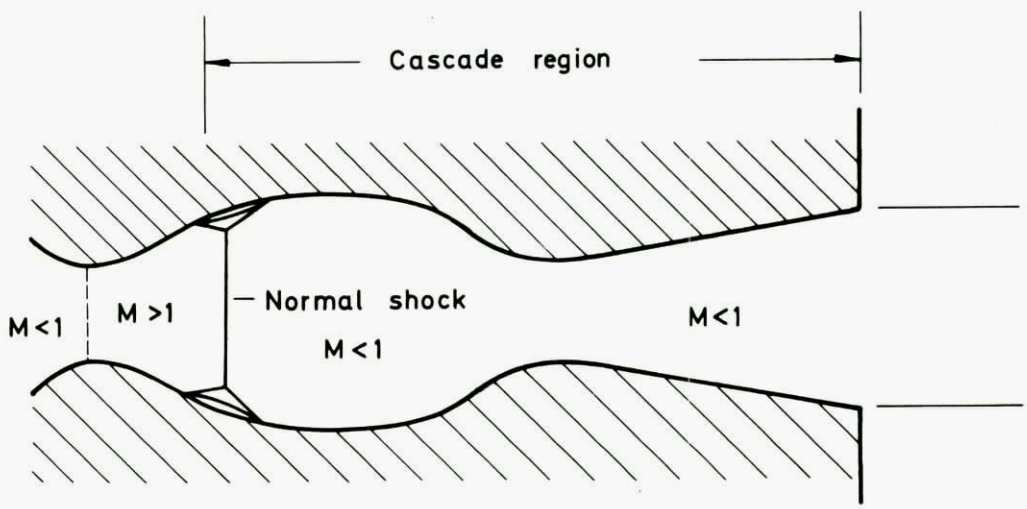

Fig.2.20 Flow patterns in a real Laval nozzle for varying back pressures.

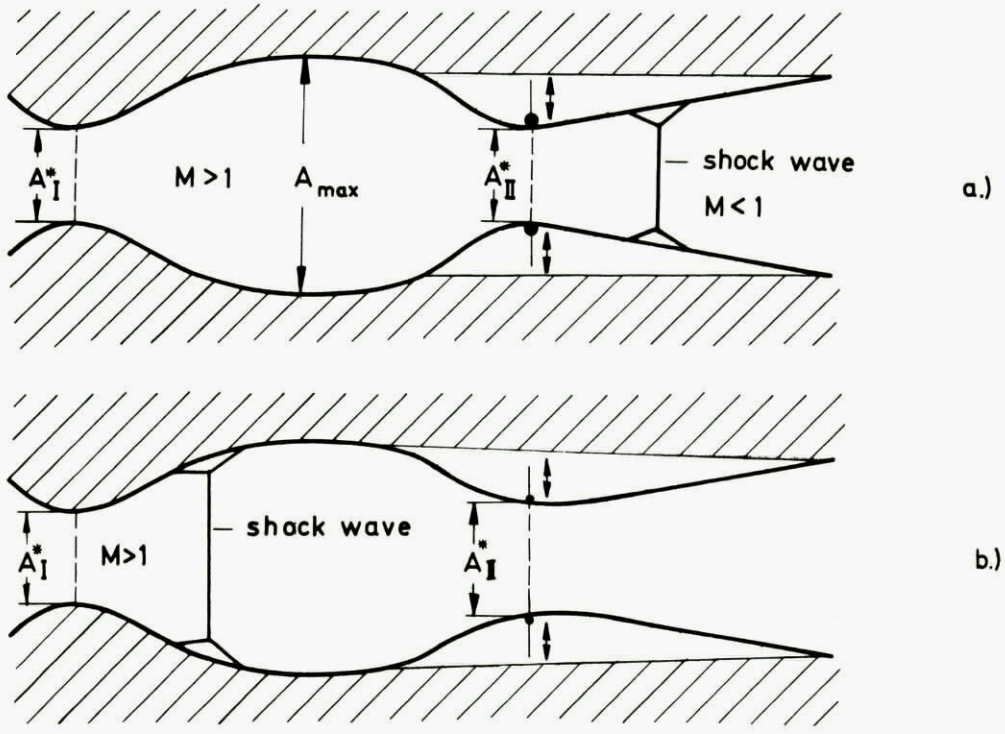

Fig.2.21: Ideal double throat supersonic Laval nozzle under different operating conditions.

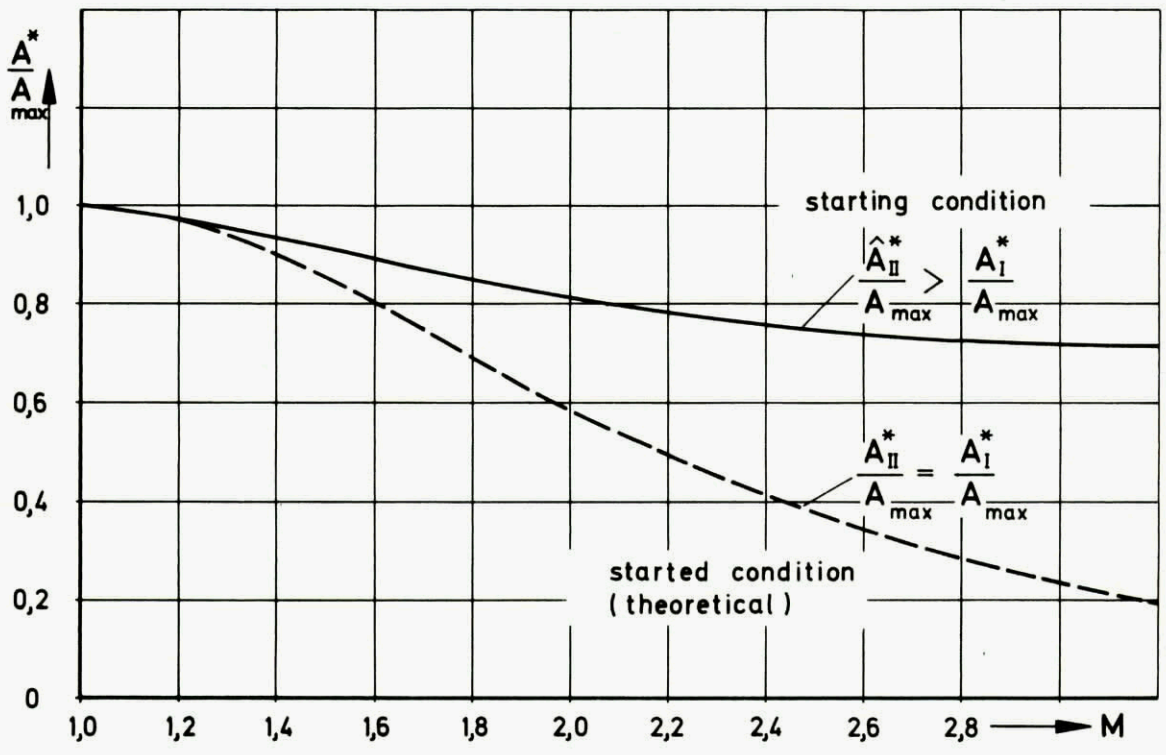

Fig.2.22: Area ratios of started and starting supersonic diffuser as a function of inlet Mach number.

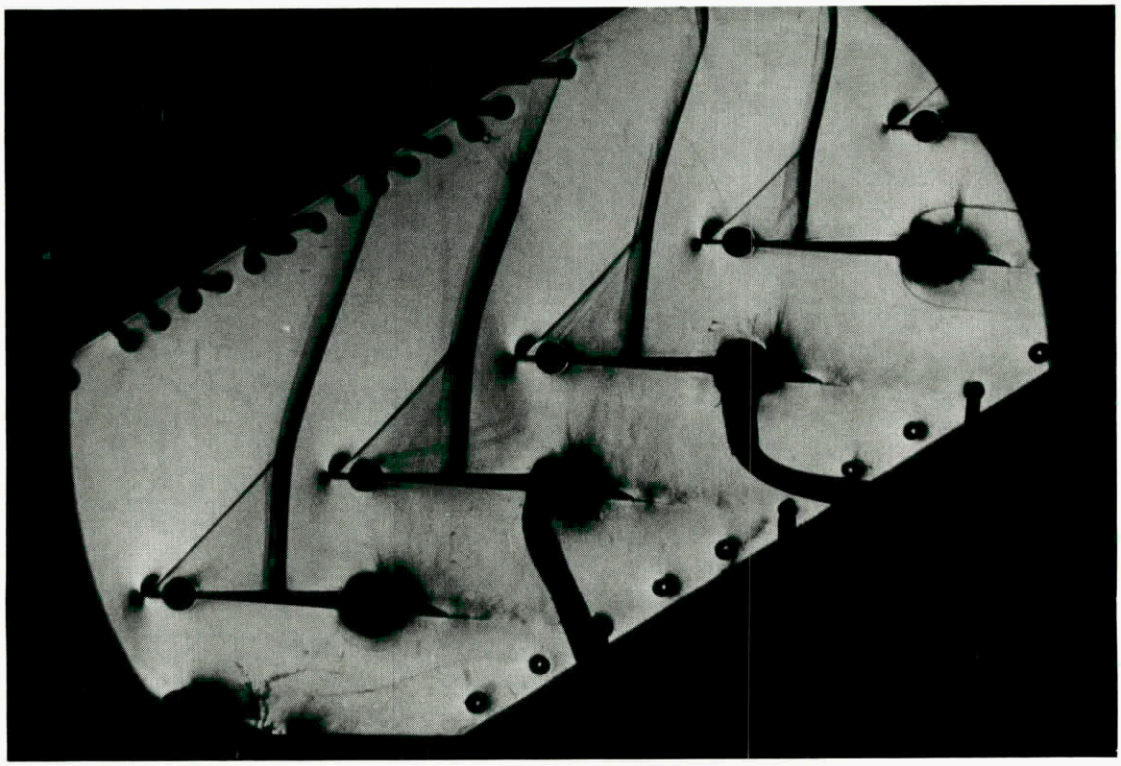

Fig.2.23: Schlieren picture of an unstarted cascade (CW1, t/l = 0.7, $\beta_s = 145^o$ and $M_\infty = 1.1$).

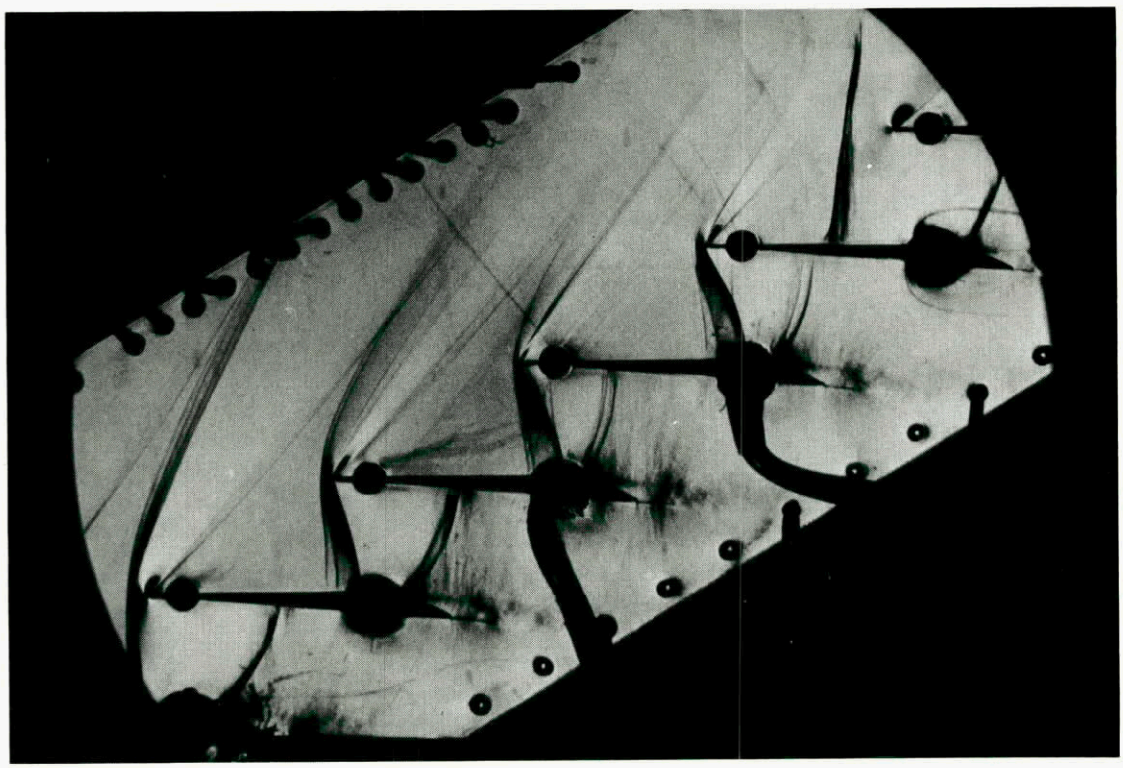

Fig.2.24: Schlieren picture of a started cascade (CW1, t/l = 0.7, $\beta_s = 145^o$ and $M_\infty = 1.24$).

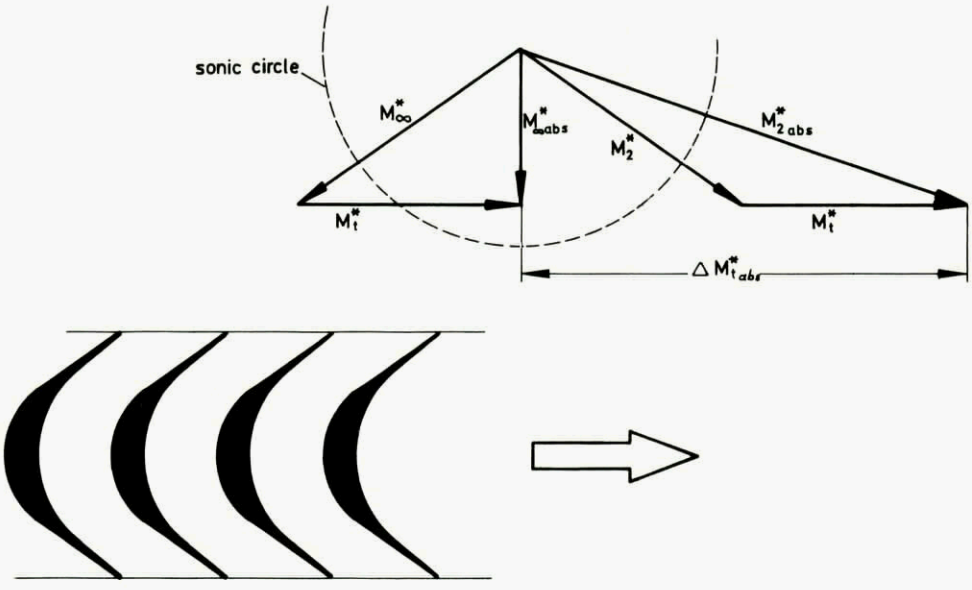

Fig.3.1a: Velocity triangles of high turning supersonic impulse cascade: $M_2^* = M_\infty^*$.

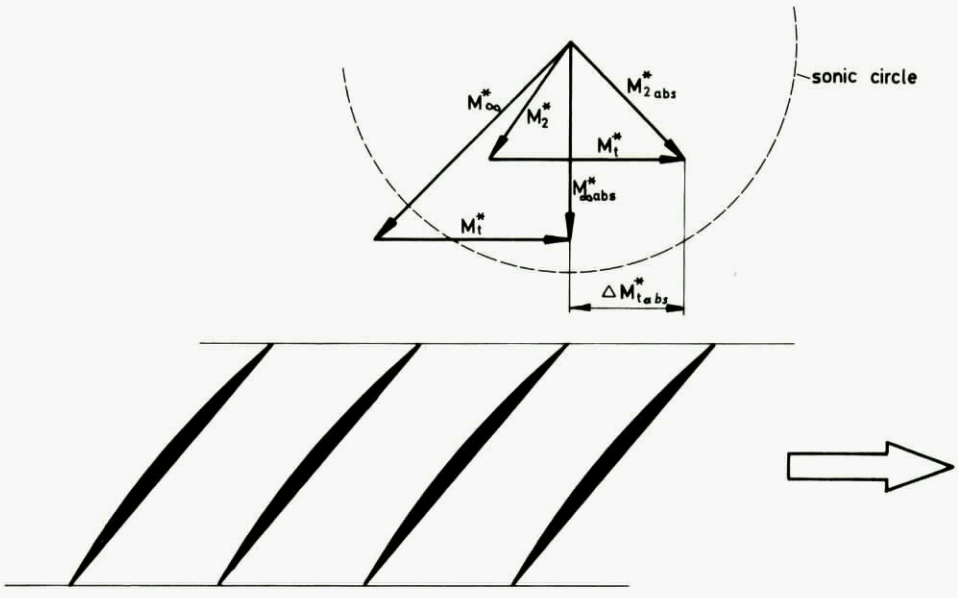

Fig.3.1b: Velocity triangles of low turning supersonic decelerating cascade: $M_2^* < M_\infty^*$.

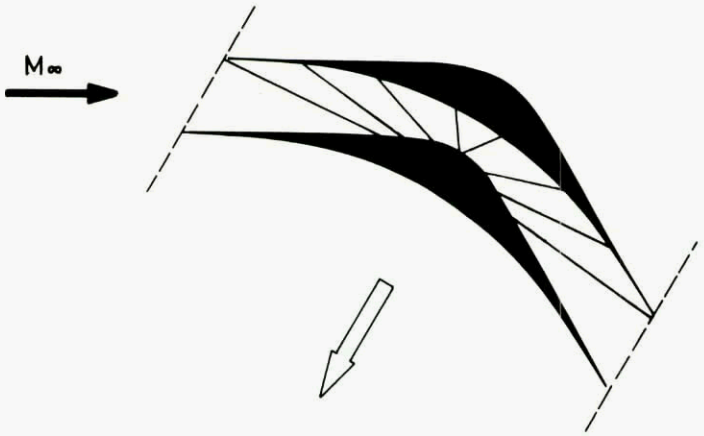

Fig.3.2: Supersonic impulse blade section of ref.(3.1).

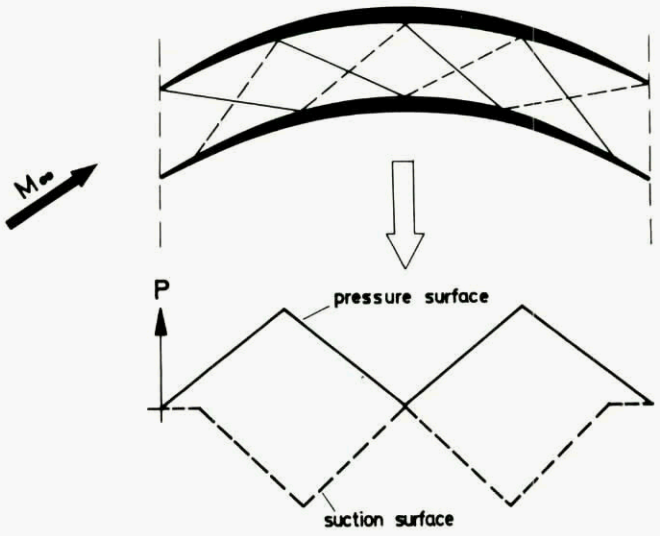

Fig.3.3: Zig-Zag pressure distribution in a blade passage of constant curvature of ref.(3.2).

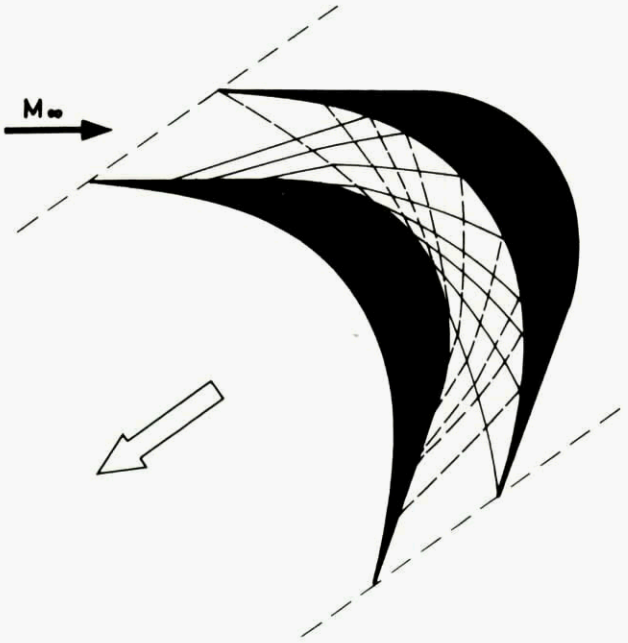

Fig.3.4: Supersonic impulse blade section with passage based on potential vortex flow of ref.(3.3).

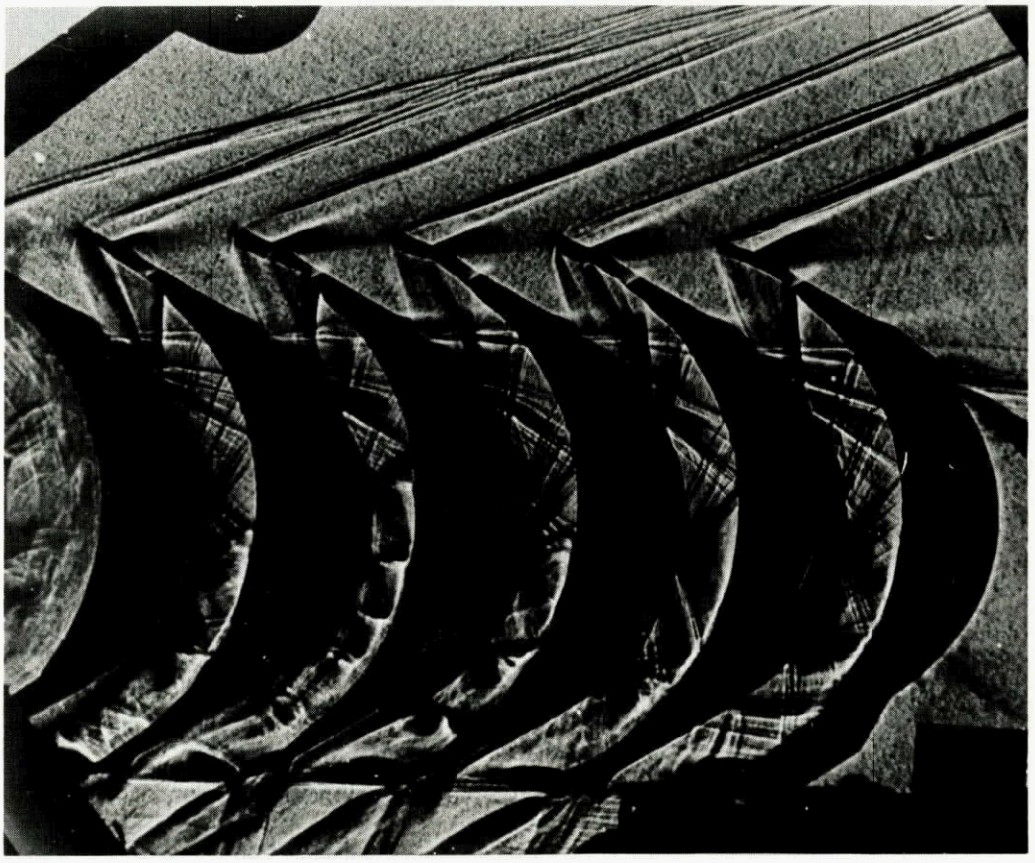

Fig.3.5: Schlieren picture of impulse type cascade, (J.R. ERWIN, NASA, Langley Field).

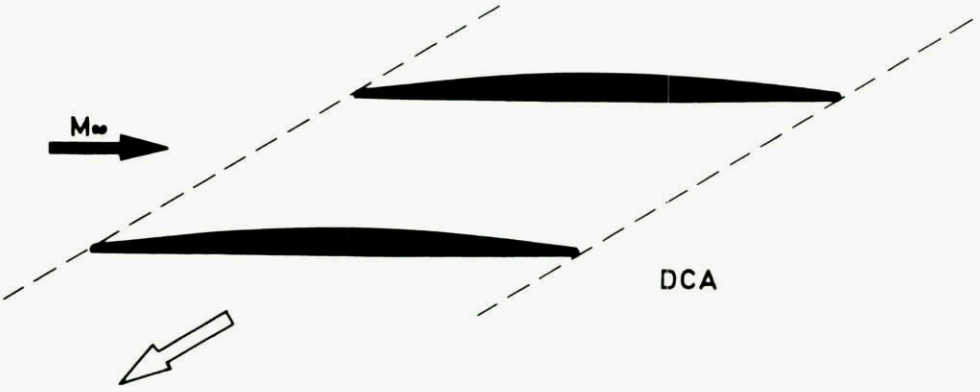

Fig.3.6: Double-circular-arc blade section.

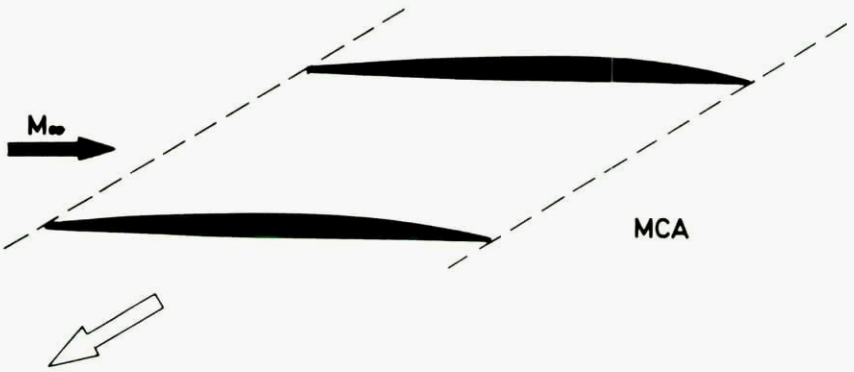

Fig.3.7: Multiple-circular-arc blade section MCA of ref.(3.11).

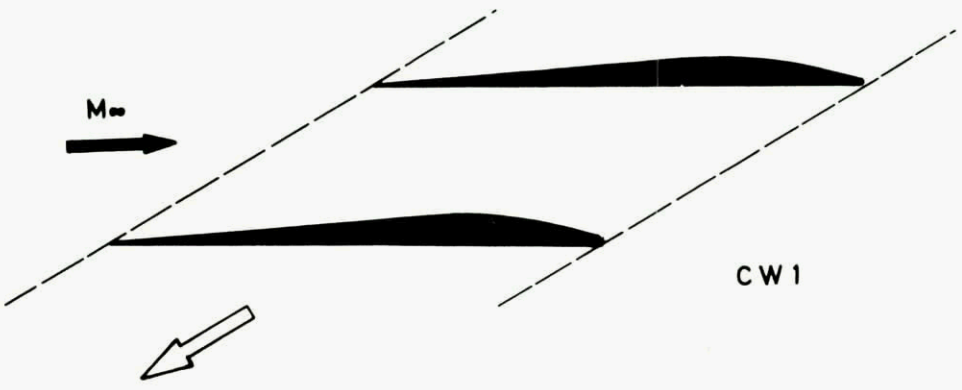

Fig.3.8: Circular-wedge blade section CW1 of ref.(3.13).

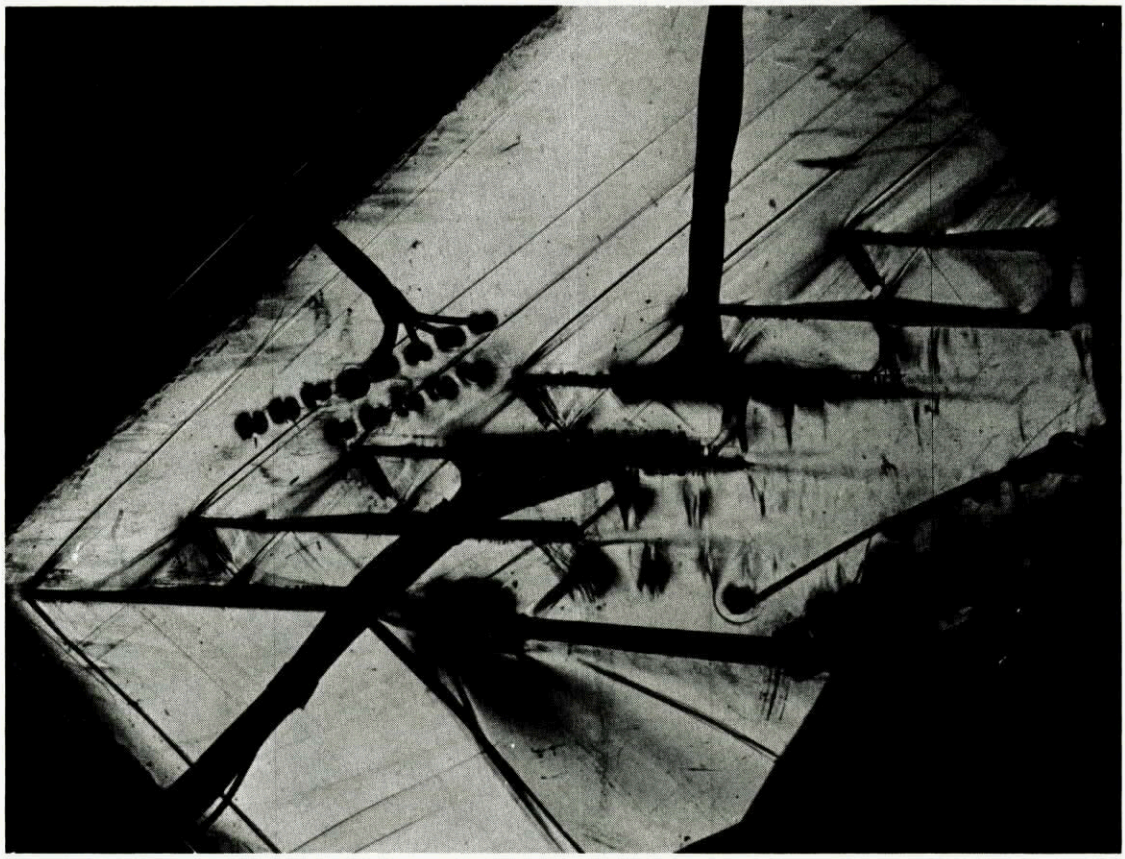

Fig.3.9: Schlieren picture of supersonic blade section with external compression of ref.(3.20).

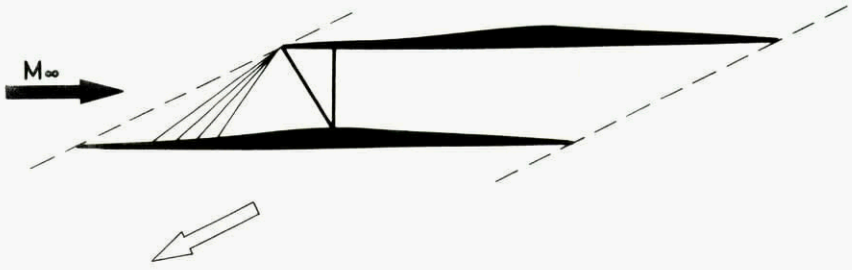

Fig.3.10: Supersonic blade section with external compression, ref.(3.20).

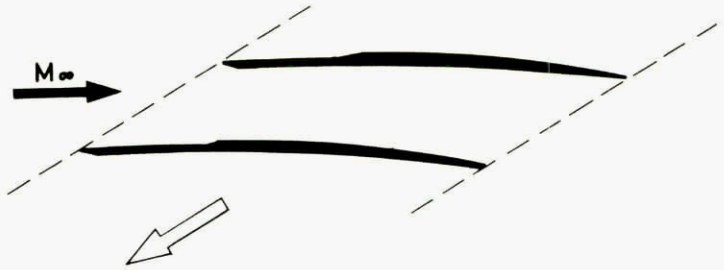

Fig.3.11: Supersonic blade section with internal compression of ref.(1.4).

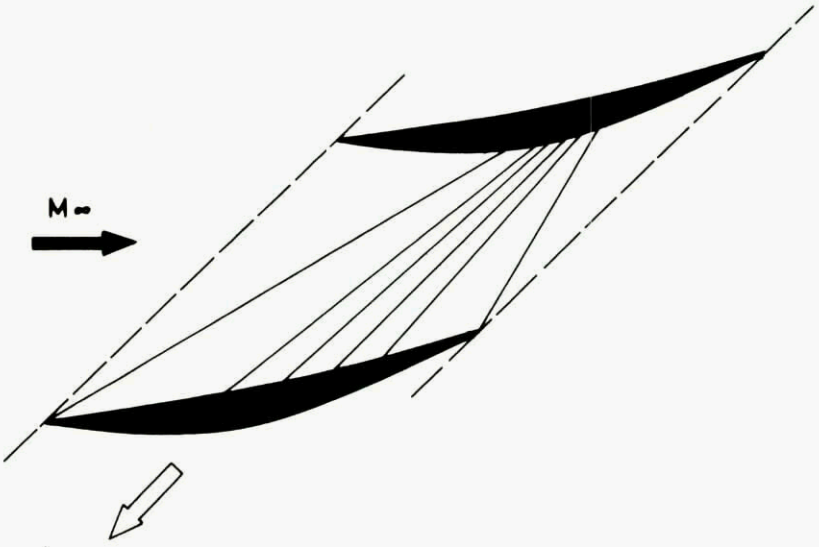

Fig.3.12: Supersonic blade section with internal compression, of ref. (3.21).

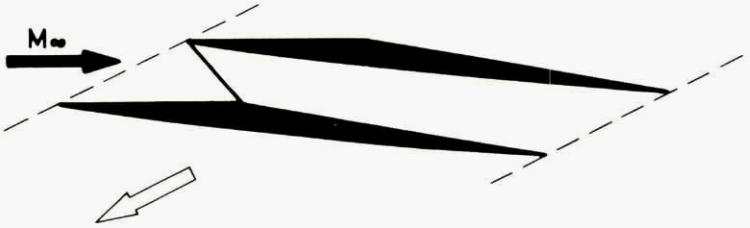

Fig.3.13: Supersonic blade section with internal compression of ref.(3.22).

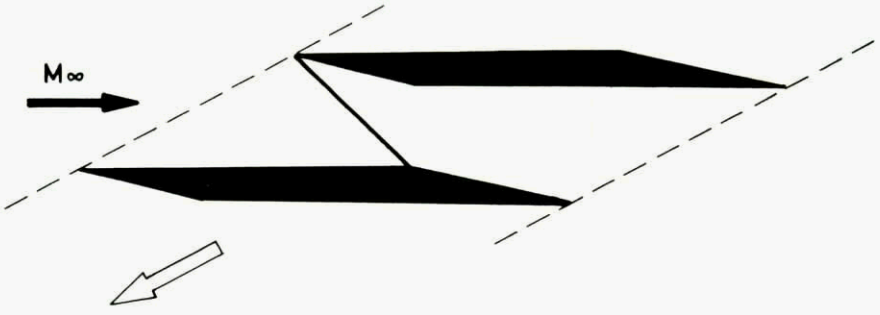

Fig.3.14: Supersonic blade section with internal compression of ref.(3.23).

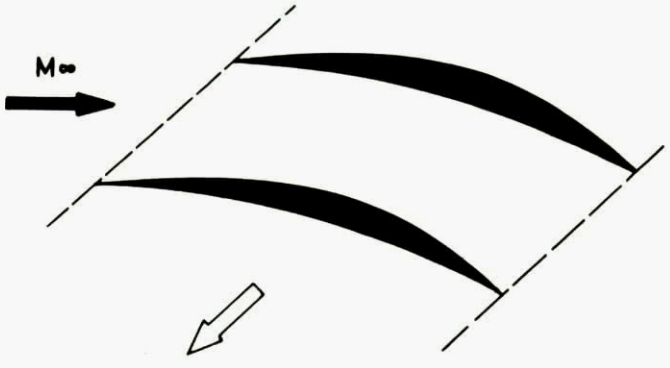

Fig.3.15: High turning supersonic decelerating blade section of ref.(3.25).

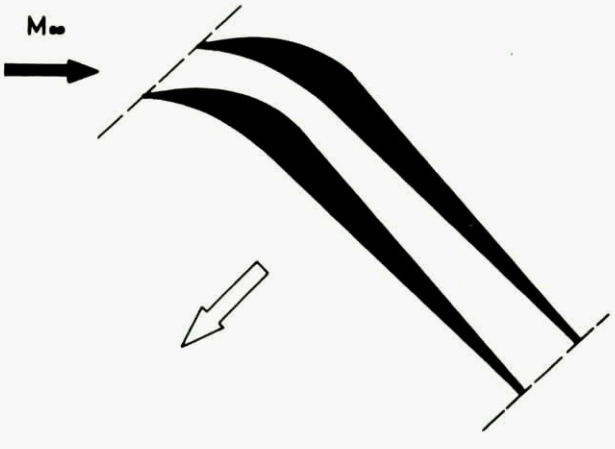

Fig.3.16a: High turning supersonic decelerating blade section of ref.(3.27).

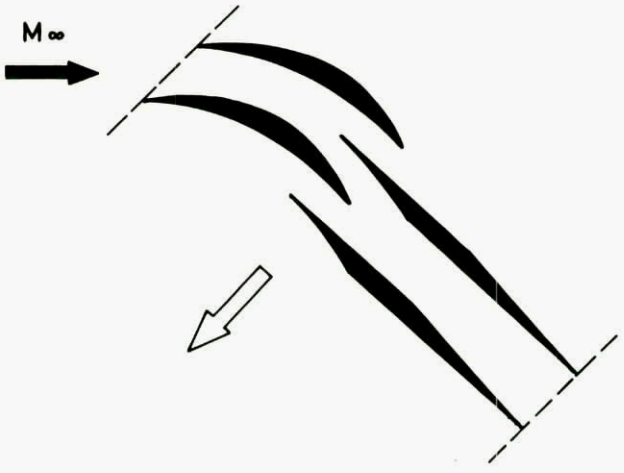

Fig.3.16b: High turning supersonic tandem cascade of ref.(3.27).

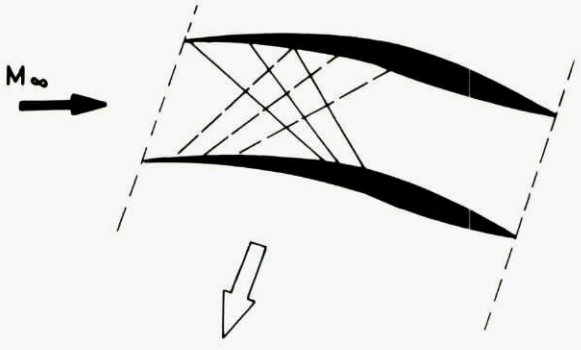

Fig.3.17: Supersonic blade section with internal compression of ref.(3.28).

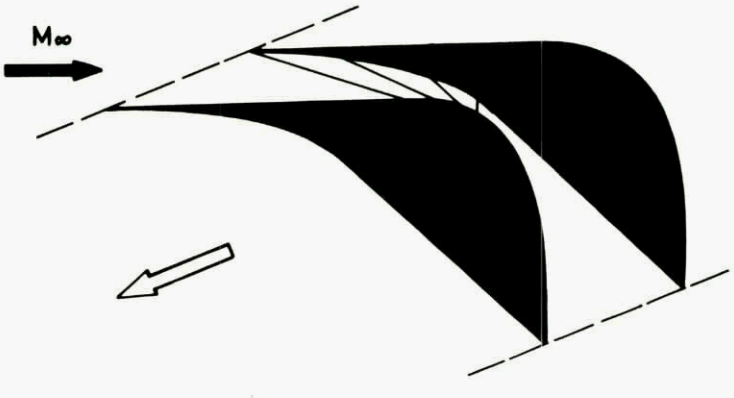

Fig.3.18: High turning supersonic blade section with internal compression of ref.(3.1).

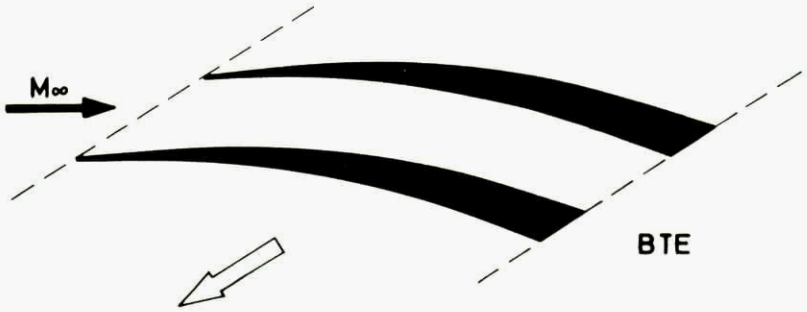

Fig.3.19: Blunt trailing edge (BTE) blade section of ref. (3.29).

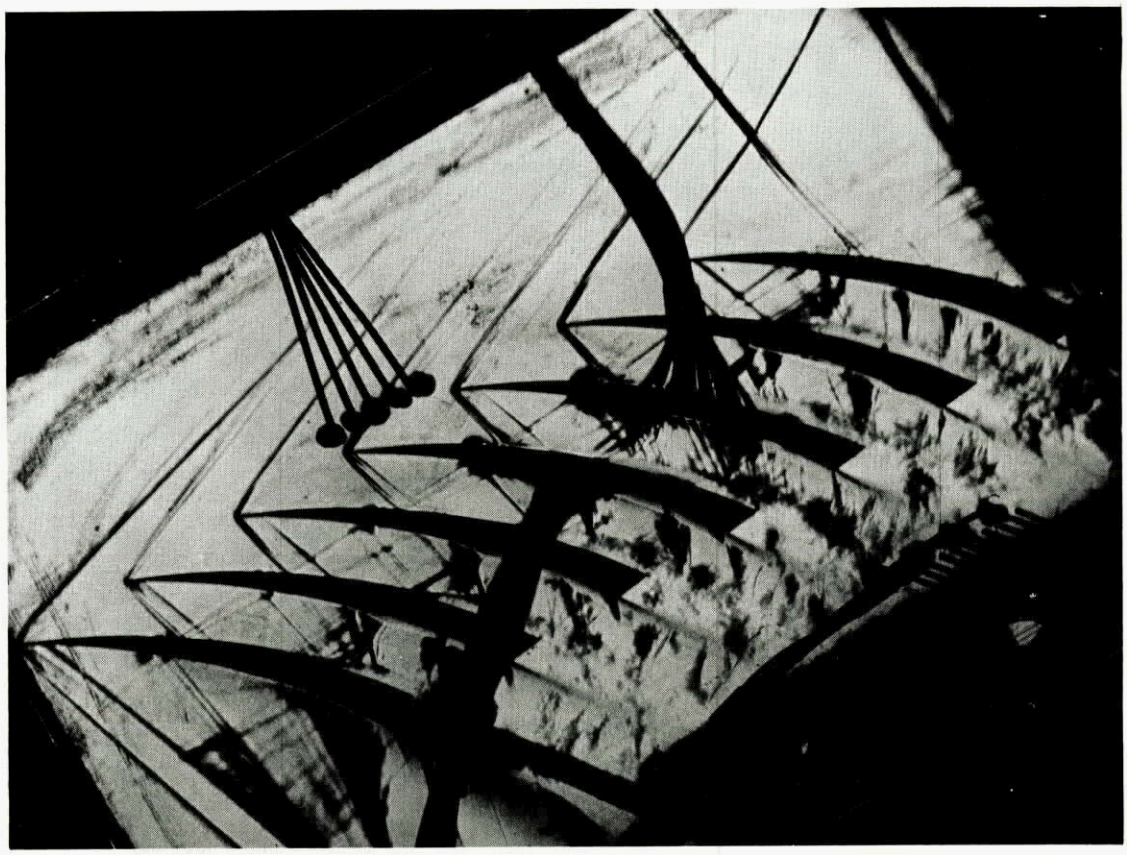

Fig.3.20: Schlieren picture of BTE-cascade at $M_\infty = 1.48$.

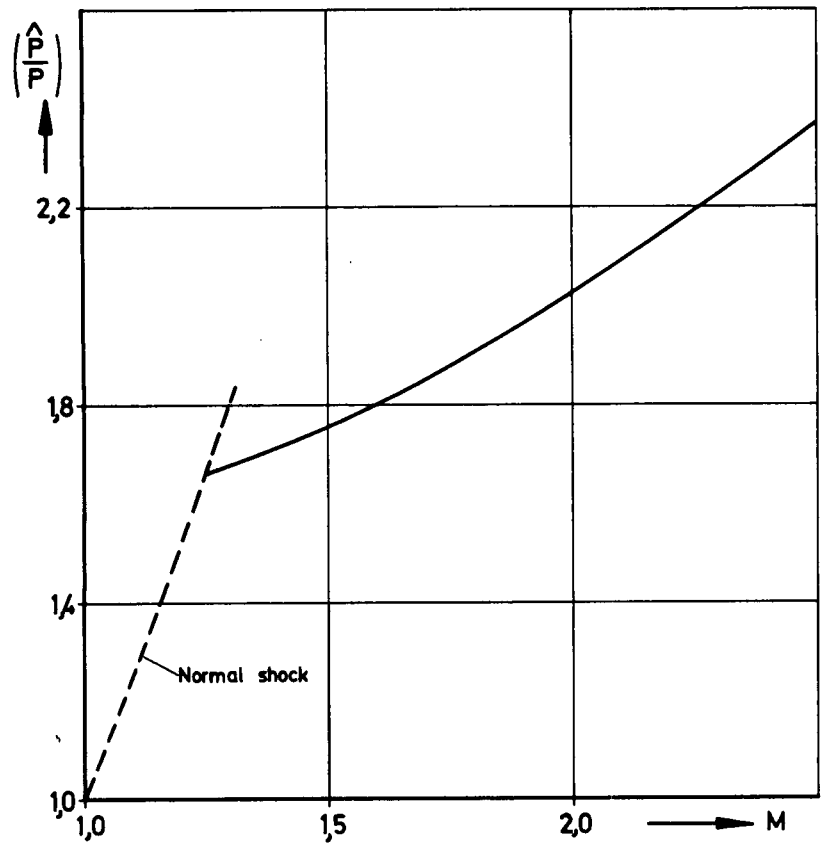

Fig.3.21: Maximum theoretical shock pressure rise in turbulent boundary layer of ref.(2.1).

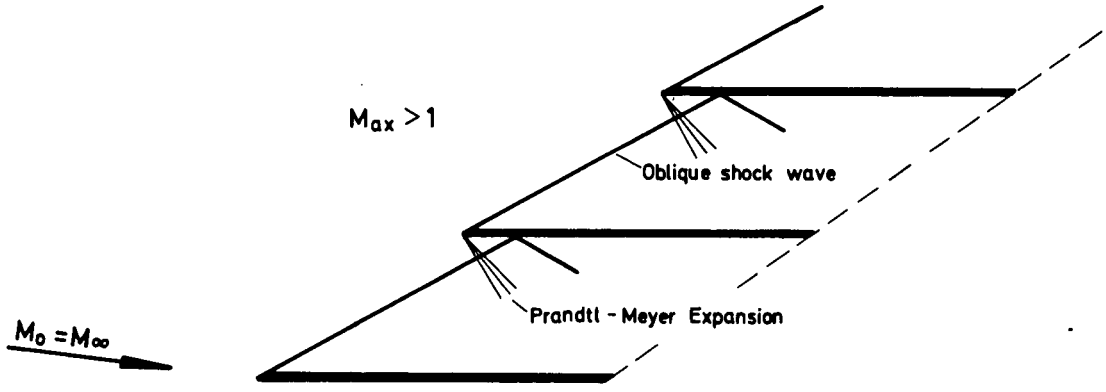

Fig.4.1: Flat-plate cascade at axial supersonic inlet velocity with suction-surface shock.

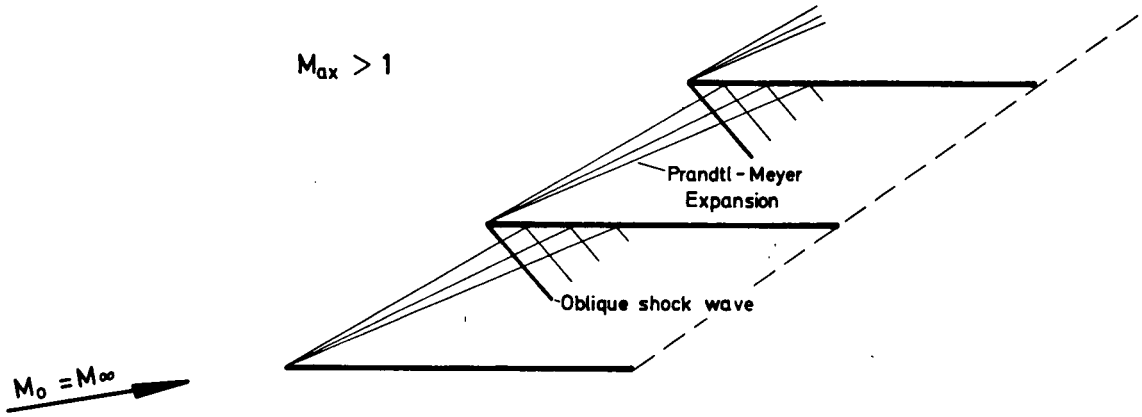

Fig.4.2: Flat-plate cascade at axial supersonic inlet velocity with pressure-surface shock.

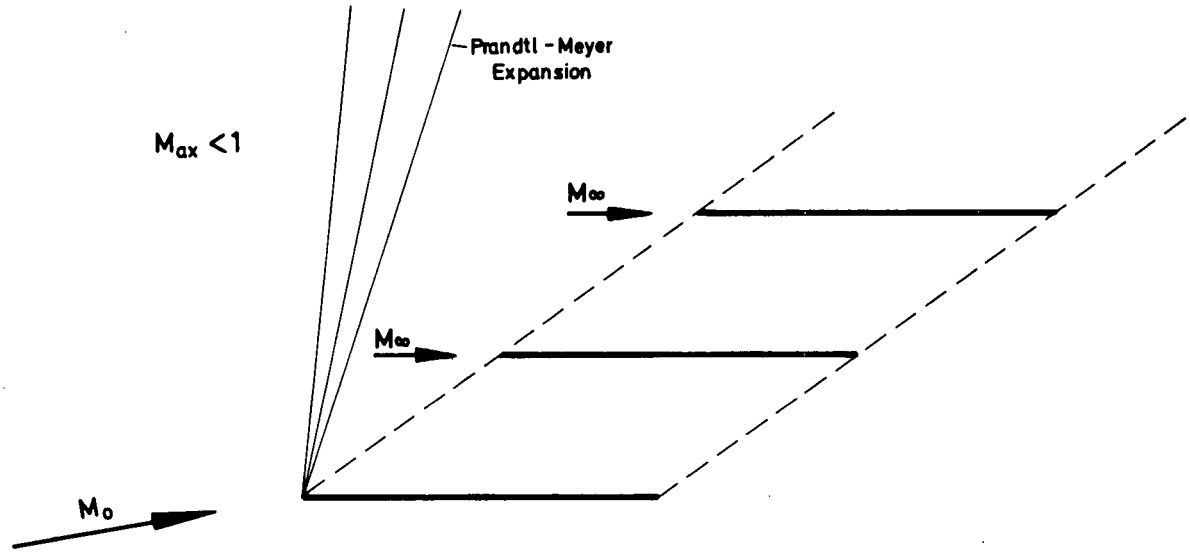

Fig.4.3: Semi-infinite flat-plate cascade at axial subsonic inlet velocity with an expansion at the first blade.

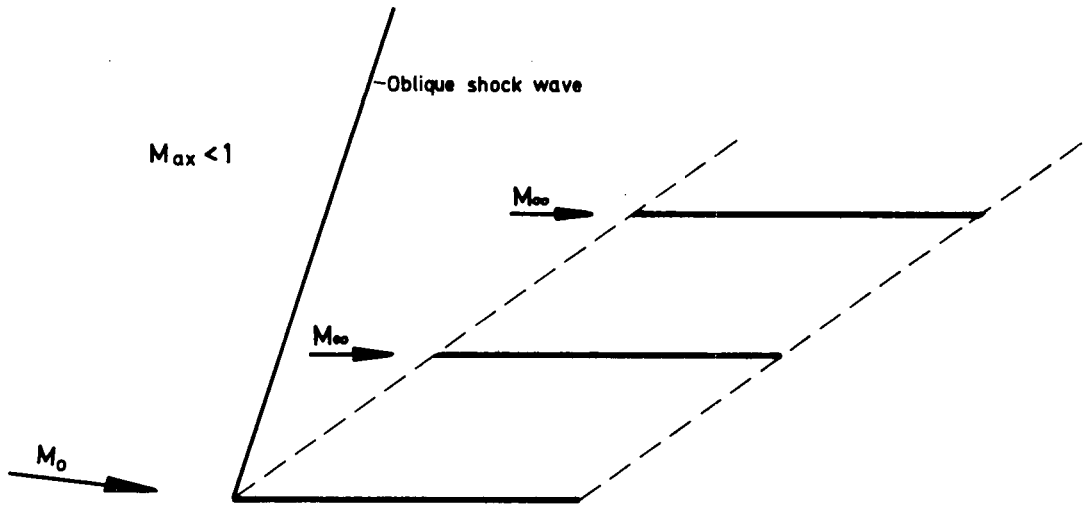

Fig.4.4: Semi-infinite flat-plate cascade at axial subsonic inlet velocity with a shock at the first blade.

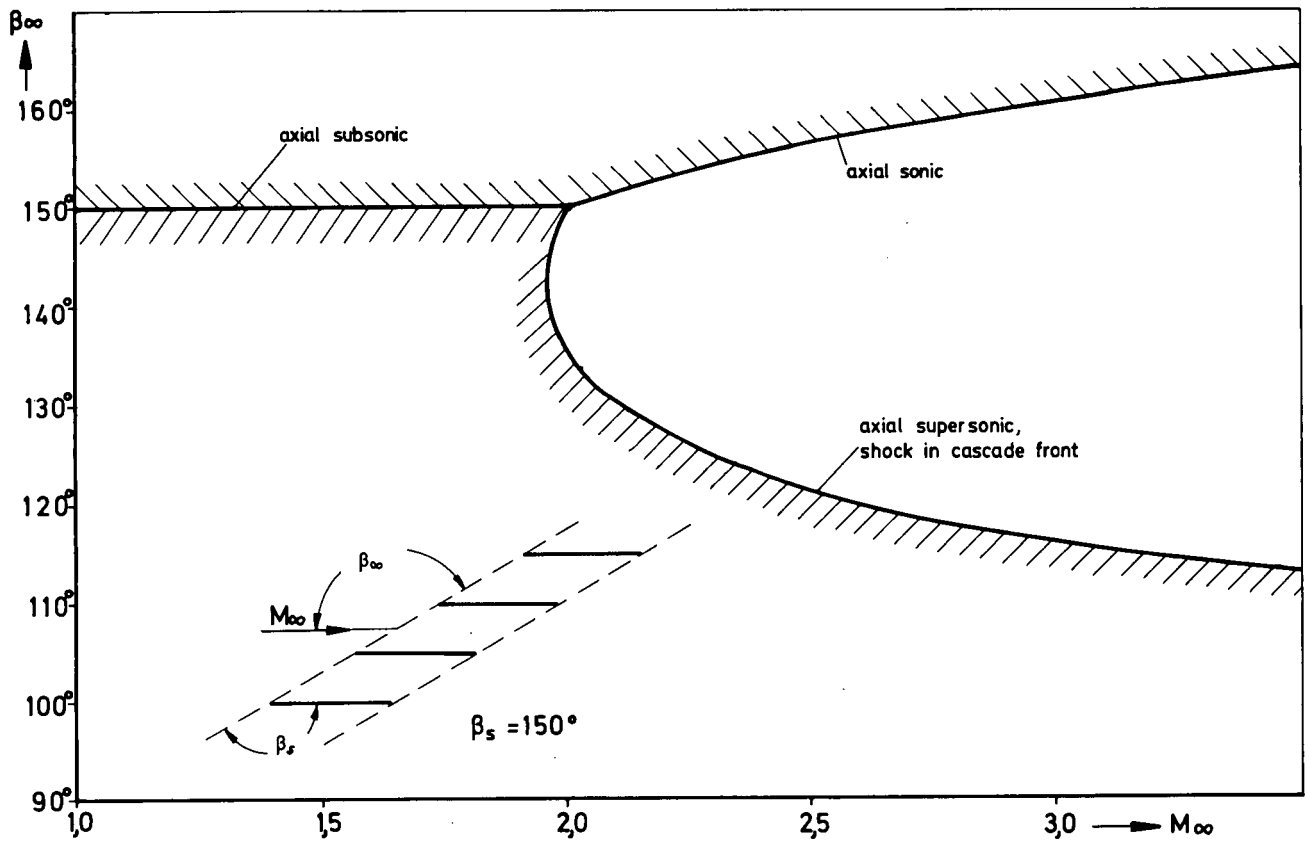

Fig.4.5: Inlet flow angle β_∞ as function of inlet Mach number M_∞ of a flat-plate cascade.

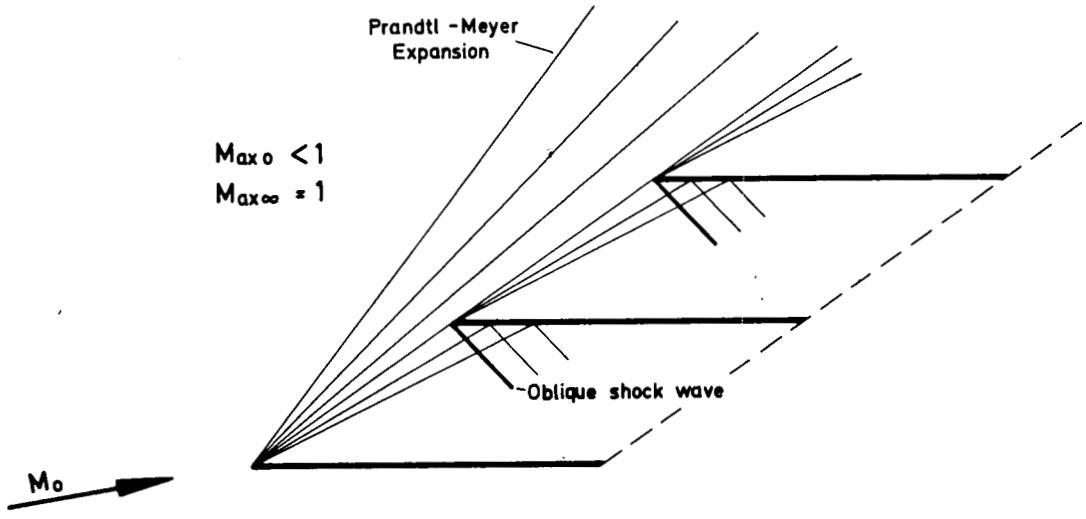

Fig.4.6: Semi-infinite flat-plate cascade at sonic axial inlet Mach number.

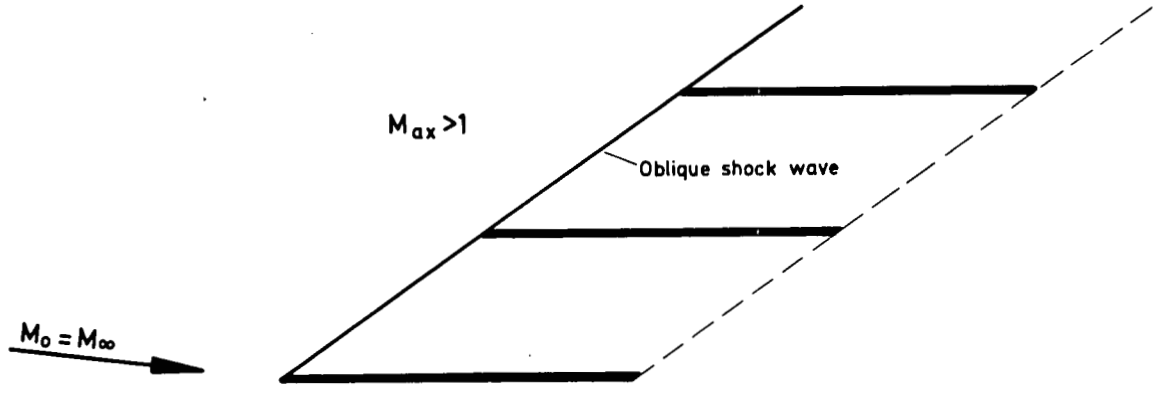

Fig.4.7: Infinite flat-plate cascade at supersonic axial inlet Mach number with shock in the cascade front.

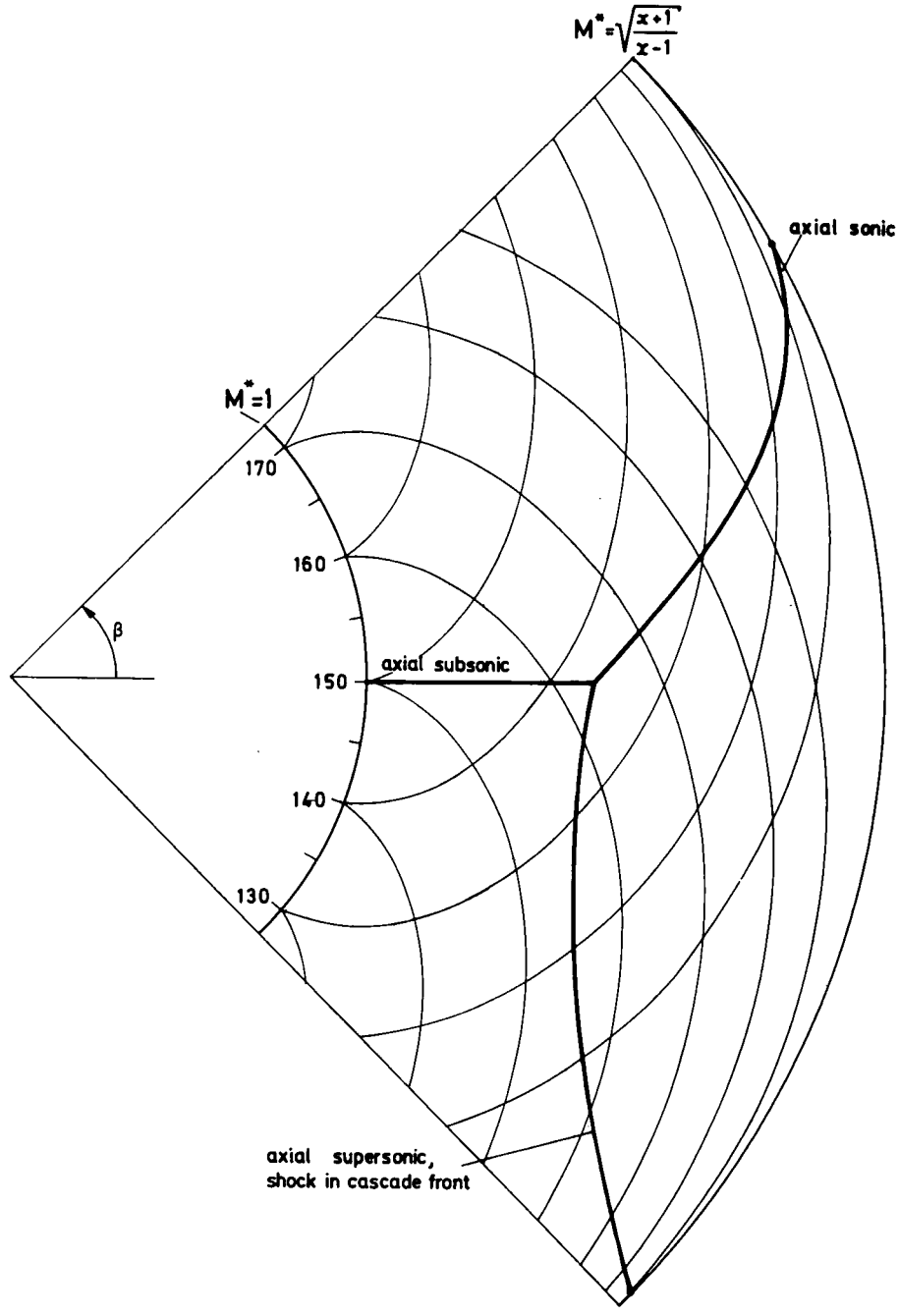

Fig.4.8: Dependency of inlet flow angle on inlet Mach number of a flat-plate cascade in hodograph plane.

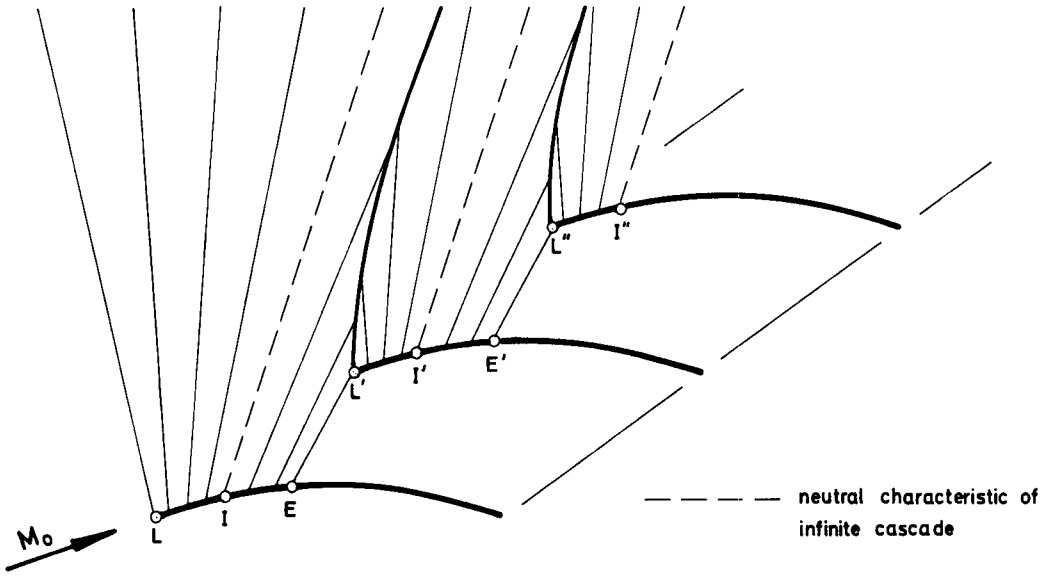

Fig.4.9: Semi-infinite cambered plate cascade at subsonic axial inlet velocity.

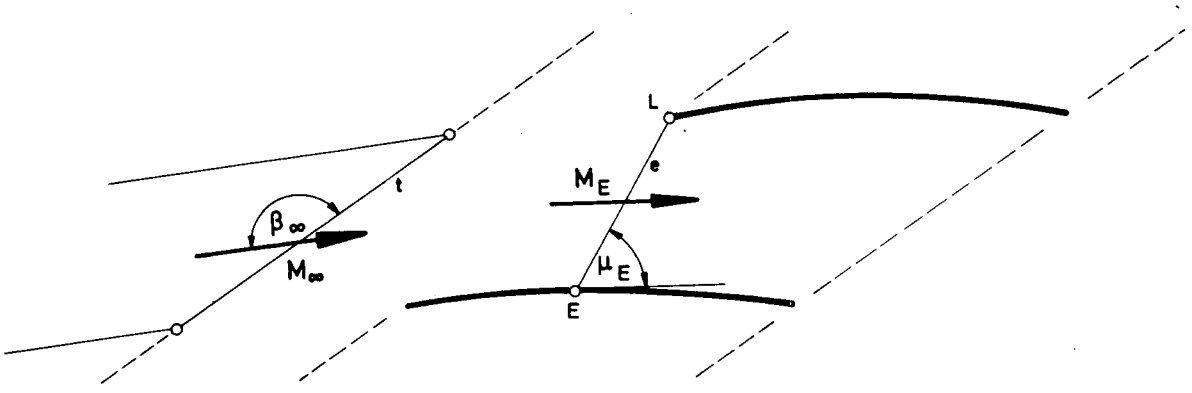

Fig.4.10: Entrance region of a supersonic cascade.

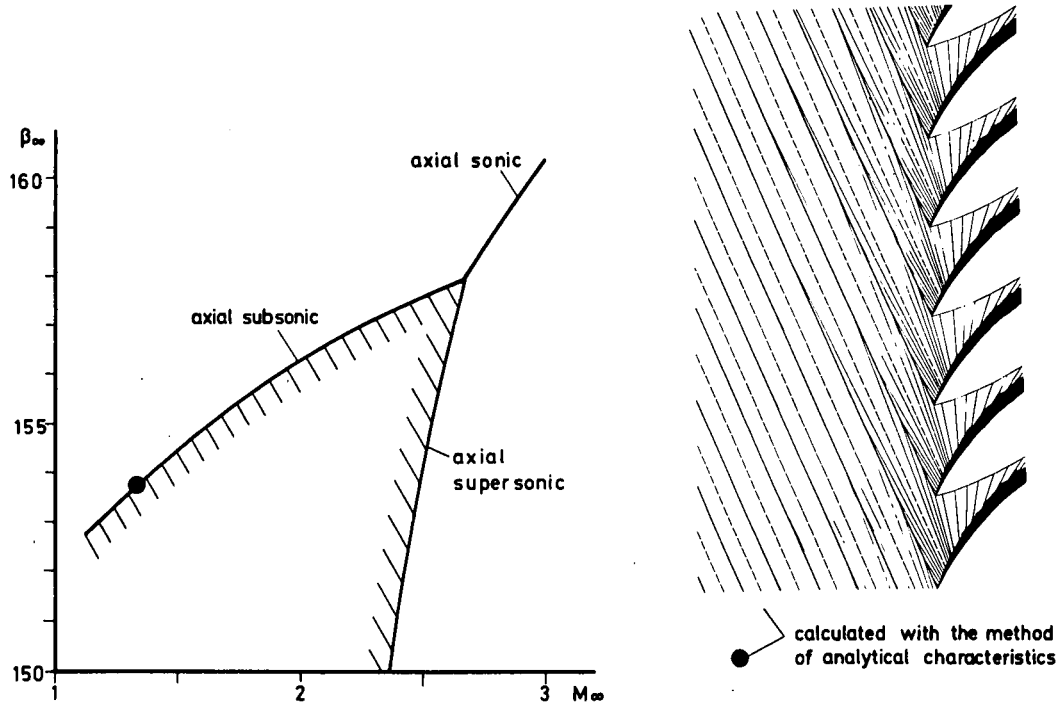

Fig.4.11: Inlet flow angle β_∞ versus inlet Mach number M_∞, together with flow pattern of a convex suction surface blade section.

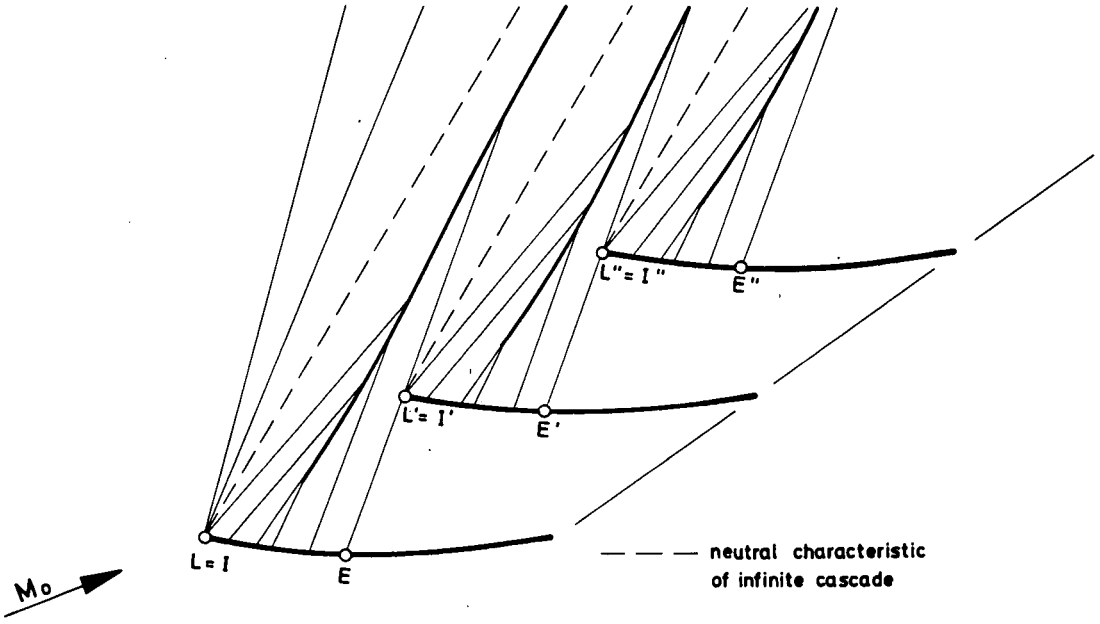

Fig.4.12: Flow pattern of semi-infinite supersonic cascade having blades with concave suction surface.

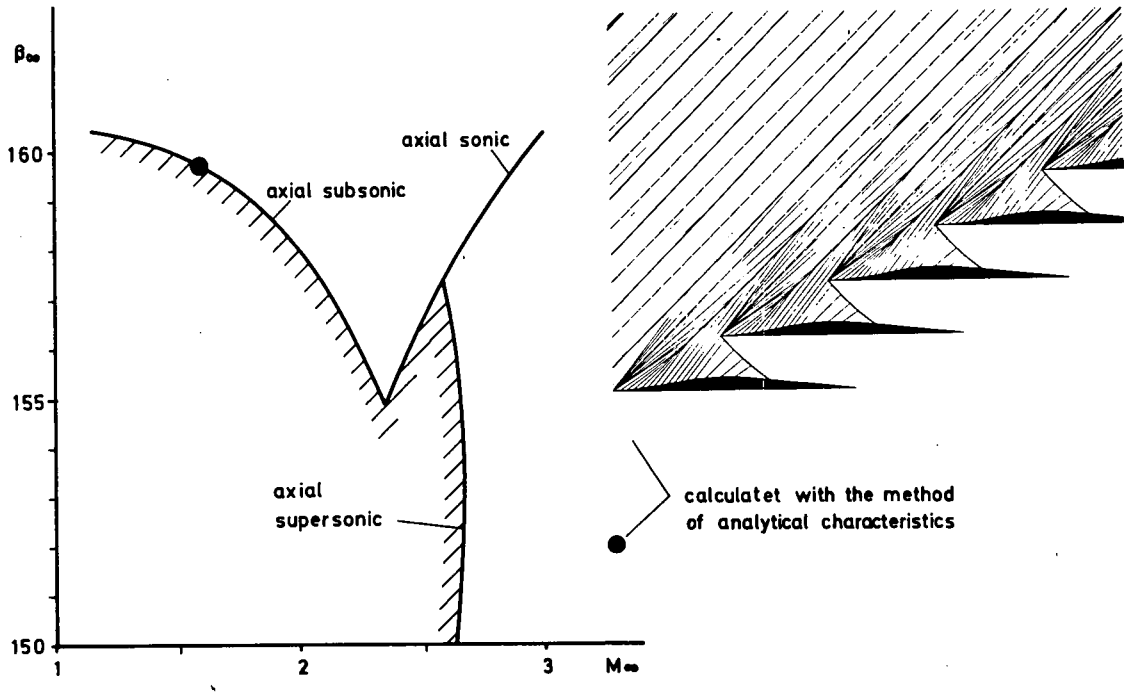

Fig.4.13: Inlet flow angle β_∞ versus inlet Mach number M_∞ together with flow pattern of a concave suction surface blade section.

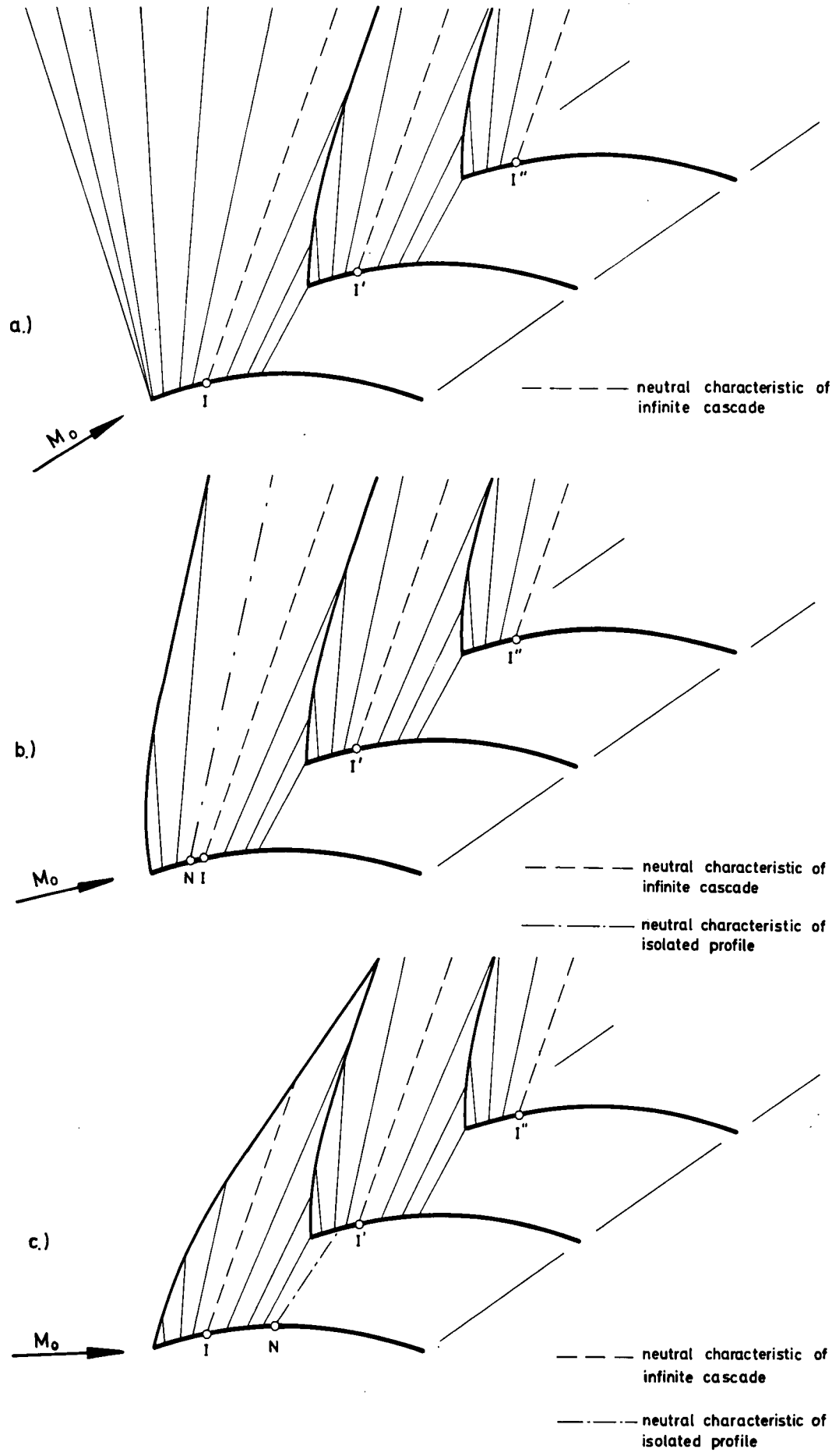

Fig.4.14: Flow pattern in front of a semi-infinite supersonic cascade at different nozzle flow conditions (M_o, β_o), but constant cascade upstream flow (M_∞, β_∞).

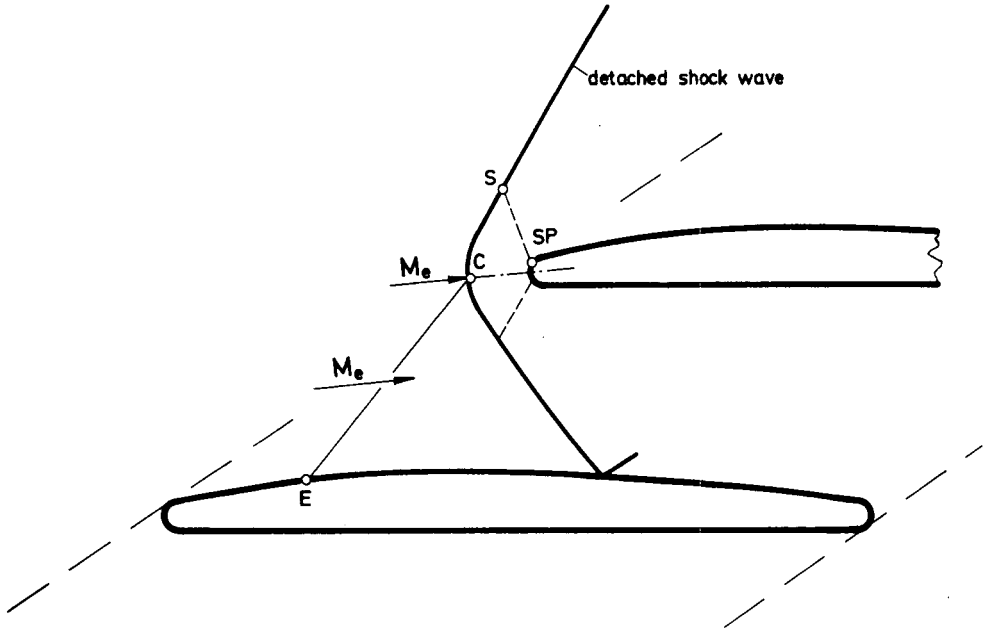

Fig.4.15: Detached shock wave in front of a cascade blade.

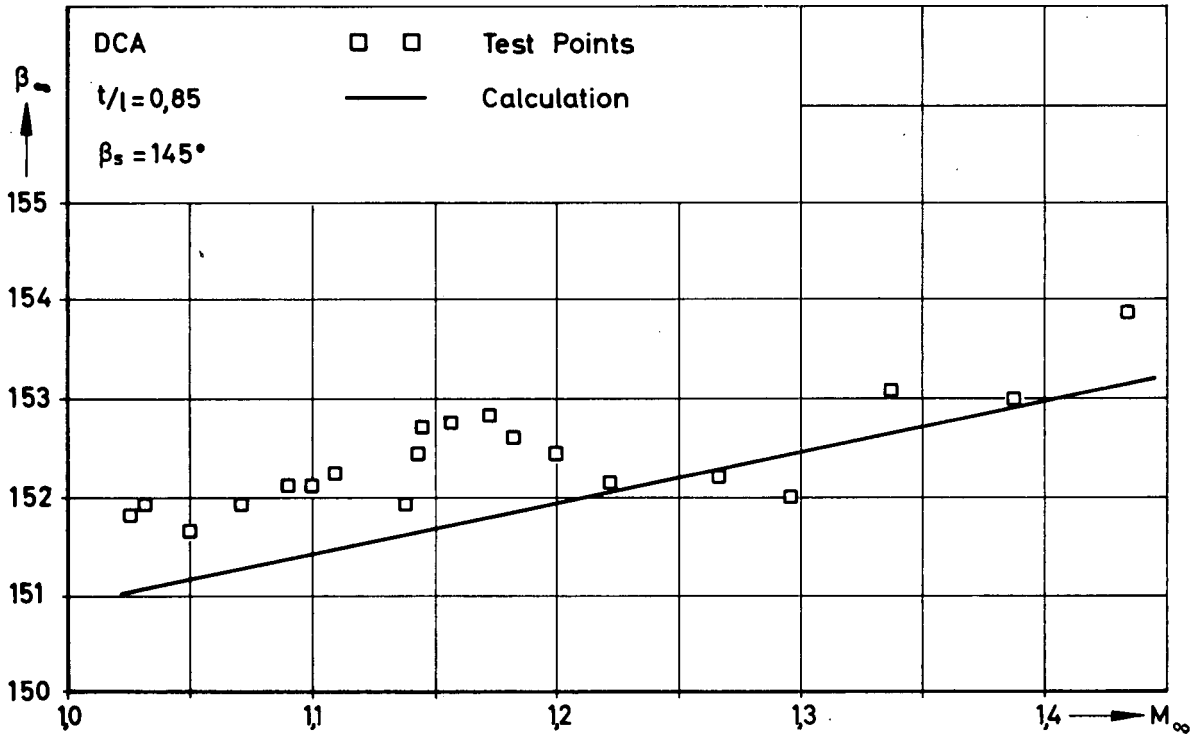

Fig.4.16: Measured and calculated inlet flow angles β_∞ as a function of inlet Mach number M_∞ for a started DCA cascade with detached shock waves.

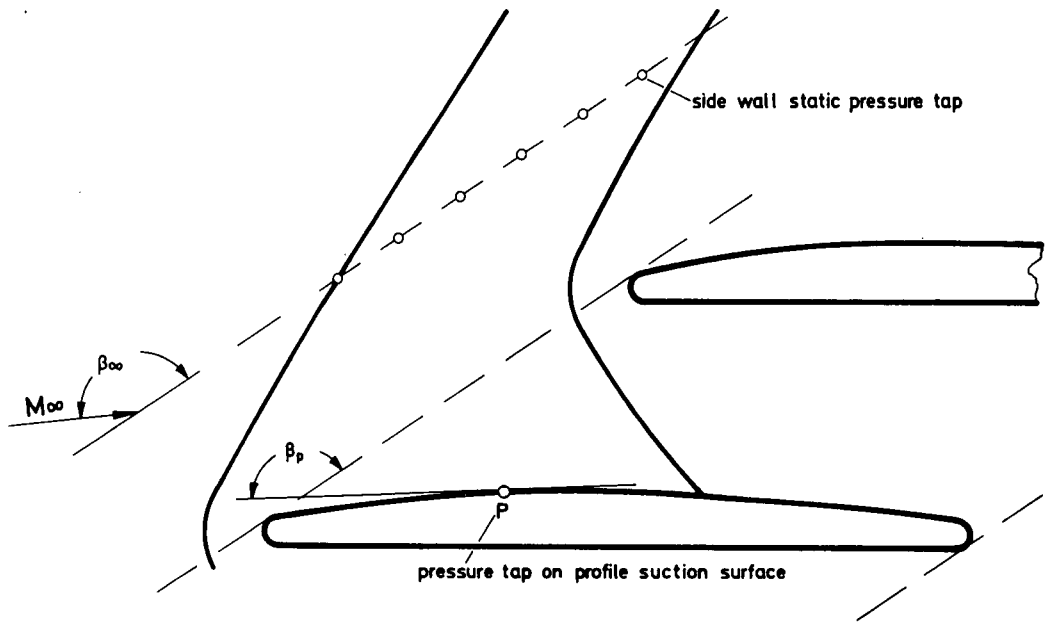

Fig.4.17: Location of pressure taps for the experimental determination of inlet Mach number M_∞ and inlet flow angle β_∞.

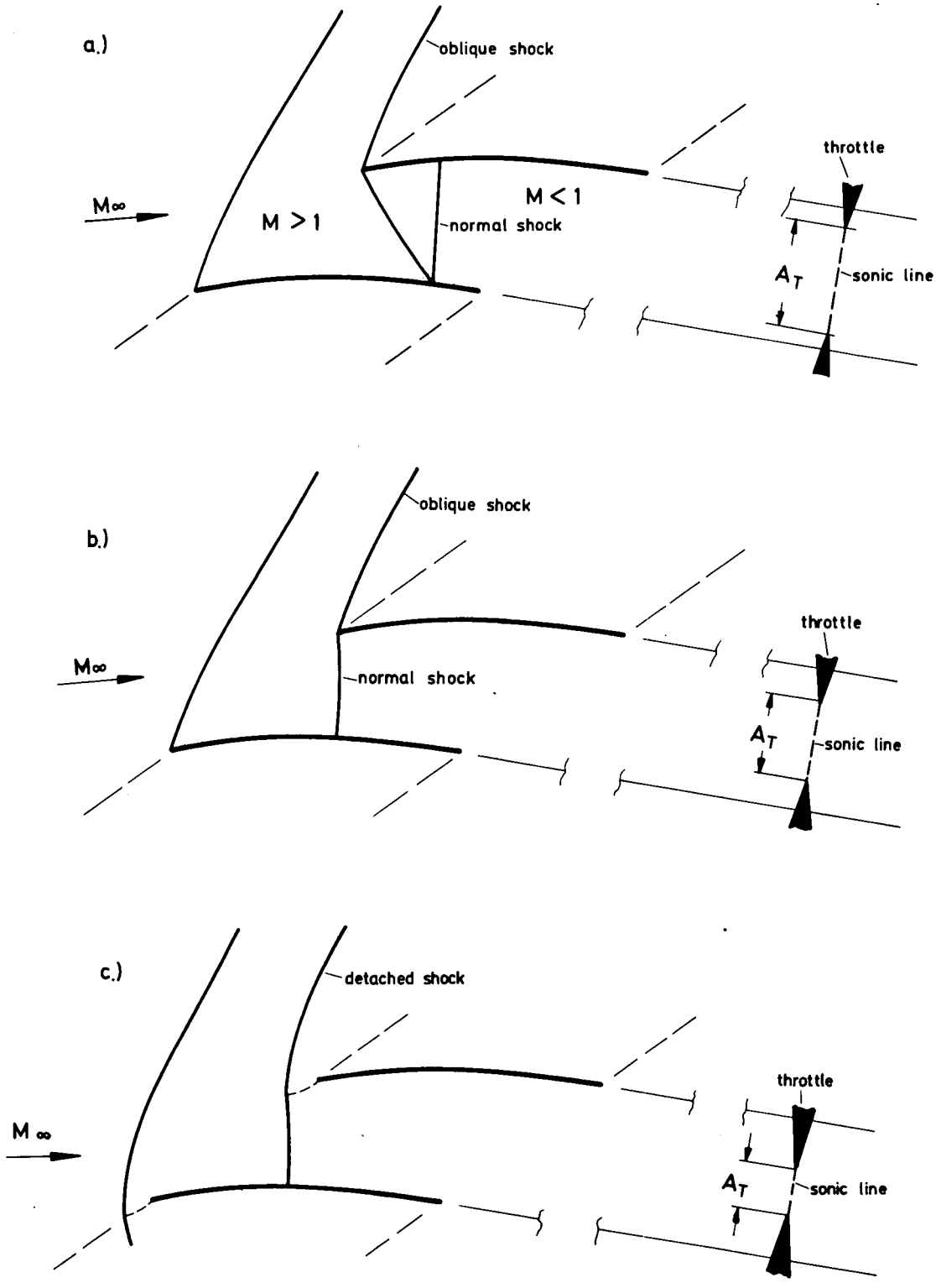

Fig.4.18: Shock pattern of supersonic cascade for three different settings of downstream throttle area A_T.

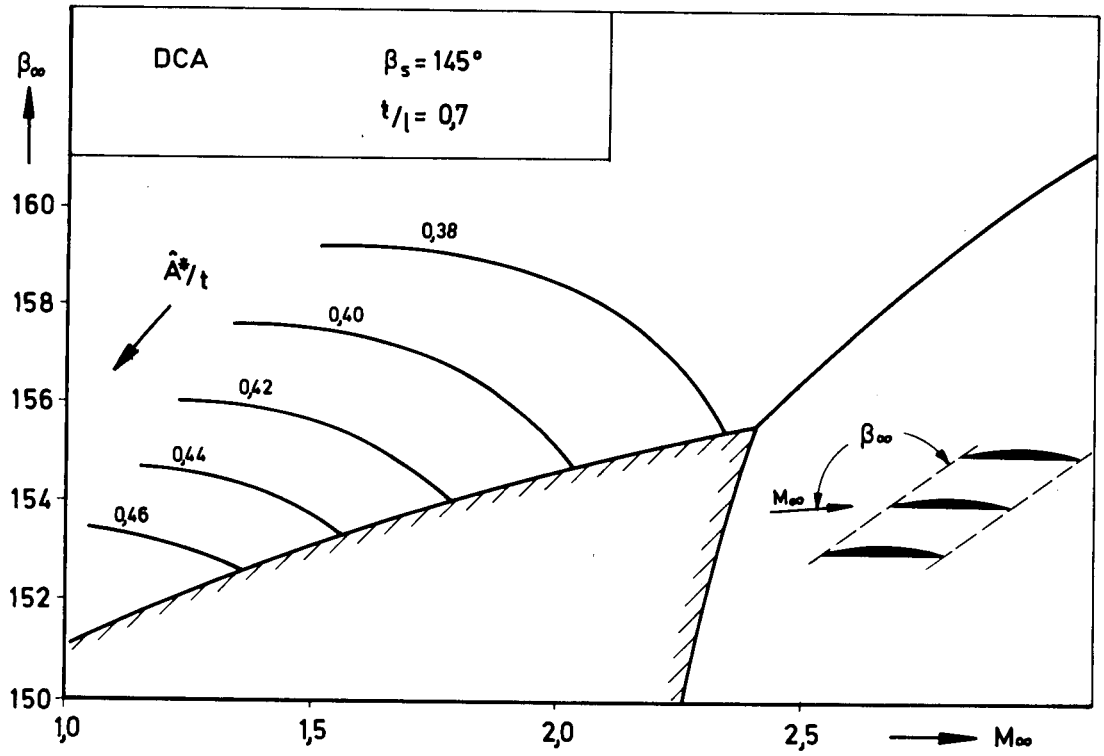

Fig.4.19: Theoretical inlet flow angle β_∞ as function of inlet Mach number M_∞ for a DCA cascade at started and unstarted operating conditions.

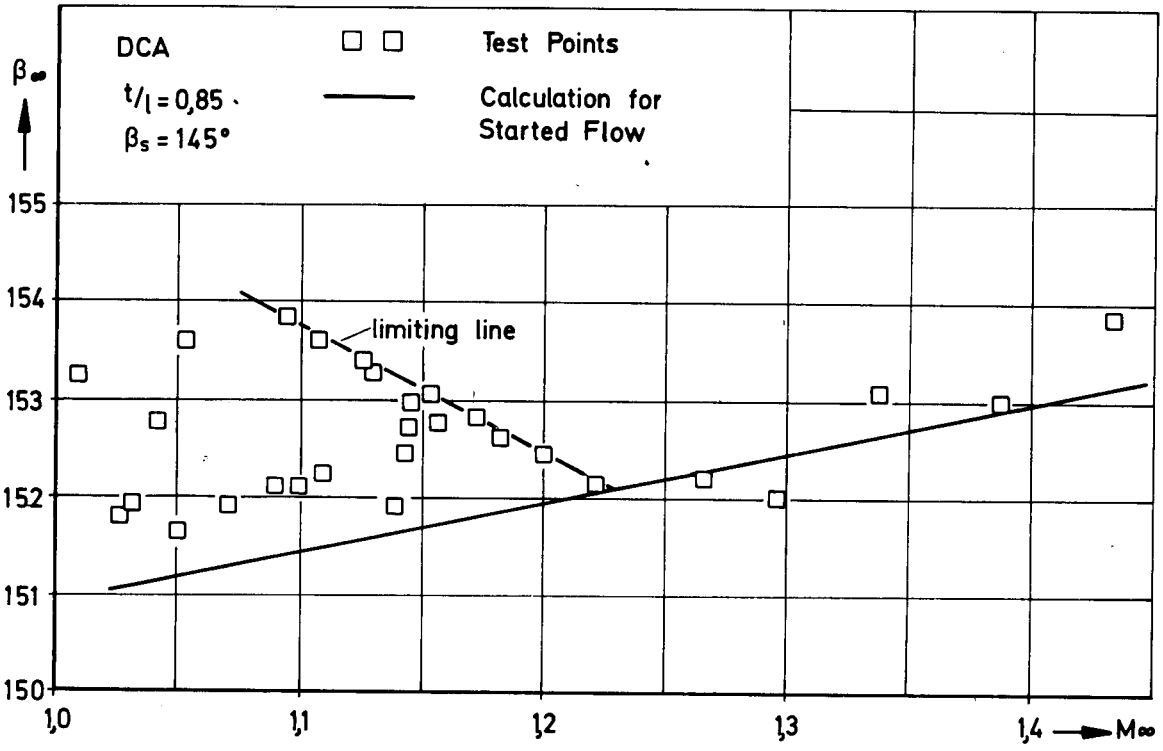

Fig.4.20: Two-dimensional cascade measurements of the inlet-flow angle of a DCA blade section (ref.(4.10)).

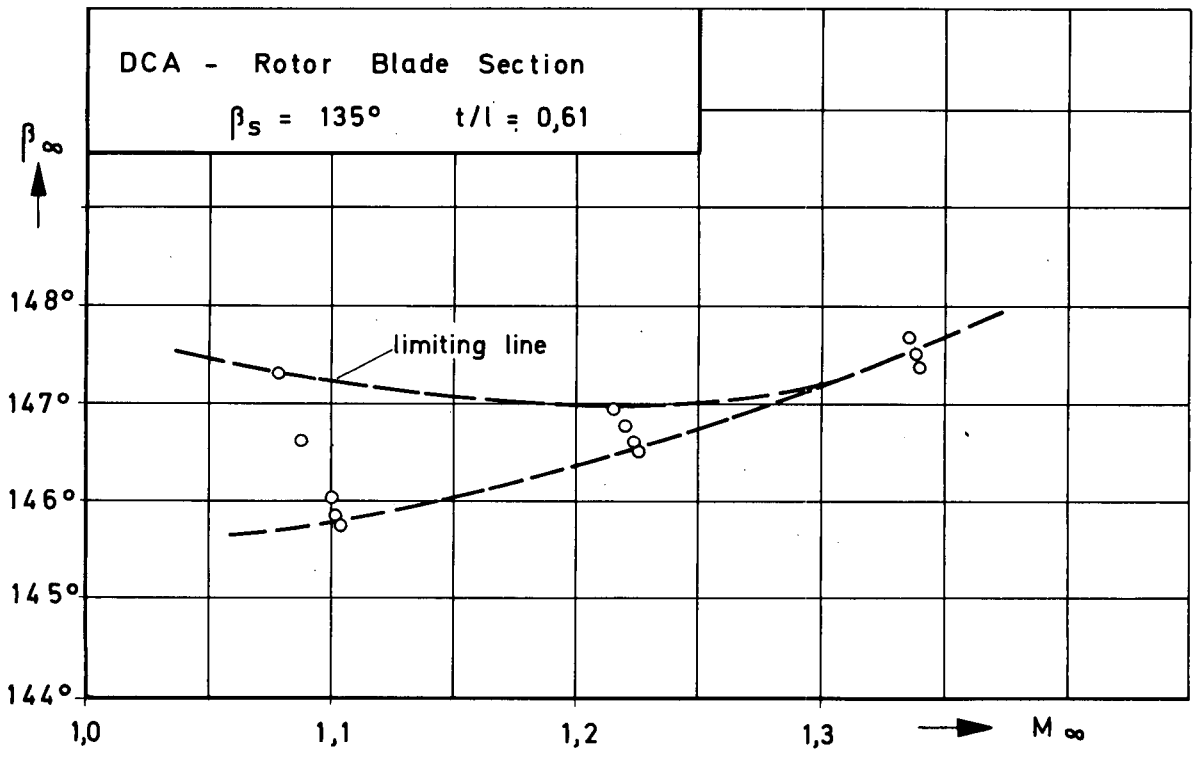

Fig.4.21: Rotor measurements of the inlet flow angle of a DCA blade section (ref.(4.12))

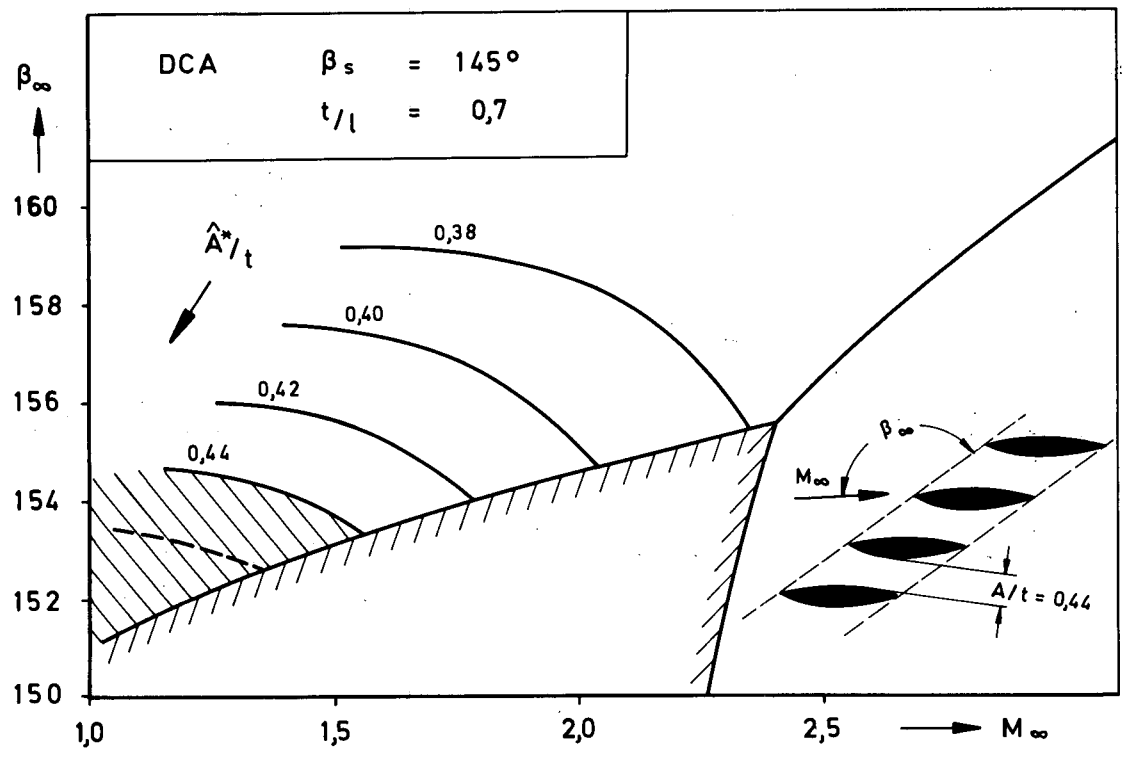

Fig.4.22: Theoretical inlet flow angle β_∞ as a function of inlet Mach number M_∞ for a DCA blade section with minimum passage area (A /t = 0.44).

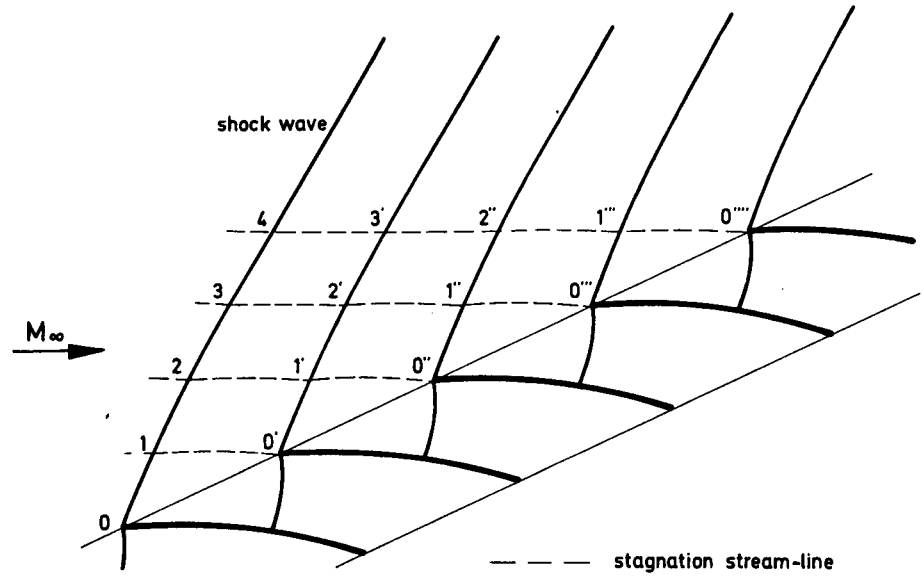

Fig.5.1: Shock pattern and stagnation streamlines in front of an infinite supersonic cascade.

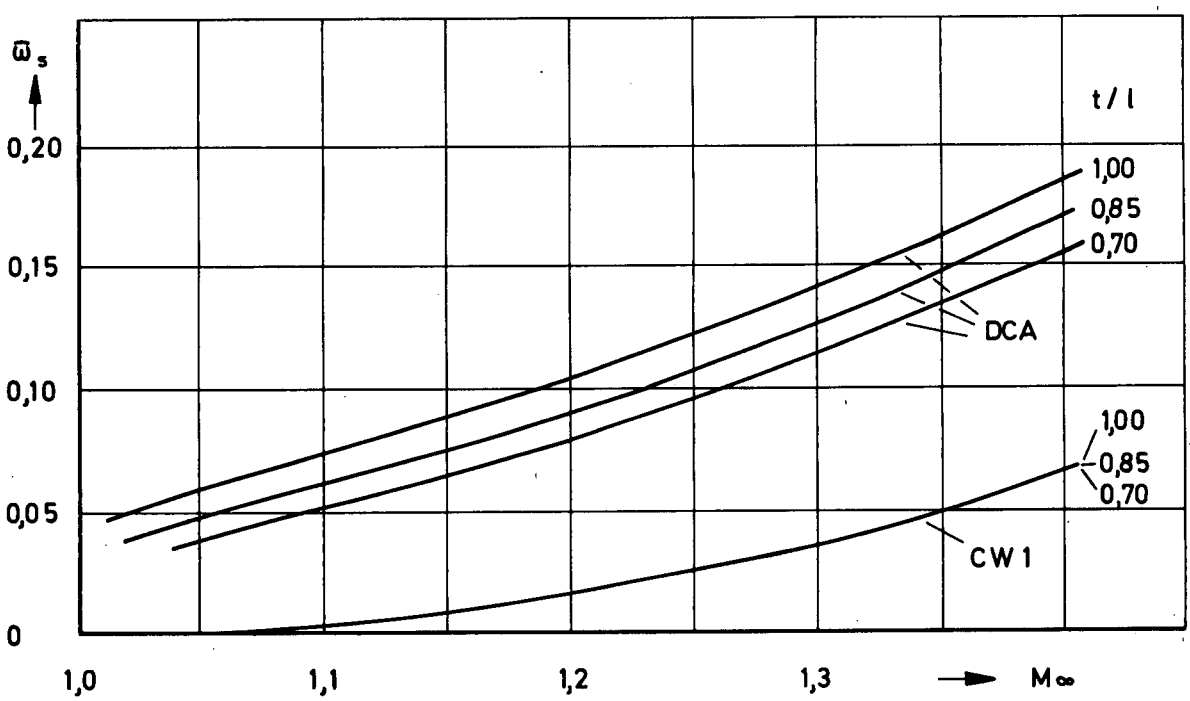

Fig.5.2: Theoretically determined shock loss coefficient $\bar{\omega}_s$ plotted against inlet Mach number M_∞ for DCA- and CW1 cascades at optimum back pressure.

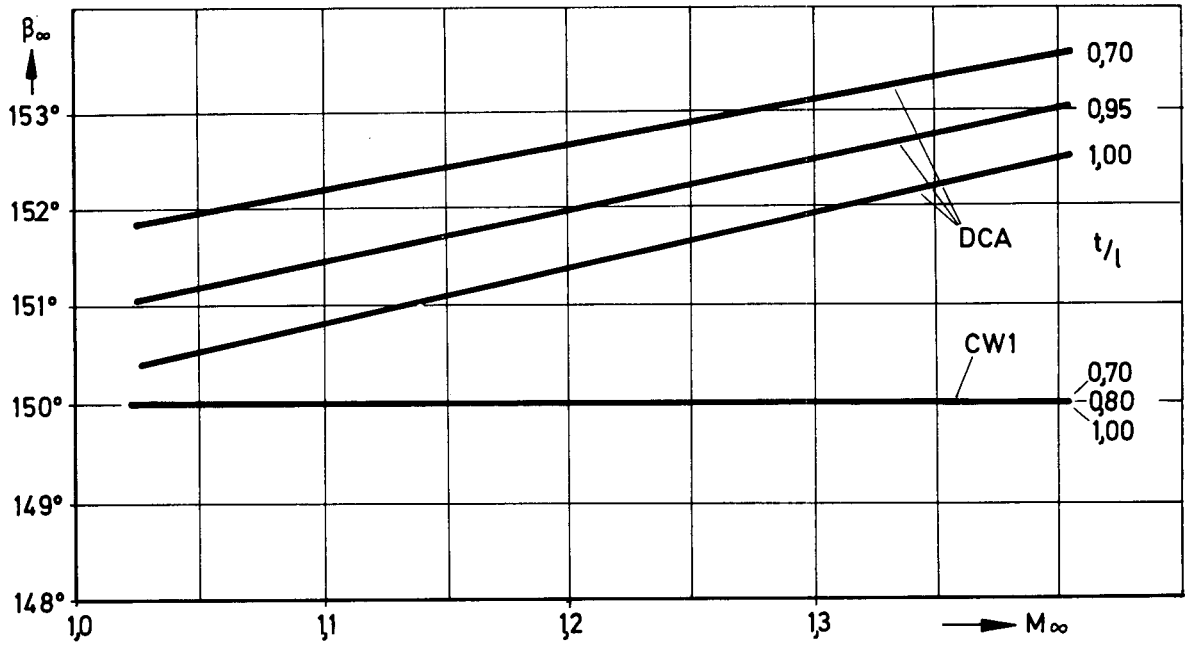

Fig.5.3: Variation of calculated inlet flow angle β_∞ with inlet Mach number M_∞ for DCA- and CW1-cascades (started condition).

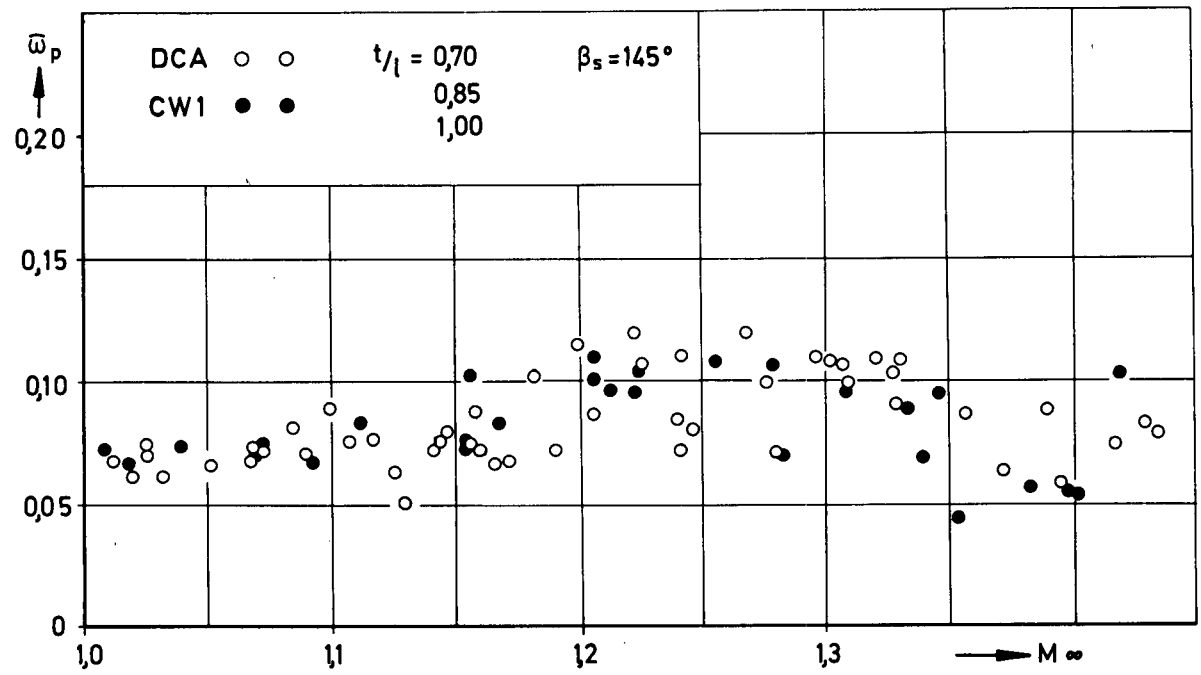

Fig.5.4: Profile loss coefficients of DCA- and CW1-blade section at supersonic inlet velocities.

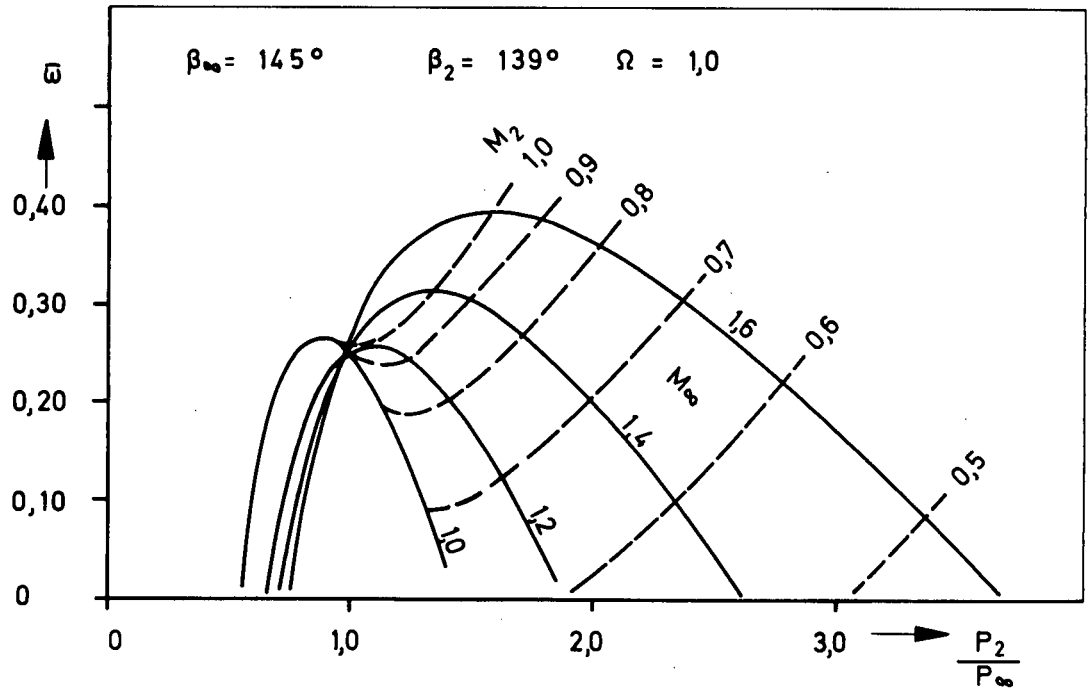

Fig.6.1: Variation of total pressure loss coefficient $\bar{\omega}$ with static pressure rise for a stream tube at different entrance Mach numbers.

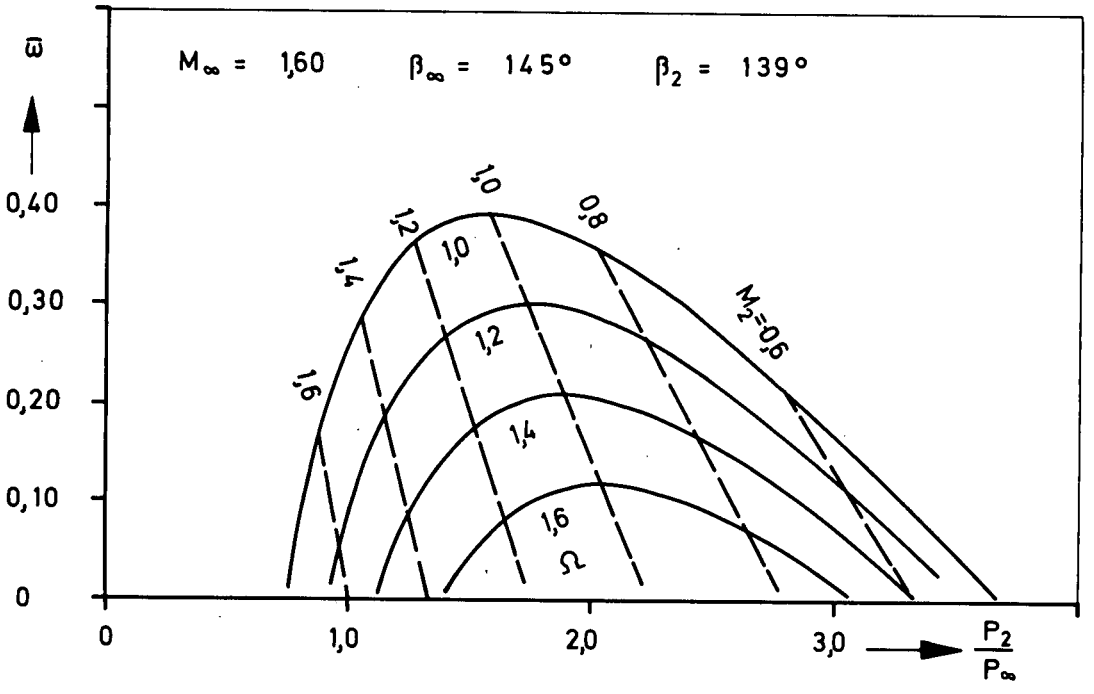

Fig.6.2: Variation of total pressure loss coefficient $\bar{\omega}$ with static pressure rise for a stream tube at different flow contraction ratios Ω.

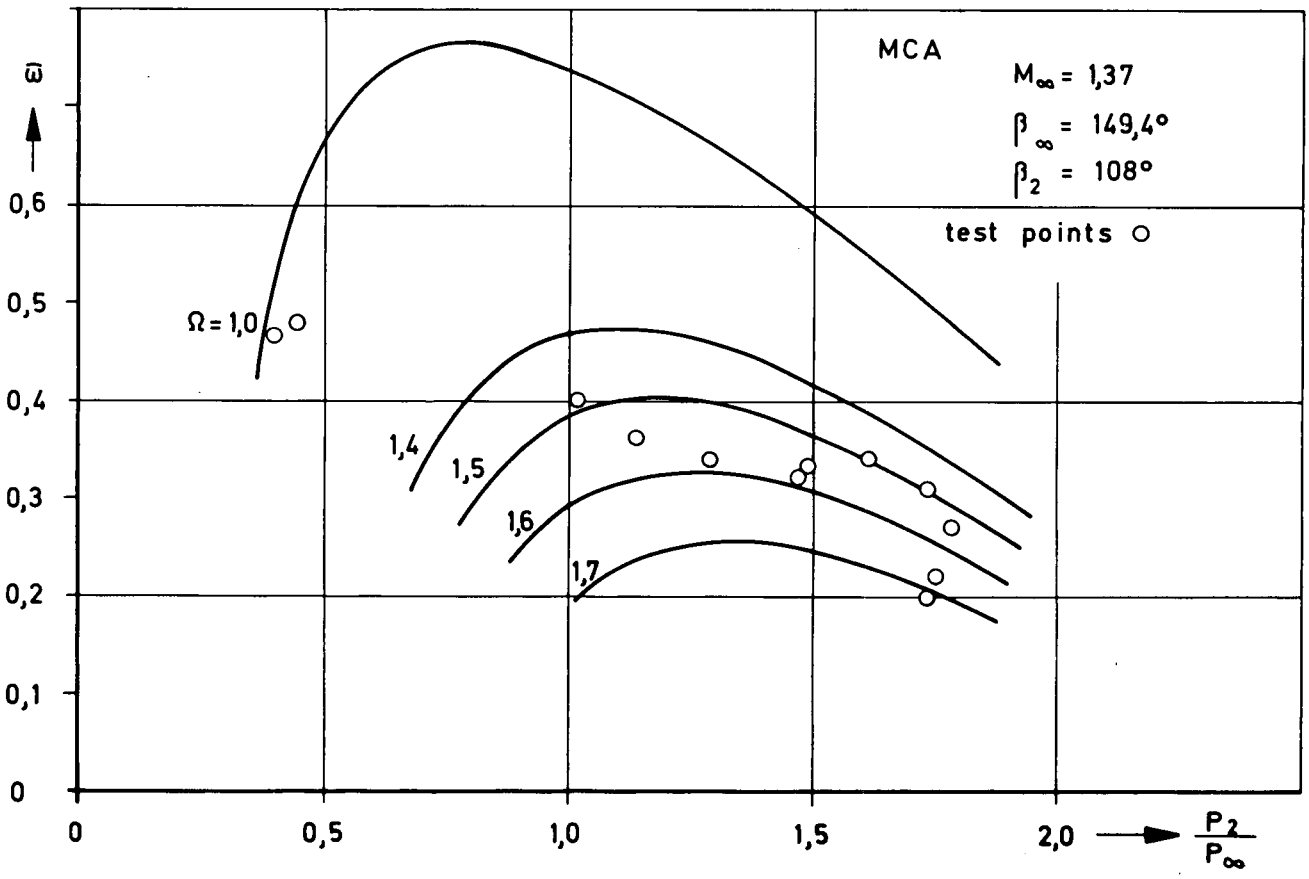

Fig.6.3: Variation of measured and calculated total pressure loss coefficients $\bar{\omega}$ with static pressure rise p_2/p_∞ and axial-velocity-density ratio Ω for a high turning supersonic blade section (MCA).

APPLICATION OF THROUGH-FLOW THEORIES

TO RADIAL WHEEL DESIGN

by

M. H. Vavra

Naval Postgraduate School
Monterey, California 93940

SUMMARY

A review is presented of the basic flow equations for the analysis of flows in rotors, together with a discussion of the effects of simplifying assumptions that are necessary to obtain solutions. Particular flows in radial compressor rotors are treated, and the approach necessary to calculate arbitrary flow patterns for given blade shapes is described. The necessity of using a correct description of the blade surface is demonstrated, and the applicability of the results to the design of compressor rotors is discussed.

APPLICATION OF THROUGH-FLOW THEORIES TO RADIAL WHEEL DESIGN

1. INTRODUCTION

The present lecture is not concerned with the procedures to calculate the flow patterns in radial compressor wheels but endeavors to discuss the effects of simplifications that have to be made in most theoretical treatments to obtain solutions.

All rigorous calculating methods must be based on the fundamental laws of fluid dynamics which are formulated in Ref. 1*. Some of the peculiarities of flows in rotors and the nature of blade-to-blade solutions are discussed in Ref. 2.*

2. FUNDAMENTAL FLOW RELATIONS

Irrespective of its particular nature or field of application, a flow will adapt itself to conditions where the laws of conservation of momentum, mass, and energy are satisfied. In addition, a flow has to meet specified boundary conditions of the field and it is also affected by the thermodynamic processes which it undergoes. If the fluid is a gas, it must satisfy the so-called condition of state, which relates its mass density to pressure and temperature.

The formulations of the three aboved-mentioned conservation laws for rotating flow channels differ from those for flows in stationary passages because of the effects of the centripetal and and Coriolis forces. If the angular velocity $\vec{\omega}$ of a rotor with fixed axis is constant, the three basic relations for the relative velocity field $\vec{W}$ of a compressible fluid in the Eulerian description are:

Equation of Motion, Eq. [7(35)]1:

$$\frac{\partial_R \vec{W}}{\partial t} + \nabla H_R = \vec{W} \times \left(\nabla \times \vec{W} + 2\vec{\omega} \right) + T \nabla s + \vec{f} \tag{1}$$

Equation of Continuity, Eq. [7(29)]1:

$$\frac{\partial_R \rho}{\partial t} + \nabla \cdot (\rho \vec{W}) = 0 \tag{2}$$

Energy Equation, Eq. [7(43)]1:

$$d_R' H_R = d_R' q_o - \frac{\partial_R}{\partial t}\left(\frac{W^2}{2}\right) dt \tag{3}$$

The derivatives $\partial_R(\ )/\partial t$ express the non-steady, or time-depending character of the flow in the rotating frame of reference, and the differentials $d_R'(\ )$ in Eq. 3 represent changes of the flow properties along the relative flow paths travelled by the fluid particles.

The so-called relative total enthalpy H_R per unit mass is defined by

$$H_R = h + \frac{W^2}{2} - \frac{U^2}{2} + g_o z \tag{4}$$

where;

- h - static enthalpy at the static pressure p and the static temperature T
- W - magnitude of relative velocity vector $\vec{W}$
- U - peripheral rotor speed
- g_o - gravitational constant
- z - elevation from a specified level surface

Also,

- s - entropy of fluid per unit mass
- T - absolute static temperature
- $\vec{f}$ - frictional force acting on fluid particle per unit mass
- ρ - mass density
- q_o - heat added to unit mass particle along its path from sources outside the flow field

For so-called absolute flows in stationary passages where ω and U are zero, the absolute total enthalpy H is obtained from Eq. 4 if W is replaced by the magnitude V of the absolute velocity vector $\vec{V}$.

---

*For simplicity, chapter, page, figure, and equation numbers, from these sources are put in square brackets with postfixes 1 or 2 pertaining to Ref. 1 or Ref. 2, respectively. E.g., Eq.[47]2 is equation 47 of reference 2.

If for $\partial_R(\ )/\partial t$ and $d'_R(\ )$ there are substituted the quantities $\partial(\ )/\partial t$ and $d'(\ )$, which represent local time rate of changes, and differential changes along the absolute flow paths of particles, respectively, in the stationary frame of reference, Eqs. 1 to 3 give the principal equations for absolute flows.

For incompressible fluids with constant mass density ρ, the internal energy, and thus the temperature of the fluid, is nearly constant and the static enthalpy h is equivalent to p/ρ, where p is the static pressure of the flow. For the same reason, it is illogical to consider entropy changes, hence $T\nabla s$ is zero. The quantities H_R and H for incompressible flows change to P_R/ρ and P_t/ρ, respectively, with P_R and P_t being the so-called relative and absolute total pressures, defined by

$$P_R = p + \frac{\rho}{2} W^2 - \frac{\rho}{2} U^2 + g_o z \tag{5}$$

and

$$P_t = p + \frac{\rho}{2} V^2 + g_o z \tag{6}$$

For relative incompressible flows, from Eq. 1

$$\frac{\partial_R \vec{W}}{\partial t} + \frac{1}{\rho}\nabla P_R = \vec{W} \times (\nabla \times \vec{W} + 2\vec{\omega}) + \vec{f} \tag{7}$$

From Eq. 2, for ρ = constant,

$$\nabla \cdot \vec{W} = 0 \tag{8}$$

The energy equation along the relative flow paths cannot be obtained directly from Eq. 3 because the work of the frictional forces reduces the relative total pressure P_R. By Eq. [7(44)]1, the energy equation for incompressible relative flows is

$$d'_R P_R = -\frac{\rho}{2} \frac{\partial_R W^2}{\partial t} dt + \rho \vec{W} \cdot \vec{f}\, dt \tag{9}$$

since heat added to the flow from sources outside the flow field does not affect the pressure P_R.

3. DISCUSSION OF SIMPLIFYING ASSUMPTIONS

Equation 1, and its counterpart for absolute flows, have general validity. Major problems occur however if attempts are made to relate the frictional force $\vec{f}$ to the velocity changes in the flow and to the physical properties of the fluid. A differentiation between laminar and turbulent flows must also be made for these formulations. For laminar flows, where the frictional forces are directly proportional to the velocity gradients and the coefficient of viscosity of the fluid, the Navier-Stokes equation is obtained. However, even for constant fluid viscosity the formulation of $\vec{f}$ for compressible flows leads to very complicated expressions (see Eq. [3(6)]1) which defy solutions for arbitrary flow fields. Even for incompressible flows, where $\vec{f} = \nu \nabla^2 \vec{V}$ for constant kinematic viscosity ν, formidable difficulties occur for general solutions, although they could be achieved with modern computers that have extremely large storage capacities. The usefulness of such results is however of questionable value, not only because of their limited application to liquids, or gases at low Mach numbers, but because of the fact that flows in turbomachines have high Reynolds numbers, and are therefore turbulent and not laminar.

Because of the complicated and not yet completely understood mechanism of turbulent motions it has not been possible to establish a generally valid mathematical formulation of the turbulent shear stresses. Approximations are available for the conditions in the vicinity of walls (see p. [39]1) but these relations cannot be used for a general three-dimensional flow field. Analyses that apply Navier-Stokes equation to turbulent flows, and use the non-steady velocity term to account for the turbulent exchange of momentum lateral to the mean flow path, are at best crude approximations of the actual conditions for simple flows and particular boundary conditions. From a rigorous point of view it is not permissible to use the equation of Navier-Stokes for turbulent motions,

It is evident from this discussion that the presently available mathematical tools are not powerful enough to analyze flows in machines with great accuracy, and it is doubtful whether much progress can be expected in the near future. Attempts have been made to study turbulent flows from a molecular viewpoint by taking account of the possible random motions that can occur. However, even if computers were available with access times by a factor of 100 smaller than present nano-second machines, a turbulent flow with simple boundaries would require years of computer time for its analysis. As in all engineering endeavors it is necessary therefore to use simplified methods. From experiments it is known that the largest shear stresses in laminar and turbulent flows occur in the boundary layers along solid walls where the greatest veolcity gradients exist, and that outside of the boundary layers the flow is nearly frictionless, particularly in turbulent motions. For the flow region away from the walls it seem possible therefore to ignore the frictional force $\vec{f}$ in Eq. 1. Moreover, because flows in turbomachines are nearly adiabatic; that is, the quantities of heat denoted by q_o in Eq. 3 are negligibly small, it seems permissible to assume that flows away from the walls are isentropic. For such flows the last two

terms on the right-hand side of Eq. 1 vanish, and the differential $d'_R q_o$ in Eq. 3 can be ignored also. It must be recognized however that the assumption of constant entropy limits the analysis to reversible processes, hence these simplified relations cannot be used for flows with irreversibilities that are caused by supersonic phenomena. In the absence of shocks, the solutions for reversible flows could then be considered to represent a good estimate of the actual conditions if the boundary layers have small thickness. Because experience shows that in boundary layers the static pressure remains nearly constant perpendicular to the walls, the theoretical pressure distributions along the guiding surfaces could be taken as those occurring in actuality. Experimental data of turbulent boundary layers and approximate calculating methods could then be used to determine the frictional forces that are exerted on the walls. Evidently this approach breaks down if flow separations occur, because they will cause major changes in the flow pattern away from the walls, which cannot be handled by the simplified equations, primarily not because it is nearly impossible to predict what boundaries a separated flow will follow.

These difficulties can be avoided if measures are taken that no flow separations occur, for instance, by more complete guiding of the flow with additional blade surfaces. However the best turbomachine always has a minimum of guiding surfaces so that, similary to wing sections, there is obtained the highest ratio of lift and drag. This optimum always occurs if the flows are nearly separated and experience even seems to indicate that radial compressor wheels operate most efficiently if they have slightly separated flows. This conjecture is supported by Fig. [14]2, where the wheel with the highest flow deceleration has the highest efficiency.

Even in the absence of flow separations, the ignoring of the frictional forces along the walls produces conditions that deviate greatly from reality if flows undergo large deflections, as for instance, in the inducer of a radial wheel. Large turnings of flows are associated with large transverse pressure gradients which the particles in the wall boundary layers can overcome only, if they follow different paths than those of the particles away from the walls. As shown in Fig. [13(22)]1, these conditions produce the so-called secondary flows which, because of the formation of the peculiar vortex pattern of Fig. [13(21)]1, cause major changes in the main body of flow outside the boundary layers, which can be responsible for a large fraction of the total losses. Although attempts have been made by many sources to establish theoretical methods for the prediction of secondary flow phenomena and the associated losses, their limited success is due to the difficulties in analyzing actual turbulent flow motions.

The non-steady character of flows in turbomachines is mostly ignored, although it is recognized that the actual flows in these machines cannot be steady. A stationary row of blades arranged after a rotor will have non-steady absolute inlet velocities, even though the relative flow at the rotor discharge is steady. These conditions occur because of the rotor blade wakes and the varying velocities in peripheral direction between neighboring blades. Axial machines with large numbers of blades will not be affected greatly by these conditions, but in radial compressors the non-steady effects can have a major influence because of the small numbers of blades in rotor and diffusor. In these machines, where an effective diffusor is necessary for high overall efficiencies, the diffusor not only has an inlet flow with great amplitude changes but also with large oscillating flow angles.

4. PARTICULAR AXISYMMETRIC FLOWS IN ROTORS

Since solutions of the equations for isentropic steady flows through finitely spaced blades are difficult to obtain, it is customary to solve the problem in two steps. For the first step it is assumed that the rotor has an infinite number of thin blades whose geometry corresponds to, say, the mean section of the actual blade. For given inlet conditions this analysis establishes a series of axisymmetric stream surfaces between the hub and the tip contours of the rotor. If these axisymmetric surfaces are intersected by the actual blades, one obtains the so-called quasi two-dimensional flows of Art. [12]1 between neighboring axisymmetric surfaces, which can be solved by a number of different methods. These methods are discussed on pp. [11]2 to [15]2, together with a comparison of the obtained results with real flow patterns in radial wheels. In this paragraph the discussion is restricted to the first step which is considered as a well defined problem for which an exact solution has to be established. Special cases will be considered only, and general solutions are discussed in paragraph 5.

An indiscriminate use of Eq. 1 for the cited assumptions would give an equation of motion of the form

$$\nabla H_R = \vec{W} \times (\nabla \times \vec{W} + 2\vec{\omega}) \tag{10}$$

For a steady absolute flow at the rotor inlet that has constant total enthalpy H, and whose peripheral velocity components V_u satisfy the relation $R\,V_u$ = constant, hence if they have the same distribution as in a free-vortex flow, it can be shown (see Art. [11.4]1) that the relative total enthalpy H_R is constant at the rotor inlet if the blade surfaces are so designed that the relative flow can enter the rotor at zero incidence angle at all stations along the leading edges. Since, by Eq. 3, H_R is constant also along the relative streamlines for adiabatic, steady conditions, it is evident that H_R must be constant everywhere in the relative flow field, or ∇H_R must vanish, hence

$$\vec{W} \times (\nabla \times \vec{W} + 2\vec{\omega}) = 0 \tag{11}$$

This equation is expressed in Table B-3, p. 15, of Ref. 3 for three-dimensional velocity fields by means of the axisymmetric, orthogonal, curvilinear system shown in Table B-1, p. 13, of Ref. 3, or by Fig. [A3(2)]1. Such coordinate systems will henceforth be called AOC-systems, for short.

For the assumed axisymmetric flows at constant total relative enthalpy H_R, Eq. 11 establishes a flow pattern of the meridional velocity components of $\vec{W}$ which is identical to that of an absolute irrotational

flow at constant total enthalpy H in the same flow channel but without blades. Therefore, it is neither affected by the blade shapes nor is it influenced by different angular rotor velocities. As shown in Art. [11.4]1, it is solely depending on the shape and the curvatures of the meridional channel contours and the generatrices of the axisymmetric stream surfaces.

At an earlier stage of the development even this approximation had a considerable impact on the design of radial wheels. Inspite of its shortcomings it showed that meridional generatrices with large and radical changes in curvature could produce considerable changes in the meridional velocity components between the inner and outer wheel contours, and could be responsible for large flow decelerations, especially along the outer wheel contour. These conditions could create the non-uniformities of rotor discharge flows that were often observed. Indeed, the introduction of wheels with larger axial extensions, giving hub and tip contours with small and gradually changing curvatures, produced the first significant increase in efficiency after many years of stagnant development.

A closer examination of the problem indicates, however, that the infinitely small pressure changes in peripheral direction between adjacent blades have a finite effect because of the infinite number of blades, which must be accounted for by introducing a blade force $\vec{F}_B$ in the equation of motion, representing the force that an element of blade surface exerts on a unit mass of fluid.

For a steady rotor flow having a free-vortex type absolute inlet flow at constant total enthalpy H, there is from Eq. 1 for isentropic conditions,

$$\vec{W} \times \left(\nabla \times \vec{W} + 2\vec{\omega} \right) + \vec{F}_B = 0 \qquad (12)$$

For the assumed frictionless flows the vector of the blade force must be perpendicular to the blade surface at all stations, and must point in such directions as to require that a compressor rotor needs to be driven by an outside source. Hence the blade surface must be known to establish $\vec{F}_B$, and it must be so arranged that the desired inlet and discharge flow conditions can be achieved without sudden changes in flow angle.

Equation 12 will now be applied to a compressor wheel of the type shown in Fig. [1]2, in particular, to the impeller with straight meridional blades arranged after the inducer. For the axisymmetric through-flow solution the actual impeller blades are replaced by an infinite number of meridional half-planes. Thus, $\vec{F}_B$ points everywhere in peripheral direction, and the relative velocities $\vec{W}$ cannot have peripheral velocity components. Expressing $\vec{W} \times (\nabla \times \vec{W} + 2\vec{\omega})$ for this condition, by using the relations of Table B-3, p. 15, of Ref. 3, it can be seen that

$$\vec{F}_B = 2\ \vec{\omega} \times \vec{W} \qquad (13)$$

and

$$\vec{W} \times (\nabla \times \vec{W}) = 0 \qquad (14)$$

Equation 13 shows that the blade force $\vec{F}_B$ per unit mass of fluid equals the Coriolis acceleration. Hence, the flow exerts a force $-\vec{F}_B$ on the blade surface. Then, if $\vec{W}$ has radial components that point away from the axis, the necessary rotor driving moment is in opposite direction to ω, as is the case for a compressor.

Equation 14 indicates that the vectors $\vec{W}$ and $\nabla \times \vec{W}$ have to be parallel without necessarily requiring that $\nabla \times \vec{W}$ must be zero. It can be shown that, for the impeller with straight meridional blades, the flow pattern specified by Eq. 14 is identical with that obtained from Eq. 11. Hence for meridional blades the velocity distributions are also not affected by ω, but depend only on the shape of the axisymmetric stream surfaces, in particular, on the curvatures of their generatrices.

5. AXISYMMETRIC FLOWS IN ROTORS WITH ARBITRARY BLADE SHAPES

Although several methods of solution are available to obtain flow patterns in rotors with arbitrary blade shapes, the present discussion is restricted to the approach of Ref. 1. Further, a limitation is made by considering only the equation of motion of Eq. 12 which is valid for steady rotor flows with constant relative total enthalpy H_R. To solve Eq. 12 correctly for the above-mentioned assumptions it is necessary that the shape of the infinitely many and infinitely thin blade surfaces be specified at all stations in the field.

Since the meridional flow channel of an arbitrary rotor is bounded by surfaces of revolution at hub and tip, and because the flows under consideration have axisymmetric stream surfaces, it is of advantage to use the earlier-mentioned AOC-coordinate systems for the evaluation of the flow patterns. Cylindrical and spherical coordinate systems are special cases of a general AOC-system. Most calculating schemes involve methods of successive approximations in the manner that axisymmetric stream surfaces are assumed, and that they are modified in the course of the calculations until the equations of motions and continuity, and the energy equation, are satisfied. These stream surfaces between hub and tip are taken as coordinate surfaces having the so-called m-generatrices, or meridians, along which the coordinates m are measured in actual lengths. Evidently, the generatrices of the inner and outer walls are m-generatrices also. They are, in fact, the only ones that are fixed. For this discussion it will be assumed that the whole family of m-generatrices is known. It is possible then to establish a net of so-called n-generatrices, or normals, that are everywhere orthogonal to the m-generatrices, and along which the coordinates n are measured. Obviously if the m-generatrices are modified during the successive approximations, the n-generatrices will have to be adjusted also to maintain the orthogonality between the two nets of curves. All AOC-systems contain further a fan of half-planes through the axis of symmetry, the so-called meridional planes, or planes with θ = constant. Each one of these planes is specified by its angle θ with respect to a fixed

reference meridional plane. Thus, stations in the flow field are completely specified by their coordinates m, n, and θ. As shown on page [514]1, it is possible to establish the differential parameters ∇, $\nabla\cdot$, $\nabla\times$, etc., for general AOC-systems. They are functions of the distance R from the axis of symmetry, the angle λ between the tangents to the n-curves and the axis, the curvatures k_m and k_n of the m- and n-curves, and the coordinates m, n, and θ. Because the m-curves are supposed to be the generatrices of the stream surfaces of the flow, no velocity components can exist in direction of the normals n. However, there do occur components W_m and W_u along the m-curves and in peripheral direction, respectively. For these components it is then possible to express the quantity $\vec{W}\times(\nabla\times\vec{W}+2\vec{\omega})$ of Eq. 12, which represents a vector field with components in directions of the coordinates m, n, and θ.

A given blade surface, that meets the inlet and discharge flow conditions of the rotor, is described completely by its intersections with a number of successive meridional planes which in turn are specified by their angles θ. The intersection of the blade surface with a particular plane θ = constant is called the θ-curve of the blade surface. All these θ-curves can be shown in a particular meridional plane and form a family of curves which, together with the pertaining angles θ of the planes θ = constant, where the blade intersection occurs in actuality, specify the blade surface in its entirety. Evidently, the θ-curves of a given blade surface remain fixed even though the nets of m-curves and n-curves have to be modified during the calculations.

Article [11.2]1 shows how the θ-curves can be used to determine the deviations of the blade surface from the radial directions to estimate, for instance, the bending stresses in the blades due to centrifugal forces, and gives relations to establish the directions of the blade forces $\vec{F}_B$ which are everywhere perpendicular to the blade surface. At all stations, the relative velocity vectors $\vec{W}$ must be tangent to the closely spaced blade surfaces. The relative flow angles β are defined as the angles of the vectors $\vec{W}$ with the meridional planes. They are not given by the blade surface alone, because the vectors $\vec{W}$ must also be tangent to the stream surfaces which have the m-curves as generatrices. However for a given set of these curves the angles β are known. Then

$$W_u = W_m \tan\beta$$

where W_u and W_m are the peripheral and meridional velocity components of $\vec{W}$. For known angles β the blade force $\vec{F}_B$ can be formulated also, and from Eq. 12 there is then obtained a differential equation of the form

$$\frac{\partial W_m}{\partial n} + \frac{\partial W_m}{\partial m} X_1 + W_m X_2 + \omega X_3 = 0 \qquad (15)$$

where X_1, X_2, X_3 are known functions of m and n that depend on the nets of the m-curves and n-curves, and on the shape of the blade surface.

Equation 15 can be used to determine the distribution of the meridional velocity component W_m in the field. It can be noted, however, that Eq. 15 contains derivates of W_m in the directions of n and m. The term with $\partial W_m/\partial m$ occurs because of the blade force. In particular the function X_1 equals

$$X_1 = \tan\delta \tan^2\beta \qquad (16)$$

where δ is the angle between the θ-curve of the blade surface and the normal n at particular stations.

The partial differential equation of Eq. 15 can be transformed into an ordinary differential equation if the method of solving along particular characteristics is applied. These characteristics are curves in the meridional plane that have the angle γ with the normals, where

$$\tan\gamma = \tan\delta \sin^2\beta \qquad (17)$$

If the lengths measured along these characteristics are denoted by x, Eq. 15 can be written as

$$\frac{dW_m}{dx} + W_m Y_1 + \omega Y_2 = 0 \qquad (18)$$

where the functions Y_1 and Y_2 are related to the functions X_1, X_2, and X_3. Equation 18 represents a linear differential equation which has the solution

$$W_m = e^{-\int Y_1\,dx}\left[C - \omega\int Y_2\left(e^{+\int Y_1\,dx}\right)dx\right] \qquad (19)$$

C is a constant that can be determined by applying the equation of continuity.

Some methods try to avoid the complications associated with the establishing of the characteristics, by limiting the analysis to particular blade shapes, namely, frequently to those which are called "normal" blade surfaces in Ref. 1, and whose angles δ of Eqs. 16 and 17 are everywhere zero. Thus, a normal blade surface has θ-curves that coincide everywhere with the normals, or n-generatrices. Then the function X_1 of Eq. 16 is zero and the velocity components W_m can be obtained directly from Eq. 19 by integration along the normals. Hence, these methods do not deal with a fixed blade surface, but with one

that changes its shape if the n-generatrices must be modified in the course of performing the successive approximations. Such methods usually specify the flow angles β along the normals. In some cases it may then occur that the blade surfaces that result, namely, those with the final n-generatrices for the chosen flow angles, have shapes which either cannot be built for manufacturing reason, or deviate so much from the radial direction that the bending stresses during rotation become excessive.

If the method of solution with characteristics is applied, it can be shown that the characteristics terminate at the leading and trailing edges of the blade surfaces, and then continue as "normals" into the non-bladed regions of the flow channel. Hence if it is assumed a priori that the blade surfaces are normal blade surfaces, the analysis cannot investigate the conditions that occur with obliquely cut-off leading edges or trailing edges of the blades, in fact, the method has difficulties in producing compatible flow conditions at the rotor inlet and discharge unless the blade terminates at locations where the correct normals can be established a priori also.

6. APPLICABILITY OF AXISYMMETRIC THROUGH-FLOW METHODS

For the analyses discussed above it is necessary to assume that the flow follows the hub and tip contours of the flow channel, hence these surfaces must be the stream surfaces that form the boundaries of the flow field. The velocity profiles of and the cushioning effects due to the boundary layers at these surfaces, and the velocity changes and disturbances that are created by the tip clearance flows and scrubbing effects in unshrouded wheels, cannot be taken into account. Although the conditions that occur with flow incidence angles at the blade leading edges can be treated in an approximate manner, primarily as far as the associated changes in relative total enthalpy are concerned, the assumption of axial flow symmetry precludes investigations to establish optimum conditions at the rotor inlet. The same assumption makes it impossible also to take account of losses. They can be considered only in the equation of continuity as a uniformly distributed effect that changes the mass density of the fluid.

Reference 2 discusses the lack of knowledge in predicting the permissible flow decelerations in compressor rotors. Equally lacking is information that gives criteria for the permissible velocity changes along the inner and outer wheel contours.

In actuality the described methods cannot take account of disturbances that are created by the flows downstream of the rotor, in fact, this situation very frequently creates incompatibilities between the calculated pressure distributions at the trailing edges of the blading and those which are imposed by elements arranged after the rotor.

It was shown earlier that the methods give only limited information about the flow in the impeller parts that have radial blades, inasmuch as the flow patterns are only influenced by the streamline curvatures and that the effects of the Coriolis accelerations have no bearing on the velocity changes. Hence small changes in the assumed net of streamlines, which can still be associated with large changes in their curvatures, may produce considerable deviations in the flow distributions which are difficult to evaluate for lack of a firm basis.

It seems to the writer that the maximum benefits of the method arise with determination of the flow conditions in the inducer part of a radial wheels, not so much as far absolute accuracy is concerned but with regard to comparison of relative effects of design changes. Limitations are however imposed because of the inability of the method to deal with supersonic flow phenomena. Reference 2 mentions the possible advantages of particular leading edge configurations, and calculations in this direction have produced interesting results by applying the method of solution with the afore-mentioned characteristic curves, in contrast to the approach with "normal" blade surfaces which cannot deal with such blade shapes. As pointed out in Ref. 2 also, the discussed method represents the only approach, at least to this date, that can provide data with regards to the effects of blade shapes of the inducer parts, since these bladings cannot be analyzed with the usual cascade theories because the flow at the inducer discharge enters the individual blade channel of the radial wheel.

Although the so-called blade-to-blade solutions are discussed in Ref. 2, it should be pointed out here that the usual approach of applying the results of the axisymmetric calculations to finite blade spacings, that is based on the moment of momentum considerations of Art. [11.12]1, gives erroneous results near the rotor discharge because it cannot take account of the equalizing of the pressures on the suction and pressure sides of the blades. However, at the discharge of the inducer, where its blades meet the impeller blades, this approach will provide interesting information which can be used for the design of improved inducer bladings.

REFERENCES

1. Vavra, M. H. — Aerothermodynamics and Flow in Turbomachines, Wiley Bros., New York 1960.

2. Vavra, M. H. — Basic Elements for Advanced Designs of Radial-Flow Compressors, AGARD Lecture Series No. 39, 1970.

3. Vavra, M. H. — "Axial Flow Turbines," Von Karman Institute, Brussels, Lecture Series 15, April 1969.

CONCLUSIONS

by

J. CHAUVIN - Lecture Series Director

The interest in advanced compressors has been shown by the number and quality of people attending the course (84 in total), representing most of the companies, research or teaching establishments coping with turbomachinery in Europe, with a small delegation from the U.S.A. and Canada.

From its initiation, the Lecture Series has been limited in time to two days in each of the host countries, Belgium and Norway. This has, in turn, limited its scope, which was arbitrarily chosen, to cover only some of the main forefront problems of the fluid mechanic design of advanced (i.e. high pressure ratio) axial and radial compressors. It is therefore fragmentary, but it is the course director's feeling that it is representative of the main area of past progress and future research.

Due to the limited time, the verbal presentations had to be rather succint, but the message was obviously carried across to the auditors. The written contributions are clearly more comprehensive, and the authors have to be thanked for providing an excellent set of notes, which cover, in most cases, hitherto unpublished or original data or approaches. Some of the verbal presentation even included additional original information gained between text publication and presentation.

Although turbomachinists can be proud of the achievement made in high performance axial and radial compressors, the Lecture Series has clearly shown the urgent need for more information and therefore more detailed research on the detailed flow behaviour between blade passages. This is valid as well for axial compressors as for inducers, impellers and diffusors of high pressure ratio, small mass flow radial compressors. The real behaviour of the flow, affected by boundary layer separation, shock boundary layer interaction, unsteady flow, coriolis and centrifugal forces is not yet fully understood. Even the apparently simple question of the validity of high speed cascade data when applied to real machine or of the way to apply them, is not satisfactorily solved, although the work carried out by the groups of Professor Vavra, Mr. Fabri and Mr. Starken is expected to throw much more light on this particular problem in the near future.

It is evident that if we want to progress further, and in particular to achieve within the next decade, the same order of increase of pressure ratio per stage, at almost constant efficiency that has been achieved in the last ten years, we need to develop more theoretical work, but particularly, better experimental techniques to explore the complicated three-dimensional, unsteady viscous compressible flow inside the turbomachines, without disturbing too much the flow by the instrumentation (laser-beam holograms, probe miniaturisation, measurements in rotation). We are confident that success can be achieved within a reasonable period of time and that the corresponding investment is worthwhile. Already, the development of advanced material has removed the limitations on peripheral speed.

As mentioned earlier, only some particular aspects of the problems associated with advanced compressors have been examined in this Lecture Series.

It would be worthwhile, as a follow-up, to envisage additional courses on subjects such as off-design performance, stall and surge evaluation, mechanical problems, such as bearings, shaft, stressing and vibrations of disks and bladings, manufacturing problems and material characteristics within a reasonable period of time.

From the experience of this course, we are confident that the initiative would be well received.

AGARD Lecture Series No.39
North Atlantic Treaty Organization, Advisory Group for Aerospace Research and Development
ADVANCED COMPRESSORS
Published August 1970
292 pages

The material in this book has been assembled to support a Lecture Series presented by the authors in Brussels (Belgium) and Bolkesjø (Norway) in June 1970.

The papers presented review the significant progress which has been made in the design and development of high performance axial and radial compressors in response to the increasing demand from jet engine and gas turbine manufacturers.

Through flow methods of calculation, cascade performance, mass flow limitation, high subsonic flow in blading with local supersonic region, are presented for axial compressors. Advanced design of radial flow compressors, supersonic vaneless and vaned diffusers are covered for radial compressors.

621.438.031.3

AGARD Lecture Series No.39
North Atlantic Treaty Organization, Advisory Group for Aerospace Research and Development
ADVANCED COMPRESSORS
Published August 1970
292 pages

The material in this book has been assembled to support a Lecture Series presented by the authors in Brussels (Belgium) and Bolkesjø (Norway) in June 1970.

The papers presented review the significant progress which has been made in the design and development of high performance axial and radial compressors in response to the increasing demand from jet engine and gas turbine manufacturers.

Through flow methods of calculation, cascade performance, mass flow limitation, high subsonic flow in blading with local supersonic region, are presented for axial compressors. Advanced design of radial flow compressors, supersonic vaneless and vaned diffusers are covered for radial compressors.

621.438.031.3

AGARD Lecture Series No.39
North Atlantic Treaty Organization, Advisory Group for Aerospace Research and Development
ADVANCED COMPRESSORS
Published August 1970
292 pages

The material in this book has been assembled to support a Lecture Series presented by the authors in Brussels (Belgium) and Bolkesjø (Norway) in June 1970.

The papers presented review the significant progress which has been made in the design and development of high performance axial and radial compressors in response to the increasing demand from jet engine and gas turbine manufacturers.

Through flow methods of calculation, cascade performance, mass flow limitation, high subsonic flow in blading with local supersonic region, are presented for axial compressors. Advanced design of radial flow compressors, supersonic vaneless and vaned diffusers are covered for radial compressors.

621.438.031.3

AGARD Lecture Series No.39
North Atlantic Treaty Organization, Advisory Group for Aerospace Research and Development
ADVANCED COMPRESSORS
Published August 1970
292 pages

The material in this book has been assembled to support a Lecture Series presented by the authors in Brussels (Belgium) and Bolkesjø (Norway) in June 1970.

The papers presented review the significant progress which has been made in the design and development of high performance axial and radial compressors in response to the increasing demand from jet engine and gas turbine manufacturers.

Through flow methods of calculation, cascade performance, mass flow limitation, high subsonic flow in blading with local supersonic region, are presented for axial compressors. Advanced design of radial flow compressors, supersonic vaneless and vaned diffusers are covered for radial compressors.

621.438.031.3

AGARD Lecture Series No.39
North Atlantic Treaty Organization, Advisory Group for Aerospace Research and Development
ADVANCED COMPRESSORS
Published August 1970
292 pages

The material in this book has been assembled to support a Lecture Series presented by the authors in Brussels (Belgium) and Bolkesjø (Norway) in June 1970.

The papers presented review the significant progress which has been made in the design and development of high performance axial and radial compressors in response to the increasing demand from jet engine and gas turbine manufacturers.

Through flow methods of calculation, cascade performance, mass flow limitation, high subsonic flow in blading with local supersonic region, are presented for axial compressors. Advanced design of radial flow compressors, supersonic vaneless and vaned diffusers are covered for radial compressors.

621.438.031.3

AGARD Lecture Series No.39
North Atlantic Treaty Organization, Advisory Group for Aerospace Research and Development
ADVANCED COMPRESSORS
Published August 1970
292 pages

The material in this book has been assembled to support a Lecture Series presented by the authors in Brussels (Belgium) and Bolkesjø (Norway) in June 1970.

The papers presented review the significant progress which has been made in the design and development of high performance axial and radial compressors in response to the increasing demand from jet engine and gas turbine manufacturers.

Through flow methods of calculation, cascade performance, mass flow limitation, high subsonic flow in blading with local supersonic region, are presented for axial compressors. Advanced design of radial flow compressors, supersonic vaneless and vaned diffusers are covered for radial compressors.

621.438.031.3

NATIONAL DISTRIBUTION CENTRES FOR UNCLASSIFIED AGARD PUBLICATIONS

Unclassified AGARD publications are distributed to NATO Member Nations through the unclassified National Distribution Centres listed below

BELGIUM
General J. DELHAYE
Coordinateur AGARD - V.S.L.
Etat Major Forces Aériennes
Caserne Prince Baudouin
Place Dailly, Bruxelles 3

CANADA
Director of Scientific Information Services
Defence Research Board
Department of National Defence - 'A' Building
Ottawa, Ontario

DENMARK
Danish Defence Research Board
Østerbrogades Kaserne
Copenhagen Ø

FRANCE
O.N.E.R.A. (Direction)
29, Avenue de la Division Leclerc
92, Châtillon-sous-Bagneux

GERMANY
Zentralstelle fur Lüftfahrtdokumentation
und Information
Maria-Theresia Str. 21
8 München 27
Attn: Dr Ing. H.J. RAUTENBERG

GREECE
Hellenic Armed Forces Command
D Branch, Athens

ICELAND
Director of Aviation
c/o Flugrad
Reykjavik

ITALY
Aeronautica Militare
Ufficio del Delegato Nazionale all' AGARD
3, P. le del Turismo
Roma/Eur

LUXEMBOURG
Obtainable through BELGIUM

NETHERLANDS
Netherlands Delegation to AGARD
National Aerospace Laboratory, NLR
Attn: Mr A.H. GEUDEKER
P.O. Box 126
Delft

NORWAY
Norwegian Defense Research Establishment
Main Library, c/o Mr P.L. EKERN
P.O. Box 25
N-2007 Kjeller

PORTUGAL
Direccao do Servico de Material
da Forca Aerea
Rua de Escola Politecnica 42
Lisboa
Attn: Brig. General Jose de Sousa OLIVEIRA

TURKEY
Turkish General Staff (ARGE)
Ankara

UNITED KINGDOM
Ministry of Technology Reports Centre
Station Square House
St. Mary Cray
Orpington, Kent BR5 3RE

UNITED STATES
National Aeronautics and Space Administration (NASA)
Langley Field, Virginia 23365
Attn: Report Distribution and Storage Unit

★ ★ ★

If copies of the original publication are not available at these centres, the following may be purchased from:

Microfiche or Photocopy

Clearinghouse for Federal
Scientific and Technical
Information (CFSTI)
Springfield
Virginia 22151, USA

Microfiche

ESRO/ELDO Space
Documentation Service
European Space
Research Organization
114, Avenue de Neuilly
92, Neuilly-sur-Seine, France

Microfiche

Ministry of Technology
Reports Centre
Station Square House
St. Mary Cray
Orpington, Kent BR5 3RE
England

The request for microfiche or photocopy of an AGARD document should include the AGARD serial number, title, author or editor, and publication date. Requests to CFSTI should include the NASA accession report number.

Full bibliographical references and abstracts of the newly issued AGARD publications are given in the following bi-monthly abstract journals with indexes:

Scientific and Technical Aerospace Reports (STAR)
published by NASA,
Scientific and Technical Information Facility,
P.O. Box 33, College Park,
Maryland 20740, USA

United States Government Research and Development Report Index (USGDRI), published by the Clearinghouse for Federal Scientific and Technical Information,
Springfield, Virginia 22151, USA

Printed by Technical Editing and Reproduction Ltd
Harford House, 7-9 Charlotte St, London. W1P 1HD